95-002D

# RR Lyrae Variable Stars in the CCD/Transit Instrument Survey



By

Charles J. Wetterer

B.S., Physics and Astronomy, University of Maryland, 1986

M.S., Physics, University of New Mexico, 1990



DISSERTATION

Submitted in Partial Fulfillment of the
Requirements for the Degree of
Doctor of Philosophy in Physics

The University of New Mexico
Albuquerque, New Mexico

July, 1995

# REPORT DOCUMENTATION PAGE

*Form Approved*
*OMB No. 0704-0188*



**1. AGENCY USE ONLY** *(Leave blank)*

**2. REPORT DATE**
Jul 95

**3. REPORT TYPE AND DATES COVERED**

**4. TITLE AND SUBTITLE**
RR Lyrae Variable Stars in the Cell/Transit Instrument Survey

**5. FUNDING NUMBERS**

**6. AUTHOR(S)**
Charles J Wetterer

**7. PERFORMING ORGANIZATION NAME(S) AND ADDRESS(ES)**
AFIT Students Attending:
Univ of New Mexico

**8. PERFORMING ORGANIZATION REPORT NUMBER**
AFIT/CI/CIA
95-002D

**9. SPONSORING/MONITORING AGENCY NAME(S) AND ADDRESS(ES)**
DEPARTNEMT OF THE AIR FORCE
AFIT/CI
2950 P STREET, BDLG 125
WRIGHT-PATTERSON AFB OH 45433-7765

**10. SPONSORING/MONITORING AGENCY REPORT NUMBER**

**11. SUPPLEMENTARY NOTES**

**12a. DISTRIBUTION/AVAILABILITY STATEMENT**
Approved for Public Release IAW AFR 190-1
Distribution Unlimited
BRIAN D. GAUTHIER, MSgt, USAF
Chief Administration

**12b. DISTRIBUTION CODE**

**13. ABSTRACT** *(Maximum 200 words)*

DTIC QUALITY INSPECTED 5

**14. SUBJECT TERMS**

**15. NUMBER OF PAGES**
343

**16. PRICE CODE**

**17. SECURITY CLASSIFICATION OF REPORT**

**18. SECURITY CLASSIFICATION OF THIS PAGE**

**19. SECURITY CLASSIFICATION OF ABSTRACT**

**20. LIMITATION OF ABSTRACT**

NSN 7540-01-280-5500

Standard Form 298 (Rev. 2-89)
Prescribed by ANSI Std. Z39-18

ACKNOWLEDGEMENTS

I would like to thank the members of my dissertation committee, primarily John T. McGraw, for their salient comments and guidance during this work. I would also like to thank Thomas R. Hess for his work with the CTI databases and programing, Randy Grashuis for many nights of observing at Capilla Peak observatory, Fritz Benedict for his help with the CTI astrometry, and Jim Kunkle for many useful conversations and insights. Thanks also to Kirsten Boudreau, Heather Vogel, and Alex Collins for help throughout this endeavor.

This dissertation builds on the work of many who worked on CTI in the past. In addition to John T. McGraw and Thomas R. Hess, the CTI group at Arizona included J.R.P. Angel, T.A. Sargent, M.G.M Cawson, M.J. Keane, and J.D. Kirkpatrick.

# RR Lyrae Variable Stars in the CCD/Transit Instrument Survey

By

Charles J. Wetterer

ABSTRACT OF DISSERTATION

Submitted in Partial Fulfillment of the
Requirements for the Degree of

Doctor of Philosophy in Physics

The University of New Mexico
Albuquerque, New Mexico

July, 1995

RR LYRAE VARIABLE STARS IN THE CCD/TRANSIT INSTRUMENT SURVEY

by

Charles J. Wetterer

BS, Physics and Astronomy, University of Maryland, 1986

MS, Physics, University of New Mexico, 1990

PhD, Physics, University of New Mexico, 1995

ABSTRACT

RR Lyrae variable stars have long been recognized as important tools in probing the mass, chemical distribution and kinematics of the Galaxy from the inner recesses of the nuclear bulge to the outer environs of the distant Galactic halo. This dissertation chronicles an RR Lyrae variable star survey from a thorough description of the initial observations with the CCD/Transit Instrument (CTI), to an examination of RR Lyrae space density and the Galactic mass using the discovered RR Lyrae stars.

The RR Lyrae space density as a function of Galactocentric distance is shown to be a power-law function ($R^{-3 \text{ to } -3.5}$) and consistant with an ellipsoidal distribution in the nuclear bulge and more spherically symmetric distribution in the Galactic halo. The unique area of the CTI survey and comparison to other RR Lyrae surveys verifies this function is valid throughout the Galactic halo and over the range of Galactocentric distances sampled ($0.6 < R < 40$ kpc). Local

underdensities and overdensities of RR Lyrae stars are discussed, including a possible resonance with the Magallenic Clouds ($R \approx 50$ kpc).

The Galactic mass estimated using radial velocities of RR Lyrae stars discovered in the CTI survey does not support the existence of a massive dark Galactic halo. This result is compared to the mass as determined from the radial velocities of other halo objects. Depending on the type of orbits assumed, the radial velocities of RR Lyrae stars, globular clusters, and dwarf elliptical galaxies can be used to support the notion that a massive dark halo exists (i.e. the mass-to-light ratio increases for increasing Galactocentric distance), or that no excessive dark matter exists in the Galactic halo (i.e. the mass-to-light ratio remains constant for increasing Galactocentric distance).

## Table of Contents

Table of Contents (continued)

Table of Contents (continued)

## List of Figures

List of Figures (continued)

## List of Figures (continued)

## List of Tables

## Chapter 1  Introduction

RR Lyrae variable stars have long been recognized as important tools in probing the mass, chemical distribution and kinematics of the Galaxy from the inner recesses of the nuclear bulge to the outer environs of the distant Galactic halo. Questions concerning dark matter, the age of the Galaxy, and the size of the universe can all be addressed using information obtained from the study of RR Lyrae stars.

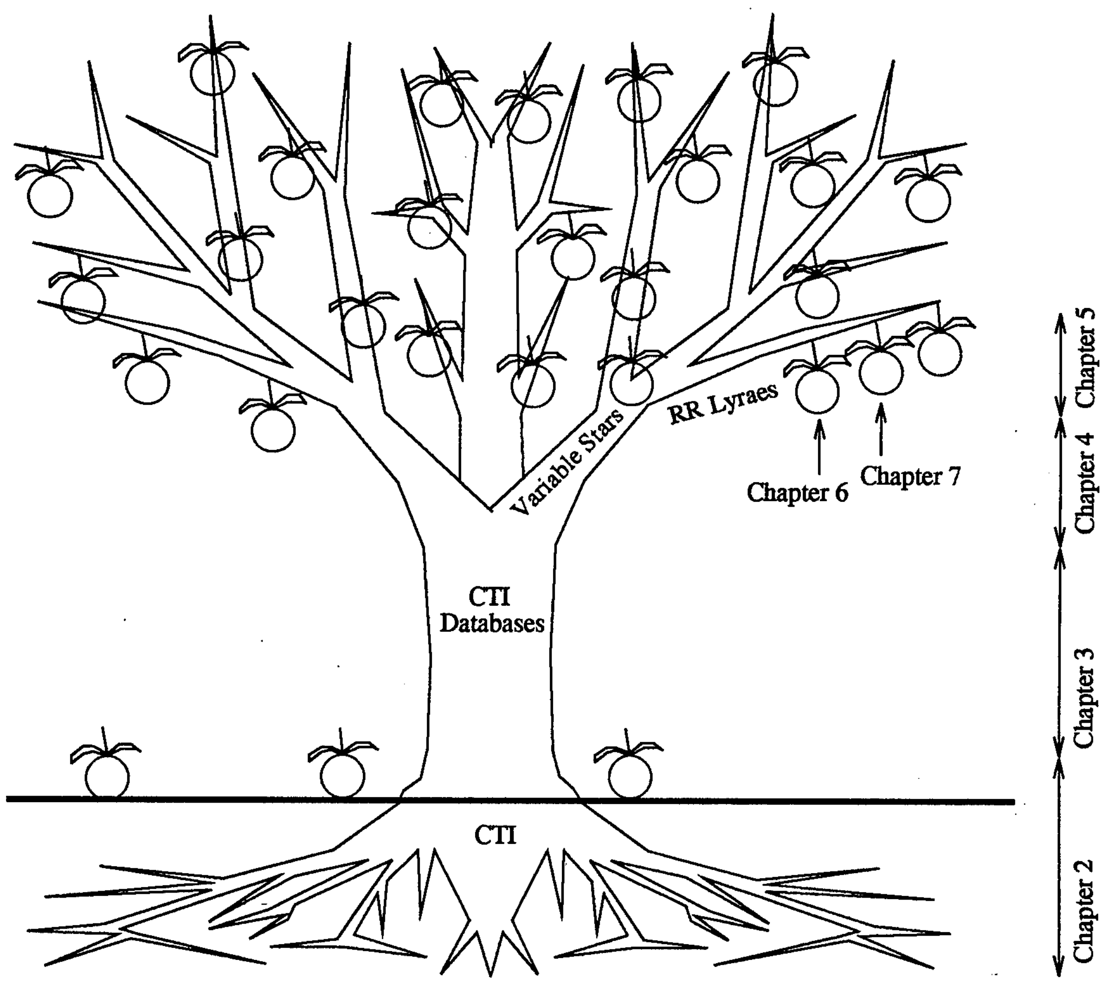


Figure 1.1 - Schematic outline of dissertation. (Not all "branches" and "fruit" shown.)

This dissertation chronicles an RR Lyrae variable star survey from its roots, in the observations of the CCD/Transit Instrument (CTI), to its fruits, in results of astrophysical significance. The outline is shown schematically in Figure 1.1. Two chapters are devoted to describing CTI and are intended to serve as a starting point for those wishing to explore other branches of the tree in Figure 1.1. Chapter 2 describes the CTI in detail as well as the portion of the sky contained in the resulting survey and Chapter 3 describes the reduction and calibration of the CTI data and contents of the survey databases. The next two chapters use the CTI survey databases to identify particular types of objects. Chapter 4 discusses the search for variable stars in the CTI survey, while Chapter 5 narrows the search to a particular type of variable star, namely RR Lyraes. Both of these chapters contain information relavent to those interested in conducting similar searches in the CTI databases. The final two chapters use the RR Lyraes discovered in the CTI survey to examine the distribution of RR Lyraes in the Galactic halo (Chapter 6) and the total mass as a function of Galactocentric radial distance of the Milky Way (Chapter 7).

## Chapter 2 The CCD/Transit Instrument

The CCD/Transit Instrument (CTI) is a stationary, meridian pointing optical telescope that images a narrow strip of the sky at all right ascensions. The telescope is rigidly mounted to point at a single declination and relies on the Earth's rotation to bring different parts of the sky into view. The databases resulting from the survey contain over 500,000 objects observed during the seven years the telescope operated on Kitt Peak. This chapter describes in detail the CTI's design and the portion of the sky CTI surveys.

## 2.1 CTI Description

CTI is a 1.8 meter, f/2.2 telescope operated on Kitt Peak in Arizona (31° 57' 41.9" north latitude, 111° 36' 00.5" west longitude, 2080 m elevation) from 1984 to 1992 (McGraw et al. 1980, 1983, 1986 and McGraw 1992a). A schematic of the optical design is shown in Figure 2.1 with optical characteristics of each element given in Table 2.1. The paraboloidal primary reflects light first to a 0.76 meter secondary, then to a 0.76 meter tertiary located just above the primary, and finally to the detectors located near the center of the structure. The secondary and tertiary are figured as a Paul-Baker two mirror corrector (Paul 1935, Baker 1969), providing achromatic correction of the primary's coma aberration and an almost diffraction limited field of view of over one degree at the focal plane. Originally designed for the Hale 5-meter telescope, this type of corrector has never been used

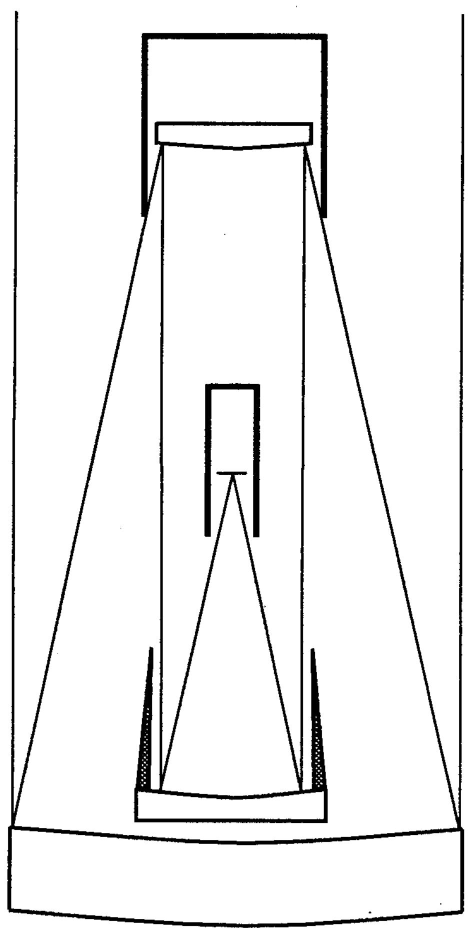

Figure 2.1 - CTI Optical Design

Table 2.1 - CTI Optical Design (dimensions in cm)

| Surface | Diameter | Radius of Curvature | Aspheric Coefs K | A6 | Distance to next surface |
|---|---|---|---|---|---|
| primary | 180 | -308.0399 | -1 | 0 | 105.1778 |
| secondary | 76 | 97.80481 | 0 | -3.15795E-11 | 97.2942 |
| tertiary | 76 | -97.19998 | 0 | 0 | 48.5404 |

before because it places the focal plane in an inconvenient position for conventional telescopes, high in the structure midway between the secondary and tertiary mirrors. Since CTI uses electronic detectors and is a dedicated transit instrument rigidly mounted in its own building to point at a single declination, it does not suffer from this limitation.

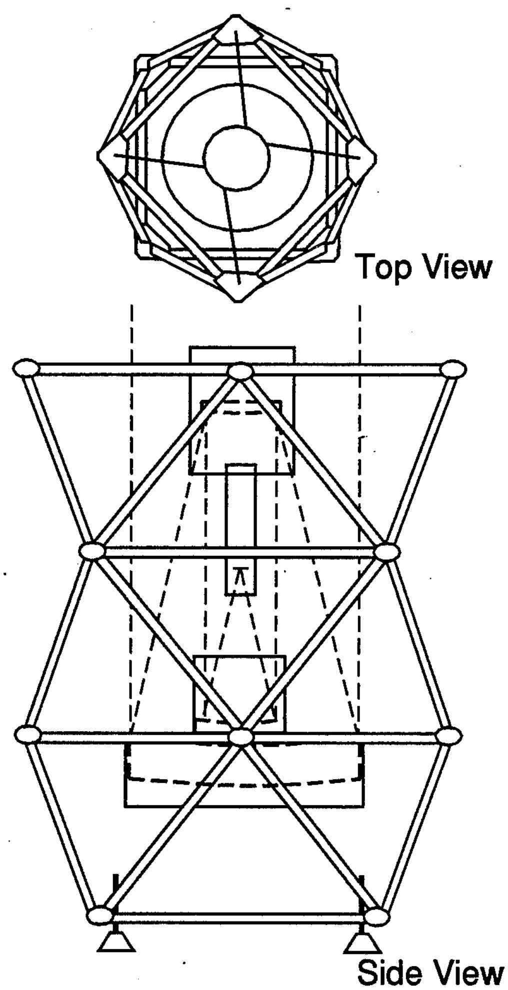

Figure 2.2 CTI Structural Design

The optics are mounted in a thermally compensating structure in which the vertically diagonal sections are made of stainless steel with a lower linear expansion coefficient than the aluminum horizontal sections. A schematic of the structure is shown in Figure 2.2. The angles at the joints were

chosen such that expansion and contraction due to temperature changes in both metals have no effect in the vertical dimension. This enables the telescope to maintain its focus throughout the night, independent of changes in temperature.

The large field of view enables the telescope to simultaneously use two side-by-side RCA charge-coupled devices (CCDs). Typically, one of the CCDs observed through a V filter while the other cycled through the B, R, and I filters. For several nights, however, an ultraviolet transparent clear filter (C) for faint galaxy and supernova detection and narrow

Table 2.2 - CTI Filter Set

| | |
|---|---|
| B | BG-12 (1 mm) + BG-18 (1 mm) + GG-385 (1 mm) |
| V | BG-18 (1 mm) + GG-495 (2 mm) |
| R | OG-570 (1 mm) + KG-3 (2 mm) |
| I | RG-9 (3 mm) |
| C | UV-28 (2.5 mm) |
| A | H-alpha 658 nm - on (>3 mm) |
| O | H-alpha 663 nm - off (>3 mm) |

band H-alpha filters were used. A summary of the CCD filter set for CTI, made up of Schott and Hoya glass filters and $H_\alpha$ interference filters, is given in Table 2.2. The CTI observing log, listing the filter combination and observational conditions of every night of operation of CTI on Kitt Peak, is summarized in Table A1.1 of Appendix 1 of this dissertation.

The RCA CCDs have 320 x 512 x 30 $\mu$m square pixels with the construction of the CCD camera and controllers following

Table 2.3 - CCD Operational Parameters

| | |
|---|---|
| CCD0 | - 72 electron readout noise |
| | - 9.18 electrons/ADU |
| CCD1 | - 40 electron readout noise |
| | - 10.78 electrons/ADU |
| CCDs have no cosmetic blemishes | |

a design first used by Kitt Peak National Observatory (Marcus et al. 1979). The CCD operational parameters are given in Table 2.3. The field scale for the telescope is 52 arcsec/mm with each pixel subtending 1.55 arcseconds. The CCDs are aligned with their columns in the east-west direction and are operated in the time-delay and integrate (TDI) mode at the apparent sidereal rate. Thus, for the stationary telescope pointed at a particular declination on the meridian, images of objects in the sky drift across the CCDs at the same rate as the electronic image is read off. This is illustrated in Figure 2.3. The effective exposure time for an object is 1 minute.

Images of the sky 8.26 arcminutes wide (320 pixels) in the north-south direction and arcminutes to more than a hundred degrees long in the east-west direction (depending on the length of the night) are obtained each night of observation. Due to interruptions by clouds or problems with the telescope's control computer, a single night's observation is not necessarily continuous, and may be segmented into several "sweeps", the term William Herschel applied to his observations made in a similar manner about 200 years ago.

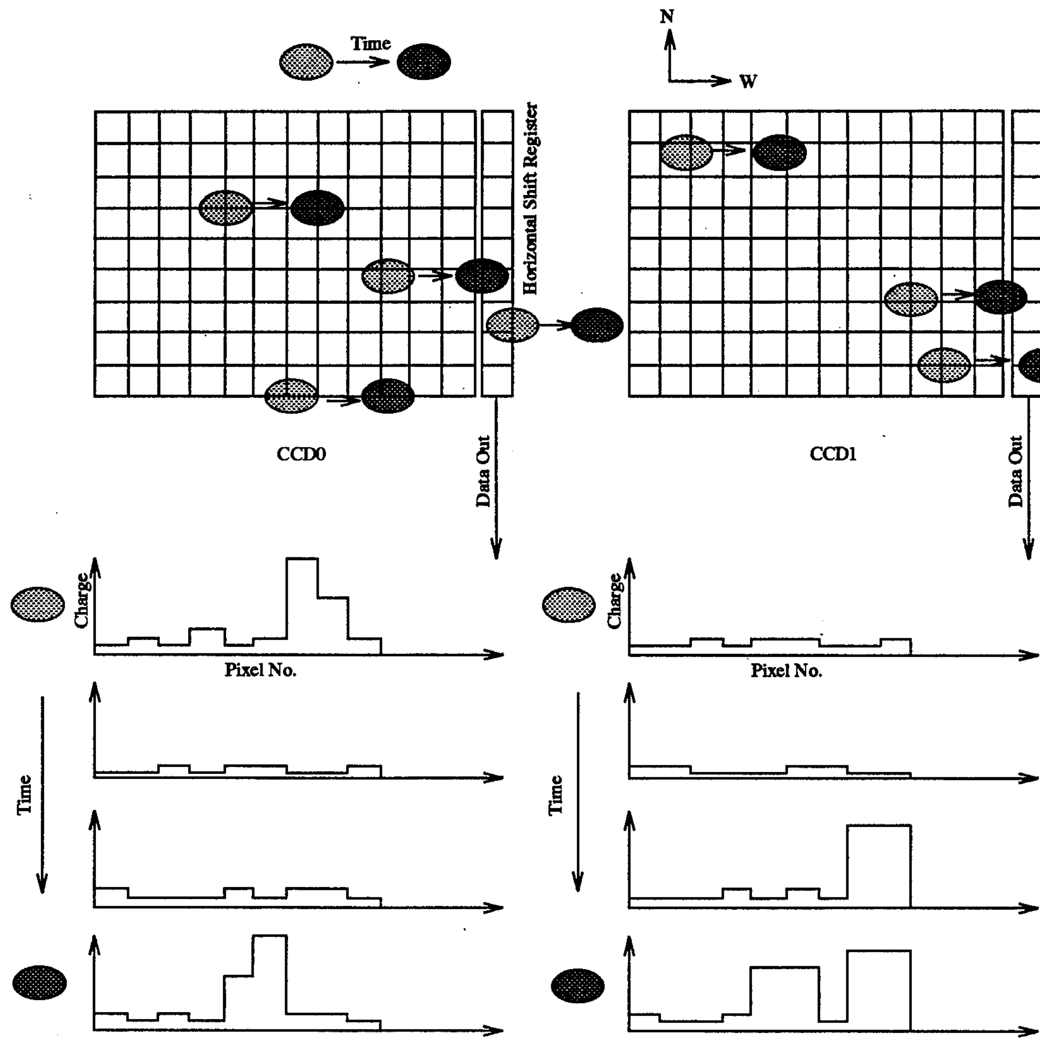


Figure 2.3 - CCD sidereal rate Time Delay and Integrate (TDI) mode. Due to the Earth's rotation, images of stars drift across the CCDs at a calculable rate. The electronic image forming in the pixels of the CCD is read out at the same rate, creating an unsmeared digitized image of the stars. The shaded dots represent stars, with the darker shade corresponding to the same stars some time later.

Additionally, due to precession and slight shifts in telescope pointing, each night's observation doesn't exactly overlap in declination, making the effective width of the CTI survey 9.5 arcminutes. The total area surveyed by CTI is approximately

50 square degrees, corresponding to 0.065% of the total sky. The CCDs saturate for stars brighter than V ≈ 12 and the nightly limiting magnitude is V ≈ 20. The resulting raw images are not unlike an image obtained from a CCD operating in its standard staring mode.

The data from the telescope goes through many steps of processing before information is merged into an object master list and history lists. A detailed description of this analysis and calibration process is given in Chapter 3. The history lists contain a day-by-day record of the time, calibrated instrumental luminosity, error in luminosity, calibrated position and size of every object observed for each filter. The history lists also reference the master list, which contains averaged positional and photometric information as well as various measures of each object's characteristics. These lists are the primary databases produced by CTI for use in scientific study, although several other intermediate databases which contain interesting information as well are produced throughout the reduction process.

CTI offers unique advantages over other types of telescopes. The stability and simplicity of the design lends itself to automation. Indeed, this telescope is the Earth-based model for the proposed Lunar Ultraviolet Telescope Experiment (LUTE) (McGraw 1992b, 1993). Additionally, by its very nature, CTI observes everything in the survey strip equally well, providing an unbiased sample of a particular

type of object. Finally, and perhaps most importantly, because CTI is a dedicated instrument, a complete, astrometrically and photometrically precise survey of all types of stars and other astronomical objects over an extended period of time is obtained. Ongoing projects include the search for and study of quasars (McGraw et al. 1988), white dwarf stars (Kirkpatrick and McGraw 1988), red dwarf stars (Kirkpatrick et al. 1990, 1994, Kirkpatrick 1992, 1994), extragalactic supernovae, high proper motion stars (Benedict et al. 1989, 1991), standard stars (McGraw et al. 1994) and all types of variable stars (McGraw 1992a, Wetterer et al. 1994, and this dissertation). Other telescopes and large surveys using techniques pioneered by CTI include the Sloan Digital Sky Survey (Kent et al. 1994, Kron 1994, Stoughton et al. 1994), new liquid mirror telescopes (Borra et al. 1989, 1992, Content et al. 1989), and standard telescopes employing the TDI mode of CCD operation (for example, Kent et al. 1993).

## 2.2 CTI Survey Area Description

CTI observed at a declination centered at +28°02′ (1987.5 epoch, J2000 equinox), four degrees from the zenith at Kitt Peak. This declination was chosen to pass within a degree of the north galactic pole ($12^h$ $50^m$), and intersects the heart of the Coma cluster of galaxies. The CTI survey strip also passes within a degree of the galactic anti-center ($5^h$ $45^m$), and within two degrees of the direction of solar motion ($18^h$ $09^m$). Figures 2.4 and 2.5 illustrate the sky coverage in

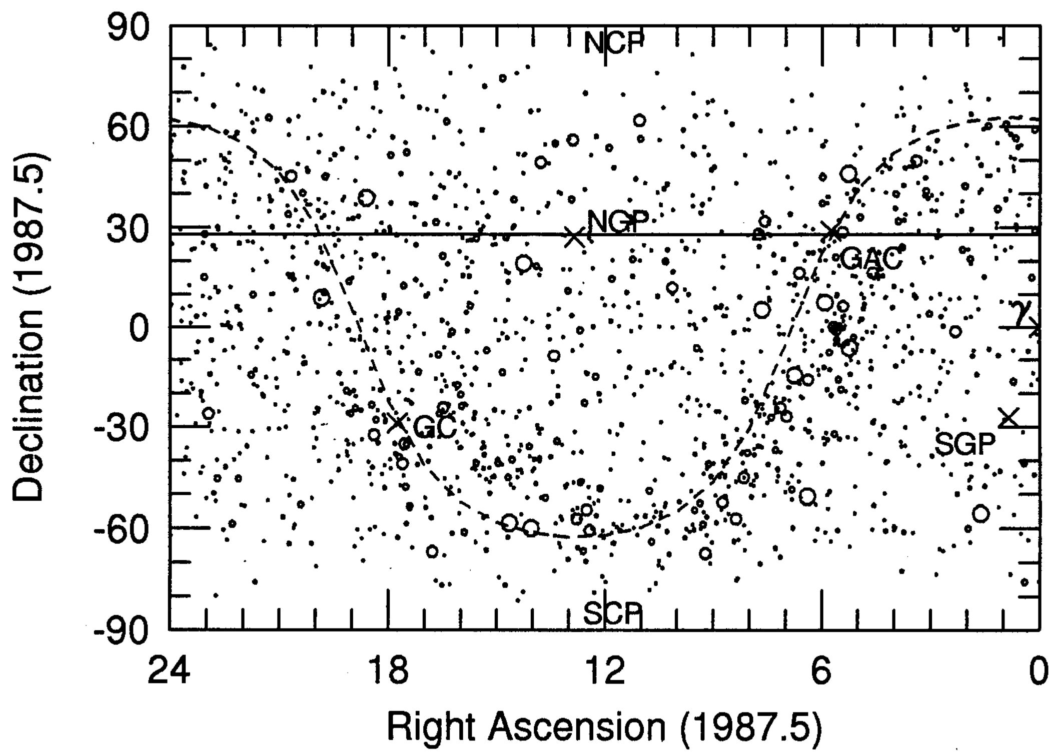


Figure 2.4 - CTI survey strip in equatorial coordinates. SAO stars brighter than 5th magnitude plotted with increasing symbol size corresponding to brighter stars. CTI survey strip (solid line) and Galactic Plane (dashed line), Galactic poles (NGP and SGP), Galactic center (GC) and anti-center (GAC), celestial poles (NCP and SCP) and first point of Aries (γ) are also marked.

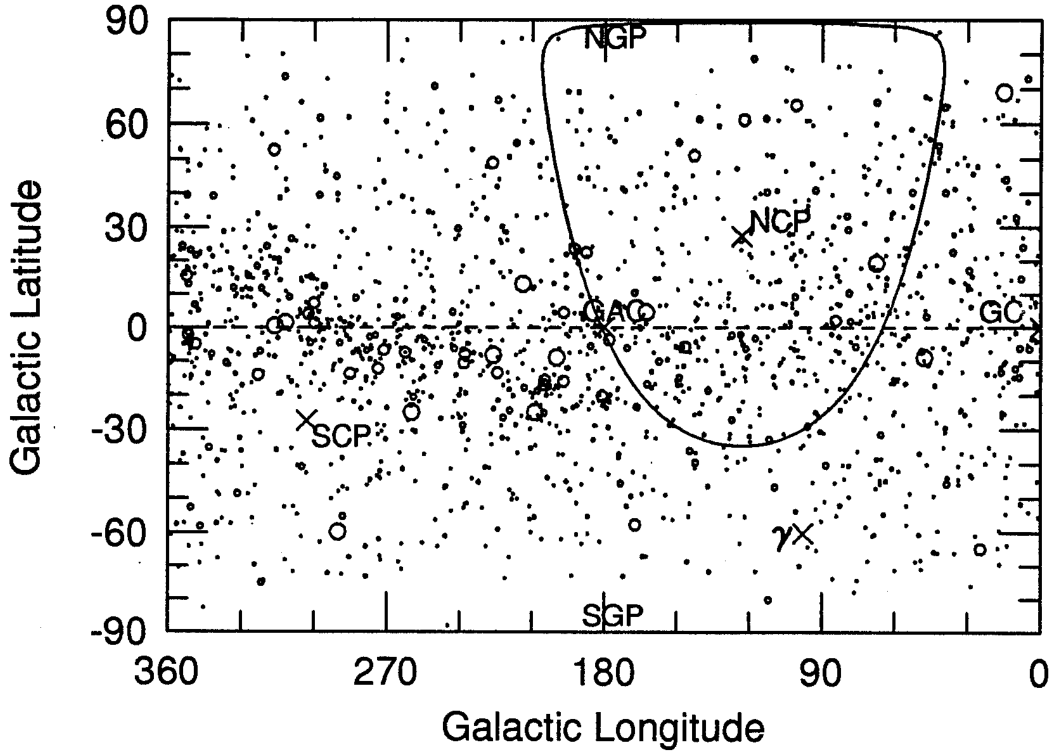


Figure 2.5 - CTI survey strip in galactic coordinates. SAO stars brighter than 5th magnitude plotted with increasing symbol size corresponding to brighter stars. CTI survey strip (solid line) and Galactic Plane (dashed line), Galactic poles (NGP and SGP), Galactic center (GC) and anti-center (GAC), celestial poles (NCP and SCP) and first point of Aries (γ) are also marked.

both equatorial and galactic coordinates. The constellation boundaries transversed by the CTI survey strip are listed in Table 2.4 (Delporte 1930). A nearly complete representation of the CTI survey strip can be found in <u>The CCD/Transit Instrument Atlas and Database Guide</u> (Wetterer 1995), written as a supplement to this dissertation.

The machine-readable versions of several different catalogs distributed by the Astronomical Data Center (ADC) were used to identify named objects within the CTI survey. All right ascensions and declinations were precessed to the

Table 2.4 - Constellation Boundaries in CTI Survey

| Constellation | Start RA (1987.5) | End RA |
|---|---|---|
| Pegasus | $21^h\ 29^m\ 57^s$ | $00^h\ 09^m\ 48^s$ |
| Andromeda | 00 09 48 | 00 49 02 |
| Pisces | 00 49 02 | 01 46 20 |
| Triangulum | 01 46 20 | 02 31 34 |
| Aries | 02 31 34 | 03 28 48 |
| Taurus | 03 28 48 | 06 00 06 |
| Gemini | 06 00 06 | 06 15 08 |
| Auriga | 06 00 06 | 06 39 05 |
| Gemini | 06 39 05 | 08 02 25 |
| Cancer | 08 02 25 | 09 21 38 |
| Leo | 09 21 38 | 10 36 16 |
| Leo Minor | 10 36 16 | 11 06 06 |
| Leo | 11 06 06 | 11 57 48 |
| Coma Berenices | 11 57 48 | 13 35 14 |
| Bootes | 13 35 14 | 15 15 46 |
| Corona Borealis | 15 15 46 | 16 24 33 |
| Hercules | 16 24 33 | 18 26 26 |
| Lyra | 18 26 26 | 19 20 01 |
| Cygnus | 19 20 01 | 19 44 34 |
| Vulpecula | 19 44 34 | 21 29 57 |

CTI epoch of 1987.5.

The 5th revised edition of the Bright Star Catalogue (BSC) (Hoffleit 1982) was used to identify all stars brighter than 6.5 magnitude whose effects are noticeable in the atlas. Stars with a V magnitude brighter than 12 will start saturating pixels in the CCDs. Diffraction effects of brighter stars in the BSC can be seen even if they lie well outside the strip. Table A1.2 in Appendix 1 lists each star's name, right ascension, declination, and visual magnitude. A total of 20 stars were identified. The Smithsonian Astrophysical Observatory (SAO) catalog (SAO Staff 1966) was used to identify other bright stars within the survey. These 311 stars, including the 20 BSC stars, are listed in Table

A1.3 in Appendix 1.

The 4th edition of the General Catalogue of Variable Stars (GCVS) (Kholopov et al. 1985-88) was used to identify known variable stars in the atlas. The papers containing the original finders for each star were also consulted to verify the identifications when needed (see references). Table A1.4 in Appendix 1 lists each star's name, right ascension, declination, magnitude range and type. A total of 35 previously known variable stars were identified.

The Revised New General Catalogue of Nonstellar Astronomical Objects (RNGC) (Sulentic and Tifft 1973), and the galaxy portion of the Catalogue of Galaxies and Clusters of Galaxies (CGCG) (Zwicky et al. 1961-68) were used to identify a selection of bright galaxies in the atlas. The Palomar Sky Survey with overlays (Dixon et al. 1981) and Volume 5 of the Webb Society Deep-Sky Observer's Handbook (Jones 1981) were consulted to verify most of the identifications, and the Catalogue of Quasars and Active Galactic Nuclei (Veron-Cetty and Veron 1989) was used to identify a bright quasar (GQ Com) and a galaxy with an active galactic nucleus (NGC 4504) falling within the boundaries of the CTI survey strip. Table A1.5 in Appendix 1 lists the name, right ascension, declination and magnitude for each of the 86 objects identified.

## Chapter 3 CTI Data Reduction and Calibration

The raw pixel data from the CTI goes through many steps of processing before it can be used in a scientific project (Cawson et al. 1986a, 1986b, McGraw et al. 1989, and McGraw 1992a). Each night of CTI observation potentially yields over 460 Mbytes of data (2 CCDs of 320 pixels per row read out every 0.12 seconds at 16 bits per pixel giving 10.67 kbytes/s). Because of the large amount of data being processed, a nearly automated data handling procedure was developed. A schematic representation of this is shown in Figure 3.1, and will be described in six steps: initial entry of night's data, removal of instrumental signature, background fitting and cosmic-ray removal, analyzing and filtering, positional and photometric calibration, and merging with the master and history databases. During each step of the analysis, one or more databases (labelled with unique two or three letter extensions) are produced for use later in the analysis, for scientific study, or for diagnostic purposes. The extension specifies the format and content of each database in the reduction system. These databases are shown as ovals in Figure 3.1.

In addition to the reduction and analysis products, one database and two text files record output from all computer routines. The *trace* file contains diagnostic information related to a single sweep (in early work this text file has a *ls* extension), while the *log* file lists the reduction and

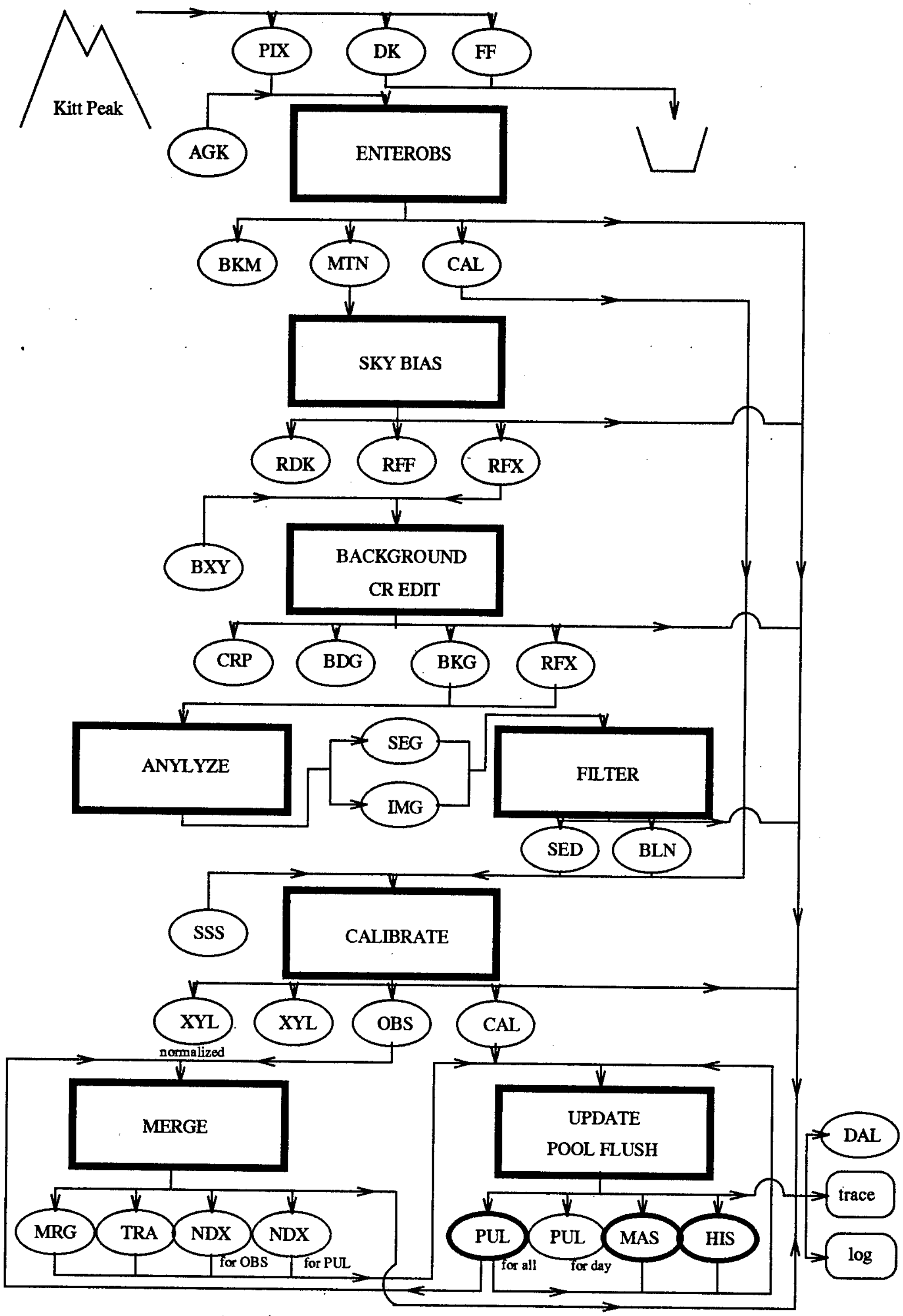


Figure 3.1 - Schematic flow chart representation of the CTI analysis process. Rectangles represent computer routines, ovals represent databases, and rounded rectangles represent text files.

analysis steps completed for all sweeps during a particular automated reduction run. These two text files are shown as rounded rectangles in Figure 3.1. The daily analysis log (**.DAL** database) records the completion of each stage of the reduction and analysis process for every sweep, and can be used to determine the sweep's present status. A complete description of the contents of each type of database can be found in The CCD/Transit Instrument Atlas and Database Guide (Wetterer 1995), written as a supplement to this dissertation.

This chapter describes the current status of the CTI data reduction and analysis process, as well as areas requiring further work. These areas include: testing and implementing a new method for determining the bias and flat field functions (see Sections 3.2 and 4.2.1), testing the cosmic ray removal algorithm under various seeing conditions and resetting the thresholds (see Sections 3.3 and 4.2.1), modifying object position determination (see Section 7.1), automating discovery and rejection of data contaminated by rapid background changes due to clouds or stray light from planets (see Sections 3.5.2 and 4.2.1), and inclusion of aperture and curve-of-growth photometry to combat difficulties with photometry of galaxies and in the Galactic plane (see Sections 3.5.2 and 4.2.1).

## 3.1 Initial Entry of Night's Data

A night's data is transferred from the CTI on magnetic tape in the format of a **.PIX** database. Each row of data contains 8 underscan pixels, 320 data pixels, and 8 overscan pixels. Using the computer routine ENTEROBS, the data are examined and several stars from the AGK-3 catalog (Dieckvoss et al. 1975) at the beginning of each sweep are identified. This is done interactively with CTI personnel verifying and choosing the centroid of stars selected by the computer from an **.AGK** database. From this information, a rough calibration of the initial right ascension and declination, the right ascension and declination scaling, and precessional coefficients are determined and written to the header of a **.CAL** database. (This **.CAL** database will later be refined during the calibration phase of the analysis.) Additionally, a **.BKM** database recording the median background value over the course of the night is created to enable a quick check of observing conditions if desired. Finally, the **.PIX** database is converted into a **.MTN** database in preparation for the next step of the analysis. A **.MTN** database contains 320 image pixels and the mean and variance of the overscan and underscan for each row of data.

## 3.2 Removal of Instrumental Signature

In the CTI CCD image, instrumental additive effects, such as the readout voltage offset (bias), and instrumental multiplicative effects, such as the pixel-to-pixel response to light (flat field), of the CCD must be removed. Because the TDI procedure requires that an image of a particular object utilize every row, the nonuniformities of the CCDs are averaged over one dimension leaving only a "simple" additive and multiplicative function to be corrected in the other dimension. Determining the correct *multiplicative* function is essential if accurate photometry is desired.

For each night of observation, the CCDs were operated under dark conditions to produce the one-dimensional "dark bias" (additive function with **.DK** extension), and while observing a uniformly illuminated screen in the telescope dome to create the "flat field" (multiplicative function with **.FF** extension) for each filter. These functions, however, proved to be inadequate in removing the CCDs instrumental signature to obtain photometry precise to our goal of 1%. The dark bias functions appear to be corrupted by a light leak or reflection off the dark slide inserted over the CCDs before acquisition and no provision was made to map out the deferred charge structure of the CCDs. The flat field functions suffered from related problems.

It was necessary to develop a new method for determining the additive and multiplicative functions for CTI's CCDs. For

the initial versions of the master and history lists, a new dark bias function was constructed (using the computer routine FIXUP) by adjusting the original dark bias function to eliminate streaks in the data created by the deferred charge structure. The flat field function was left unchanged. Unfortunately, the flat field function from the mountain is not perfect and introduces systematic errors in the photometry of up to $\approx$0.02 magnitudes in V and $\approx$0.1 magnitudes in B.

Another method, where both the dark bias and flat field functions are obtained directly from the data, was needed. This is possible because during a night's observation, the CCDs are primarily measuring the background light level, which is recording the structure of the additive and multiplicative functions. In order for the method to work, however, the background light level must be *flat* in declination. This means that nights when the moon is above the horizon or when the strip is crossing the Galactic plane must be handled very carefully. The second condition, which seems almost incompatible with the first, is that there must be a change in the background light level over the course of the night. If the additive and multiplicative functions remain stable, however, several night's worth of data could be used to accomplish the necessary background change. Finally, the overall bias level can't be determined and thus a guess must be made to start the process. These last two points will be explained below.

For CTI's CCDs, a pixel value can be calculated using the equation

$$p_{ij}=a_i+m_i\times k_j, \tag{3.1}$$

where $a_i$ is the additive terms (bias, deferred charge, self illumination), $m_i$ are the multiplicative terms (flat field), $k_j$ is the background light level (stars having been removed), and i and j are declination and right ascension respectively. It has been assumed that k is a function of right ascension only to meet the first condition stated in the above paragraph. The background light level can be determined by taking the mean of Equation 3.1 over all columns (declination) and solving for $k_j$, remembering that $m_i$ is normalized ($\sum m_i = n_{col}$),

$$k_j=\frac{\sum_{i=1}^{n_{col}} p_{ij}-\sum_{i=1}^{n_{col}} a_i}{n_{col}}. \tag{3.2}$$

If a guess of the additive function is made, the multiplicative function can be calculated by combining Equations 3.1 and 3.2,

$$m_{i(j)}=\frac{n_{col}(p_{ij}-a_i)}{\sum_i p_{ij}-\sum_i a_i}. \tag{3.3}$$

As the background light level (or equivalently $p_{ij}$) changes, $m_i$ should remain the same if the correct values for the $a_i$'s relative to $\sum a_i$ were used. If a slope exists when comparing the calculated $m_{i(j)}$ for a particular column against the

background light level, the $a_i$ for that column is incorrect. A positive slope indicates $a_i$ is too low while a negative slope indicates $a_i$ is too high. All $a_i$'s can thus be adjusted to minimize these slopes for all columns to approach the correct solution. As stated earlier, however, the background light level must change to give leverage in determining the slopes, and the changes in the $a_i$'s are made relative to the average bias level ($\sum a_i$).

Stars, truncation noise (the fact that the $p_{ij}$'s are integerized), random error (including readout noise), low background levels, and a small background change over the night will all reduce the quality of the resulting additive and multiplicative functions. In addition, most nights had the original **.DK** and **.FF** applied, and then were *reintegerized*, resulting in additional systematic errors above the original truncation noise.

This entire process is accomplished by several programs managed by the computer routine SKY_BIAS. The resulting additive function is written to a **.RDK** database while the multiplicative function is written to a **.RFF** database, both recorded as real (i.e. non-integer) numbers. Currently, however, the resulting dark bias and flat field functions using this method are inadequate in improving the existing calibration.

For the next incarnation of CTI, the method used to determine the additive and multiplicative functions will be

crucial in improving CTI's photometry. The best alternative might be to start acquiring data during astronomical twilight. As the twilight deepens, the changing background starting from a high initial value would give the factors necessary in making the method described above to work optimally. Because all the CTI raw data are recorded on magnetic tape, regenerating all databases from the current data is possible, though time consuming.

These functions (**.RFF** and **.RDK**), however determined, are applied to the pixel information in the **.MTN** database to remove the CCD's instrumental signature, with the result entered into a new **.RFX** database made up of real numbers. (Reductions using FIXUP, described earlier, reintegerized the data and saved it to a **.FIX** database.)

## 3.3 Background Fitting and Cosmic Ray Removal

The next step involves fitting the background sky brightness in the **.RFX** database. Accurate photometry depends on being able to fit the background well. This is accomplished with the computer routine BACKGROUND. The background fitting algorithm divides the strip into five overlapping sub-strips of 106 columns each and calculates the modal pixel value (in initial reductions, the biased median pixel value was calculated) for each sub-strip in a particular row. A **.BXY** database is accessed to identify regions of the strip where possible problems might occur. The resulting median values are entered into a least squared regression of the form

$$Back=A+Bx+Cy+Dx^2 \tag{3.4}$$

where x is the column number (declination), and y is the row number (right ascension). In the fit, the five modal values of each sub-strip are weighted by the inverse of the difference between the median (50-percentile point) and the 80-percentile point of that particular substrip. The larger the difference, the more stars present in the region, and the less weight that region's value is given in the regression. For each row (y), these coefficients (A,B,C, and D) are saved to a **.BKG** database. Additionally, a **.BDG** database containing the modal values and weights used in the regression for each row of data is produced.

Next, cosmic rays are detected and removed by the

computer routine CR_EDIT. The technique is based on the fact that the ionization trails deposited in the detectors by charged particles are basically single (or few) pixel events. This signature has a contrast much higher than the point spread function and can be isolated by simply selecting pixels greater than a certain pre-set value above the background level while requiring the mean of the surrounding eight pixels be below another lower pre-set value, (both these thresholds are listed in the header of the **.CRP** database for that particular sweep). A cosmic ray pixel in the **.RFX** database is assigned the mean value of the surrounding eight pixels, with the result of all pixel substitutions sent to the **.CRP** database. All cosmic ray events are thus fully recoverable.

The search for variable stars in the CTI survey strip turned up photometry anomalies related to cosmic ray removal. For a few nights entered into the current databases, the CR_EDIT algorithm removed the peak pixel of several faint stars resulting in either non-detections or anomalously low luminosity values for these stars on those nights. For the purposes of finding RR Lyrae type variable stars, these nights were easy to remove from the data (see Section 4.2.1). It will be necessary, however, to test the cosmic ray removal algorithm under various seeing conditions and reset the thresholds to distinguish between the actual short lived dimming of a star (e.g. Algol type variable stars) and a false dimming or non-detection created by cosmic ray removal.

## 3.4 Analyzing and Filtering

The pixel data in the **.RFX** database can now be background subtracted (using the **.BKG** database) and partitioned into images (group of pixels above some threshold) and segments (individual peaks within an image). This is accomplished by the computer routine ANALYZE. The pixel information is transformed into attributes associated with each segment's position, luminosity, shape and blending with other segments.

First, all pixels below a pre-set isophotal threshold (listed in the header of the **.IMG** database for the particular sweep) are ignored, with the pixels above the threshold forming groups, connected either adjacently or diagonally. All pixels in each group are considered part of the same "image." The luminosity, centroid, radius of gyration, ellipticity, and position angle of each image are calculated from the first and second moments of the group of pixels from which it is composed. For images above a preset luminosity threshold (listed in the header of the **.IMG** database), this information is output to the **.IMG** database.

Next, all pixels are grouped, connecting either adjacently or diagonally, to their nearest local peak. All pixels in each group formed are now considered part of the same "segment." Segments can be thought of as individual peaks in a mountain range, where the mountain range itself is an image. The properties of each segment are calculated in the same way as an image and output to a **.SEG** database.

Again, because the way segments are found guarantees to produce a segment from noise for about one pixel in nine over the entire background, segments below a preset luminosity threshold (listed in the header of the **.SEG** database) are not considered. The **.IMG** and **.SEG** databases also contain information specifying which segments refer to each image.

The **.IMG** and **.SEG** databases are then processed by the computer routine FILTER to produce a final list of recognized detections for that particular night's data. Segments representing real detections must be separated from the remaining noise-produced segments with the use of a contrast filter. If the log of the peak luminosity is plotted against the log of the mean luminosity for each segment, as in Figure 3.2(a), noise-produced segments lie close to the y=x line representing the case where the peak and mean luminosity are equal. Additionally, noise segments lie closer to the y=x line for segments with higher mean luminosities. If the axes in Figure 3.2(a) are rotated by 45°, an empirically determined division between the noise segments and potentially "real" segments can be set, represented by an exponential asymptote to the new x-axis, which is simply the y=x line in Figure 3.2(a). Figure 3.2(b) shows this plot, with the log of the y-axis used to display the exponential asymptote division between noise and real segments as a straight line. This division is also plotted in Figure 3.2(a).

The y-axis of Figure 3.2(b) is defined as the contrast,

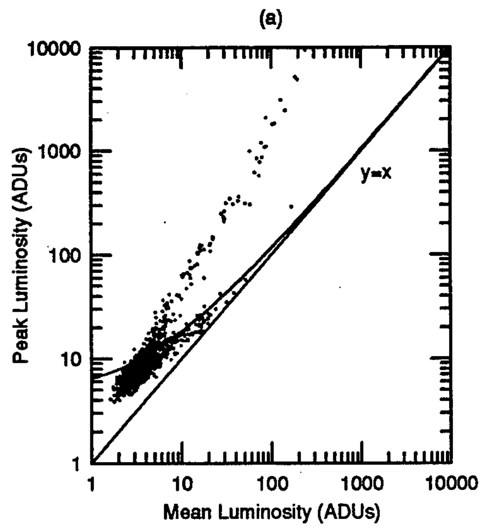


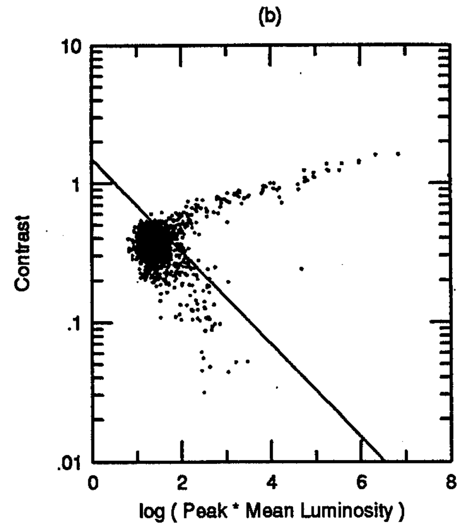


Figure 3.2 (a) peak luminosity versus mean luminosity for a single night's data, (b) log of the contrast versus log(peak luminosity × mean luminosity) for a single night's data. Empirically determined division between noise and real segments shown as solid line.

and can be represented by the simple equation

$$contrast = \log\left(\frac{peak}{mean}\right), \tag{3.5}$$

where *peak* and *mean* are the peak and mean luminosity respectively. The x-axis is now log(peak×mean), which is related to the brightness of the segment. All segments below the empirically defined division are thrown out, while an unnormalized probability of reality value is assigned to each real segment determined using the distance of the segment above the empirically defined division.

All information about each real segment, as well as its

unnormalized probability value, are output to the **.SED** database. Additionally, the information regarding what segments in the **.SED** database make up a particular image is entered into a **.BLN** database. For the rest of the analysis, only segments entered into the **.SED** database are considered, although the parent images are trace-recoverable by using the **.BLN** database.

### 3.5. Calibration

Each segment must now be fixed in a positional and photometric standard calibration to prepare the night's data for merging with other nights. This calibration is critical in determining the usefulness of the CTI data. We must be confident that each night has been calibrated such that changes in luminosity for an object over time or between two different objects anywhere in the CTI survey strip are actual differences in the brightness of the object or between the objects. The instrumental calibration is achieved by several programs managed by the CTI routine AUTO_CALIBRATE.

#### 3.5.1. Positional Calibration

A rough positional calibration was carried out at the start of the analysis with the identification of bright stars from the AGK-3 catalog at the beginning of each sweep. This is improved by using a set of secondary positional standard stars selected from the Space Telescope Guide Star Catalog (Lasker et al. 1990). These secondary standard stars are contained in a database with a **.SSS** extension. The observed positions of each segment are first converted to the CTI epoch of 1987.5, taking into account proper motion, parallax, precession, nutation, aberration of starlight due to the Earth's revolution around the sun, and diurnal aberration due to the Earth's rotation. The resulting positions are compared with the list of the expected positions for the positional

standards within the list of secondary standard stars. Typically a 2 x 2 pixel window centered on the expected star position is used to determine a positive identification. The matching routine, however, is not rigid and will follow uniform smooth deviations greater than 2 pixels over the course of the sweep to accommodate possible shifts in telescope pointing. Each standard star identified, as well as the x and y displacements (in pixels) for each, are annotated in a newly created **.XYL** database.

The standard star identifications in the **.XYL** database are then used to produce a minute-by-minute (temporal) positional calibration to be contained in the **.CAL** database for the sweep. This is achieved by taking the median of the x and y displacements for every standard within a three minute window about each minute of observation to determine the global displacements to be used for that minute. Interpolations between two of these global displacements in the **.CAL** database will then be applied to all stars during the sweep. The **.CAL** database contains this, as well as the nine parameter conversion of the observed coordinates for the sweep's epoch to the CTI's 1987.5 epoch.

During this phase of the analysis, a problem was discovered that necessitated additional processing of each star's position. It was found that standard stars of similar right ascension had systematic x and y displacements dependent on their declination. The standard stars appeared closer

together than they should in declination, while there appeared to be a shearing present in right ascension. For example, a situation existed where standard stars on the north edge of the strip required a positive displacement of two pixels in right ascension to put the observed position of the star to where it was expected, while stars on the south edge required a negative displacement of two pixels, and stars in the center of the strip required no displacement at all. The resulting median displacement written to the **.CAL** database would thus be zero and only be valid for stars near the center of the strip, resulting in an incorrect positional determination for stars on each edge. Because the severity of this effect was different for the two CCDs and changed from night to night, double images of stars near the edges were formed in the master list producing spurious variable stars that appeared to blink on and off.

The severity was very different in magnitude for the two CCDs, and positively correlated between the two as the severity of the problem changed. Errors in any of the astrometric routines could not explain what was observed. The problem was eventually diagnosed as coming from two different causes. The first involves a misalignment of CCD0's columns from the east-west direction. This has the effect of elongating images in the north-south direction, and also creates most of the shearing effect observed. Indeed, it is with this CCD that the problem is most evident. The second

and more subtle cause involves an astigmatism in CTI's optics caused by a misalignment of either the secondary mirror, the tertiary mirror, or both. The astigmatism effects the declination scale as well as producing additional shearing in right ascension, and also elongates the images along the axis of the astigmatism, all of which are observed in the data.

To combat the misalignment and astigmatism, the positional displacements versus declination are analyzed for each sweep. The calculated slopes (x and y displacement versus declination) and intercepts were then used to remove the dependence from the data. An iterative process was necessary to entirely correct the data with the final slopes and intercepts used for each sweep saved in the header of the **.CAL** database. Additionally, a second normalized **.XYL** database is produced which is simply the original displacements in the previous **.XYL** database with the global corrections from the **.CAL** database applied. This database is used to check the quality of the global corrections. Currently, no correction has been made to the shapes of the objects. As a result, virtually every object observed with CCD0 (primarily through the B, R, and I filters) will be elongated north-south with a non-zero ellipticity, while objects observed with CCD1 (primarily through the V filter) will also be elongated, but along the axis of the astigmatism, and also have a non-zero, but smaller, ellipticity.

Early work with CTI data included the program STANDARDS,

which was used to modify the expected position for the standard stars in the **.SSS** database. It compared positions in the **.SSS** database with positions in a sweep's **.XYL** database, and output relevant information regarding changes to a **.RES** database. The program was used both before and after the positional calibration. It was eventually decided to discontinue using this program because any changes to a standard's position must be accompanied by a recalibration of the history and master lists in order to reflect those changes, and this was considered impractical.

### 3.5.2 Photometric Calibration

Concurrently with the positional calibration, a photometric calibration is also carried out. Certain secondary standard stars appear constant and thus have expected luminosities. For each of these standard stars, the **.XYL** database contains the multiplicative luminosity factor needed to match the expected luminosity with the observed. For example, if the observed luminosity was half that expected, the luminosity factor would be 0.5. As with positional displacements, the median of all luminosity factors is taken for standard stars within a three minute window to produce a minute-by-minute luminosity calibration for the **.CAL** database. It is an interpolation between two of these global luminosity factors that will be used to adjust the luminosities of all stars within the sweep.

Because the quality of the photometric calibration depends entirely on the accuracy of the expected luminosities in the standard star list, the method developed to compile and test this list once the difficulties with the dark bias and flat field functions are solved will be described in detail. It was found early on that the luminosities in the Space Telescope Guide Star Catalog were not accurate enough for CTI's calibration, making it necessary for the expected luminosities to be determined from the CTI data itself.

Several night's observations under photometric conditions were linked together over the full CTI survey strip to produce an initial estimate for the expected luminosities. The resulting closure error was 0.02 magnitudes in V, possibly related to the systematic error introduced by the incorrect flat field function. Currently, the master and history lists use this calibration to derive all instrumental magnitudes. This can be improved by processing all the nights and examining the luminosity factors of each standard star for every night the star was observed. A systematic offset indicates the star's initial estimate for the expected luminosity was incorrect. These offsets can be calculated for each standard, and the expected luminosity adjusted to eliminate them. Before this calculation can be done, however, the effects of dimming caused by dust settling on the optics, dimming caused by background overestimation during poor seeing in confused regions of the sky, dimming caused by clouds, and

inaccurate photometry caused by background fitting or other problems must be eliminated from the data. Each of these will be addressed in turn.

For a particular night of observation, there will be a mean luminosity factor related to the amount of dust on the optics. Essentially, the more dust on the optics, the dimmer stars will appear, and the lower the luminosity factor. Using the **.XYL** or **.CAL** databases for a large number of V observations, these luminosity offsets as a function of time can be examined.

The effective reflecting (or refracting) area of a telescope, and thus the flux from a standard source, will slowly decrease over time as dust settles onto the optics. For example, if the initial reflecting area of a mirror is $A_o$, a given time interval later, the effective area will be $A_1 = A_o - [nA_o]A_d = A_o(1 - nA_d)$, where n is the number of dust particles deposited per unit area in the given time interval and $A_d$ is the effective obscuration area of one dust particle. After another time interval, $A_2 = A_1 - [nA_1]A_d = A_o(1 - nA_d)^2$. Given that the rate at which dust settles onto the optics is constant and the time interval between calculations is short enough, the flux reflecting from this mirror as a function of time can be represented by the equation

$$F(t) = F_o(1-nA_d)^{t/T}, \qquad (3.6)$$

where $F_o$ is some arbitrary initial flux, and T is the time interval over which n was calculated. Notice that the

relationship between flux and time is not linear because dust particles that land on other dust particles do not degrade the performance of the mirror. Equation 3.6 can be manipulated to express the above relationship in magnitudes as a function of time. The resulting equation is

$$\Delta m=[(-2.5/T)\log(1-nA_d)]\,t. \tag{3.7}$$

Here, the equation is linear in time. The constants in square brakets of Equation 3.7 are independent of the size of the mirror, so for telescopes with several reflective (or refractive) surfaces, each surface contributes an identical term. The "constant" $n$, of course, will be different for each surface. If the constants in square brakets and contributions from all surfaces are lumped together into a single constant, we obtain the simple result

$$\Delta m=K\times t. \tag{3.8}$$

where K is in units of magnitudes per unit time.

For several photometric V nights of observation with CTI, the average magnitude offset was calculated from the luminosity offset (dm = -2.5*log(dl)). Figure 3.3 plots this magnitude offset versus time. Notice that there are four distinct breaks in an otherwise linear trend. By looking back in the CTI logs, these breaks were found to correspond to times when the telescope mirrors were washed. (1988 Sep 13, 1989 Apr 25, assumed washing during summer of 1989, and 1991 Apr 22). The slope of the line for each interval was

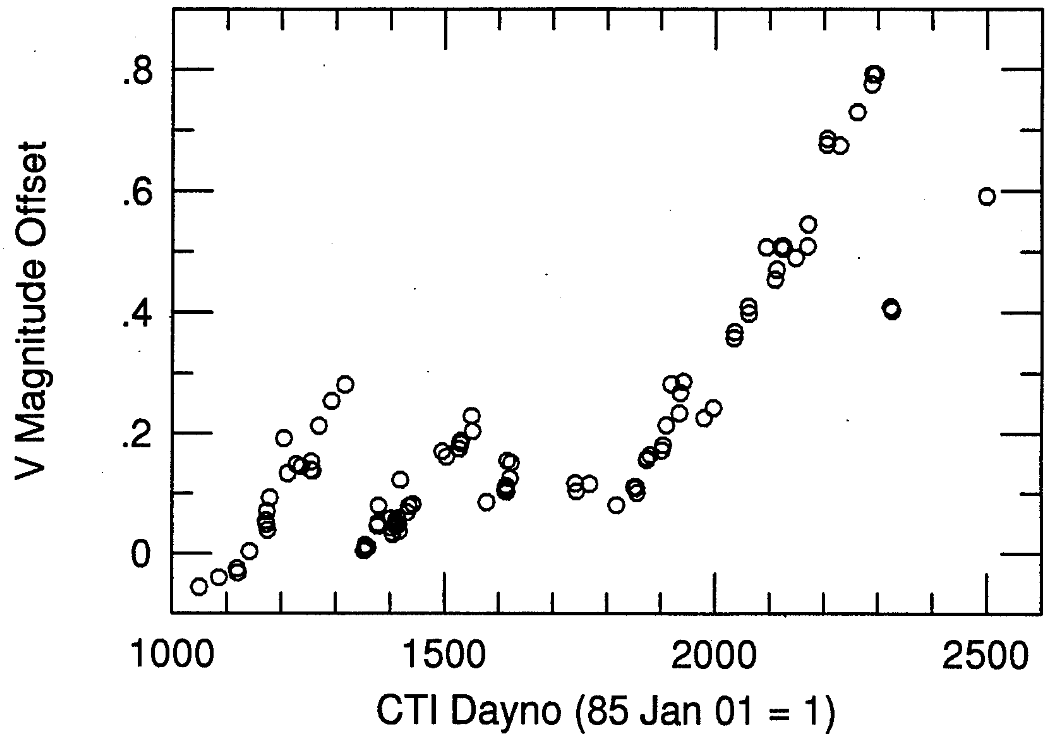


Figure 3.3 - V magnitude offset versus CTI dayno

calculated and the data adjusted such that the best fit lines for each segment yield the same value at the midpoint between them. The resulting plot of magnitude offset versus time is shown in Figure 3.4. The best fit to this scaled data is also plotted. The slope of this line is 0.001239 +/- 0.000010 mags/day which corresponds to 0.452 +/- 0.004 mags/year. This means that the CTI is only 65% as sensitive to light after only one year of observing without any cleaning! Generally, K appears to remain fairly constant over the four years of observing represented. Slight variations in the slope, however, indicate the presence of seasonal variations.

A similar calculation using Capilla Peak data acquired

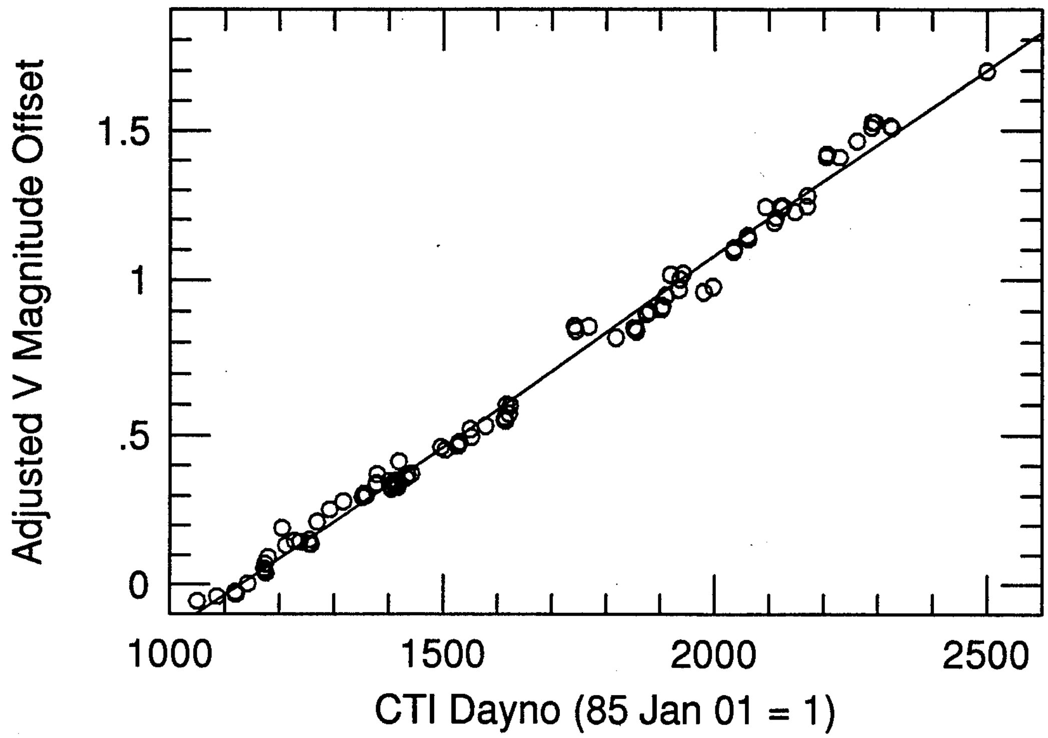


Figure 3.4 - Adjusted V magnitude offset versus CTI dayno.

over one year for three separate variable star fields gives K = 0.101 +/- 0.011 mags/year. The fact that CTI has three reflective surfaces collecting dust and that the primary and tertiary mirror are always horizontal while Capilla Peak's telescope is stored with the primary vertical probably accounts for most of the difference.

The effect of dust settling on the optics can thus be eliminated by scaling each night's observation to the mode (to eliminate the effects of clouds) of all luminosity offsets for that particular night. This is exactly what is done in calculating the normalizing factor used in adjusting each star's dl in the normalized **.XYL** database.

Next, the effect of dimming caused by background overestimation during poor seeing in regions of high confusion must be dealt with. In examining the **.CAL** databases for several nights of observation in the V bandpass, there appear systematic variations in magnitude offset at certain right ascensions. Figure 3.5(a) plots the magnitude offset versus right ascension for a number of nights for right ascensions between $18^h$ and $22^h$. An individual night's magnitude offset as a function of right ascension has been normalized to zero to eliminate the effect of dust settling on the optics. Figure 3.5(b) plots the average background intensity in V (as contained in the **.CAL** database) versus right ascension for several observation nights over the same right ascension interval. The summer galactic plane at approximately $19^h40^m$ is clearly visible. The increase in background intensity at the galactic plane indicates that stars are included in the background estimate. This suggests a possible link between the magnitude offset calculated for a particular star and the concentration of background stars.

The "confusion," proportional to the concentration of background stars, was calculated to compare with the magnitude offset (determined from the luminosity factor) and seeing for several night's observations as contained in **.CAL** databases. To calculate the confusion, a histogram of all objects with two or more observations in the declination slice from +28°00' to +28°03' (1987.5 epoch) contained in the CTI master list was

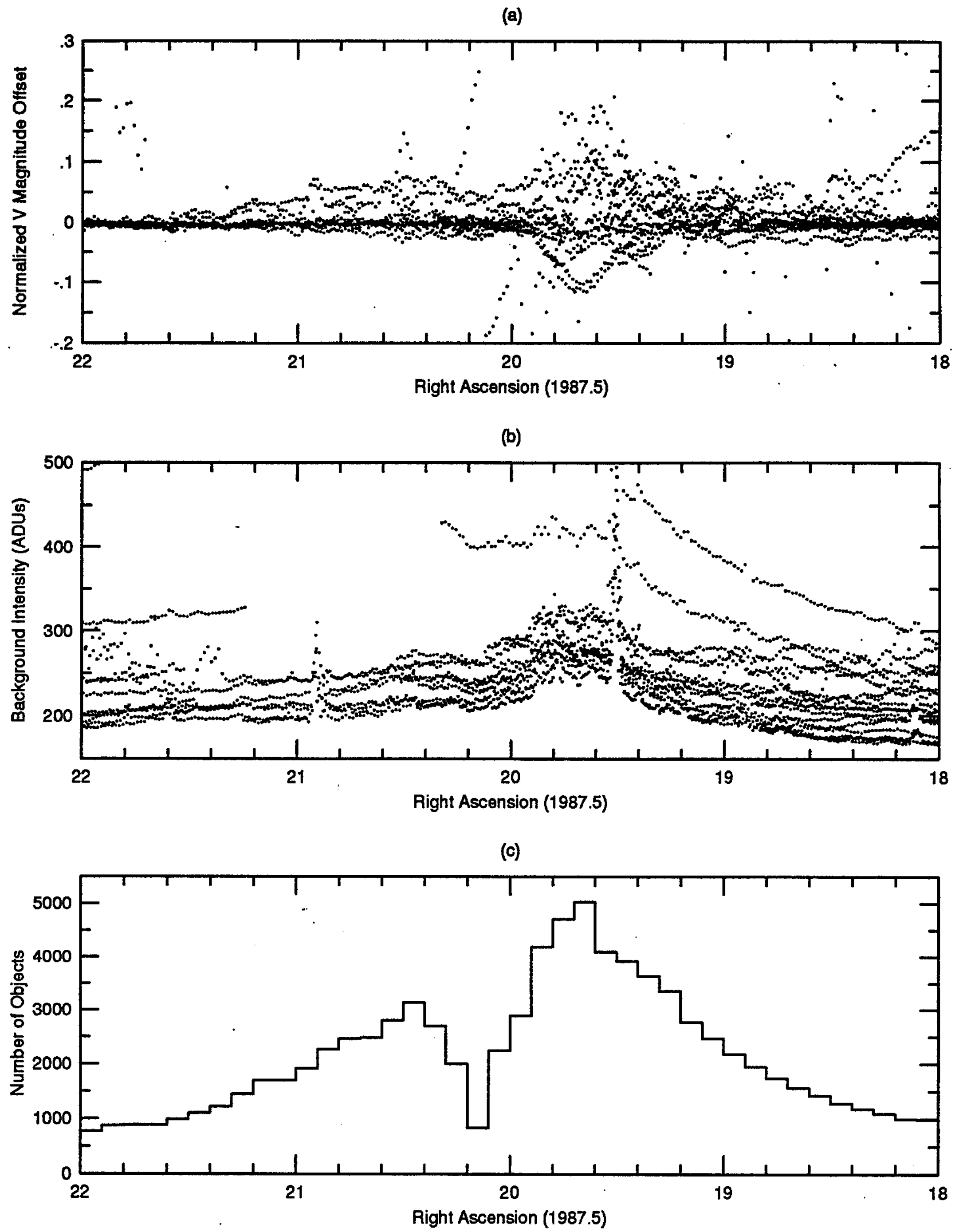


Figure 3.5 - (a) Normalized magnitude offsets versus right ascension, (b) Background intensity versus right ascension, (c) Number of stars per 3 arcminutes declination by $6^m$ right ascension versus right ascension for several nights crossing the summer Galactic plane.

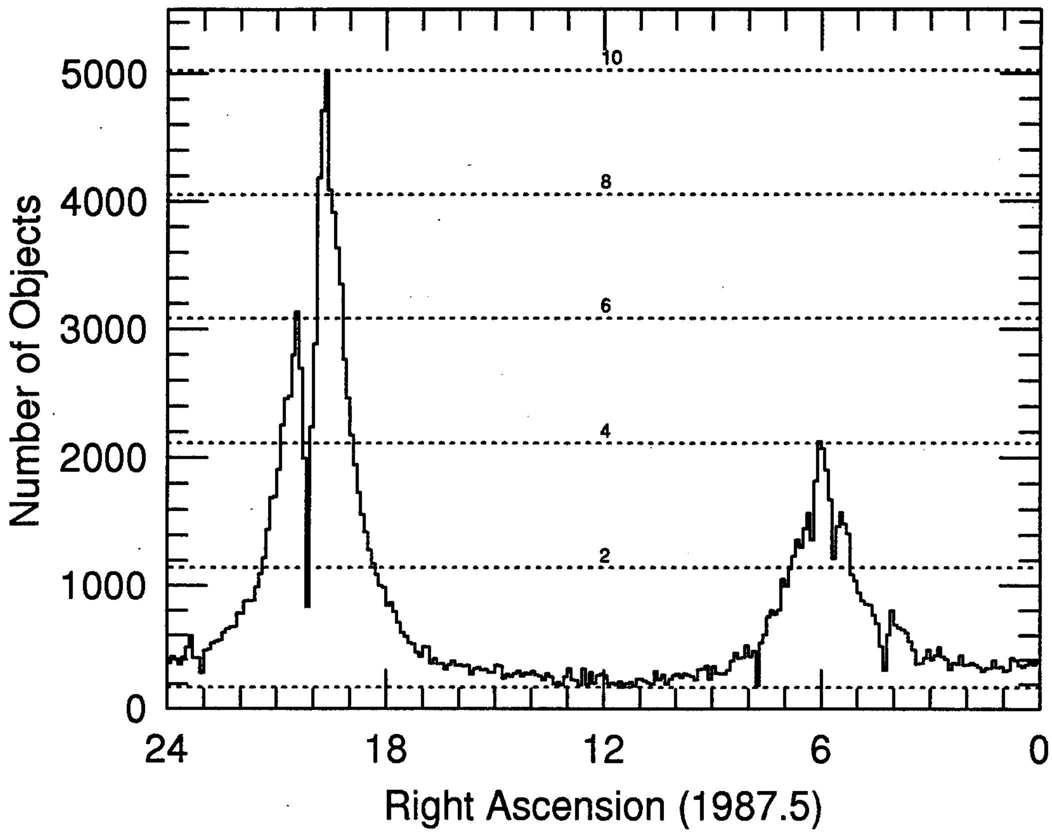


Figure 3.6 - Histogram in right ascension of the number of objects in CTI survey strip between 28°00' and 28°03' declination. Each bin corresponds to $6^m$ right ascension. Even confusion levels shown as horizontal dashed lines.

taken with respect to right ascension. Figure 3.6 shows this histogram, with every bin corresponding to $6^m$ of right ascension. The confusion was defined as a real number between 0 and 10 directly proportional to the concentration of stars, with confusion equal to zero for the minimum concentration, and confusion equal to ten for the maximum concentration.

Figures 3.7(a) through (c) display the magnitude offset versus seeing for increasing confusion. For each plot there

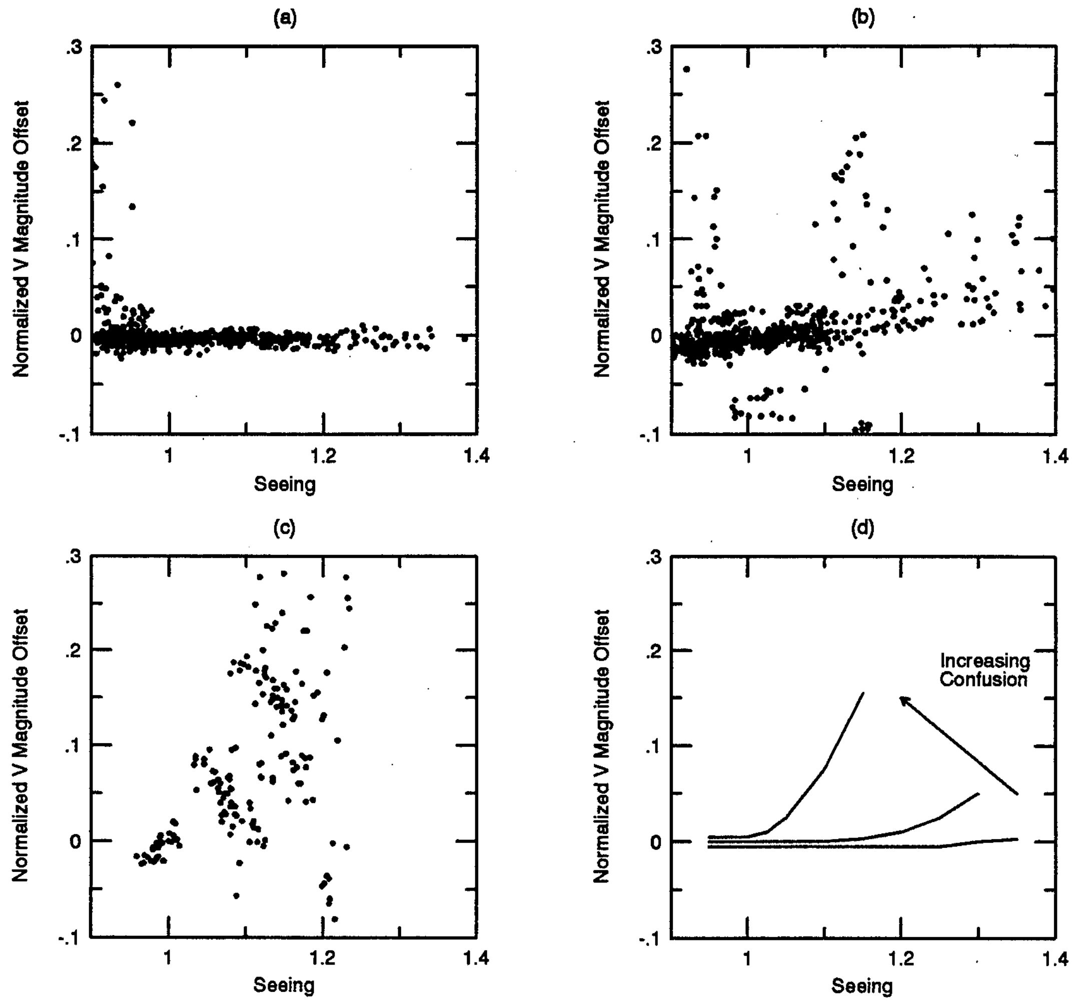


Figure 3.7 - Normalized magnitude offset versus seeing for (a) confusion < 1 in region near the north Galactic pole, (b) 3 < confusion < 4 in winter Galactic plane, (c) confusion > 9 in summer Galactic plane, and (d) trend summarized.

is a value of seeing above which the magnitude offset begins to increase. As the confusion increases, this value of seeing decreases. The trend is summarized schematically in Figure 3.7(d). Points far from the given standard trend for a particular confusion level most likely represent clouds.

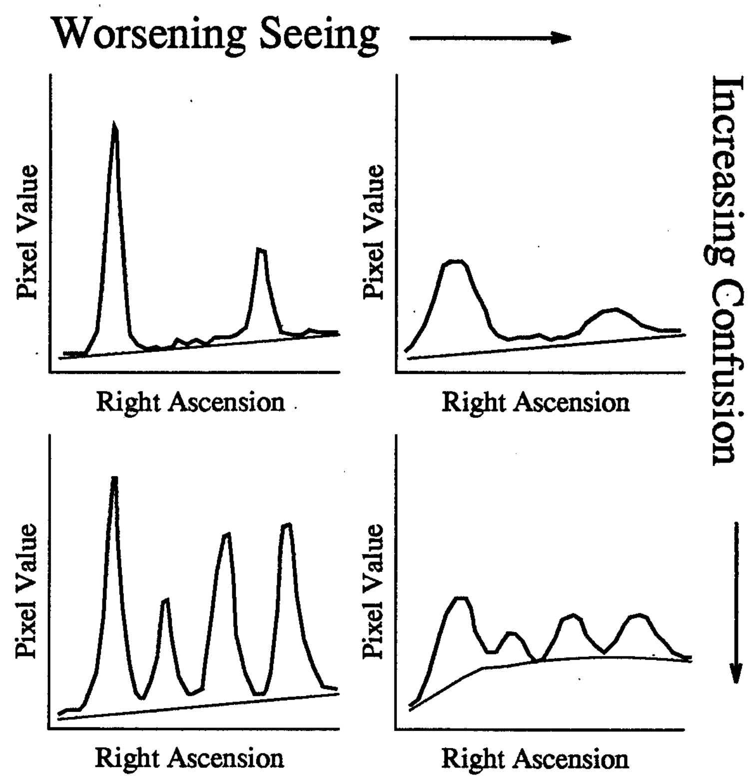


Figure 3.8 - Relationship between confusion, seeing, and magnitude offset explained. Worsening seeing is to the right. Increasing confusion is towards the bottom.

The explanation for why there is a relationship between magnitude offset and seeing for a given confusion level lies in how the background is determined. Figure 3.8 illustrates in one-dimension how the background level is affected for variable seeing and confusion conditions. Low confusion is on top with high confusion on bottom, and good seeing is to the left with bad seeing to the right. Changes in seeing have little or no effect in areas of low confusion because there are still large areas of sky that essentially remain unperturbed. The background can thus follow the true sky

brightness to determine the level consistently. In areas of high confusion, however, as seeing gets worse, stars begin to merge. There is no longer any sky for the background to trace. In effect, the background level rises because it begins to trace the very stars for which we wish to estimate magnitudes. The stars thus appear dimmer, and the magnitude offset increases in order to compensate for the elevated background.

In order for the systematic variations caused by incorrect standard star luminosities to be examined and corrected, the data from the **.XYL** databases must first be cleaned of all seeing/confusion effects. This can be done using the above definition for confusion and setting seeing limits as determined from a process analogous to that described by Figure 3.7.

The only other effects to be addressed are clouds, photometry anomolies such as those created by CR_EDIT (see Section 3.3) and inaccurate photometry due to incorrect background determinations. An example of the latter would be photometry in a portion of the sky contaminated by diffracted or reflected light where the background fitting algorithm was unable to follow the background changes. Most of the these effects occur near bright stars, and thus the region of the CTI survey strip contaminated by their effects can be easily eliminated (see Section 4.2.1). One notable exception, however, is a diffraction effect or reflection from a bright

Table 3.1 - Possible Contamination of CTI Survey Strip by Mars and Jupiter during 1987-1992.

| Date of Opposition | Planet | RA (1987.5) | Dec |
|---|---|---|---|
| 1987 Oct 25 | Jupiter | $1^h\ 31^m$ | $+8°$ |
| 1988 Nov 29 | Jupiter | $3^h\ 52^m$ | $+19°$ |
| 1990 Jan 06 | Jupiter | $6^h\ 19^m$ | $+23°$ |
| 1990 Dec 05 | Mars | $3^h\ 59^m$ | $+22°$ |
| 1991 Feb 11 | Jupiter | $8^h\ 38^m$ | $+20°$ |
| 1992 Mar 13 | Jupiter | $10^h\ 40^m$ | $+10°$ |

planet. The effect of Jupiter, for instance, is clearly evident in data taken during the fall and winter of 1988 at right ascensions about $3^h$, although other regions of the CTI survey strip passing close to the ecliptic can be affected in much the same way by other planets or the Moon. Table 3.1 lists possible occurances for contamination from Mars and Jupiter during the period from 1987 to 1992. The planet Saturn was never in a position to affect the CTI survey strip during this period.

Assuming that most observations of a particular standard star are free from clouds, photometry anomolies and the effects of solar system objects, by simply taking the mode instead of the mean to find systematic offsets, the effect of these outliers are eliminated.

The final result of the calibration process is an **.OBS** database, identical in form to the **.SED** database, but containing the *calibrated* position, luminosity, and second moments of every object observed in the particular sweep.

As a side note, if the expected luminosities in the **.SSS**

database were correct, the **.RDK** and **.RFF** databases could be determined by simply examining the **.XYL** or **.CAL** databases for systematic trends in standard star luminosities as a function of declination, and adjusting them accordingly to eliminate those trends. Unfortunately, at this stage we can't be sure if the trends in declination are caused by an incorrect flat field application or incorrect standard star luminosities. This could be remedied by obtaining luminosities to the desired precision for all standard stars located in a small section of the CTI survey strip using another telescope. These expected luminosities could be used to correct the flat-field function for a single night's data, thus obtaining correct expected luminosities for many more standards. Other overlapping nights of data could then be corrected until the entire set of CTI standard star luminosities are free from systematic errors created by incorrect flat-field application.

## 3.6. Merging Data into Master and History Databases

The day's data can now be merged into the history list of the particular color filter and the master list using the computer routines AUTO_MERGE, AUTO_UPDATE and AUTO_FLUSH.

AUTO_MERGE compares the existing **.PUL** database (containing a right ascension-sorted record of every object observed) with the **.OBS** database of a particular day and matches the records of objects found in both. A **.MRG** database containing the data for each match, and two **.NDX** databases containing a pointer to the record of any unmatched records in the **.PUL** and **.OBS** databases are produced. Additionally, a **.TRA** database containing information relevant to all matches to trace possible mismatches is produced.

Next, AUTO_UPDATE uses the **.MRG** database to refine the information on existing objects in the **.PUL**, **.MAS**, and **.HIS** databases, and uses the **.OBS** combined with the **.NDX** pointer to add new objects. Only objects with a probability value of 0.5 or above are added to the **.MAS** and **.HIS** databases while all new objects, regardless of the probability value, are listed in a newly created **.PUL** database. Including all objects in the **.PUL** database retains the possibility of a very faint object building on its probability value with subsequent detections to eventually be inculded in the **.MAS** and **.HIS** databases. The **.HIS** database contains the day-to-day record of the time, calibrated instrumental luminosity, and error in luminosity of every object observed. The **.HIS** databases also

reference the **.MAS** database, which contains variance-weighted average positional and photometric information as well as various measures of the object's shape and blending. The **.PUL** database contains information similar to the **.MAS** database, but retains all detections regardless of the probability value of detection and is sorted by right ascension for ease in comparing the next day's data. The **.MAS** and **.HIS** databases are not sorted by right ascension, with new detections being added to the end.

Finally, AUTO_FLUSH combines the existing **.PUL** file with the new objects contained in the day's **.PUL** file. The probability value of all non-detections are adjusted downward, and the entire database is sorted by right ascension in preparation for the next day's data.

Currently, data from 77 V nights, 8 B nights, 8 R nights, and 8 I nights have been entered into the **.MAS** and **.HIS** databases. The solid lines in Figure 3.9 displays the distribution of the V and B observations in right ascension for the **.MAS** and **.HIS** databases. The lack of observations about $21^h$ corresponds to the summer observing season where clear nights were hard to come by. An additional 68 V nights, 26 B nights, 39 R nights, and 23 I nights have been analyzed but not yet merged into these databases.

A second analysis of all 145 V nights and 34 B nights was made for this dissertation with the output entered into new versions of the master and history databases (**.NML** and **.NHL**

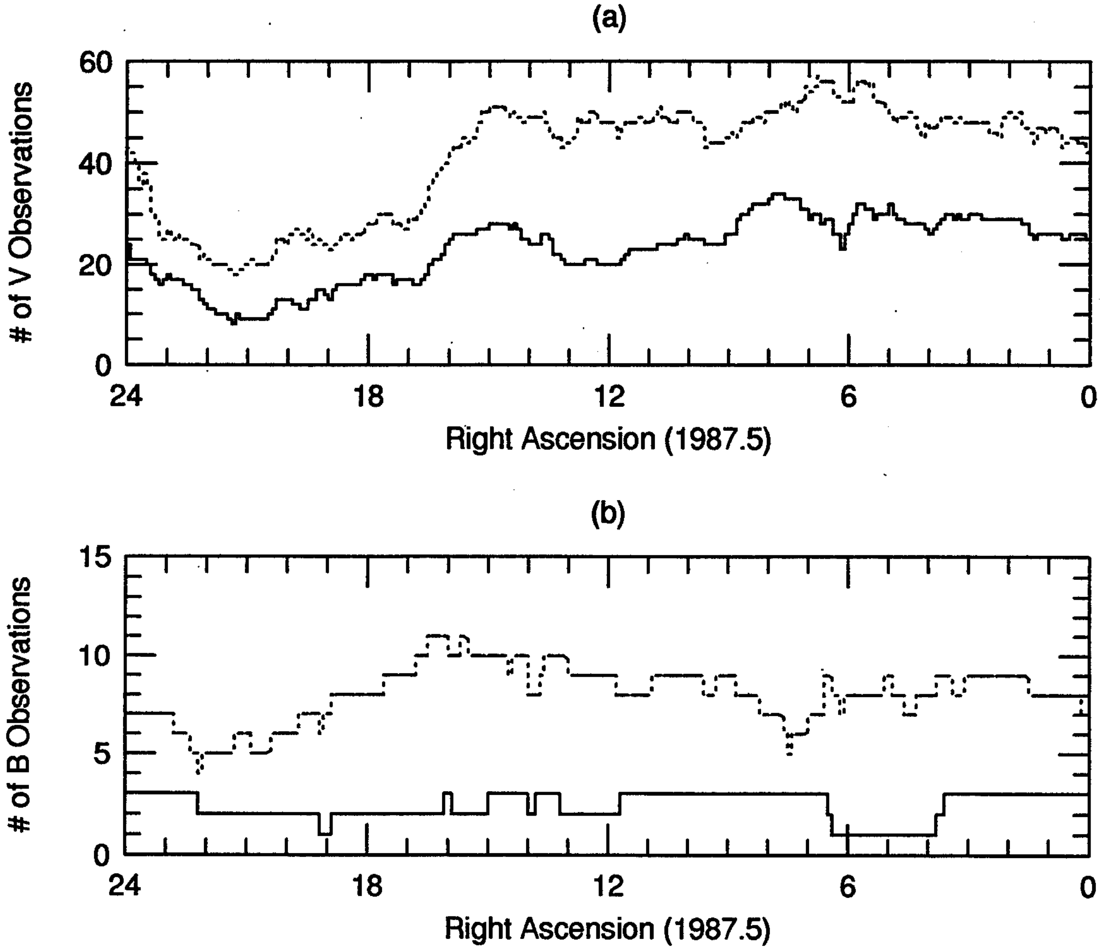


Figure 3.9 - (a) Number of V observations and (b) number of B observations as a function of right ascension. Solid line represents those days merged into the current **.MAS** and **.HIS** databases. Dashed line represents those days merged into the current **.NML** and **.NHL** databases.

respectively). The primary difference between these new databases and the old versions is that the **.NHL** database now contains a day-to-day record of the position of every object in addition to its luminosity. Also, the positional calibration of the data used to create these new databases employed the misalignment and astigmatism correction procedure (see Section 3.5.1) not used previously. The dashed line in

Figure 3.9 displays the distribution of the V and B observations versus right ascension for the **.NML** and **.NHL** databases.

We are now ready to query the information contained in the master (**.MAS** or **.NML**), pool (**.PUL**), and history (**.HIS** or **.NHL**) databases, or any of the other databases produced during the analysis process. This is accomplished using the computer program PSI, which was specifically developed for use with the CTI survey. A user's guide to this and other CTI database programs can be found in <u>The CCD/Transit Instrument Atlas and Database Guide</u> (Wetterer 1995), written as a supplement to this dissertation.

# Chapter 4 Variable stars in the CTI survey

The CTI observes over 500,000 objects, many of which vary in luminosity as a function of time. This chapter describes the discovery of variable stars in the CTI survey. First, a short history of the study of variable stars is given. Next, the method for finding variable stars and the completeness of the variable star list is presented with the issues of spurious variables and blind spots discussed. Finally, a description of the resulting variable star index database is presented.

## 4.1 Variable Stars

A variable star refers to a star where one or more of its physical properties change with time. Typically it is the star's luminosity in a certain wavelength range that is examined to determine variability, although it may be another property, such as spectral type (or color), radial velocity, or details within the spectra that vary with or without a luminosity variation. The simple fact that stars have finite lifetimes make all stars variable at some level. Over time, certain stars become variable due to evolutionary changes. Helium core burning RR Lyrae variable stars were quiet members of the main-sequence earlier in life. Even if time restraints are specified, small scale variability, such as the Sun's 11-year sunspot cycle, are probably present in most stars. In the following discussion, however, I will restrict the definition of a variable star to those for which luminosity in visible light (V bandpass) changes appreciably over a time interval detectable by CTI (a few minutes to a few years).

The history of the study of variable stars spans nearly four centuries (see, for instance, Campbell and Jacchia 1941). Although many novae and supernovae had been detected beforehand, such as the supernova leading to the Crab Nebula in Taurus recorded by the Chinese in 1054 AD, the first star to be classified as a periodic variable was a star in the constellation Cetus. The star was designated o Ceti by Bayer in 1603, who was unaware of its variability, and later also

named Mira. Fabricius first noted its presence and disappearance in August 1596 and February 1609, although it was not until 1638 that Holwarda noted the star was periodic in its brightening and dimming (Allen 1963). By the end of the 18th century, sixteen stars were classified as variables. There were four Mira variables, two eclipsing variables (the star Algol being the prototype), two Cepheid variables (named after one of the two, $\delta$ Cephei), five novae, and three others stars that exhibited their own unique variations ($\alpha$ Herculis with a small and irregular variation, R Scuti with a semi-regular periodicity, and R Coronae Borealis with erratic and large variations). By the end of the 19th century, the number of identified variable stars had grown to over 1000. With improvements in photography, the discovery rate of variable stars greatly increased. By the middle of the 20th century, 10000 variables had been identified, and as we near the 21st century, nearly 30000 are known and cataloged in the Milky Way (Kholopov et al. 1985-88) with many more variable stars identified in other nearby galaxies (see, for example, Saha et al. 1990). As with the advent of photographic surveys, in the coming years, CCD surveys such as the CTI survey will undoubtedly continue the dramatic increase in the number of detected variable stars.

Because of similarities between variable stars, astronomers have continually attempted to group them into

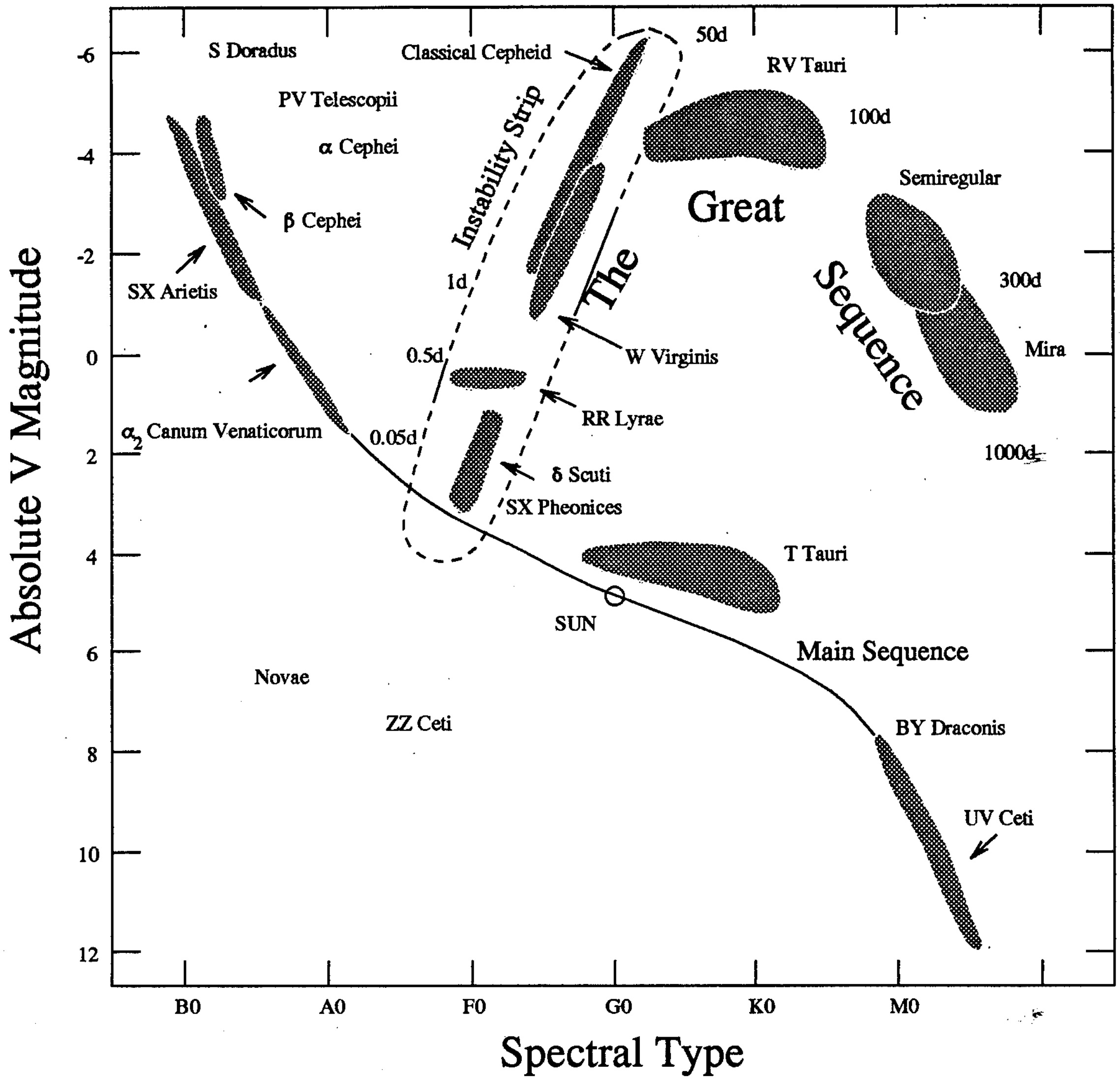


Figure 4.1 - Positions of variable star types on Hertzsprung-Russell (H-R) diagram, (Adapted from Cox 1980). Variable stars in the "Instability Strip" are radially pulsating stars and share a common mechanism that drives their pulsations. Variable stars in "The Great Sequence" (SX Pheonices to Mira) are pulsational variables of decreasing density and increasing size and period (typical periods shown in days).

different categories and types. Whereas the number of recognized variable star types in 1800 were 7, there are currently nearly 50. The first division used in the

classifications of the General Catalog of Variable Stars (GCVS) (Kholopov et al. 1985-88) are between *cataclysmic* (thermonuclear burst processes deep in star's interiors, in surface layers, or in surrounding space), *eruptive* (violent processes and flares occurring in the chromosphere or corona), *pulsating* (periodic radial or nonradial contractions and expansions of surface layers), *rotating* (nonuniform surface brightness and/or ellipsoidal shapes), and *eclipsing* (close binary geometric effects) variables. Other broad distinctions can be made between *intrinsic* variables where the variability is the result of changes within the star itself, and *extrinsic* variables where the variability is a result of an interaction with another star or interstellar medium. Also, light curve morphology is often used to make distinctions between variables. Confusing matters still further, several stars exhibit variability from more than one source, presenting the possibility of multiple classifications. Table A1.6 in Appendix 1 (adapted from the GCVS and Petit 1987) attempts to summarize all the types represented in the GCVS detectable by the CTI. Many of these variables occupy specific parts of the Hertzsprung-Russell (H-R) diagram, as shown in Figure 4.1 (adapted from Cox 1980).

Variable stars are stars in certain phases of their evolution, or undergoing rapid changes. The study of variable stars has improved our understanding of stellar structure and evolution. Perhaps the most important result to come from the

study of variable stars, however, involves using certain types of variable stars as "standard candles" or distance indicators. The famous period-luminosity relationship of classical Cepheid variable stars allows their distance to be accurately calculated given knowledge of their period and apparent magnitude (see, for example, Madore and Freedman 1991, Jacoby et al. 1992). With absolute magnitudes of $M_V$ = -2 to -7, Cepheid variable stars can be detected in galaxies out to 10 Mpc. Most other types of pulsating variable stars also exhibit a similar relationship. One of these types, RR Lyrae stars, are abudent in the old population of the Galaxy, enabling astronomers to probe the properties of the Milky Way's halo as well as the properties of globular clusters. The study of RR Lyrae variable stars, and subsequent search for this type of star within the CTI survey, is discussed in more detail in the next chapter.

## 4.2 Finding variable stars in CTI survey

The obvious CTI database to use in order to start our search for variable stars in the CTI survey is the V filter's history list (**.HIS** or **.NHL** database). The history list contains the time, luminosity (*lum*) and luminosity error ($\sigma_{lum}$) for every observation with the V filter of each object in the survey. The scatter in luminosity measurements is approximated well by a Gaussian distribution, and thus a simple test can determine if the observed variability of the luminosity is statistically significant (Chapter 10, Bevington 1969).

The error estimates should follow a $\chi^2$ distribution. The reduced $\chi^2$ is given by

$$\chi_{\upsilon}^{2}=\sum_{i=1}^{n}\frac{(lum-\langle lum\rangle)^{2}}{\upsilon\sigma_{lum}^{2}}, \tag{4.1}$$

where $\langle lum \rangle$ is the mean luminosity, n is the number of observations and $\nu$ = n-1. It is evident that for a given number of observations, the larger $\chi_{\nu}^{2}$, the more probable the object's variability is a result of an actual change in its luminosity rather than from random errors. This probability can be calculated using the equation

$$P_{\chi}(\chi_{\upsilon}^{2})=\int_{\chi_{\upsilon}^{2}}^{\infty}P(x^{2},\nu)\,dx^{2}, \tag{4.2}$$

where

$$P(x^2, \nu) = \frac{(x^2)^{1/2(\nu-2)} e^{-x^2/2}}{2^{\nu/2}\Gamma(\nu/2)} \tag{4.3}$$

is the probability distribution function for $\chi_\nu^2$. In the search for variable stars in the CTI survey, only those objects were selected for which this probability of the observed distribution being a product of the calculated random error is less than 1%.

Due to photometry errors, if this test is applied to objects in the current **.HIS** or **.NHL** databases, approximately 60% pass the test and are considered variable. It is thus necessary to screen the photometry data before testing for variability to eliminate sources of spurious variables.

### 4.2.1 Spurious Variables

There are several sources of systematic error that affect the photometry of objects in the CTI survey. Before the above test for variability can be conducted, the data contaminated by these photometry errors must be eliminated.

Stars surrounding a bright star may all appear variable as the amount of contamination from the diffraction spikes of the bright star varies. These night-to-night variations are caused by different observing conditions, such as seeing, transparency, and estimated background level. To reduce this problem, a region surrounding each bright star was removed from the survey corresponding to the area visually

contaminated by false objects produced by the star's diffraction spikes and charge bleeding. The biggest offenders are Pollux, Scheat, and Alberio for which it was necessary to remove 0.24%, 0.17% and 0.07% of the CTI survey area respectively. Another 308 stars contained in the SAO catalog (see Table A1.5 in Appendix 1), and 2060 stars determined to be brighter that V = 12 from CTI's **.MAS** database were also removed. The CTI selected stars were carefully screened to exclude bright objects in the database created by meteor or satellite trails. The size of the regions masked around each star varied as a function of the magnitude of the star. The formulas used in calculating the size and shape of the mask were determined empirically using a small selection of representative stars and are given in Table A1.7 of Appendix 1. The total area removed because of bright star contamination was approximately 1.0 square degree, or 1.93% of the CTI survey area. The remaining CTI survey area contains 532,878 objects with four or more V observations.

The luminosity data of an object may also be contaminated by isolated events, such as meteor trails, systematic errors caused by photometry in regions where the background was not accurately calculated (see Chapter 3.5.2), and accidental non-detections caused by the cosmic ray removal algorithm (see Chapter 3.3). For a nonvariable star, these effects will create anomalously bright or faint data in an otherwise constant luminosity light curve. As a first cut, the minimum

and maximum luminosity for a particular star is not considered. Next, luminosity measurements which deviate more than 3$\sigma$ above the mean luminosity and 2$\sigma$ below the mean luminosity for each object, ($\sigma$ being the standard deviation of the luminosity from the mean not considering the minimum and maximum luminosities) were removed from consideration. Finally, $\sigma$ and the mean were recalculated, with any more extreme luminosity data removed as in the first pass. The limits used in this prescreening were chosen empirically to remove the bulk of the spurious variables created. This prescreening of the luminosity data does bias the resulting variable object list against stars that vary by exhibiting an occasional short-lived brightening (e.g. some eruptive-type variables) or dimming (e.g. Algol type eclipsing variables). This bias, however, does not affect the detection of RR Lyrae variable stars with good phase coverage, which was the primary goal of the present search. A total of 39,334 objects (7.4%) pass the variability test after employing the above prescreening.

Figure 4.2 plots the variable fraction of the total number of objects as a function of mean instrumental V magnitude (solid line labeled $\sigma$ = 0%) after prescreening. Also plotted in Figure 4.2 is the total number of objects as a function of mean V magnitude (dashed line). Only objects outside the Galactic plane with 9 or more V observations were used in making this plot to reduce the effects of other

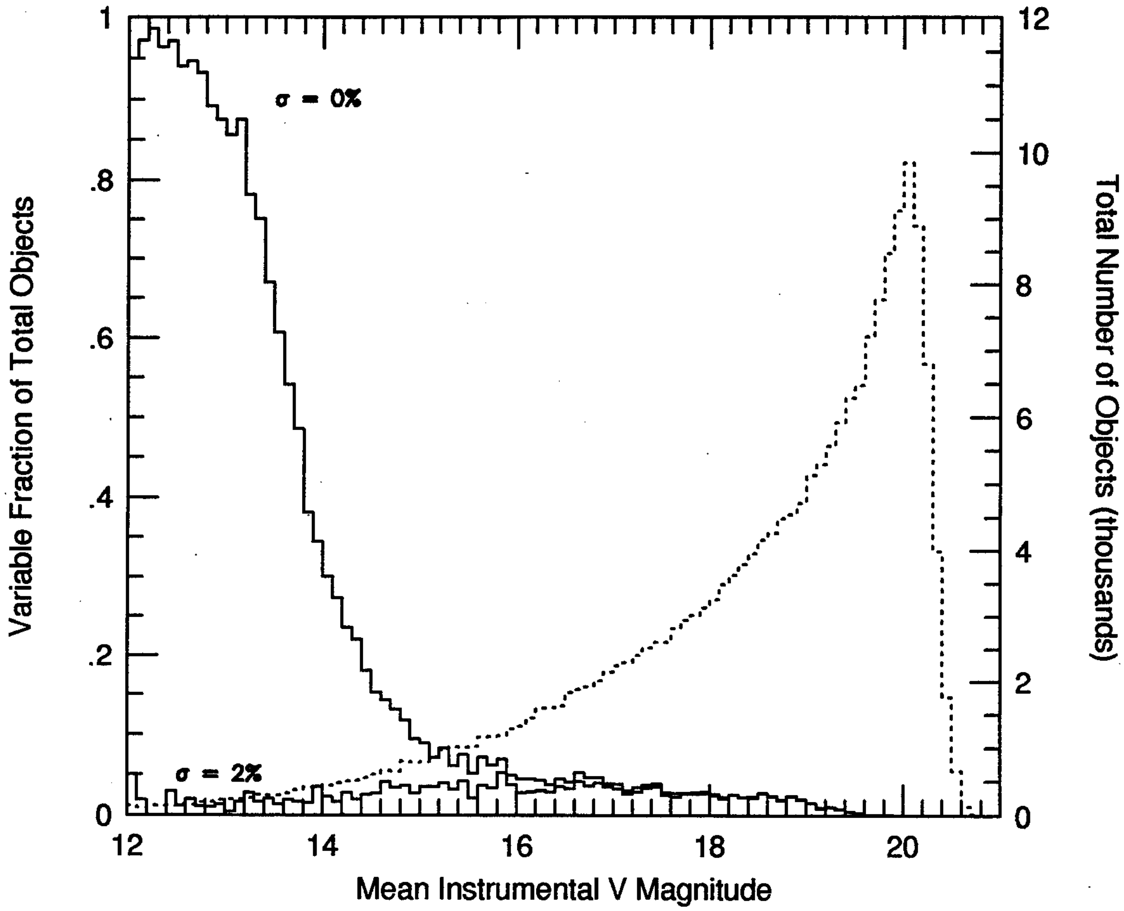


Figure 4.2 - Variable fraction of objects outside Galactic plane with 9 or more V observations versus mean instrumental V magnitude for additional systematic errors of 0.00 and 0.02 times the luminosity (solid lines). Total number of objects outside the Galactic Plane with 9 or more V observations versus mean instrumental V magnitude also shown as dashed line and using scale on right.

sources of spurious variables. The most striking feature in Figure 4.2 is the dramatic increase of the variable fraction of objects for stars with V < 15. For brighter stars, the error in luminosity relative to the luminosity decreases, making the variability test more sensitive to lower amplitudes of variation in magnitudes. The increase in the fraction of

variable objects for V < 15 could simply be an actual detection of more variables due to the increased sensitivity. An additional luminosity-dependent error not accounted for in the calculated luminosity error, however, would produce the same effect. A possible source for this type of error is incorrect flat-field application (see Chapter 3.2). An error in the flat-field would directly manifest itself as a systematic error in the calculated luminosity of an object. The calculated error in the luminosity for the object, however, is not affected. If the position and magnitude of these flat-field errors vary from night-to-night, the induced systematic errors for a particular object would be similar to increasing the random error in luminosity. The variable fraction of the total number of objects as a function of mean instrumental V magnitude after adding in quadrature an additional error of 2% the object's luminosity to the existing random error (solid line labeled $\sigma = 2\%$) is also plotted in Figure 4.2. The variable fraction of objects is now virtually independent of magnitude. Unfortunately increasing the error in the luminosities to remove spurious variables created by flat-field application (or from another source of a luminosity dependent error) undoubtedly removes true variables as well, just as using the existing error undoubtedly includes spurious variables. The former represents a conservative estimate of what objects are variable, while the latter a liberal estimate.

If the additional error as described above is applied, an effective lower limit in amplitude of about $\Delta V \approx 0.1$ magnitudes for detecting variables is set. For fainter magnitudes, the increasing random error requires ever greater amplitude variations to be detected as a variable star. This sets a faint limit to the detection of variable stars and will be discussed in more detail in the next section. A total of 25,325 objects (4.7%) pass the variability test after employing the prescreening and additional error.

Another source of spurious variables are stars that are very close together or segments of extended objects such as galaxies. These objects might appear variable because the photometry splits the light between them differently under different conditions. Thus, sometimes one star appears dimmer while the other brighter, while at other times the reverse is true. Both stars appear variable when in fact they are not. For all stars passing the variability test using the prescreening and additional error, and with 9 or more V observations, the linear correlation coefficient was calculated between the star's luminosity and the luminosity of its nearest variable neighbor (Chapter 7, Bevington 1969)

$$r \equiv \frac{N\Sigma x_i y_i - \Sigma x_i \Sigma y_i}{\sqrt{N\Sigma x_i^2 - (\Sigma x_i)^2}\sqrt{N\Sigma y_i^2 - (\Sigma y_i)^2}}, \qquad (4.4)$$

where $x_i$ is the star's luminosity, $y_i$ is the neighboring star's luminosity, and N is the number of observation dates common to

both. The light curves of the two stars are inversely correlated for $r < 0$. The probability that a random sample of N uncorrelated experimental data points would yield an experimental linear-correlation coefficient $|r|$ as large as or larger than the observed value was calculated with

$$P_c(r,N) = 2\int_{|r|}^{1} P_r(\rho,\nu)\,d\rho, \tag{4.5}$$

where

$$P_r(r,\nu) = \frac{1}{\sqrt{\pi}}\frac{\Gamma[(\nu+1)/2]}{\Gamma(\nu/2)}(1-r^2)^{(\nu-2)/2}, \tag{4.6}$$

$\nu = N - 2$, and $\Gamma$ is the Gamma function. If $r < 0$ and $P_c(r,N)$ less than 1%, the two stars in question were not considered variable. A total of 19,412 (4.3%) stars pass the variability test after employing the prescreening, additional error, and correlation test.

Galaxies may still appear variable due to a dependence of the photometry on the seeing or the throughput of the telescope (see, for instance, Hawkins 1984 and Stobie et al. 1986). For example, as dust settles on the mirror reducing the throughput of the telescope, the contribution of a galaxy's faint outer structure may slowly be lost in the noise of the surrounding background. Because the luminosity calibration is determined by stars, a spurious long period variable could thus be created from the photometry of a galaxy. An indication that this may indeed be happening is

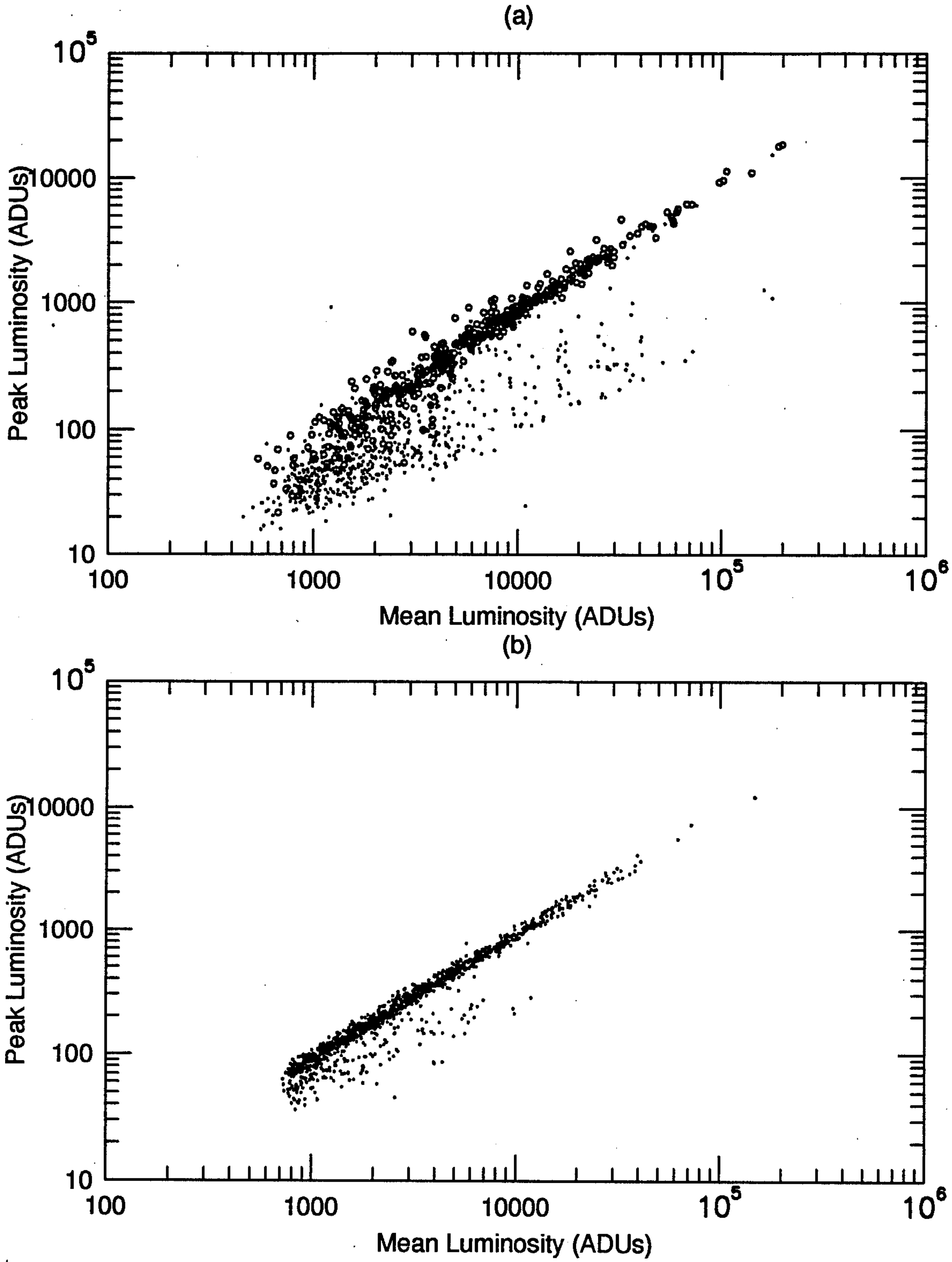


Figure 4.3 - Peak luminosity versus mean luminosity for (a) variable objects with 9 or more V observations and a right ascension between $7^h$ and $18^h$, and, (b) non-variable objects with 9 or more V observations and a right ascension between $7^h$ and $18^h$. Circles in (a) are for objects with V_COMB = 0.

illustrated in Figure 4.3. The peak luminosity is plotted versus the mean luminosity for (a) variable objects and (b) the same number of non-variable objects. Only objects with 9 or more V observations and a right ascensions between $7^h$ and $18^h$ are plotted to reduce the effect of other sources of spurious variables. All stars have the same point spread function and thus fall on a straight line in these plots. Extended objects such as galaxies will have a lower peak luminosity as compared to the same mean luminosity for a star, and will thus fall below the line tracing stars. As seen when comparing Figure 4.3(a) to 4.3(b), it is clear there is a higher percentage of galaxies that are variable.

A useful CTI database attribute that can be used to eliminate galaxies as well as other blended stars and artifacts surrounding bright stars not previously masked is V_COMB. V_COMB is related to possible matching errors, with a non-zero V_COMB indicating that at some time the automated matching accomplished during AUTO_MERGE (see Chapter 3.6) had trouble matching the observed object(s) with the records contained in the **.PUL** database. The more complicated the matching problem (corresponding to greater values of V_COMB), the greater fraction of these objects are detected as variable. The circles plotted in Figure 4.3(a) are variable objects with V_COMB = 0 (i.e. no matching problem), with nearly all falling close to the line representing stars. Requiring V_COMB to equal zero appears to eliminate galaxies,

but is also reducing the effective CTI survey area by eliminating stars from consideration. A total of 13,547 (3.5%) stars pass the variability test after employing the prescreening, additional error, correlation test, and requiring V_COMB = 0. The last condition also reduces the total number of observed stars to 387,998.

Figure 4.4 plots the variable fraction of objects as a function of the number of V observations using (a) all the screening described above except the restriction on V_COMB, and (b) all the screening described above including V_COMB = 0 (solid line). Only objects outside the Galactic plane between right ascensions $1^h$ and $15^h$, corresponding to regions of the CTI survey strip with approximately the same maximum number of V observations, were used in making this plot to reduce the effects of other sources of spurious variables. The total number of objects as a function of the number of V observations for this region is also plotted (dashed line). The increase in the fraction of variables for objects with less than 15 detections in Figure 4.4(a) can be explained by comparing this to Figure 4.4(b). The majority of these objects with less than 15 detections and variable have also experienced a matching problem (V_COMB ≠ 0). It is likely that most of these objects are segments of extended objects or noise segments in the diffraction halos of bright stars not previously masked. Since changing observing conditions will change the positions of these false objects, many such objects

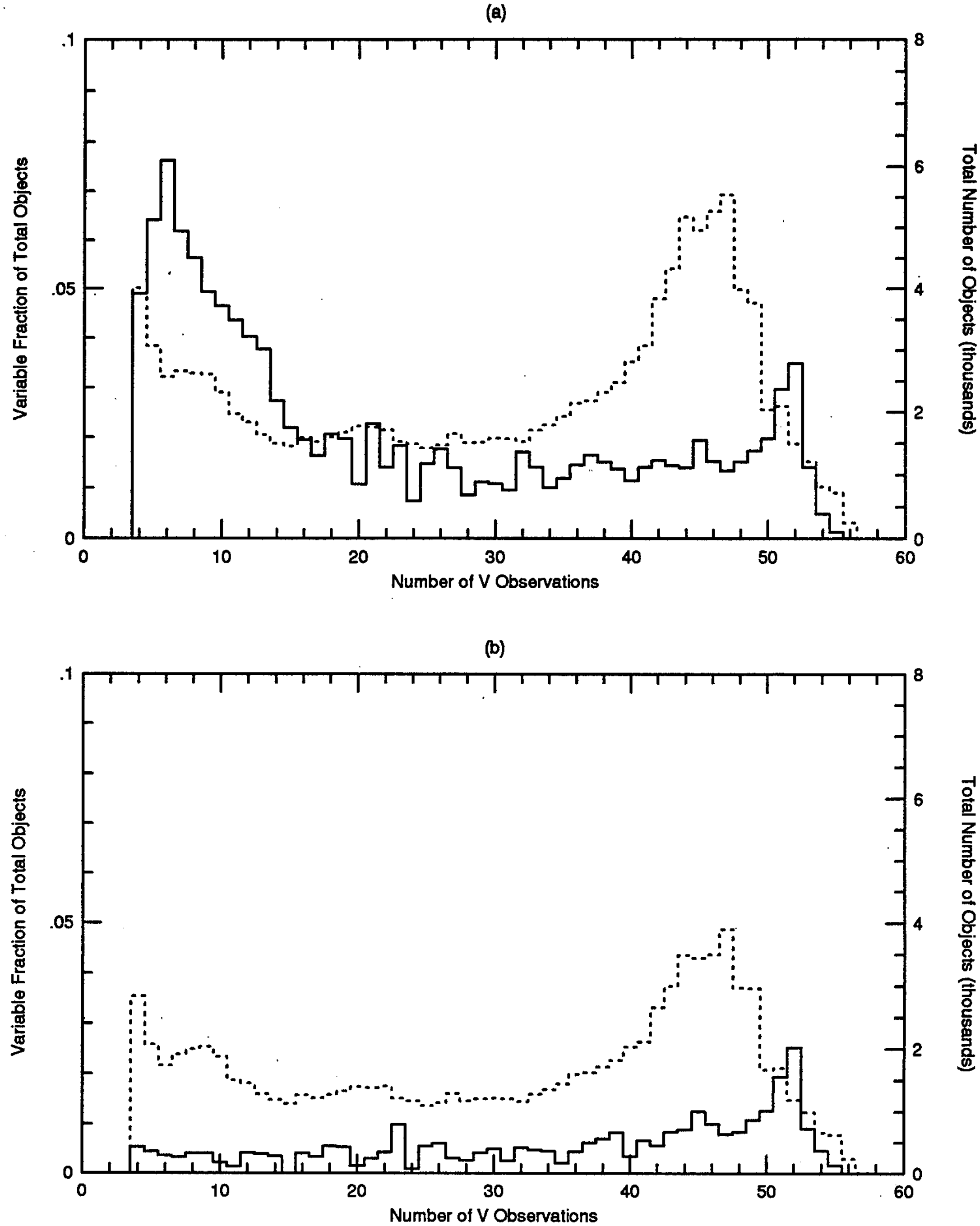


Figure 4.4 - Variable fraction of objects outside Galactic plane between right ascensions $1^h$ - $15^h$ versus number of V observations (a) no restriction on V_COMB and (b) V_COMB = 0 shown as solid line. Total number of objects outside the Galactic plane between right ascensions $1^h$ to $15^h$ versus number of V observations also shown as dashed line and using scale on right.

are created, with a particular object being "observed" only on a fraction of the total number of nights. The rise in the variable fraction of objects when the number of V observations is above 50 is related to confusion near the Galactic plane.

Figure 4.5 plots the variable fraction of objects as a function of right ascension using (a) all the screening described above except the restriction on V_COMB, and (b) all the screening described above including V_COMB = 0 (solid line). Only objects with 9 or more V observations were used in making the plot. Also plotted is the total number of objects as a function of right ascension (dashed line). In general, the fraction of variable objects remains reasonably constant, except in the Galactic plane where there is a sharp rise directly correlated to the density of objects (i.e. confusion), and in highly localized regions outside the Galactic plane. The first effect is most probably a result of photometry errors created by the link between background estimation and observing conditions in regions of high confusion (see Chapter 3.5.2). Figure 4.6 plots the fraction of variable objects as a function of V magnitude for objects in the heart of the summer Galactic plane. The photometry errors resulting from the background estimation clearly increase the scatter in the luminosity data such that nearly all bright stars pass the variability test because this error is not reflected in the luminosity error. The increased fraction of variables in highly localized regions outside the

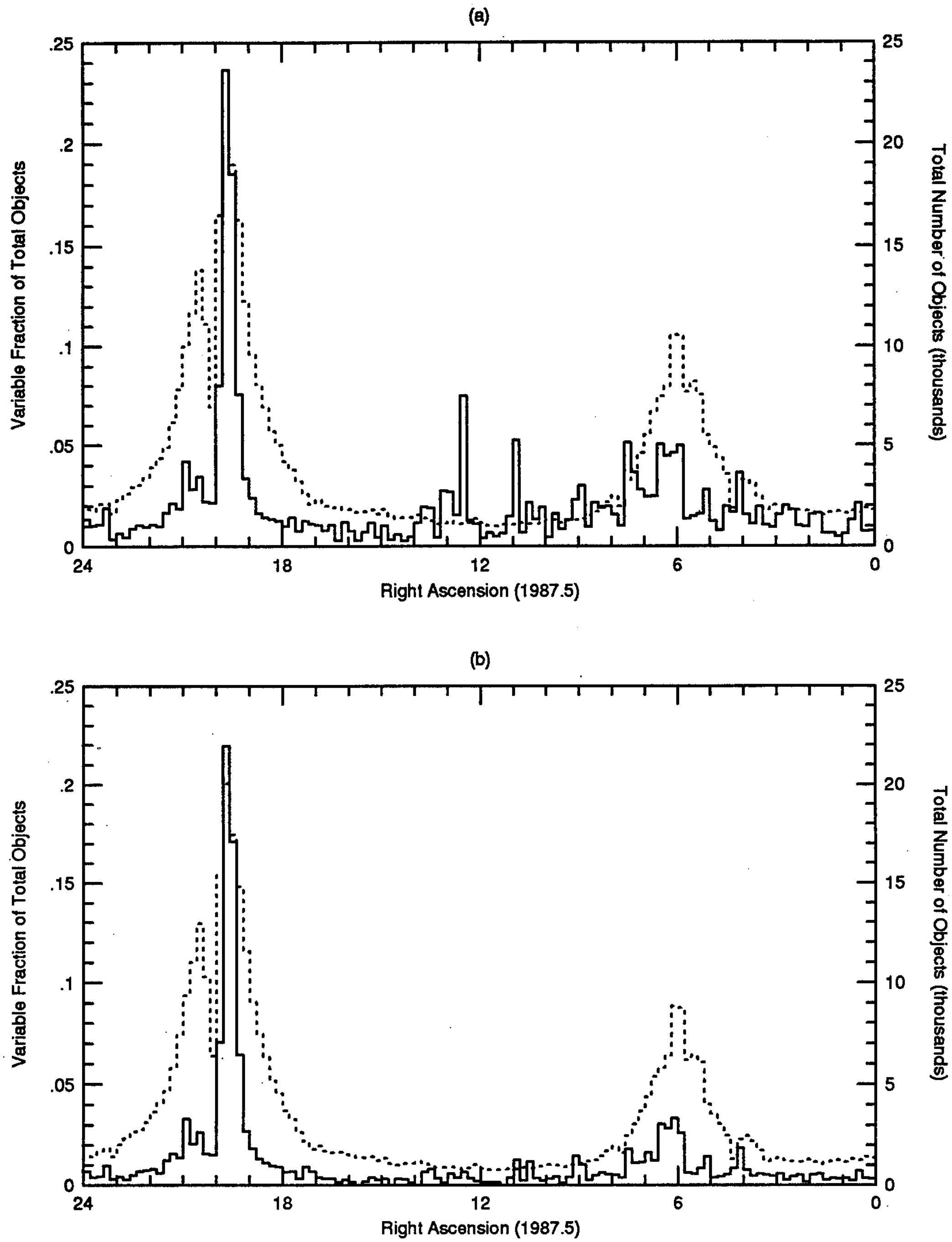


Figure 4.5 - Variable fraction of objects with 9 or more V observations versus right ascension (a) no restriction on V_COMB and (b) V_COMB = 0 shown as solid line. Total number of objects with 9 or more V observations versus right ascension also shown as dashed line and using scale on right.

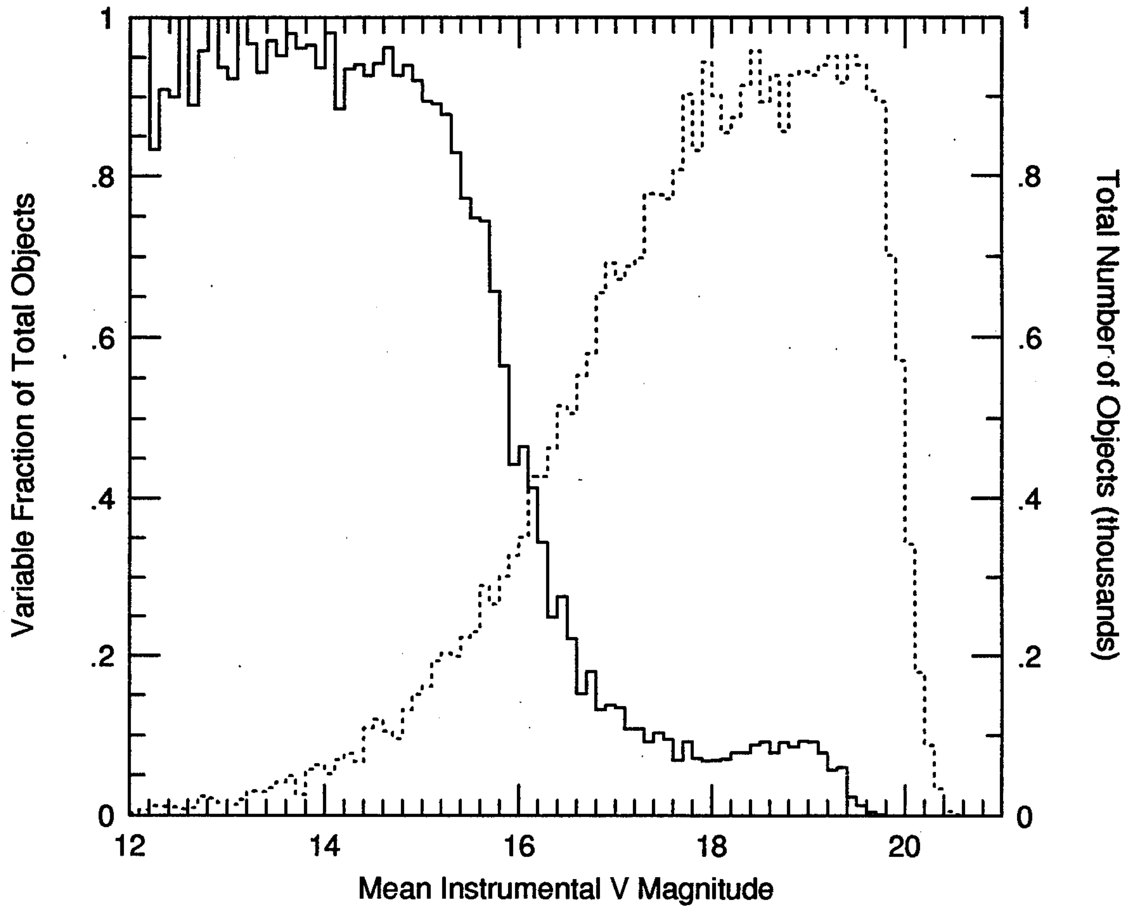


Figure 4.6 - Variable fraction of objects in Galactic plane (right ascensions 19.4h to 19.8h) with 9 or more V observations versus mean instrumental V magnitude shown as solid line. Total number of objects in this region versus mean instrumental V magnitude also shown as dashed line and using scale on right.

Galactic plane are possibly due to spurious variables created by extended objects or bright stars. This is supported by the fact that these high variable fraction regions are eliminated by requiring V_COMB = 0, as shown in Figure 4.5(b).

In summary, searching for variable stars in the CTI

databases also exposes sources of photometry errors that create spurious variables. Indeed, many of the sources discussed above were discovered due to clues left in the "light curves" of the spurious variables created. Each solution employed to eliminate spurious variables has unfortunately eliminated true variables as well, and depending on the type of variable star being sought, will effect the completeness of the resulting sample.

### 4.2.2 Blind Spots (Completeness)

There are certain variable stars that CTI will not be able to detect. As stated above, with the addition of a systematic error to account for flat-fielding problems, variable stars with changes in luminosity less than $\approx 0.1$ magnitudes will not be detected. For fainter stars, this minimum detectable magnitude difference increases as the observational error increases. This is illustrated in Figure 4.7 which plots the average random error (solid line) and average adjusted error (including the 2% systematic error discussed in previous section, dashed line) in the instrumental V magnitude versus the average instrumental V magnitude. It is clear that the fainter the object, the greater the average error, and thus the greater amplitude in variability needed for detection. This is evident in Figure 4.2 as a decline in the variable fraction of objects for V > 19. Using synthesized sinusoidal light curves, the minimum

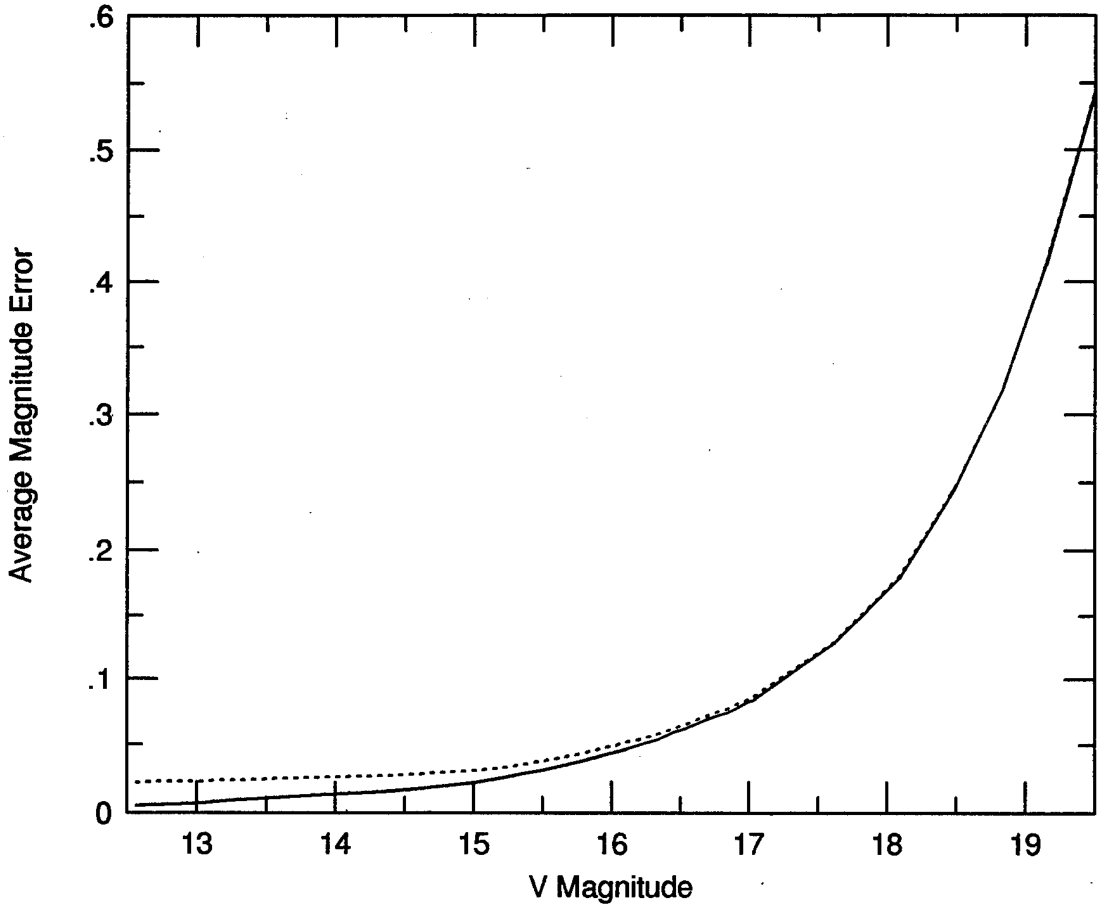


Figure 4.7 - Average V magnitude random error (solid line) and total error (dashed line) as a function of average instrumental V magnitude.

amplitude limit as a function of magnitude was determined to be between 3 and 4 times the total error.

Another blind spot involves variable stars of specific periods. As an obvious example, a variable star with a period of exactly one sidereal day will appear constant due to the fact that CTI *observes* with exactly a one sidereal day period. Depending on the type of variability, variable stars with

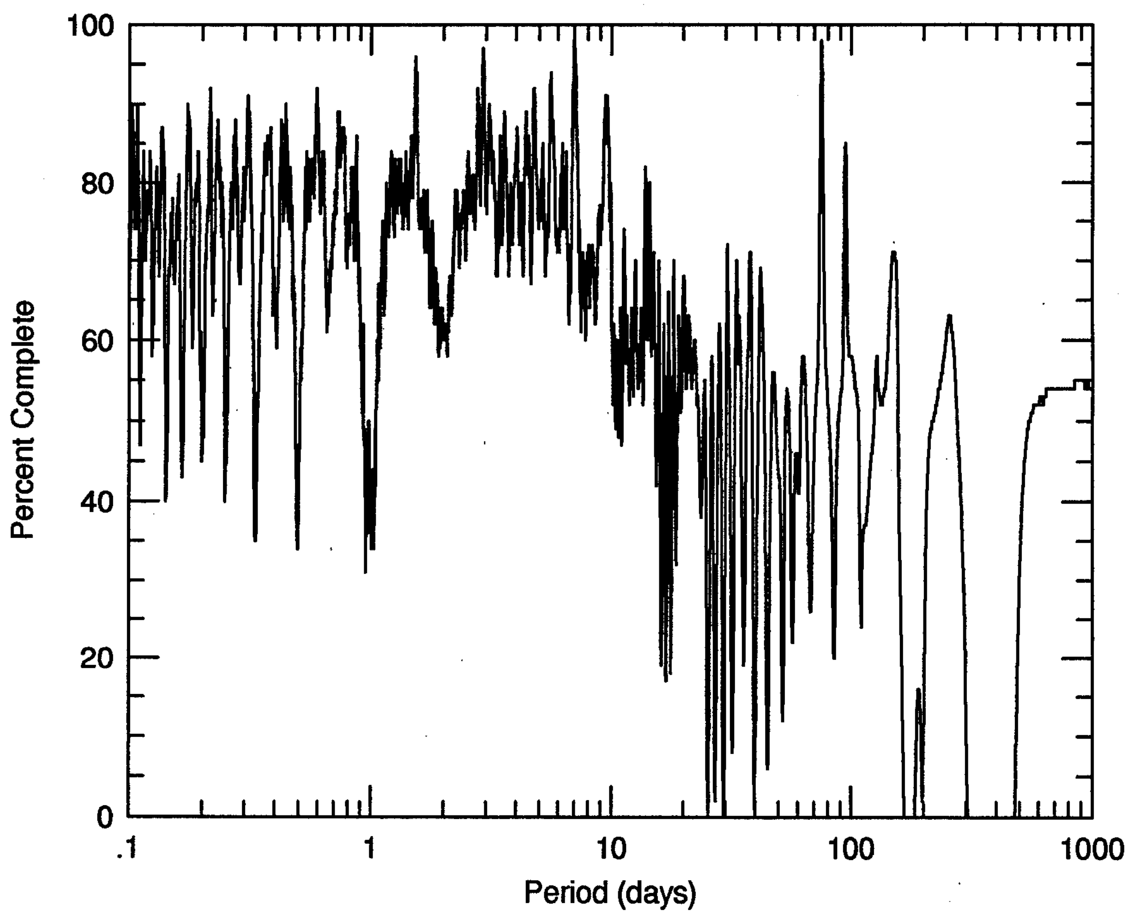


Figure 4.8 - Percent detectability as a function of period as calculated from the observation times of a typical star with 19 observations.

periods close to fractions or multiples of a sidereal day will also not be detected. These period-specific blind spots can be identified and an estimate of the completeness of detecting a certain type of variable star can be made.

Figure 4.8 maps out these blind spots for periods between a tenth of a day to 1000 days. This graph was produced using a typical list of observation times and assuming a sinusoidal

light curve with an amplitude four times that of the observational error. The observation times were first converted to heliocentric observation times to account for varying arrival times of the light from stars during different times of the year. Given the heliocentric observation times and period, the phase distribution of observations was calculated. Given some initial phase, luminosities were calculated and the resulting data was tested for variability using the same test as described above. For each period, the detections were averaged over all initial phases to determine the detection rate for that period. Fractions and multiples of the sidereal day and the tropical year are clearly visible. Any serious completeness estimate, however, should take into account minimum and maximum periods, light curve shape, and minimum and maximum amplitude of the particular variable in question.

## 4.3 CTI Variable Star Index Description

All entries in the CTI survey's **.NML** database with at least one V observation are listed in the CTI variable star index (**.VNX** database). This database can be used to produce index listings for the **.NML** or **.NHL** databases of potential variable stars by setting limits on the various other attributes. The following is a description of the information contained in the **.VNX** database.

The first two attributes are pointers to the **.NML** database (MLINK) and the B and V **.NHL** databases (HLINK). Positional information is contained in the next two attributes, YCTI (right ascension in centipixels) and XCTI (declination in centipixels). These values are given using CTI's epoch of 1987.5, and can be easily converted to hours of right ascension and degrees of declination using

$$RA = \frac{YCTI}{3.0\times10^{6}} \tag{4.7}$$

and

$$Dec = 28.0 + \cos(28.0) \times \frac{XCTI}{2.0\times10^{5}}. \tag{4.8}$$

When referring to a listing, the object name is "CTI" plus the right ascension (HHMMSS.S) and declination (+DDMMSS.S) (e.g. CTI025001.4+280123.3). The **.VNX** database is sorted by increasing YCTI.

The next attribute, NDET, refers to the number of V observations, including those observations that might suffer

from photometry errors. The next two attributes were calculated for all objects using the data prescreening procedure described in Section 4.2.1. V refers to the average instrumental V magnitude and AMP refers to the amplitude of variation in V magnitude. In both cases, the minimum and maximum luminosities were considered if they fell within the specified luminosity limits determined by the prescreening procedure.

Finally, the last attribute, FLAG, contains information pertaining to the search for variable stars. The first number in the array corresponds to whether the object passed the variability test or not. There are four possible values: 0 refers to a star that has never passed, 100 refers to stars that only pass with no prescreening of the data (must have at least 2 V observations), 110 refers to stars that pass with prescreening of the data but no additional error (must have at least 4 V observations), and 111 refer to stars that pass with prescreening and additional error (must have at least 4 V observations). The second number in the array corresponds to whether the object is close to a bright star (value equal to 1) or not (value equal to 0). The third number in the array is simply V_COMB as contained in the .NML database. Finally, the fourth number in the array corresponds to whether the luminosity data of the object is anti-correlated with the luminosity data of it's nearest variable neighbor (value equal to 1) or not (value equal to 0).

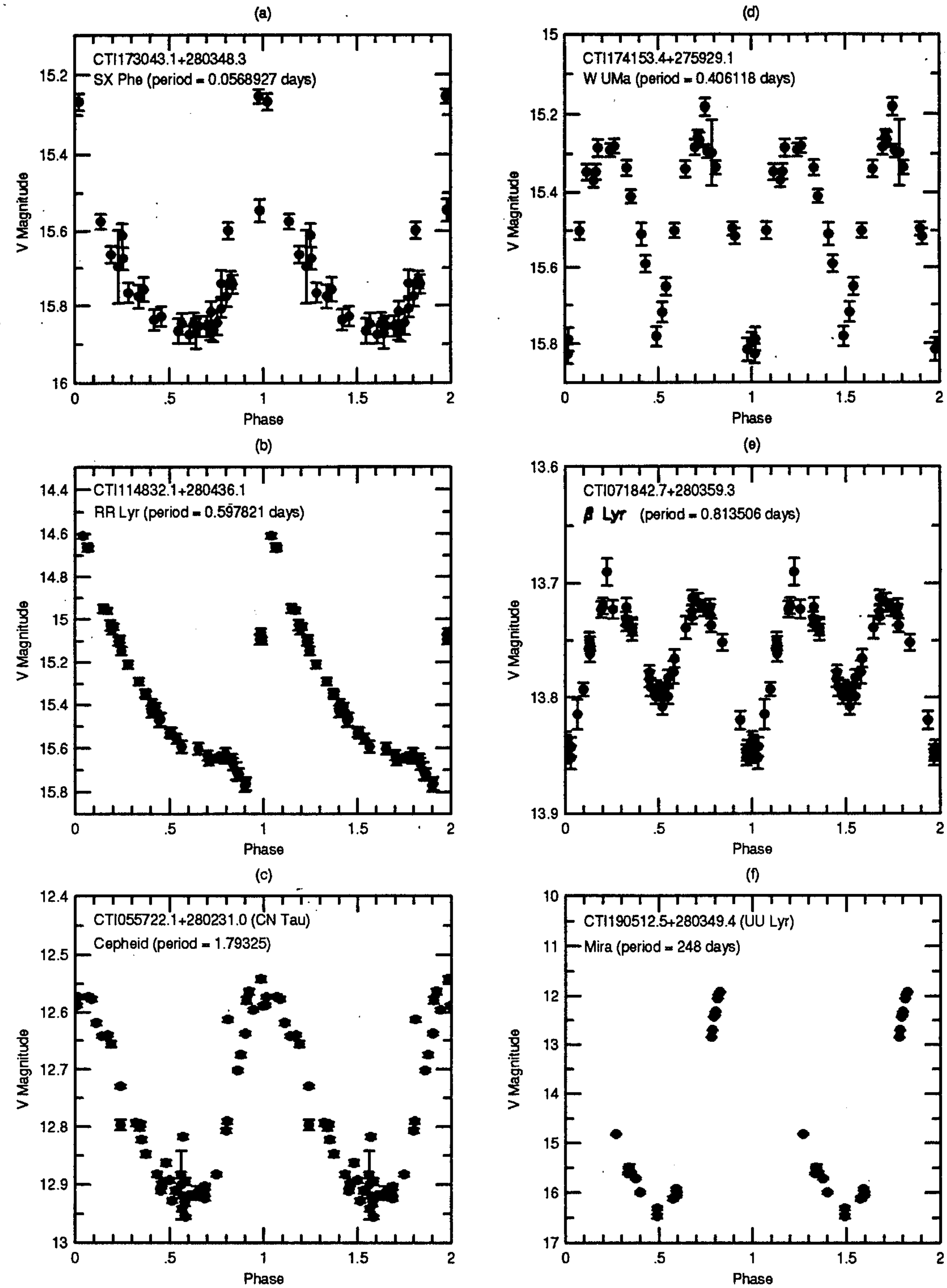


Figure 4.9 - Light curves of different types of variable stars found in CTI survey. Periods for (a) - (c) determined using additional observations at Capilla Peak (not shown). Periods for (d) and (e) potentially aliased. Period for (f) from GCVS.

The CTI survey can provide samples of many different types of variable stars (see Figure 4.9). An index created using the **.VNX** database is just the starting point in discovering examples of a particular type of variable star. In addition to V_COMB, the size and shape information in the **.NML** database can be used to eliminate or select galaxies. The **.NHL** databases can be used to find periodicity, calculate colors, and ultimately classify stars as a particular type of variable. The completeness of a given sample can then be estimated using information provided in this chapter and details concerning the limits used in the search. This is done for RR Lyrae type variable stars in the next chapter.

## Chapter 5  RR Lyrae Variable Stars in CTI Survey

This chapter describes the search for and identification of RR Lyrae variable stars contained in the CTI survey. First, a short history of the study of RR Lyraes is presented. Next, a description of the search for RR Lyraes through the CTI survey databases is given with a discussion of the completeness of the resulting RR Lyrae variable star list. Confirmation and alias-breaking observations at Capilla Peak observatory of the RR Lyrae variable star candidates are also described. Finally, the characteristics of the resulting list of RR Lyrae variable stars is compared to those contained in other surveys of field RR Lyrae variables.

## 5.1 RR Lyrae Variable Stars

In 1895, Bailey discovered several short period Cepheid-like variables in the globular cluster ω Cen (Tsesevich 1975). He divided the variables into three subclasses corresponding to differences primarily in the rise time from minimum to maximum light as compared to the total period. The subclasses also showed differences, however, in their amplitude of variation and period of variation. These variable stars were found to be common in globular clusters, occupying the intersection of the horizontal branch and the instability strip of the H-R diagram.

It was soon discovered that these "cluster Cepheids" were not limited to globular clusters. In 1899, Fleming discovered a star in the constellation Lyra that exhibited the same characteristics as the cluster Cepheids but was unassociated with a cluster. This star was designated RR Lyrae, with this name eventually referring to all stars of this type.

Horizontal branch stars are highly evolved Population II stars, having already passed through their giant phase, and are burning helium in their core (Mihalas and Binney 1981). These stars have masses less than half the solar mass and radii 4-5 times greater than the Sun. RR Lyrae stars also reside in the instability strip of the H-R diagram, as do classical Cepheids, W Virginis, δ Scuti, and SX Phoenices type variable stars (see Figure 4.1). Gravity and pressure provide the counteracting forces for radial oscillations. The

resulting oscillations would be damped and disappear, however, if it were not for a driving mechanism. The second ionization layer of helium for stars within this region of the H-R diagram is at the correct depth such that changes in temperature of this layer changes the opacity in such a way as to drive the radial oscillations. Specifically, when $He^+$ first begins to ionize, its opacity increases with increasing temperature. When the star contracts and the temperature increases, the opacity increases. The $He^+ \rightarrow He^{++}$ layer traps radiation, building up a reservoir of extra thermal energy. The radiative pressure outward slows the contraction and eventually reverses it. As the star expands, the extra energy stored in the thermal reservoir is released, accelerating the gas to a higher velocity than would have been realized without the trapped energy. The expansion overshoots the equilibrium radius of the star. The opacity of the layer decreases as the temperature decreases, and at maximum expansion, the radiative pressure is not enough to support the star. The star begins to contract once more. For hotter stars, the ionization layer is too far out in the star's atmosphere, and for cooler stars, the ionization layer is too deep within the star for the oscillations to be sustained.

The resulting light curves range from a rapid increase to maximum light followed by a slower decline (RRa type) to a nearly sinusoidal light curve (RRc type), as shown in Figure 5.1. Bailey types a and b (commonly lumped together as type

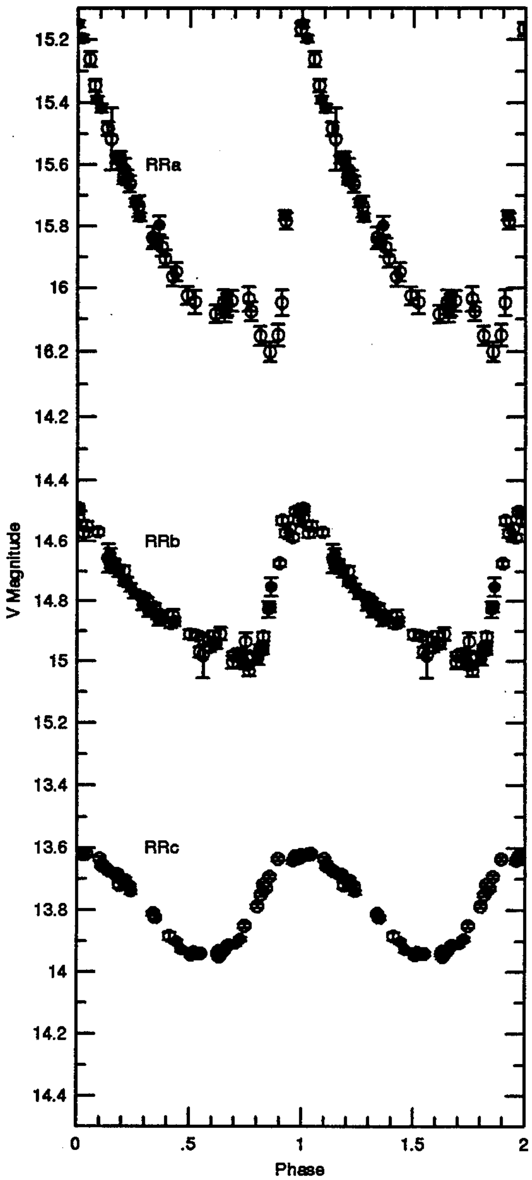


Figure 5.1 - RR Lyrae variable star light curves (combined CTI and Capilla Peak data).

ab) correspond to stars oscillating in the fundamental mode, while Bailey type c correspond to stars oscillating in the first harmonic. The mode of oscillation a star will attain depends on the depth of the $He^{+}$ layer in the star. Some RR Lyrae variable stars oscillate in both modes simultaneously, resulting in what is known as the Blazhko effect where the light curve shape and amplitude vary periodically (Tsesevich 1975). Approximately 15 - 30% of all RR Lyrae variables exhibit the Blazhko effect to some degree, with the fraction increasing for stars with decreasing metal abundance. Additionally, some RR Lyrae variable stars exhibit gradual or sudden period changes probably due to evolution. When very short period (< 0.1 days) Cepheid-like variables were discovered, they were originally designated as RRs type

variables. These variables have since been renamed δ Scuti or SX Phoenices type stars (depending on the star's Population type) although the RRs reference still shows up in the literature.

The radial velocity curve of an RR Lyrae variable star has a shape similar to the light curve (positive velocity corresponding to expansion). Maximum light occurs when the expansion velocity is maximum. The hydrogen absorption lines observed in the spectra occur higher in the star's atmosphere where higher radial velocities are observed resulting in a larger amplitude of variation than the metal lines. In addition, hydrogen line emission and line splitting can occur during the ascending part of the light curve when a shock is produced as the old contracting hydrogen layer meets a new expanding layer. Maximum light also corresponds to the time when the star exhibits its earliest spectral type (about A2). The RR Lyrae star's latest spectral type (about F2) occurs at minimum light. The maximum radius of the star occurs after maximum light, during the descending part of the light curve, while minimum radius is obtained during the ascending part of the light curve.

RR Lyrae variable stars exhibit a relationship similar to the famous period-luminosity relationship of classical Cepheids. The RR Lyrae relationship takes many forms, from a simple constant absolute magnitude (Hawley et al. 1986, Barnes and Hawley 1986, Layden et al. 1994), to a dependence on

metallicity (Carney et al. 1992), to a more complex period-luminosity-amplitude relationship (Sandage 1981a, 1981b, 1982a, 1982b, Sandage et al. 1981) or period-luminosity-metallicity relationship (Nemec et al. 1994). Using these relationships, RR Lyrae variable stars have been used extensively as standard candles to determine the distance to globular clusters as well as probe the mass distribution of the galactic halo (see Chapters 6 and 7). With the improvement of imaging technology, RR Lyraes have now been observed in nearby galaxies and can be used as yet another yardstick of extragalactic distances (see, for instance, Saha 1990). Due to advances in theoretical modeling of stellar evolution tracks, RR Lyrae variable stars can also now be used to help determine the age of globular clusters (Carney et al. 1992, Lee 1992 and references therein) and help answer questions regarding the formation of the Galaxy.

## 5.2 Search for RR Lyrae Variable Stars

After prescreening the data for photometric outliers and application of an additional error of amplitude 2% times the luminosity, all objects passing the variability test were considered. Additionally, objects near bright stars, with light curves correlated with their nearest variable neighbor, within the Galactic plane (defined below), with average V magnitudes > 18.5, or with less than 9 V observations were removed. Finally, only objects with V_COMB ≤ 20 (related to blending with other objects) were retained. A combined B and V history list (**.BVH** database) was created for these variables, and conditions were placed on various attributes of each object to discover the RR Lyrae variable stars contained in the list.

The first such condition was on average color. RR Lyrae variable stars are of spectral type A2-F2, with $\langle B \rangle - \langle V \rangle \approx 0.26$ for RRab type stars (Hawley et al. 1986). The reddest an RRab type star will appear, however, is at minimum light, and can be calculated using (McDonald 1977)

$$B_{\mathrm{min}} - V_{\mathrm{min}} = 0.40 + 0.25 \times (P - 0.5) \qquad (5.1)$$

This gives a maximum B-V of approximately 0.5 for RRab type stars. Due to the limited number of B observations, it is possible that many of the RR Lyraes were observed at or near minimum light, and thus this upper limit must be used. RRc type variables are bluer than RRab types, so this color limit will apply to them as well.

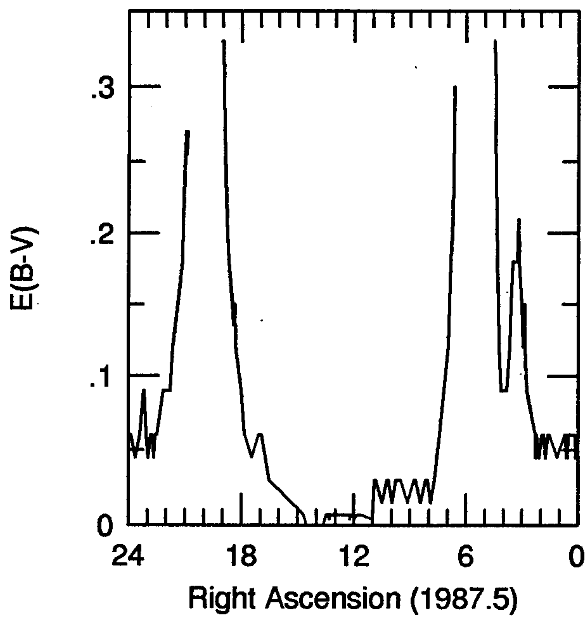


Figure 5.2 - E(B-V) versus right ascension for CTI survey strip.

Because of reddening by dust in the Galactic disk, the <B-V> of each star must first be corrected using the Galactic HI maps of Burstein and Heiles (1982). The E(B-V) as determined from these maps as a function of right ascension on the CTI survey strip is shown in Figure 5.2. No reddening information is given for galactic latitudes less than 10°. The Galactic plane, corresponding to the region excluded from this search, was defined as the region where E(B-V) > 0.24 (right ascensions $4.4^h$ to $6.7^h$ and $18.8^h$ to $21.1^h$). The resulting RR Lyrae survey area is shown in Figure 5.3. The declination boundaries are determined by the requirement that the star have 9 or more V observations and at least one B observation. The search for RR Lyrae variable stars was conducted using two different compilations of the CTI databases: the current **.MAS** and **.HIS** databases (hereafter, referred to as list 1, with boundaries shown as solid lines in Figure 5.3), and the recently compiled **.NML** and **.NHL** databases (list 2, dashed lines in Figure 5.3). Due to bright star masking, the percentage coverage as a function of right ascension varies. This percentage, smoothed to intervals of

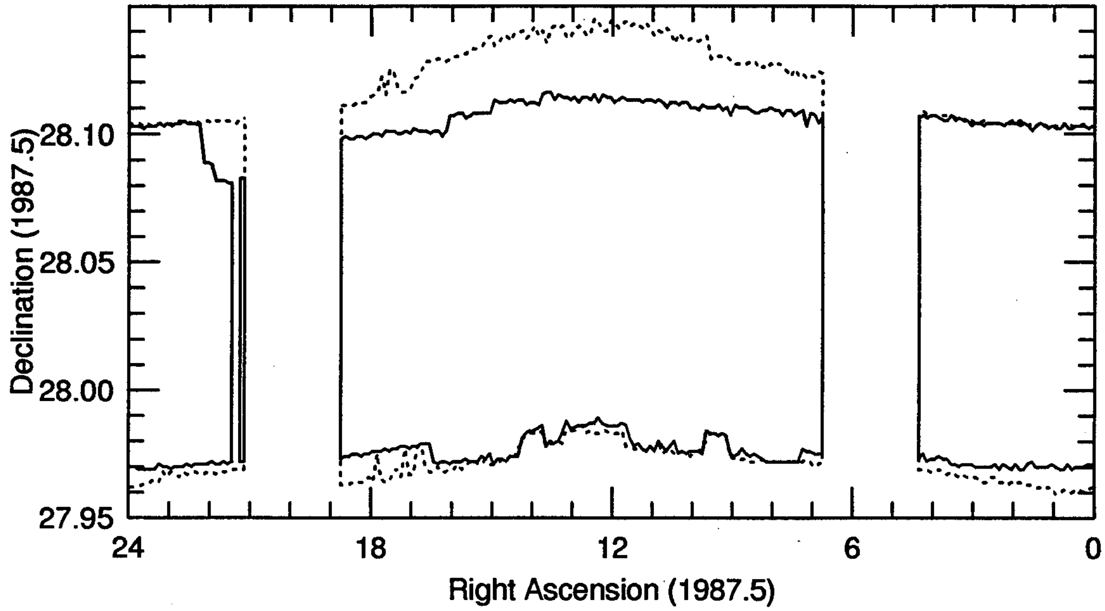


Figure 5.3 - CTI RR Lyrae survey area. Solid line for list 1 and dashed line for list 2.

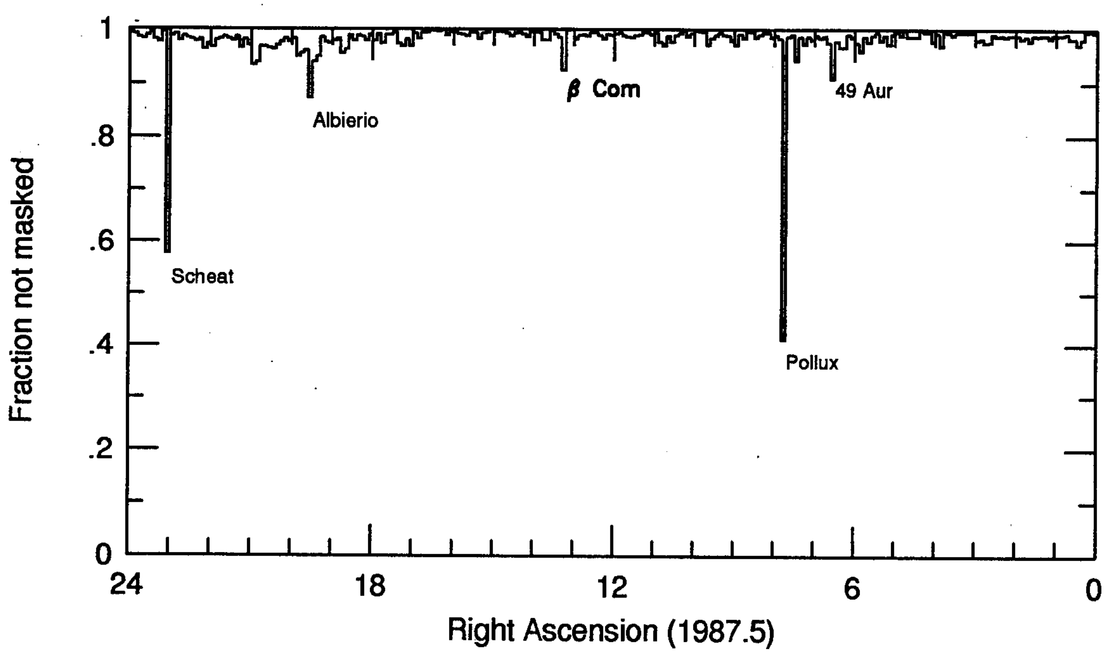


Figure 5.4 - Fraction of survey area masked by bright stars as a function of right ascension. Smoothed to 6m intervals. Five stars masking the greatest area are labeled.

$6^m$ in right ascension, is shown in Figure 5.4.

Next, a limit on the amplitude of variation was set. Several searches were conducted. For both lists, the first search used a color limit of $\langle B-V \rangle < 0.6$ and an amplitude limit of $\Delta V > 0.2$. A total of 5 variables listed as RR Lyrae variable stars in the GCVS have amplitudes less than 0.2, corresponding to less than 0.08%, and these stars are probably misclassified anyway. Due to possible systematic errors created by the flat field (see Chapter 3.2) of up to 0.2 magnitudes for the B magnitude, another search using a limit of $\langle B-V \rangle < 0.7$ and an amplitude limit of $\Delta V > 0.6$ was made. No new confirmed RR Lyrae type stars were found with this search using both list 1 and list 2. A final search, only conducted on list 1, used a color limit of $\langle B-V \rangle < 0.8$ and an amplitude limit of $\Delta V > 0.2$. Again, no new confirmed RR Lyrae type stars were found.

The best period for each object passing the above criteria within the range of 0.2 to 1.2 days was determined using a standard period finding algorithm (see Lafler and Kinman 1965 or Stellingwerf 1978) and the light curve shape was examined. This period range ensures that for an RR Lyrae variable star, the best period found corresponds to the actual period or an alias to the actual period. Objects with sinusoidal (RRc) to sawtooth (RRab) light curves were included in the final candidate list.

The sidereal day alias inherent to the CTI data has

several unfortunate consequences pertaining to period selection and light curve shape. Noisy RRab-like light curves with periods close to 1/2 or 1/3 a sidereal day can be created for many variables. This occurs for most "long period" variables displaying systematic shifts in their mean magnitude from one year to the next. The source of this group of variables is unknown, although it's possible they're spurious and related to the photometry of galaxies (see Chapter 4.2.1). Another group of variables with bimodal magnitude distributions will often produce noisy RRc-like light curves at fractional sidereal day periods. Again, the nature of these variables is unknown and it's possible they are also spurious. Considering the fact it is unlikely a large population of RR Lyrae variable stars exist at these specific fractional sidereal day periods, noisy RR Lyrae-like light curves with these periods were not selected duing the search for candidates. Another problem related to the sidereal day alias in the CTI data occurs for variables with only a few V observations. These variables display a multitude of periods and a wide range of light curve shapes can be found. This problem becomes so severe that for variables with less than ≈9 observations, a period search yields no useful information relative to classification by light curve shape.

The resulting final RR Lyrae candidate lists contain 52 objects each (list1 and list2), with 39 candidates in common. Thirteen candidates in list 1 were not in list 2. Seven of

these are W UMa type variables rejected due to the improved phase coverage offered by the additional observations contained in the **.NHL** database, four of these are non-RR Lyrae type variables not contained in list 2 due to color considerations, and two are RR Lyrae type variables whose light curves degraded with the additional observations, possibly due to a changing period or the Blazhko effect. Thirteen candidates in list 2 were not in list 1, all of which either had poor phase coverage or were near the edge of the CTI survey area and had less than 9 V observations in the **.HIS** database. Eight of these are confirmed RR Lyrae variable stars, three are possible RR Lyrae variable stars, and two are probable W UMa variable stars.

Six of the final candidates are previously known RR Lyrae variable stars listed in the GCVS (GR Com, GS Com, DV Com, EZ Com, V385 Her and V532 Her). All previously known RR Lyrae variable stars within the RR Lyrae search area were found. Another previously known variable star (V375 Her), classified as a semiregular type variable star in the GCVS, is also on both final candidate lists. In addition to those candidates found in the above searches, four other previously known variable stars outside the RR Lyrae search area but within the CTI survey strip were included in the final combined RR Lyrae candidate list for a total of 69 objects. CN Tau, V427 Lyr and V926 Cyg are designated as RR Lyrae stars in the GCVS, and GS Lyr is listed as an irregular variable in the GCVS, but has

an RR Lyrae shape light curve for a particular period using the data contained in the **.HIS** database. Table 5.1 lists each object's right ascension, declination, number of B and V observations (from list 2), E(B-V) as determined from Burstein and Heiles (1982), average B-V as initially determined from CTI data (from list 2), master list number for list 1 (**.MAS** database) and list 2 (**.NML** database), and variable type as determined from subsequent observations at Capilla Peak observatory (see Chapter 5.4). The list 1 and 2 mlink columns also indicate whether or not the star was found during that particular search. Table 5.2 identifies all previously known variable stars.

## Table 5.1 - RR Lyrae final candidate list

| # | RA (1987.5 epoch) | Dec | # B | # V | E(B-V) | <B-V> | list 1 mlink | list 2 mlink | Type |
|---|---|---|---|---|---|---|---|---|---|
| 1 | 00 21 01.3 | 28 05 18.0 | 8 | 39 | 0.060 | 0.672 | 1770* | 1770 | W UMa |
| 2 | 01 13 58.1 | 28 02 47.1 | 8 | 46 | 0.049 | 0.519 | 5890* | 5890* | W UMa |
| 3 | 01 26 59.2 | 28 03 54.3 | 7 | 44 | 0.057 | 0.835 | 6829+ | 6829 | W UMa |
| 4 | 01 58 55.9 | 27 58 09.5 | 5 | 48 | 0.055 | 0.466 | 9134 | 9134* | RRab |
| 5 | 02 01 50.4 | 28 04 22.6 | 7 | 46 | 0.050 | 0.260 | 9353* | 9353* | RRab(B) |
| 6 | 02 31 40.3 | 27 59 47.3 | 9 | 45 | 0.076 | 0.789 | 11615+ | 11615 | W UMa |
| 7 | 03 46 21.7 | 28 01 24.7 | 6 | 46 | 0.101 | -0.226 | 18722 | 18722* | RRab |
| 8 | 04 02 57.9 | 28 01 30.5 | 7 | 46 | 0.090 | 0.607 | 21446* | 21446 | W UMa |
| 9 | 05 57 22.1 | 28 02 31.0 | 7 | 50 | INDEF | 0.879 | 48925 | 48925 | Cδs |
| 10 | 06 49 46.1 | 28 04 59.5 | 6 | 54 | 0.181 | 0.862 | 105847* | 112136 | W UMa |
| 11 | 07 53 50.3 | 28 01 58.2 | 7 | 49 | 0.016 | 0.385 | 117092* | 122309* | RRab |
| 12 | 08 46 51.7 | 28 02 45.3 | 8 | 45 | 0.030 | 0.299 | 122995* | 130077* | RRab(B) |
| 13 | 09 01 17.7 | 28 01 31.3 | 9 | 45 | 0.020 | 0.261 | 140537* | 143625* | RRab(B) |
| 14 | 09 56 59.1 | 28 02 02.6 | 8 | 49 | 0.016 | 0.126 | 152725* | 164491* | RRc |
| 15 | 10 26 04.7 | 28 02 51.5 | 8 | 44 | 0.018 | 0.290 | 153914* | 165680* | RRab |
| 16 | 10 36 17.2 | 27 59 07.7 | 3 | 14 | 0.020 | 0.211 | 154337* | 166103* | RRab |
| 17 | 10 57 41.6 | 28 02 46.0 | 7 | 48 | 0.012 | 0.165 | 155137* | 166905* | RRc |
| 18 | 11 48 32.1 | 28 04 36.1 | 8 | 45 | 0.007 | 0.318 | 163979* | 174580* | RRab |
| 19 | 12 04 40.4 | 28 01 08.5 | 9 | 48 | 0.007 | 0.244 | 164643* | 175244* | RRab |
| 20 | 12 05 25.4 | 28 03 28.8 | 9 | 47 | 0.007 | 0.340 | 164674 | 175275* | RRab |
| 21 | 12 24 18.6 | 28 03 17.4 | 9 | 50 | 0.007 | 0.382 | 165395* | 175996* | RRab |
| 22 | 12 43 17.6 | 28 05 21.7 | 9 | 45 | 0.007 | 0.372 | 166086* | 176687* | RRab |
| 23 | 13 14 03.3 | 28 00 26.7 | 7 | 35 | 0.007 | 0.105 | 167332* | 177933* | RRc |
| 24 | 13 17 32.5 | 28 01 39.4 | 9 | 45 | 0.007 | 0.299 | 167472* | 178073* | RRab |
| 25 | 13 23 46.7 | 28 06 32.5 | 7 | 37 | 0.007 | 0.708 | 167695+ | 178296 | Galaxy |
| 26 | 14 33 13.2 | 28 01 17.0 | 8 | 49 | 0.014 | 0.174 | 178400* | 194872* | RRab |
| 27 | 14 54 39.0 | 28 05 32.8 | 10 | 51 | 0.010 | 0.354 | 179503* | 195975* | RRab |
| 28 | 15 16 28.1 | 28 00 41.6 | 6 | 47 | 0.014 | 0.137 | 187650 | 203872* | RRab |
| 29 | 16 23 17.6 | 27 58 28.9 | 3 | 13 | 0.028 | 0.568 | 196711 | 212616* | W UMa |
| 30 | 16 50 08.8 | 27 59 55.0 | 6 | 29 | 0.053 | 0.346 | 203356* | 221010* | RRab |
| 31 | 16 58 30.7 | 28 06 00.7 | 6 | 20 | 0.060 | 0.297 | 204123 | 221777* | RRc? |
| 32 | 17 13 10.9 | 28 00 10.3 | 6 | 27 | 0.055 | 0.388 | 205617* | 223271* | RRab |
| 33 | 17 15 23.9 | 28 00 43.0 | 6 | 27 | 0.053 | 0.234 | 205868* | 223522* | RRab |
| 34 | 17 15 57.0 | 28 06 44.6 | 3 | 15 | 0.053 | 0.609 | 433757 | 556381* | RRab |
| 35 | 17 19 06.6 | 28 06 28.2 | 3 | 17 | 0.051 | 0.645 | 433799 | 556429* | RRab? |
| 36 | 17 20 58.6 | 28 01 15.2 | 8 | 27 | 0.049 | 0.141 | 206532* | 224186* | RRc |
| 37 | 17 30 43.1 | 28 03 48.3 | 8 | 30 | 0.047 | 0.268 | 207769* | 225423* | SX Phe |
| 38 | 17 41 51.5 | 28 03 53.2 | 7 | 30 | 0.055 | 0.311 | 209299* | 226953* | RRab |
| 39 | 17 42 40.2 | 28 04 44.7 | 7 | 30 | 0.055 | 0.275 | 209407* | 227060* | RRab |
| 40 | 17 44 19.7 | 28 01 21.6 | 7 | 30 | 0.056 | 0.266 | 209648* | 227302 | RRc? |
| 41 | 17 50 17.0 | 28 01 00.0 | 7 | 25 | 0.061 | 0.412 | 216980* | 234109* | W UMa |
| 42 | 18 11 01.2 | 27 59 27.4 | 6 | 26 | 0.108 | 0.374 | 221799* | 238926* | RRab |
| 43 | 18 11 26.7 | 28 03 45.4 | 8 | 25 | 0.109 | 0.436 | 221928* | 239057* | RRab |
| 44 | 18 36 06.3 | 28 03 21.6 | 7 | 25 | 0.170 | 0.416 | 229745* | 246872* | RRab |
| 45 | 18 39 18.3 | 28 04 16.6 | 7 | 25 | 0.178 | 0.453 | 230978* | 248106* | RRab |
| 46 | 18 40 18.8 | 28 00 54.1 | 8 | 25 | 0.181 | 0.571 | 231410+ | 248537 | W UMa |
| 47 | 18 43 15.3 | 28 01 14.7 | 8 | 24 | 0.196 | 0.644 | 232642 | 249768* | W UMa? |
| 48 | 18 44 20.6 | 27 59 36.6 | 6 | 24 | 0.202 | 0.549 | 233103+ | 250230* | W UMa? |
| 49 | 18 47 46.9 | 28 04 47.0 | 4 | 24 | 0.223 | 0.556 | 234619* | 251747* | RRab(B) |
| 50 | 19 03 50.4 | 28 00 44.9 | 7 | 23 | INDEF | 1.757 | 252097 | 269174 | L |
| 51 | 19 13 11.8 | 28 00 51.5 | 6 | 24 | INDEF | 0.733 | 259179 | 276256 | RRab |
| 52 | 19 38 06.6 | 27 59 09.9 | 7 | 25 | INDEF | 0.653 | 318729 | 336159 | RRc |
| 53 | 21 07 16.1 | 28 02 29.2 | 6 | 19 | 0.206 | 0.531 | 385417* | 415882 | W UMa |
| 54 | 21 20 11.2 | 28 06 09.3 | 2 | 13 | 0.154 | 0.611 | 505079 | 477321* | RRc? |
| 55 | 21 21 10.2 | 28 05 56.5 | 2 | 13 | 0.152 | 0.176 | 468466 | 477369* | RRc |
| 56 | 21 34 29.8 | 28 01 56.9 | 5 | 18 | 0.127 | 0.687 | 403397* | 431575 | W UMa |
| 57 | 21 46 11.6 | 28 00 57.2 | 4 | 20 | 0.093 | 0.382 | 405697* | 433874* | RRab |

**Table 5.1 - RR Lyrae final candidate list (continued)**

| # | RA (1987.5 epoch) | Dec | # B | # V | E(B-V) | <B-V> | list 1 mlink | list 2 mlink | Type |
|---|---|---|---|---|---|---|---|---|---|
| 58 | 21 57 35.4 | 28 02 37.5 | 3 | 20 | 0.090 | 0.472 | 407892* | 436069* | RRab |
| 59 | 21 58 55.9 | 27 58 09.5 | 5 | 20 | 0.090 | 0.240 | 407995 | 436173* | RRab |
| 60 | 22 00 54.8 | 28 00 20.1 | 5 | 21 | 0.090 | 0.471 | 408475* | 436652* | RRab |
| 61 | 22 02 44.8 | 27 59 04.0 | 5 | 21 | 0.090 | 0.888 | 408775+ | 436953 | W UMa |
| 62 | 22 10 22.8 | 28 04 16.2 | 3 | 20 | 0.088 | 0.314 | 410030 | 438208* | RRab B |
| 63 | 22 20 36.4 | 27 59 39.2 | 5 | 23 | 0.072 | 0.478 | 60633* | 60635* | W UMa |
| 64 | 22 36 18.9 | 27 58 38.4 | 5 | 24 | 0.056 | 0.526 | 63071* | 63069 | RRab |
| 65 | 22 47 34.7 | 28 01 20.8 | 6 | 24 | 0.060 | 0.504 | 64566* | 64569* | W UMa |
| 66 | 23 05 19.7 | 28 05 44.1 | 3 | 21 | 0.068 | 0.206 | 67062* | 66402* | RRab |
| 67 | 23 21 38.0 | 28 01 25.6 | 2 | 21 | 0.063 | 0.535 | 68710* | 68049 | W UMa |
| 68 | 23 32 06.7 | 28 02 10.9 | 5 | 37 | 0.051 | 0.477 | 80409* | 89389* | RRab |
| 69 | 23 52 26.0 | 28 01 18.9 | 7 | 40 | 0.060 | 0.447 | 82132* | 91112* | RRab |

Notes to Table 5.1
In list 1 and list 2 mlink column:
* = discovered in RR Lyrae search
+ = discovered in extended color (<B-V> < 0.8) RR Lyrae search of list 1
In Type column:
RRab - type ab RR Lyrae
RRc - type c RR Lyrae
RRab(B) - type ab RR Lyrae exhibiting Blazhko effect
SX Phe - SX Phoenices type variable star
C$\delta$s - short period classical Cepheid
W UMa - W Ursa Majoris
L - Irregular

**Table 5.2 - GCVS name for stars in RR Lyrae candidate list**

| # | GCVS name |
|---|---|
| 9 | CN Tau |
| 19 | GR Com |
| 21 | GS Com |
| 22 | DV Com |
| 24 | EZ Com |
| 27 | NSV 06854* |
| 32 | V375 Her |
| 34 | V385 Her |
| 43 | V532 Her |
| 50 | GS Lyr |
| 51 | V427 Lyr |
| 52 | V926 Cyg |

Notes to Table 5.2
* - from New Catalogue of Suspected Variable Stars (Kukarkin et al. 1982)

## 5.3 - Completeness

In estimating the completeness of the resulting RR Lyrae variable star list, each step in the search must be examined to determine how it affects the discovery of RR Lyraes. The final result will be estimated functions for completeness versus position and completeness versus magnitude.

During the initial testing for variability, stars with poor phase coverage due to having a small number of observations and a period close to 1/2 or 1/3 a sidereal day may not even pass the variability test. More likely, however, is that the resulting light curve for the star will not be recognized as an RR Lyrae during the final selection. The completeness as a function of position was estimated by first calculating the detectable fraction of variable stars as a function of period. Typical observation times were used to calculate the phase ($\phi$) of all observations for all periods (0.0005 day bins) cycled through all initial phases. If at least two observations fell during maximum light ($\phi$ = 0.0 - 0.2), at least two observations during the descending part of the light curve ($\phi$ = 0.2 - 0.5), at least two observations at minimum light ($\phi$ = 0.5 - 0.9), and at least one more observation during minimum or the ascending part of the light curve ($\phi$ = 0.5 - 1.0), it was considered detectable. This ensures a well distributed sample in phase and requires that the full amplitude of the variable is observed. Figure 5.5 plots the resulting detectable fraction of RR Lyraes as a

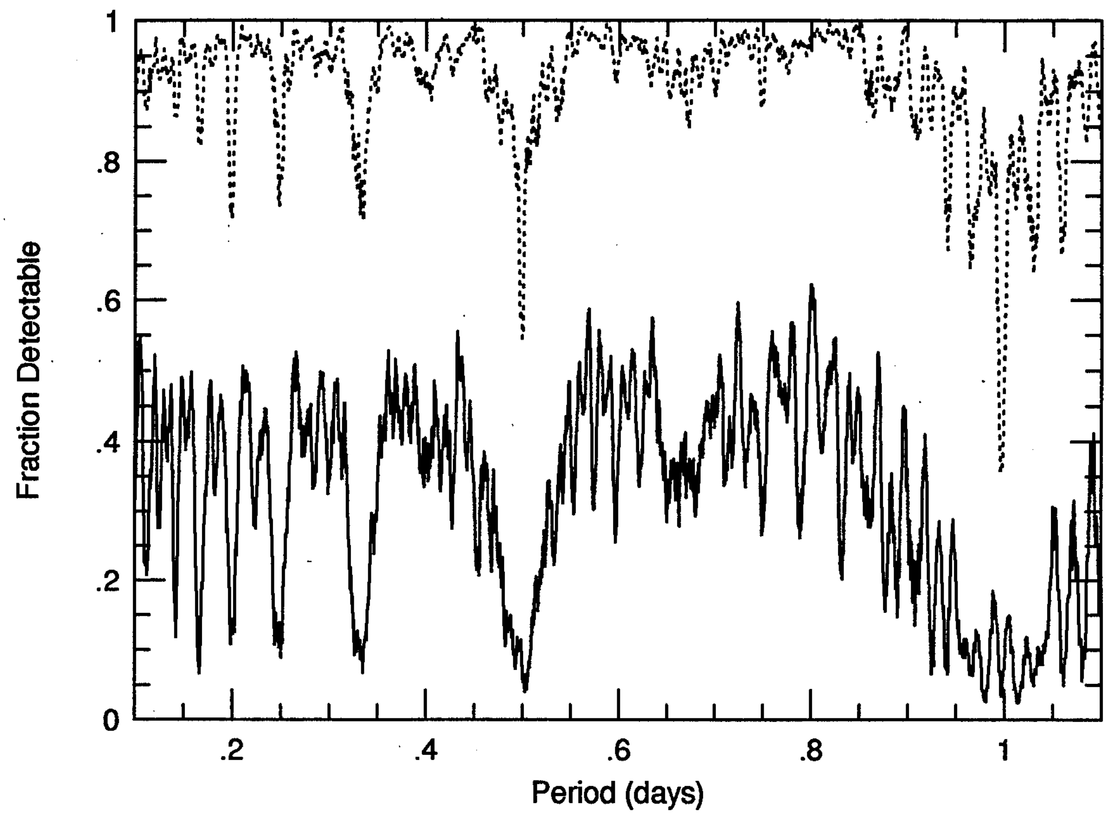


Figure 5.5 - Detectable fraction of RR Lyrae variable stars versus period for 9 observations (solid line) and 20 observations (dashed line). Original bins 0.0005 days, smoothed to 0.005 days.

function of period for 9 and 20 V observations. For RRab type variables, the average percentage in the interval from 0.4 to 0.7 days was then calculated for a number of cases with the number of V observations ranging from 9 to 60. The resulting detectable percentage as a function of the number of V observations is shown in Figure 5.6. The same calculation for RRc type variables with periods ranging from 0.25 to 0.4 days yields an almost identical curve. Using the information from Figure 5.6, as well as the maximum number of V observations as

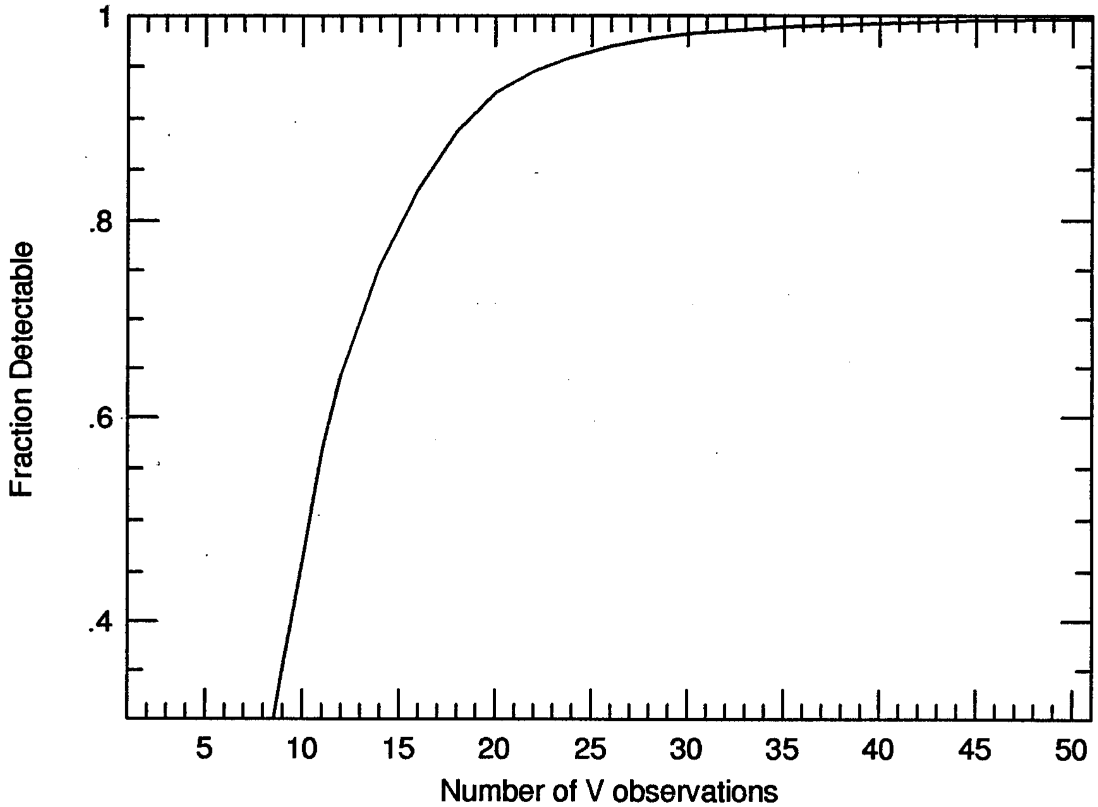


Figure 5.6 - Detectable fraction of RR Lyrae variable stars as a function of the number of V observations.

a function of right ascension (see Figure 3.7) and the number of objects as a function of the number of V observations and right ascension (see, for example, Figure 4.4), the completeness of the CTI RR Lyrae Survey as a function of position was calculated and is shown in Figure 5.7. The solid and dashed lines represent the completeness of list 1 and list 2 respectively.

The completeness as a function of magnitude was calculated considering the fact that the amplitude of variability needs to be four times the average error for a

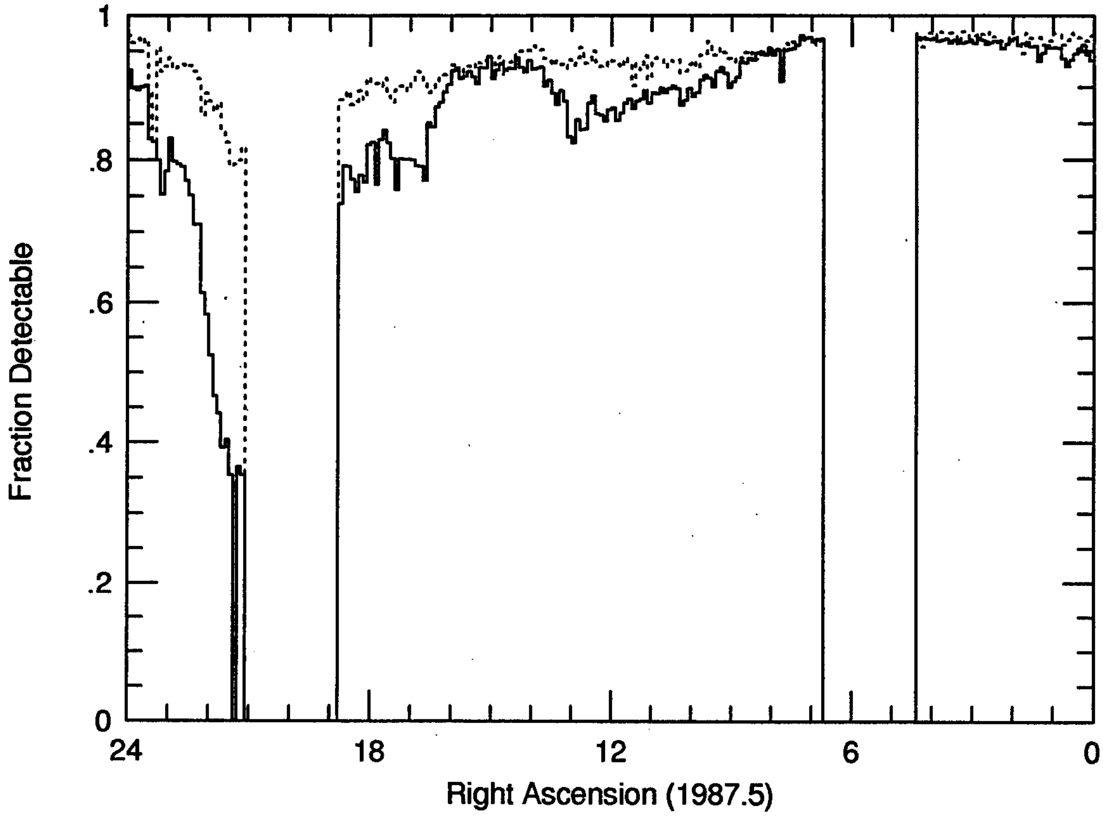


Figure 5.7 - Detectable fraction of RR Lyrae variables as a function of right ascension for list 1 (solid line) and list 2 (dashed line).

positive detection (see Chapter 4.2.2). This can be accomplished by using the information from the plot of average error versus mean instrumental magnitude (Figure 4.6), and knowing the distribution of RR Lyrae stars as a function of amplitude. The Palomar-Groningen Variable Star survey provides a large homogeneous sample of RR Lyrae variable stars to estimate this last function.

It was first necessary to convert each star's amplitude in B ($\Delta$B) as listed in the Palomar-Groningen survey to a corresponding amplitude in V ($\Delta$V) to compare to the CTI RR

Lyrae survey. For RRab type stars, this was done by combining Equation 5.1 ($B_{min}-V_{min}$ as a function of period where $B_{min}$ and $V_{min}$ are magnitudes at minimum light), $\langle B\rangle - \langle V\rangle \approx 0.26$ (Hawley et al. 1986), and the empirical equation (from Barnes and Hawley 1986)

$$\langle V\rangle = V_{min} - 0.375\times\Delta V - 0.04. \quad (5.2)$$

Using these equations, and assuming a similar relation for $\langle B\rangle$ as in Equation 5.2, the color at maximum light can be calculated using

$$B_{max} - V_{max} = 0.03 - 0.42\times(P-0.5), \quad (5.3)$$

and the amplitude in V can be calculated using

$$\Delta V = \Delta B - 0.37 - 0.67\times(P-0.5). \quad (5.4)$$

For RRc type variable stars, the V and B observations of RRc type variable stars in the CTI survey were examined yielding the relationship, $\Delta V \approx \Delta B - 0.115$.

The resulting histogram of V amplitude for RR Lyrae stars in the Palomar-Groningen Variable Star survey is shown in Figure 5.8. The distribution of RRab and RRc type variables are shown with a solid and dashed line respectively. The completeness as a function of average instrumental V magnitude is shown in Figure 5.9 for RRab (solid line) and RRc (dashed line) type variable stars in the CTI RR Lyrae survey.

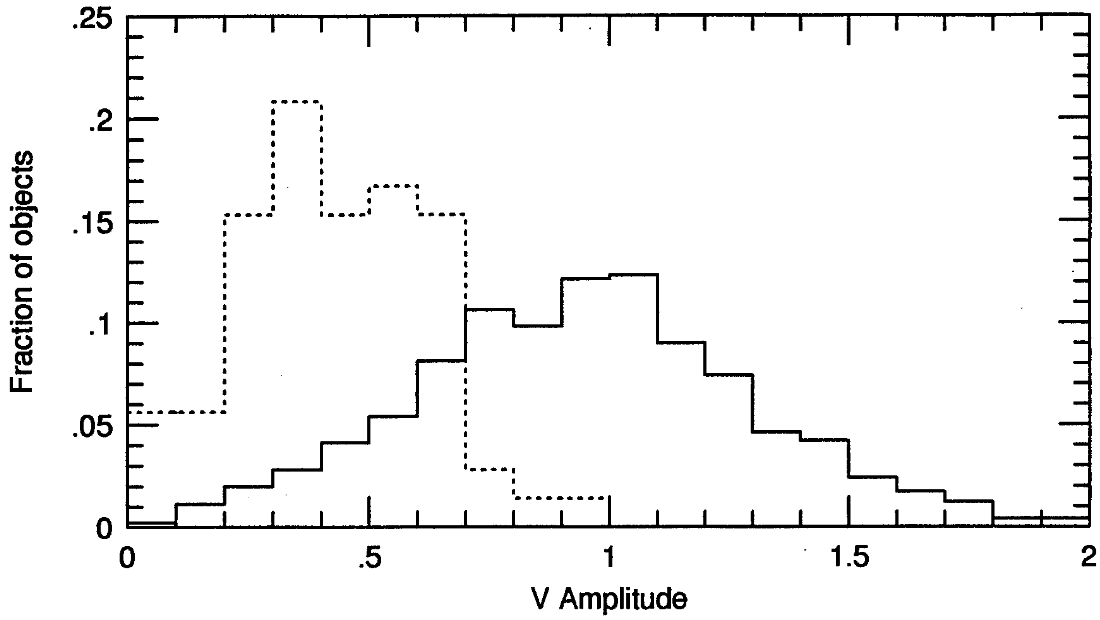


Figure 5.8 - Percentage of RR Lyrae variable stars in Palomar-Groningen Variable Star survey (regions 1, 2, and 3) as a function of amplitude of variation in V (using Equation 5.4). RRab type (solid line) and RRc type (dashed line).

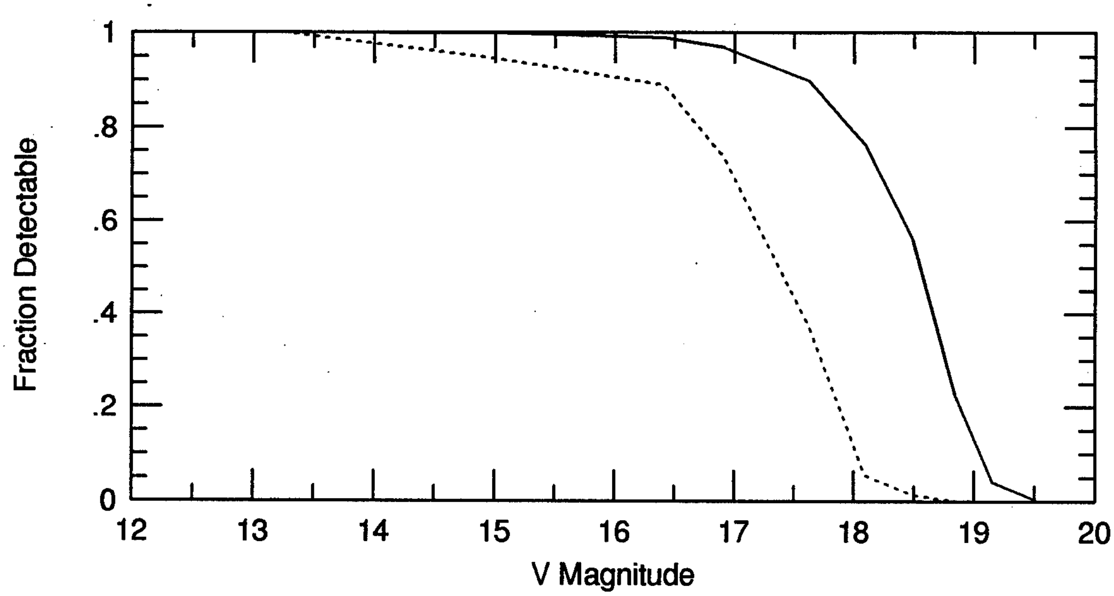


Figure 5.9 - Detectable fraction of RR Lyrae variable stars as a function of average V magnitude for RRab type variables (solid line) and RRc type variables (dashed line).

## 5.4 Alias Breaking Observations at Capilla Peak

Complementary observations of the candidate RR Lyrae stars are necessary to determine their correct pulsational period. This is due to CTI's built in frequency of observation, the sidereal day, and the fact that RR Lyrae variable star periods are typically less than a sidereal day. Thus, for each variable with a true period P, many aliased periods exist, given by

$$P_{alias}=\left|\frac{1}{\frac{1}{P}+nf_{sd}}\right| \tag{5.5}$$

where $f_{sd}$ = 1.002740 day$^{-1}$ is the sidereal day frequency and n is a positive or negative integer.

The telescope at Capilla Peak Observatory was used to make alias breaking observations. What follows is a short description of the telescope and CCD at Capilla Peak and a description of the image reduction process, which is also intended to serve as a guide to future users of Capilla Peak. Finally, the method used in combining CTI and Capilla Peak data is described.

### 5.4.1 Capilla Peak Telescope/CCD Description

Operated by the Institute for Astrophysics at the University of New Mexico, Capilla Peak is a small observatory located in the Manzano Mountains, 30 miles south of Albuquerque, New Mexico. The observatory is located at latitude 34° 41' 53" and longitude 106° 24' 13", and elevation

of 2842 meters. It is the 15th highest observatory in the world as listed in the The Astronomical Almanac for the year 1993.

Located at the observatory is a single 61-cm Boller and Chivens telescope equipped with a RCA 320 x 512 x 30 $\mu$m SID50EX CCD (Laubscher et al. 1988). With a system f/# of 15.2, the image field scale is 0.67 arcsecs/pixel which produces an image size of 3.57' x 5.72'. The CCD operates with a gain of 15.6 electrons/ADU, 14-bit digitization, and has a readout noise of 57 electrons. The current filter set includes $H_\alpha$ filters centered at 657, 665 and 673 nm, an OIII filter (manufactured by Barr Associates), polarization filters, and BVRI filters (described in Beckert and Newberry 1989). The telescope is also equipped with an additional CCD camera with a microchannel plate amplifier used for real-time guiding on off-axis stars during lengthy exposures.

The telescope operates year round as a research and instructional instrument. Published scientific papers using data collected at Capilla Peak include studies of variable stars (Zeilik et al. 1994 and references therein, Wetterer et al. 1994 and this dissertation), standard stars (Odewahn et al. 1992), brown dwarfs (Bryja and Lawrence 1991, Bryja et al. 1992), galaxies (Gregory et al. 1990, Odewahn 1991, Hayes et al. 1993, Laubscher and Gregory 1993, Taylor et al. 1995, and others), extragalactic supernova (Schmidt et al. 1993, 1994), and the SL-9 impact on Jupiter (Gisler et al. 1994).

### 5.4.2 Capilla Peak Image Reduction

CCD images obtained at Capilla Peak must go through several reduction steps before useful photometry can be done (Newberry 1991, Tyson 1990). These steps include bias subtraction, removal of the deferred charge structure, preflash subtraction (if used), dark current subtraction (if desired), division by a flat-field frame, and cosmic ray removal. Several steps require that additional CCD images be acquired at the time of observation. What follows is a discussion of each step, which includes both the observational and reduction procedures required.

Every image has a device-specific baseline level, known as the bias, created by the CCD camera's electronics. The bias level does not represent charge contained in individual pixels, but is rather a baseline voltage added to the image as the image is being read out of the CCD array. A bias frame, simply a zero second exposure, can be taken and examined at the telescope by using the *bias* command. Ideally, the bias level should be constant and uniform over the entire CCD frame. The CCD at Capilla Peak has a nearly constant bias structure, but a bias level that changes during the course of the night. The bias level has short-term fluctuations of about 8 electrons, and can have a drift greater than 90 electrons during the night. The bias structure also changes with changing bias level, primarily in the first 50 columns. These changes are probably due to changes in the ambient

temperature of the CCD camera's electronics located in the observatory dome. To accurately subtract the bias requires that the bias structure and level be tracked and recorded during observations. This can be accomplished in two ways. If the preflash is used, the bias and preflash are recorded in the same frames and can be subtracted from other images together. This will be described later. Otherwise, "superbias" frames can be made between observations to track the structure and bias level. A superbias is simply the average of several bias frames and can be made at the telescope using the *addup* command. Averaging is done in order to reduce the effect of readout noise in the final product. Two or more of these superbias frames bracketing your observations can then be used to create the final reduction bias. The bias level immediately before each image can also be recorded in the image header by using the *bobs* command at the telescope instead of *obs*. The noise added to all other images by bias subtraction is

$$RB=\sqrt{\frac{\frac{R^2}{n_b}+T^2}{n_{sb}}+BL^2} \qquad (5.6)$$

where R = 57 electrons is the readout noise, $n_b$ (typically 25) is the number of bias frames used in creating a superbias, T = 4.5 electrons is the truncation noise as determined from the gain, $n_{sb}$ (typically 2) is the number of superbias frames used in creating the final reduction bias, and BL = 8 electrons is

the empirically determined short term bias level uncertainty.

Next, the horizontal band structure created by deferred charge within the horizontal shift register must be eliminated. This is accomplished by mapping out the structure with the preflash or a low light level sky flat (approximately 100 ADUs or 1560 electrons) known as a skim flat. If the latter method is used, only a single skim flat is required and can be taken through any filter during astronomical twilight. To create the final frame used in reducing all other images, a high light level sky flat (approximately 8000 ADUs) taken through the same filter and scaled to the level of the skim flat must first be subtracted off the skim flat in order to remove the CCD's response to light. The remaining feature is simply the deferred charge structure. Exposure times for the skim flat and sky flat should either be identical or greater than 3 seconds in order to eliminate the effect of the shutter speed on the final images. To reduce noise, the skim flat is sliced into 512 one-dimensional rows, all containing the deferred charge structure. These rows are averaged column by column, and 512 of the resulting average slice are then stacked back together to create the final "superskim". The noise added to all other images by deferred charge subtraction is

$$RS=\sqrt{\frac{R^2+T^2+L_{skim}(1+RK^2\times L_{skim})+RB^2}{512}} \qquad (5.7)$$

where $L_{skim}$ is the skim flat light level in electrons, and RK

is the superskyflat error, to be discussed later. Two aspects of using a superskim frame for deferred charge subtraction should be noted. First, in order for the deferred charge structure to be accurately eliminated by using a superskim, the background sky level must be greater than the maximum deferred charge structure. Although this corresponds to about 10 ADUs, in practice the background sky level must be greater than about 50 ADUs for the superskim to work. Also, since a sky flat (containing the deferred charge structure) is used to make the superskim, a residual deferred charge structure on the order of 1% will remain. This can be remedied by creating the superskim in an iterative manner, or by using the preflash on the sky flats in order to eliminate the deferred charge structure beforehand. The deferred charge structure remains nearly constant, and thus a superskim frame from one night was typically used for several months of data.

Bias subtraction and correction of deferred charge structure can be accomplished in a single step if the preflash is used. A preflash is simply the addition of a specific number of electrons to each pixel in the CCD prior to an exposure. At Capilla Peak, the preflash consists of 6 light emitting diodes (LEDs) located inside the shutter and arranged to uniformly illuminate the CCD array. This is currently manually applied. To examine the preflash, a preflashed dark exposure can be taken at the telescope by using the *dark* command. A dark exposure is an exposure of a certain length

without opening the shutter. A 2 to 5 second exposure is necessary to accurately record the preflash. The resulting image will show the deferred charge structure superimposed on the bias and preflash structure. As with creating a superbias, several of these frames are averaged together to reduce noise. This is accomplished by taking several preflashbias frames and storing each in one of the eight different caches (using *ci* command to move between caches) of the CCD control computer memory, and then averaging them together using the *median* command. Because of bias and preflash level changes during the night, these superpreflashbias frames should be taken throughout the night to track the changes. Two or more superpreflashbiases bracketing your observations can be used later to create the final reduction preflashbias. The noise added to an object frame by preflashbias subtraction is

$$RP=\sqrt{\frac{\frac{R^2+L_{preflash}}{n_p}+T^2}{n_{sp}}+BL^2+PL^2} \tag{5.8}$$

where $L_{preflash}$ is the preflash light level (about 50 - 100 ADUs = 780 - 1560 electrons), $n_p$ (up to 7) is the number of preflashbias frames used in making the superpreflashbias, $n_{sp}$ (typically 2) is the the number of superpreflashbias frames used in making the final reduction preflashbias, and PL = 16 electrons is the empirically determined preflash level uncertainty.

The final additive term in the reduction process is the dark current of the CCD. Several dark frames as long as or longer than all other image frames must be taken. A pixel-by-pixel median of these dark frames, after bias and deferred charge subtraction, must then be taken to eliminate the effect of pixels contaminated by cosmic rays. The resulting superdark can now be scaled to the exposure length of the remaining images, and subtracted. The noise per second of observation added to all other frames by dark current subtraction is

$$SD=\frac{\sqrt{\frac{R^2+T^2+P^2}{n_d}}}{t_d} \tag{5.9}$$

where P = RP for preflashbias subtracted dark frames or P = $(RB^2 + RS^2)^{1/2}$ for bias and skim flat subtracted dark frames, $n_d$ (3 or greater) is the number of dark frames used in creating the superdark, and $t_d$ is the exposure length of the dark frames. The dark current for nearly the entire CCD is less than the bias level uncertainty and can thus not be determined accurately. The dark current is thus ignored in further calculations.

Next, the response of the CCD to light must be estimated. This requires images of a uniform background in order to map out the pixel-to-pixel response. Typically, sky flats are taken during evening or morning twilight. The resulting images, specific to the particular filter used, are combined

and normalized, and then used to divide out the response of the CCD from all the remaining images. The sky flats must first be bias and skim flat subtracted, (or preflashbias subtracted), before the final superskyflat can be produced. Additionally, as with the skim flat, the exposure time for a sky flat must be greater than 3 seconds to reduce the residual shutter structure to a tolerable level. Also, sky flats show up to 1% variations depending on the pointing of the telescope. This is probably due to flexing of the telescope as it is moved. If feasible, sky flats should thus be taken at different telescope pointings with the resulting superskyflats used for images of similar hour angle, and the filters and CCD window should be cleaned regularly. The noise contained in the superskyflat frame is

$$RK=\frac{\sqrt{\frac{R^2+T^2+P^2+L_{flat}}{n_k}}}{L_{flat}} \tag{5.10}$$

where $L_{flat}$ is the sky flat light level (typically 10,000 ADUs or 156,000 electrons), and $n_k$ (3 or greater) is the number of sky flats used to create superskyflat.

Finally, corrupted pixels from cosmic rays or decay events in the radioactive glass used in the construction of the CCD must be removed. A cosmic ray or decay event impinging on the CCD during an exposure will corrupt the pixel value where it passes through the array. An average of 18 pixels per minute of observation are effected in this way.

Typically, only a single pixel is effected per event. Because of this unique signature, each CCD image can be examined for these cosmic ray pixels, with the pixel value of the resulting cosmic ray detections replaced with the average of the surrounding pixel values. This works well for cosmic rays located in areas of the CCD that measure background sky. If a cosmic ray happens to coincide with your object of interest, however, the image is essentially useless for accurate photometry.

Using equations 5.6 to 5.10, the total noise in a reduced image is

$$N=\sqrt{n(R^2+T^2+P^2)+L\times(1+RK^2L)} \tag{5.11}$$

where $L = L_{object} + nL_{sky}$, $L_{object}$ is the total signal level of the object of interest in electrons, $L_{sky}$ is the background sky level per pixel in electrons, and n is the number of pixels used in the photometry (depends on the seeing during the night of observation). $L_{object}$ can be calculated in electrons for the V filter using

$$L_{object}=15.6\times10^{((V_{limit}-V)/2.5)}\times t \tag{5.12}$$

where $V_{limit}$ = (19.224 ± 0.018) - (0.101 ± 0.011) × (years since last cleaning), V is the object's V magnitude, and t is the exposure length in seconds. For moonless nights, $L_{sky}$ is approximately 0.87 x t electrons per pixel in V. This corresponds to a sky brightness of 22.3 magnitudes in V. A moonlit sky will have a $L_{sky}$ value approximately 5 times

greater, corresponding to a sky brightness of 20.5 magnitudes in V. Table A1.8 of Appendix 1 gives sample signal to noise calculations using Equation 5.8 for various magnitude stars, exposure lengths, and conditions.

### 5.4.3 Combining CTI and Capilla Peak Data

The next step in determining an accurate period for a candidate RR Lyrae star is to combine the Capilla Peak data with the CTI data. Within arcminutes of every candidate variable, the CTI database also contains information on stars determined to be nonvariable from CTI light curves. Several stars of similar magnitude and color to the variable and close enough to the variable to fit within a Capilla Peak image are picked to be used as standard comparison stars. Differential Capilla Peak instrumental magnitudes ($\Delta V_{Capilla}$) are found for all standard pairs and between each standard and the variable using the photometry package in IRAF. Using the standard stars, differential CTI instrumental magnitudes ($\Delta V_{CTI}$) are used to create a Capilla Peak to CTI conversion factor ($K_V = |\Delta V_{CTI}/\Delta V_{Capilla}|$), with the resulting CTI instrumental magnitude for the variable calculated by

$$V_{CTI}(var) = V_{CTI}(std) + K_V \times \Delta V_{Capilla}(var-std) . \qquad (5.13)$$

Due to the similarity of the CTI and Capilla Peak's V filter and CCD, the value $K_V$ is essentially equal to 1. This was verified using several standard star pairs and calculating $K_V$ directly. A similar calculation can be done for each of the

other filters.

By selecting standard stars of similar color and magnitude, effects created by extinction in the Earth's atmosphere are practically eliminated. Where suitable standard stars do not exist for a particular variable, care was taken to observe only at low airmasses.

### 5.4.4 Summary of Observations

Each variable star required an average of two nights of observing to accurately determine its period with two to four variable stars observed per night. Several cloudy nights were also used to test the CCD system and aspects of the reduction and analysis process. Table A1.9 in Appendix 1 lists each night of observation at Capilla Peak used in this dissertation. The date, CTI dayno (1 = 85 Jan 01), percentage of the night used, observers, and cumulative percentage of nights observed are given. Tables A1.10 and A1.11 summarize all the images obtained and reduced.

Table 5.2 summarizes the results for all stars listed on the final RR Lyrae candidate list. The number of CTI and Capilla observations through the V filter, the maximum, minimum, flux averaged instrumental V magnitudes, and error in the flux averaged instrumental V magnitude, amplitude of variation in V, (M-m)/P (rise time in fraction of the period), period (in days), heliocentric epoch of maximum light (for RR Lyrae) or primary minimum light (for eclipsing), and type of

each variable star is given. The flux averaged instrumental magnitude was calculated using

$$\langle V\rangle=-2.5\times\log\sum_{i=1}^{N}0.5(\phi_{i+1}-\phi_{i-1})10^{\frac{V_i}{-2.5}} \tag{5.14}$$

where $\phi_i$ is the phase of the $i$th observation in order of increasing $\phi$, $\phi_0 = \phi_N$ and $\phi_{N+1} = \phi_1$. Photometry, finder charts, and light curves for each variable is supplied in Appendix 3.

Individual standard V magnitudes were determined using

$$V_{std}=V_{inst}+0.084\times(B-V)_{std}-0.054 \tag{5.15}$$

and

$$(B-V)_{std}=1.007\times(B-V)_{inst}+0.089, \tag{5.16}$$

where the subscript *std* is for the standard Johnson system and *inst* is for instrumental magnitudes (McGraw et al. 1989). The $(B-V)_{std}$ as a function of phase for each RR Lyrae star was calculated by first determining the minimum B-V and the B magnitude amplitude of variation ($\Delta B$) using the CTI B observations. The B-V at any phase can then be calculated using

$$B-V=(B-V)_{min}-\frac{(\Delta B-\Delta V)}{\Delta V}\times(V-V_{min}). \tag{5.17}$$

Equation 5.4 was used for stars where the number of B observations or the distribution in phase of the B observations was insufficient to determine $\Delta B$. The error in $(B-V)_{min}$ ranges from 0.03 to 0.2 magnitudes, while the error in

$\Delta B$ ranges from 0.1 to 0.4 magnitudes. At most, this results in an additional systematic error of <0.02 magnitudes for the amplitude, minimum and mean magnitudes, and <0.04 magnitudes for the maximum magnitude. The (B-V) of all eclipsing variable stars was assumed to be constant. Table 5.4 summarizes the results for all stars listed on the final RR Lyrae candidate list. The instrumental B-V at minimum light, amplitude in instrumental V and B magnitudes, standard B-V at minimum light, the minimum, maximum, and flux averaged standard V magnitudes, and the amplitude in standard V magnitudes are listed.

## Table 5.3 - Photometry results for RR Lyrae survey stars

| # | CTI | CAP | Max | Min | Mean | Err | Amp | m-M | Period | Epoch | Type |
|---|---|---|---|---|---|---|---|---|---|---|---|
| | | | \|<-Instrumental magnitudes ->\| | | | | | | | | |
| 1 | 39 | 10 | 16.67 | 17.09 | 16.837 | 0.0090 | 0.42 | 0.50 | 0.276682 | 3539.373 | W UMa |
| 2 | 45 | 16 | 16.23 | 16.73 | 16.415 | 0.0091 | 0.50 | 0.50 | 0.383472 | 3539.565 | W UMa |
| 3 | 43 | 10 | 16.43 | 16.73 | 16.580 | 0.0076 | 0.30 | 0.50 | 0.349120 | 3546.520 | W UMa |
| 4 | 48 | 29 | 16.33 | 17.59 | 17.081 | 0.0094 | 1.26 | 0.20 | 0.497854 | 3641.220 | RRab |
| 5 | 46 | 51 | 16.71 | 18.00 | 17.517 | 0.0088 | 1.29 | 0.20 | 0.461291 | 3559.380 | RRab B |
| 6 | 44 | 10 | 13.83 | 14.06 | 13.947 | 0.0015 | 0.23 | 0.50 | 0.265461 | 3539.429 | W UMa |
| 7 | 46 | 20 | 17.29 | 18.41 | 17.905 | 0.0219 | 1.12 | 0.15 | 0.561891 | 3685.125 | RRab |
| 8 | 46 | 19 | 17.40 | 18.13 | 17.711 | 0.0185 | 0.73 | 0.50 | 0.319400 | 3546.455 | W UMa |
| 9 | 50 | 32 | 12.56 | 12.91 | 12.739 | 0.0008 | 0.35 | 0.25 | 1.79325 | 3299.884 | Cδs |
| 10 | 51 | 17 | 18.02 | 18.81 | 18.267 | 0.0228 | 0.79 | 0.50 | 0.269392 | 3622.235 | W UMa |
| 11 | 48 | 20 | 15.80 | 16.29 | 16.085 | 0.0058 | 0.49 | 0.20 | 0.632536 | 3308.300 | RRab |
| 12 | 45 | 28 | 15.55 | 16.74 | 16.344 | 0.0053 | 1.19 | 0.10 | 0.552704 | 3307.320 | RRab B |
| 13 | 45 | 23 | 15.44 | 16.73 | 16.255 | 0.0048 | 1.29 | 0.20 | 0.513581 | 3331.312 | RRab B |
| 14 | 49 | 15 | 16.32 | 16.88 | 16.571 | 0.0074 | 0.56 | 0.35 | 0.286813 | 3342.322 | RRc |
| 15 | 44 | 28 | 17.75 | 18.70 | 18.250 | 0.0167 | 0.95 | 0.20 | 0.552801 | 3666.438 | RRab |
| 16 | 13 | 32 | 17.50 | 18.44 | 18.037 | 0.0140 | 0.94 | 0.15 | 0.707095 | 3641.348 | RRab |
| 17 | 47 | 16 | 16.47 | 17.04 | 16.740 | 0.0064 | 0.57 | 0.30 | 0.327640 | 3363.304 | RRc |
| 18 | 43 | 16 | 14.56 | 15.80 | 15.305 | 0.0029 | 1.24 | 0.10 | 0.597821 | 3356.253 | RRab |
| 19 | 48 | 12 | 15.61 | 16.79 | 16.364 | 0.0065 | 1.18 | 0.10 | 0.521823 | 3361.121 | RRab |
| 20 | 47 | 16 | 14.97 | 16.19 | 15.737 | 0.0078 | 1.22 | 0.10 | 0.508702 | 3683.373 | RRab |
| 21 | 50 | 10 | 15.76 | 16.91 | 16.470 | 0.0068 | 1.15 | 0.10 | 0.529449 | 3361.268 | RRab |
| 22 | 45 | 10 | 14.22 | 15.24 | 14.820 | 0.0022 | 1.02 | 0.10 | 0.540837 | 3361.347 | RRab |
| 23 | 34 | 10 | 13.67 | 14.00 | 13.825 | 0.0012 | 0.33 | 0.40 | 0.314639 | 3361.432 | RRc |
| 24 | 45 | 12 | 16.44 | 17.09 | 16.770 | 0.0090 | 0.65 | 0.25 | 0.568389 | 3468.281 | RRab |
| 25 | 36 | 11 | 16.75 | 17.41 | 17.056 | 0.0240 | 0.66 | ---- | -------- | -------- | Galaxy |
| 26 | 49 | 20 | 17.63 | 18.34 | 17.995 | 0.0271 | 0.71 | 0.20 | 0.437536 | 3481.155 | RRab |
| 27 | 50 | 17 | 14.52 | 15.06 | 14.810 | 0.0028 | 0.54 | 0.20 | 0.622135 | 3112.203 | RRab |
| 28 | 46 | 7 | 17.52 | 18.24 | 17.897 | 0.0218 | 0.72 | 0.15 | 0.571900 | 3685.029 | RRab |
| 29 | 13 | 4 | 15.13 | 15.36 | 15.234 | 0.0055 | 0.23 | 0.50 | 0.343670 | 3685.451 | W UMa |
| 30 | 28 | 20 | 14.77 | 15.76 | 15.368 | 0.0035 | 0.99 | 0.15 | 0.570831 | 3113.209 | RRab |
| 31 | 20 | 5 | 14.64 | 15.15 | 14.884 | 0.0042 | 0.51 | 0.50 | 0.272711 | 3685.586 | RRc? |
| 32 | 27 | 19 | 15.54 | 16.62 | 16.202 | 0.0064 | 1.08 | 0.15 | 0.531433 | 3481.184 | RRab |
| 33 | 27 | 20 | 17.28 | 18.59 | 17.998 | 0.0187 | 1.31 | 0.05 | 0.516250 | 3474.160 | RRab |
| 34 | 15 | 16 | 14.67 | 15.42 | 15.090 | 0.0034 | 0.75 | 0.25 | 0.528145 | 3385.207 | RRab |
| 35 | 17 | 0 | 17.22 | 17.99 | 17.637 | 0.0304 | 0.77 | 0.10 | 0.47259 | 3385.248 | RRab? |
| 36 | 26 | 25 | 14.60 | 14.94 | 14.768 | 0.0031 | 0.34 | 0.40 | 0.295405 | 3469.480 | RRc |
| 37 | 30 | 27 | 15.28 | 15.91 | 15.686 | 0.0044 | 0.63 | 0.20 | 0.0568927 | 3385.429 | SX Phe |
| 38 | 30 | 13 | 15.18 | 16.23 | 15.807 | 0.0052 | 1.05 | 0.10 | 0.566966 | 3113.194 | RRab |
| 39 | 30 | 33 | 16.08 | 16.98 | 16.642 | 0.0074 | 0.90 | 0.20 | 0.526354 | 3186.109 | RRab |
| 40 | 30 | 16 | 15.46 | 15.87 | 15.666 | 0.0041 | 0.41 | 0.40 | 0.377069 | 3487.309 | RRc? |
| 41 | 25 | 20 | 13.15 | 13.37 | 13.244 | 0.0014 | 0.22 | 0.50 | 0.695000 | 3474.190 | W UMa |
| 42 | 26 | 27 | 16.36 | 17.50 | 17.072 | 0.0224 | 1.14 | 0.20 | 0.454185 | 3181.102 | RRab |
| 43 | 25 | 16 | 15.19 | 15.98 | 15.610 | 0.0047 | 0.79 | 0.15 | 0.541466 | 3169.122 | RRab |
| 44 | 25 | 22 | 15.84 | 17.06 | 16.621 | 0.0074 | 1.22 | 0.10 | 0.484114 | 3175.196 | RRab |
| 45 | 25 | 19 | 16.30 | 17.07 | 16.698 | 0.0114 | 0.77 | 0.15 | 0.709921 | 3516.300 | RRab |
| 46 | 25 | 12 | 14.21 | 14.75 | 14.427 | 0.0023 | 0.54 | 0.50 | 0.366912 | 3473.422 | W UMa |
| 47 | 24 | 0 | 16.19 | 16.60 | 16.373 | 0.0101 | 0.41 | 0.50 | 0.656278 | 3473.717 | W UMa? |
| 48 | 24 | 10 | 16.90 | 17.38 | 17.103 | 0.0133 | 0.48 | 0.50 | 0.345930 | 3481.409 | W UMa? |
| 49 | 24 | 44 | 16.85 | 17.52 | 17.175 | 0.0081 | 0.67 | 0.25 | 0.764461 | 3488.260 | RRab B |
| 50 | 23 | 94 | 12.47 | 13.41 | 12.976 | 0.0058 | 0.94 | ---- | -------- | (3174) | L |
| 51 | 24 | 21 | 15.74 | 16.83 | 16.359 | 0.0064 | 1.09 | 0.20 | 0.424599 | 3474.433 | RRab |
| 52 | 25 | 22 | 14.93 | 15.43 | 15.131 | 0.0043 | 0.50 | 0.45 | 0.306999 | 3488.337 | RRc |
| 53 | 18 | 17 | 12.73 | 13.17 | 12.894 | 0.0014 | 0.44 | 0.50 | 0.438854 | 3517.448 | W UMa |
| 54 | 13 | 0 | 16.34 | 16.66 | 16.493 | 0.0150 | 0.32 | 0.20 | 0.448676 | 3517.381 | RRc? |
| 55 | 13 | 0 | 15.18 | 15.61 | 15.423 | 0.0075 | 0.43 | 0.30 | 0.325160 | 3517.511 | RRc |
| 56 | 18 | 17 | 16.69 | 17.27 | 16.892 | 0.0104 | 0.58 | 0.50 | 0.333247 | 3516.360 | W UMa |
| 57 | 20 | 18 | 14.79 | 15.47 | 15.233 | 0.0038 | 0.68 | 0.20 | 0.592806 | 3517.220 | RRab |

## Figure 5.3 - Photometry Results (continued)

| # | CTI | CAP | Min | Max | Mean | Err | Amp | m-M | Period | Epoch | Type |
|---|---|---|---|---|---|---|---|---|---|---|---|
| | | | \|<-Instrumental Magnitudes ->\| | | | | | | | | |
| 58 | 20 | 26 | 16.33 | 17.77 | 17.137 | 0.0104 | 1.44 | 0.05 | 0.464627 | 3234.243 | RRab |
| 59 | 21 | 13 | 14.62 | 15.63 | 15.192 | 0.0049 | 1.01 | 0.25 | 0.525361 | 3660.060 | RRab |
| 60 | 21 | 29 | 15.01 | 16.02 | 15.630 | 0.0037 | 1.01 | 0.10 | 0.529309 | 3517.108 | RRab |
| 61 | 21 | 8 | 13.81 | 14.07 | 13.927 | 0.0016 | 0.26 | 0.50 | 0.279144 | 3478.351 | W UMa |
| 62 | 20 | 19 | 15.92 | 16.85 | 16.566 | 0.0089 | 0.93 | 0.05 | 0.554907 | 3673.098 | RRab B |
| 63 | 23 | 17 | 15.05 | 15.35 | 15.185 | 0.0032 | 0.30 | 0.50 | 0.426090 | 3517.356 | W UMa |
| 64 | 24 | 32 | 16.44 | 16.88 | 16.693 | 0.0069 | 0.44 | 0.10 | 0.611901 | 3622.260 | RRab |
| 65 | 24 | 8 | 13.40 | 13.68 | 13.525 | 0.0016 | 0.28 | 0.50 | 0.379380 | 3480.338 | W UMa |
| 66 | 21 | 21 | 16.28 | 17.51 | 17.064 | 0.0094 | 1.23 | 0.15 | 0.522284 | 3174.327 | RRab |
| 67 | 27 | 24 | 16.24 | 16.72 | 16.411 | 0.0055 | 0.48 | 0.50 | 0.394387 | 3545.638 | W UMa |
| 68 | 37 | 24 | 16.69 | 17.67 | 17.265 | 0.0113 | 0.98 | 0.10 | 0.692859 | 3187.329 | RRab |
| 69 | 40 | 28 | 17.10 | 17.90 | 17.565 | 0.0141 | 0.80 | 0.15 | 0.589192 | 3545.372 | RRab |

Notes to Table 5.3

1 - Other short periods possible.
3 - Other short periods possible.
5 - A period of 0.461300 days fits CTI data well, while a period of 0.461877 days fits Capilla data well. Possible example of period changing with time.
9 - CN Tau previously classified as RRab with period of 0.642062 days.
24 - EZ Com period listed as 0.568404 days in GCVS.
25 - Systematic shifts in mean magnitude from one year to the next possibly indicate this galaxy is a spurious variable (see Chapter 4.2.1 and 5.2), although an actual variability can't be ruled out.
28 - Other aliased periods possible.
29 - Other short periods possible.
31 - Other aliased periods possible. Possibly W UMa.
32 - V375 Her previously classified as SR with period of 84.1 days.
35 - Not observed at Capilla Peak. Many aliased periods possible. B-V color redder than other RR Lyraes.
40 - CTI data from 1990 and 1991 does not agree well with chosen period. No good periods were found with this data included, and so it did not pass the search for RR Lyraes in list 2. Color consistent with RRc classification. Possibly changing period with time.
43 - V532 Her had no period listed in GCVS.
47 - Not observed at Capilla Peak. Many aliased periods possible. B-V color redder than other RR Lyraes, but possibly RRc.
48 - Short period so not classified RRc although asymmetry possibly present. Other short periods possible.
51 - V427 Lyr combined with other fainter stars in photometry (see finder chart in Appendix 3).
52 - V926 Cyg period given as 0.30697965 days in GCVS. Combined with other fainter stars in photometry (see finder chart in Appendix 3).
54 - Not observed at Capilla Peak. Many aliased periods possible. Asymmetric light curve, possibly RRc.
55 - Not observed at Capilla Peak. Many aliased periods possible. Asymmetric light curve and color consistent with RRc type.
61 - Some CTI data does not agree well with chosen period. Other short periods possible.
64 - Combined with other star of equal brightness in photometry (see finder chart in Appendix 3).

## Figure 5.4 - Standard Magnitudes for RR Lyrae survey stars

| | | | | \|<- | Standard | magnitudes | | ->\| |
|---|---|---|---|---|---|---|---|---|
| # | (B-V) | Vamp | Bamp | (B-V) | Max | Min | Mean | Vamp |
| 1 | 0.60 | 0.42 | 0.42 | 0.69 | 16.67 | 17.09 | 16.841 | 0.42 |
| 2 | 0.47 | 0.50 | 0.50 | 0.56 | 16.22 | 16.72 | 16.408 | 0.50 |
| 3 | 0.80 | 0.30 | 0.30 | 0.89 | 16.45 | 16.75 | 16.601 | 0.30 |
| 4 | 0.20 | 1.26 | 1.45 | 0.29 | 16.29 | 17.56 | 17.045 | 1.27 |
| 5 | 0.40 | 1.29 | 1.60 | 0.49 | 16.67 | 18.00 | 17.495 | 1.33 |
| 6 | 0.78 | 0.23 | 0.23 | 0.87 | 13.85 | 14.08 | 13.966 | 0.23 |
| 7 | 0.45 | 1.12 | 1.30 | 0.54 | 17.27 | 18.40 | 17.889 | 1.13 |
| 8 | 0.60 | 0.73 | 0.73 | 0.69 | 17.40 | 18.13 | 17.715 | 0.73 |
| 9 | 0.80 | 0.35 | 0.50 | 0.89 | 12.56 | 12.92 | 12.755 | 0.36 |
| 10 | 0.75 | 0.79 | 0.79 | 0.84 | 18.04 | 18.83 | 18.284 | 0.79 |
| 11 | 0.33 | 0.49 | 0.60 | 0.42 | 15.77 | 16.30 | 16.063 | 0.53 |
| 12 | 0.21 | 1.19 | 1.40 | 0.30 | 15.51 | 16.71 | 16.310 | 1.20 |
| 13 | 0.30 | 1.29 | 1.60 | 0.39 | 15.40 | 16.71 | 16.226 | 1.31 |
| 14 | 0.07 | 0.56 | 0.69 | 0.16 | 16.27 | 16.84 | 16.525 | 0.57 |
| 15 | 0.32 | 0.95 | 1.10 | 0.41 | 17.71 | 18.68 | 18.224 | 0.97 |
| 16 | 0.24 | 0.94 | 1.20 | 0.33 | 17.46 | 18.42 | 18.003 | 0.96 |
| 17 | 0.12 | 0.57 | 0.65 | 0.21 | 16.42 | 17.00 | 16.700 | 0.58 |
| 18 | 0.36 | 1.24 | 1.62 | 0.45 | 14.52 | 15.78 | 15.278 | 1.26 |
| 19 | 0.20 | 1.18 | 1.25 | 0.29 | 15.58 | 16.77 | 16.332 | 1.19 |
| 20 | 0.32 | 1.18 | 1.50 | 0.41 | 14.92 | 16.17 | 15.705 | 1.25 |
| 21 | 0.33 | 1.15 | 1.50 | 0.42 | 15.72 | 16.89 | 16.442 | 1.17 |
| 22 | 0.35 | 1.02 | 1.29 | 0.44 | 14.19 | 15.23 | 14.794 | 1.04 |
| 23 | 0.05 | 0.33 | 0.43 | 0.14 | 13.62 | 13.95 | 13.779 | 0.33 |
| 24 | 0.35 | 0.65 | 1.00 | 0.44 | 16.40 | 17.07 | 16.743 | 0.67 |
| 25 | 0.60 | 0.66 | 0.66 | 0.69 | 16.75 | 17.41 | 17.060 | 0.66 |
| 26 | 0.40 | 0.71 | 1.05 | 0.49 | 17.60 | 18.32 | 17.972 | 0.72 |
| 27 | 0.36 | 0.54 | 0.75 | 0.45 | 14.49 | 15.04 | 14.787 | 0.55 |
| 28 | 0.30 | 0.72 | 1.10 | 0.39 | 17.47 | 18.22 | 17.860 | 0.75 |
| 29 | 0.47 | 0.23 | 0.23 | 0.56 | 15.12 | 15.35 | 15.227 | 0.23 |
| 30 | 0.33 | 0.99 | 1.25 | 0.42 | 14.73 | 15.74 | 15.341 | 1.01 |
| 31 | 0.30 | 0.51 | 0.80 | 0.39 | 14.59 | 15.13 | 14.850 | 0.54 |
| 32 | 0.30 | 1.08 | 1.50 | 0.39 | 15.49 | 16.60 | 16.170 | 1.11 |
| 33 | 0.35 | 1.31 | 1.55 | 0.44 | 17.25 | 18.57 | 17.972 | 1.32 |
| 34 | 0.45 | 0.75 | 1.20 | 0.54 | 14.64 | 15.41 | 15.071 | 0.77 |
| 35 | 0.60 | 0.77 | 0.77 | 0.69 | 17.22 | 17.99 | 17.641 | 0.77 |
| 36 | 0.15 | 0.34 | 0.48 | 0.24 | 14.56 | 14.91 | 14.730 | 0.35 |
| 37 | 0.15 | 0.63 | 0.75 | 0.24 | 15.23 | 15.88 | 15.649 | 0.65 |
| 38 | 0.30 | 1.05 | 1.30 | 0.39 | 15.14 | 16.21 | 15.779 | 1.07 |
| 39 | 0.30 | 0.90 | 1.25 | 0.39 | 16.04 | 16.96 | 16.612 | 0.92 |
| 40 | 0.22 | 0.41 | 0.50 | 0.31 | 15.43 | 15.84 | 15.634 | 0.41 |
| 41 | 0.28 | 0.22 | 0.22 | 0.37 | 13.13 | 13.35 | 13.221 | 0.22 |
| 42 | 0.38 | 1.14 | 1.30 | 0.47 | 16.33 | 17.48 | 17.052 | 1.15 |
| 43 | 0.43 | 0.79 | 0.90 | 0.52 | 15.18 | 15.97 | 15.595 | 0.79 |
| 44 | 0.49 | 1.22 | 1.70 | 0.58 | 15.80 | 17.05 | 16.604 | 1.25 |
| 45 | 0.55 | 0.77 | 1.00 | 0.64 | 16.29 | 17.07 | 16.690 | 0.78 |
| 46 | 0.52 | 0.54 | 0.54 | 0.61 | 14.21 | 14.75 | 14.424 | 0.54 |
| 47 | 0.66 | 0.41 | 0.41 | 0.75 | 16.20 | 16.61 | 16.382 | 0.41 |
| 48 | 0.45 | 0.48 | 0.48 | 0.54 | 16.89 | 17.37 | 17.095 | 0.48 |
| 49 | 0.65 | 0.67 | 1.00 | 0.74 | 16.84 | 17.53 | 17.174 | 0.69 |
| 50 | 1.75 | 0.94 | 0.94 | 1.85 | 12.57 | 13.51 | 13.078 | 0.94 |
| 51 | 0.60 | 1.09 | 1.50 | 0.69 | 15.90 | 17.44 | 16.694 | 1.54 |
| 52 | 0.60 | 0.50 | 0.70 | 0.69 | 15.03 | 15.63 | 15.258 | 0.60 |
| 53 | 0.42 | 0.44 | 0.44 | 0.51 | 12.72 | 13.16 | 12.883 | 0.44 |
| 54 | 0.43 | 0.32 | 0.32 | 0.52 | 16.33 | 16.65 | 16.483 | 0.32 |
| 55 | 0.25 | 0.43 | 0.55 | 0.34 | 15.15 | 15.58 | 15.394 | 0.43 |
| 56 | 0.70 | 0.58 | 0.58 | 0.79 | 16.70 | 17.28 | 16.905 | 0.58 |
| 57 | 0.45 | 0.68 | 1.00 | 0.54 | 14.76 | 15.46 | 15.214 | 0.70 |
| 58 | 0.38 | 1.44 | 1.78 | 0.47 | 16.29 | 17.76 | 17.107 | 1.47 |

## Figure 5.4 - Standard Magnitudes (continued)

| # | (B-V) | Vamp | Bamp | \|<- (B-V) | Standard Max | Magnitudes Min | Mean | ->\| Vamp |
|---|---|---|---|---|---|---|---|---|
| 59 | 0.35 | 1.01 | 1.31 | 0.44 | 14.58 | 15.61 | 15.162 | 1.03 |
| 60 | 0.38 | 1.01 | 1.50 | 0.47 | 14.96 | 16.01 | 15.597 | 1.05 |
| 61 | 0.79 | 0.26 | 0.26 | 0.88 | 13.83 | 14.09 | 13.947 | 0.26 |
| 62 | 0.30 | 0.93 | 1.10 | 0.39 | 15.88 | 16.83 | 16.540 | 0.95 |
| 63 | 0.35 | 0.30 | 0.30 | 0.44 | 15.03 | 15.33 | 15.168 | 0.30 |
| 64 | 0.45 | 0.44 | 0.60 | 0.54 | 16.84 | 17.54 | 17.245 | 0.70 |
| 65 | 0.40 | 0.28 | 0.28 | 0.49 | 13.39 | 13.67 | 13.512 | 0.28 |
| 66 | 0.30 | 1.23 | 1.60 | 0.39 | 16.23 | 17.48 | 17.030 | 1.25 |
| 67 | 0.40 | 0.48 | 0.48 | 0.49 | 16.23 | 16.71 | 16.398 | 0.48 |
| 68 | 0.44 | 0.98 | 1.25 | 0.53 | 16.65 | 17.66 | 17.241 | 1.01 |
| 69 | 0.48 | 0.80 | 1.00 | 0.57 | 17.08 | 17.89 | 17.549 | 0.81 |

Notes to Table 5.4

35 - Particularly poor B observations.

51 - Luminosity of blended stars ($V = 18.008 \pm 0.056$ and $V = 19.497 \pm 0.133$ as determined by Capilla Peak photometry) removed. Random error in standard magnitude 0.0092.

52 - Luminosity of blended stars ($V = 18.273 \pm 0.040$ and $V = 18.093 \pm 0.025$ as determined by Capilla Peak photometry) removed. Random error in standard magnitude 0.0048.

64 - Luminosity of blended star ($V = 17.718 \pm 0.035$ as determined by Capilla Peak photometry) removed. Random error in standard magnitude 0.0115.

## 5.5 CTI RR Lyrae Survey Statistics

Equation 5.2 (from Barnes and Hawley 1986), which empirically accounts for changing light curve shape with increasing amplitude when comparing the mean, minimum, and maximum magnitudes, will be used in Chapter 6 to calculate mean magnitudes for RR Lyrae stars in surveys where only the minimum and maximum magnitudes are listed. Equation 5.2 can be checked using the CTI data. Figure 5.10 plots ($V_{min}$ - <V>) versus $\Delta$V for the twenty-five brightest RR Lyrae variable

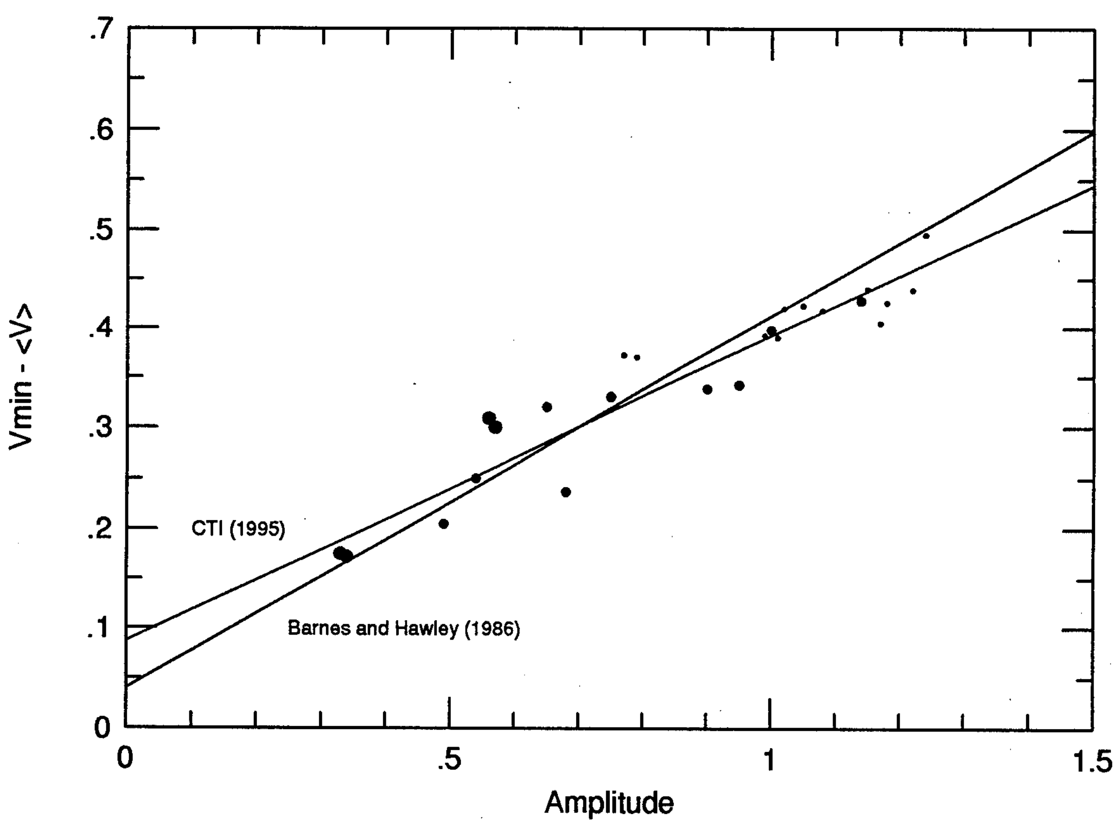


Figure 5.10 - Vmin - <V> versus $\Delta$V for bright RR Lyrae variable stars in CTI survey. Increasing symbol size corresponds to increasing (m-M)/P. Barnes and Hawley 1986 relation and CTI regression fit also plotted.

stars in the CTI survey with increasing symbol size corresponding to increasing (m-M)/P (a measure of light curve shape). The Barnes and Hawley 1986 relation ($V_{min} - \langle V \rangle = 0.04 + 0.375 \times \Delta V$) and the regression fit to the CTI data ($V_{min} - \langle V \rangle = (0.087 \pm 0.030) + (0.305 \pm 0.021) \times \Delta V$) are also plotted. For stars of identical light curve shape, the intercept of $V_{min} - \langle V \rangle$ versus $\Delta V$ must be equal to zero. This is the case for RRc type variables (represented by the largest symbols in Figure 5.10), where the resulting slope is close to 0.5 (as would be expected for a sinusoidal light curve). For the more asymmetric light curves of RRab type stars, a slope between 0.35 and 0.45 fits the data best with zero intercept. The fact that increasing asymmetry is correlated with amplitude makes it possible for a relation like Equation 5.2 to be calculated using all types of RR Lyraes. The slight difference in slope and intercept between the Barnes and Hawley 1986 and CTI best fit lines are comparable to the scatter of the CTI data from the best fit lines. The CTI best fit line, however, was calculated using over three times the number of stars, and is thus more representative of the actual relationship.

Equation 5.1 (McDonald 1977), an empirical relation between B-V at minimum light and period for RRab type variable stars, was used earlier to establish a color limit in selecting RR Lyrae variables. This relation can also be checked using CTI data. Figure 5.11 plots the B-V at minimum

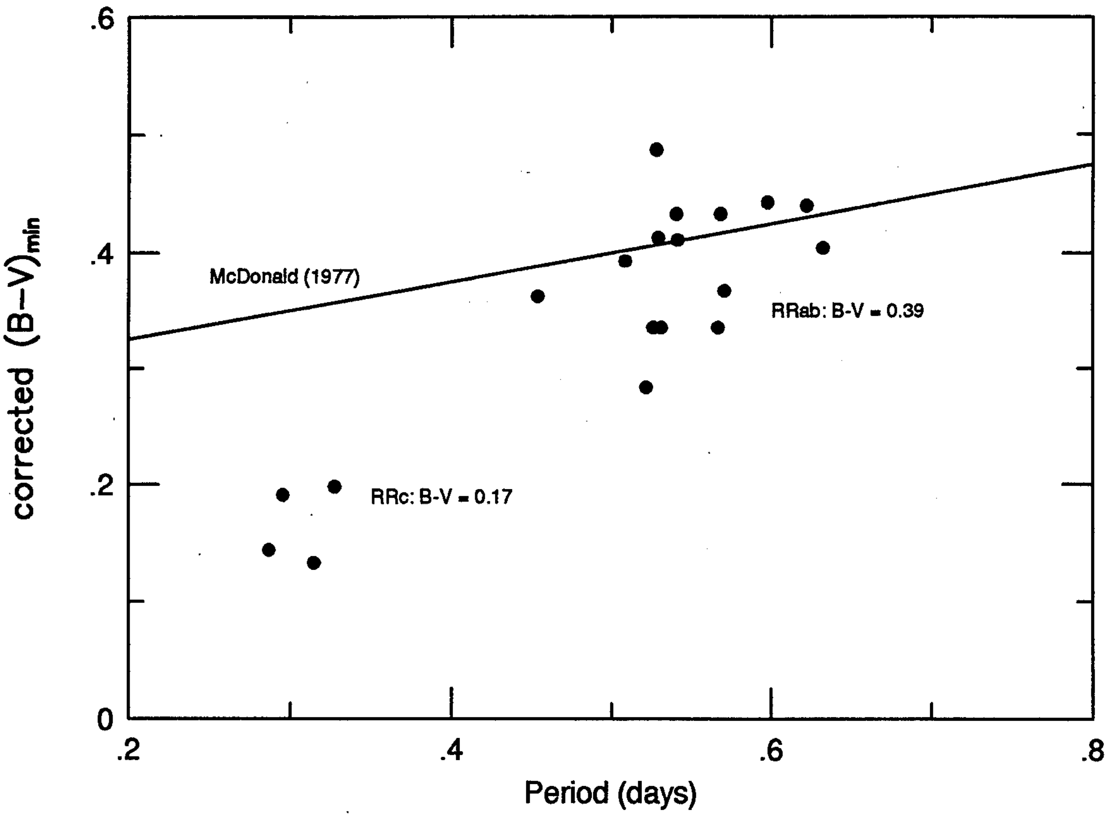


Figure 5.11 - B-V at minimum light (corrected for Galactic reddening) versus period for bright RR Lyrae variable stars in CTI survey. McDonald 1977 relation also plotted.

light versus period for nineteen of the brightest RR Lyrae stars with more than 5 B observations and little Galactic reddening. The reddening corrected mean B-V at minimum light of the RRab type variables is 0.39 ± 0.05. There is only the slightest hint of a dependence on period, although this dependence might manifest itself more clearly if the sample included RRab type stars with a larger range of periods. If the four RRc type variables are included (having a mean B-V at minimum light of 0.17 ± 0.03), Figure 5.11 clearly displays

the trend of redder colors for longer periods.

Finally, Figure 5.12 compares the period and amplitude distribution of the CTI RR Lyrae variable stars to that of the RR Lyrae variable stars contained in the Palomar-Groningen Variable Star survey. Despite the fact that the CTI survey covers a large range of Galactic latitude and longitude as compared to the Palomar-Groningen survey, there are no significant deviations between the period and amplitude distributions for these surveys and thus it can be assumed they are subsets of the same parent population.

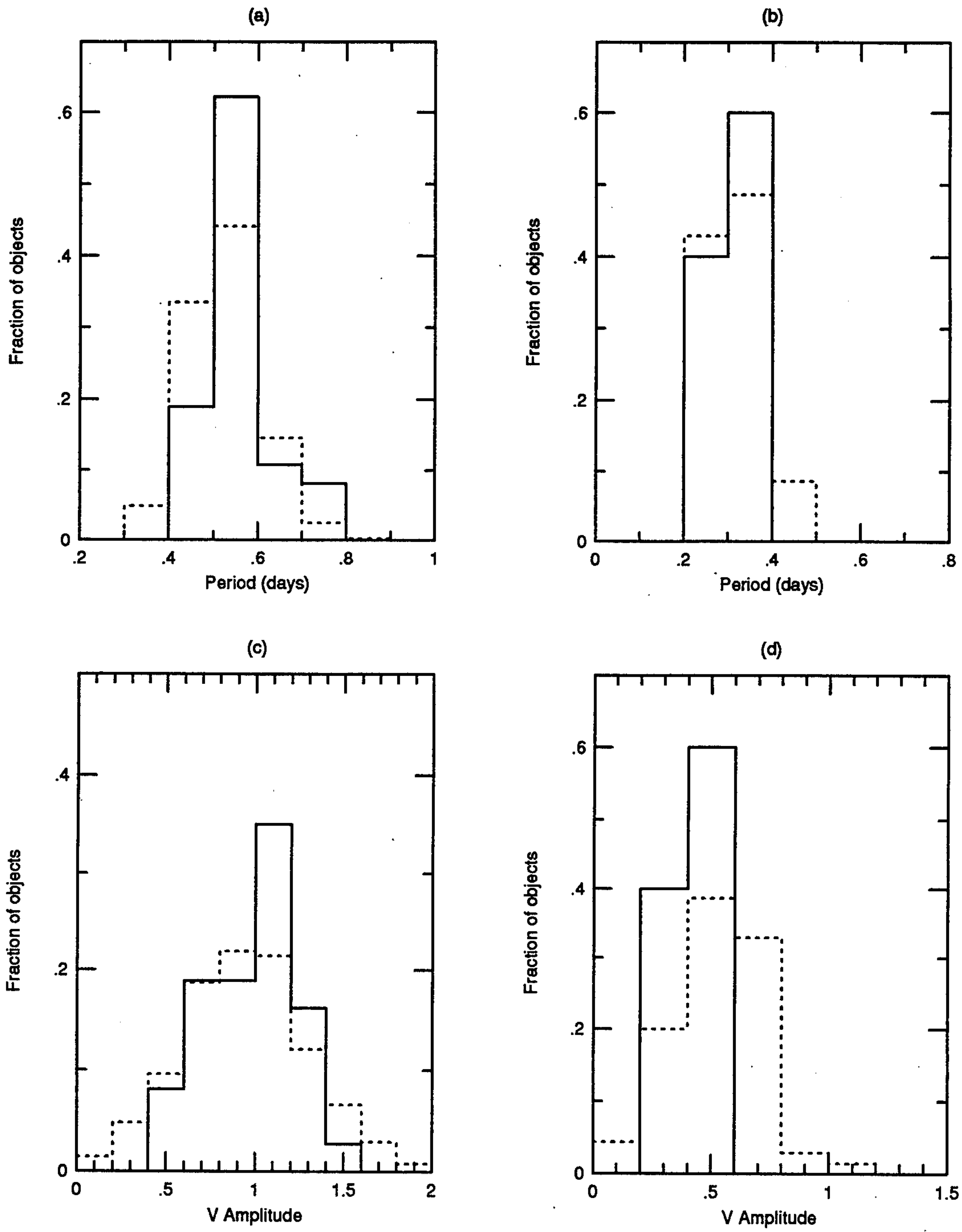


Figure 5.12 - Distribution in (a),(b) period and (c),(d) amplitude for the CTI RR Lyrae stars (solid lines) and the RR Lyrae stars contained in the Palomar-Groningen Variable Star survey (dashed lines). RRab type stars are shown in (a) and (c) while RRc type stars are shown in (b) and (d).

## Chapter 6 RR Lyrae Variable Star Space Densities

The space density of RR Lyrae variable stars in the Galactic halo can now be examined. RR Lyrae variable stars exhibit a period-luminosity relationship similar to the period-luminosity relationship of Classical Cepheids. Knowing the absolute magnitude ($M_V$, $M_B$), Galactic absorption ($A_V = 3 \times E(B-V)$, $A_B = 4 \times E(B-V)$), and apparent magnitude ($\langle V \rangle$, $\langle B \rangle$), the heliocentric distance (r) to the RR Lyrae star can be readily calculated using

$$r=10^{\frac{\langle V\rangle-M_V+5-A_V}{5}} \tag{6.1}$$

In this chapter the simplest luminosity function, namely that all RR Lyraes have an absolute magnitude of $M_V = 0.74 \pm 0.12$ (Layden et al. 1994) will be used. This is necessary because metallicity measurements have not been made for all the RR Lyrae stars in the CTI survey, nor in most of the other surveys with which the calculated CTI RR Lyrae space densities will be compared. Given that $\langle B \rangle - \langle V \rangle \approx 0.26$ (Hawley et al. 1986), $M_B = 1.00$.

Knowing the Galactic latitude ($b$), Galactic longitude ($l$) and heliocentric distance (r) leads directly to a calculation of the Galactocentric coordinates ((x,y,z) or ($R,\theta,\phi$)). Figure 6.1 displays this coordinate system with $R_0$ the distance from the Sun (S) to the Galactic center (O) defined to be along the positive x-axis, and P marking an arbitrary position for an RR Lyrae Star.

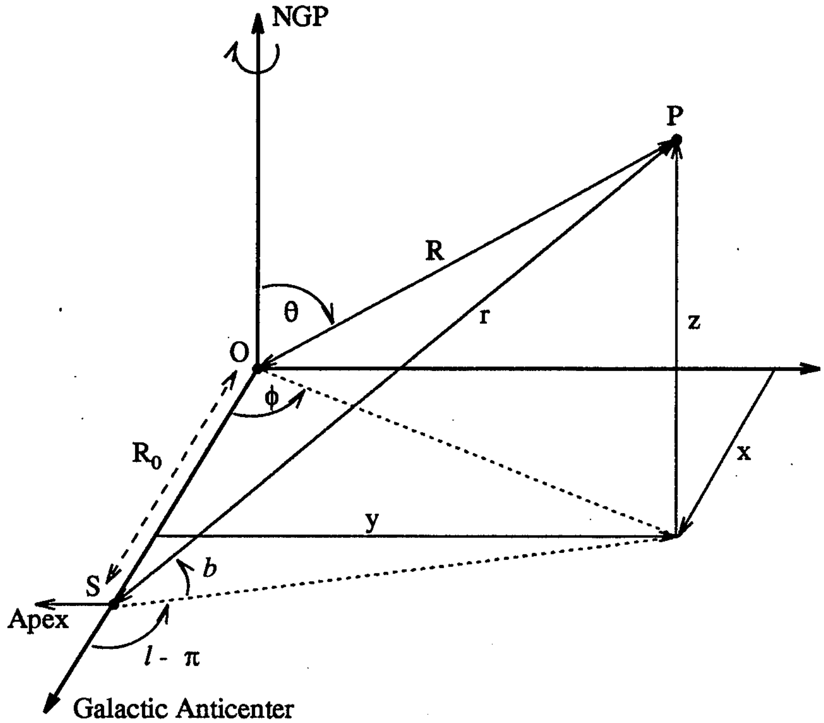


Figure 6.1 - Galactocentric coordinates. O is the Galactic center, S is the Sun's position, NGP is the north Galactic pole.

Oort and Plaut (1975) calculated $R_0$ with the RR Lyrae space density data from the Palomar-Groningen variable star survey and Baade's Window. Their value of $R_0 = 8.7 \pm 0.6$ kpc, however, was calculated assuming $M_{pg} = 0.7$ (or equivalently, $M_V = 0.44$). If this distance is recalculated using $M_V = 0.74$, $R_0 = 7.6 \pm 0.5$ kpc. This value of $R_0$ will be used when calculating distances in this chapter and agrees well with recent calculations using the rotation curve of HI in the solar neighborhood ($R_0 = 7.9 \pm 0.8$ kpc, Merrifield 1992), and an analysis based on the weighted average of several methods ($R_0 = 7.7 \pm 0.7$ kpc, Reid 1989).

Table 6.1 lists <V>, $\sigma_{<V>}$, E(B-V), the heliocentric coordinates (r, b, and l), the Galactocentric coordinates (x, y, z, R, $\theta$, and $\phi$) and the error in the Galactocentric radial distance ($\sigma_R$) for all confirmed RRab type stars in the CTI Survey. This last value was calculated using

$$\sigma_R^2 = (1+KR_0^2)\,r^2 \ln(10)^2 (\sigma_{<V>}^2 + \sigma_{M_V}^2 + \sigma_{A_V}^2) + (1+Kr^2)\,\sigma_{R_0}^2, \qquad (6.2)$$

where K = (cos(b)cos(l) - 1)/$R^2$ and $\sigma_{AV} \geq 0.03$ (Burstein and Heiles 1982). Due to the different completeness estimates for RRab and RRc type variables in the CTI as well as all other RR Lyrae surveys, the contribution to the space density from RRc type variables will not be considered.

Using the Galactocentric radial distances for the RRab type variable stars in the CTI survey, the RR Lyrae space density as a function of distance can be calculated. Due to the unique shape of the CTI survey field, covering a large range of both Galactic latitude and longitude, a method for determining the RR Lyrae space density must first be developed. The RR Lyrae space density will be calculated for the CTI survey and then compared to several other surveys of RR Lyrae variable stars.

## Table 6.1 - CTI RR Lyrae Galactocentric coordinates

| # | <V> | $\sigma_{<V>}$ | E(B-V) | r | l | b | x | y | z | R | $\sigma_R$ | $\theta$ | $\phi$ |
|---|---|---|---|---|---|---|---|---|---|---|---|---|---|
| 4 | 17.045 | 0.0094 | 0.055 | 16904.4 | 140.8 | -32.5 | 18652.4 | 9014.8 | -9074.0 | 22616.7 | 4454.4 | 113.7 | 25.8 |
| 5 | 17.495 | 0.0088 | 0.050 | 20941.1 | 141.5 | -32.2 | 21469.6 | 11040.2 | -11148.0 | 26591.5 | 5683.1 | 114.8 | 27.2 |
| 7 | 17.889 | 0.0219 | 0.101 | 23399.1 | 163.8 | -20.6 | 28634.5 | 6127.6 | -8217.2 | 30413.9 | 6497.5 | 105.7 | 12.1 |
| 11 | 16.063 | 0.0058 | 0.016 | 11350.1 | 193.0 | 25.3 | 17595.8 | -2306.1 | 4857.1 | 18398.9 | 2740.1 | 74.7 | 352.5 |
| 12 | 16.310 | 0.0053 | 0.030 | 12473.8 | 196.9 | 36.6 | 17189.5 | -2906.6 | 7429.0 | 18950.4 | 3085.3 | 66.9 | 350.4 |
| 13 | 16.226 | 0.0048 | 0.020 | 12167.5 | 197.9 | 39.6 | 16518.3 | -2873.8 | 7762.3 | 18476.1 | 2991.9 | 65.2 | 350.1 |
| 15 | 18.224 | 0.0167 | 0.018 | 30619.6 | 202.9 | 58.0 | 22532.5 | -6296.9 | 25979.4 | 34961.4 | 8671.6 | 42.0 | 344.4 |
| 16 | 18.003 | 0.0140 | 0.020 | 27580.4 | 203.5 | 60.3 | 20140.9 | -5454.8 | 23950.9 | 31765.7 | 7736.6 | 41.1 | 344.8 |
| 18 | 15.278 | 0.0029 | 0.007 | 8005.7 | 205.7 | 76.2 | 9322.7 | -828.7 | 7774.1 | 12167.0 | 1726.0 | 50.3 | 354.9 |
| 19 | 16.332 | 0.0065 | 0.007 | 13007.7 | 205.7 | 79.7 | 9686.8 | -1003.5 | 12799.9 | 16083.5 | 3274.5 | 37.3 | 354.1 |
| 20 | 15.705 | 0.0078 | 0.007 | 9745.4 | 205.4 | 79.9 | 9142.0 | -733.1 | 9594.7 | 13272.9 | 2260.6 | 43.7 | 355.4 |
| 21 | 16.442 | 0.0068 | 0.007 | 13683.6 | 203.1 | 84.1 | 8901.5 | -555.2 | 13610.2 | 16272.2 | 3490.1 | 33.2 | 356.4 |
| 22 | 14.794 | 0.0022 | 0.007 | 6406.2 | 184.4 | 88.1 | 7811.0 | -16.1 | 6402.7 | 10099.8 | 1261.6 | 50.7 | 359.9 |
| 24 | 16.743 | 0.0090 | 0.007 | 15718.1 | 42.5 | 84.0 | 6393.4 | 1105.1 | 15632.7 | 16925.7 | 4146.6 | 22.5 | 9.8 |
| 26 | 17.972 | 0.0271 | 0.014 | 27415.7 | 41.0 | 67.3 | -369.3 | 6929.6 | 25300.1 | 26234.5 | 7923.0 | 15.3 | 93.1 |
| 27 | 14.787 | 0.0028 | 0.010 | 6359.2 | 42.1 | 62.6 | 5431.3 | 1959.4 | 5647.7 | 8076.8 | 1256.0 | 45.6 | 19.8 |
| 28 | 17.860 | 0.0218 | 0.014 | 26037.6 | 43.0 | 57.8 | -2532.7 | 9453.1 | 22043.7 | 24118.4 | 7463.2 | 23.9 | 105.0 |
| 30 | 15.341 | 0.0035 | 0.053 | 7733.9 | 48.7 | 37.5 | 3549.2 | 4604.6 | 4711.9 | 7483.4 | 1645.2 | 51.0 | 52.4 |
| 32 | 16.170 | 0.0064 | 0.055 | 11298.0 | 50.3 | 32.6 | 1519.0 | 7318.5 | 6091.3 | 9642.2 | 2798.8 | 50.8 | 78.3 |
| 33 | 17.972 | 0.0187 | 0.053 | 25977.7 | 50.4 | 32.2 | -6404.6 | 16956.7 | 13826.7 | 22797.5 | 7456.7 | 52.7 | 110.7 |
| 34 | 15.071 | 0.0034 | 0.053 | 6829.7 | 50.6 | 32.1 | 3926.5 | 4472.2 | 3626.1 | 6969.0 | 1386.5 | 58.6 | 48.7 |
| 38 | 15.779 | 0.0052 | 0.055 | 9436.3 | 52.5 | 26.6 | 2460.8 | 6692.3 | 4224.3 | 8287.7 | 2184.3 | 59.4 | 69.8 |
| 39 | 16.612 | 0.0074 | 0.055 | 13848.4 | 52.6 | 26.4 | 60.3 | 9845.8 | 6163.7 | 11616.1 | 3637.2 | 58.0 | 89.6 |
| 42 | 17.052 | 0.0224 | 0.108 | 15761.6 | 54.7 | 20.5 | -922.7 | 12054.7 | 5520.3 | 13290.7 | 4342.5 | 65.5 | 94.4 |
| 43 | 15.595 | 0.0047 | 0.109 | 8046.4 | 54.8 | 20.4 | 3258.8 | 6164.6 | 2810.0 | 7517.9 | 1756.3 | 68.1 | 62.1 |
| 44 | 16.604 | 0.0074 | 0.170 | 11770.6 | 57.0 | 15.4 | 1413.8 | 9514.4 | 3123.4 | 10113.2 | 3217.0 | 72.0 | 81.5 |
| 45 | 16.690 | 0.0114 | 0.178 | 12111.6 | 57.3 | 14.7 | 1267.1 | 9853.0 | 3082.5 | 10401.4 | 3383.6 | 72.8 | 82.7 |
| 49 | 17.174 | 0.0081 | 0.223 | 14223.3 | 58.1 | 13.0 | 267.6 | 11757.8 | 3208.2 | 12190.5 | 4427.9 | 74.7 | 88.7 |
| 57 | 15.214 | 0.0038 | 0.093 | 6902.4 | 80.5 | -19.2 | 6529.5 | 6429.1 | -2272.4 | 9441.0 | 1402.7 | 103.9 | 44.6 |
| 58 | 17.107 | 0.0104 | 0.090 | 16573.0 | 82.6 | -20.9 | 5595.7 | 15354.7 | -5905.8 | 17376.9 | 4423.0 | 109.9 | 70.0 |
| 59 | 15.162 | 0.0049 | 0.090 | 6767.1 | 82.6 | -21.0 | 6790.2 | 6264.1 | -2428.5 | 9552.2 | 1364.5 | 104.7 | 42.7 |
| 60 | 15.597 | 0.0037 | 0.090 | 8268.0 | 83.1 | -21.4 | 6679.7 | 7643.7 | -3014.3 | 10589.2 | 1806.0 | 106.5 | 48.9 |
| 62 | 16.540 | 0.0089 | 0.088 | 12799.7 | 84.9 | -22.7 | 6554.8 | 11765.9 | -4929.8 | 14342.4 | 3229.9 | 110.1 | 60.9 |
| 64 | 17.245 | 0.0069 | 0.056 | 18509.7 | 90.0 | -26.1 | 7587.4 | 16625.0 | -8137.6 | 20004.5 | 4998.2 | 114.0 | 65.5 |
| 66 | 17.030 | 0.0094 | 0.068 | 16489.2 | 96.3 | -29.2 | 9173.5 | 14308.8 | -8042.2 | 18803.5 | 4368.2 | 115.3 | 57.3 |
| 68 | 17.241 | 0.0113 | 0.051 | 18603.7 | 102.5 | -31.6 | 11033.4 | 15464.0 | -9755.7 | 21355.2 | 5017.9 | 117.2 | 54.5 |
| 69 | 17.549 | 0.0141 | 0.060 | 21173.9 | 107.6 | -33.0 | 12955.3 | 16924.4 | -11542.0 | 24238.3 | 5811.4 | 118.4 | 52.6 |

## 6.1 Calculating RR Lyrae Space Densities

In most previous RR Lyrae surveys, space densities were calculated by determining the volume of space occupied by a certain number of stars of increasing *heliocentric* distance (based on Kinman et al. 1965). The space density at particular Galactocentric distances are then obtained by converting a given heliocentric distance to its corresponding Galactocentric distance. This method works fine for surveys covering a small solid angle at a fixed Galactic latitude and longitude where a given heliocentric distance corresponds to a single Galactocentric distance. This method will not work, however, with the CTI survey because of the unique shape of the CTI survey area.

Saha (1985) proposed a similar method for calculating space densities using the relationship

$$N=\int \omega \rho(r) r^2 dr \tag{6.2}$$

where N is the total number of RR Lyrae stars found in a solid angle $\omega$ along a given direction, r is the heliocentric distance, and $\rho$ is the RR Lyrae space density. Equation 6.2 can be solved for $\rho$ giving

$$\rho(r)=\frac{1}{\omega r^2}\frac{dN}{dr} \tag{6.3}$$

By using a plot of N versus r, dN/dr can be estimated as a function of r, and Equation 6.3 used to calculate the RR Lyrae space density as a function of heliocentric distance. As

before, the space density as a function of Galactocentric distance is found by converting heliocentric distances to Galactocentric distances. Again, because of the unique shape of CTI's survey area, this method will not work for the CTI survey. A variation on this method, however, can be used. An equivalent expression to Equation 6.2 is

$$N=\int f(R)\,\rho(R)\,4\pi R^2 dR \tag{6.4}$$

where f(R) is the fraction of the volume of space at Galactocentric distance R the survey samples, and ρ is now measured as a function of Galactocentric distance. The function 4πf(R) is analogous to ω in Equation 6.3, but whereas ω is constant with increasing heliocentric distance, f(R) varies with increasing Galactocentric distance and must be calculated numerically knowing the magnitude limits and borders of the survey area. Equation 6.4 can be solved for ρ giving

$$\rho(R)=\frac{1}{f(R)\,4\pi R^2}\frac{dN}{dR} \tag{6.5}$$

By using a plot of N versus R, the RR Lyrae space density as a function of Galactocentric distance can be calculated directly (assuming a spherically symmetric distribution).

A similar derivation can be done for any type of distribution. For a distribution where the density is constant on ellipsoids with a semi-major axis of *a* in the plane of the Galaxy, and a semi-minor axis of *c* perpendicular

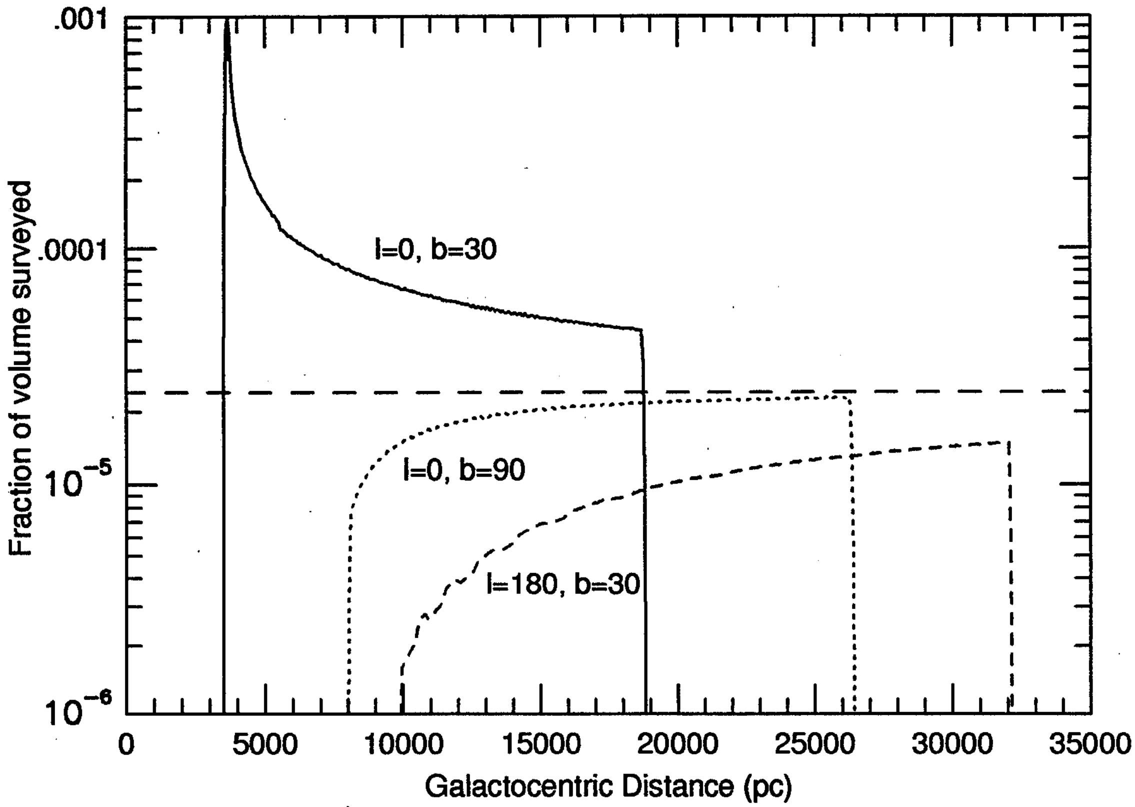


Figure 6.2 - Fraction of total volume as function of Galactocentric distance surveyed for three different 1 square degree pointings for <B> = 14 - 18: solid line for l=0° and b=30°, dotted line for l=0° and b=90°, and short dashed line for l=180° and b=30°. Long dashed line is asymptotic limit.

to the plane of the Galaxy, the resulting equation for space density is

$$\rho(a) = \frac{1}{f(a) \times \frac{c}{a}(a) \times 4\pi a^2} \frac{dN}{da} \qquad (6.6)$$

where f(a) is the fraction of the volume of space at Galactocentric semi-major axis distance $a$ sampled by the survey.

In order to determine RR Lyrae space densities, the

functions f(R) and f(a) in Equations 6.5 and 6.6 respectively must be calculated. This was done by numerically integrating over the volume of space surveyed. Figure 6.2 plots f(R) as a function of Galactocentric distance for three 1 square degree pointings with magnitude limits B = 14 to 18 and assuming no Galactic reddening. All three pointings asymptotically approach the value of (solid angle of 1 square degree)/4π representing the case where $R_0 = 0$.

Due to the different completeness estimates for RRab and RRc type variables as a function of magnitude, only RRab type variables are considered. The ellipsoidal distribution described in Preston et al. 1991, namely

$$\frac{c}{a}(a) = \begin{matrix} (\frac{c}{a})_0 + [1-(\frac{c}{a})_0]\,(\frac{a}{a_u}),\, a<a_u \\ 1,\, a>a_u \end{matrix} \qquad (6.7)$$

where $(c/a)_0 = 0.5$ and $a_u = 20$ kpc, was used.

The result for the CTI survey and a spherically symmetric distribution are shown in Figure 6.3. The survey area used in the calculations is that for list 2 shown in Figure 5.4, as modified by Figure 5.3 (bright star masking) and Figure 5.7 (completeness as a function of right ascension), and requiring E(B-V) (Figure 5.2) to be less than 0.15. The magnitude limits used were $\langle V \rangle = 13.0$ to 18.5. This faint magnitude limit corresponds to the point where the CTI survey becomes 50% complete (see Figure 5.9).

The values (dN/dR) and (dN/da) as functions of

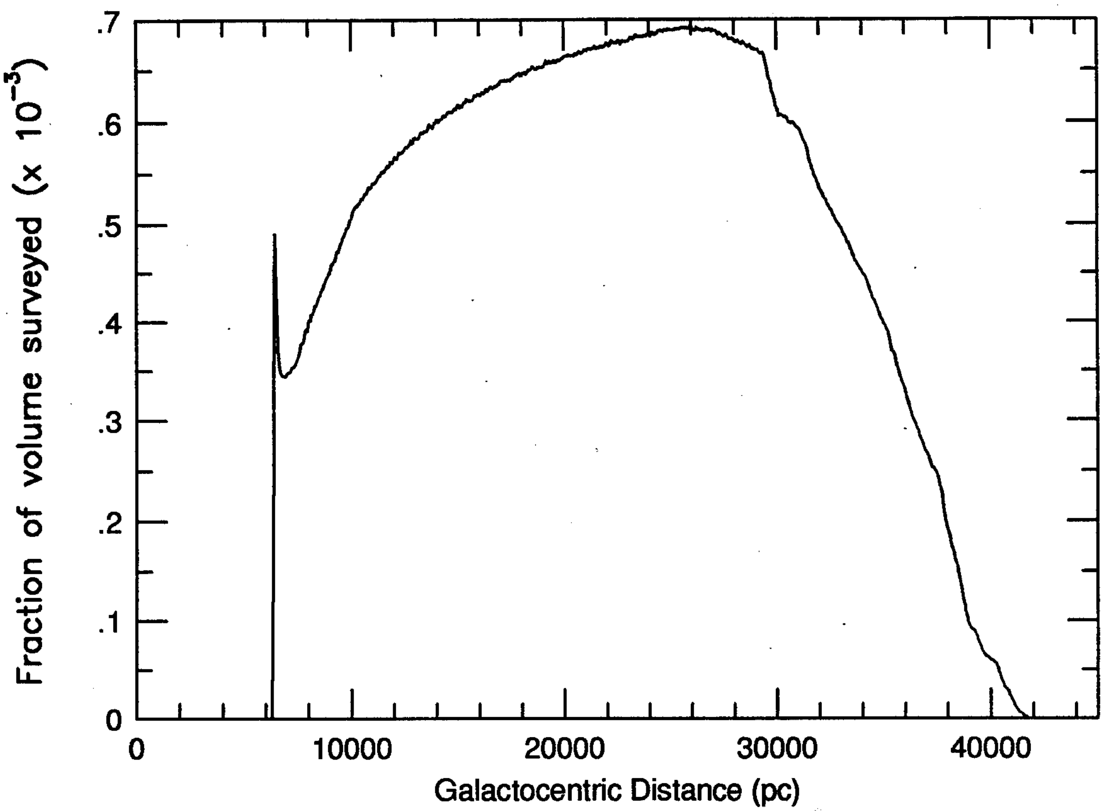


Figure 6.3 - Fraction of total volume surveyed by CTI RR Lyrae survey (× $10^{-5}$) as a function of Galactocentric distance.

Galactocentric distance and semi-major axis distance respectively must also be calculated. Figure 6.4 plots the number of RR Lyrae stars out to a certain Galactocentric distance (N) versus the Galactocentric distance (R). The value (dN/dR) for each RR Lyrae was estimated by calculating the slope of five consecutive points, two on either side of the point in question. For the two most distant and two closest to the Galactic center, only three or four points were used to calculate the slope. Similar calculations were done to determine (dN/da) as a function of the semi-major axis distance.

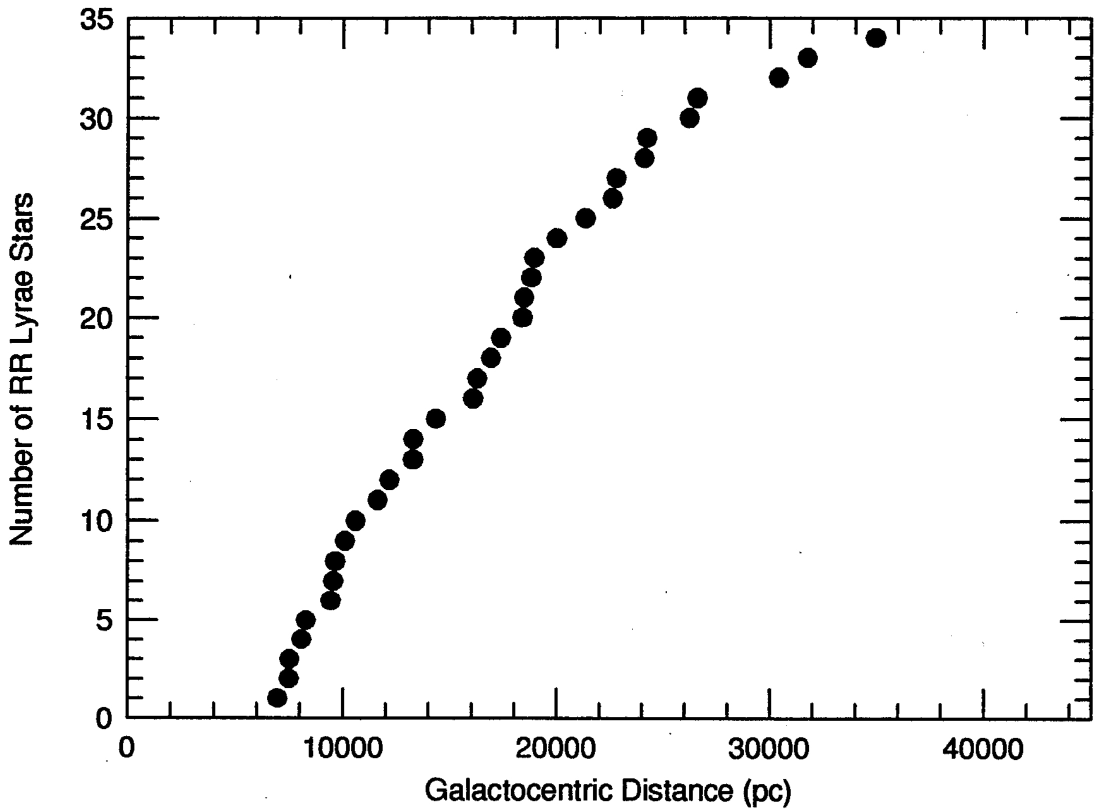


Figure 6.4 - Cumulative number of RRab type stars in the CTI RR Lyrae survey as a function of Galactocentric distance.

The method described above for calculating space densities was tested using generated N versus R plots for different spherically symmetric power-law distributions and the f(R) function appropriate for the CTI RR Lyrae survey. The resulting calculated functions matched the input functions to within the calculated errors.

The space density was calculated at the position of every RRab type star using Equations 6.5 and 6.6. The errors in R and *a* were taken to be the standard deviation of the individual distances going into the calculation. The error in

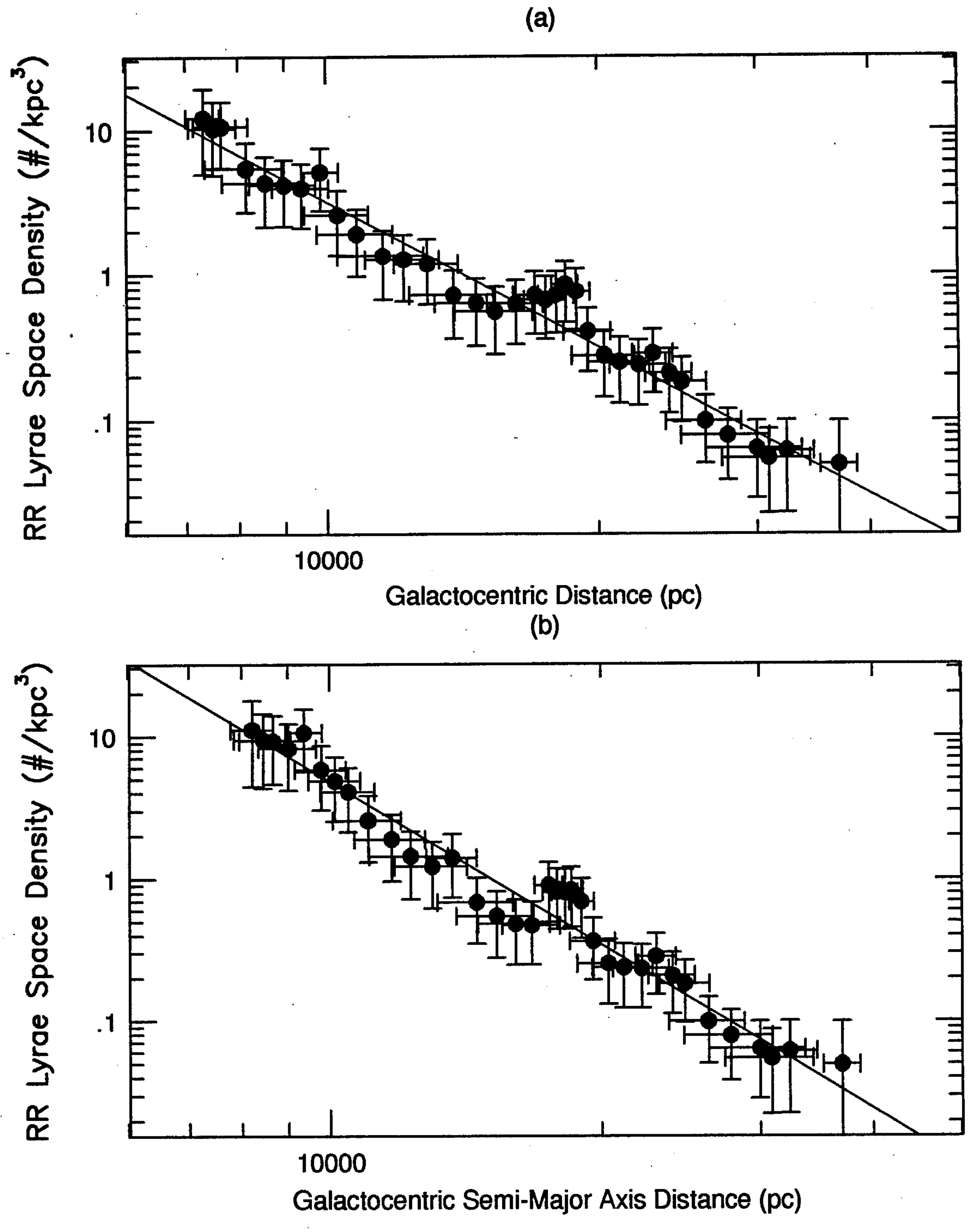


Figure 6.5 - RR Lyrae Space Density in #/kpc$^3$ versus (a) Galactocentric radial distance and (b) Galactocentric semi-major axis distance for the CTI RR Lyrae survey. Solid lines correspond to best-fit linear regression.

$\rho$ was calculated from the errors in R or $a$, the error in f (taken to be the standard deviation of the values of f for the stars used in calculating (dN/dR) or (dN/da)), and in (dN/dR) or (dN/da) (taken to be 100%/sqrt(# of points)). Figure 6.5 plots the calculated space densities as a function of Galactocentric radial distance and Galactocentric semi-major axis distance for RRab type variables in the CTI survey.

The most distant data points in Figure 6.5 correspond to an estimated most probable value given the faint limiting magnitude of the CTI survey. In other words, what must the space density be for no RR Lyrae stars to have been observed to the faint limiting magnitude. This space density was calculated by taking one over the volume of space surveyed beyond a distance midway between the two faintest RR Lyrae stars observed. The error in this space density is assumed to be 100%.

The solid lines in Figure 6.5 correspond to the best fit linear regression to the data, and are $\log(\rho) = (13.861 \pm 0.471) - (3.336 \pm 0.112)\times\log(R)$ and $\log(\rho) = (15.705 \pm 0.557) - (3.757 \pm 0.132)\times\log(a)$ for Figure 6.5(a) and (b) respectively. These results are commensurate with other RR Lyrae surveys (see Chapter 6.3), and because of the wide range of Galactic latitude and longitude covered by the CTI survey, demonstrates the large scale homogeneity of the Galactic halo.

## 6.2 Other RR Lyrae Variable Star Surveys

Several other variable star surveys have calculated RR Lyrae space densities. These include the Lick RR Lyrae Survey (Kinman et al. 1965a, Lafler and Kinman 1965, Kinman et al. 1965b, 1966, 1982, 1984, hereafter papers L1 - L6), the Palomar-Groningen Variable Star Survey (Plaut 1966, 1968a, 1968b, 1970, 1971, 1973a, and Oort and Plaut 1975, papers P-G1 - P-G7), surveys of Baade's Window (Blanco 1984 and references therein), an RR Lyrae survey by Saha (Saha 1984, Saha and Oke 1985, Saha 1985, Papers S1 - S3), and an RR Lyrae survey by Hawkins (Hawkins 1984 and references therein). Table 6.2 lists the area in square degrees, the central right ascension

Table 6.2 - RR Lyrae Space Density Surveys

| Survey/Field | Area sq deg | RA | Dec | l | b | Paper |
|---|---|---|---|---|---|---|
| Lick | | | | | | |
| RR1 (MWF 361) | 29.2 | $16^h\ 22^m$ | -3° 30' | 11.0 | +29.4 | L3, L6 |
| RR2 | 29.2 | $12^h\ 26^m$ | +31° 16' | 172.7 | +84.3 | L4 |
| RR3 | 22.2 | $12^h\ 47^m$ | +28° 35' | 121.1 | +89.1 | L4 |
| RR4 | 29.2 | $13^h\ 04^m$ | +29° 55' | 64.8 | +85.9 | L4 |
| RR5 | 29.2 | $02^h\ 26^m$ | +40° 35' | 142.6 | -18.0 | L5 |
| RR6 | 29.2 | $07^h\ 38^m$ | +39° 49' | 180.0 | +26.5 | L5 |
| RR7 | 29.2 | $08^h\ 30^m$ | +39° 46' | 182.4 | +36.4 | L5 |
| Palomar-Groningen | | | | | | |
| PG1 | 42.3 | $16^h\ 04^m$ | -12° 15' | 359.0 | +28.5 | P-G1 |
| PG2 | 33.6 | $17^h\ 07^m$ | -19° 25' | 3.5 | +12.5 | P-G2, P-G3 |
| PG3 | 19.1 | $18^h\ 24^m$ | -34° 00' | 0.0 | -10.0 | P-G4, P-G5 |
| Saha | | | | | | |
| SII | 43.6 | $07^h\ 29^m$ | +39° 00' | 180.0 | +24.1 | S1-3 |
| SIII | 43.6 | $07^h\ 58^m$ | +40° 17' | 180.2 | +30.0 | S1-3 |
| SIV | 43.6 | $23^h\ 56^m$ | +32° 06' | 110.2 | -29.2 | S1-3 |
| Hawkins (H) | 16.0 | $21^h\ 28^m$ | -45° 00' | 355.0 | -47.0 | |
| Baade's Window (BW) | 0.14 | $18^h\ 00^m$ | -30° 02' | 1.0 | -3.9 | |
| CTI | 35.6 | $12^h\ 00^m$ | +28° 01' | - | - | |

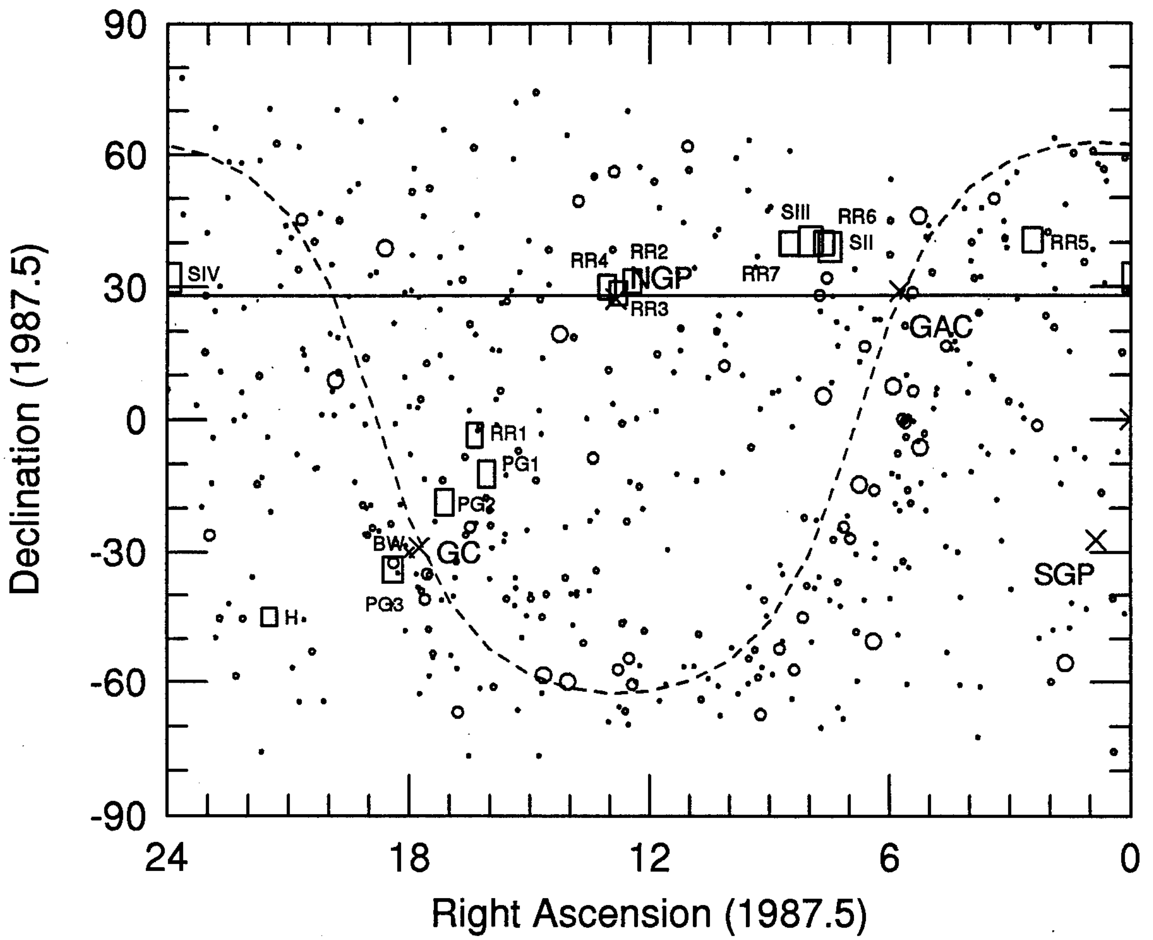


Figure 6.6 - Location of all fields listed in Table 6.2 in right ascension and declination. CTI survey strip (solid line), Galactic plane (dashed line), Galactic poles (NGP and SGP), Galactic center (GC) and Galactic anti-center (GAC) also marked.

and declination (1950 epoch), and the central Galactic longitude and latitude for each field in these surveys.

Figure 6.6 plots the position of all fields in the above surveys in right ascension and declination. Fields RR3 and RR4 in the Lick survey are slightly overlapped, thus reducing the overall area of field RR3. As done with the CTI survey, the E(B-V) maps of Burstein and Heiles (1982) were used to estimate the Galactic reddening for all fields except Baade's

Window. As a result, it was necessary to exclude from consideration portions of fields PG2 and PG3 in the Palomar-Groningen survey closer than 10° to the Galactic plane.

### 6.2.1 Lick RR Lyrae Star Survey

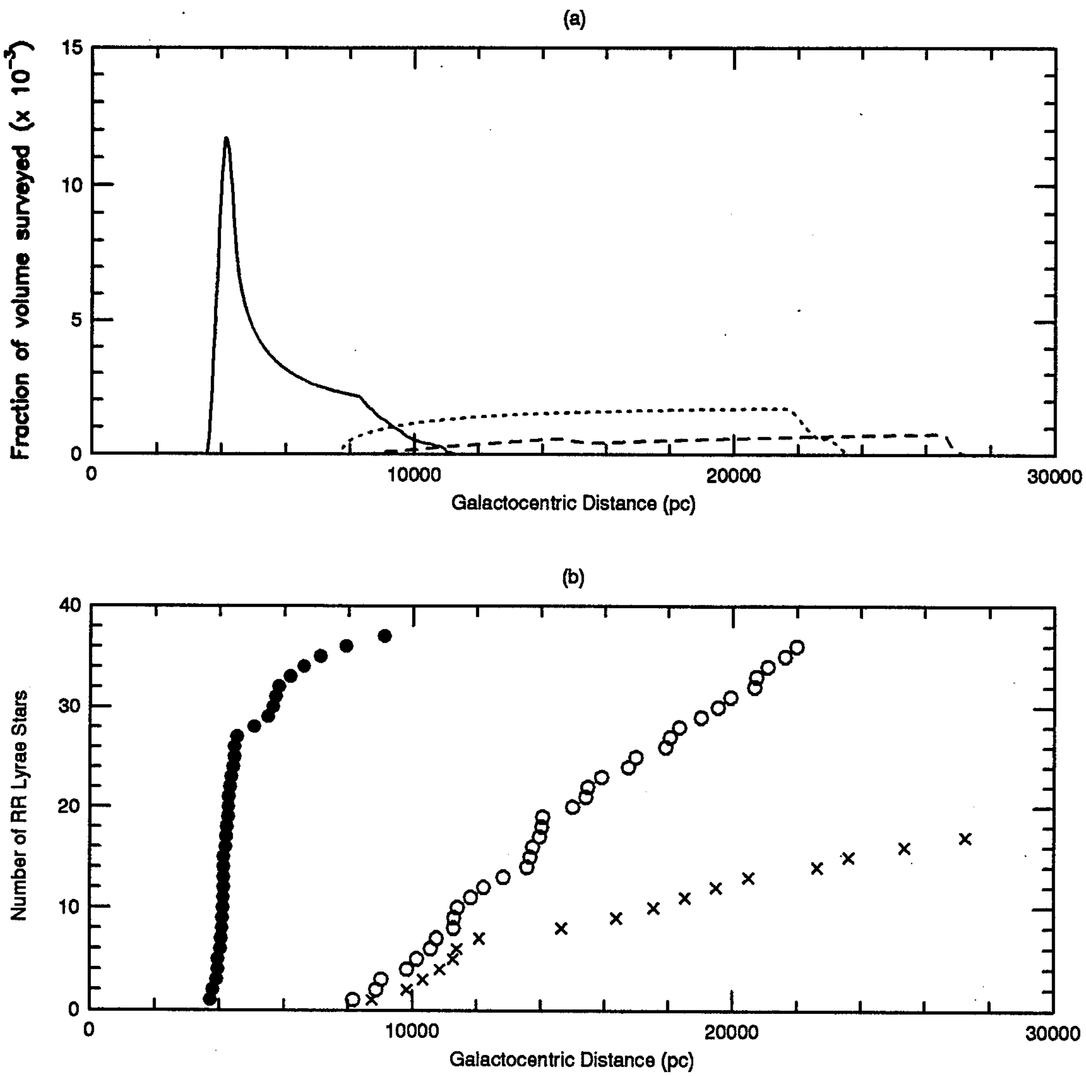


Figure 6.7 - (a) Fraction volume surveyed and (b) cumulative number of RRab stars versus Galactocentric radial distance. RR1 (solid, filled), RR2+RR3+RR4 (dotted, open) and RR5+RR6+RR7 (dashed, x's)

The Lick RR Lyrae Star Survey used the 20-inch Carnegie Astrograph at Lick Observatory and 14 x 14-inch plates to cover an area of the sky 5° 26' square for each field. The seven Lick fields listed in Table 6.2 will be considered in three separate groups corresponding to Papers L3 and L6 (RR1), Paper L4 (RR2+RR3+RR4), and Paper L5 (RR5+RR6+RR7).

Completeness as a function of magnitude for the Lick survey is described in detail in Paper L1. For RRab type variables with amplitudes greater than 0.75, the survey is 100% complete to $\langle m_{pg} \rangle = 17.0$ and reduces to 50% complete at $\langle m_{pg} \rangle = 17.7$. By not considering variables with amplitudes less than 0.75, the overall completeness for each field is 92% when compared to the Palomar-Groningen survey (taken to be the standard, as done with the CTI survey). Additionally, from the discussion in Paper L1, photographic magnitudes ($\langle m_{pg} \rangle$) will be considered identical to $\langle B \rangle$.

Figure 6.7 plots (a) the fraction of space surveyed and (b) the cumulative number of RRab type variable stars as a function of Galactocentric radial distance for RR1 (solid line and filled circles), RR2+RR3+RR4 (dotted line and open circles), and RR5+RR6+RR7 (dashed line and x's).

### 6.2.2 Palomar-Groningen Variable Star Survey

The plates for the Palomar-Groningen Variable Star Survey were all taken with the 48" Palomar Schmidt telescope. The three survey fields listed in Table 6.2 will be considered

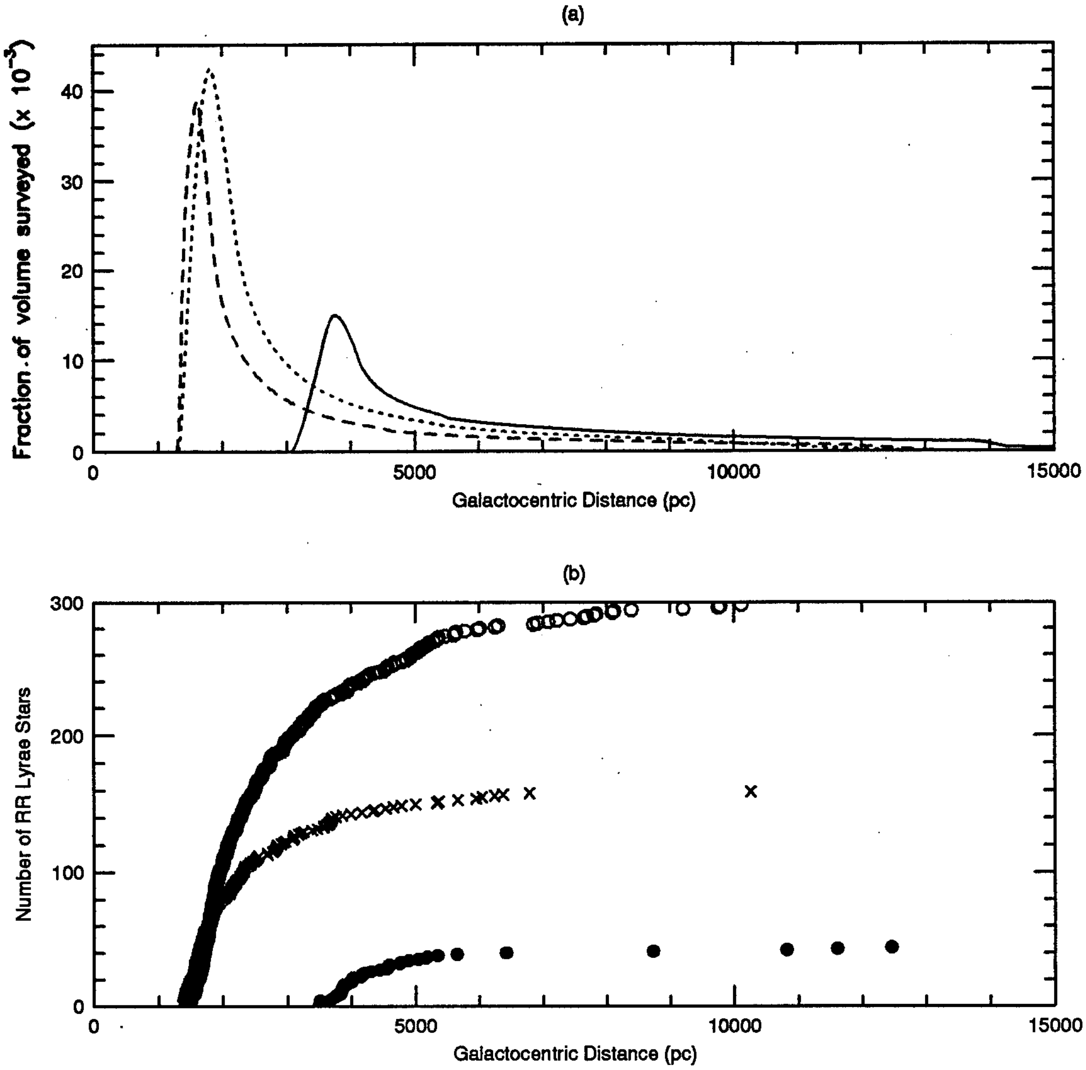


Figure 6.8 - (a) Fraction volume surveyed and (b) cumulative number of RRab stars versus Galactocentric radial distance. PG1 (solid, filled), PG2 (dotted, open) and PG3 (dashed, x's).

separately. The boundaries of fields PG2 and PG3 were modified to eliminate the region with $|b| < 10°$.

In Papers P-G1 and P-G7, the completeness as a function of amplitude and magnitude are discussed in detail. Table 3 of Paper P-G7 summarizes the results. The completeness as a

function of magnitude as outlined in Table 3 of Paper P-G7 will be used. The magnitude limits of $<m_{pg}> = 14 - 18.5$ for fields PG1 and PG2, and $<m_{pg}> = 14 - 18.0$ for field PG3, as detailed in the same paper, will also be used. As with the Lick survey, photographic magnitudes will be considered identical to $<B>$.

Only the minimum and maximum photographic magnitudes were listed for each star, and so Equation 5.2 (using the CTI values detailed in Chapter 5.5) was used to calculate a mean magnitude for each RRab type variable star.

Figure 6.8 plots (a) the fraction of space surveyed and (b) the cumulative number of RRab type variable stars as a function of Galactocentric radial distance for field 1 (solid line and filled circles), field 2 (dotted line and open circles), and field 3 (dashed line and x's).

### 6.2.3 Saha's RR Lyrae Survey

The 1.2-m Schmidt telescope at Palomar with 14 x 14-inch photographic plates was used to observe each field in Saha's RR Lyrae survey. The resulting fields covered an area of sky 6° 36' square. All three of Saha's fields will be considered together.

Saha describes completeness calculations in detail with the final results of completeness as a function of period shown in Figure 2 of Paper S1 (similar to Figure 5.5 of this dissertation). Using this figure for periods 0.4 to 0.7 days

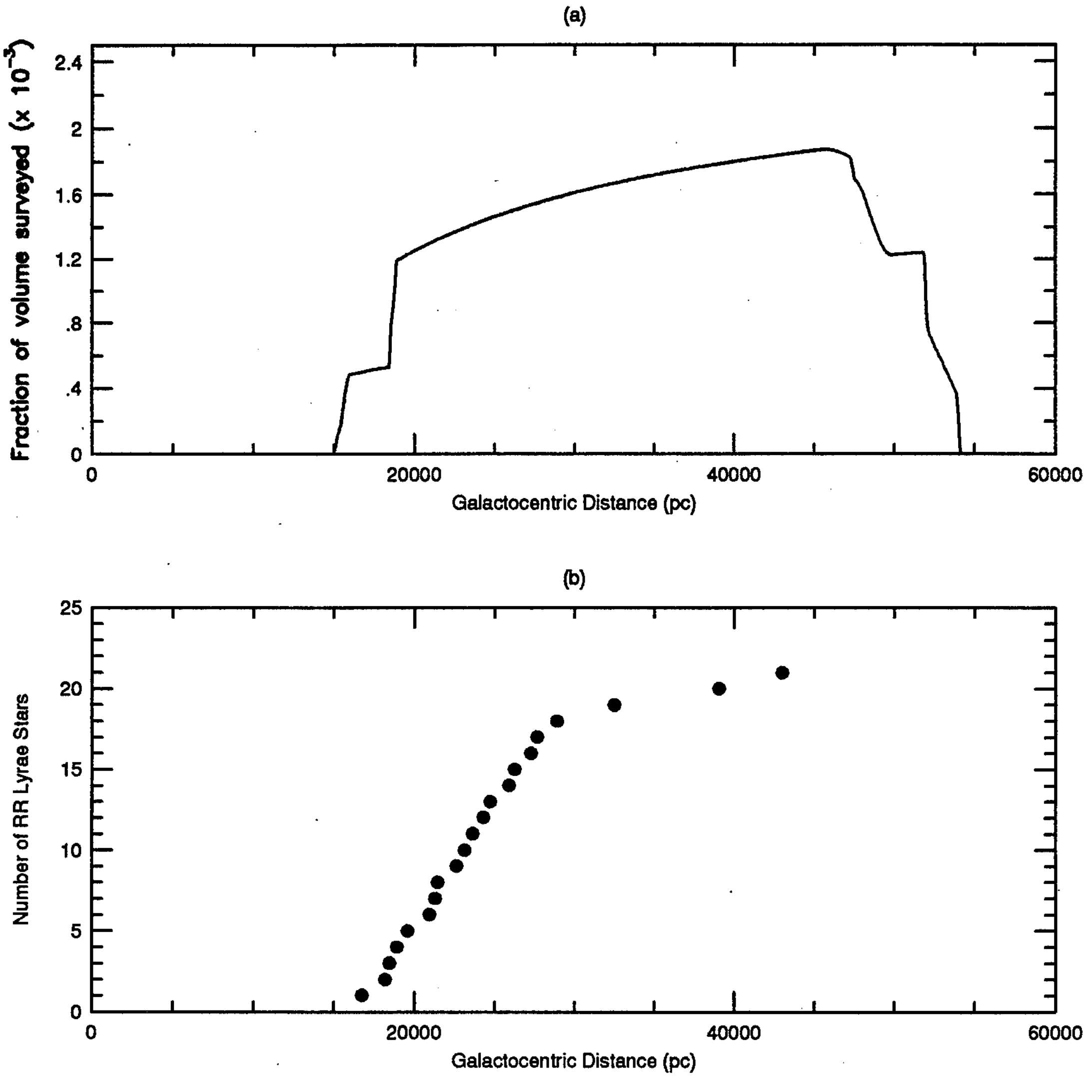


Figure 6.9 - (a) Fraction volume surveyed and (b) cumulative number of RRab stars versus Galactocentric radial distance for Saha's survey.

(as done with the CTI survey), Fields SII, SIII, and SIV are estimated to be 85%, 78%, and 73% complete respectively. The magnitude limits for all three fields are <B> = 16.5 - 19.5.

Figure 6.9 plots (a) the fraction of space surveyed and

(b) the cumulative number of RRab type variable stars as a function of Galactocentric radial distance for all of Saha's fields.

### 6.2.4 Hawkins' RR Lyrae Survey

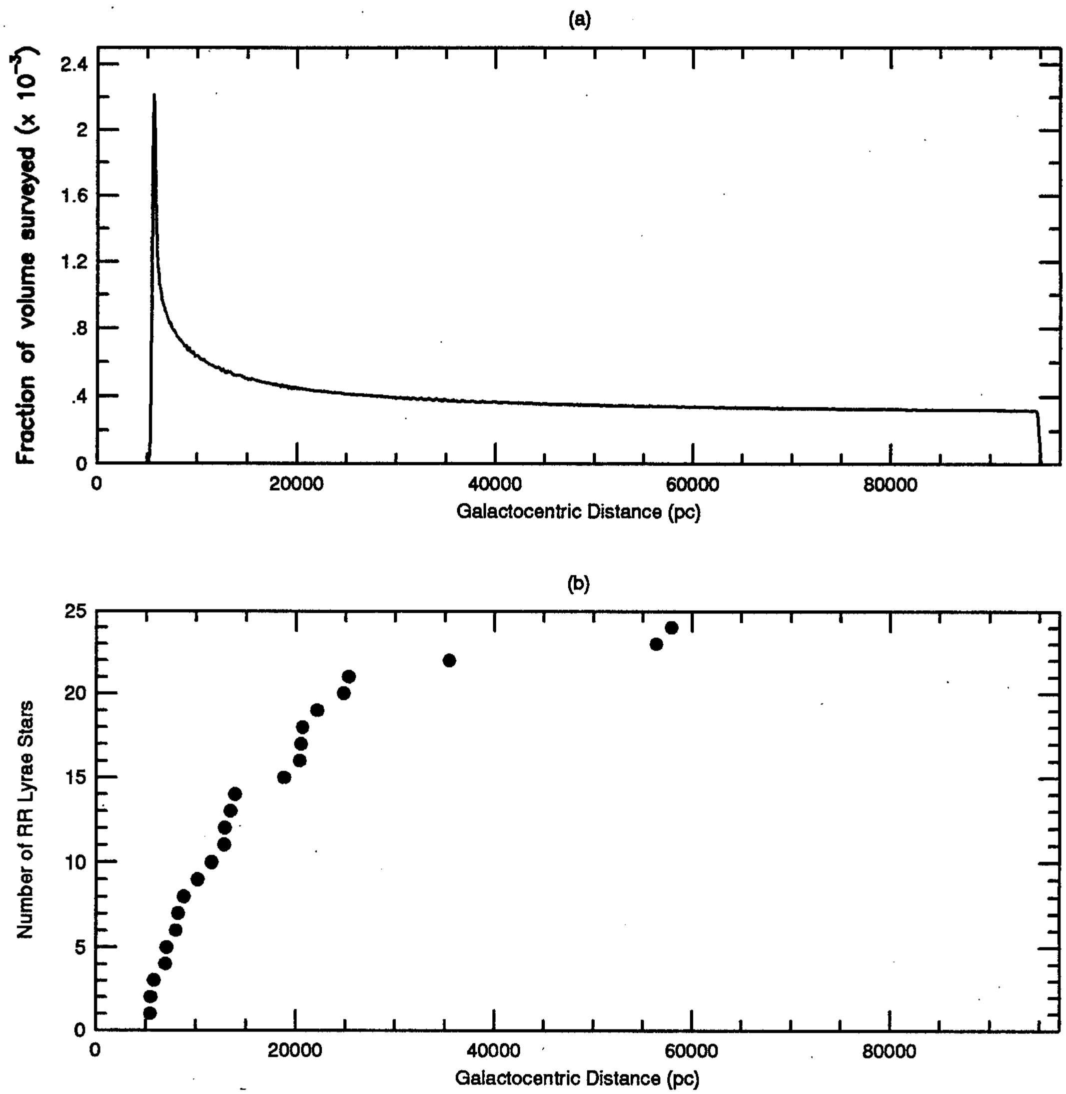


Figure 6.10 - (a) Fraction volume surveyed and (b) cumulative number of RRab stars versus Galactocentric radial distance for Hawkins' survey.

Photographic plates taken with the UK 1.2-m Schmidt telescope in Australia and scanned with the COSMOS measuring machine were used by Hawkins to detect RR Lyrae variable stars (Hawkins 1984). The magnitude limits of his survey are <B> = 14.0 - 21.0, but no discussion of completeness is given.

To estimate the completeness, the detectable fraction of RR Lyrae stars as a function of period for different amplitudes of variation was first calculated. This was done using a synthetic RRab type variable star of a particular amplitude observed at the times listed in Table 1 of Hawkins 1984, and requiring the rms variation in magnitude with the extreme data point removed to be greater than 0.2 (Hawkins' selection criteria as described in Hawkins 1984). Using the distribution of RRab type variables as a function of amplitude of variation from the RR Lyraes in the Palomar-Groningen survey as representing the true distribution (as done with the CTI survey), the completeness of Hawkins' survey is 74%.

Figure 6.10 plots (a) the fraction of space surveyed and (b) the cumulative number of RRab type variable stars as a function of Galactocentric radial distance for Hawkins' survey field.

### 6.2.5 Baade's Window RR Lyrae Survey

Baade's Window is a region of relatively small Galactic absorption centered on the globular cluster NGC 6522 approximately 4° from the Galactic center. Baade's original

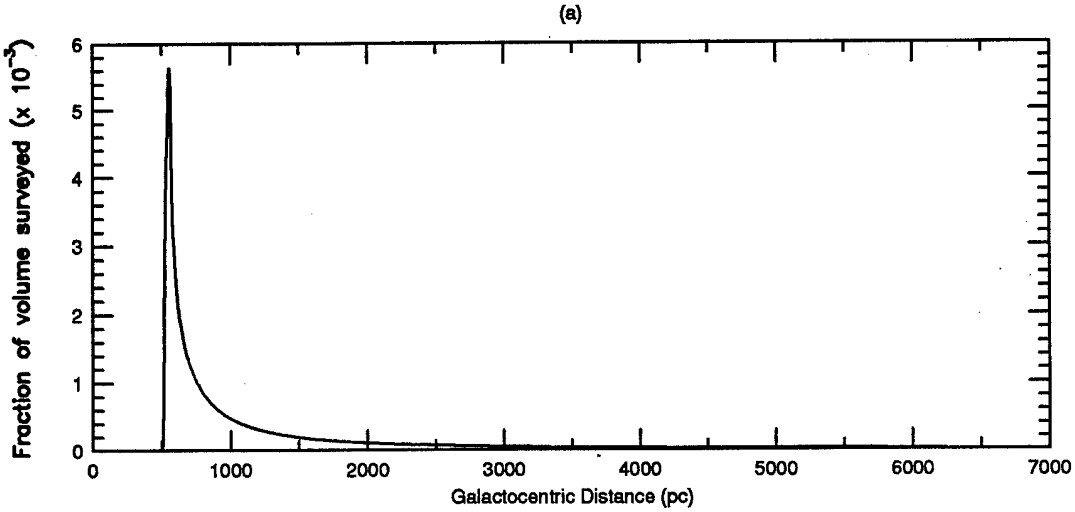


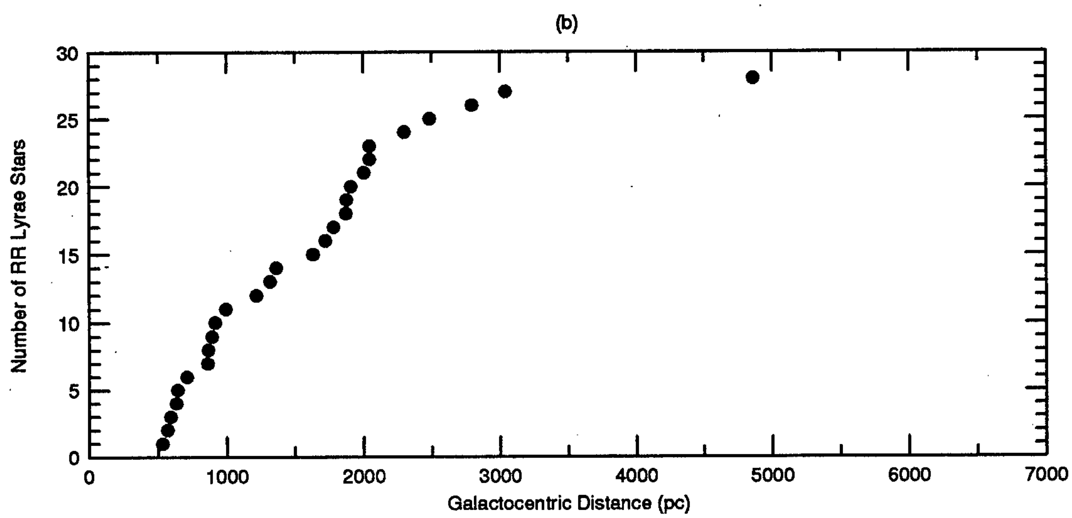


Figure 6.11 - (a) Fraction volume surveyed and (b) cumulative number of RRab stars versus Galactocentric radial distance for region W of Blanco's survey of Baade's window.

survey for RR Lyrae variable stars was from Mt. Wilson Observatory and suffered from incorrect period determinations due to period aliasing to the sidereal day. Many investigators have accomplished subsequent observations in order to redetermine the RR Lyrae periods (Blanco 1984 and

references therein). Blanco's survey was accomplished using photographic plates with the CTIO's 1.5-m telescope.

The Galactic reddening of the globular cluster NGC 6522 has been estimated at 0.45 ± 0.03 (van den Bergh 1971). Because of a possible east-west absorption gradient (van den Bergh 1971), only region W in Figure 1 of Blanco (1984), corresponding to the NGC 6522 field, is considered. Blanco (1984) gives a faint magnitude limit of $\langle B \rangle = 18.5$, and argues that the completeness is ≈100% in light of the great deal of attention given to discovering RR Lyrae stars in this region.

Figure 6.11 plots (a) the fraction of space surveyed and (b) the cumulative number of RRab type variable stars as a function of Galactocentric radial distance for region W of Blanco's survey.

### 6.2.6 Local RR Lyrae Space Density

The local RR Lyrae space density, (or at least a lower limit to the local space density due to possible incompleteness), can be calculated and compared to the results obtained from the other surveys by using RR Lyrae data contained in the General Catalog of Variable Stars (GCVS) (Kholopov 1985-88). First, a list of all RR Lyrae stars in the GCVS with a minimum apparent magnitude brighter than 11.5 and greater than 10° from the Galactic plane was made. After calculating the average apparent magnitude with Equation 5.2 and estimating the Galactic reddening of each star from the

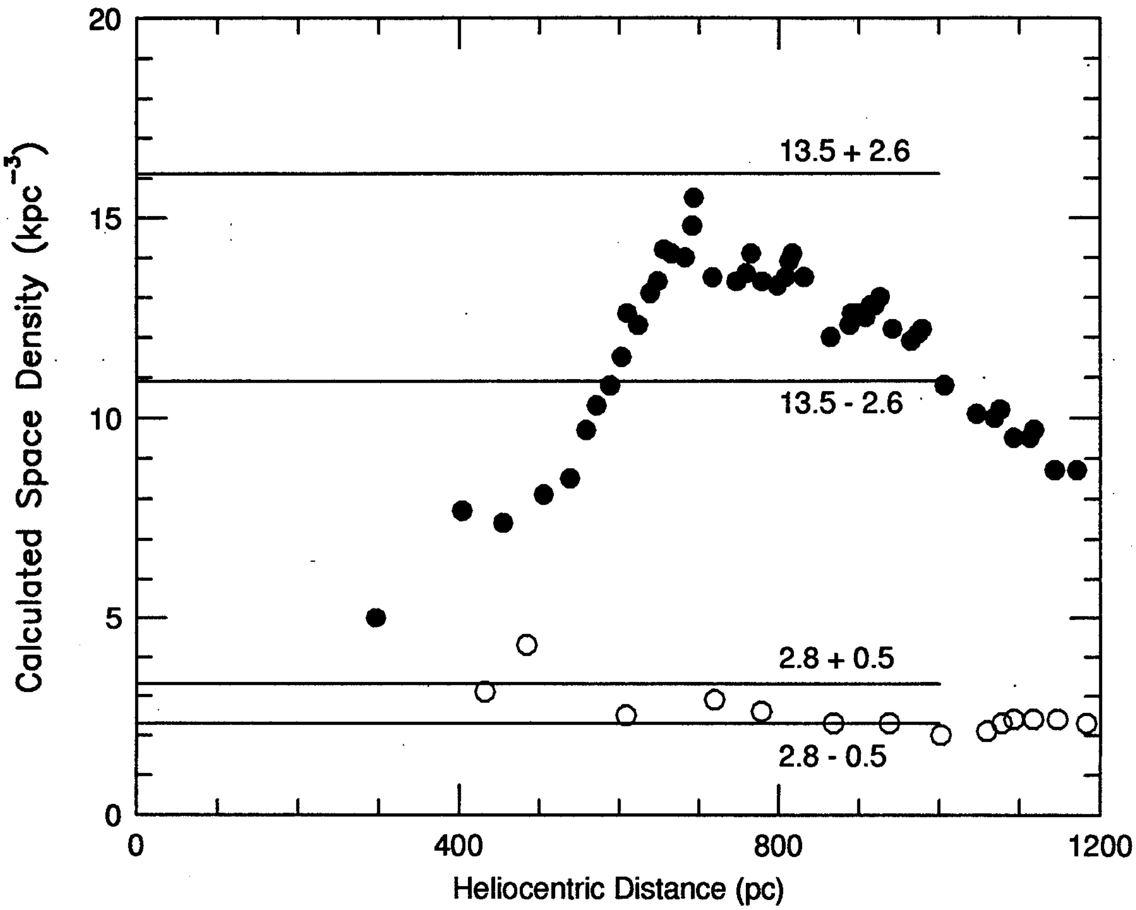


Figure 6.12 - RR Lyrae space density in kpc$^{-3}$ versus heliocentric distance for bright RRab type variables (filled circles) and bright RRc type variables (open circles) in GCVS.

E(B-V) maps of Burstein and Heiles (1982), a heliocentric distance was calculated to each. Since the magnitudes of all these stars are listed as visual estimates in the GCVS, an absolute magnitude of $\langle M_V \rangle = 0.74$ was assumed. For each RR Lyrae, the space density was determined by dividing the number of stars interior to the RR Lyrae's heliocentric distance by the volume enclosed by the star. This was done for RRab and RRc type variables seperately. The variable star name, right

ascension, declination, type, minimum, maximum and mean magnitude, Galactic absorption, and heliocentric distance are listed in Table A1.12 of Appendix 1.

Figure 6.12 plots the calculated space density versus heliocentric distance for these bright RRab type variables (filled circles) and RRc type variables (open circles). The decreasing space density for the RRab type variables with heliocentric distances greater than 800 pc is probably due to incompleteness of the GCVS for fainter magnitudes. The local RR Lyrae space density was estimated by simply taking the number of RR Lyrae stars within 800 pc divided by the volume enclosed, resulting in 13.5 +/- 2.6 $kpc^{-3}$ for RRab type variables, and 2.8 +/- 0.5 $kpc^{-3}$ for RRc type variables. The error in these values was taken to be 100%/sqrt(# of stars). These values include both halo and potential "thick disk" (Zinn 1985, Suntzeff et al. 1991) RR Lyrae stars (see Chapter 6.3), and are commensurate with similar calculations in Paper L3 (10.8 $kpc^{-3}$ for RRab using $M_B = 1.0$ with $\Delta B > 0.75$) and by Preston et al. 1991 (10-13 $kpc^{-3}$ for all RR Lyrae stars using $M_V = 0.6$ and [Fe/H] < -1.0).

### 6.2.7 Miscellaneous Surveys

A few RR Lyrae surveys were not considered due to a lack of information in the corresponding paper necessary to calculate the completeness of the survey. These are a survey centered on the globular cluster NGC 6304 at l=356°, b=+5°

(Hartwick et al. 1981), a survey centered on a Galactic bulge window at $l=1°$, $b=-6°$ (Blanco 1992), and a survey centered on the south Galactic cap (Stobie et al. 1986). The second survey listed also does not currently have any information concerning the Galactic reddening in the field.

## 6.3 RR Lyrae Space Densities

Calculations identical to those described in Section 6.1 for the CTI survey can be carried out for all the other surveys listed in Table 6.2. The different completeness of each survey was accounted for when calculating the functions f(R) and f(a) of Equations 6.5 and 6.6 respectively. The most distant space density in the Saha and Hawkins surveys correspond to most probable values determined in the same way as for the CTI survey.

To lessen the confusion, data from individual stars in each survey were divided into bins equally spaced in log(R) (or log(a)) and averaged. Figure 6.13 plots the RR Lyrae space density as a function of Galactocentric radial distance for RRab type variables in the CTI survey (open circles), Lick survey (open squares), Palomar-Groningen survey (filled triangles), Saha's survey (open triangles), Hawkins' survey (x's), Baade's Window survey (filled circles) and the local space density (filled square). The best-fit least squares linear regression for the data is

$$\log(\rho)=12.237(0.299)-3.024(0.077)\times\log(R) \qquad (6.8)$$

where the calculated error for the intercept and slope is given in parentheses.

Figure 6.14 plots the same data as a function of Galactocentric semi-major axis distance. Clearly, using an ellipsoidal distribution for smaller Galactocentric distances yields greater agreement among surveys. This is most

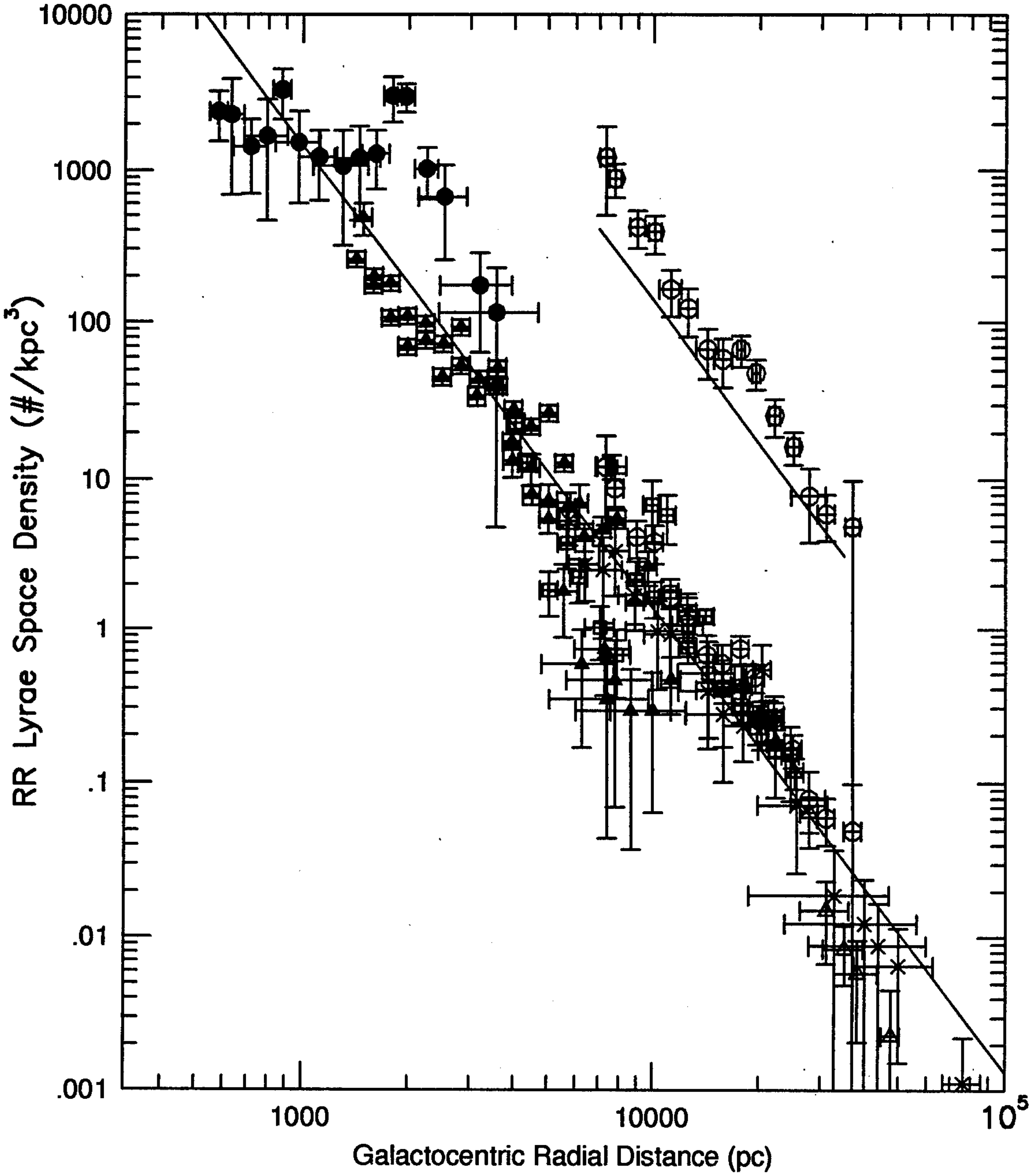


Figure 6.13 - RR Lyrae space density in #/kpc$^3$ versus Galactocentric radial distance for CTI survey (open circles), Lick survey (open squares), Palomar-Groningen survey (closed triangles), Saha's survey (open triangles), Hawkins' survey (x's), Baade's Window survey (closed circles) and the local space density as determined from the GCVS (open square). Solid line corresponds to best-fit linear regression. A second set of CTI survey points two orders of magnitude above actual value are also plotted for clarity.

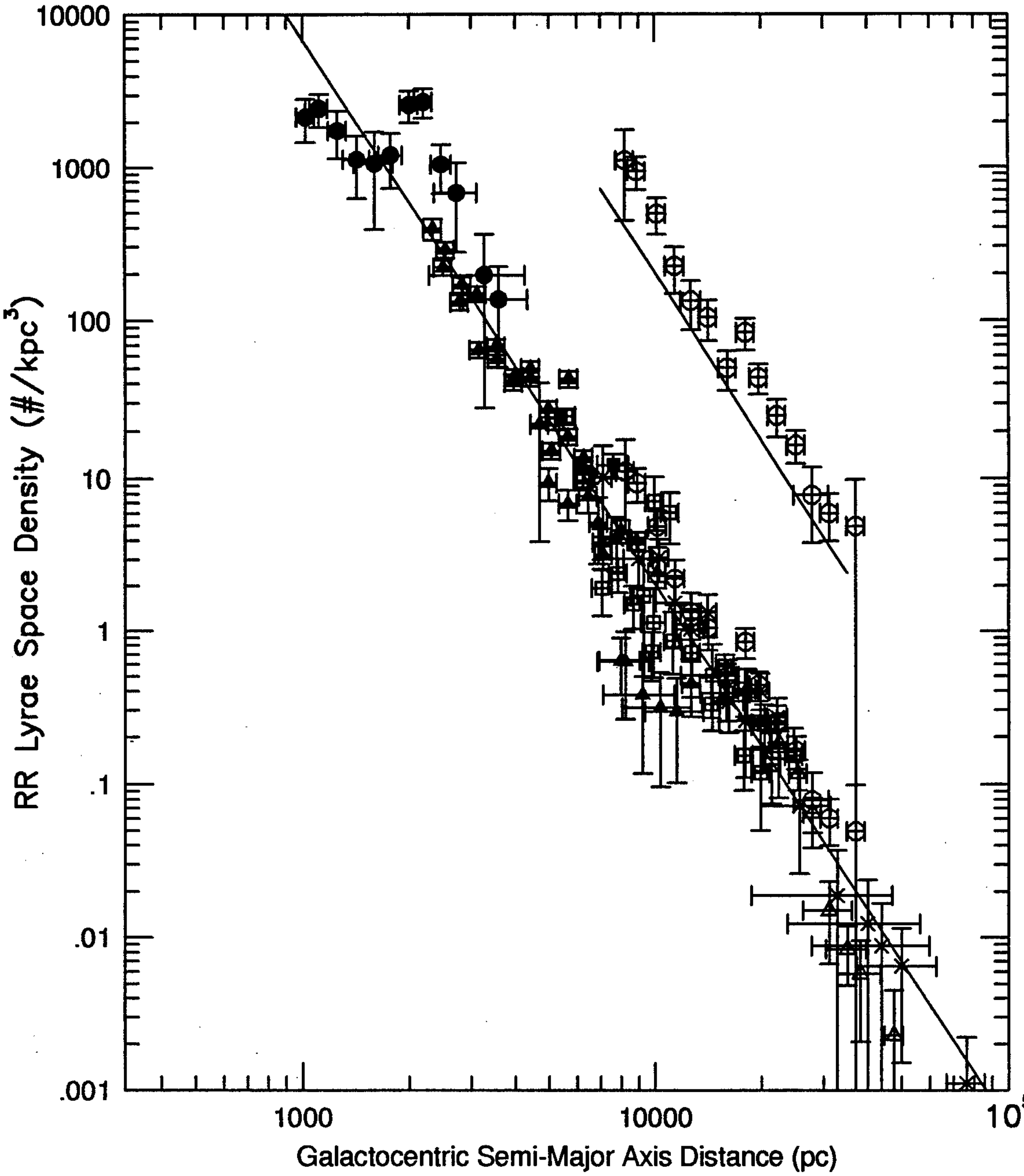


Figure 6.14 - RR Lyrae space density in #/kpc$^3$ versus Galactocentric semi-major axis distance for CTI survey (open circles), Lick survey (open squares), Palomar-Groningen survey (closed triangles), Saha's survey (open triangles), Hawkins' survey (x's), Baade's Window survey (closed circles) and the local space density as determined from the GCVS (open square). Solid line corresponds to best-fit linear regression. A second set of CTI survey points two orders of magnitude above actual value are also plotted for clarity.

evident between the Baade's Window and Palomar-Groningen surveys (~1-3 kpc). The best fit linear regression for this

$$\log(\rho)=14.425(0.307)-3.530(0.077)\times\log(a) \qquad (6.9)$$

data is

where again the calculated error is given in parentheses.

Although it is clear the mean RR Lyrae space density falls off with a power law distribution, the RR Lyrae space density does vary locally. Kinman noticed in field RR5 of the Lick survey (Paper L5), that all the RR Lyrae variable stars were concentrated on one half of the field. All the survey fields display systematic deviations from the best-fit linear regression at certain distances, suggesting a halo distribution that is clumpy, with locally overdense and underdense regions of RR Lyraes, but retaining an overall power law decrease with increasing distance.

The space densities at the Sun's Galactocentric distance (7.6 kpc) is of particular interest, spanning nearly two orders of magnitude. The local space density as calculated from the GCVS is 4.2 and 2.5 times above that expected for the spherically symmetric (Equation 6.8) and ellipsoidal (Equation 6.9) distributions respectively. If the local RR Lyrae stars are divided into halo and "thick disk" (defined as [Fe/H] > -0.8 with z < 1.5 kpc) components (Suntzeff et al. 1991), the space density of the halo RR Lyrae stars is still 3.0 or 1.8 times that expected. To explain this anomalously high value,

it has been suggested there exists a new population of metal-poor ([Fe/H] < -0.8) RR Lyrae stars with very low scale height from the Galactic disk (Preston et al. 1991). The CTI survey space density at R = 7.6 kpc (z > 4 kpc and well outside the thick disk), however, agrees well with the GCVS value, indicating that the local space density of RR Lyrae stars is not as anomalous as once thought. The space density at 7.6 kpc as calculated from Hawkins' survey and field PG2 of the Palomar-Groningen survey agree well with Equations 6.8 and 6.9, while the space densities for field RR1 of the Lick survey and fields PG1 and PG3 of the Palomar-Groningen survey are about 1/10th that expected. Because this distance roughly corresponds to the faint magnitude limits of the Lick and Palomar-Groningen fields, it's possible the measured underdensities are an artifact of incorrectly estimating the completeness as a function of magnitude. The other fields of the Lick survey and field PG2 of the Palomar-Groningen survey, however, do not show a commensurate underdensity at their faint magnitude limit. It's also possible the underdensities are caused by difficulties in discovering faint RR Lyraes in a crowded field, although again, field PG2 is very crowded and does not show an underdensity. The space density as calculated from field PG1 of the Palomar-Groningen survey even displays a flattening out and increase near its faint magnitude limit that would possibly bring it back to the best-fit line if the survey was extended to fainter magnitudes.

Although it's not possible from the present data to know for certain, the evidence suggests these deviations may indeed be real.

Another example of a significant underdensity can be found in Saha's survey beyond 25 kpc where the calculated space densities are systematically lower than the best fit power law. It is possible this underdensity is similar in origin to the underdensities found at 10 kpc, although as Saha suggested, the distribution beyond 25 kpc may be expressed by a different power law than that of the inner halo. Indeed at some distance, the space density would be expected to fall off precipitously as the effects of other galaxies begin to strip the Milky Way of its most distant members. The Large and Small Magellanic Clouds (LMC and SMC) are suggestively only twice the distance from the Galactic center as the distance where Saha's RR Lyrae space density begins to drop. The globular cluster distribution displays a similar underdensity starting at $\approx$20 kpc, with no globular clusters in the region 33 kpc $< R <$ 60 kpc, again corresponding to the LMC and SMC Galactocentric distance. The globular clusters beyond 60 kpc, however, display space densities consistent with the $R^{-3.5}$ densities calculated for clusters at 4 $< R <$ 20 kpc (Harris 1976, Zinn 1985). Due to this underdensity as well as chemical and structural differences between the distant and nearby globular clusters, Harris (1976) has even suggested that the Milky Way's globular cluster system ends at $R \approx$ 40

kpc and that the more distant clusters constitute a separate group perhaps related to the dwarf elliptical galaxies at similar distances. Although it's conceivable the underdensity of globular clusters and possible underdensity of RR Lyrae stars at the LMC and SMC's Galactocentric distance is the result of chance, it is equally plausible the underdensity is the direct result of a dynamical interaction. If the latter is correct, the underdensity could simply be the 1:1 resonance gap created by the Magellanic Clouds. The RR Lyrae space density as calculated from Hawkins' survey and the CTI survey do not fully support the conclusion of an RR Lyrae underdensity beyond 25 kpc. Due to the small number of RR Lyraes discovered at these distances (nine with R > 30 kpc in these surveys), however, clearly other deep surveys for RR Lyraes are needed.

Indeed, deep surveys can clear up many of the questions addressed above. Of particular interest would be extending the search for RR Lyrae variable stars in and near the RR1 field of the Lick survey and field PG1 of the Palomar-Groningen survey to see if the calculated space densities indeed return to the calculated best fit power law, or if more RR Lyraes are found to fill in the underdensity if it is indeed caused by incompleteness. As stated in the last paragraph, deeper surveys will also add to the number of stars past 25 kpc to better define the space densities at these distances. Perhaps the most promising survey would be one at

$-30^{\circ}$ declination using a CTI-like telescope. This survey would pass over Baade's Window, close to the Galactic center and Galactic south pole, providing consistent photometry and completeness over a much larger range of Galactocentric radial distances than provided by any previous survey field.

## Chapter 7 Mass Distribution of the Milky Way

In the previous chapter, the Galactocentric position of each RR Lyrae variable star in the CTI RR Lyrae survey was calculated. If in addition to this positional information, the star's velocity is determined for all three dimensions, an estimation of the mass interior to the star's orbit can be accomplished.

The total energy of a star in orbit about the center of the Milky Way is simply

$$E=\frac{1}{2}mv^2-\frac{GM(R)\,m}{R}, \tag{7.1}$$

where m is the star's mass, v is the star's velocity, and M(R) is the Milky Way's mass at Galactocentric distance R. If for a given star's orbit the Milky Way's mass can be approximated as being concentrated at the Galactic center, Equation 7.1 and the energy of a Keplerian orbit of given eccentricity ($E = -GMm(1 - e^2)/2R$, where e is the eccentricity of the star's orbit) can be combined and solved for M(R) giving,

$$M(R)=\frac{Rv^2}{(1+e^2)\,G}. \tag{7.2}$$

With a precise knowledge of R and v, the mass of the Milky Way at the Galactocentric distance R can be calculated to within a factor of two, assuming the star is in a bound orbit with a value of e between e = 0 (circular orbit) and e = 1 (parabolic orbit).

The calculation of R from the magnitude and position of

each star was accomplished in the previous chapter. In this chapter, preliminary results calculating the space velocity for RR Lyrae variable stars will be presented. First, the possibility of using astrometry to determine the proper motion of the RR Lyrae stars relative to the local standard of rest is examined. Next, radial velocity measurements of CTI RR Lyrae stars are presented. Finally, the mass of the Milky Way as a function of Galactocentric distance as calculated using Equations 7.2 is given.

## 7.1 - RR Lyrae Astrometry

In addition to the photometric information compiled in the CTI databases for each star in the CTI survey strip, there exists astrometric information as well. Seasonal variance-weighted positions for a given object can be calculated using the nightly luminosity weighted positions (YCTI and XCTI), second moments (XX and YY), and calibrated luminosity and luminosity error (LUM and LUMERR), all contained in the CTI **.NHL** database.

The variance of the position in right ascension (YCTI) or declination (XCTI), however, is the second moment (XX or YY respectively) divided by the *uncalibrated* total luminosity. It was necessary to calculate the uncalibrated total luminosity from the calibrated luminosity and luminosity error. The uncalibrated luminosity and error (L and $\sigma_L$) and the calibrated luminosity and error (C and $\sigma_C$) are related through the luminosity scaling factor (dl, contained in the **.CAL** database on a minute-by-minute basis, see Chapter 3.5.2), namely, $C = dl \times L$ and $\sigma_C = dl \times \sigma_L$. Using $\sigma_L^2 \propto L$, this leads to $L \propto C^2/\sigma_C^2$, resulting in a positional variance of $\sigma_{XCTI}^2 \propto (XX \times \sigma_C^2)/C^2$. The error in the seasonal position was calculated by taking the standard deviation of the individual measurements from the calculated weighted mean added in quadrature to a measurement error of 0.5 centipixels.

Figure 7.1 plots the total positional error $(\sigma_{XCTI}^2 + \sigma_{YCTI}^2)^{1/2}$ of the seasonal position in centipixels versus

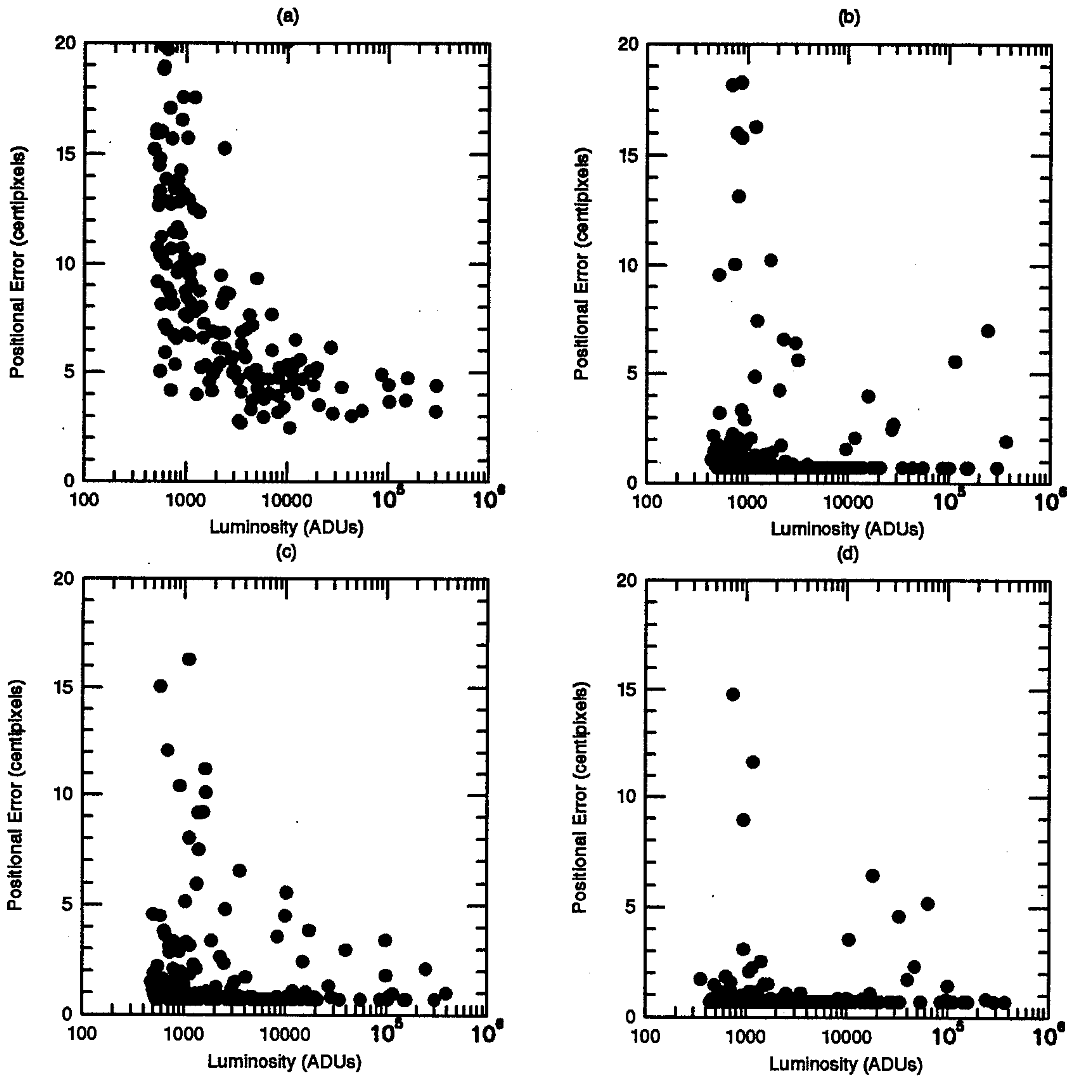


Figure 7.1 - Positional error in centipixels versus instrumental luminosity in ADUs for field near north Galactic pole. (a) 1987-1988 observing season, (b) 1988-1989 observing season, (c) 1989-1990 observing season, (d) 1990-1991 observing season.

instrumental luminosity (in ADUs) for several objects with more than one observation in a sample field for (a) the 1987-1988 observing season, through (d) the 1990-1991 observing season. As expected, the error in position decreases for

increasing luminosity. Previous astrometry with CTI (Benedict et al. 1991), using early uncalibrated CTI data reported errors commensurate with those seen in Figure 7.1(a). It is not clear why the positional calibration improved after the first full year of operation, as seen in Figures 7.1(b) through (d). A number of stars in these seasons actually show no scatter in position. Either the scatter is sub-centipixel, or the position has somehow been quantized during data reduction. An in-depth analysis of positions throughout the reduction process is required to examine this question, although is not necessary for the present purposes.

The positions of objects in the CTI Survey strip for all four seasons of CTI operation can be compared to positions obtained from the Palomar Observatory-National Geographic Sky Survey (POSS). The copies of the E and O POSS plates at the University of Texas at Austin were scanned with the McDonald Observatory PDS Microdensiomter Automated Inventory System (Benedict and Shelus 1978). The scanned image was then ported into IRAF to measure the centroids of all the stars. These measurements were kindly carried out by Dr. G. F. Benedict and associates.

The process of overlapping the CTI and POSS positional data is described in detail in Benedict et al. 1991. The program GAUSSFIT (Jeffreys et al. 1989) is used to determine simultaneously the least-squares fit of all plate parameters (scale, offset and rotation) and relative proper motions for

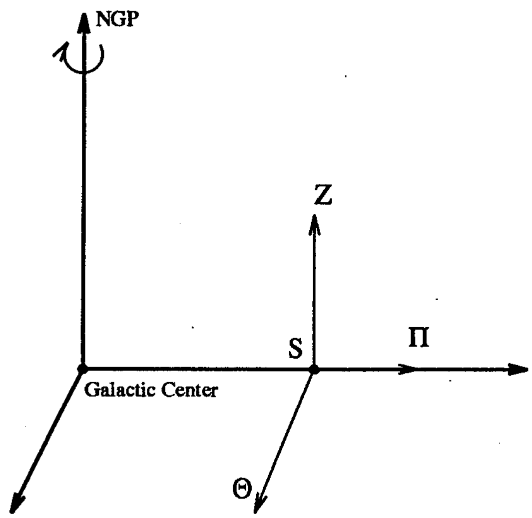


Figure 7.2 - Definition of velocity components in Galactocentric cylindrical coordinate system

all stars, where the "plates" are the four CTI positions and the two POSS positions (from the E and O POSS plates separately).

The measured relative proper motions are relative to the mean motion of the sample of stars within the field used in the calculations. If this sample is dominated by nearby disk stars, the resulting sample's space motion can be approximated by the motion of the local standard of rest (LSR). A cylindrical coordinate system centered at the Galactic center (R, θ, z), with Π, Θ, and Z the respective velocities, will be used, as shown in Figure 7.2. The LSR velocity at a given radius is defined as the velocity of a circular orbit ($\Pi = 0$, $Z = 0$, $\Theta = \Theta_0$) for an axisymmetric time-independent Galactic mass distribution (resulting in only a constant radial gravitational force). Peculiar velocities are defined as the velocities relative to the LSR ($u = \Pi - \Pi_{LSR}$, $v = \Theta - \Theta_{LSR}$, and $w = Z - Z_{LSR}$). It is the tangential component of these peculiar velocities of the RR Lyrae stars (as measured against the Sun's local standard of rest) combined with the peculiar velocity of the Sun with respect to the LSR that is measured astrometrically for each

star. It is necessary to transform to the rest frame of the Galactic center using knowledge of the space velocity of the LSR and the Sun's peculiar velocity. Many studies have been done using measured radial velocities of objects in the Galactic halo as well as external galaxies, yielding an LSR space velocity of $\Theta_0 = 250 \pm 25$ km/s (Mihalas and Binney 1981). The Sun's peculiar motion (as calculated against the most commonly measured velocities for stars in the solar neighborhood) is u = -9 km/s, v = 11 km/s and w = 6 km/s (Mihalas and Binney 1981).

The CTI field surrounding the RR Lyrae star DV Com was used to test the astrometric accuracy and precision of combined CTI and POSS data. This star was chosen because it is the brightest RR Lyrae variable star near the north Galactic pole, and a halo star near the Galactic poles represents the best chance of measuring a RR Lyrae proper motion relative to the LSR. For a $\Theta_{LSR} = 250$ km/s, r = 6.36 kpc and assuming $\Theta_{halo} = 0$ km/s, DV Com's relative proper motion should be ≈8 mas/year (milliarcseconds per year) directed away from b = 0°, l = 90°.

No significant relative proper motion was measured for DV Com. The standard deviation in all relative proper motions for the DV Com field was 9 mas/year (as compared to Benedict et al.'s 5 mas/year calculation). This higher value may be a result of actual relative proper motions within the field. Disk stars with peculiar velocities comparable to the Sun's

would have relative proper motions of up to 7 mas/year at 500 pc and up to 33 mas/year at 100 pc. Taking Benedict et al.'s value of 5 mas/year as the obtainable accuracy and precision for combined CTI and POSS data, the error in a space velocity measurement as a function of heliocentric distance would be $\sigma = (0.023 \times r)$ km/s where r is measured in parsecs. This corresponds to a 150 km/s error for the closest RR Lyrae in the CTI survey strip. In light of this, and the further research necessary regarding CTI position measurements, space velocity measurements from relative proper motions will not be pursued for the CTI RR Lyrae stars in this dissertation.

## 7.2 - RR Lyrae Spectroscopy

Several RR Lyrae stars discovered in the CTI survey were observed with McDonald Observatory's 2.7-m (f/18) telescope using the Large Cass Spectrometer (LCS) on UT 94 Oct 7 - 10 to measure radial velocities. RR Lyrae metallicity standards, (Liu and Janes 1989, Layden 1994) SW And, XX And, DX Del, RR Cet, and RR Gem were observed for future calculation of the metallicity index $\Delta S$, and will also serve as RR Lyrae velocity standards. All RR Lyraes were observed at a phase near minimum light. The velocity standards HR-458 and HR-2047 and flux standard G191-B2B were also observed.

Because of the low throughput of the LCS, it was necessary to use a low dispersion grating (300 l/mm). Details of the instrumentation and resulting coverage of the spectra are given in Table 7.1. Every object spectra (RR Lyraes and standards) were bracketed by argon comparison lamp spectra.

The data were reduced using IRAF with the final spectra

Table 7.1 - McDonald Observatory Operating Parameters

Telescope: McDonald Observatory's 2.7-m
    f/18
Instrument: Large Cass Spectrometer
Detector: TI1V5C
    800 x 800 x 15 $\mu$m pixels
    15 $e^-$ readout noise
Grating: #40 (1st order)
    300 l/mm
    420 nm blaze
Wavelength coverage: 320 - 600 nm
Dispersion: 0.3379 nm/pixel
Slit width: 1 arcsecond

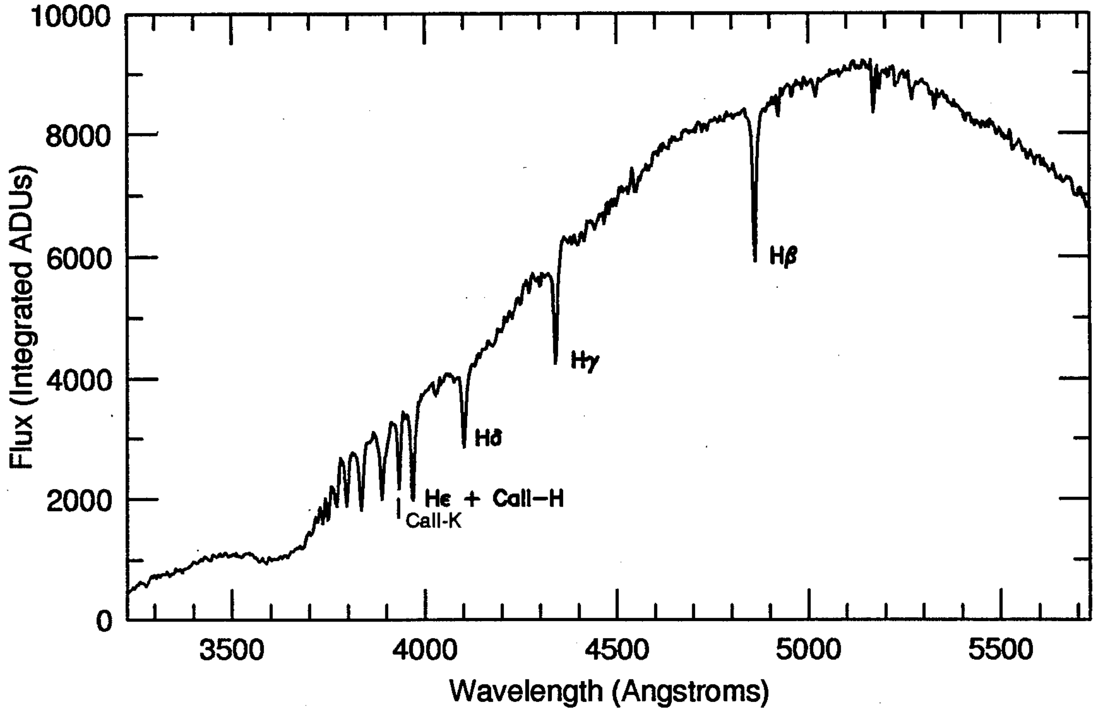


Figure 7.3 - Flux (arbitrary units) versus wavelength for RR Lyrae metallicity standard star XX And.

collapsed to one dimension. The reduction process included bias subtraction, application of flat field, distortion correction and wavelength calibration using the argon comparison lamp spectra, and sky subtraction. Figure 7.3 gives an example of an RR Lyrae spectrum (not corrected for atmospheric extinction and not flux calibrated).

The radial velocities of the RR Lyrae stars from these low resolution spectra can be determined by finding the wavelength centers of the hydrogen and CaII K lines. However, because the hydrogen and metal lines originate from different altitudes in the star's atmosphere, only the hydrogen lines

were used. The regions surrounding Hβ, Hγ, and Hδ of each spectrum were cross-correlated with the spectra of SW And, RR Cet and DX Del, producing relative velocity measurements between each star's spectrum and the templates. For all RRab type variable stars, the center-of-mass velocity ($v_{cm}$) and heliocentric velocity at a particular phase ($v(\phi)$) can be determined from one another if $v(\phi)$ is measured in the phase interval ≈0.15 - 0.85 (Saha and Oke 1984). By examining the radial velocity curves for X Ari (Oke, Giver, and Searle 1962) and SU Dra (Oke 1966), the center-of-mass velocity can be calculated using

$$v_{cm}=v(\varphi)+b\times(\varphi-a) \tag{7.3}$$

where b and a are empirically determined constants. For the Hγ spectral line in the above two radial velocity curves, a = 0.44 ± 0.03 and b = -104 ± 4 km/s. Published values of $v_{cm}$ for SW And, RR Cet and DX Del (Layden 1994) and the observation times were used to calculate $v(\phi)$ for the template spectra. The measured relative velocities for all other stars were then converted to heliocentric velocities and averaged, and using Equation 7.3, the center-of-mass velocities were determined. The error in the heliocentric velocities was taken to be the standard deviation of the calculated values. Table 7.2 lists the heliocentric radial velocity, radial velocity error and phase, and the resulting center-of-mass radial velocity and error for the observed stars. The SW And, RR Cet and DX Del spectra were not cross-correlated with themselves, so the

listed center-of-mass velocity is that determined from cross-correlation with the other two. The values listed for SW And and DX Del also represent the average of two spectra.

Table 7.2 - Center-of-mass velocity measurements

| #/name | $v_{hel}$ | $\sigma_v$ | $\phi$ | $v_{cm}$ | $\sigma_v$ |
|---|---|---|---|---|---|
| 5 | -62 | 27 | 0.59 | -77 | 27 |
| 11 | 61 | 27 | 0.45 | 60 | 28 |
| 36 | -368 | 25 | 0.31 | -354 | 25 |
| 39 | -358 | 30 | 0.56 | -371 | 30 |
| 42 | -265 | 25 | 0.56 | -277 | 25 |
| 51 | -200 | 23 | 0.58 | -215 | 23 |
| 57 | -288 | 28 | 0.51 | -295 | 28 |
| 58 | -246 | 27 | 0.27 | -229 | 27 |
| 66 | -368 | 30 | 0.29 | -352 | 30 |
| 68 | -299 | 29 | 0.55 | -311 | 29 |
| 69 | -110 | 28 | 0.38 | -103 | 29 |
| SW And | 60 | 9 | 0.81 | 21 | 10 |
| RR Cet | -118 | 25 | 0.35 | -108 | 25 |
| DX Del | -30 | 29 | 0.59 | -45 | 30 |

The metallicity standards XX And and RR Gem were also observed, but due to an error in predicting the phase of observation, these stars were observed during the ascending part of their light curve or at maximum light (phase between 0.9 to 0.1). The measured velocities for SW And, RR Cet, DX Del, and HR 458 agree reasonably well with the published values, with the differences consistant with $\sigma$ = 32 km/s. The measured velocity for HR 2047, however, is 60 km/s off.

## 7.3 Galactic Mass versus Radial Distance

With only radial velocity measurements, the Galaxy's mass interior to a particular orbit can't be determined on a star-by-star basis. The radial velocities of a collection of stars at a particular Galactocentric radial distance must be used to make this estimate. Equation 7.2 thus becomes

$$M(R)=\frac{R\langle v^2\rangle}{G(1+\langle e^2\rangle)}. \tag{7.4}$$

Certain assumptions must be made about the types of orbits in order to calculate the total space velocity from the observed heliocentric radial velocity.

The kinematics of a collection of halo RR Lyrae stars can be described by systemic motion in each dimension ($V_R$, $V_\theta$, and $V_\phi$ for R, θ and ϕ in Figure 6.1) and the average square of the peculiar motion in each dimension ($\langle v_R^2\rangle$, $\langle v_\theta^2\rangle$, and $\langle v_\phi^2\rangle$). The systemic velocities can be measured directly by taking the average radial velocity for a number of RR Lyrae stars at particular Galactic coordinates. For example, $V_R$ can be calculated using heliocentic radial velocities for stars towards the Galactic anticenter (see Saha 1985). Currently, however, the detected systemic motion of halo RR Lyrae variable stars has been of the order of or less than the error in the measurement. It will thus be assumed that $V_R = V_\theta = V_\phi = 0$. If the RR Lyrae orbits are distributed isotropically, then the average of the three peculiar velocity components squared are equal ($\langle v_R^2\rangle = \langle v_\theta^2\rangle = \langle v_\phi^2\rangle$). In this situation,

the measurement of one component of the space velocity, on average, would equal the space velocity divided by the square root of 3. Since the averaging is over the velocity squared, the high velocity RR Lyrae stars at a given distance have the largest leverage in determining the mass. Errors in these velocities could dramatically increase the mass estimate. To allow for velocity errors, the average of $(v+\sigma)(v-\sigma)$ will be used instead of $v^2$ (Lynden-Bell et al. 1983). The average total space velocity squared for N RR Lyrae stars is then

$$\langle v^2\rangle=\frac{3}{N}\sum_{i=1}^{N}(v_r^2-\sigma_v^2)_i \tag{7.5}$$

where $v_r$ is the heliocentric radial velocity corrected for the Sun's motion about the Galactic center and $\sigma_v$ is the corresponding error. For isotropic orbits, all eccentricities are equally probable, so $\langle e^2\rangle$ will be taken to be

$$\langle e^2\rangle=\int_0^1 e^2 de=\frac{1}{3} \tag{7.6}$$

If the RR Lyrae stars instead have radial orbits ($\langle v_R^2\rangle \gg \langle v_\theta^2\rangle \approx \langle v_\phi^2\rangle$), $\langle v_R^2\rangle$ (and thus $\langle v^2\rangle$) can be easily calculated from the heliocentric radial velocity measurements and knowledge of each star's Galactocentric position (see Figure 6.1) using

$$\langle v^2\rangle=\frac{1}{N}\sum_{i=1}^{N}\frac{(v_r^2-\sigma_v^2)_i}{\cos^2\beta_i}, \tag{7.7}$$

where $\beta$ is the angle subtended by the Sun and the Galactic

center as seen from the RR Lyrae star. The average eccentricity squared will be taken to be $<e^2> = 1$ for radial orbits. For both cases, Equation 7.4 can now be used to estimate the Galaxy's mass interior to the average Galactocentric radial distance. It is interesting to note that for large Galactocentric distances, $\cos(\beta)$ approaches 1 resulting in $<v^2>_{isotropic} = 3\times<v^2>_{radial}$ and $M(R)_{isotropic} = 4.5\times M(R)_{radial}$.

Other methods for determining the mass of the Galaxy from the dynamics of halo objects are similar to the one described above, but not identical. Hartwick and Sargent (1978) approximated globular clusters as a collisionless spherically symmetric system of mass points and used the collisionless Boltzmann equation to derive the mass. The resulting equation is

$$M(R) = \frac{R<v_r^2>}{G}\left[-\frac{d\ln\rho(R)}{d\ln R} - \frac{d\ln<v_r^2>}{d\ln R} + (\lambda-2) + \frac{V_\phi^2}{<v_r^2>}\right], \qquad (7.8)$$

where $\rho(R)$ is the globular cluster space density, $\lambda = (<v_\theta^2> + <v_\phi^2>)/<v_R^2>$ ($\lambda = 0$ for radial orbits and $\lambda = 2$ for isotropic orbits), and $V_\phi$ is the systemic rotation. Saha (1985) used a similar equation for a sample of RR Lyrae variable stars. Lynden-Bell et al. (1983) derived a mass formula to use with globular cluster radial velocities by time averaging the radial distance times the square of the radial velocity observed from the focus over one orbit. The Galaxy's mass interior to the orbit was approximated as a point mass. The

resulting equation is

$$M(R) = \frac{2\langle R(v_r^2 - \sigma_v^2)\rangle}{G\langle e^2\rangle}, \tag{7.9}$$

where it is implicitly assumed that the average heliocentric radial velocity corrected for the Sun's motion is a good approximation to the average radial velocity measured from the focus of the orbit. Other investigators of globular cluster and dwarf elliptical galaxy dynamics (Peterson 1985, Olszewski et al. 1986) have also used Equation 7.9 to estimate the mass of the Galaxy. Little and Tremaine (1987) devised an entirely different method employing Bayes' theorem with an assumed point potential, later used by Zaritsky et al. (1989). Mass estimates using this method are nearly identical to those using Equations 7.8 or 7.9. Finally, Kulessa and Lynden-Bell (1992) employed a maximum likelihood method with results indicating a massive dark halo. The Galactic mass estimates for the dynamical studies described above are shown in Figure 7.4. Open and closed symbols indicate masses calculated assuming isotropic and radial orbits respectively. All studies, including Frenk and White's (1980) study testing kinematical models of the globular clusters in the inner and outer Galactic halo against observational data, have concluded a massive dark halo exists in the Milky Way.

The radial velocity measurements for the CTI RR Lyrae stars were divided into two groups corresponding to Galactocentric radial distance. This was also done for those

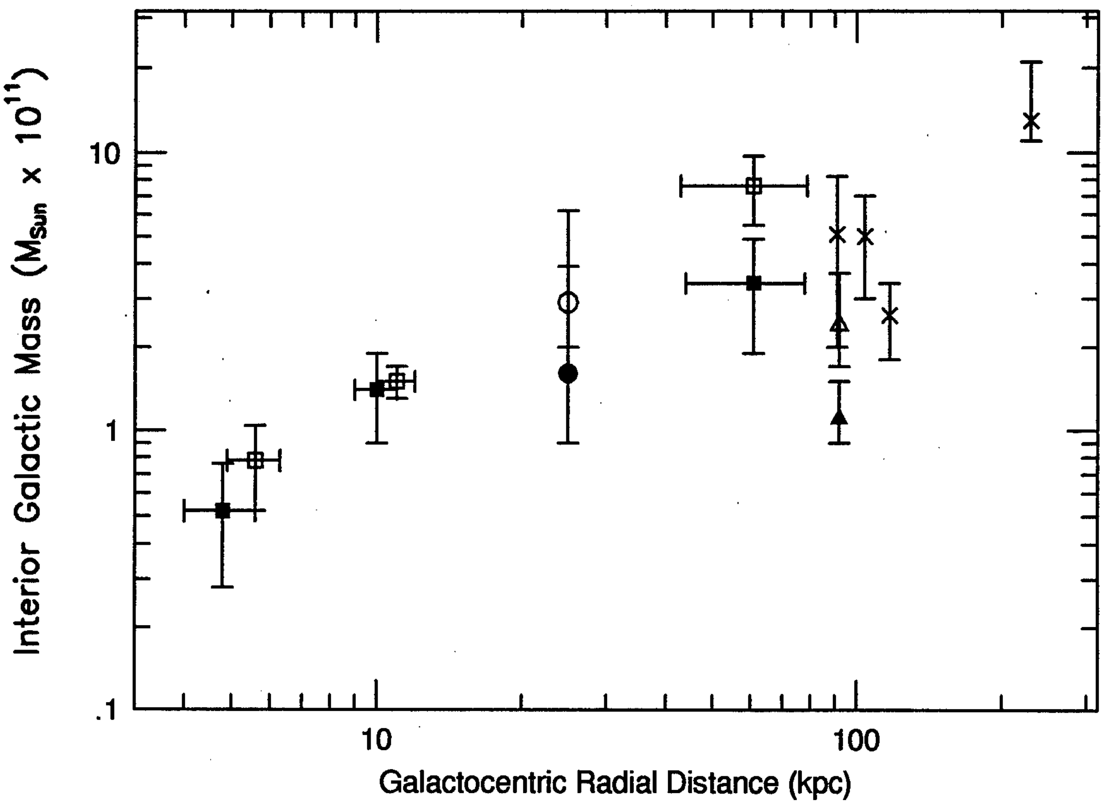


Figure 7.4 - Interior Galactic mass versus Galactocentric radial distance. Hartwick and Sargent 1978 (squares), Lynden-Bell et al. 1983 (x at 120 kpc), Peterson 1985 (x at 90 kpc) Saha 1985 (circles), Olszweski et al. 1986 (x at 100 kpc), Little and Tremaine 1987 (triangles), Zaritsky et al. 1989 (diamonds), and Kulessa and Lynden-Bell (x at 230 kpc).

stars with radial velocity measurements in Saha's (Saha and Oke 1985, Saha 1985) and Hawkins' (Hawkins 1984) RR Lyrae surveys. The two most distant stars in Hawkins' survey were not included due to their isolation from the rest. One of these stars is reported to have a very large radial velocity, and if it is assumed this star is bound to the Galaxy, requires a Galactic mass at 60 kpc of over $1.5 \times 10^{12}$ $M_{Sun}$

(Hawkins 1983). The bright RRab-type stars in the GCVS with velocity measurements (Layden 1994) were used to calculate the mass interior to the Sun's orbit. Additionally, radial velocities for 38 distant globular clusters in four distance ranges and 9 distant dwarf elliptical galaxies in two distance ranges were used to calculate the mass of the Galaxy using the identical method as for RR Lyrae stars. The velocity and distance data for the globular clusters and dwarf elliptical galaxies are those listed in Table 1 of Kulessa and Lynden-Bell's (1992) study, except for Pal 15 (Peterson and Latham 1989) and Eridanus, Pal 14, Leo I, and Leo II (Zaritsky et al. 1989). The velocity errors for the other objects were obtained from the original papers (Webbink 1981, Lynden-Bell et al. 1983, Peterson 1985, Hesser et al. 1986, Armandroff and DaCosta 1986, Olszewski et al. 1986). Figure 7.5 plots the calculated mass versus Galactocentric radial distance assuming (a) isotropic orbits and (b) radial orbits. The error in the average radial distance is the standard deviation of the distances of the individual RR Lyrae stars, globular clusters, or dwarf elliptical galaxies. The error in the calculated average space velocity was calculated using 100% / sqrt (# of objects). The upper and lower error bars for the mass were calculated using $(\sqrt{<v^2>} + \sigma_v)^2$ and $(\sqrt{<v^2>} - \sigma_v)^2$ in Equation 7.4 respectively. Also plotted is the expected mass as a function of distance if the mass is proportional to the space density of RR Lyrae stars (Equation 6.8), pinned to a mass derived at

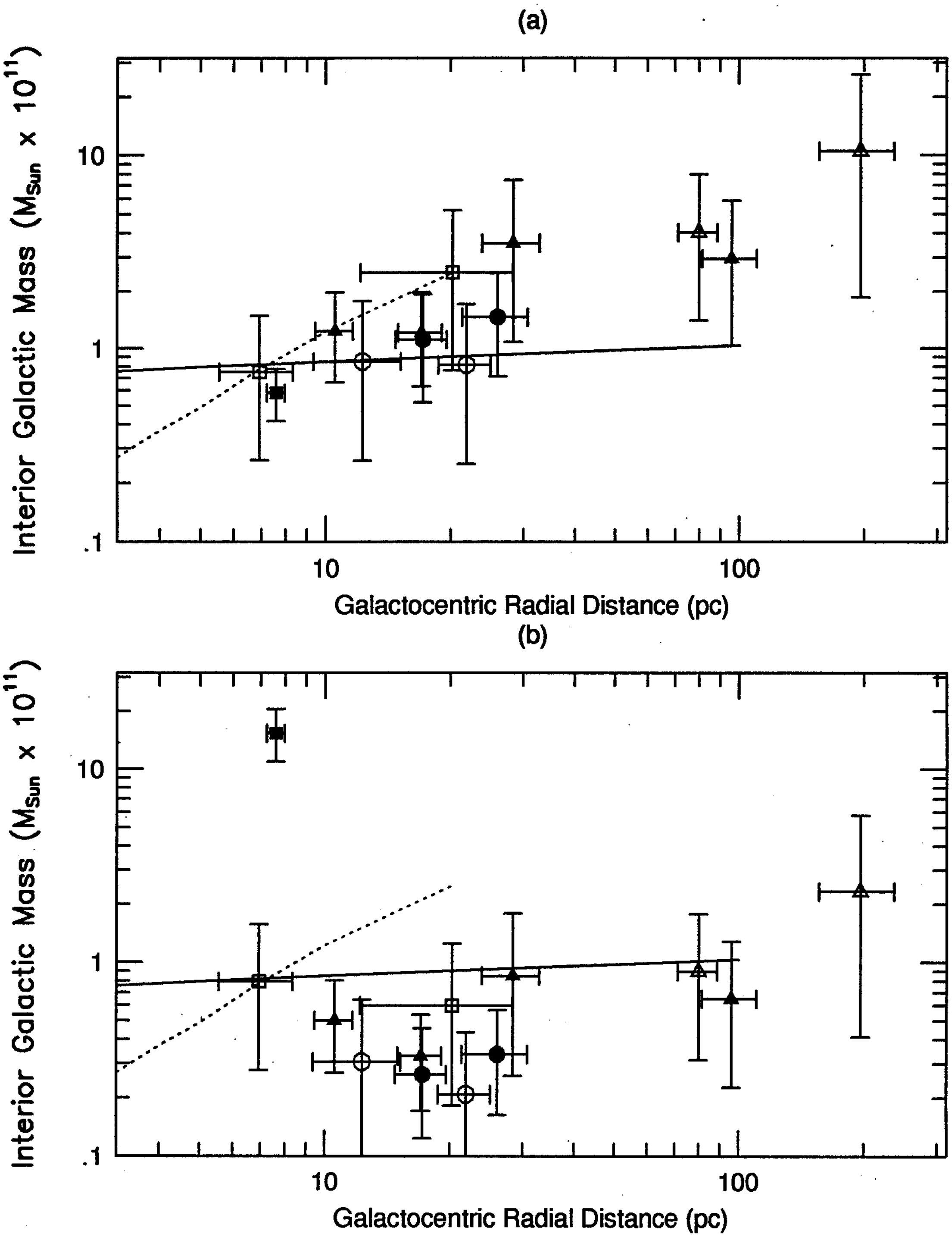


Figure 7.5 - Interior Galactic mass versus Galactocentric radial distance for (a) isotropic orbits and (b) radial orbits. CTI (open circles), Saha (filled circles), Hawkins (open squares), GCVS (filled square), globular clusters (filled triangles), dwarf elliptical galaxies (open triangles) data shown. Expected mass as derived from Equation 6.8 shown as solid line. Expected mass as derived from HI rotation curve shown as dashed line.

the Sun's distance using $\theta_{LSR}$ = 250 km/s (solid line), and the mass as calculated from the HI rotation curve of the Milky Way assuming circular orbits (dashed line, Merrifield 1992). The solid line in Figure 7.5 assumes the mass of the entire Galaxy (both halo and disk) is described by a single power law distribution. This of course may become a very poor approximation for decreasing Galactocentric distances.

The large error bars are due to the fact that the radial velocities of 3 (farthest dwarf elliptical point) to 15 (closest globular cluster point) objects were used to calculate all of these masses except the GCVS point. For isotropic orbits, all the RR Lyrae data and the nearby globular clusters ($R < 25$ kpc), are consistent with a mass distribution traced by the RR Lyrae distribution in the outer halo (i.e. no dark matter necessary). The more distant globular clusters, the dwarf elliptical galaxies, and the HI rotation curve, however, are consistent with a mass distribution requiring a massive dark halo. This of course assumes these distant globular clusters and dwarf elliptical galaxies are bound to the Milky Way, and the mass of the Galaxy can be calculated from the HI rotation curve by assuming circular orbits. For radial orbits, the distant globular clusters and dwarf elliptical galaxies are now more consistent with a near constant interior mass. The calculated masses from the RR Lyrae radial velocities are also approximately one-fourth that calculated assuming isotropic

orbits, except for the GCVS data point. The large mass calculated for this point indicates that radial orbits are not appropriate for these stars. The low mass for the Galaxy (less than the mass interior to the Sun's orbit) determined for the other RR Lyrae stars and the inner globular clusters indicate that radial orbits are probably not appropriate for these objects as well.

Depending on the type of orbits assumed, the radial velocity data for RR Lyrae stars, globular clusters, and dwarf elliptical galaxies can be used to support the notion that a massive dark halo exists (i.e. the mass-to-light ratio increases for increasing Galactocentric distance), or that no excessive dark matter exists at all in the Galaxy (i.e. the mass-to-light ratio is constant). The latter argument requires that the orbits for objects with $R < 25$ kpc are isotropic while the orbits for objects with $R > 25$ kpc are predominantly radial. Additionally, some other explanation for the HI rotation curve would need to be found.

Some have claimed that the orbits of globular clusters and dwarf elliptical galaxies in the distant Galactic halo are actually more circular (Lynden-Bell et al. 1983). They argue that globular clusters and dwarf elliptical galaxies with central densities typical with these systems and on highly eccentric orbits do not survive their perigalactic encounter due to tidal disruption, leaving intact the systems in the outer halo with near circular orbits. This would support a

massive dark halo if these objects were indeed bound to the Milky Way. As discussed in the previous chapter, however, these distant globular clusters and dwarf elliptical galaxies might constitute a distinct population ($R > 40$ kpc) completely separate from the Milky Way's globular clusters (Harris 1976). This population, although perhaps bound to the Local Group, may not be bound to the Milky Way at all. Indeed, the dynamics of this group may be described well by radial orbits as the objects fall into the Milky Way's gravitational potential, perhaps for the first time.

Whereas the number of globular clusters available to make mass estimates of the Milky Way is nearly complete, a large number of known and yet to be found RR Lyrae stars exist in the distant Galactic halo. By combining radial velocity data from many surveys and increasing the number of RR Lyrae stars with radial velocity measurements, the error in the mass for all distances in Figure 7.5 can be decreased. In addition to discovering and observing spectroscopically more distant RR Lyrae variable stars to extend the mass estimates to larger radial distances, RR Lyrae variables in the inner halo and nuclear bulge could be sampled as well. The mass function, independent of the HI rotation curve, could then be calculated for a large range of Galactocentric distances.

This dissertation has used a unique sample of RR Lyrae stars to estimate their space density and to derive a mass for the Milky Way. Our dynamical results do not require a massive

dark halo. It is clear that additional work is necessary on several fronts, including the dynamics of Galactic stars and stellar systems, the Galactic HI rotation curve, and the distribution of stellar populations, to arrive at a robust, rationalized estimate of the mass distribution of the Milky Way.

**Appendix 1 - Tables**

Table A1.1 - CTI Observing Log

Key
filters:
- B - Johnson B
- V - Johnson V
- R - Johnson R
- I - Johnson I
- C - UV transparent clear
- A - H-alpha on
- O - H-alpha off

codes:
- * - Merged into current **.NML** and **.NHL** databases (B and V filters), calibrated, but not merged (R and I filters)
- ** - Merged into current **.MAS** and **.HIS** databases, and **.NML** and **.NHL** databases

| Date | Dayno | CCD0 | CCD1 | Comments |
|---|---|---|---|---|
| 84dec09 | -23 | I | V | test of sky |
| 84dec10 | -22 | I | V | Cirrus at start, marginal night |
| 85jan04 | 4 | R | V | |
| 85jan17 | 17 | R | V | |
| 85feb06 | 37 | I | V | mostly clear with light cirrus to NW |
| 85feb07 | 38 | R | V | Clear with cirrus to NW at sunset |
| 85feb13 | 44 | B | V | |
| 85mar18 | 77 | - | V | light cirrus at sunset, CCD0 in for repair |
| 85mar19 | 78 | - | V | Closed due to high winds |
| 85may18 | 138 | ? | ? | some clouds |
| 85may19 | 139 | ? | ? | |
| 85may20 | 140 | ? | ? | moderate cirrus, extremely marginal |
| 85may21 | 141 | ? | ? | |
| 85may22 | 142 | ? | ? | |
| 85may26 | 146 | ? | ? | |
| 85jun18 | 169 | ? | ? | worked on dewar rotation |
| 85jun19 | 170 | ? | ? | light clouds at sunset, clouds later |
| 85jun20 | 171 | ? | ? | |
| 85jun21 | 172 | ? | ? | light cirrus to SW at sunset, marginal data |
| 85jun27 | 178 | ? | ? | Clear |
| 85jun28 | 179 | ? | ? | light cirrus throughout night |
| 85aug14 | 226 | R | V | poor seeing |
| 85aug15 | 227 | R | V | |
| 85aug16 | 228 | ? | ? | |

Table A1.1 - CTI Observing Log (continued)

| Date | Dayno | CCD0 | CCD1 | Comment |
|---|---|---|---|---|
| 85aug23 | 235 | ? | ? | Close to photometric |
| 85sep05 | 248 | ? | ? | Very windy, rest of mountain closed, high variable background |
| 85sep13 | 256 | ? | ? | Clear and calm |
| 85sep22 | 265 | ? | ? | Cirrus early, bad seeing, clear later |
| 85sep23 | 266 | ? | ? | Clear, beautiful night |
| 86mar01 | 425 | ? | ? | Clouds, close early due to clouds |
| 86mar06 | 430 | ? | ? | Clear, late start, calm |
| 86mar08 | 432 | ? | ? | much cirrus |
| 86mar09 | 433 | ? | ? | Very cloudy, no data acquired |
| 86mar20 | 444 | ? | ? | photometric |
| 86mar21 | 445 | ? | ? | photometric, high background |
| 86apr04 | 459 | ? | ? | Clear and calm, some dust |
| 86apr05 | 460 | ? | ? | Clear, photometric, may have cirrus in early A.M. |
| 86apr10 | 465 | ? | ? | Clear,photometric, some cirrus in west |
| 86apr17 | 472 | ? | ? | windy, cleared late, photometric |
| 86apr18 | 473 | ? | ? | photometric, thick clouds |
| 86apr20 | 475 | ? | ? | Clear |
| 86may10 | 495 | ? | ? | photometric, clear and calm |
| 86jun10 | 526 | ? | ? | Clear photometric, try to realign telescope |
| 86jun11 | 527 | ? | ? | photometric |
| 86jun14 | 530 | ? | ? | Clear and calm |
| 87may20 | 870 | ? | ? | TROUBLE |
| 87may23 | 873 | ? | ? | flashlight at start, data screwed up |
| 87may24 | 874 | V | R | photometric |
| 87may25 | 875 | ? | ? | Cirrus, close early due to clouds |
| 87may27 | 877 | ? | ? | |
| 87may28 | 878 | ? | ? | photometric |
| 87jun08 | 889 | ? | ? | Clear, possibly photometric |
| 87jun17 | 898 | ? | ? | Clear |
| 87jun19 | 900 | B | V | photometric |
| 87jun27 | 908 | ? | ? | warm night |
| 87jun28 | 909 | ? | ? | photometric |
| 87jun29 | 910 | ? | ? | windy and photometric |
| 87jun30 | 911 | ? | ? | photometric |
| 87jul03 | 914 | ? | ? | |
| 87jul07 | 918 | ? | ? | warm, fans on all night |
| 87jul09 | 920 | ? | ? | telescope moved |
| 87jul14 | 925 | ? | ? | Clouds on horizon, clear overhead, close early due to clouds |
| 87sep28 | 1001 | I | V | dewar pumped, filters cleaned, variable clouds all night |
| 87sep29 | 1002 | I | V | Clear at start, some clouds in morning |

Table A1.1 - CTI Observing Log (continued)

| Date | Dayno | CCD0 | CCD1 | Comment |
|---|---|---|---|---|
| 87oct17 | 1020 | R** | V** | Clear |
| 87oct04 | 1007 | O | A | Clear and photometric all night, refocused for H-alpha filters |
| 87oct05 | 1008 | O | A | Clear |
| 87oct06 | 1009 | O | A | Clear, large gradients in data, closed early due to WWVB error |
| 87oct12 | 1015 | I | V | light cirrus throughout night |
| 87oct15 | 1018 | I | V | Clear all night, power supply on DMC crapped out |
| 87oct16 | 1019 | R | V | partly cloudy all night, use with caution |
| 87oct18 | 1021 | R** | V | Clear |
| 87oct20 | 1023 | B** | V** | photometric |
| 87oct21 | 1024 | B | V | Clear, clouds in morning |
| 87nov09 | 1043 | I | V | Clear, no data |
| 87nov10 | 1044 | I | V | Clear, maybe problem with data due to computer |
| 87nov11 | 1045 | I | V | light cirrus, first use of MgFe coating on filters |
| 87nov12 | 1046 | I | V | light cirrus, |
| 87nov13 | 1047 | I | V | Clear, occasional light cirrus |
| 87nov15 | 1049 | R | V | Clear |
| 87nov16 | 1050 | R* | V** | Clear |
| 87nov17 | 1051 | R | V | Clear, no good data |
| 87nov20 | 1054 | R | V** | Clear, windy, poor seeing |
| 87nov21 | 1055 | R* | V** | Clear, cirrus in morning |
| 87nov22 | 1056 | B | V* | Clear, technical problems |
| 87nov23 | 1057 | B | V | technical problems |
| 87nov25 | 1059 | B | V | Clear |
| 87dec09 | 1073 | A | O | Clear |
| 87dec11 | 1075 | O | A | photometric, changed focus |
| 87dec12 | 1076 | O | A | Clear |
| 87dec22 | 1086 | B* | V** | Clear, maybe photometric |
| 87dec23 | 1087 | B | V* | Clear, windy |
| 87dec28 | 1092 | R | V | Clear, clouded out at end |
| 87dec29 | 1093 | R | V | Cirrus |
| 88jan07 | 1102 | I | V | Clear, cirrus at end, telescope turned off incorrectly |
| 88jan10 | 1105 | I | V | Clear, maybe photometric |
| 88jan11 | 1106 | I | V | Clear, maybe photometric |
| 88jan22 | 1117 | B | V | Clear, technical problems |
| 88jan24 | 1119 | B** | V** | Clear, maybe photometric, use caution |
| 88jan25 | 1120 | B | V** | Clear |
| 88jan26 | 1121 | R* | V** | Clear, light cirrus |
| 88feb01 | 1127 | R | V | Clear, |
| 88feb08 | 1134 | R | V | Clear, technical problems, no data |
| 88feb15 | 1141 | B | V | Clear, maybe photometric |

Table A1.1 - CTI Observing Log (continued)

| Date | Dayno | CCD0 | CCD1 | Comment |
|---|---|---|---|---|
| 88feb16 | 1142 | B** | V** | Clear, maybe photometric |
| 88feb17 | 1143 | B | V | Clear, slight wind |
| 88feb18 | 1144 | R** | V** | Clear |
| 88feb21 | 1147 | B | V | Clear, cirrus at morning |
| 88mar11 | 1166 | I | V | Clear, then cloudy |
| 88mar12 | 1167 | I | V | Clear, maybe photometric, slight wind |
| 88mar13 | 1168 | R | V | Cirrus |
| 88mar14 | 1169 | B | V | Clear, cloudy later |
| 88mar15 | 1170 | B | V | Clear |
| 88mar16 | 1171 | R | V | Clear, very windy |
| 88mar17 | 1172 | R** | V** | Clear, windy |
| 88mar18 | 1173 | I* | V** | Clear |
| 88mar19 | 1174 | B* | V** | Clear maybe photometric |
| 88mar20 | 1175 | B | V** | Clear, windy |
| 88mar21 | 1176 | R | V | Cirrus |
| 88mar22 | 1177 | R | V | slight clouds |
| 88mar24 | 1179 | B | V** | Clear, maybe high dust |
| 88mar25 | 1180 | R | V | Clear, near photometric |
| 88mar26 | 1181 | I | V | Clear, bright moon |
| 88mar27 | 1182 | I | V | Clouded out, no data |
| 88mar29 | 1184 | I | V | Clear, windy |
| 88mar30 | 1185 | O | A | Clear, refocused |
| 88apr08 | 1194 | O | A | Clear |
| 88apr09 | 1195 | I | V | Clear |
| 88apr10 | 1196 | R | V | light cirrus |
| 88apr19 | 1205 | B | V** | Clear |
| 88apr20 | 1206 | R | V | Clear, scattered cirrus, wind gusts |
| 88apr22 | 1208 | I | V | Clear |
| 88apr24 | 1210 | R | V | scattered clouds. wind gusts, dusty |
| 88apr25 | 1211 | B | V | Clear, data out of focus, something is amiss |
| 88apr26 | 1212 | R* | V** | Clear, maybe photometric |
| 88apr27 | 1213 | I | V | Clear. |
| 88may05 | 1221 | I | V | Clear, windy, gusts, no data |
| 88may06 | 1222 | I | V | Cloudy |
| 88may11 | 1227 | R | V | no information on conditions, possible computer trouble |
| 88may12 | 1228 | B** | V** | Clear |
| 88may13 | 1229 | B | V | Clear, slight clouds |
| 88may21 | 1237 | B** | V** | Clear, photometric, slight wind |
| 88may24 | 1240 | R | V | Cloudy |
| 88may25 | 1241 | I | V | slight haze |

Table A1.1 - CTI Observing Log (continued)

| Date | Dayno | CCD0 | CCD1 | Comment |
|---|---|---|---|---|
| 88may26 | 1242 | R | V | Clear |
| 88may27 | 1243 | I | V | slight cirrus, questionable data |
| 88may28 | 1244 | I | V | slight cirrus |
| 88jun07 | 1254 | I* | V** | Clear |
| 88jun08 | 1255 | R* | V** | Clear |
| 88jun09 | 1256 | I | V | Clear, occasional cirrus |
| 88jun10 | 1257 | I | V* | Clear, maybe photometric |
| 88jun11 | 1258 | R* | V** | Clear |
| 88jun12 | 1259 | R | V | Clear |
| 88jun13 | 1260 | R | V | Clear, windy |
| 88jun14 | 1261 | R* | V | Clear, some cirrus |
| 88jun15 | 1262 | I* | V | Clear, slight haze, maybe photometric |
| 88jun16 | 1263 | I | V* | Clear, some cirrus |
| 88jun17 | 1264 | B | V | Clear, scattered clouds |
| 88jun20 | 1267 | B | V | scattered clouds |
| 88jun21 | 1268 | B* | V | scattered clouds, cleared latter, flashlights around 2:00am |
| 88jun22 | 1269 | R* | V** | Clear |
| 88jun23 | 1270 | R | V | Cloudy, windy |
| 88jun24 | 1271 | R | V | Cloudy |
| 88jun26 | 1273 | I | V | Clear, scattered clouds, poor data |
| 88jun27 | 1274 | I | V | scattered clouds |
| 88jun28 | 1275 | R | V | Clear |
| 88jul05 | 1282 | I | V | (dewar pumped Jul 03) scattered clouds, 4 july fireworks, no data |
| 88jul06 | 1283 | V | R | Cloudy, only 1/2 hour of data |
| 88jul12 | 1289 | R | V | scattered clouds |
| 88jul13 | 1290 | B | V | no information on conditions |
| 88jul15 | 1292 | B | V** | slight clouds |
| 88jul16 | 1293 | R* | V | Clear |
| 88jul17 | 1294 | R | V | scattered clouds |
| 88aug09 | 1317 | R** | V** | Clear |
| 88sep13 | 1352 | I* | V** | Clear, maybe photometric, mirrors washed since last data |
| 88sep14 | 1353 | B | V | Clear, probably photometric, focusing procedures |
| 88sep15 | 1354 | B** | V** | Clear, probably photometric |
| 88sep16 | 1355 | B** | V** | Clear |
| 88sep17 | 1356 | R** | V | Clear, probably photometric |
| 88sep18 | 1357 | R | V | Clear, KPNO "fun-night" (problems with car lights) |
| 88sep19 | 1358 | R | V | Clear, data doesn't look that good |
| 88sep20 | 1359 | I* | V** | Clear, dust in atmosphere?, stayed closed due to high winds |
| 88sep24 | 1363 | O | A | Clear, probably photometric |
| 88sep26 | 1365 | O | A | Clear, data looks good |

Table A1.1 - CTI Observing Log (continued)

| Date | Dayno | CCD0 | CCD1 | Comment |
|---|---|---|---|---|
| 88nov04 | 1404 | I | V** | Clear, data looks O.K. |
| 88sep27 | 1366 | O | A | scattered clouds |
| 88sep28 | 1367 | O | A | Clear, slightly hazy, data quality poor |
| 88oct02 | 1371 | O | A | Clear |
| 88oct03 | 1372 | O | A | Clear, poor seeing |
| 88oct04 | 1373 | I | V | Cloudy, no data |
| 88oct08 | 1377 | I | V** | Clear, probably photometric |
| 88oct09 | 1378 | I | V** | Clear, cirrus visible at sunset |
| 88oct10 | 1379 | I | V** | Cloudy to east, clear overhead |
| 88oct18 | 1387 | B | V | Clear after afternoon thunderstorms, no data recorded |
| 88oct19 | 1388 | R | V | low cirrus, thunderstorms in area, not photometric |
| 88oct23 | 1392 | I | V | Clear, very bright moon, high background |
| 88oct24 | 1393 | I | V | Clear, very bright moon, data quality much better than yesterday |
| 88nov01 | 1401 | I* | V** | Clear, probably photometric, high moon background at end |
| 88nov02 | 1402 | I | V | scattered clouds, good seeing |
| 88nov03 | 1403 | I | V** | Clouds on horizon, not photometric |
| 88nov05 | 1405 | I | V** | Clear, definitely photometric |
| 88nov06 | 1406 | R | V | patchy cirrus and hazy |
| 88nov07 | 1407 | B | V | some cirrus, hazy and very windy, data quality questionable |
| 88nov08 | 1408 | R | V | Cirrus all over |
| 88nov10 | 1410 | B | V** | Clear, clouds by morning |
| 88nov11 | 1411 | B | V** | Clear, clouds in morning, data looks good |
| 88nov12 | 1412 | B* | V** | possibly photometric |
| 88nov13 | 1413 | B | V** | Clear, photometric at start, images elongated by wind at times |
| 88nov14 | 1414 | R | V** | Clear |
| 88nov16 | 1416 | R | V** | Clear, data looks good |
| 88nov17 | 1417 | R | V** | high cirrus |
| 88nov18 | 1418 | R | V* | Clear but very foggy in early morning |
| 88nov19 | 1419 | R | V** | Intermittent cloudiness, data useless and not recorded |
| 88nov20 | 1420 | R | V | high cirrus very bad |
| 88dec02 | 1432 | I | V** | Clear, data looks good |
| 88dec04 | 1434 | R | V | scattered cirrus, images fuzzy but cleared up later |
| 88dec05 | 1435 | R | V** | scattered cirrus and hazy, data looks O.K. |
| 88dec06 | 1436 | R | V** | Clear with cirrus in west at sunset |
| 88dec07 | 1437 | R | V | Cirrus overcast with brief openings, no data taken |
| 88dec12 | 1442 | B | V** | Very clear, data looks O.K. |
| 88dec13 | 1443 | B | V | Clear, possibly photometric, clouds in east at sunrise |
| 88dec14 | 1444 | B | V | Clear, data looks good |
| 89jan06 | 1467 | B | V | not photometric, closed by clouds |
| 89jan09 | 1470 | I | V | Clear, probably photometric, dewar problems |

Table A1.1 - CTI Observing Log (continued)

| Date | Dayno | CCD0 | CCD1 | Comment |
|---|---|---|---|---|
| 89jan11 | 1472 | R | V | Clear, elongated images because of strong winds |
| 89jan12 | 1473 | R | V | hazy with cirrus to north, high humidity |
| 89jan14 | 1475 | R | V | Clear |
| 89jan15 | 1476 | I | V | Cirrus, not photometric |
| 89jan16 | 1477 | I | V | scattered cirrus and hazy, high background at start |
| 89jan17 | 1478 | R* | V | Clear with some haze, high background |
| 89jan31 | 1492 | I* | V | Clear overhead,clouds to south, closed by heavy cloud cover later |
| 89feb03 | 1495 | R | V | Clear, possibly photometric, images elongated due to wind |
| 89feb04 | 1496 | R | V** | Clear with clouds on horizon, cirrus at sunrise, data looks good |
| 89feb12 | 1504 | B* | V** | Clear, data looks O.K. |
| 89feb13 | 1505 | R | V | some cirrus |
| 89feb14 | 1506 | I | V | Cirrus at sunset, closed early due to clouds |
| 89feb16 | 1508 | I | V | Clear |
| 89mar02 | 1522 | I | V | scattered cirrus and very hazy, complete cloud cover at end |
| 89mar05 | 1525 | I | V | Cirrus all night, no data recorded |
| 89mar06 | 1526 | I | V** | Clear |
| 89mar07 | 1527 | I* | V** | Clear, data looks good |
| 89mar08 | 1528 | B** | V** | Clear |
| 89mar09 | 1529 | B | V** | Clear, data looks O.K. |
| 89mar10 | 1530 | R* | V** | scattered cirrus on horizons all night |
| 89mar11 | 1531 | R | V** | Clear |
| 89mar12 | 1532 | R | V | light cirrus, look carefully at data |
| 89mar13 | 1533 | R* | V | some cirrus at sunset, mostly clear |
| 89mar15 | 1535 | R | V | Cirrus throughout night |
| 89mar16 | 1536 | I | V | some scattered cirrus, cleared somewhat during night |
| 89mar30 | 1550 | R* | V* | Clear, data looks good |
| 89apr01 | 1552 | I* | V* | Clear, data looks good |
| 89apr02 | 1553 | I | V | Clear, data looks good despite wind, some clouds in morning |
| 89apr03 | 1554 | ? | ? | moderate cirrus at sunset, wind causing severe data smearing |
| 89apr05 | 1556 | R | C | Clear, probably photometric, r data out of focus |
| 89apr06 | 1557 | I | C | Clear, data looks good |
| 89apr07 | 1558 | I | C | Clear, probably photometric, good sweep! |
| 89apr08 | 1559 | R | C | Clear, data looks O.K. |
| 89apr09 | 1560 | R | C | Clear, data looks O.K. |
| 89apr10 | 1561 | R | C | no information on conditions |
| 89apr11 | 1562 | R | C | Clear, probably photometric |
| 89apr25 | 1576 | R | V | (mirrors washed Apr 24) clear, pumped dewar |
| 89apr26 | 1577 | R | V | Clear, closed early due to wind |
| 89apr27 | 1578 | I | V** | Clear, data looks O.K. |
| 89apr28 | 1579 | R | V | Clear |

Table A1.1 - CTI Observing Log (continued)

| Date | Dayno | CCD0 | CCD1 | Comment |
|---|---|---|---|---|
| 89apr29 | 1580 | I | V | some scattered cirrus, data looks O.K. with some coma |
| 89may03 | 1584 | B | V | Cirrus but good seeing, coma present at end of data |
| 89may04 | 1585 | I | V | some scattered cirrus |
| 89may09 | 1590 | B* | V* | Clear at start, data looks reasonable, closed early due to clouds |
| 89may11 | 1592 | B | V | partly cloudy, ragged images perhaps due to wind, coma present |
| 89may12 | 1593 | R | V** | Cirrus on horizon at sunset, clear overhead, images look good |
| 89may13 | 1594 | R | V | Clear, data looks good at start, ghost images later |
| 89may14 | 1595 | R | V | Clear, data looks good at start, ghost images later |
| 89may15 | 1596 | I | V | Clear with some cirrus to north, high wind and bad seeing |
| 89may30 | 1611 | B | V | Cirrus to west, not transparent, images elongated by wind |
| 89may31 | 1612 | B | V** | Clear, images look fairly good |
| 89jun01 | 1613 | R** | V** | Clear all night |
| 89jun02 | 1614 | R* | V** | scattered cirrus and slightly hazy |
| 89jun03 | 1615 | I* | V** | Clear, data looks O.K. |
| 89jun04 | 1616 | I* | V** | Clear, data looks good |
| 89jun05 | 1617 | B | V* | scattered cirrus, not photometric, windy |
| 89jun06 | 1618 | I | V | Cirrus at start |
| 89jun07 | 1619 | B | V | scattered clouds |
| 89jun08 | 1620 | B* | V** | Clear, bright moon, data looks good |
| 89jun09 | 1621 | R | V** | Clear, data looks quite good! |
| 89jun11 | 1623 | R | V** | Clear, data looks pretty good |
| 89jun13 | 1625 | I | V | no go |
| 89jun26 | 1638 | I | V | Cloudy, pumped dewar |
| 89jun27 | 1639 | I | V | partly cloudy, questionable data because of clouds |
| 89jul01 | 1643 | B | V | Clear but slightly hazy, stars out of focus |
| 89jul02 | 1644 | B | V | scattered cirrus, data reasonable but focus still a problem |
| 89jul03 | 1645 | B* | V | Clear, stars still out of focus, coma also exists |
| 89jul04 | 1646 | B* | V | Clear with slight haze, continued focus problems |
| 89jul06 | 1648 | B | V | thunderclouds and lightning, did not open |
| 89oct08 | 1742 | I | V** | Clear, possibly photometric, ran well and images look good |
| 89oct09 | 1743 | R* | V* | Clear, probably photometric, data looks good |
| 89oct10 | 1744 | I | V** | Clear, probably photometric, moved telescope closer to strip |
| 89oct11 | 1745 | R | V | Clear, scattered cirrus by morning, data looks O.K. |
| 89oct18 | 1752 | R | V | Clear, stars slightly out of focus |
| 89oct19 | 1753 | I | V | slight haziness, cirrus in morning, stars slightly unfocused |
| 89oct20 | 1754 | I | V | Clouds to east and south, closed early due to increasing clouds |
| 89oct24 | 1758 | R* | V** | Clear, data looks O.K. |
| 89oct25 | 1759 | I | V | scattered cirrus, data looks O.K. |
| 89oct28 | 1762 | B | V | Clear, data looks good, power outage |
| 89oct29 | 1763 | B | V | Clear |

Table A1.1 - CTI Observing Log (continued)

| Date | Dayno | CCD0 | CCD1 | Comment |
|---|---|---|---|---|
| 89oct30 | 1764 | B | V | Cirrus to south, windy, data pretty good |
| 89nov03 | 1768 | I* | V* | Clear, probably photometric, moved telescope |
| 89nov04 | 1769 | I | V | Clear, data very good |
| 89nov05 | 1770 | R* | V | Clear, data pretty good |
| 89nov23 | 1788 | I | V | scattered cirrus, closed early due to clouds |
| 89nov24 | 1789 | I | V | scattered cirrus, hazy, very windy, cloud cover in morning |
| 89nov25 | 1790 | I | V | Variable high clouds, elongated images due to wind, closed early clouds |
| 89nov28 | 1793 | B | V | Cloudy at start, cleared later, power failure during night |
| 89dec01 | 1796 | B | V | Clear with haze on horizon, data good |
| 89dec02 | 1797 | I | V | Clear, early shutdown due to high winds |
| 89dec03 | 1798 | R | V | Clear, did not open due to high winds |
| 89dec04 | 1799 | R | V | Clear, data good |
| 89dec05 | 1800 | I | V | Clear, still trying to fix A/D problems |
| 89dec06 | 1801 | R | V | Clear with patches of cirrus, data O.K. |
| 89dec07 | 1802 | R | V | Clear |
| 89dec09 | 1804 | R | V | some scattered cirrus, data is acceptable |
| 89dec21 | 1816 | I* | V** | (fixed computer hard disk Dec 11) clear, data good |
| 89dec23 | 1818 | I* | V** | Clear, data promising |
| 89dec24 | 1819 | B | V | scattered cirrus, heavy cirrus in morning, data is acceptable |
| 90jan05 | 1831 | R | V | Clear, problems with WWVB signal, cannot open telescope |
| 90jan06 | 1832 | R* | V** | Clear, data O.K. |
| 90jan21 | 1847 | B | V | scattered cirrus, hazy, data good, moderate cloud cover in morning |
| 90jan22 | 1848 | B | V | scattered cirrus, very hazy, data acceptable, closed early due to clouds |
| 90jan24 | 1850 | B* | V** | Clear, data good, images slightly out of focus, power failure |
| 90jan25 | 1851 | B* | V** | Clear, very windy, data does not look too bad |
| 90jan26 | 1852 | R | V** | Clear, data good, slightly hazy with cirrus in morning |
| 90jan28 | 1854 | R* | V** | scattered cirrus, data looks O.K., stars slightly unfocused |
| 90jan29 | 1855 | R* | V* | Clear, data very good |
| 90jan30 | 1856 | I* | V* | Clear, data very good |
| 90feb04 | 1861 | I | V | Clear, data O.K., partly cloudy in morning |
| 90feb17 | 1874 | I* | V* | Clear, data good |
| 90feb18 | 1875 | I* | V* | Clear with some clouds to north, data good |
| 90feb21 | 1878 | I | V | Clear with clouds on horizon, same in morning, may be a good night |
| 90feb22 | 1879 | R* | V* | Clear with clouds on horizon, clear in morning, data fairly good |
| 90feb23 | 1880 | R* | V* | Clear with cirrus to north, data good, clear all night |
| 90feb24 | 1881 | B | V | Clear with cirrus to west, telescope refused to open |
| 90mar01 | 1886 | B* | V* | Clear with cumulus to east, data O.K., clear throughout night |
| 90mar08 | 1893 | R | V | widely scattered cirrus throughout night |
| 90mar17 | 1902 | R* | V* | widely scattered cirrus, closed early due to clouds and moon |

Table A1.1 - CTI Observing Log (continued)

| Date | Dayno | CCD0 | CCD1 | Comment |
|---|---|---|---|---|
| 90mar19 | 1904 | R* | V* | Clear, data looks good, excellent night, closed early due to moon |
| 90mar20 | 1905 | I | V | Clear, clouds to west, closed early due to moon, lots of cirrus in morning |
| 90mar23 | 1908 | I | V | scattered cirrus and hazy throughout night, data looks O.K. |
| 90mar24 | 1909 | B | V | Clear with cirrus on horizon, data looks good, lots of cirrus in morning |
| 90mar25 | 1910 | B* | V* | Clear all night, data looks good |
| 90apr03 | 1919 | I* | V* | Clear, data looks O.K. |
| 90apr14 | 1930 | I | V | Cirrus throughout night, data looks acceptable |
| 90apr16 | 1932 | I | V* | Very clear early but also windy, closed due to moon |
| 90apr18 | 1934 | I | V* | windy, closed early due to fog and moon |
| 90apr19 | 1935 | I | V* | good night, clear and calm |
| 90apr20 | 1936 | R | V* | good night |
| 90apr21 | 1937 | R | V | Cirrus, humid, breezy, Grinnell problem |
| 90apr26 | 1942 | R | V* | Clear, good night |
| 90apr27 | 1943 | B | V | Breezy, clouds on horizon, low moon |
| 90apr29 | 1945 | B | V | Very windy, distortion, early shutdown for wind, possible Grinnell problem |
| 90apr30 | 1946 | B | V | windy, 35deg moon, distortion |
| 90may15 | 1961 | R | V | Breezy, early shutdown for moon |
| 90may16 | 1962 | R | V | windy, clear, early shutdown for moon |
| 90may17 | 1963 | I | V | Cloudy, poor seeing, diagnostic data only |
| 90may22 | 1968 | B | V | Cloudy, diagnostic data, cleared up later |
| 90may24 | 1970 | B | V | diagnostic data only |
| 90may25 | 1971 | B* | V | windy, distorted |
| 90may27 | 1973 | B* | V | Clear, calm |
| 90may28 | 1974 | B | V | Cirrus, setting moon, data fair |
| 90may30 | 1976 | I | V | moon 30deg, cirrus, SEVERE data shearing |
| 90may31 | 1977 | R | V | moon 30deg, slight cirrus, possible data smearing |
| 90jun01 | 1978 | I* | V | gusty wind, 30deg moon, good data |
| 90jun02 | 1979 | I | V | 40deg moon, very good night |
| 90jun03 | 1980 | R** | V* | 40deg moon, clear, calm |
| 90jun05 | 1982 | I | V | late open for moon, wind, dewar drift |
| 90jun20 | 1997 | I* | V* | (pumped dewar Jun 18) clear, slight breeze, good data |
| 90jun21 | 1998 | I | V | Clear, calm, but dewar failed during night |
| 90jun22 | 1999 | R | V | Bad dewar, no data, power supply check |
| 90jun26 | 2003 | B | V | system fixed, some clouds, got data |
| 90jun28 | 2005 | R | V* | Clear after midnight |
| 90jul28 | 2035 | R* | V* | 15deg moon, clear, very good data |
| 90jul29 | 2036 | I* | V* | Calm, clear, moon and lightning on horizon, good data |
| 90aug19 | 2057 | R | V* | Calm, clear with morning cirrus, high humid, good data |
| 90aug20 | 2058 | I | V | Clear, light wind, humid 37%, Grinnell problem, close early for clouds |
| 90aug21 | 2059 | I | V | slight breeze, good data in spite of tape drive failure |

Table A1.1 - CTI Observing Log (continued)

| Date | Dayno | CCD0 | CCD1 | Comment |
|---|---|---|---|---|
| 90aug22 | 2060 | B | V | good night, good data |
| 90aug23 | 2061 | B | V* | Clear,calm , good data |
| 90aug24 | 2062 | I* | V* | Clear, windy, good data |
| 90aug25 | 2063 | R | V* | Clear, windy, good data |
| 90aug26 | 2064 | I | V | Clear, windy, Grinnell problem in middle, good data |
| 90sep13 | 2082 | R* | V* | Breezy, close early for storm, very good data in spite of tape drive failure |
| 90sep20 | 2089 | I* | V* | Clouds on horizon, close early for clouds, good data |
| 90sep22 | 2091 | I | V | Clear, windy, early close for clouds, good data |
| 90sep25 | 2094 | I | V* | some clouds, low moon, data problems |
| 90sep26 | 2095 | R | V | hazy, cirrus, fair data |
| 90sep27 | 2096 | R* | V* | Clear, calm, 25deg moon, good data |
| 90sep28 | 2097 | R | V | scattered cirrus, windy, good data |
| 90oct11 | 2110 | I | V* | Breezy, hazy, close early for moon, good data (long flat) |
| 90oct12 | 2111 | I | V | Clear, close early for moon, good data |
| 90oct13 | 2112 | I | V | data problems |
| 90oct14 | 2113 | R | V* | Clear, calm good data |
| 90oct15 | 2114 | R | V | Clear, Grinnell problem, close early for humid, good data |
| 90oct16 | 2115 | B | V | good data |
| 90oct18 | 2117 | B | V | Clear calm, becoming windy, data fuzzy and distorted |
| 90oct19 | 2118 | B | V | Clear, breezy to windy, humid |
| 90oct21 | 2120 | B | V | Clear, breezy, data problems |
| 90oct22 | 2121 | I | V* | Clear, calm good data |
| 90oct23 | 2122 | I | V | Beautiful night, good data |
| 90oct24 | 2123 | R* | V* | Clear, calm, data problems |
| 90oct25 | 2124 | R* | V* | Clear, breezy, good data |
| 90oct26 | 2125 | R* | V* | Clear, calm, 10deg moon, good data |
| 90oct27 | 2126 | I | V* | Clear, good seeing, good data |
| 90nov10 | 2140 | I | V | Clear, windy, focus fuzzy, good data, power supply problem |
| 90nov11 | 2141 | I | V | Bad power supply, no data |
| 90nov15 | 2145 | I | V | Clear, breezy, good data |
| 90nov16 | 2146 | I | V | Cirrus, calm, fair data |
| 90nov17 | 2147 | B* | V* | Clear, humid good data |
| 90nov18 | 2148 | B | V* | Cloudy, fair data |
| 90nov19 | 2149 | B | V | Clear with cirrus later, good data |
| 90nov22 | 2152 | I | V | some cirrus, good data |
| 90nov23 | 2153 | I | V | Clear, breezy to windy, stuck filter, fair data |
| 90dec10 | 2170 | R | V* | Clear, breeze, good data |
| 90dec11 | 2171 | R* | V* | Clear, breeze, good data |
| 90dec18 | 2178 | B | V* | Clear, windy, bad focus, good data |
| 90dec19 | 2179 | B | V | Clear, windy, bad focus, Grinnell problem, needs realignment |

Table A1.1 - CTI Observing Log (continued)

| Date | Dayno | CCD0 | CCD1 | Comment |
|---|---|---|---|---|
| 91jan08 | 2199 | I | V* | cirrus, closed-moon, O.K data |
| 91jan11 | 2202 | I | V* | Clear, O.K. data |
| 91jan13 | 2204 | I | V | cirrus, good data |
| 91jan14 | 2205 | B | V | partly cloudy, good data |
| 91jan15 | 2206 | B* | V* | Clear, clouds, O.K. data |
| 91jan16 | 2207 | B | V* | Clear, breeze, good data |
| 91jan19 | 2210 | I | V | Clear, good data |
| 91jan24 | 2215 | R | V | Cirrus early, hazy at start |
| 91jan25 | 2216 | R* | V* | Clear, haze |
| 91feb07 | 2229 | R | V | Clear, windy, hazy, closed-clouds, good data |
| 91feb08 | 2230 | R* | V* | Clear, clouds in East, calm, closed-moon, O.K. data |
| 91feb09 | 2231 | I | V | cirrus, breezy, closed-cirrus, data marginal |
| 91feb15 | 2237 | B | V* | cirrus, breeze, closed-clouds, good data |
| 91feb20 | 2242 | I | V | Clear, very windy, monitor blank in A.M., good data |
| 91feb21 | 2243 | I* | V* | Clear, cold, breezy, images not focused |
| 91mar09 | 2259 | V | I | Clear, ccd and dewar temp high, stop early |
| 91mar12 | 2262 | I* | V* | Clear, clouds in East, slight breeze, images not focused, data acceptable |
| 91mar13 | 2263 | R | V* | Clear, breeze, scattered cirrus in A.M., data good |
| 91apr08 | 2289 | R* | V* | Clear, very windy, closed-moon, calm, data O.K. |
| 91apr09 | 2290 | I* | V* | Clear, breezy, closed-moon, data O.K. |
| 91apr10 | 2291 | B | V | Clear, Grinnell problem, data good |
| 91apr13 | 2294 | I | V | (changed ccd voltages Apr 11) clear, breeze, data O.K. |
| 91apr14 | 2295 | B* | V* | Clear, good data |
| 91apr15 | 2296 | B | V | Clear, data O.K. |
| 91apr16 | 2297 | I | V | hazy, thin cirrus, closed-wind and clouds, data mediocre |
| 91apr20 | 2301 | R | V | thin cirrus, slight wind, data O.K. |
| 91apr21 | 2302 | I | V | Clear, very windy, closed-winds, images distorted |
| 91apr22 | 2303 | I | V | mirrors washed, Grinnell re-installed, clear, cirrus, data good |
| 91apr24 | 2305 | R | V* | Clear, calm, good data |
| 91may07 | 2318 | I* | V* | Clear, breeze, closed-moon, data good |
| 91may08 | 2319 | R | V | cirrus, breeze, closed-moon, data acceptable |
| 91may09 | 2320 | R | V | Cloudy, windy, closed-clouds and wind, data fair |
| 91may10 | 2321 | I | V | Clear, windy, distorted images, closed-wind |
| 91may11 | 2322 | I | V | Clear, windy, haze, data acceptable |
| 91may12 | 2323 | B* | V* | Clear, data good |
| 91may14 | 2325 | R | V | Clear, windy, distorted images, closed-wind |
| 91may15 | 2326 | I | V* | Clear, data good |
| 91may16 | 2327 | B | V | Clear, data good |
| 91may17 | 2328 | I | V | Clear, wind later, data good |
| 91may18 | 2329 | R | V | Clear, windy, data O.K. |

Table A1.1 - CTI Observing Log (continued)

| Date | Dayno | CCD0 | CCD1 | Comment |
|---|---|---|---|---|
| 91may19 | 2330 | I | V | Clear and breezy, good data |
| 91jun05 | 2347 | B | V | (adjusted current ccd0 May 30, ccd tests Jun 03) clear and breezy, data good |
| 91jun06 | 2348 | V | I | Clear, close early |
| 91jun07 | 2349 | R | V | Clear and calm, data looks good, close early due to moon |
| 91jun08 | 2350 | I | V | Clear, slight breeze, data looks good, close early due to moon |
| 91jun15 | 2357 | I | V | (test dewar hold time Jun 09) clear and slight breeze, data looks good |
| 91jun16 | 2358 | B | V | Clear and calm, data looks O.K. |
| 91jun17 | 2359 | R | V | Clear, slight breeze, Grinnell problem early |
| 91jun18 | 2360 | I | V | Clear, clouds in horizon, hazy in A.M., data looks O.K. |
| 91jun20 | 2362 | R | V | Clear, data looks O.K. |
| 91jun21 | 2363 | I | V | Clear and breezy, data looks O.K. |
| 91jun22 | 2364 | R | V | Clear and breezy, calm in A.M. |
| 91jul09 | 2381 | I | V | thick clouds, clearing, lightning in South, close early due to clouds |
| 91jul10 | 2382 | B | V | Install two new tape drives, clear |
| 91jul13 | 2385 | B | V | Clear and slight breeze |
| 91aug06 | 2409 | I | V | Clear, clouds in East, breezy, data looks good |
| 91aug07 | 2410 | R | V | Clear and breezy, data looks good, close early due to moon |
| 91aug08 | 2411 | R | V | Clear, data looks good, close early due to clouds and moon |
| 91aug13 | 2416 | B | V | (dewar pumped Aug 11) clear but hazy, data looks good |
| 91aug14 | 2417 | B | V | patchy clouds, lightning in SE |
| 91aug18 | 2421 | I | V | hazy, scattered cirrus, clearing, data marginally O.K. |
| 91aug19 | 2422 | R | V | hazy, close early due to clouds |
| 91oct06 | 2470 | C | R | down past months due to lightning strike, clear and calm, no data |
| 91oct07 | 2471 | C | R* | Clear and slightly breezy, data very good, close early |
| 91oct08 | 2472 | C | R* | Clear and calm, data very good, close early |
| 91oct09 | 2473 | C | B | scattered cirrus, breezy, close early due to clouds, data questionable |
| 91oct10 | 2474 | C | B* | scattered cirrus, slight breeze, close early, data looks good |
| 91oct11 | 2475 | C | B | Clear and windy, data looks good |
| 91oct14 | 2478 | C | B* | Clear and breezy, data good |
| 91oct15 | 2479 | C | I* | Clear and slight breeze, data looks good |
| 91oct16 | 2480 | C | I | Clear and calm, data looks good |
| 91oct17 | 2481 | C | I | Clear and breezy, data looks good |
| 91oct18 | 2482 | C | I | Clear and calm |
| 91oct29 | 2493 | C | I | Clear, slight breeze, data looks good, close early due to moon |
| 91oct31 | 2495 | C | I | Clear, data O.K., close early due to humidity |
| 91nov01 | 2496 | C | R* | Clear, slight breeze, data looks good, stars slightly out-of-focus |
| 91nov02 | 2497 | C | R* | Clear and calm, data looks good |
| 91nov03 | 2498 | C | R* | scattered cirrus, calm, data looks good |
| 91nov04 | 2499 | C | B* | Clear, occasional breeze, gusts, data good |
| 91nov05 | 2500 | C | V* | Clear and calm, mirror focused, data looks good |

Table A1.1 - CTI Observing Log (continued)

| Date | Dayno | CCD0 | CCD1 | Comment |
|---|---|---|---|---|
| 91nov07 | 2502 | C | B | Clear and calm, data very good |
| 91nov08 | 2503 | C | V | Clear and calm, data looks good |
| 91nov09 | 2504 | C | V | Clear and calm, data looks good, close early due to clouds |
| 91nov12 | 2507 | C | B | Clear, data has many horizontal streaks, close early |
| 91nov13 | 2508 | C | R* | scattered cirrus, calm, data good, close early due to clouds and rain |
| 91nov26 | 2521 | C | R | scattered cirrus, data looks good, close early due to moon, Grinnell problems |
| 91nov27 | 2522 | C | I | Clear and calm, software problem, close early due to moon |
| 91nov30 | 2525 | C | I | Clear but very windy, no data acquired |
| 91dec03 | 2528 | C | I | Clear, slight breeze, data looks good, close early due to winds |
| 91dec04 | 2529 | C | I | scattered cirrus, windy, data looks O.K. |
| 91dec07 | 2532 | C | V* | Clear and calm, lightning in South, data looks good |
| 91dec08 | 2533 | C | B* | Clear and windy, data looks O.K. |
| 91dec14 | 2539 | C | I | Clear and windy, data looks O.K., close early due to wind |
| 91dec15 | 2540 | C | R* | Clear and windy, data looks O.K., moonlight strong |
| 91dec16 | 2541 | C | I | Cloudy, close early due to clouds, data poor |
| 92jan02 | 2558 | C | V | Clear and breezy, Grinnell problem, close early due to clouds |
| 92jan09 | 2565 | C | I | scattered cirrus and windy, no data acquired |
| 92jan10 | 2566 | C | I* | Clear and breezy, data good |
| 92jan13 | 2569 | C | V* | Clear and breezy, data looks good |
| 92jan14 | 2570 | C | I* | Clear and calm, strong moonlight, data looks good |
| 92jan15 | 2571 | C | I* | |
| 92jan25 | 2581 | C | R* | Clear and breezy, data looks good |
| 92jan26 | 2582 | C | I | scattered cirrus, windy, data probably O.K. |
| 92jan27 | 2583 | C | V | thin cirrus, calm, data looks good |
| 92jan28 | 2584 | C | V | thin cirrus, calm, data looks good |
| 92jan29 | 2585 | C | V | Clear and breezy, data good |
| 92jan30 | 2586 | C | I* | Clear and breezy, data good |
| 92jan31 | 2587 | C | I | Clear and very breezy, images slightly distorted, data O.K. |
| 92feb01 | 2588 | C | B* | Clear and calm |
| 92feb10 | 2597 | C | V | partial clouds, high humidity, no data acquired |
| 92feb24 | 2611 | C | I | Clear and breezy, data looks O.K., close early due to moon |
| 92feb25 | 2612 | C | R | Clear and breezy, data very good, close early due to moon |
| 92feb26 | 2613 | C | V | Clear and breezy, data looks good |
| 92feb27 | 2614 | C | V | Clear and windy, data O.K., |
| 92feb28 | 2615 | C | B | Clear and breezy, A/D problems, data O.K. |
| 92feb29 | 2616 | C | B | A/D converters test, clear and breezy, data looks good, thick cirrus later |
| 92mar06 | 2622 | C | B | (voltage test Mar 04) clear and calm, horizontal bars in data, data marginal |
| 92mar11 | 2627 | C | V | Clear and calm, 100% humidity, no data acquired |
| 92mar12 | 2628 | C | R | Clear and breezy, no data on screen |
| 92mar25 | 2640 | C | I | Clear and calm, data looks good, close early due to moon |

Table A1.1 - CTI Observing Log (continued)

| Date | Dayno | CCD0 | CCD1 | Comment |
|---|---|---|---|---|
| 92mar26 | 2641 | C | I | scattered cirrus, calm, data marginal, close early due to clouds |
| 92apr06 | 2652 | C | V | Clear and slight breeze, data looks good |
| 92apr07 | 2653 | C | B | Clear and calm, data looks good |
| 92apr08 | 2654 | C | I | scattered cirrus, calm, data O.K., close early due to clouds |
| 92apr09 | 2656 | C | V | Clear and calm, data looks good |
| 92apr10 | 2657 | C | I | Clear and calm, data looks good |
| 92apr11 | 2658 | C | I | Cirrus everywhere, calm |
| 92apr25 | 2672 | C | R | traces of cirrus, data looks very good |
| 92apr26 | 2673 | C | I | scattered cirrus at start, data looks good |
| 92apr27 | 2674 | C | V | Clear with slight cirrus, data looks very good |
| 92apr28 | 2675 | C | V | Clear overhead, data looks good |
| 92apr29 | 2676 | C | V | Clear but very windy, data looks good |
| 92apr30 | 2677 | C | B | scattered cirrus throughout night, data looks O.K. |
| 92may02 | 2679 | C | B | some cirrus, heavier in morning, data looks O.K. |
| 92may03 | 2680 | C | B | thin cirrus with heavy clouds to east, data looks O.K. |
| 92may07 | 2684 | C | V | Clear overhead with clouds on horizon, data looks very good |
| 92may08 | 2685 | C | R | Clear overhead, clouds to east, data looks good, early closing due to clouds |

Table A1.2 - Bright Stars in CTI Survey

| name | RA (1987.5) | Dec | visual mag |
|---|---|---|---|
| SAO 76990 | $05^h\ 08^m\ 57.8^s$ | $28^\circ\ 00'\ 57.6''$ | 6.01 |
| SAO 77121 | 05 20 12.2 | 27 56 44.3 | 6.33 |
| SAO 77625 | 05 50 10.8 | 27 57 53.4 | 5.56 |
| 49 Aur | 06 34 24.8 | 28 01 58.7 | 5.27 |
| $\iota$ Gem | 07 24 57.4 | 27 49 28.4 | 3.79 |
| 64 Gem | 07 28 33.9 | 28 08 43.8 | 5.05 |
| 65 Gem | 07 29 02.2 | 27 56 34.6 | 5.01 |
| $\beta$ Gem (Pollux) | 07 44 34.9 | 28 03 27.3 | 1.14 |
| $\psi_1$ Cnc | 08 25 42.3 | 27 56 11.3 | 5.57 |
| $\rho_2$ Cnc | 08 54 54.9 | 27 58 33.8 | 5.22 |
| 67 Cnc | 09 01 04.4 | 27 57 11.8 | 6.07 |
| 44 LMi | 10 49 12.6 | 28 02 23.4 | 6.04 |
| $\beta$ Com | 13 11 19.7 | 27 55 55.5 | 4.26 |
| SAO 82944 | 13 40 04.7 | 28 07 41.1 | 6.23 |
| SAO 84015 | 15 48 03.4 | 28 11 40.9 | 5.85 |
| SAO 87165 | 19 23 52.3 | 28 03 46.0 | 6.53 |
| $\beta_1$ Cyg (Albireo-A) | 19 30 13.0 | 27 55 58.5 | 3.08 |
| $\beta_2$ Cyg (Albireo-B) | 19 30 15.1 | 27 56 18.8 | 5.11 |
| 32 Vul | 20 54 01.6 | 28 00 34.9 | 5.01 |
| $\beta$ Peg (Scheat) | 23 03 09.4 | 28 00 48.4 | 2.42 |

Table A1.3 - SAO stars in CTI Survey

| SAO #/ name | RA (1987.5) | Dec | visual mag |
|---|---|---|---|
| 73878 | $00^h\ 17^m\ 27.1^s$ | $28^\circ\ 06'\ 12.5''$ | 9.4 |
| 73901 | 00 19 44.7 | 28 05 04.7 | 9.1 |
| 73920 | 00 20 47.2 | 28 06 20.0 | 9.4 |
| 73923 | 00 20 59.7 | 28 00 53.7 | 9.0 |
| 73965 | 00 24 31.5 | 28 00 29.8 | 8.6 |
| 74015 | 00 27 09.0 | 28 06 18.1 | 8.0 |
| 74022 | 00 27 37.2 | 27 59 29.4 | 8.0 |
| 74045 | 00 29 47.9 | 28 00 15.6 | 8.2 |
| 74053 | 00 30 09.2 | 28 02 33.8 | 9.0 |
| 74075 | 00 31 39.3 | 28 02 54.0 | 9.1 |
| 74124 | 00 34 58.7 | 28 05 38.0 | 9.2 |
| 74198 | 00 40 45.3 | 27 58 27.5 | 8.2 |
| 74337 | 00 52 43.2 | 28 00 07.8 | 9.3 |
| 74380 | 00 55 54.4 | 28 00 44.8 | 9.0 |
| 74403 | 00 57 43.9 | 28 04 16.5 | 9.0 |
| 74528 | 01 09 26.4 | 27 58 37.8 | 8.9 |
| 74555 | 01 11 53.4 | 27 59 43.1 | 9.0 |
| 74584 | 01 13 55.9 | 28 00 33.3 | 8.3 |
| 74711 | 01 25 07.7 | 28 01 13.1 | 8.9 |
| 74733 | 01 26 39.5 | 28 01 58.8 | 9.2 |
| 74794 | 01 33 03.4 | 27 57 53.8 | 9.5 |
| 74835 | 01 37 02.7 | 28 05 53.9 | 9.3 |
| 74857 | 01 38 51.9 | 28 02 45.8 | 7.9 |
| 74876 | 01 41 07.3 | 28 03 46.5 | 8.6 |
| 74891 | 01 42 33.9 | 27 59 47.9 | 9.1 |
| 74937 | 01 47 05.0 | 28 00 23.0 | 9.1 |
| 74998 | 01 52 28.8 | 27 57 39.0 | 8.3 |
| 75027 | 01 54 58.8 | 27 59 10.9 | 9.0 |
| 75105 | 02 01 54.8 | 28 02 57.5 | 9.0 |
| 75137 | 02 05 11.5 | 28 02 31.5 | 9.0 |
| 75206 | 02 12 13.5 | 27 57 36.1 | 9.3 |
| 75230 | 02 14 39.5 | 28 00 38.7 | 9.0 |
| 75301 | 02 20 36.4 | 28 00 51.8 | 8.9 |
| 75328 | 02 22 35.7 | 28 05 06.3 | 8.6 |
| 75365 | 02 25 57.8 | 27 59 35.3 | 8.8 |
| 75402 | 02 28 51.3 | 27 59 08.9 | 9.0 |
| 75475 | 02 36 54.1 | 27 57 43.9 | 9.0 |
| 75484 | 02 37 17.0 | 27 59 37.8 | 8.6 |
| 75520 | 02 40 49.2 | 27 59 35.1 | 8.8 |
| 75538 | 02 43 04.8 | 28 05 31.2 | 8.9 |
| 75543 | 02 43 45.6 | 27 57 46.6 | 7.9 |
| 75561 | 02 45 41.8 | 28 00 19.1 | 9.0 |
| 75617 | 02 52 07.3 | 28 01 33.3 | 8.6 |
| 75640 | 02 54 40.9 | 28 05 43.9 | 8.2 |
| 75678 | 02 59 16.9 | 27 57 59.7 | 9.4 |
| 76223 | 03 48 10.5 | 28 01 36.1 | 9.0 |
| 76278 | 03 51 13.8 | 27 58 39.9 | 8.8 |
| 76288 | 03 51 41.5 | 28 05 49.5 | 8.6 |

Table A1.3 (continued) - SAO stars in CTI Survey

| SAO #/ name | RA (1987.5) | Dec | visual mag |
|---|---|---|---|
| 76298 | 03 52 33.4 | 27 59 44.2 | 8.5 |
| 76304 | 03 52 51.3 | 28 06 42.5 | 7.8 |
| 76354 | 03 56 52.8 | 28 03 48.6 | 9.2 |
| 76403 | 04 01 28.7 | 28 05 33.2 | 7.5 |
| 76418 (RW Tau) | 04 03 08.1 | 28 05 32.6 | 8.0 |
| 76540 | 04 17 40.8 | 28 04 23.9 | 8.7 |
| 76634 | 04 29 32.9 | 28 06 17.1 | 6.6 |
| 76659 | 04 34 07.1 | 28 02 23.8 | 9.0 |
| 76673 | 04 36 15.8 | 27 59 11.2 | 9.3 |
| 76690 | 04 38 45.5 | 27 59 52.5 | 8.8 |
| 76781 | 04 49 35.5 | 28 05 04.6 | 8.9 |
| 76805 | 04 52 13.7 | 28 05 15.6 | 8.2 |
| 76918 | 05 02 06.7 | 28 01 20.3 | 9.8 |
| 76990 | 05 08 57.8 | 28 00 57.6 | 6.0 |
| 76991 | 05 08 58.2 | 28 01 07.8 | 8.1 |
| 77093 | 05 17 55.1 | 28 04 41.8 | 8.4 |
| 77114 | 05 19 47.5 | 28 03 20.3 | 9.0 |
| 77121 | 05 20 12.2 | 27 56 44.3 | 6.3 |
| 77130 | 05 21 47.5 | 28 05 26.3 | 8.8 |
| 77268 | 05 33 51.8 | 28 02 35.9 | 8.1 |
| 77346 | 05 37 56.0 | 28 00 27.2 | 9.3 |
| 77351 | 05 38 19.9 | 27 59 41.2 | 9.0 |
| 77401 | 05 40 59.0 | 28 06 40.1 | 9.1 |
| 77625 | 05 50 10.8 | 27 57 53.4 | 5.6 |
| 77638 | 05 50 45.6 | 28 05 22.4 | 8.0 |
| 77662 | 05 52 08.3 | 27 59 45.5 | 9.0 |
| 77728 | 05 55 05.9 | 27 58 28.7 | 9.2 |
| 77818 | 05 59 17.6 | 28 07 33.0 | 7.0 |
| 78126 | 06 13 35.8 | 28 01 57.9 | 8.7 |
| 78185 | 06 16 54.9 | 28 04 33.5 | 9.1 |
| 78191 | 06 17 12.6 | 28 00 44.0 | 7.4 |
| 78206 | 06 17 59.9 | 28 03 39.7 | 8.0 |
| 78240 | 06 19 34.1 | 28 04 59.6 | 8.6 |
| 78291 | 06 22 00.6 | 27 59 36.9 | 7.5 |
| 78334 | 06 24 12.1 | 28 02 22.7 | 7.7 |
| 78483 | 06 32 17.7 | 28 05 33.6 | 7.6 |
| 78488 | 06 32 32.1 | 28 05 44.4 | 8.7 |
| 78496 | 06 32 54.2 | 27 59 25.3 | 7.8 |
| 78524 (49 Aur) | 06 34 24.8 | 28 01 58.7 | 5.0 |
| 78533 | 06 34 57.3 | 28 02 58.4 | 9.3 |
| 78553 | 06 36 34.3 | 27 59 14.2 | 8.9 |
| 79050 | 07 05 19.9 | 28 00 58.7 | 8.9 |
| 79112 | 07 08 29.4 | 28 04 25.2 | 8.4 |
| 79184 | 07 12 59.2 | 27 59 18.9 | 8.8 |
| 79270 | 07 17 55.7 | 28 00 55.2 | 9.0 |
| 79283 | 07 18 41.0 | 27 59 31.8 | 9.3 |
| 79374 (ι Gem) | 07 24 57.4 | 27 49 28.4 | 3.9 |
| 79390 | 07 26 17.8 | 28 03 18.0 | 9.0 |
| 79427 (64 Gem) | 07 28 33.8 | 28 08 43.0 | 5.0 |

Table A1.3 (continued) - SAO stars in CTI Survey

| SAO #/ name | RA (1987.5) | Dec | visual mag |
|---|---|---|---|
| 79434 (65 Gem) | 07 29 02.2 | 27 56 34.6 | 5.1 |
| 79457 | 07 30 22.6 | 28 01 42.5 | 9.0 |
| 79602 | 07 40 03.3 | 27 58 30.1 | 8.7 |
| 79666 ($\beta$ Gem) | 07 44 34.9 | 28 03 27.3 | 1.2 |
| 79772 | 07 52 34.7 | 28 05 07.0 | 6.7 |
| 79807 | 07 55 31.2 | 28 05 31.8 | 9.4 |
| 79891 | 08 02 26.1 | 27 58 02.1 | 8.2 |
| 80118 | 08 20 21.1 | 28 07 40.9 | 9.0 |
| 80181 ($\psi_1$ Cnc) | 08 25 42.3 | 27 56 11.3 | 5.8 |
| 80183 | 08 25 55.3 | 28 06 17.9 | 8.5 |
| 80214 | 08 29 24.5 | 28 07 26.1 | 8.7 |
| 80430 | 08 47 09.1 | 28 01 38.4 | 8.4 |
| 80464 | 08 51 00.8 | 28 04 08.4 | 9.0 |
| 80511 ($\rho_2$ Cnc) | 08 54 54.9 | 27 58 33.8 | 5.3 |
| 80584 | 09 01 00.2 | 27 58 37.1 | 9.0 |
| 80585 (67 Cnc) | 09 01 04.4 | 27 57 11.8 | 6.0 |
| 80646 | 09 06 55.0 | 28 03 23.8 | 8.3 |
| 80854 | 09 28 23.2 | 27 59 18.0 | 8.9 |
| 80911 | 09 34 25.1 | 27 59 23.4 | 8.2 |
| 80922 | 09 35 52.3 | 28 01 17.1 | 8.9 |
| 80926 | 09 36 07.0 | 28 01 50.4 | 8.9 |
| 80941 | 09 37 44.0 | 28 03 45.4 | 7.9 |
| 80969 | 09 40 52.8 | 28 00 47.2 | 8.6 |
| 81194 | 10 06 51.0 | 28 06 38.1 | 8.8 |
| 81209 | 10 08 43.4 | 28 02 39.7 | 8.7 |
| 81272 | 10 16 41.1 | 28 07 51.4 | 9.1 |
| 81308 | 10 20 44.3 | 28 04 00.3 | 9.2 |
| 81395 | 10 30 52.4 | 28 06 21.5 | 9.0 |
| 81423 | 10 34 07.8 | 28 01 39.7 | 6.9 |
| 81429 | 10 34 47.1 | 28 01 58.4 | 9.2 |
| 81461 | 10 39 32.1 | 28 04 54.6 | 8.9 |
| 81462 | 10 39 39.5 | 28 04 36.1 | 8.9 |
| 81503 | 10 45 00.9 | 28 01 52.4 | 8.5 |
| 81542 (44 LMi) | 10 49 12.6 | 28 02 23.4 | 6.1 |
| 81663 | 11 04 55.0 | 28 05 21.7 | 9.0 |
| 81666 | 11 05 32.0 | 28 07 05.9 | 9.1 |
| 81695 | 11 08 15.9 | 28 03 18.3 | 8.3 |
| 81814 | 11 24 40.0 | 28 00 43.1 | 8.8 |
| 81892 | 11 35 23.8 | 27 58 20.3 | 8.2 |
| 81932 | 11 39 31.7 | 27 58 32.8 | 9.1 |
| 81955 | 11 42 43.7 | 28 07 27.3 | 7.3 |
| 82041 | 11 53 23.4 | 28 01 58.4 | 8.7 |
| 82100 | 12 00 26.7 | 28 01 55.8 | 8.6 |
| 82121 | 12 03 26.9 | 28 07 48.9 | 8.4 |
| 82149 | 12 07 47.0 | 28 03 11.3 | 8.9 |
| 82208 | 12 15 24.8 | 28 07 05.1 | 8.2 |
| 82236 | 12 18 23.9 | 28 07 08.3 | 9.0 |
| 82241 | 12 18 43.3 | 27 59 39.6 | 9.2 |

Table A1.3 (continued) - SAO stars in CTI Survey

| SAO #/ name | RA (1987.5) | Dec | visual mag |
|---|---|---|---|
| 82359 | 12 31 12.1 | 28 02 52.1 | 9.2 |
| 82430 | 12 39 30.0 | 27 58 43.4 | 9.3 |
| 82445 | 12 41 46.1 | 28 00 51.2 | 9.3 |
| 82465 | 12 43 43.9 | 28 03 00.8 | 7.8 |
| 82560 | 12 54 14.1 | 27 58 51.3 | 9.3 |
| 82561 | 12 54 20.5 | 28 03 37.7 | 8.9 |
| 82595 | 12 58 56.6 | 28 07 58.6 | 7.1 |
| 82706 (β Com) | 13 11 19.7 | 27 55 55.5 | 4.3 |
| 82763 | 13 17 23.0 | 28 07 51.6 | 9.0 |
| 82793 | 13 20 08.4 | 28 02 37.9 | 9.3 |
| 82826 | 13 24 31.7 | 28 02 41.0 | 8.3 |
| 82904 | 13 36 19.5 | 28 01 41.8 | 7.9 |
| 82944 | 13 40 04.7 | 28 07 41.1 | 6.4 |
| 82983 | 13 44 32.8 | 28 07 25.7 | 9.1 |
| 82992 | 13 46 00.2 | 28 00 17.6 | 8.1 |
| 83009 | 13 48 25.3 | 28 01 29.7 | 9.4 |
| 83142 | 14 02 39.0 | 28 03 50.3 | 9.0 |
| 83209 | 14 10 37.9 | 28 03 54.1 | 9.1 |
| 83213 | 14 11 00.2 | 28 05 39.4 | 8.3 |
| 83218 | 14 11 52.5 | 28 06 55.4 | 9.3 |
| 83237 | 14 13 34.6 | 27 59 29.6 | 9.0 |
| 83386 | 14 30 30.6 | 28 03 52.9 | 9.0 |
| 83439 | 14 36 29.2 | 28 03 12.6 | 8.5 |
| 83519 | 14 46 46.3 | 28 07 16.1 | 9.0 |
| 83791 | 15 21 23.0 | 28 05 07.4 | 9.0 |
| 83797 | 15 22 14.4 | 28 06 04.2 | 7.5 |
| 83855 | 15 29 39.7 | 28 05 53.8 | 9.0 |
| 83860 | 15 30 15.9 | 28 07 21.7 | 9.1 |
| 83949 | 15 41 05.1 | 28 02 05.0 | 8.0 |
| 83967 | 15 43 02.5 | 28 07 07.8 | 9.0 |
| 84015 | 15 48 03.4 | 28 11 40.9 | 5.8 |
| 84050 | 15 51 47.1 | 28 07 37.1 | 8.9 |
| 84215 | 16 08 42.8 | 28 05 12.5 | 8.7 |
| 84648 | 16 50 57.4 | 28 08 31.6 | 6.9 |
| 84810 | 17 04 15.9 | 28 06 27.9 | 7.2 |
| 84822 | 17 05 00.6 | 28 06 16.2 | 8.6 |
| 84857 | 17 06 58.8 | 28 08 13.1 | 8.0 |
| 84859 | 17 07 01.6 | 28 03 28.1 | 9.0 |
| 84870 | 17 07 53.0 | 28 03 13.5 | 9.0 |
| 84920 | 17 11 56.6 | 28 00 51.6 | 9.0 |
| 84946 | 17 13 46.8 | 28 00 14.6 | 8.9 |
| 84949 | 17 14 12.1 | 27 59 19.7 | 8.4 |
| 85006 | 17 18 54.1 | 28 02 18.5 | 7.1 |
| 85011 | 17 19 09.4 | 28 05 47.9 | 9.0 |
| 85056 | 17 22 52.9 | 28 03 15.1 | 9.0 |
| 85059 | 17 23 08.1 | 28 02 39.0 | 9.4 |
| 85173 | 17 30 41.8 | 28 08 43.6 | 8.6 |
| 85220 | 17 34 08.1 | 27 59 50.4 | 8.8 |
| 85378 | 17 44 28.5 | 28 00 40.4 | 8.7 |

Table A1.3 (continued) - SAO stars in CTI Survey

| SAO #/ name | RA (1987.5) | Dec | visual mag |
|---|---|---|---|
| 85405 | 17 46 12.7 | 27 59 13.6 | 8.7 |
| 85407 | 17 46 24.0 | 28 05 55.2 | 8.0 |
| 85581 | 17 57 05.1 | 27 59 36.7 | 8.5 |
| 85598 | 17 57 50.4 | 27 59 23.7 | 8.4 |
| 85803 | 18 10 19.4 | 27 58 30.5 | 8.5 |
| 85830 | 18 12 26.7 | 28 03 11.4 | 9.1 |
| 85981 | 18 22 02.7 | 28 06 47.4 | 9.1 |
| 86027 | 18 24 50.7 | 28 04 30.7 | 8.0 |
| 86269 | 18 37 52.5 | 28 00 21.4 | 8.9 |
| 86301 | 18 39 25.6 | 28 04 58.9 | 9.1 |
| 86306 | 18 39 39.1 | 28 00 01.0 | 9.1 |
| 86340 | 18 41 54.4 | 28 06 44.0 | 7.5 |
| 86376 | 18 43 11.7 | 28 05 53.7 | 8.7 |
| 86388 | 18 43 51.6 | 28 05 17.4 | 7.3 |
| 86402 | 18 44 50.8 | 28 00 41.3 | 9.2 |
| 86410 | 18 45 12.8 | 27 59 44.1 | 9.4 |
| 86718 | 19 01 13.0 | 28 05 53.3 | 8.3 |
| 87059 | 19 18 29.1 | 28 01 57.8 | 9.0 |
| 87108 | 19 20 46.5 | 28 02 32.4 | 9.0 |
| 87165 | 19 23 52.3 | 28 03 46.0 | 6.4 |
| 87229 | 19 26 47.4 | 27 59 45.2 | 9.0 |
| 87301 ($\beta_1$ Cyg) | 19 30 13.0 | 27 55 58.5 | 3.2 |
| 87302 ($\beta_2$ Cyg) | 19 30 15.1 | 27 56 18.8 | 5.4 |
| 87500 | 19 38 16.0 | 28 03 24.4 | 9.3 |
| 87503 | 19 38 22.4 | 28 03 00.2 | 9.2 |
| 87520 | 19 39 02.5 | 28 07 01.7 | 8.5 |
| 87590 | 19 41 31.1 | 28 04 29.6 | 8.9 |
| 87614 | 19 42 21.8 | 28 01 30.8 | 8.7 |
| 87651 | 19 43 59.9 | 28 03 20.0 | 9.3 |
| 87716 | 19 46 27.8 | 28 00 50.4 | 8.6 |
| 87769 | 19 48 47.5 | 28 04 34.5 | 9.4 |
| 87842 | 19 51 33.7 | 28 04 08.3 | 8.5 |
| 87877 | 19 52 45.3 | 28 03 59.9 | 7.8 |
| 87890 | 19 53 08.3 | 28 03 48.5 | 9.3 |
| 87931 | 19 54 48.5 | 28 04 58.2 | 9.2 |
| 88180 | 20 05 17.2 | 28 05 43.9 | 7.7 |
| 88197 | 20 05 37.1 | 28 05 23.2 | 8.3 |
| 88265 | 20 08 56.7 | 28 02 05.7 | 8.5 |
| 88357 | 20 12 12.0 | 28 02 11.0 | 8.9 |
| 88474 | 20 17 01.8 | 28 02 37.1 | 9.4 |
| 88475 | 20 17 03.9 | 28 04 21.2 | 9.0 |
| 88537 | 20 19 50.0 | 28 02 30.3 | 9.0 |
| 88563 | 20 20 44.3 | 28 04 08.5 | 8.5 |
| 88568 | 20 21 02.2 | 28 07 02.7 | 8.5 |
| 88627 | 20 23 36.9 | 28 04 26.4 | 9.3 |
| 88634 | 20 23 53.6 | 27 59 03.6 | 9.0 |
| 88684 | 20 26 15.0 | 28 01 34.4 | 8.8 |
| 88702 | 20 27 01.7 | 28 00 57.6 | 8.6 |

Table A1.3 (continued) - SAO stars in CTI Survey

| SAO #/ name | RA (1987.5) | Dec | visual mag |
|---|---|---|---|
| 88760 | 20 29 13.1 | 27 58 09.7 | 8.7 |
| 88854 | 20 33 50.6 | 27 59 45.3 | 9.4 |
| 88857 | 20 34 03.1 | 28 03 16.0 | 8.5 |
| 88948 | 20 38 01.1 | 27 58 01.7 | 9.2 |
| 88970 | 20 38 58.2 | 28 02 39.7 | 8.0 |
| 89100 | 20 44 58.3 | 28 05 59.0 | 9.2 |
| 89102 | 20 45 01.8 | 28 01 35.9 | 9.2 |
| 89108 | 20 45 19.1 | 28 01 18.8 | 9.2 |
| 89118 | 20 46 17.3 | 28 04 54.0 | 8.3 |
| 89125 | 20 46 31.7 | 28 05 54.6 | 9.2 |
| 89160 | 20 48 24.5 | 28 06 32.6 | 9.2 |
| 89169 | 20 48 55.5 | 28 03 16.2 | 9.1 |
| 89262 | 20 53 44.5 | 28 04 35.6 | 9.0 |
| 89272 (32 Vul) | 20 54 01.6 | 28 00 34.9 | 5.2 |
| 89276 | 20 54 09.0 | 28 00 49.9 | 9.2 |
| 89278 | 20 54 29.9 | 28 02 36.4 | 8.0 |
| 89279 | 20 54 32.8 | 28 05 06.0 | 9.3 |
| 89359 | 20 59 44.5 | 28 01 48.3 | 9.2 |
| 89378 | 21 01 09.4 | 28 03 08.8 | 7.6 |
| 89433 | 21 04 06.6 | 28 04 52.1 | 9.1 |
| 89455 | 21 05 31.9 | 27 58 13.5 | 9.3 |
| 89534 | 21 12 26.7 | 28 06 14.0 | 8.1 |
| 89558 | 21 14 01.6 | 28 06 09.6 | 8.4 |
| 89562 | 21 14 35.7 | 28 05 10.0 | 9.0 |
| 89567 | 21 14 49.2 | 28 05 34.4 | 9.0 |
| 89569 | 21 15 04.0 | 27 57 26.4 | 8.1 |
| 89717 | 21 26 52.4 | 27 57 44.3 | 9.0 |
| 89816 | 21 34 47.5 | 27 57 51.4 | 8.8 |
| 89900 | 21 40 20.9 | 28 00 41.8 | 8.8 |
| 89996 | 21 46 45.5 | 28 02 01.3 | 8.4 |
| 90063 | 21 51 53.1 | 27 59 56.1 | 9.0 |
| 90152 | 21 59 02.8 | 28 04 50.0 | 8.5 |
| 90168 | 22 00 17.6 | 27 59 14.6 | 8.2 |
| 90172 | 22 00 48.8 | 27 58 22.9 | 9.3 |
| 90221 | 22 05 21.0 | 27 58 52.4 | 9.2 |
| 90253 | 22 07 14.0 | 28 04 19.2 | 9.3 |
| 90261 | 22 07 47.6 | 27 59 02.7 | 9.0 |
| 90264 | 22 08 02.4 | 28 05 06.4 | 8.6 |
| 90268 | 22 08 23.8 | 28 01 24.9 | 9.2 |
| 90272 | 22 08 42.0 | 28 01 01.6 | 9.0 |
| 90286 | 22 09 48.3 | 28 05 16.1 | 8.5 |
| 90369 | 22 15 21.6 | 28 04 22.4 | 9.2 |
| 90394 | 22 16 46.3 | 28 02 42.0 | 8.8 |
| 90464 | 22 23 05.0 | 27 57 31.1 | 9.5 |
| 90479 | 22 23 55.7 | 28 01 21.1 | 9.0 |
| 90534 | 22 27 58.1 | 28 04 48.9 | 9.0 |
| 90561 | 22 30 08.5 | 28 05 08.6 | 8.5 |
| 90617 | 22 34 20.2 | 28 01 27.2 | 9.0 |
| 90675 | 22 38 25.9 | 28 06 14.7 | 9.0 |

Table A1.3 (continued) - SAO stars in CTI Survey

| SAO #/ name | RA (1987.5) | Dec | visual mag |
|---|---|---|---|
| 90715 | 22 41 06.4 | 27 59 34.0 | 8.6 |
| 90732 (BD Peg) | 22 42 23.3 | 28 05 30.2 | 8.9 |
| 90762 | 22 44 52.2 | 28 02 06.0 | 8.7 |
| 90799 | 22 47 54.2 | 28 03 22.2 | 8.1 |
| 90905 | 22 57 32.6 | 28 00 36.1 | 9.1 |
| 90929 | 22 59 21.8 | 28 04 15.9 | 9.0 |
| 90981 (β Peg) | 23 03 09.4 | 28 00 48.4 | 2.6 |
| 91118 | 23 14 21.1 | 28 00 10.4 | 7.0 |
| 91153 | 23 17 14.0 | 27 57 31.8 | 8.5 |
| 91193 | 23 20 17.3 | 27 59 56.7 | 8.8 |
| 91214 | 23 21 43.8 | 28 03 20.9 | 8.5 |
| 91224 | 23 22 20.5 | 27 58 58.0 | 9.0 |
| 91252 | 23 24 43.2 | 28 07 23.7 | 8.6 |
| 91363 | 23 34 51.4 | 27 57 06.2 | 8.7 |
| 91406 | 23 39 02.8 | 27 57 19.4 | 9.1 |
| 91421 | 23 41 05.7 | 27 58 38.6 | 9.3 |
| 91472 | 23 45 10.8 | 28 06 29.5 | 7.9 |
| 91505 | 23 48 03.4 | 27 58 41.7 | 9.1 |

Table A1.4 - Previously known variable stars in CTI Survey

| name | RA (1987.5) | Dec | mag range | Type |
|---|---|---|---|---|
| RW Tri | $02^h\ 24^m\ 52.4^s$ | $28°\ 02'\ 30.0''$ | 12.5 - 12.61 | Algol |
| EP Tau | 03 29 18.6 | 28 04 20.5 | 11 - >13 | SR |
| RW Tau | 04 03 08 | 28 05 37 | 7.98 - 11.59 | Algol |
| AB Tau | 05 40 14 | 28 06 06 | 10.4 - 12.0 | SR |
| SV Tau | 05 51 20 | 28 06 36 | 9.68 - 10.78 | Algol |
| CN Tau | 05 57 22.1 | 28 02 23.1 | 13.1 - 13.7 | RR Lyr |
| AH Aur | 06 25 17 | 28 00 26 | 10.2 - 10.70 | W UMa |
| IR Gem | 06 46 52 | 28 05 34 | 10.7 - >14.5 | U Gem |
| GR Com | 12 04 40.4 | 28 01 08.6 | 15.4 - 16.7 | RR Lyr |
| GS Com | 12 24 18.6 | 28 03 17.2 | 15.9 - 16.9 | RR Lyr |
| DV Com | 12 43 18.6 | 28 05 21.5 | 14.2 - 15.5 | RR Lyr |
| EZ Com | 13 17 32.6 | 28 01 39.6 | 16.5 - 17.5 | RR Lyr |
| V375 Her | 17 13 11.0 | 28 00 10.2 | 15.8 - 17.2 | SR |
| V385 Her | 17 15 57.0 | 28 06 44.6 | 14.9 - 15.9 | RR Lyr |
| V532 Her | 18 11 26.7 | 28 03 45.4 | 14.8 - 16.0 | RR Lyr |
| CE Lyr | 18 36 22.8 | 28 03 39.5 | 11.7 - 14.5 | Mira |
| CV Lyr | 18 50 06.0 | 28 05 59.7 | 10.8 - 13.1 | SR |
| DF Lyr | 18 53 04.5 | 28 03 22.6 | 13.1 - 13.5 | W UMa |
| GS Lyr | 19 03 50.3 | 28 00 44.9 | 14.4 - 14.8 | L |
| UU Lyr | 19 05 12.5 | 28 03 49.3 | 11.5 - >16.1 | Mira |
| TY Lyr | 19 09 17.7 | 28 03 04.6 | 9.0 - 14.6 | Mira |
| V427 Lyr | 19 13 11.8 | 28 00 51.6 | 15.3 - 17.3 | RR Lyr |
| PP Lyr | 19 17 13.8 | 28 06 06.6 | 13.3 - >15.6 | Mira |
| V1129 Cyg | 19 33 21.9 | 28 03 16.9 | 15.3 - >17 | Mira |
| V911 Cyg | 19 35 24.5 | 27 57 20.9 | 14.4 - 16.5 | Algol |
| EH Cyg | 19 36 18.5 | 28 06 00.1 | 11.8 - 16.5 | Mira |
| V926 Cyg | 19 38 06.6 | 27 59 09.9 | 15.2 - 15.9 | RR Lyr |
| V1140 Cyg | 19 39 16.7 | 28 03 26.4 | 15.3 - >20 | Mira |
| AI Vul | 19 46 17 | 28 05 55 | 13.2 - >17.5 | Mira |
| EQ Vul | 19 57 52.6 | 27 59 05.2 | 11.8 - 12.5 | Algol |
| KW Vul | 20 20 34.3 | 27 57 35.0 | 15 - >19 | Mira |
| BY Peg | 21 38 18.9 | 28 02 21.6 | 12.9 - 13.6 | W UMa |
| CW Peg | 21 47 54.0 | 28 02 59.1 | 11.8 - 16.1 | Algol |
| BD Peg | 22 42 23 | 28 05 28 | 9.4 - 10.3 | SR |
| β Peg | 23 03 09 | 28 00 43 | 2.31 - 2.74 | Slow Irg |

Table A1.5 - Bright galaxies in CTI Survey

| name | RA (1987.5) | Dec | mag |
|---|---|---|---|
| Z 499020 | $00^h$ $09.3^m$ | $28°$ $06'$ | 15.7 |
| Z 501011 | 00 46.4 | 28 00 | 15.4 |
| Z 504093 | 02 28.3 | 28 05 | 15.7 |
| Z 505003 (NGC 962) | 02 32.0 | 28 01 | 14.2 |
| Z 505052 | 02 45.2 | 27 58 | 15.6 |
| Z 144002 | 06 19.8 | 27 59 | 15.6 |
| Z 148026 | 07 47.3 | 28 03 | 15.6 |
| Z 148028 | 07 47.5 | 28 03 | 15.5 |
| Z 148056 | 07 53.1 | 28 04 | 15.6 |
| Z 148116 | 08 07.9 | 28 06 | 15.4 |
| Z 148117 | 08 08.4 | 28 02 | 15.3 |
| Z 149014 | 08 18.2 | 28 03 | 15.6 |
| Z 149026 | 08 27.5 | 28 07 | 15.2 |
| Z 150004 | 08 35.5 | 28 06 | 14.9 |
| Z 151008 | 09 03.7 | 28 00 | 14.4 |
| Z 151044 | 09 16.1 | 28 07 | 15.7 |
| Z 151054 | 09 18.0 | 28 01 | 15.7 |
| Z 152042 | 09 37.4 | 28 07 | 14.8 |
| Z 152071 | 09 49.3 | 28 05 | 15.3 |
| Z 153027 | 10 09.7 | 28 01 | 14.6 |
| Z 154004 | 10 20.6 | 27 59 | 15.2 |
| Z 154008 (NGC 3232) | 10 23.6 | 28 05 | 15.4 |
| Z 154010 (NGC 3235) | 10 24.2 | 28 05 | 14.7 |
| Z 154039 | 10 41.7 | 28 05 | 15.5 |
| Z 155004 | 10 44.5 | 28 03 | 15.7 |
| Z 155020 | 10 48.5 | 27 59 | 15.3 |
| Z 155029 (NGC 3414) | 10 50.6 | 28 02 | 12.0 |
| Z 155049 (NGC 3504) | 11 02.6 | 28 03 | 11.5 |
| Z 155051 (NGC 3512) | 11 03.4 | 28 06 | 12.9 |
| Z 156021 | 11 11.8 | 28 06 | 15.7 |
| Z 156022 | 11 12.1 | 20 08 | 15.7 |
| Z 156024 | 11 12.2 | 28 03 | 15.5 |
| Z 156098 | 11 31.7 | 28 07 | 15.0 |
| GQ Com | 12 04.1 | 27 58 | 14.7-16.1 |
| Z 158021 | 12 05.7 | 28 01 | 15.7 |
| Z 158022 | 12 05.9 | 28 00 | 15.4 |
| Z 158076 | 12 19.4 | 28 03 | 14.9 |
| Z 158079 | 12 19.7 | 28 00 | 15.7 |
| Z 159024 (NGC 4559) | 12 35.3 | 28 02 | 10.7 |
| Z 159051 | 12 40.3 | 28 03 | 15.4 |
| NGC 4828 | 12 56.1 | 28 05 | 15.5 |
| NGC 4850 | 12 57.4 | 28 02 | 15.5 |
| NGC 4864 | 12 58.6 | 28 03 | 15.0 |
| NGC 4867 | 12 58.7 | 28 04 | 15.5 |
| NGC 4871 | 12 58.9 | 28 02 | 15.0 |
| NGC 4872 | 12 59.0 | 28 01 | 15.5 |
| NGC 4873 | 12 58.9 | 28 03 | 15.5 |
| NGC 4874 | 12 59.0 | 28 02 | 13.5 |

Table A1.5 (continued) - Bright galaxies in CTI Survey

| name | RA (1987.5) | Dec | mag |
|---|---|---|---|
| NGC 4883 | 12 59.3 | 28 06 | 15.0 |
| NGC 4886 | 12 59.5 | 28 03 | 15.0 |
| NGC 4889 | 12 59.5 | 28 03 | 12.5 |
| NGC 4894 | 12 59.7 | 28 02 | 15.5 |
| NGC 4898 | 12 59.7 | 28 01 | 14.5 |
| NGC 4906 | 13 00.1 | 28 00 | 15.0 |
| NGC 4908 | 13 00.2 | 28 07 | 15.0 |
| NGC 4927 | 13 01.4 | 28 04 | 15.0 |
| Z 160113 (NGC 4929) | 13 02.1 | 28 06 | 14.9 |
| Z 160118 (NGC 4931) | 13 02.4 | 28 06 | 14.4 |
| Z 160120 (NGC 4934) | 13 02.7 | 28 05 | 15.0 |
| Z 160123 | 13 03.3 | 28 03 | 15.4 |
| Z 160141 | 13 06.6 | 28 06 | 15.5 |
| Z 160149 | 13 08.4 | 28 06 | 15.6 |
| Z 161065 | 13 28.6 | 28 06 | 15.7 |
| Z 161092 | 13 57.1 | 28 04 | 15.7 |
| Z 162039 | 13 58.5 | 28 05 | 15.6 |
| Z 162040 | 13 58.5 | 28 07 | 15.6 |
| Z 162041 | 13 58.6 | 28 02 | 15.7 |
| Z 162044 | 13 59.0 | 28 08 | 15.3 |
| Z 162053 | 14 02.4 | 28 05 | 14.7 |
| Z 163055 | 14 27.5 | 28 00 | 15.7 |
| Z 163079 | 14 33.0 | 28 06 | 15.3 |
| Z 163081 | 14 33.5 | 28 00 | 15.2 |
| Z 165021 | 15 07.4 | 28 01 | 15.5 |
| Z 165024 | 15 08.7 | 28 02 | 15.7 |
| Z 166036 | 15 40.9 | 28 02 | 15.2 |
| Z 166052 | 15 45.1 | 28 08 | 14.9 |
| Z 167021 | 16 04.2 | 28 08 | 15.6 |
| Z 167030 | 16 09.1 | 28 05 | 14.7 |
| Z 167048 (NGC 6092) | 16 12.2 | 28 00 | 15.0 |
| Z 169013 (NGC 6261) | 16 56.0 | 28 01 | 15.2 |
| Z 170028 | 17 24.3 | 28 05 | 15.7 |
| Z 171030 | 17 56.3 | 28 05 | 15.6 |
| Z 496043 (NGC 7487) | 23 08.3 | 28 07 | 15.0 |
| Z 498037 | 23 51.5 | 28 01 | 15.7 |
| Z 499102 | 23 58.1 | 28 02 | 15.7 |

Table A1.6 - Variable star types (adapted from GCVS)

**Cataclysmic** (Characterized by thermonuclear processes in the interior of a star, the surface layers of star, or the surrounding space volume.)

| | |
|---|---|
| Nova | Close binary system with one component a hot dwarf star. Mass transfer from cooler component excites a thermonuclear burst in dwarf's surface layers. Brightness increases of 7 to 19 magnitudes in V. Distinctions made between fast (fading of 3 magnitudes in V in < 100 days), slow (fading of 3 magnitudes in V in > 150 days), very slow (also called pseudonova, fading takes place over 10 years or longer) and recurrent (two or more outbursts observed) nova. |
| Supernova | Thermonuclear burst of entire star triggered by collapse of core. Brightness increases by 20 magnitudes or more in V. Distinctions made between Type I (no hydrogen lines present in spectra) and Type II (hydrogen lines present in spectra) supernova. |
| U Geminorum | (Also called dwarf nova.) Close binary with one component a white dwarf star surrounded by an accretion disk. Mass transfer excites periodic bursts in space surrounding white dwarf. Brightness increases from 2 to 6 magnitudes in V. Distinctions made between SS Cygni-type (cyclic), SU Ursae Majoris-type (cyclic with occasional larger outbursts), and Z Camelopardalis-type (cyclic with occasional variations in maximum and minimum brightness) variables. |
| Z Andromedae | Close binary of hot and late-type star with extended envelope excited by hot star's radiation. Irregular variations of up to 4 magnitudes in V. |

**Eruptive** (Characterized by violent processes or flares in the star's chromosphere and coronae.)

| | |
|---|---|
| Orion | Stars connected with diffuse nebulae and probably evolving to the zero-age main sequence. Variations of up to 6 magnitudes caused by star's interaction with surrounding circumstellar material. Irregular or cyclic variations observed. Distinctions made between early spectral types, intermediate and late spectral types, T Tauri-type (spectral type Fe-Me), YY Orionis-type (infall of matter observed in spectra), FU Orionis-type (large and sustained outburst), and flaring (identical to UV Ceti and related to nebulosity). |
| Rapid irregular | Similar to Orion variables, but with no apparent connection with diffuse nebulae. Brightness variations between 0.5 and 1.0 magnitudes in V. Distinctions made between early, intermediate, and late-type stars. |

Table A1.6 (continued) - Variable star types (adapted from GCVS)

| | |
|---|---|
| S Doradus | High luminosity stars connected with diffuse nebula and surrounded by expanding envelopes. Irregular, (although sometimes cyclic), brightness increases of 1 to 7 magnitudes in V. |
| G Cassiopeiae | Rapidly rotating stars with mass outflow from equatorial zone. Brightness variations of up to 1.5 magnitudes in V. Equatorial rings and disks often present. |
| Wolf-Rayet | Irregular brightness changes of up to 0.1 magnitudes in V probably caused by nonstable mass outflow from their atmospheres (stellar wind). Broadband emission features present. |
| UV Ceti | K-M stars displaying flare activity with brightness increases of tenths to 6 magnitudes in V. Flares peak rapidly and last from minutes to hours. |
| R Coronae Borealis | Hydrogen-poor, carbon- and helium-rich, high luminosity stars showing slow nonperiodic fading (1 to 9 magnitudes in V) and cyclic pulsations (tenths of magnitudes over 30-100 days). |

**Pulsating** (Characterized by periodic radial or nonradial contractions and expansions of surface layers. Those variables within the "instability strip" of the H-R diagram are thought to all owe their pulsation to a variable opacity of the second ionization state of helium. Many types of pulsating variables also form the "Great Sequence" on the H-R diagram.)

| | |
|---|---|
| δ Scuti | Both radial and non-radial pulsations of amplitudes from 0.003 to 0.9 magnitudes in V over periods of 0.01 to 0.2 days. Stars are of Population I with spectral types A0-F5, and are contained in the "instability strip" of the H-R diagram near the Main Sequence. |
| SX Pheonices | (Previously called dwarf Cepheid or RRs.) Similar to δ Scuti variables except stars are of Population II. |
| RR Lyrae | Radially pulsating giant (A2-F2) helium core burning stars of amplitudes from 0.2 to 2 magnitudes in V over periods of 0.3 to 1.2 days. Stars are of Population II and are in the "instability strip" of the H-R diagram. Distinctions made between ab-type (steep ascending branch), c-type (nearly symmetric with shorter periods and smaller light amplitudes), and stars with more than one pulsational mode present. |
| Classical Cepheids | (Also known as δ Cephei-type variables.) Population I, massive, high luminosity stars that have left the main sequence and evolved into the "instability strip" of the H-R diagram. Radial pulsations produce brightness variations of hundredths to 2 magnitudes in V |

Table A1.6 (continued) - Variable star types (adapted from GCVS)

| | |
|---|---|
| | over periods of 1 to 135 days. Exhibits relation between period and absolute luminosity. Distinctions made between stars with single and multiple pulsation modes. |
| W Virginis | Similar to Classical Cepheids, except stars are of Population II. Radial pulsations produce brightness variations of 0.3 to 1.2 magnitudes in V over periods of 0.8 to 35 days. |
| RV Tauri | Radially pulsating supergiant exhibiting two pulsations of unequal maxima and minima. Occasional shifts between primary and secondary minima observed. Periods between two primary minima range form 30 to 150 days with a brightness variation of up to 4 magnitudes in V. Distinctions made between stars whose mean magnitude also changes over periods of 600 to 1500 days and those that do not change. |
| Semi-regular | Giants and supergiants of intermediate to late spectral types showing noticeable periodicity accompanied by various irregularities. Shape of light curve is also variable. Brightness amplitudes range from hundredths to several magnitudes over periods of 20 to over 2000 days. Distinctions made between late-type giants, late-type giants with poor periodicity, late-type supergiants, and earlier-type giants and supergiants. |
| Slow Irregular | Late-type giants or supergiants showing no evidence of periodicity. |
| Mira | Giants with late-type emission spectra. Brightness amplitudes from 2.5 to 11 magnitudes in V over periods from 80 to 1000 days. Periodicity well pronounced. |
| α Cygni | Nonradially pulsating supergiant (B-A spectral type) with brightness variations of approximately 0.1 magnitudes in V. Superposition of many oscillations with close periods and cycles from several days to several weeks. |
| β Cephei | (Also known as β Canis Majoris variables.) Radially pulsating stars of spectral type O8-B6 with brightness variations of 0.01 to 0.3 magnitudes in V over periods from 0.1 to 0.6 days. Many of these stars exhibit multiple periods and nonradial pulsations. |
| PV Telescopium | B spectral type supergiant with weak hydrogen lines and enhanced helium and carbon lines. Brightness variations of up to 0.1 mags in V over periods from 0.1 to 1 day. |

Table A1.6 (continued) - Variable star types (adapted from GCVS)

| | |
|---|---|
| ZZ Ceti | Nonradially pulsating white dwarfs with brightness variations of 0.001 to 0.2 in V over periods of 30 seconds to 25 minutes. Many close oscillation modes are present. Distinctions made between those having hydrogen absorption lines and those having helium absorption lines. |

**Rotating** (Characterized by stars with nonuniform surface brightness or ellipsoidal shapes. Variability caused by star's rotation.)

| | |
|---|---|
| $\alpha_2$ Canum Venaticorum | Main sequence B8-A7 stars having strong variable magnetic fields. Brightness variations of 0.01 to 0.1 magnitudes in V over periods from 0.5 to >160 days. Distinction made between those also displaying nonradial pulsations of about 0.01 magnitudes in V over 0.004 to 0.01 days and those that do not. |
| RS Canum Venaticorum | CaII H and K emission line of stars in close binary system showing nonuniform surface brightness (star spots) and chromospheric activity. Brightness variations on the order of 0.2 magnitudes in V. |
| BY Draconis | CaII H and K emission line dwarfs of K-M spectral type showing nonuniform surface brightness (star spots) and chromospheric activity. Brightness variations of hundredths to 0.5 magnitudes in V over periods from hours to 120 days. Some stars also exhibit flares, and are simultaneously classified as UV Ceti stars. Similar to RS Canum Venaticorum variable stars. |
| FK Comae Bernices | Giants of G-K spectral type with broad H and K CaII emission. Brightness variations of tenths of magnitudes in V over periods up to several days. Possibly related to W Ursa Majoris eclipsing variables. |
| SX Arietis | Main sequence B0-B9 stars with variable spectral features and magnetic fields. Brightness variations of about 0.1 magnitudes in V over periods of about 1 day. Similar to $\alpha_2$ Canum Venaticorum type variables. |
| ellipsoidal | Close binary system with ellipsoidal components. Brightness variations caused by varying projection of stars as seen by observer. No eclipses are present. |
| pulsars | Rapidly rotating neutron stars with strong magnetic fields emitting narrow beams of synchrotron radiation (radio, visible, X-ray). Brightness variations of up to 0.8 magnitudes in V over periods from 0.004 to 4 seconds. |

Table A1.6 (continued) - Variable Star Types (adapted from GCVS)

**Eclipsing** (Characterized by close binary systems where variation is primarily caused by eclipses of one star by the other.)

| | |
|---|---|
| Algol | Spherical or near spherical components where it is possible to specify the beginning and end of the eclipses. Spectral types of components and degree of filling of inner Roche lobes are also often specified in classification. (This is true for **β** Lyrae-type and W Ursae Majoris-type variables as well.) |
| **β** Lyrae | Ellipsoidal components where it is impossible to specify the beginning and end of the eclipses. Depth of secondary minimum is considerably smaller than primary minimum. |
| W Ursae Majoris | Ellipsoidal components almost in contact with each other where it is impossible to specify the beginning and end of the eclipses. Depths of primary and secondary minima are almost equal. |

Table A1.7 - Bright Star Masks

| | |
|---|---|
| **SAO stars with V < 5 (individually masked)** | |
| $\iota$ Gem | $7^h\ 24^m\ 50^s$ - $7^h\ 25^m\ 00^s$ (south of $28^\circ\ 03'\ 00''$) |
| Pollux | $7^h\ 42^m\ 45^s$ - $7^h\ 46^m\ 15^s$ |
| $\beta$ Com | $13^h\ 10^m\ 45^s$ - $13^h\ 12^m\ 00^s$ (south of $28^\circ\ 25'\ 12''$) |
| Albireo | $19^h\ 29^m\ 30^s$ - $19^h\ 31^m\ 00^s$ (south of $28^\circ\ 03'\ 36''$) |
| Scheat | $23^h\ 02^m\ 00^s$ - $23^h\ 04^m\ 30^s$ |
| **SAO stars with 5 < V < 7.6** | |
| radius | $43 + (4.037 \times 10^{-7}) \times 10^{((25.75-V)/2.5)}$ pixels |
| centered | on star |
| additionally | 10 pixel wide region in RA for all declinations |
| additionally | 10 pixel wide region in declination, 1.6 times mask radius to east if radius > 60 |
| **SAO stars with V > 7.6** | |
| radius | $27 + (1.287 \times 10^{-6}) \times 10^{((25.75-V)/2.5)}$ pixels |
| centered | on star |
| additionally | 10 pixel wide region in RA for all northern declinations |
| additionally | 10 pixel wide region in RA, 1.5 times mask radius for southern declinations if radius > 35 |
| **CTI stars with V < 12** | |
| radius | 22 pixels (V < 11), or<br>22 - 10 × (V - 11) pixels (V > 11) |
| centered | 10 × (12 - V) pixels north and east of star |

Table A1.8 - Sample S/N Calculations for Capilla Peak

## I. Signal to Noise Calculation Parameters

| | | |
|---|---|---|
| gain = | 15.6 | electrons/ADU |
| Readout Noise = | 57.0 | electrons |
| Truncation Noise = | 4.5 | electrons |
| Bias level Noise = | 8.0 | electrons |
| Preflash level Noise = | 16.0 | electrons |

photometry area = 380.12 (11 pixel radius)
3 flat field frames at 10000 ADU level
flat field noise = 0.001478 electrons per pixel per ADU

OPTION #1: superbias and superskim subtracted frames
2 superbiases with 25 bias frames per superbias
3 skimflats at 100 ADU level
Baseline Noise = **58.49** electrons

OPTION #2: superpreflashbias subtracted frames
2 superpreflashbiases with 7 preflashbiases per superpreflashbias, preflash at 100 ADU level
Baseline Noise = **74.25** electrons

OPTION #3: superpreflashbias subtracted frames
1 superpreflashbias made up of 2 preflashbiases
preflash at 100 ADU level
Baseline Noise = **82.43** electrons

Table A1.8 - Sample S/N Calculations (continued)

**II. Moonless night**

sky brightness = 0.87 #electrons per pixel per second
= 22.3 V mag

OPTION #1 Signal to Noise

| V | 30 | 60 | 120 | 180 | 300 | 600 | 900 | 1200 | 1500 | 1800 |
|---|---|---|---|---|---|---|---|---|---|---|
| | time (seconds) | | | | | | | | | |
| 12 | 258.1 | 402.0 | | | | | | | | |
| 13 | 117.7 | 214.4 | 348.5 | 428.1 | | | | | | |
| 14 | 49.0 | 94.7 | 175.0 | 240.3 | 334.0 | | | | | |
| 15 | 19.8 | 39.1 | 75.6 | 109.2 | 167.8 | 269.2 | 327.7 | 363.0 | | |
| 16 | 7.9 | 15.7 | 30.9 | 45.5 | 72.8 | 129.1 | 170.3 | 200.1 | 221.9 | 238.1 |
| 17 | 3.2 | 6.3 | 12.4 | 18.4 | 29.9 | 55.2 | 75.8 | 92.2 | 105.2 | 115.6 |
| 18 | 1.3 | 2.5 | 5.0 | 7.4 | 12.0 | 22.6 | 31.5 | 38.9 | 45.1 | 50.1 |
| 19 | | 1.0 | 2.0 | 2.9 | 4.8 | 9.1 | 12.8 | 15.9 | 18.5 | 20.7 |
| 20 | | | 0.8 | 1.2 | 1.9 | 3.6 | 5.1 | 6.4 | 7.4 | 8.3 |
| 21 | | | | | 0.8 | 1.4 | 2.0 | 2.5 | 3.0 | 3.3 |
| 22 | | | | | | | | 1.0 | 1.2 | 1.3 |

OPTION #2 Signal to Noise:

| V | 30 | 60 | 120 | 180 | 300 | 600 | 900 | 1200 | 1500 | 1800 |
|---|---|---|---|---|---|---|---|---|---|---|
| | time (seconds) | | | | | | | | | |
| 12 | 218.0 | 360.5 | | | | | | | | |
| 13 | 95.2 | 178.8 | 306.9 | 391.8 | | | | | | |
| 14 | 39.0 | 76.4 | 144.8 | 204.2 | 296.6 | | | | | |
| 15 | 15.7 | 31.1 | 60.9 | 89.1 | 140.5 | 238.4 | 301.5 | 342.3 | | |
| 16 | 6.3 | 12.5 | 24.7 | 36.6 | 59.3 | 109.1 | 148.9 | 179.7 | 203.5 | 222.0 |
| 17 | 2.5 | 5.0 | 9.9 | 14.7 | 24.1 | 45.7 | 64.4 | 80.2 | 93.5 | 104.5 |
| 18 | 1.0 | 2.0 | 3.9 | 5.9 | 9.7 | 18.5 | 26.4 | 33.4 | 39.4 | 44.6 |
| 19 | | 0.8 | 1.6 | 2.3 | 3.9 | 7.4 | 10.7 | 13.5 | 16.0 | 18.2 |
| 20 | | | | 0.9 | 1.5 | 3.0 | 4.3 | 5.4 | 6.4 | 7.3 |
| 21 | | | | | 0.6 | 1.2 | 1.7 | 2.2 | 2.6 | 2.9 |
| 22 | | | | | | | | 0.9 | 1.0 | 1.2 |

OPTION #3 Signal to Noise:

| V | 30 | 60 | 120 | 180 | 300 | 600 | 900 | 1200 | 1500 | 1800 |
|---|---|---|---|---|---|---|---|---|---|---|
| | time (seconds) | | | | | | | | | |
| 12 | 201.1 | 340.6 | | | | | | | | |
| 13 | 86.5 | 164.1 | 287.8 | 373.7 | | | | | | |
| 14 | 35.3 | 69.3 | 132.6 | 188.7 | 279.1 | | | | | |
| 15 | 14.2 | 28.1 | 55.2 | 81.2 | 129.1 | 224.1 | 288.3 | 331.2 | | |
| 16 | 5.7 | 11.3 | 22.3 | 33.1 | 54.0 | 100.7 | 139.2 | 170.0 | 194.3 | 213.6 |
| 17 | 2.3 | 4.5 | 8.9 | 13.3 | 21.9 | 41.8 | 59.5 | 74.9 | 88.0 | 99.1 |
| 18 | 0.9 | 1.8 | 3.6 | 5.3 | 8.8 | 16.9 | 24.3 | 31.0 | 36.8 | 42.0 |
| 19 | | 0.7 | 1.4 | 2.1 | 3.5 | 6.8 | 9.8 | 12.5 | 14.9 | 17.1 |
| 20 | | | | 0.8 | 1.4 | 2.7 | 3.9 | 5.0 | 6.0 | 6.9 |
| 21 | | | | | 0.6 | 1.1 | 1.6 | 2.0 | 2.4 | 2.7 |
| 22 | | | | | | | | 0.8 | 1.0 | 1.1 |

Table A1.8 - Sample S/N Calculations (continued)

**III. Bright Moon night**

**sky brightness = 4.33 #electrons per pixel per second**

**= 20.5 V mag**

OPTION #1 Signal to Noise

time (seconds)

| V | 30 | 60 | 120 | 180 | 300 | 600 | 900 | 1200 | 1500 | 1800 |
|---|---|---|---|---|---|---|---|---|---|---|
| 12 | 251.4 | 382.0 | | | | | | | | |
| 13 | 115.1 | 203.5 | 313.9 | 372.4 | | | | | | |
| 14 | 48.1 | 90.5 | 157.7 | 204.8 | 260.7 | | | | | |
| 15 | 19.5 | 37.5 | 68.8 | 93.8 | 128.7 | 169.3 | 185.3 | 193.3 | | |
| 16 | 7.8 | 15.2 | 28.4 | 39.5 | 56.2 | 78.0 | 87.4 | 92.3 | 95.2 | 97.1 |
| 17 | 3.1 | 6.1 | 11.4 | 16.1 | 23.2 | 33.1 | 37.5 | 39.9 | 41.3 | 42.2 |
| 18 | 1.2 | 2.4 | 4.6 | 6.4 | 9.4 | 13.5 | 15.4 | 16.4 | 17.0 | 17.4 |
| 19 | | 1.0 | 1.8 | 2.6 | 3.8 | 5.4 | 6.2 | 6.6 | 6.9 | 7.1 |
| 20 | | | 0.7 | 1.0 | 1.5 | 2.2 | 2.5 | 2.7 | 2.8 | 2.8 |
| 21 | | | | | 0.6 | 0.9 | 1.0 | 1.1 | 1.1 | 1.1 |
| 22 | | | | | | | | 0.4 | 0.4 | 0.4 |

OPTION #2 Signal to Noise:

time (seconds)

| V | 30 | 60 | 120 | 180 | 300 | 600 | 900 | 1200 | 1500 | 1800 |
|---|---|---|---|---|---|---|---|---|---|---|
| 12 | 213.9 | 345.8 | | | | | | | | |
| 13 | 93.8 | 172.3 | 282.5 | 347.8 | | | | | | |
| 14 | 38.5 | 74.1 | 134.6 | 181.0 | 241.7 | | | | | |
| 15 | 15.5 | 30.3 | 57.2 | 80.1 | 115.1 | 160.8 | 180.2 | 189.9 | | |
| 16 | 6.2 | 12.2 | 23.3 | 33.2 | 49.2 | 72.9 | 84.1 | 90.0 | 93.6 | 95.9 |
| 17 | 2.5 | 4.9 | 9.4 | 13.4 | 20.2 | 30.6 | 35.9 | 38.7 | 40.5 | 41.6 |
| 18 | 1.0 | 1.9 | 3.7 | 5.4 | 8.1 | 12.5 | 14.7 | 15.9 | 16.7 | 17.2 |
| 19 | | 0.8 | 1.5 | 2.1 | 3.2 | 5.0 | 5.9 | 6.4 | 6.7 | 6.9 |
| 20 | | | | 0.9 | 1.3 | 2.0 | 2.4 | 2.6 | 2.7 | 2.8 |
| 21 | | | | | 0.5 | 0.8 | 0.9 | 1.0 | 1.1 | 1.1 |
| 22 | | | | | | | | 0.4 | 0.4 | 0.4 |

OPTION #3 Signal to Noise:

time (seconds)

| V | 30 | 60 | 120 | 180 | 300 | 600 | 900 | 1200 | 1500 | 1800 |
|---|---|---|---|---|---|---|---|---|---|---|
| 12 | 197.8 | 328.2 | | | | | | | | |
| 13 | 85.5 | 159.1 | 267.4 | 334.9 | | | | | | |
| 14 | 34.9 | 67.6 | 124.6 | 170.0 | 232.0 | | | | | |
| 15 | 14.0 | 27.5 | 52.4 | 74.2 | 108.6 | 156.2 | 177.2 | 188.0 | | |
| 16 | 5.6 | 11.0 | 21.3 | 30.6 | 46.1 | 70.2 | 82.2 | 88.7 | 92.6 | 95.2 |
| 17 | 2.2 | 4.4 | 8.5 | 12.3 | 18.8 | 29.4 | 35.0 | 38.1 | 40.0 | 41.2 |
| 18 | 0.9 | 1.8 | 3.4 | 4.9 | 7.6 | 11.9 | 14.3 | 15.6 | 16.5 | 17.0 |
| 19 | | 0.7 | 1.4 | 2.0 | 3.0 | 4.8 | 5.8 | 6.3 | 6.6 | 6.9 |
| 20 | | | | 0.8 | 1.2 | 1.9 | 2.3 | 2.5 | 2.7 | 2.8 |
| 21 | | | | | 0.5 | 0.8 | 0.9 | 1.0 | 1.1 | 1.1 |
| 22 | | | | | | | | 0.4 | 0.4 | 0.4 |

Table A1.9 - Capilla Peak Observation Dates

| date | dayno | %used | observers | nights |
|---|---|---|---|---|
| 93Jun20 | 3093 | 5% | Wetterer, Boudreau | 0.05 |
| 93Jun24 | 3097 | 70% | Boudreau | 0.75 |
| 93Jun26 | 3099 | 55% | McGraw, Kunkle, Boudreau, Vogel | 1.30 |
| 93Jul06 | 3109 | 45% | Grashuis, Boudreau | 1.75 |
| 93Jul09 | 3112 | 50% | Wetterer, Grashuis | 2.25 |
| 93Jul10 | 3113 | 85% | Grashuis | 3.10 |
| 93Jul23 | 3126 | 50% | Wetterer, Kunkle | 3.60 |
| 93Jul25 | 3128 | 100% | Wetterer, Grashuis | 4.60 |
| 93Jul26 | 3129 | 100% | Grashuis | 5.60 |
| 93Jul27 | 3130 | 30% | Grashuis, Kunkle | 5.90 |
| 93Sep04 | 3169 | 50% | Grashuis | 6.40 |
| 93Sep09 | 3174 | 100% | Wetterer, Grashuis, Weichman | 7.40 |
| 93Sep10 | 3175 | 70% | Grashuis | 8.10 |
| 93sep15 | 3180 | 100% | Wetterer, Grashuis | 9.10 |
| 93Sep16 | 3181 | 100% | Grashuis | 10.10 |
| 93Sep21 | 3186 | 60% | Grashuis | 10.70 |
| 93Sep22 | 3187 | 60% | Grashuis, Adams | 11.30 |
| 93Sep24 | 3189 | 40% | Grashuis, Kunkle, Vogel, Collette | 11.70 |
| 93Sep29 | 3194 | 40% | Grashuis | 12.10 |
| 93Sep30 | 3195 | 40% | Grashuis | 12.50 |
| 93Oct06 | 3201 | 5% | Grashuis | 12.55 |
| 93Oct08 | 3203 | 5% | Grashuis | 12.60 |
| 93Oct09 | 3204 | 15% | Grashuis, Boudreau | 12.75 |
| 93Oct10 | 3205 | 45% | Grashuis, Boudreau | 13.20 |
| 93Oct11 | 3206 | 10% | Grashuis, Adams | 13.30 |
| 93Oct14 | 3209 | 20% | Boudreau | 13.50 |
| 93Oct15 | 3210 | 0% | Boudreau (Sky flats only) | 13.50 |
| 93Oct16 | 3211 | 20% | Boudreau | 13.70 |
| 93Oct22 | 3217 | 10% | Grashuis, Fairweather, Malahkov | 13.80 |
| 93Oct23 | 3218 | 5% | Grashuis, Fairweather, Gregory, + | 13.85 |
| 93Oct28 | 3223 | 5% | Grashuis | 13.90 |
| 93Nov05 | 3231 | 40% | Grashuis | 14.30 |
| 93Nov06 | 3232 | 25% | Grashuis, McGraw, McGraw's class | 14.55 |
| 93Nov08 | 3234 | 100% | Wetterer, Grashuis | 15.55 |
| 93Nov19 | 3245 | 30% | Grashuis, Boudreau | 15.85 |
| 93Nov20 | 3246 | 25% | Grashuis, Kunkle | 16.10 |
| 93Nov21 | 3247 | 12% | Boudreau, Fairweather, Kraybill | 16.22 |
| 93Dec06 | 3262 | 5% | Grashuis, Adams | 16.27 |
| 93Dec09 | 3265 | 0% | Wetterer, Grashuis, Miller (tests) | 16.27 |
| 93Dec17 | 3273 | 25% | Grashuis, Adams | 16.52 |
| 94Jan10 | 3297 | 0% | Wetterer, Grashuis (CCD tests) | 16.52 |
| 94Jan11 | 3298 | 100% | Wetterer, Grashuis | 17.52 |
| 94Jan14 | 3301 | 0% | Grashuis, Adams (CCD tests) | 17.52 |
| 94Jan20 | 3307 | 40% | Grashuis | 17.92 |
| 94Jan21 | 3308 | 60% | Grashuis | 18.52 |
| 94Feb13 | 3331 | 80% | Grashuis, Boudreau | 19.32 |
| 94Feb17 | 3335 | 0% | Grashuis (CCD tests) | 19.32 |
| 94Feb24 | 3342 | 90% | Grashuis, Adams | 20.22 |
| 94Mar05 | 3355 | 30% | Boudreau | 20.52 |

Table A1.9 - Capilla Peak Observation Dates (continued)

| date | dayno | %used | observers | nights |
|---|---|---|---|---|
| 94Mar06 | 3356 | 5% | Boudreau | 20.57 |
| 94Mar10 | 3360 | 75% | Grashuis, Adams | 21.32 |
| 94Mar11 | 3361 | 10% | Grashuis | 21.42 |
| 94Mar15 | 3365 | 100% | Grashuis | 22.42 |
| 94Mar17 | 3367 | 90% | Grashuis | 23.32 |
| 94Apr07 | 3384 | 2% | Wetterer | 23.34 |
| 94Apr08 | 3385 | 90% | Wetterer, Grashuis | 24.24 |
| 94Jun15 | 3453 | 100% | Wetterer, Grashuis | 25.24 |
| 94Jun16 | 3454 | 100% | Wetterer, Grashuis | 26.24 |
| 94Jun25 | 3463 | 35% | Boudreau, Chavot, Lopshire, Rivers | 26.59 |
| 94Jun26 | 3464 | 16% | Boudreau | 27.75 |
| 94Jun27 | 3465 | 35% | Boudreau | 28.10 |
| 94Jun30 | 3468 | 100% | Grashuis, Boudreau | 29.10 |
| 94Jul01 | 3469 | 60% | Grashuis, Boudreau | 29.70 |
| 94Jul05 | 3473 | 60% | Wetterer, Kunkle | 30.30 |
| 94Jul06 | 3474 | 100% | Wetterer, Grashuis | 31.30 |
| 94Jul10 | 3478 | 60% | Boudreau | 31.90 |
| 94Jul12 | 3480 | 60% | Grashuis, Kunkle | 32.50 |
| 94Jul13 | 3481 | 95% | Wetterer, Grashuis | 33.45 |
| 94Jul16 | 3484 | 20% | Boudreau | 33.65 |
| 94Jul19 | 3487 | 50% | Grashuis | 34.15 |
| 94Jul20 | 3488 | 60% | Grashuis | 34.75 |
| 94Aug04 | 3503 | 20% | Boudreau, Kunkle, Rivers | 34.95 |
| 94Aug13 | 3512 | 80% | Wetterer, Kraybill | 35.75 |
| 94Aug17 | 3516 | 90% | Wetterer, Rivers | 36.65 |
| 94Aug18 | 3517 | 100% | Wetterer, Oetiker | 37.65 |
| 94Sep09 | 3539 | 100% | Grashuis | 38.65 |
| 94Sep10 | 3540 | 65% | Grashuis | 39.30 |
| 94Sep15 | 3545 | 100% | Wetterer, Grashuis | 40.30 |
| 94Sep16 | 3546 | 65% | Wetterer, Grashuis | 40.95 |
| 94Sep29 | 3559 | 30% | Grashuis | 41.25 |
| 94Oct03 | 3563 | 40% | Wetterer, Grashuis | 41.55 |
| 94Oct09 | 3569 | 100% | Grashuis, Boudreau | 42.55 |
| 94Nov15 | 3606 | 15% | Grashuis | 42.70 |
| 94Nov16 | 3607 | 30% | Grashuis | 43.00 |
| 94Dec01 | 3622 | 100% | Wetterer, Grashuis | 44.00 |
| 94Dec20 | 3641 | 90% | Wetterer, Grashuis | 44.90 |
| 95Jan08 | 3660 | 20% | Wetterer, Grashuis | 45.10 |
| 95Jan14 | 3666 | 90% | Grashuis | 46.00 |
| 95Jan15 | 3667 | 15% | Grashuis | 46.15 |
| 95Jan21 | 3673 | 2% | Grashuis, Adams | 46.17 |
| 95Jan29 | 3681 | 33% | Grahsuis, Adams | 46.50 |
| 95Jan31 | 3683 | 15% | Grashuis | 46.65 |
| 95Feb02 | 3685 | 95% | Wetterer, Grashuis | 47.60 |

Table A1.10 - Capilla Peak Observer Log Summary

| observer | # V images |
|---|---|
| Grashuis | 1227 |
| Wetterer | 644 |
| Boudreau | 266 |
| Kunkle | 104 |
| Adams | 53 |
| Rivers | 45 |
| Oetiker | 41 |
| Vogel | 33 |
| Weichman | 30 |
| Kraybill | 25 |
| McGraw | 23 |
| Collette | 10 |
| Chavot | 10 |
| Lopshire | 10 |
| Fairweather | 10 |
| Malahkov | 6 |
| Gregory | 2 |
| Anderson | 2 |
| TOTAL | 1465 |

Table A1.11 - Capilla Peak Image Log

| images | description |
|---|---|
| 1465 | images through V filter (RR Lyr candidates) |
| 35 | images through V filter (Mira variables) |
| 44 | images through V filter (calibration) |
| 83 | images through V filter (CCD tests) |
| 33 | images through B filter (RR Lyr candidates) |
| 360 | bias or superbias images |
| 615 | V and B sky flats |
| 46 | V skim flats |
| 367 | preflash darks |
| 18 | superpreflashbias-7s |
| 13 | darks |
| 1 | pretty picture |
| 3036 | TOTAL |

## Table A1.12 - Bright RR Lyrae stars in GCVS

RRab

| | Name | RA | Dec | Type | Max | Min | Mean | Av | r(pc) |
|---|---|---|---|---|---|---|---|---|---|
| 1 | RR Lyr | 19 23 52 | 42 41.2 | RRAB | 7.06 | 8.12 | 7.68 | 0.36 | 207 |
| 2 | FW Lup | 15 19 07 | -40 44.9 | RR | 8.82 | 9.22 | 9.03 | 0.36 | 385 |
| 3 | X Ari | 03 05 48 | 10 15.4 | RRAB | 8.97 | 9.95 | 9.54 | 0.68 | 422 |
| 4 | UV Oct | 16 20 24 | -83 47.5 | RRAB | 8.70 | 9.97 | 9.45 | 0.27 | 488 |
| 5 | XZ Cyg | 19 31 27 | 56 16.8 | RRAB | 8.90 | 10.16 | 9.65 | 0.32 | 523 |
| 6 | ST Pic | 06 13 30 | -61 27.3 | RR | 9.29 | 9.77 | 9.55 | 0.09 | 555 |
| 7 | XZ Cet | 01 57 53 | -16 35.3 | RRAB | 9.24 | 9.71 | 9.49 | 0.00 | 563 |
| 8 | SW And | 00 21 06 | 29 07.5 | RRAB | 9.14 | 10.09 | 9.69 | 0.14 | 580 |
| 9 | RX Eri | 04 47 29 | -15 49.6 | RRAB | 9.17 | 10.10 | 9.71 | 0.09 | 597 |
| 10 | RR Cet | 01 29 34 | 01 05.1 | RRAB | 9.10 | 10.10 | 9.69 | 0.02 | 609 |
| 11 | DX Del | 20 45 06 | 12 16.7 | RRAB | 9.52 | 10.26 | 9.94 | 0.27 | 612 |
| 12 | SV Eri | 03 09 28 | -11 32.6 | RRAB | 9.56 | 10.23 | 9.94 | 0.18 | 636 |
| 13 | SU Dra | 11 35 07 | 67 36.4 | RRAB | 9.18 | 10.27 | 9.82 | 0.05 | 642 |
| 14 | TU UMa | 11 27 10 | 30 20.6 | RRAB | 9.26 | 10.24 | 9.83 | 0.01 | 655 |
| 15 | TT Lyn | 08 59 49 | 44 47.1 | RRAB | 9.42 | 10.21 | 9.87 | 0.05 | 657 |
| 16 | V Ind | 21 08 11 | -45 16.7 | RRAB | 9.12 | 10.48 | 9.93 | 0.05 | 675 |
| 17 | IK Hya | 12 02 14 | -27 23.9 | RR | 9.96 | 10.42 | 10.21 | 0.27 | 691 |
| 18 | XZ Dra | 19 09 24 | 64 46.6 | RRAB | 9.59 | 10.65 | 10.21 | 0.27 | 693 |
| 19 | V440 Sgr | 19 29 20 | -23 57.6 | RRAB | 9.60 | 10.80 | 10.31 | 0.36 | 695 |
| 20 | VY Ser | 15 28 30 | 01 51.2 | RRAB | 9.73 | 10.46 | 10.15 | 0.06 | 740 |
| 21 | SS For | 02 05 36 | -27 06.1 | RRAB | 9.45 | 10.60 | 10.13 | 0.00 | 755 |
| 22 | S Ara | 17 55 19 | -49 25.8 | RRAB | 9.96 | 11.20 | 10.70 | 0.54 | 764 |
| 23 | RU Scl | 00 00 14 | -25 13.4 | RRAB | 9.35 | 10.75 | 10.19 | 0.02 | 767 |
| 24 | SV Hya | 12 27 53 | -25 46.3 | RRAB | 9.78 | 11.00 | 10.50 | 0.27 | 792 |
| 25 | BH Peg | 22 50 32 | 15 30.8 | RRAB | 9.99 | 10.79 | 10.45 | 0.18 | 805 |
| 26 | AT And | 23 40 02 | 42 44.3 | RRAB | 10.42 | 10.92 | 10.69 | 0.41 | 812 |
| 27 | V413 CrA | 18 44 34 | -37 47.6 | RRAB | 10.23 | 10.90 | 10.61 | 0.32 | 814 |
| 28 | AV Peg | 21 49 47 | 22 19.3 | RRAB | 9.88 | 10.92 | 10.49 | 0.18 | 820 |
| 29 | RS Boo | 14 31 25 | 31 58.4 | RRAB | 9.69 | 10.84 | 10.37 | 0.00 | 843 |
| 30 | SW Dra | 12 15 26 | 69 47.3 | RRAB | 9.94 | 10.94 | 10.53 | 0.05 | 887 |
| 31 | V445 Oph | 16 22 00 | -06 25.3 | RRAB | 10.53 | 11.39 | 11.03 | 0.54 | 890 |
| 32 | VX Her | 16 28 28 | 18 28.1 | RRAB | 9.89 | 11.21 | 10.68 | 0.18 | 893 |
| 33 | V341 Aql | 20 29 58 | 00 24.9 | RRAB | 10.13 | 11.39 | 10.88 | 0.36 | 903 |
| 34 | XX And | 01 14 36 | 38 41.3 | RRAB | 10.08 | 11.13 | 10.70 | 0.15 | 915 |
| 35 | U Lep | 04 54 09 | -21 17.6 | RRAB | 9.84 | 11.11 | 10.59 | 0.05 | 916 |
| 36 | W CVn | 14 04 21 | 38 04.0 | RRAB | 10.03 | 10.96 | 10.57 | 0.00 | 925 |
| 37 | UU Vir | 12 06 01 | 00 12.5 | RRAB | 9.89 | 11.07 | 10.59 | 0.01 | 928 |
| 38 | WY Ant | 10 13 48 | -29 28.2 | RRAB | 10.27 | 11.22 | 10.82 | 0.18 | 957 |
| 39 | WZ Hya | 10 10 59 | -12 53.6 | RRAB | 10.27 | 11.28 | 10.86 | 0.18 | 973 |
| 40 | RR Leo | 10 04 56 | 24 14.2 | RRAB | 9.94 | 11.27 | 10.73 | 0.05 | 976 |
| 41 | RV UMa | 13 31 21 | 54 14.7 | RRAB | 9.81 | 11.30 | 10.70 | 0.00 | 982 |
| 42 | RV Cet | 02 12 49 | -11 02.0 | RRAB | 10.35 | 11.22 | 10.85 | 0.05 | 1031 |
| 43 | KX Lyr | 18 31 45 | 40 08.0 | RRAB | 10.38 | 11.47 | 11.02 | 0.15 | 1062 |
| 44 | UY Boo | 13 56 20 | 13 11.7 | RRAB | 10.25 | 11.35 | 10.90 | 0.00 | 1075 |
| 45 | RY Col | 05 13 33 | -41 41.1 | RRAB | 10.44 | 11.24 | 10.90 | 0.00 | 1076 |
| 46 | AN Ser | 15 51 11 | 13 07.1 | RRAB | 10.40 | 11.44 | 11.01 | 0.05 | 1109 |
| 47 | ST Boo | 15 28 44 | 35 57.3 | RRAB | 10.49 | 11.41 | 11.03 | 0.05 | 1117 |
| 48 | VW Scl | 01 15 59 | -39 28.6 | RRAB | 10.40 | 11.40 | 10.99 | 0.00 | 1119 |
| 49 | SX For | 03 28 26 | -36 13.3 | RRAB | 10.68 | 11.38 | 11.08 | 0.00 | 1168 |
| 50 | BB Vir | 13 49 11 | 06 40.7 | RRAB | 10.70 | 11.42 | 11.11 | 0.02 | 1174 |

RRc

| | | | | | | | | | |
|---|---|---|---|---|---|---|---|---|---|
| 1 | MT Tel | 18 58 31 | -46 43.5 | RRC | 8.68 | 9.28 | 8.98 | 0.18 | 409 |
| 2 | CS Eri | 02 35 11 | -43 10.8 | RRC | 8.75 | 9.31 | 9.03 | 0.00 | 455 |
| 3 | DH Peg | 22 12 55 | 06 34.4 | RRC | 9.15 | 9.80 | 9.48 | 0.18 | 514 |
| 4 | T Sex | 09 50 53 | 02 17.6 | RRC | 9.81 | 10.32 | 10.07 | 0.09 | 703 |
| 5 | RU Psc | 01 11 42 | 24 09.1 | RRC | 9.93 | 10.40 | 10.17 | 0.09 | 736 |

Table A1.12 (continued) - Bright RR Lyrae stars in GCVS

| | Name | RA | Dec | Type | Max | Min | Mean | Av | r(pc) |
|---|---|---|---|---|---|---|---|---|---|
| 6 | BB CMi | 07 48 46 | 05 02.8 | RRC | 10.00 | 10.80 | 10.40 | 0.09 | 820 |
| 7 | XZ Gru | 22 44 43 | -39 19.8 | RRC | 10.40 | 10.70 | 10.55 | 0.00 | 916 |
| 8 | AE Boo | 14 45 15 | 17 03.3 | RRC | 10.44 | 10.88 | 10.66 | 0.01 | 959 |
| 9 | SS Psc | 01 18 10 | 21 28.5 | RRC | 10.73 | 11.21 | 10.97 | 0.14 | 1045 |
| 10 | SX UMa | 13 24 17 | 56 31.0 | RRC | 10.58 | 11.21 | 10.90 | 0.00 | 1074 |
| 11 | LS Her | 15 59 49 | 17 37.2 | RRC | 10.79 | 11.12 | 10.96 | 0.05 | 1081 |
| 12 | BV Aqr | 22 00 07 | -21 46.1 | RRC | 10.80 | 11.20 | 11.00 | 0.05 | 1104 |
| 13 | TV Boo | 14 14 37 | 42 35.5 | RRC | 10.71 | 11.30 | 11.01 | 0.00 | 1130 |
| 14 | AP Ser | 15 11 37 | 10 10.0 | RRC | 10.85 | 11.38 | 11.12 | 0.05 | 1164 |
| 15 | AO Tuc | 00 01 34 | -59 45.8 | RRC | 10.88 | 11.40 | 11.14 | 0.00 | 1202 |
| RR Lyrae stars within 10° of Galactic plane | | | | | | | | | |
| | V1719Cyg | 21 02 56 | 50 35.1 | RRC | 7.95 | 8.33 | 8.23 | | |
| | RZ Cep | 22 37 28 | 64 35.7 | RRC | 9.11 | 9.75 | 9.55 | | |
| | V675 Sgr | 18 10 16 | -34 19.9 | RRAB | 9.80 | 10.76 | 10.36 | | |
| | AR Per | 04 13 38 | 47 16.7 | RRAB | 9.92 | 10.83 | 10.45 | | |
| | V363 Cas | 00 12 33 | 60 03.8 | RRAB | 10.29 | 10.73 | 10.53 | | |
| | CZ Lac | 22 17 33 | 51 13.2 | RRAB | 10.77 | 11.26 | 11.04 | | |
| | BN Vul | 19 25 50 | 24 14.7 | RRAB | 10.63 | 11.40 | 11.07 | | |
| | UY Cyg | 20 54 22 | 30 14.1 | RRAB | 10.59 | 11.46 | 11.09 | | |
| Possible additional RR Lyrae variable stars | | | | | | | | | |
| | S Eri | 04 57 36 | -12 36.6 | RRC | 4.77 | 4.80 | | | |
| | V819 Cen | 13 16 12 | -57 55.9 | RR | 9.00 | 9.07 | | | |
| | AW Mic | 21 16 02 | -34 07.8 | RRC | 9.04 | 9.13 | | | |
| | V429 Ori | 04 53 44 | -03 36.5 | RRAB | 10.00 | 11.00 | | | |
| | V753 Cen | 11 48 44 | -55 31.3 | RRC | 10.24 | 10.64 | | | |
| | V1356Aql | 19 44 23 | -02 11.5 | RRC | 10.30 | 10.50 | | | |
| | IV Pav | 20 29 23 | -72 47.2 | RR | 10.40 | 10.80 | | | |

## Appendix 2 - Database Descriptions

Descriptions for those databases created specifically for this dissertation and used frequently are listed in this appendix. Descriptions for CTI data reduction and analysis databases can be found in The CCD/Transit Instrument Atlas and Database Guide (Wetterer 1995). Descriptions for other user defined databases must be found elsewhere. The contents of all databases and all attribute titles are available by using the CTI program DBDESC. The database descriptions in this appendix are listed in alphabetical order. Each listing contains the database extension, date and time of creation, database title, listing of header attributes and main attributes with attribute type (e.g. integer) and array size (e.g. scalar), and a short description of each main attribute. If the internal and external type differ or there exists a mapping, this is listed as well. All databases with headers have essentially the same attributes in their header. The descriptions for these header attributes are:

NRECS - number of records contained in the database
DATE - date file was produced (yy/mm/dd)
PROGNAME- program used to create database
ORIGIN - description of database's origin
PARM - Twenty three to eighty three parameters. Described for particular database type if appropriate. (For example, the parameters for the .CAL database are defined in CALPARMS.INC, and the parameters for all other databases in the pipeline are defined in PCP.INC.)

```
Database: .BSA    Version:   (94/02/11|09:08:03)
Description: bright star mask areas

Header attributes...
NRECS       type: INTEGER                (scalar)
DATE        type: STRING* 8              (scalar)
PROGNAME    type: STRING*12              (scalar)
ORIGIN      type: STRING*44              (scalar)
PARM        type: REAL                   (23)

Record attributes...
YCTI        ext: DOUBLE int: INTEGER map: LINEAR     (scalar)
P_AREA      type: REAL                               (scalar)

YCTI     - right ascension of bright star in centipixels
P_AREA   - Area in square pixels masked by star
```

```
Database: .BSM    Version:   (93/11/29|10:28:39)
Description: bright star masks

Header attributes...
NRECS       type: INTEGER                (scalar)
DATE        type: STRING* 8              (scalar)
PROGNAME    type: STRING*12              (scalar)
ORIGIN      type: STRING*44              (scalar)
PARM        type: REAL                   (23)

Record attributes...
XCTI        ext: DOUBLE int: INTEGER map: LINEAR (scalar)
YCTI        ext: DOUBLE int: INTEGER map: LINEAR (scalar)
RMASK       type: INTEGER                (scalar)
CATID       type: INTEGER                (scalar)

XCTI     - Declination of bright star in centipixels
YCTI     - Right ascension of bright star in centipixels
RMASK    - Radius of mask in pixels
CATID    - Identification of bright star (SAO number or mlink)
```

**Database: .BVH** Version: (94/01/28|14:13:15)
Description: B and V history list

```
Header attributes...
NRECS      type: INTEGER                  (scalar)
DATE       type: STRING* 8                (scalar)
PROGNAME   type: STRING*12                (scalar)
ORIGIN     type: STRING*44                (scalar)
PARM       type: REAL                     (23)

Record attributes...
MLINK      ext: POINT int: INTEGER   (scalar)
HLINK      ext: POINT int: INTEGER   ( 2)
YCTI       ext: DOUBLE int: INTEGER map: LINEAR (scalar)
XCTI       ext: DOUBLE int: INTEGER map: LINEAR (scalar)
BDAYVAL    type: INTEGER                  (21)
BLUM       type: REAL                     (21)
BLUMERR    type: REAL                     (21)
VDAYVAL    type: INTEGER                  (63)
VLUM       type: REAL                     (63)
VLUMERR    type: REAL                     (63)
```

MLINK - Pointer to master list (**.NML** database)
HLINK - Pointers to B and V history lists (**.NHL** databases)
YCTI - Right Ascension in centipixels
XCTI - Declination in centipixels
BDAYVAL - B Observation times in CTI dayno $\times 10^5$
BLUM - B Luminosities in ADUs
BLUMERR - B Luminosity errors in ADUs
VDAYVAL - V Observation times in CTI dayno $\times 10^5$
VLUM - V Luminosities in ADUs
VLUMERR - V Luminosity errors in ADUs

Note: older versions of this database using the **.MAS** and **.HIS** databases used 42 number arrays for BDAYVAL, BLUM, BLUMERR, VDAYVAL, VLUM, and VLUMERR and have the **.OBV** extension.

**Database: .CAT** Version: (93/11/22|08:02:56)
Description: Catalog

Header attributes...

| | | |
|---|---|---|
| NRECS | type: INTEGER | (scalar) |
| DATE | type: STRING* 8 | (scalar) |
| PROGNAME | type: STRING*12 | (scalar) |
| ORIGIN | type: STRING*44 | (scalar) |
| PARM | type: REAL | (23) |

Record attributes...

| | | |
|---|---|---|
| CATID | type: INTEGER | (scalar) |
| RA_HOUR | type: SHORT | (scalar) |
| RA_MIN | type: SHORT | (scalar) |
| RA_SEC | type: REAL | (scalar) |
| DEC_DEG | type: SHORT | (scalar) |
| DEC_MIN | type: SHORT | (scalar) |
| DEC_SEC | type: REAL | (scalar) |
| EPOCH | type: REAL | (scalar) |
| V | type: REAL | (scalar) |
| CATCODE | type: INTEGER | (scalar) |

CATID - Identification of object in catalog (SAO number, Zwicky number, etc..)
RA_HOUR - Hour of right ascension
RA_MIN - Minute of right ascension
RA_SEC - Second of right ascension
DEC_DEG - Degree of declination
DEC_MIN - Arcminute of declination
DEC_SEC - Arcsecond of declination
EPOCH - Epoch of right ascension and declination
V - Magnitude
CATCODE - Identification of catalog (unique integer)

**Database: .HST** Version: (94/02/04|07:54:16)
Description: Histogram Result

Header attributes...

| | | |
|---|---|---|
| NRECS | type: INTEGER | (scalar) |
| DATE | type: STRING* 8 | (scalar) |
| PROGNAME | type: STRING*12 | (scalar) |
| ORIGIN | type: STRING*44 | (scalar) |
| PARM | type: REAL | (23) |

Record attributes...

| | | |
|---|---|---|
| BINID | type: REAL | (scalar) |
| BINTOTAL | type: INTEGER | (scalar) |
| BINSHADED | type: INTEGER | (scalar) |

```
BINID    - Center of bin in histogram
BINTOTAL- Total number of records in bin
BINSHADED Total number of records shaded in bin
```

---

**Database: .NPL** Version:
Description: Normal Point List

```
Header attributes...
NRECS      type: INTEGER              (scalar)
DATE       type: STRING* 8            (scalar)
PROGNAME   type: STRING*12            (scalar)
ORIGIN     type: STRING*44            (scalar)
PARM       type: REAL                 (23)

Record attributes...
RYCTI      type: DOUBLE               (scalar)
RXCTI      type: DOUBLE               (scalar)
RYCTIERR   type: DOUBLE               (scalar)
RXCTIERR   type: DOUBLE               (scalar)
LUM        type: REAL map: LOG        (scalar)
LUMERR     type: REAL map: LOG        (scalar)
DAY        type: REAL                 (scalar)
RANGE      type: INTEGER              (scalar)
V_NDET     ext: INTEGER int: SHORT    (scalar)

RYCTI    - Right ascension in centipixels
RXCTI    - Declination in centipixels
RYCTIERR- Error in right ascension in centipixels
RXCTIERR- Error in declination in centipixels
LUM      - Luminosity in ADUs
LUMERR   - Error in luminosity in ADUs
DAY      - Mean CTI dayno of position measurement
RANGE    - Range of days going into position measurement
V_NDET   - Number of days going into position measurement
```

---

**Database: .NPT** Version: (95/02/16|12:59:03)
Description: Normal Point Table

```
Header attributes...
NRECS      type: INTEGER              (scalar)
DATE       type: STRING* 8            (scalar)
PROGNAME   type: STRING*12            (scalar)
ORIGIN     type: STRING*44            (scalar)
PARM       type: REAL                 (23)

Record attributes...
SET        type: REAL                 (scalar)
ITEM       type: REAL                 (scalar)
```

| | | |
|---|---|---|
| RYCTI | type: DOUBLE | (scalar) |
| RXCTI | type: DOUBLE | (scalar) |
| LUM | type: REAL map: LOG | (scalar) |
| MAG | type: REAL | (scalar) |
| RYCTIERR | type: DOUBLE | (scalar) |
| RXCTIERR | type: DOUBLE | (scalar) |
| YEAR | type: REAL | (scalar) |

SET - Number to distinguish between plates used in astrometry.
ITEM - Number to distinguish between stars on all plates used in astrometry.
RYCTI - Right ascension in centipixels
RXCTI - Declination in centipixels
LUM - Luminosity in ADUs
MAG - Magnitude
RYCTIERR- Error in right ascension in centipixels
RXCTIERR- Error in declination in centipixels
YEAR - Mean year of plate observation

---

**Database: .NPP** Version: (95/02/18|08:01:41)
Description: Normal Point POSS positions

Header attributes...

| | | |
|---|---|---|
| NRECS | type: INTEGER | (scalar) |
| DATE | type: STRING* 8 | (scalar) |
| PROGNAME | type: STRING*12 | (scalar) |
| ORIGIN | type: STRING*44 | (scalar) |
| PARM | type: REAL | (23) |

Record attributes...

| | | |
|---|---|---|
| E_X | type: REAL | (scalar) |
| E_Y | type: REAL | (scalar) |
| EX_ERR | type: REAL | (scalar) |
| EY_ERR | type: REAL | (scalar) |
| E_SIGMA | type: REAL | (scalar) |
| O_X | type: REAL | (scalar) |
| O_Y | type: REAL | (scalar) |
| OX_ERR | type: REAL | (scalar) |
| OY_ERR | type: REAL | (scalar) |
| O_SIGMA | type: REAL | (scalar) |

E_X - Right ascension in 20-$\mu$m pixels for POSS E plate
E_Y - Declination in 20-$\mu$m pixels for POSS E plate
EX_ERR - Error in E_X
EY_ERR - Error in E_Y
E_SIGMA - Related to luminosity for POSS E plate
O_X - Right ascension in 20-$\mu$m pixels for POSS O plate
O_Y - Declination in 20-$\mu$m pixels for POSS O plate
OX_ERR - Error in O_X

```
OY_ERR   - Error in O_Y
O_SIGMA  - Related to luminosity for POSS O plate
```

---

**Database: .R01** Version: (93/12/01|14:55:11)

```
Header attributes...
NRECS     type: INTEGER          (scalar)
DATE      type: STRING* 8        (scalar)
PROGNAME  type: STRING*12        (scalar)
ORIGIN    type: STRING*44        (scalar)
PARM      type: REAL             (23)

Record attributes...
RNUM      type: REAL             (scalar)
```

RNUM - Real number (used for sorting a list of real numbers to be used in an application).

---

**Database: .R03** Version: (94/11/07|13:56:08)

```
Header attributes...
NRECS     type: INTEGER          (scalar)
DATE      type: STRING* 8        (scalar)
PROGNAME  type: STRING*12        (scalar)
ORIGIN    type: STRING*44        (scalar)
PARM      type: REAL             (23)

Record attributes...
RNUM      type: REAL             (3)
```

RNUM - Array of three real number (used for creating data files of real numbers in preparation for printing a data table).

---

**Database: .R06** Version: (95/02/06|11:33:33)
Description: Six real numbers

```
Header attributes...
NRECS     type: INTEGER          (scalar)
DATE      type: STRING* 8        (scalar)
PROGNAME  type: STRING*12        (scalar)
ORIGIN    type: STRING*44        (scalar)
PARM      type: REAL             (23)

Record attributes...
RNUM      type: REAL             ( 6)
```

RNUM - Array of six real number

```
Database: .RRL    Version:    (94/09/01|08:41:37)
Description: RR Lyrae List

Header attributes...
NRECS       type: INTEGER            (scalar)
DATE        type: STRING* 8          (scalar)
PROGNAME    type: STRING*12          (scalar)
ORIGIN      type: STRING*44          (scalar)
PARM        type: REAL               (23)

Record attributes...
RA1987_HOUR    type: SHORT           (scalar)
RA1987_MIN     type: SHORT           (scalar)
RA1987_SEC     type: REAL            (scalar)
DEC1987_DEG    type: SHORT           (scalar)
DEC1987_MIN    type: SHORT           (scalar)
DEC1987_SEC    type: REAL            (scalar)
RA1950_HOUR    type: SHORT           (scalar)
RA1950_MIN     type: SHORT           (scalar)
RA1950_SEC     type: REAL            (scalar)
DEC1950_DEG    type: SHORT           (scalar)
DEC1950_MIN    type: SHORT           (scalar)
DEC1950_SEC    type: REAL            (scalar)

RA1987_HOUR  - Hour of right ascension (1987.5 epoch)
RA1987_MIN   - Minute of right ascension (1987.5 epoch)
RA1987_SEC   - Second of right ascension (1987.5 epoch)
DEC1987_DEG  - Degrees of declination (1987.5 epoch)
DEC1987_MIN  - Arcminute of declination (1987.5 epoch)
DEC1987_SEC  - Arcsecond of declination (1987.5 epoch)
RA1950_HOUR  - Hour of right ascension (1950 epoch)
RA1950_MIN   - Minute of right ascension (1950 epoch)
RA1950_SEC   - Second of right ascension (1950 epoch)
DEC1950_DEG  - Degrees of declination (1950 epoch)
DEC1950_MIN  - Arcminute of declination (1950 epoch)
DEC1950_SEC  - Arcsecond of declination (1950 epoch)
```

---

```
Database: .RRM    Version:    (94/08/04|13:50:31)
Description: RR Lyrae Magnitudes

Header attributes...
NRECS       type: INTEGER            (scalar)
DATE        type: STRING* 8          (scalar)
PROGNAME    type: STRING*12          (scalar)
ORIGIN      type: STRING*44          (scalar)
PARM        type: REAL               (23)

Record attributes...
DAY         type: REAL               (scalar)
```

```
PHASE     type: REAL              (scalar)
MAG       type: REAL              (scalar)
MAGERR    type: REAL              (scalar)

DAY      - CTI dayno of observation
PHASE    - Phase of observation given period and epoch
MAG      - Magnitude of observation
MAGERR   - Error in magnitude of observation
```

---

**Database: .RRP** Version: (94/08/03|16:50:28)
Description: RR Lyrae Space Densities

```
Header attributes...
NRECS     type: INTEGER           (scalar)
DATE      type: STRING* 8         (scalar)
PROGNAME  type: STRING*12         (scalar)
ORIGIN    type: STRING*44         (scalar)
PARM      type: REAL              (23)

Record attributes...
RR_SD     type: REAL              (scalar)
RR_DIST   type: REAL              (scalar)
SURVEY    type: INTEGER           (scalar)
DRR_SD    type: REAL              (scalar)
DRR_DIST  type: REAL              (scalar)

RR_SD    - RR Lyrae space density in number per cubic kpc
RR_DIST  - RR Lyrae Galactocentric distance in pc
SURVEY   - Identification of survey
DRR_SD   - Error in RR Lyrae space density
DRR_DIST- Error in RR Lyrae Galactocentric distance
```

---

**Database: .RRT** Version: (94/08/03|16:56:05)
Description: RR Lyrae Tables

```
Header attributes...
NRECS     type: INTEGER           (scalar)
DATE      type: STRING* 8         (scalar)
PROGNAME  type: STRING*12         (scalar)
ORIGIN    type: STRING*44         (scalar)
PARM      type: REAL              (23)

Record attributes...
RA1987_HOUR    type: SHORT             (scalar)
RA1987_MIN     type: SHORT             (scalar)
RA1987_SEC     type: REAL              (scalar)
DEC1987_DEG    type: SHORT             (scalar)
DEC1987_MIN    type: SHORT             (scalar)
```

| | | |
|---|---|---|
| DEC1987_SEC | type: REAL | (scalar) |
| NDET | type: INTEGER | ( 2) |
| MAG_MAX | type: REAL | (scalar) |
| MAG_MIN | type: REAL | (scalar) |
| MAG_MEAN | type: REAL | (scalar) |
| MAG_MEANERR | type: REAL | (scalar) |
| AMP | type: REAL | (scalar) |
| SKEW | type: REAL | (scalar) |
| B_V | type: REAL | (scalar) |
| EBV | type: REAL | (scalar) |
| RDIST | type: REAL | (scalar) |
| GLONG | type: REAL | (scalar) |
| GLAT | type: REAL | (scalar) |
| XDIST | type: REAL | (scalar) |
| YDIST | type: REAL | (scalar) |
| ZDIST | type: REAL | (scalar) |
| RCENT | type: REAL | (scalar) |
| RCENTERR | type: REAL | (scalar) |
| TCENT | type: REAL | (scalar) |
| PCENT | type: REAL | (scalar) |
| VARPERIOD | type: DOUBLE | (scalar) |
| VAREPOCH | type: DOUBLE | (scalar) |
| EBV | type: REAL | (scalar) |
| MLINK | ext: POINT int: INTEGER | (scalar) |

| | |
|---|---|
| RA1987_HOUR | - Hour of right ascension (1987.5 epoch) |
| RA1987_MIN | - Minute of right ascension |
| RA1987_SEC | - Second of right ascension |
| DEC1987_DEG | - Degree of declination (1987.5 epoch) |
| DEC1987_MIN | - Arcminute of declination |
| DEC1987_SEC | - Second of declination |
| NDET | - Number of V observations with CTI and at Capilla Peak observatory |
| MAG_MAX | - Magnitude of star at maximum light |
| MAG_MIN | - Magnitude of star at minimum light |
| MAG_MEAN | - Average magnitude of star |
| MAG_MEANERR | - Error in MAG_MEAN |
| AMP | - Amplitude of Variability |
| SKEW | - (M-m)/P of star. Skewness of light curve |
| B_V | - B-V color of star |
| EBV | - Galactic reddening of star |
| RDIST | - Heliocentric distance in parsecs |
| GLONG | - Galactic Longitude |
| GLAT | - Galactic Latitude |
| XDIST | - Galactocentric x distance in parsecs |
| YDIST | - Galactocentric y distance in parsecs |
| ZDIST | - Galactocentric z distance in parsecs |
| RCENT | - Galactocentric radial distance in parsecs |
| RCENTERR | - Error in RCENT |
| TCENT | - Galactic polar angle $\theta$ in degrees |
| PCENT | - Galactic azimuthal angle $\phi$ in degrees |
| VARPERIOD | - Period of variable star in days |

```
VAREPOCH       - Epoch of variable star at maximum light
EBV            - E(B-V) of star.  Reddening.
MLINK          - Pointer to .MAS and .NML databases
```

---

**Database: .VNX** Version: (94/11/27|16:08:54)
Description: Variable Star Index file

```
Header attributes...
NRECS      type: INTEGER            (scalar)
DATE       type: STRING* 8          (scalar)
PROGNAME   type: STRING*12          (scalar)
ORIGIN     type: STRING*44          (scalar)
PARM       type: REAL               (23)

Record attributes...
MLINK      ext: POINT int: INTEGER  (scalar)
HLINK      ext: POINT int: INTEGER  (2)
YCTI       ext: DOUBLE int: INTEGER map: LINEAR (scalar)
XCTI       ext: DOUBLE int: INTEGER map: LINEAR (scalar)
NDET       type: INTEGER            (scalar)
V          type: REAL               (scalar)
AMP        type: REAL               (scalar)
FLAG       ext: INTEGER int: SHORT  (4)
```

| | |
|---|---|
| MLINK | - Pointer to master list (.NML database) |
| HLINK | - Pointer to history lists (B and V .NHL databases) |
| YCTI | - Right Ascension in centipixels |
| XCTI | - Declination in centipixels |
| NDET | - Number of V observations |
| V | - Mean instrumental V magnitude |
| AMP | - Amplitude of variation in V magnitude |
| FLAG | - Results of variability testing. 1st number: 0 = never variable, 100 = only variable with no prescreening, 110 = variable with prescreening but no additional error, and 111 = variable with prescreening and additional error. 2nd number: 0 = not masked by nearby bright star, 1 = masked by nearby bright star. 3rd number: V_COMB. 4th number: 0 = not correlated with nearest variable neighbor, 1 = correlated with nearest variable neighbor. |

## Appendix 3 - Photometry, Light Curves, and Finder Charts for CTI RR Lyrae Survey Stars

In the first part of this appendix, the combined CTI and Capilla Peak photometry is given for each candidate RR Lyrae variable star. The dayval (dayval = 1.0 corresponds to 85 Jan 01 0:00 UT), phase (using period and epoch listed in Table 5.3), instrumental V magnitude and error in this magnitude are listed. Stars identified with number from Table 5.1 and RR+right ascension (e.g. RR002101) or GCVS variable star name when applicable. All data after dayval = 3000 is from Capilla Peak Observatory.

In the second part of this appendix, a finder chart for each candidate RR Lyrae variable star is given along with the combined CTI and Capilla Peak light curve. Finder charts are CTI images, 8.25 arcminutes square with north towards the top of the page. For three stars blended with other stars, a 1' x 1' schematic finder chart with increased resolution is also given. CTI and Capilla Peak data are plotted as open and closed circles respectively in the light curve. Zero phase refers to maximum light for the pulsational variables, and primary minimum light for the eclipsing variables. The magnitudes listed are instrumental magnitudes.

1. RR002101

| | Dayval | Phase | Vint | Vinterr |
|---|---|---|---|---|
| 1 | 1020.25500 | 0.259 | 16.718 | 0.038 |
| 2 | 1023.24670 | 0.072 | 16.982 | 0.048 |
| 3 | 1055.15784 | 0.407 | 16.915 | 0.044 |
| 4 | 1354.34302 | 0.739 | 16.694 | 0.040 |
| 5 | 1355.34033 | 0.343 | 16.859 | 0.043 |
| 6 | 1377.27783 | 0.631 | 16.816 | 0.047 |
| 7 | 1378.27502 | 0.235 | 16.771 | 0.046 |
| 8 | 1379.27307 | 0.843 | 16.810 | 0.053 |
| 9 | 1401.21143 | 0.133 | 16.905 | 0.052 |
| 10 | 1403.20605 | 0.342 | 16.846 | 0.049 |
| 11 | 1404.20325 | 0.947 | 17.016 | 0.059 |
| 12 | 1405.20032 | 0.550 | 17.011 | 0.053 |
| 13 | 1410.18616 | 0.571 | 16.937 | 0.050 |
| 14 | 1411.18384 | 0.176 | 16.835 | 0.049 |
| 15 | 1413.17786 | 0.383 | 16.888 | 0.053 |
| 16 | 1414.17542 | 0.989 | 17.087 | 0.065 |
| 17 | 1416.16968 | 0.196 | 16.783 | 0.067 |
| 18 | 1417.16711 | 0.801 | 16.753 | 0.079 |
| 19 | 1418.16406 | 0.405 | 17.017 | 0.175 |
| 20 | 1432.12549 | 0.865 | 16.736 | 0.050 |
| 21 | 1435.11731 | 0.678 | 16.794 | 0.046 |
| 22 | 1436.11450 | 0.282 | 16.755 | 0.049 |
| 23 | 1442.09802 | 0.908 | 16.867 | 0.054 |
| 24 | 1768.20618 | 0.547 | 17.018 | 0.062 |
| 25 | 2061.40869 | 0.256 | 16.694 | 0.054 |
| 26 | 2063.40210 | 0.461 | 16.848 | 0.065 |
| 27 | 2094.31543 | 0.190 | 16.669 | 0.059 |
| 28 | 2095.30981 | 0.784 | 16.750 | 0.064 |
| 29 | 2110.27100 | 0.857 | 16.775 | 0.071 |
| 30 | 2113.26270 | 0.670 | 16.585 | 0.063 |
| 31 | 2121.24048 | 0.504 | 16.874 | 0.084 |
| 32 | 2123.23462 | 0.711 | 16.649 | 0.065 |
| 33 | 2124.23193 | 0.316 | 16.744 | 0.069 |
| 34 | 2125.22925 | 0.920 | 16.998 | 0.090 |
| 35 | 2147.16821 | 0.214 | 16.680 | 0.083 |
| 36 | 2170.10498 | 0.113 | 16.721 | 0.078 |
| 37 | 2171.10229 | 0.717 | 16.626 | 0.070 |
| 38 | 2178.08301 | 0.947 | 16.920 | 0.081 |
| 39 | 2499.20215 | 0.554 | 16.696 | 0.086 |
| 40 | 3539.13892 | 0.154 | 16.797 | 0.020 |
| 41 | 3539.14990 | 0.193 | 16.756 | 0.020 |
| 42 | 3539.23486 | 0.500 | 17.070 | 0.022 |
| 43 | 3539.24512 | 0.538 | 17.053 | 0.021 |
| 44 | 3539.32153 | 0.814 | 16.726 | 0.018 |
| 45 | 3539.33154 | 0.850 | 16.757 | 0.018 |
| 46 | 3539.38818 | 0.055 | 17.020 | 0.022 |
| 47 | 3539.39844 | 0.092 | 16.917 | 0.021 |
| 48 | 3539.44360 | 0.255 | 16.703 | 0.019 |
| 49 | 3539.45361 | 0.292 | 16.708 | 0.020 |

2. RR011358

| | Dayval | Phase | Vint | Vinterr |
|---|---|---|---|---|
| 1 | 1020.29187 | 0.360 | 16.368 | 0.031 |
| 2 | 1023.28363 | 0.161 | 16.343 | 0.032 |
| 3 | 1055.19482 | 0.378 | 16.444 | 0.031 |
| 4 | 1056.19165 | 0.977 | 16.716 | 0.121 |
| 5 | 1352.38440 | 0.375 | 16.406 | 0.035 |
| 6 | 1354.37988 | 0.578 | 16.520 | 0.031 |
| 7 | 1355.37720 | 0.179 | 16.312 | 0.031 |
| 8 | 1377.31482 | 0.387 | 16.459 | 0.036 |
| 9 | 1378.31189 | 0.987 | 16.600 | 0.040 |
| 10 | 1379.30994 | 0.590 | 16.494 | 0.041 |
| 11 | 1401.24829 | 0.800 | 16.356 | 0.030 |
| 12 | 1403.24292 | 0.001 | 16.686 | 0.041 |
| 13 | 1404.24011 | 0.602 | 16.432 | 0.036 |
| 14 | 1405.23718 | 0.202 | 16.296 | 0.031 |
| 15 | 1410.22290 | 0.203 | 16.304 | 0.030 |
| 16 | 1411.22070 | 0.805 | 16.400 | 0.034 |
| 17 | 1413.21472 | 0.005 | 16.686 | 0.051 |
| 18 | 1414.21179 | 0.605 | 16.414 | 0.038 |
| 19 | 1416.20654 | 0.807 | 16.355 | 0.043 |
| 20 | 1417.20398 | 0.408 | 16.552 | 0.062 |
| 21 | 1418.20093 | 0.008 | 16.731 | 0.130 |
| 22 | 1432.16235 | 0.416 | 16.474 | 0.039 |
| 23 | 1435.15430 | 0.218 | 16.297 | 0.029 |
| 24 | 1436.15137 | 0.818 | 16.343 | 0.036 |
| 25 | 1442.13501 | 0.422 | 16.533 | 0.039 |
| 26 | 1742.31604 | 0.220 | 16.241 | 0.033 |
| 27 | 1744.30969 | 0.419 | 16.488 | 0.061 |
| 28 | 1758.27124 | 0.827 | 16.353 | 0.039 |
| 29 | 1768.24304 | 0.831 | 16.357 | 0.040 |
| 30 | 2061.44556 | 0.430 | 16.509 | 0.043 |
| 31 | 2063.43896 | 0.629 | 16.314 | 0.044 |
| 32 | 2094.35229 | 0.243 | 16.232 | 0.048 |
| 33 | 2095.34668 | 0.837 | 16.520 | 0.056 |
| 34 | 2110.30786 | 0.851 | 16.334 | 0.059 |
| 35 | 2113.29956 | 0.653 | 16.303 | 0.046 |
| 36 | 2121.27734 | 0.457 | 16.530 | 0.064 |
| 37 | 2123.27148 | 0.658 | 16.247 | 0.046 |
| 38 | 2124.26587 | 0.250 | 16.358 | 0.049 |
| 39 | 2126.26294 | 0.458 | 16.546 | 0.175 |
| 40 | 2147.20508 | 0.070 | 16.436 | 0.057 |
| 41 | 2169.14160 | 0.275 | 16.440 | 0.054 |
| 42 | 2171.13916 | 0.484 | 16.570 | 0.064 |
| 43 | 2178.11987 | 0.688 | 16.272 | 0.045 |
| 44 | 2500.23853 | 0.694 | 16.228 | 0.058 |
| 45 | 2532.15063 | 0.913 | 16.406 | 0.076 |
| 46 | 3539.16724 | 0.963 | 16.616 | 0.020 |
| 47 | 3539.17798 | 0.991 | 16.634 | 0.020 |
| 48 | 3539.25732 | 0.197 | 16.335 | 0.016 |
| 49 | 3539.26733 | 0.224 | 16.296 | 0.017 |
| 50 | 3539.35547 | 0.454 | 16.619 | 0.019 |
| 51 | 3539.36475 | 0.478 | 16.677 | 0.019 |
| 52 | 3539.41016 | 0.597 | 16.490 | 0.019 |
| 53 | 3539.41968 | 0.621 | 16.426 | 0.018 |
| 54 | 3539.46582 | 0.741 | 16.275 | 0.017 |
| 55 | 3539.47534 | 0.766 | 16.251 | 0.018 |
| 56 | 3546.15967 | 0.197 | 16.284 | 0.023 |
| 57 | 3546.16919 | 0.222 | 16.266 | 0.021 |
| 58 | 3546.20410 | 0.313 | 16.332 | 0.018 |
| 59 | 3546.21338 | 0.337 | 16.313 | 0.020 |
| 60 | 3546.25146 | 0.437 | 16.588 | 0.023 |
| 61 | 3546.26074 | 0.461 | 16.641 | 0.021 |

3. RR012659

| | Dayval | Phase | Vint | Vinterr |
|---|---|---|---|---|
| 1 | 1020.30090 | 0.038 | 16.678 | 0.039 |
| 2 | 1023.29266 | 0.607 | 16.627 | 0.034 |
| 3 | 1055.20386 | 0.012 | 16.671 | 0.038 |
| 4 | 1056.20068 | 0.867 | 16.542 | 0.090 |
| 5 | 1352.39343 | 0.265 | 16.481 | 0.037 |
| 6 | 1354.38892 | 0.981 | 16.669 | 0.036 |
| 7 | 1355.38623 | 0.838 | 16.536 | 0.034 |
| 8 | 1377.32385 | 0.675 | 16.554 | 0.036 |
| 9 | 1378.32092 | 0.531 | 16.684 | 0.039 |
| 10 | 1379.31897 | 0.389 | 16.532 | 0.044 |
| 11 | 1401.25732 | 0.228 | 16.528 | 0.035 |
| 12 | 1403.25195 | 0.942 | 16.640 | 0.042 |
| 13 | 1404.24927 | 0.798 | 16.460 | 0.041 |
| 14 | 1405.24622 | 0.654 | 16.602 | 0.034 |
| 15 | 1410.23206 | 0.935 | 16.614 | 0.042 |
| 16 | 1411.22974 | 0.793 | 16.536 | 0.037 |
| 17 | 1413.22388 | 0.505 | 16.671 | 0.055 |
| 18 | 1414.22083 | 0.360 | 16.544 | 0.053 |
| 19 | 1416.21558 | 0.074 | 16.665 | 0.053 |
| 20 | 1417.21301 | 0.931 | 16.598 | 0.066 |
| 21 | 1418.21008 | 0.787 | 16.435 | 0.098 |
| 22 | 1432.17151 | 0.777 | 16.517 | 0.033 |
| 23 | 1435.16333 | 0.347 | 16.525 | 0.041 |
| 24 | 1436.16040 | 0.203 | 16.522 | 0.039 |
| 25 | 1442.14404 | 0.342 | 16.515 | 0.041 |
| 26 | 1742.32507 | 0.164 | 16.562 | 0.040 |
| 27 | 1744.31860 | 0.874 | 16.542 | 0.062 |
| 28 | 1758.28027 | 0.865 | 16.523 | 0.043 |
| 29 | 1768.25220 | 0.428 | 16.631 | 0.046 |
| 30 | 2061.45337 | 0.257 | 16.488 | 0.049 |
| 31 | 2063.44800 | 0.971 | 16.654 | 0.055 |
| 32 | 2095.35596 | 0.366 | 16.461 | 0.050 |
| 33 | 2110.31689 | 0.220 | 16.525 | 0.067 |
| 34 | 2113.30859 | 0.788 | 16.535 | 0.055 |
| 35 | 2121.28638 | 0.640 | 16.563 | 0.065 |
| 36 | 2123.28052 | 0.352 | 16.434 | 0.059 |
| 37 | 2124.27734 | 0.207 | 16.506 | 0.059 |
| 38 | 2126.27197 | 0.920 | 16.570 | 0.182 |

| | | | | |
|---|---|---|---|---|
| 39 | 2147.21411 | 0.906 | 16.611 | 0.062 |
| 40 | 2171.14819 | 0.461 | 16.644 | 0.063 |
| 41 | 2178.12891 | 0.456 | 16.602 | 0.058 |
| 42 | 2500.24756 | 0.115 | 16.586 | 0.080 |
| 43 | 2532.15967 | 0.522 | 16.646 | 0.086 |
| 44 | 3540.20020 | 0.898 | 16.632 | 0.043 |
| 45 | 3540.20947 | 0.925 | 16.735 | 0.037 |
| 46 | 3540.28882 | 0.152 | 16.587 | 0.026 |
| 47 | 3540.29834 | 0.179 | 16.536 | 0.026 |
| 48 | 3546.18213 | 0.032 | 16.707 | 0.026 |
| 49 | 3546.19165 | 0.059 | 16.718 | 0.026 |
| 50 | 3546.23145 | 0.174 | 16.558 | 0.024 |
| 51 | 3546.24097 | 0.201 | 16.504 | 0.027 |
| 52 | 3546.33960 | 0.483 | 16.676 | 0.026 |
| 53 | 3546.34937 | 0.511 | 16.684 | 0.025 |

4. RR015856

| | Dayval | Phase | Vint | Vinterr |
|---|---|---|---|---|
| 1 | 1020.32318 | 0.612 | 17.145 | 0.052 |
| 2 | 1050.23987 | 0.703 | 17.264 | 0.059 |
| 3 | 1054.22852 | 0.715 | 17.281 | 0.078 |
| 4 | 1055.22607 | 0.718 | 17.283 | 0.060 |
| 5 | 1056.22302 | 0.721 | 17.547 | 0.199 |
| 6 | 1086.13916 | 0.811 | 17.303 | 0.063 |
| 7 | 1352.41565 | 0.660 | 17.281 | 0.062 |
| 8 | 1354.41125 | 0.668 | 17.219 | 0.050 |
| 9 | 1355.40710 | 0.668 | 17.236 | 0.059 |
| 10 | 1377.34607 | 0.735 | 17.351 | 0.065 |
| 11 | 1378.34314 | 0.738 | 17.375 | 0.068 |
| 12 | 1379.34131 | 0.743 | 17.378 | 0.085 |
| 13 | 1401.27954 | 0.809 | 17.246 | 0.076 |
| 14 | 1403.27417 | 0.815 | 17.432 | 0.064 |
| 15 | 1404.27148 | 0.818 | 17.348 | 0.080 |
| 16 | 1405.26843 | 0.821 | 17.331 | 0.070 |
| 17 | 1410.25427 | 0.835 | 17.409 | 0.069 |
| 18 | 1411.25195 | 0.839 | 17.466 | 0.095 |
| 19 | 1412.24866 | 0.841 | 17.442 | 0.541 |
| 20 | 1413.24573 | 0.844 | 17.375 | 0.074 |
| 21 | 1414.24316 | 0.847 | 17.244 | 0.076 |
| 22 | 1416.23779 | 0.854 | 17.367 | 0.093 |
| 23 | 1417.23535 | 0.858 | 17.160 | 0.106 |
| 24 | 1418.23230 | 0.860 | 17.590 | 0.251 |
| 25 | 1432.19373 | 0.903 | 17.130 | 0.057 |
| 26 | 1435.18555 | 0.913 | 16.988 | 0.061 |
| 27 | 1436.18262 | 0.916 | 17.077 | 0.056 |
| 28 | 1442.16626 | 0.934 | 16.682 | 0.045 |
| 29 | 1742.34741 | 0.885 | 17.376 | 0.067 |
| 30 | 1744.34094 | 0.889 | 17.426 | 0.092 |
| 31 | 1758.30261 | 0.932 | 17.531 | 0.080 |
| 32 | 1768.27441 | 0.962 | 16.833 | 0.048 |
| 33 | 2061.47559 | 0.892 | 17.334 | 0.088 |
| 34 | 2063.47021 | 0.899 | 17.537 | 0.095 |
| 35 | 2096.37769 | 0.997 | 16.365 | 0.042 |
| 36 | 2110.33911 | 0.041 | 16.747 | 0.080 |
| 37 | 2113.33081 | 0.050 | 16.720 | 0.065 |
| 38 | 2121.30811 | 0.073 | 16.697 | 0.072 |
| 39 | 2123.30298 | 0.080 | 16.789 | 0.062 |
| 40 | 2124.29980 | 0.082 | 16.716 | 0.075 |
| 41 | 2126.29419 | 0.088 | 16.819 | 0.203 |
| 42 | 2147.23608 | 0.152 | 17.007 | 0.079 |
| 43 | 2148.23315 | 0.155 | 17.117 | 0.068 |
| 44 | 2170.17285 | 0.224 | 17.147 | 0.095 |
| 45 | 2178.15112 | 0.249 | 17.407 | 0.105 |
| 46 | 2199.09375 | 0.315 | 17.245 | 0.103 |
| 47 | 2500.26978 | 0.263 | 17.437 | 0.123 |
| 48 | 2532.18188 | 0.363 | 17.382 | 0.129 |
| 49 | 3641.08423 | 0.728 | 17.401 | 0.026 |
| 50 | 3641.09863 | 0.756 | 17.427 | 0.025 |
| 51 | 3641.11279 | 0.785 | 17.424 | 0.025 |
| 52 | 3641.12720 | 0.813 | 17.372 | 0.025 |
| 53 | 3641.14258 | 0.844 | 17.230 | 0.023 |
| 54 | 3641.15967 | 0.879 | 17.066 | 0.021 |
| 55 | 3641.17383 | 0.907 | 16.894 | 0.018 |
| 56 | 3641.18823 | 0.936 | 16.661 | 0.016 |
| 57 | 3641.20239 | 0.965 | 16.381 | 0.014 |
| 58 | 3641.21655 | 0.993 | 16.331 | 0.014 |
| 59 | 3641.23071 | 0.022 | 16.451 | 0.015 |
| 60 | 3641.24487 | 0.050 | 16.518 | 0.015 |
| 61 | 3641.25928 | 0.079 | 16.682 | 0.018 |
| 62 | 3660.08008 | 0.883 | 17.187 | 0.021 |
| 63 | 3660.09082 | 0.904 | 16.917 | 0.022 |
| 64 | 3660.13818 | 0.999 | 16.454 | 0.038 |
| 65 | 3660.15234 | 0.028 | 16.487 | 0.067 |
| 66 | 3666.12524 | 0.025 | 16.597 | 0.015 |
| 67 | 3666.13965 | 0.054 | 16.684 | 0.017 |
| 68 | 3666.18774 | 0.151 | 16.943 | 0.020 |
| 69 | 3666.20825 | 0.192 | 16.971 | 0.024 |
| 70 | 3666.25342 | 0.282 | 17.142 | 0.028 |
| 71 | 3666.26758 | 0.311 | 17.255 | 0.030 |
| 72 | 3685.06470 | 0.067 | 16.882 | 0.022 |
| 73 | 3685.07886 | 0.096 | 16.970 | 0.017 |
| 74 | 3685.13965 | 0.218 | 17.124 | 0.019 |
| 75 | 3685.15405 | 0.247 | 17.149 | 0.020 |
| 76 | 3685.19995 | 0.339 | 17.237 | 0.021 |
| 77 | 3685.21411 | 0.368 | 17.233 | 0.022 |

5. RR020150

| | Dayval | Phase | Vint | Vinterr |
|---|---|---|---|---|
| 1 | 1020.32520 | 0.763 | 17.878 | 0.091 |
| 2 | 1023.31696 | 0.249 | 17.434 | 0.061 |
| 3 | 1050.24194 | 0.618 | 17.902 | 0.087 |
| 4 | 1054.23047 | 0.264 | 17.615 | 0.098 |
| 5 | 1055.22815 | 0.427 | 17.939 | 0.081 |
| 6 | 1056.22498 | 0.588 | 18.187 | 0.327 |
| 7 | 1086.14111 | 0.441 | 17.764 | 0.080 |
| 8 | 1352.41772 | 0.683 | 17.900 | 0.106 |
| 9 | 1354.41321 | 0.009 | 17.039 | 0.049 |
| 10 | 1355.40918 | 0.168 | 17.332 | 0.064 |
| 11 | 1377.34814 | 0.728 | 17.902 | 0.094 |
| 12 | 1378.34521 | 0.890 | 18.151 | 0.123 |
| 13 | 1379.34326 | 0.053 | 16.797 | 0.063 |
| 14 | 1401.28162 | 0.612 | 18.072 | 0.115 |
| 15 | 1403.27625 | 0.936 | 17.957 | 0.102 |
| 16 | 1404.27344 | 0.098 | 16.815 | 0.050 |
| 17 | 1405.27051 | 0.259 | 17.375 | 0.070 |
| 18 | 1410.25623 | 0.067 | 16.710 | 0.043 |
| 19 | 1411.25403 | 0.230 | 17.315 | 0.067 |
| 20 | 1413.24768 | 0.552 | 17.964 | 0.114 |
| 21 | 1414.24512 | 0.715 | 17.961 | 0.109 |
| 22 | 1416.23987 | 0.039 | 16.726 | 0.051 |
| 23 | 1417.23730 | 0.201 | 17.202 | 0.097 |
| 24 | 1432.19568 | 0.628 | 17.877 | 0.095 |
| 25 | 1435.18762 | 0.114 | 17.186 | 0.059 |
| 26 | 1436.18469 | 0.276 | 17.645 | 0.084 |
| 27 | 1442.16833 | 0.247 | 17.605 | 0.081 |
| 28 | 1742.34937 | 0.988 | 17.124 | 0.056 |
| 29 | 1744.34290 | 0.310 | 17.704 | 0.113 |
| 30 | 1758.30457 | 0.576 | 17.807 | 0.099 |
| 31 | 1768.27649 | 0.194 | 17.299 | 0.072 |
| 32 | 2061.47754 | 0.804 | 17.952 | 0.131 |
| 33 | 2063.47241 | 0.128 | 16.940 | 0.065 |
| 34 | 2096.37964 | 0.466 | 17.755 | 0.129 |
| 35 | 2113.33276 | 0.217 | 17.537 | 0.110 |
| 36 | 2121.31006 | 0.510 | 17.769 | 0.164 |
| 37 | 2123.30493 | 0.835 | 17.300 | 0.110 |
| 38 | 2124.30176 | 0.996 | 17.058 | 0.092 |
| 39 | 2126.29614 | 0.319 | 17.590 | 0.373 |
| 40 | 2147.23804 | 0.718 | 17.852 | 0.146 |
| 41 | 2148.23511 | 0.879 | 17.671 | 0.121 |
| 42 | 2170.17505 | 0.441 | 17.661 | 0.141 |
| 43 | 2178.15332 | 0.737 | 17.833 | 0.143 |
| 44 | 2199.09570 | 0.136 | 16.799 | 0.088 |
| 45 | 2500.27173 | 0.035 | 17.199 | 0.107 |
| 46 | 2532.18384 | 0.214 | 17.502 | 0.161 |
| 47 | 3175.26636 | 0.307 | 17.706 | 0.033 |
| 48 | 3175.28052 | 0.338 | 17.743 | 0.044 |
| 49 | 3175.32812 | 0.441 | 17.793 | 0.045 |
| 50 | 3175.34570 | 0.479 | 17.516 | 0.037 |
| 51 | 3181.28955 | 0.365 | 17.742 | 0.032 |
| 52 | 3181.30444 | 0.397 | 17.765 | 0.035 |
| 53 | 3181.37085 | 0.541 | 17.758 | 0.042 |
| 54 | 3181.38501 | 0.572 | 17.814 | 0.039 |
| 55 | 3181.43237 | 0.674 | 17.891 | 0.037 |
| 56 | 3181.44678 | 0.705 | 17.901 | 0.033 |
| 57 | 3181.46118 | 0.737 | 17.804 | 0.034 |
| 58 | 3186.25195 | 0.122 | 17.419 | 0.025 |

| | | | | |
|---|---|---|---|---|
| 59 | 3186.26636 | 0.154 | 17.481 | 0.025 |
| 60 | 3186.28076 | 0.184 | 17.508 | 0.028 |
| 61 | 3186.29565 | 0.217 | 17.544 | 0.030 |
| 62 | 3186.30981 | 0.248 | 17.543 | 0.033 |
| 63 | 3186.32397 | 0.278 | 17.618 | 0.033 |
| 64 | 3187.28662 | 0.365 | 17.741 | 0.028 |
| 65 | 3187.30151 | 0.397 | 17.673 | 0.033 |
| 66 | 3189.23584 | 0.591 | 17.859 | 0.052 |
| 67 | 3189.25146 | 0.625 | 17.851 | 0.032 |
| 68 | 3189.26611 | 0.656 | 17.735 | 0.041 |
| 69 | 3189.28442 | 0.696 | 17.838 | 0.026 |
| 70 | 3189.30322 | 0.737 | 17.823 | 0.030 |
| 71 | 3189.32251 | 0.778 | 17.716 | 0.027 |
| 72 | 3189.34180 | 0.821 | 17.530 | 0.039 |
| 73 | 3189.39209 | 0.930 | 17.137 | 0.072 |
| 74 | 3232.27197 | 0.886 | 18.072 | 0.041 |
| 75 | 3232.28638 | 0.917 | 17.819 | 0.048 |
| 76 | 3234.07812 | 0.801 | 17.966 | 0.041 |
| 77 | 3234.09229 | 0.832 | 17.970 | 0.049 |
| 78 | 3234.13940 | 0.934 | 17.703 | 0.031 |
| 79 | 3234.15356 | 0.965 | 17.277 | 0.023 |
| 80 | 3234.20166 | 0.069 | 16.831 | 0.019 |
| 81 | 3234.21606 | 0.100 | 16.931 | 0.022 |
| 82 | 3234.27173 | 0.221 | 17.270 | 0.028 |
| 83 | 3234.28589 | 0.252 | 17.439 | 0.028 |
| 84 | 3234.31836 | 0.322 | 17.539 | 0.032 |
| 85 | 3234.33252 | 0.353 | 17.564 | 0.040 |
| 86 | 3234.38989 | 0.477 | 17.790 | 0.046 |
| 87 | 3234.40430 | 0.508 | 17.739 | 0.046 |
| 88 | 3234.42700 | 0.558 | 17.854 | 0.040 |
| 89 | 3546.30371 | 0.653 | 17.889 | 0.046 |
| 90 | 3546.36108 | 0.777 | 17.850 | 0.042 |
| 91 | 3546.37207 | 0.801 | 17.689 | 0.035 |
| 92 | 3559.28125 | 0.786 | 17.689 | 0.028 |
| 93 | 3559.29199 | 0.809 | 17.391 | 0.025 |
| 94 | 3559.36499 | 0.968 | 17.055 | 0.023 |
| 95 | 3559.37573 | 0.991 | 17.093 | 0.022 |
| 96 | 3559.44727 | 0.146 | 17.505 | 0.027 |
| 97 | 3559.45801 | 0.169 | 17.489 | 0.027 |

6. RR023140

| | Dayval | Phase | Vint | Vinterr |
|---|---|---|---|---|
| 1 | 1020.34595 | 0.534 | 14.003 | 0.007 |
| 2 | 1023.33771 | 0.804 | 13.871 | 0.006 |
| 3 | 1050.26270 | 0.232 | 13.828 | 0.006 |
| 4 | 1054.25134 | 0.257 | 13.836 | 0.007 |
| 5 | 1055.24890 | 0.015 | 14.028 | 0.007 |
| 6 | 1086.16199 | 0.465 | 14.011 | 0.006 |
| 7 | 1352.43848 | 0.538 | 14.044 | 0.007 |
| 8 | 1354.43396 | 0.055 | 14.049 | 0.006 |
| 9 | 1355.42993 | 0.806 | 13.871 | 0.006 |
| 10 | 1377.36890 | 0.451 | 14.020 | 0.007 |
| 11 | 1378.36597 | 0.207 | 13.898 | 0.007 |
| 12 | 1379.36401 | 0.967 | 14.043 | 0.009 |
| 13 | 1401.30237 | 0.609 | 13.960 | 0.008 |
| 14 | 1403.29700 | 0.123 | 13.958 | 0.007 |
| 15 | 1404.29431 | 0.880 | 13.978 | 0.007 |
| 16 | 1405.29126 | 0.636 | 13.922 | 0.007 |
| 17 | 1410.27710 | 0.417 | 13.997 | 0.007 |
| 18 | 1412.27148 | 0.930 | 13.957 | 0.011 |
| 19 | 1413.26843 | 0.686 | 13.887 | 0.007 |
| 20 | 1414.26587 | 0.443 | 13.990 | 0.008 |
| 21 | 1416.26013 | 0.955 | 14.041 | 0.008 |
| 22 | 1417.25806 | 0.715 | 13.860 | 0.008 |
| 23 | 1418.25513 | 0.471 | 13.888 | 0.023 |
| 24 | 1432.21655 | 0.064 | 14.014 | 0.007 |
| 25 | 1435.20837 | 0.334 | 13.900 | 0.007 |
| 26 | 1436.20544 | 0.090 | 13.978 | 0.008 |
| 27 | 1442.18909 | 0.631 | 13.922 | 0.007 |
| 28 | 1742.37024 | 0.422 | 13.967 | 0.007 |
| 29 | 1744.36365 | 0.932 | 14.009 | 0.008 |
| 30 | 1758.32434 | 0.522 | 13.992 | 0.008 |
| 31 | 1768.29724 | 0.090 | 13.957 | 0.008 |
| 32 | 2096.40039 | 0.066 | 14.042 | 0.009 |
| 33 | 2113.35352 | 0.929 | 14.025 | 0.010 |
| 34 | 2121.33081 | 0.979 | 14.008 | 0.005 |
| 35 | 2123.32568 | 0.494 | 14.034 | 0.011 |
| 36 | 2124.32251 | 0.249 | 13.872 | 0.010 |
| 37 | 2147.25879 | 0.651 | 13.904 | 0.011 |
| 38 | 2148.25586 | 0.407 | 14.000 | 0.009 |
| 39 | 2170.19580 | 0.055 | 14.029 | 0.011 |
| 40 | 2171.19263 | 0.810 | 13.922 | 0.010 |
| 41 | 2178.17407 | 0.109 | 13.980 | 0.009 |
| 42 | 2199.11646 | 0.000 | 14.025 | 0.012 |
| 43 | 2500.29248 | 0.540 | 14.009 | 0.011 |
| 44 | 2532.20459 | 0.754 | 13.869 | 0.011 |
| 45 | 3539.21875 | 0.208 | 13.901 | 0.008 |
| 46 | 3539.22412 | 0.228 | 13.877 | 0.008 |
| 47 | 3539.27612 | 0.425 | 13.985 | 0.009 |
| 48 | 3539.28076 | 0.441 | 14.003 | 0.009 |
| 49 | 3539.37402 | 0.793 | 13.855 | 0.008 |
| 50 | 3539.37842 | 0.810 | 13.860 | 0.008 |
| 51 | 3539.42969 | 0.003 | 14.062 | 0.009 |
| 52 | 3539.43433 | 0.020 | 14.058 | 0.009 |
| 53 | 3539.48438 | 0.209 | 13.889 | 0.009 |
| 54 | 3539.48877 | 0.226 | 13.889 | 0.008 |

7. RR034622

| | Dayval | Phase | Vint | Vinterr |
|---|---|---|---|---|
| 1 | 1020.39801 | 0.573 | 18.101 | 0.117 |
| 2 | 1023.38971 | 0.897 | 18.185 | 0.104 |
| 3 | 1050.31458 | 0.816 | 18.152 | 0.119 |
| 4 | 1054.30334 | 0.915 | 17.983 | 0.138 |
| 5 | 1055.30090 | 0.690 | 18.040 | 0.115 |
| 6 | 1056.29785 | 0.464 | 18.061 | 0.271 |
| 7 | 1086.21362 | 0.705 | 18.262 | 0.115 |
| 8 | 1120.12292 | 0.054 | 17.435 | 0.136 |
| 9 | 1352.49048 | 0.600 | 18.179 | 0.119 |
| 10 | 1377.42090 | 0.968 | 17.532 | 0.077 |
| 11 | 1378.41797 | 0.743 | 18.100 | 0.121 |
| 12 | 1379.41614 | 0.519 | 18.196 | 0.161 |
| 13 | 1401.35327 | 0.561 | 18.133 | 0.188 |
| 14 | 1403.34790 | 0.111 | 17.611 | 0.085 |
| 15 | 1404.34631 | 0.888 | 18.080 | 0.129 |
| 16 | 1405.34326 | 0.662 | 18.213 | 0.129 |
| 17 | 1410.32910 | 0.535 | 17.991 | 0.124 |
| 18 | 1411.32593 | 0.309 | 17.914 | 0.118 |
| 19 | 1412.32349 | 0.085 | 17.606 | 0.088 |
| 20 | 1413.32043 | 0.859 | 18.228 | 0.159 |
| 21 | 1414.31750 | 0.633 | 18.412 | 0.166 |
| 22 | 1416.31213 | 0.183 | 17.589 | 0.104 |
| 23 | 1417.31018 | 0.959 | 17.647 | 0.085 |
| 24 | 1432.26855 | 0.581 | 18.030 | 0.118 |
| 25 | 1436.25745 | 0.680 | 18.125 | 0.132 |
| 26 | 1442.24109 | 0.329 | 17.919 | 0.121 |
| 27 | 1742.42224 | 0.563 | 18.412 | 0.139 |
| 28 | 1744.41565 | 0.111 | 17.641 | 0.091 |
| 29 | 1758.37634 | 0.957 | 17.638 | 0.103 |
| 30 | 1768.34924 | 0.705 | 18.117 | 0.146 |
| 31 | 1816.21643 | 0.895 | 18.140 | 0.133 |
| 32 | 2096.45239 | 0.632 | 18.166 | 0.151 |
| 33 | 2121.38281 | 0.001 | 17.295 | 0.066 |
| 34 | 2123.37769 | 0.551 | 17.941 | 0.194 |
| 35 | 2124.37451 | 0.325 | 17.917 | 0.162 |
| 36 | 2125.37134 | 0.099 | 17.670 | 0.128 |
| 37 | 2126.36890 | 0.874 | 18.142 | 0.515 |
| 38 | 2147.31055 | 0.144 | 17.688 | 0.134 |
| 39 | 2148.30786 | 0.919 | 17.768 | 0.155 |
| 40 | 2170.24731 | 0.965 | 17.445 | 0.124 |
| 41 | 2171.24438 | 0.740 | 18.046 | 0.201 |
| 42 | 2178.22534 | 0.164 | 17.797 | 0.157 |
| 43 | 2199.16846 | 0.436 | 17.877 | 0.231 |
| 44 | 2206.14917 | 0.860 | 18.153 | 0.203 |
| 45 | 2500.34448 | 0.441 | 18.206 | 0.194 |
| 46 | 2532.25659 | 0.235 | 18.070 | 0.198 |
| 47 | 3666.16357 | 0.254 | 17.744 | 0.037 |
| 48 | 3666.17090 | 0.267 | 17.888 | 0.042 |
| 49 | 3666.28296 | 0.467 | 18.125 | 0.050 |
| 50 | 3666.29736 | 0.492 | 18.106 | 0.073 |
| 51 | 3666.33032 | 0.551 | 18.099 | 0.066 |
| 52 | 3666.34448 | 0.576 | 18.145 | 0.066 |
| 53 | 3681.09570 | 0.829 | 18.279 | 0.037 |
| 54 | 3681.11035 | 0.855 | 18.289 | 0.039 |
| 55 | 3681.17871 | 0.977 | 17.534 | 0.027 |
| 56 | 3681.19312 | 0.002 | 17.449 | 0.030 |
| 57 | 3681.22900 | 0.066 | 17.599 | 0.063 |

| | | | | |
|---|---|---|---|---|
| 58 | 3685.09399 | 0.945 | 17.660 | 0.027 |
| 59 | 3685.10840 | 0.970 | 17.573 | 0.023 |
| 60 | 3685.12256 | 0.996 | 17.449 | 0.023 |
| 61 | 3685.16870 | 0.078 | 17.600 | 0.025 |
| 62 | 3685.18311 | 0.103 | 17.642 | 0.025 |
| 63 | 3685.22900 | 0.185 | 17.777 | 0.028 |
| 64 | 3685.24316 | 0.210 | 17.812 | 0.029 |
| 65 | 3685.28198 | 0.279 | 17.965 | 0.035 |
| 66 | 3685.29614 | 0.305 | 17.905 | 0.031 |

8. RR040258

| | Dayval | Phase | Vint | Vinterr |
|---|---|---|---|---|
| 1 | 1020.40955 | 0.279 | 17.635 | 0.074 |
| 2 | 1023.40131 | 0.646 | 17.795 | 0.078 |
| 3 | 1050.32593 | 0.943 | 17.829 | 0.085 |
| 4 | 1054.31482 | 0.432 | 17.957 | 0.106 |
| 5 | 1055.31250 | 0.556 | 18.003 | 0.117 |
| 6 | 1056.30933 | 0.677 | 17.741 | 0.209 |
| 7 | 1086.22510 | 0.339 | 17.619 | 0.071 |
| 8 | 1120.13452 | 0.505 | 17.925 | 0.177 |
| 9 | 1377.43250 | 0.072 | 18.002 | 0.111 |
| 10 | 1378.42957 | 0.193 | 17.655 | 0.079 |
| 11 | 1379.42761 | 0.318 | 17.659 | 0.104 |
| 12 | 1401.36475 | 0.001 | 18.054 | 0.167 |
| 13 | 1403.35950 | 0.246 | 17.732 | 0.097 |
| 14 | 1404.35779 | 0.371 | 17.513 | 0.079 |
| 15 | 1405.35486 | 0.493 | 17.994 | 0.108 |
| 16 | 1410.34070 | 0.103 | 17.708 | 0.088 |
| 17 | 1411.33740 | 0.224 | 17.585 | 0.097 |
| 18 | 1412.33508 | 0.347 | 17.436 | 0.089 |
| 19 | 1413.33203 | 0.469 | 17.775 | 0.111 |
| 20 | 1414.32910 | 0.590 | 17.814 | 0.096 |
| 21 | 1416.32373 | 0.835 | 17.443 | 0.094 |
| 22 | 1417.32166 | 0.960 | 17.812 | 0.098 |
| 23 | 1432.28003 | 0.792 | 17.477 | 0.078 |
| 24 | 1435.27197 | 0.159 | 17.591 | 0.178 |
| 25 | 1436.26904 | 0.281 | 17.543 | 0.084 |
| 26 | 1442.25269 | 0.015 | 18.052 | 0.125 |
| 27 | 1496.10547 | 0.621 | 17.764 | 0.112 |
| 28 | 1742.43213 | 0.838 | 17.606 | 0.086 |
| 29 | 1744.42725 | 0.085 | 17.962 | 0.114 |
| 30 | 1758.38757 | 0.793 | 17.593 | 0.088 |
| 31 | 1768.36084 | 0.018 | 18.112 | 0.137 |
| 32 | 1816.22803 | 0.883 | 17.555 | 0.097 |
| 33 | 2121.39453 | 0.320 | 17.657 | 0.153 |
| 34 | 2123.38843 | 0.563 | 17.799 | 0.174 |
| 35 | 2124.38599 | 0.687 | 17.468 | 0.127 |
| 36 | 2125.38281 | 0.807 | 17.628 | 0.124 |
| 37 | 2126.38013 | 0.929 | 17.799 | 0.396 |
| 38 | 2147.32202 | 0.496 | 17.974 | 0.214 |
| 39 | 2148.31934 | 0.618 | 17.664 | 0.129 |
| 40 | 2170.25903 | 0.308 | 17.618 | 0.126 |
| 41 | 2171.25586 | 0.430 | 17.758 | 0.155 |
| 42 | 2178.23706 | 0.287 | 17.250 | 0.115 |
| 43 | 2199.18018 | 0.857 | 17.522 | 0.147 |
| 44 | 2206.16089 | 0.713 | 17.543 | 0.131 |
| 45 | 2500.35620 | 0.800 | 17.617 | 0.148 |
| 46 | 2532.26831 | 0.713 | 17.610 | 0.139 |
| 47 | 3540.31470 | 0.776 | 17.621 | 0.037 |
| 48 | 3540.32544 | 0.809 | 17.573 | 0.035 |
| 49 | 3545.29443 | 0.366 | 17.408 | 0.040 |
| 50 | 3545.30542 | 0.401 | 17.632 | 0.046 |
| 51 | 3545.35010 | 0.541 | 17.886 | 0.055 |
| 52 | 3545.35962 | 0.571 | 17.829 | 0.049 |
| 53 | 3545.43408 | 0.803 | 17.547 | 0.036 |
| 54 | 3545.44409 | 0.835 | 17.544 | 0.033 |
| 55 | 3546.27515 | 0.437 | 17.780 | 0.043 |
| 56 | 3546.28613 | 0.471 | 18.100 | 0.051 |
| 57 | 3546.38501 | 0.781 | 17.411 | 0.070 |
| 58 | 3622.13574 | 0.947 | 17.913 | 0.035 |
| 59 | 3622.14990 | 0.991 | 18.132 | 0.038 |
| 60 | 3622.19751 | 0.140 | 17.635 | 0.029 |
| 61 | 3622.21143 | 0.184 | 17.589 | 0.027 |
| 62 | 3622.26880 | 0.363 | 17.622 | 0.029 |
| 63 | 3622.28174 | 0.404 | 17.810 | 0.032 |
| 64 | 3622.39844 | 0.769 | 17.607 | 0.026 |
| 65 | 3622.41284 | 0.814 | 17.623 | 0.027 |

9. CN Tau

| | Dayval | Phase | Vint | Vinterr |
|---|---|---|---|---|
| 1 | 1020.48920 | 0.903 | 12.617 | 0.003 |
| 2 | 1023.48096 | 0.571 | 12.900 | 0.004 |
| 3 | 1050.40503 | 0.585 | 12.937 | 0.003 |
| 4 | 1054.39453 | 0.810 | 12.593 | 0.004 |
| 5 | 1056.38818 | 0.922 | 12.545 | 0.005 |
| 6 | 1086.30481 | 0.605 | 12.899 | 0.004 |
| 7 | 1120.21375 | 0.514 | 12.908 | 0.004 |
| 8 | 1121.21118 | 0.070 | 12.553 | 0.004 |
| 9 | 1142.15466 | 0.749 | 12.863 | 0.003 |
| 10 | 1144.14929 | 0.862 | 12.683 | 0.003 |
| 11 | 1401.44434 | 0.341 | 12.781 | 0.006 |
| 12 | 1403.43909 | 0.454 | 12.891 | 0.004 |
| 13 | 1404.43750 | 0.010 | 12.568 | 0.003 |
| 14 | 1405.43457 | 0.566 | 12.922 | 0.004 |
| 15 | 1410.41919 | 0.346 | 12.777 | 0.004 |
| 16 | 1411.41711 | 0.903 | 12.619 | 0.003 |
| 17 | 1412.41467 | 0.459 | 12.879 | 0.004 |
| 18 | 1413.41089 | 0.014 | 12.553 | 0.003 |
| 19 | 1414.40869 | 0.571 | 12.798 | 0.004 |
| 20 | 1416.40259 | 0.683 | 12.892 | 0.004 |
| 21 | 1417.40137 | 0.240 | 12.710 | 0.003 |
| 22 | 1419.39429 | 0.351 | 12.803 | 0.004 |
| 23 | 1432.35974 | 0.581 | 12.914 | 0.004 |
| 24 | 1436.34875 | 0.806 | 12.771 | 0.004 |
| 25 | 1442.33228 | 0.142 | 12.622 | 0.003 |
| 26 | 1496.18506 | 0.173 | 12.621 | 0.003 |
| 27 | 1504.16333 | 0.622 | 12.899 | 0.005 |
| 28 | 1758.46729 | 0.434 | 12.864 | 0.004 |
| 29 | 1768.43933 | 0.995 | 12.569 | 0.003 |
| 30 | 1816.30762 | 0.688 | 12.904 | 0.004 |
| 31 | 1818.30188 | 0.801 | 12.787 | 0.004 |
| 32 | 1832.26367 | 0.586 | 12.875 | 0.006 |
| 33 | 1874.15063 | 0.944 | 12.576 | 0.003 |
| 34 | 1875.14795 | 0.501 | 12.873 | 0.004 |
| 35 | 2124.46484 | 0.531 | 12.892 | 0.005 |
| 36 | 2125.46265 | 0.088 | 12.557 | 0.004 |
| 37 | 2126.45947 | 0.644 | 12.895 | 0.012 |
| 38 | 2147.40161 | 0.322 | 12.774 | 0.005 |
| 39 | 2148.39868 | 0.878 | 12.656 | 0.004 |
| 40 | 2170.33813 | 0.112 | 12.599 | 0.004 |
| 41 | 2171.33545 | 0.669 | 12.901 | 0.006 |
| 42 | 2178.31641 | 0.561 | 12.864 | 0.005 |
| 43 | 2199.25977 | 0.240 | 12.777 | 0.009 |
| 44 | 2202.25098 | 0.908 | 12.559 | 0.006 |
| 45 | 2207.23755 | 0.689 | 12.885 | 0.005 |
| 46 | 2230.17554 | 0.481 | 12.843 | 0.005 |
| 47 | 2237.15674 | 0.374 | 12.828 | 0.005 |
| 48 | 2500.43530 | 0.190 | 12.637 | 0.005 |
| 49 | 2532.34692 | 0.985 | 12.522 | 0.005 |
| 50 | 2569.24634 | 0.562 | 12.881 | 0.059 |
| 51 | 3231.36523 | 0.791 | 12.813 | 0.007 |
| 52 | 3231.36768 | 0.792 | 12.813 | 0.007 |
| 53 | 3231.45020 | 0.838 | 12.722 | 0.007 |
| 54 | 3231.45264 | 0.839 | 12.716 | 0.007 |
| 55 | 3231.50244 | 0.867 | 12.668 | 0.007 |
| 56 | 3231.50488 | 0.869 | 12.666 | 0.007 |
| 57 | 3234.25928 | 0.405 | 12.841 | 0.007 |
| 58 | 3234.26172 | 0.406 | 12.849 | 0.007 |
| 59 | 3234.29810 | 0.426 | 12.864 | 0.007 |
| 60 | 3234.30054 | 0.428 | 12.855 | 0.007 |
| 61 | 3234.34302 | 0.451 | 12.868 | 0.007 |
| 62 | 3234.34546 | 0.453 | 12.875 | 0.007 |
| 63 | 3234.41431 | 0.491 | 12.898 | 0.007 |
| 64 | 3234.41675 | 0.492 | 12.895 | 0.007 |
| 65 | 3234.46777 | 0.521 | 12.903 | 0.007 |
| 66 | 3234.47021 | 0.522 | 12.901 | 0.007 |
| 67 | 3234.51611 | 0.548 | 12.902 | 0.007 |
| 68 | 3234.51880 | 0.549 | 12.912 | 0.007 |
| 69 | 3298.05249 | 0.979 | 12.552 | 0.007 |
| 70 | 3298.05518 | 0.980 | 12.553 | 0.007 |
| 71 | 3298.10889 | 0.010 | 12.563 | 0.006 |
| 72 | 3298.11133 | 0.011 | 12.551 | 0.006 |
| 73 | 3298.14014 | 0.028 | 12.561 | 0.006 |
| 74 | 3298.14282 | 0.029 | 12.560 | 0.006 |
| 75 | 3298.22412 | 0.074 | 12.573 | 0.006 |
| 76 | 3298.22656 | 0.076 | 12.570 | 0.006 |

| | | | |
|---|---|---|---|
| 77 3298.30469 | 0.119 | 12.602 | 0.006 |
| 78 3298.30737 | 0.121 | 12.593 | 0.006 |
| 79 3298.38428 | 0.164 | 12.642 | 0.007 |
| 80 3298.38672 | 0.165 | 12.642 | 0.007 |
| 81 3298.43921 | 0.194 | 12.662 | 0.007 |
| 82 3298.44165 | 0.196 | 12.669 | 0.007 |

10. RR064946

| Dayval | Phase | Vint | Vinterr |
|---|---|---|---|
| 1 1050.44299 | 0.347 | 18.206 | 0.127 |
| 2 1054.43274 | 0.157 | 18.403 | 0.179 |
| 3 1055.42883 | 0.854 | 18.216 | 0.119 |
| 4 1056.42627 | 0.557 | 18.736 | 0.465 |
| 5 1086.34167 | 0.605 | 18.088 | 0.122 |
| 6 1119.25159 | 0.769 | 18.059 | 0.100 |
| 7 1120.24915 | 0.472 | 18.472 | 0.161 |
| 8 1121.24658 | 0.174 | 18.094 | 0.193 |
| 9 1142.18909 | 0.914 | 18.685 | 0.150 |
| 10 1144.18372 | 0.318 | 18.110 | 0.123 |
| 11 1403.47766 | 0.834 | 18.238 | 0.150 |
| 12 1404.47400 | 0.532 | 18.463 | 0.184 |
| 13 1405.47302 | 0.241 | 18.048 | 0.108 |
| 14 1410.45764 | 0.744 | 18.066 | 0.104 |
| 15 1412.45312 | 0.151 | 18.110 | 0.131 |
| 16 1413.44922 | 0.849 | 18.170 | 0.149 |
| 17 1414.44702 | 0.553 | 18.377 | 0.181 |
| 18 1416.44080 | 0.954 | 18.659 | 0.173 |
| 19 1417.43958 | 0.661 | 18.061 | 0.142 |
| 20 1419.43237 | 0.058 | 18.228 | 0.135 |
| 21 1442.36951 | 0.203 | 18.089 | 0.111 |
| 22 1496.22009 | 0.099 | 18.468 | 0.208 |
| 23 1504.19812 | 0.714 | 18.147 | 0.156 |
| 24 1527.13574 | 0.860 | 18.169 | 0.140 |
| 25 1528.13306 | 0.562 | 18.259 | 0.149 |
| 26 1529.13025 | 0.264 | 18.055 | 0.118 |
| 27 1530.12756 | 0.966 | 18.561 | 0.185 |
| 28 1758.50549 | 0.719 | 17.959 | 0.146 |
| 29 1768.47791 | 0.737 | 18.193 | 0.150 |
| 30 1816.34448 | 0.421 | 18.507 | 0.200 |
| 31 1818.33862 | 0.823 | 18.146 | 0.176 |
| 32 1832.29968 | 0.648 | 18.246 | 0.252 |
| 33 1850.25024 | 0.281 | 17.963 | 0.133 |
| 34 1851.24744 | 0.983 | 18.685 | 0.239 |
| 35 1854.23926 | 0.089 | 18.153 | 0.157 |
| 36 1855.23657 | 0.791 | 18.042 | 0.127 |
| 37 1874.18506 | 0.129 | 17.961 | 0.129 |
| 38 1875.18250 | 0.832 | 18.185 | 0.145 |
| 39 1880.16870 | 0.341 | 18.111 | 0.144 |
| 40 2125.50122 | 0.031 | 18.818 | 0.302 |
| 41 2126.49805 | 0.731 | 18.006 | 0.482 |
| 42 2147.43994 | 0.468 | 18.459 | 0.254 |
| 43 2171.37256 | 0.308 | 18.322 | 0.205 |
| 44 2178.35327 | 0.220 | 18.438 | 0.235 |
| 45 2199.29492 | 0.957 | 18.765 | 0.280 |
| 46 2202.28662 | 0.063 | 18.140 | 0.245 |
| 47 2207.27319 | 0.573 | 18.142 | 0.201 |
| 48 2230.21045 | 0.717 | 17.919 | 0.182 |
| 49 2237.19116 | 0.630 | 18.075 | 0.223 |
| 50 2500.47314 | 0.950 | 18.439 | 0.313 |
| 51 2532.38403 | 0.405 | 18.728 | 0.256 |
| 52 3331.11255 | 0.335 | 18.140 | 0.033 |
| 53 3331.13062 | 0.402 | 18.410 | 0.039 |
| 54 3331.21558 | 0.718 | 18.014 | 0.032 |
| 55 3331.23340 | 0.784 | 18.043 | 0.028 |
| 56 3331.29663 | 0.018 | 18.542 | 0.041 |
| 57 3331.34644 | 0.204 | 18.116 | 0.036 |
| 58 3331.36426 | 0.269 | 18.098 | 0.036 |
| 59 3342.08936 | 0.082 | 18.460 | 0.072 |
| 60 3342.10010 | 0.122 | 18.204 | 0.064 |
| 61 3342.11084 | 0.162 | 18.184 | 0.053 |
| 62 3342.12476 | 0.213 | 18.258 | 0.058 |
| 63 3342.13550 | 0.253 | 18.092 | 0.045 |
| 64 3342.14624 | 0.293 | 18.108 | 0.054 |
| 65 3622.30273 | 0.252 | 17.994 | 0.036 |
| 66 3622.31763 | 0.307 | 18.104 | 0.031 |
| 67 3622.36890 | 0.497 | 18.670 | 0.052 |
| 68 3622.38306 | 0.550 | 18.555 | 0.047 |

11. RR075350

| Dayval | Phase | Vint | Vinterr |
|---|---|---|---|
| 1 1050.48743 | 0.539 | 16.229 | 0.029 |
| 2 1054.47607 | 0.845 | 16.118 | 0.033 |
| 3 1055.47339 | 0.422 | 16.179 | 0.027 |
| 4 1086.38538 | 0.291 | 16.065 | 0.027 |
| 5 1119.29626 | 0.321 | 16.094 | 0.027 |
| 6 1120.29382 | 0.899 | 15.940 | 0.029 |
| 7 1121.29114 | 0.475 | 16.184 | 0.042 |
| 8 1142.23376 | 0.584 | 16.174 | 0.028 |
| 9 1144.22827 | 0.738 | 16.301 | 0.029 |
| 10 1173.14978 | 0.460 | 16.206 | 0.027 |
| 11 1174.14709 | 0.037 | 15.876 | 0.024 |
| 12 1405.51770 | 0.820 | 16.245 | 0.031 |
| 13 1410.50220 | 0.700 | 16.222 | 0.037 |
| 14 1412.49768 | 0.855 | 16.068 | 0.037 |
| 15 1413.49390 | 0.430 | 16.187 | 0.031 |
| 16 1414.49158 | 0.007 | 15.797 | 0.031 |
| 17 1416.48547 | 0.159 | 15.984 | 0.025 |
| 18 1417.48413 | 0.738 | 16.252 | 0.032 |
| 19 1419.47693 | 0.888 | 15.977 | 0.029 |
| 20 1436.43079 | 0.691 | 16.289 | 0.029 |
| 21 1442.41418 | 0.151 | 15.981 | 0.027 |
| 22 1496.26465 | 0.285 | 16.008 | 0.035 |
| 23 1504.24268 | 0.898 | 15.981 | 0.031 |
| 24 1527.18030 | 0.161 | 15.970 | 0.029 |
| 25 1528.17761 | 0.737 | 16.305 | 0.036 |
| 26 1529.17480 | 0.314 | 16.100 | 0.031 |
| 27 1530.17224 | 0.891 | 15.988 | 0.027 |
| 28 1816.38904 | 0.382 | 16.149 | 0.036 |
| 29 1818.38269 | 0.534 | 16.201 | 0.034 |
| 30 1832.34436 | 0.606 | 16.211 | 0.056 |
| 31 1851.29211 | 0.561 | 16.225 | 0.043 |
| 32 1854.28394 | 0.291 | 16.112 | 0.067 |
| 33 1855.28125 | 0.868 | 16.008 | 0.026 |
| 34 1874.22974 | 0.824 | 16.138 | 0.034 |
| 35 1875.22717 | 0.401 | 16.174 | 0.033 |
| 36 1880.21313 | 0.284 | 16.094 | 0.032 |
| 37 1902.15405 | 0.971 | 15.897 | 0.027 |
| 38 1904.14868 | 0.124 | 15.957 | 0.028 |
| 39 2148.48071 | 0.398 | 16.183 | 0.039 |
| 40 2178.39746 | 0.694 | 16.199 | 0.051 |
| 41 2199.33911 | 0.802 | 16.256 | 0.074 |
| 42 2202.33105 | 0.532 | 16.264 | 0.053 |
| 43 2207.31787 | 0.416 | 16.236 | 0.044 |
| 44 2230.25464 | 0.677 | 16.335 | 0.050 |
| 45 2237.23560 | 0.714 | 16.262 | 0.059 |
| 46 2262.16821 | 0.131 | 15.950 | 0.056 |
| 47 2532.42847 | 0.396 | 16.225 | 0.049 |
| 48 2569.32642 | 0.729 | 16.293 | 0.537 |
| 49 3298.12085 | 0.907 | 15.904 | 0.025 |
| 50 3298.13184 | 0.925 | 15.904 | 0.022 |
| 51 3298.20288 | 0.037 | 15.845 | 0.021 |
| 52 3298.21338 | 0.054 | 15.837 | 0.021 |
| 53 3298.28369 | 0.165 | 16.011 | 0.024 |
| 54 3298.29443 | 0.182 | 16.045 | 0.024 |
| 55 3298.36401 | 0.292 | 16.094 | 0.021 |
| 56 3298.37476 | 0.309 | 16.074 | 0.021 |
| 57 3298.45630 | 0.438 | 16.169 | 0.022 |
| 58 3298.46704 | 0.455 | 16.179 | 0.021 |
| 59 3298.50366 | 0.512 | 16.185 | 0.025 |
| 60 3298.51440 | 0.530 | 16.180 | 0.027 |
| 61 3308.11060 | 0.700 | 16.274 | 0.028 |
| 62 3308.12134 | 0.717 | 16.276 | 0.026 |
| 63 3308.20459 | 0.849 | 16.089 | 0.023 |
| 64 3308.21533 | 0.866 | 16.016 | 0.023 |
| 65 3308.29883 | 0.998 | 15.877 | 0.023 |
| 66 3308.30933 | 0.015 | 15.802 | 0.022 |
| 67 3308.39404 | 0.149 | 15.946 | 0.022 |
| 68 3308.40503 | 0.166 | 15.992 | 0.022 |

12. RR084652

| Dayval | Phase | Vint | Vinterr |
|---|---|---|---|
| 1 1054.51318 | 0.027 | 15.550 | 0.022 |
| 2 1055.51062 | 0.831 | 16.698 | 0.037 |
| 3 1086.42249 | 0.760 | 16.704 | 0.038 |
| 4 1119.33313 | 0.304 | 16.366 | 0.029 |
| 5 1121.32800 | 0.914 | 16.306 | 0.040 |

| | | | | |
|---|---|---|---|---|
| 6 | 1142.27026 | 0.804 | 16.579 | 0.035 |
| 7 | 1144.26501 | 0.413 | 16.489 | 0.034 |
| 8 | 1172.18896 | 0.936 | 15.899 | 0.026 |
| 9 | 1173.18640 | 0.740 | 16.688 | 0.041 |
| 10 | 1174.18372 | 0.545 | 16.685 | 0.041 |
| 11 | 1175.18091 | 0.349 | 16.455 | 0.046 |
| 12 | 1417.52136 | 0.812 | 16.586 | 0.044 |
| 13 | 1419.51416 | 0.418 | 16.453 | 0.042 |
| 14 | 1435.47083 | 0.288 | 16.361 | 0.039 |
| 15 | 1436.46802 | 0.092 | 15.900 | 0.024 |
| 16 | 1442.45129 | 0.918 | 16.056 | 0.030 |
| 17 | 1496.30151 | 0.348 | 16.441 | 0.047 |
| 18 | 1504.27869 | 0.781 | 16.681 | 0.046 |
| 19 | 1527.21692 | 0.283 | 16.375 | 0.038 |
| 20 | 1528.21423 | 0.088 | 16.190 | 0.034 |
| 21 | 1529.21143 | 0.892 | 16.232 | 0.033 |
| 22 | 1530.20886 | 0.696 | 16.603 | 0.042 |
| 23 | 1552.14941 | 0.393 | 16.572 | 0.046 |
| 24 | 1816.42615 | 0.546 | 16.680 | 0.055 |
| 25 | 1818.41980 | 0.153 | 16.323 | 0.035 |
| 26 | 1832.38135 | 0.413 | 16.585 | 0.067 |
| 27 | 1850.33154 | 0.890 | 16.238 | 0.035 |
| 28 | 1851.32898 | 0.695 | 16.659 | 0.063 |
| 29 | 1854.32080 | 0.108 | 16.236 | 0.055 |
| 30 | 1855.31799 | 0.912 | 15.781 | 0.022 |
| 31 | 1874.26648 | 0.195 | 16.428 | 0.037 |
| 32 | 1875.26379 | 1.000 | 16.048 | 0.034 |
| 33 | 1880.24988 | 0.021 | 16.112 | 0.030 |
| 34 | 1886.23340 | 0.847 | 16.513 | 0.047 |
| 35 | 1902.19067 | 0.718 | 16.698 | 0.054 |
| 36 | 1904.18530 | 0.327 | 16.590 | 0.038 |
| 37 | 2148.51782 | 0.395 | 16.543 | 0.053 |
| 38 | 2202.36792 | 0.825 | 16.045 | 0.043 |
| 39 | 2207.35474 | 0.847 | 15.769 | 0.041 |
| 40 | 2230.29150 | 0.347 | 16.513 | 0.068 |
| 41 | 2237.27222 | 0.977 | 16.102 | 0.052 |
| 42 | 2262.20483 | 0.087 | 16.355 | 0.055 |
| 43 | 2263.20190 | 0.891 | 16.088 | 0.048 |
| 44 | 2532.46558 | 0.066 | 16.233 | 0.052 |
| 45 | 2569.36328 | 0.825 | 15.865 | 0.450 |
| 46 | 3234.36548 | 0.004 | 15.792 | 0.026 |
| 47 | 3234.37622 | 0.024 | 15.771 | 0.023 |
| 48 | 3234.44409 | 0.147 | 16.058 | 0.024 |
| 49 | 3234.45483 | 0.166 | 16.101 | 0.020 |
| 50 | 3234.49829 | 0.245 | 16.240 | 0.023 |
| 51 | 3234.50903 | 0.264 | 16.277 | 0.023 |
| 52 | 3298.15479 | 0.418 | 16.517 | 0.026 |
| 53 | 3298.16577 | 0.437 | 16.503 | 0.028 |
| 54 | 3298.23584 | 0.564 | 16.658 | 0.026 |
| 55 | 3298.24658 | 0.584 | 16.705 | 0.024 |
| 56 | 3298.31616 | 0.710 | 16.697 | 0.024 |
| 57 | 3298.32690 | 0.729 | 16.676 | 0.024 |
| 58 | 3298.39551 | 0.853 | 16.741 | 0.025 |
| 59 | 3298.40649 | 0.873 | 16.735 | 0.025 |
| 60 | 3298.47949 | 0.005 | 15.598 | 0.020 |
| 61 | 3298.52686 | 0.091 | 15.873 | 0.024 |
| 62 | 3307.14551 | 0.684 | 16.616 | 0.028 |
| 63 | 3307.15625 | 0.704 | 16.621 | 0.027 |
| 64 | 3307.19971 | 0.782 | 16.598 | 0.024 |
| 65 | 3307.21045 | 0.802 | 16.599 | 0.026 |
| 66 | 3307.25049 | 0.874 | 16.679 | 0.034 |
| 67 | 3307.25781 | 0.887 | 16.695 | 0.027 |
| 68 | 3307.31763 | 0.996 | 15.645 | 0.020 |
| 69 | 3307.32837 | 0.015 | 15.603 | 0.020 |
| 70 | 3307.38892 | 0.125 | 15.968 | 0.022 |
| 71 | 3307.39966 | 0.144 | 15.994 | 0.022 |
| 72 | 3307.47119 | 0.273 | 16.323 | 0.024 |
| 73 | 3307.48169 | 0.293 | 16.310 | 0.023 |

13. RR090118

| | Dayval | Phase | Vint | Vinterr |
|---|---|---|---|---|
| 1 | 1055.52075 | 0.778 | 16.529 | 0.036 |
| 2 | 1086.43250 | 0.967 | 15.680 | 0.018 |
| 3 | 1119.34314 | 0.048 | 16.026 | 0.024 |
| 4 | 1121.33813 | 0.932 | 15.855 | 0.029 |
| 5 | 1142.28027 | 0.709 | 16.612 | 0.032 |
| 6 | 1172.19897 | 0.964 | 15.984 | 0.025 |
| 7 | 1173.19641 | 0.906 | 15.864 | 0.021 |
| 8 | 1174.19373 | 0.848 | 16.155 | 0.028 |
| 9 | 1175.19092 | 0.790 | 16.507 | 0.039 |
| 10 | 1435.48096 | 0.604 | 16.698 | 0.045 |
| 11 | 1436.47803 | 0.545 | 16.732 | 0.042 |
| 12 | 1442.46143 | 0.195 | 16.226 | 0.029 |
| 13 | 1496.31152 | 0.048 | 15.957 | 0.035 |
| 14 | 1504.28870 | 0.580 | 16.549 | 0.038 |
| 15 | 1526.22913 | 0.301 | 16.398 | 0.035 |
| 16 | 1527.22693 | 0.243 | 16.327 | 0.031 |
| 17 | 1528.22424 | 0.185 | 16.242 | 0.030 |
| 18 | 1529.22144 | 0.127 | 16.131 | 0.029 |
| 19 | 1530.21887 | 0.069 | 15.977 | 0.029 |
| 20 | 1531.21570 | 0.010 | 15.859 | 0.025 |
| 21 | 1550.16467 | 0.906 | 15.866 | 0.028 |
| 22 | 1552.15942 | 0.790 | 16.641 | 0.042 |
| 23 | 1816.43616 | 0.366 | 16.397 | 0.044 |
| 24 | 1818.42981 | 0.248 | 16.289 | 0.034 |
| 25 | 1832.39136 | 0.433 | 16.603 | 0.056 |
| 26 | 1850.34155 | 0.384 | 16.433 | 0.042 |
| 27 | 1851.33899 | 0.326 | 16.388 | 0.046 |
| 28 | 1854.33081 | 0.151 | 16.122 | 0.048 |
| 29 | 1855.32800 | 0.093 | 16.111 | 0.030 |
| 30 | 1856.32483 | 0.034 | 16.122 | 0.028 |
| 31 | 1874.27649 | 0.988 | 15.777 | 0.023 |
| 32 | 1875.27380 | 0.930 | 15.530 | 0.021 |
| 33 | 1880.25989 | 0.638 | 16.690 | 0.048 |
| 34 | 1886.24341 | 0.289 | 16.351 | 0.040 |
| 35 | 1902.20068 | 0.359 | 16.388 | 0.042 |
| 36 | 1904.19519 | 0.243 | 16.220 | 0.032 |
| 37 | 1910.17883 | 0.894 | 16.085 | 0.033 |
| 38 | 2202.37769 | 0.838 | 16.294 | 0.056 |
| 39 | 2207.36475 | 0.548 | 16.498 | 0.056 |
| 40 | 2230.30151 | 0.209 | 16.271 | 0.053 |
| 41 | 2237.28223 | 0.801 | 16.599 | 0.083 |
| 42 | 2262.21484 | 0.348 | 16.317 | 0.060 |
| 43 | 2263.21191 | 0.289 | 16.427 | 0.095 |
| 44 | 2289.14209 | 0.778 | 16.615 | 0.069 |
| 45 | 2569.37329 | 0.420 | 16.517 | 0.626 |
| 46 | 3298.17896 | 0.486 | 16.396 | 0.028 |
| 47 | 3298.18970 | 0.507 | 16.358 | 0.027 |
| 48 | 3298.26001 | 0.644 | 16.427 | 0.026 |
| 49 | 3298.27075 | 0.665 | 16.455 | 0.025 |
| 50 | 3298.34033 | 0.800 | 16.377 | 0.025 |
| 51 | 3298.35107 | 0.821 | 16.360 | 0.025 |
| 52 | 3298.41895 | 0.954 | 15.868 | 0.022 |
| 53 | 3298.42969 | 0.975 | 15.877 | 0.020 |
| 54 | 3298.49121 | 0.094 | 16.026 | 0.023 |
| 55 | 3298.53882 | 0.187 | 16.137 | 0.028 |
| 56 | 3308.18140 | 0.962 | 15.842 | 0.026 |
| 57 | 3308.19214 | 0.983 | 15.874 | 0.024 |
| 58 | 3308.22778 | 0.053 | 15.985 | 0.025 |
| 59 | 3308.23877 | 0.074 | 16.051 | 0.024 |
| 60 | 3308.32227 | 0.236 | 16.120 | 0.025 |
| 61 | 3308.33301 | 0.257 | 16.110 | 0.023 |
| 62 | 3308.41797 | 0.423 | 16.311 | 0.023 |
| 63 | 3308.42871 | 0.444 | 16.314 | 0.025 |
| 64 | 3331.15259 | 0.690 | 16.609 | 0.026 |
| 65 | 3331.16333 | 0.711 | 16.561 | 0.026 |
| 66 | 3331.25293 | 0.885 | 16.233 | 0.023 |
| 67 | 3331.26367 | 0.906 | 15.884 | 0.022 |
| 68 | 3331.31421 | 0.004 | 15.442 | 0.023 |

14. RR095659

| | Dayval | Phase | Vint | Vinterr |
|---|---|---|---|---|
| 1 | 1086.47302 | 0.774 | 16.648 | 0.034 |
| 2 | 1119.38208 | 0.515 | 16.819 | 0.041 |
| 3 | 1121.37671 | 0.469 | 16.756 | 0.049 |
| 4 | 1142.31836 | 0.484 | 16.802 | 0.041 |
| 5 | 1172.23608 | 0.795 | 16.618 | 0.037 |
| 6 | 1173.23340 | 0.272 | 16.579 | 0.038 |
| 7 | 1174.23071 | 0.750 | 16.689 | 0.042 |
| 8 | 1175.22791 | 0.226 | 16.519 | 0.041 |
| 9 | 1179.21667 | 0.134 | 16.414 | 0.048 |
| 10 | 1435.52185 | 0.765 | 16.750 | 0.045 |
| 11 | 1436.51892 | 0.242 | 16.482 | 0.038 |
| 12 | 1442.50208 | 0.103 | 16.318 | 0.034 |
| 13 | 1496.34900 | 0.845 | 16.408 | 0.054 |
| 14 | 1504.32715 | 0.661 | 16.796 | 0.049 |

| | | | | |
|---|---|---|---|---|
| 15 | 1526.26660 | 0.155 | 16.440 | 0.039 |
| 16 | 1527.26440 | 0.634 | 16.859 | 0.041 |
| 17 | 1528.26111 | 0.109 | 16.370 | 0.036 |
| 18 | 1529.25879 | 0.588 | 16.876 | 0.048 |
| 19 | 1530.25610 | 0.065 | 16.348 | 0.037 |
| 20 | 1531.25293 | 0.540 | 16.790 | 0.051 |
| 21 | 1550.20142 | 0.606 | 16.800 | 0.052 |
| 22 | 1552.19604 | 0.561 | 16.826 | 0.055 |
| 23 | 1816.47668 | 0.999 | 16.346 | 0.043 |
| 24 | 1818.47021 | 0.950 | 16.365 | 0.037 |
| 25 | 1832.43127 | 0.627 | 16.800 | 0.055 |
| 26 | 1850.38074 | 0.209 | 16.487 | 0.043 |
| 27 | 1851.37805 | 0.686 | 16.812 | 0.069 |
| 28 | 1854.36926 | 0.115 | 16.405 | 0.043 |
| 29 | 1855.36694 | 0.594 | 16.850 | 0.044 |
| 30 | 1856.36365 | 0.069 | 16.374 | 0.035 |
| 31 | 1874.31458 | 0.656 | 16.737 | 0.051 |
| 32 | 1875.31189 | 0.134 | 16.409 | 0.044 |
| 33 | 1880.29773 | 0.517 | 16.789 | 0.050 |
| 34 | 1886.28101 | 0.379 | 16.666 | 0.050 |
| 35 | 1902.23767 | 0.013 | 16.375 | 0.036 |
| 36 | 1904.23218 | 0.967 | 16.407 | 0.034 |
| 37 | 1932.15625 | 0.327 | 16.591 | 0.053 |
| 38 | 1935.14819 | 0.759 | 16.790 | 0.052 |
| 39 | 1910.21558 | 0.829 | 16.574 | 0.046 |
| 40 | 2202.41699 | 0.616 | 16.875 | 0.078 |
| 41 | 2207.40430 | 0.004 | 16.418 | 0.048 |
| 42 | 2230.33984 | 0.972 | 16.366 | 0.051 |
| 43 | 2237.32031 | 0.310 | 16.612 | 0.104 |
| 44 | 2262.25195 | 0.236 | 16.549 | 0.055 |
| 45 | 2263.24902 | 0.713 | 16.763 | 0.108 |
| 46 | 2289.17871 | 0.118 | 16.444 | 0.068 |
| 47 | 2290.17578 | 0.595 | 16.752 | 0.103 |
| 48 | 2295.16235 | 0.981 | 16.385 | 0.061 |
| 49 | 2569.41284 | 0.181 | 16.454 | 0.644 |
| 50 | 3331.18237 | 0.161 | 16.386 | 0.015 |
| 51 | 3331.19751 | 0.214 | 16.427 | 0.015 |
| 52 | 3331.27954 | 0.499 | 16.806 | 0.018 |
| 53 | 3331.32983 | 0.675 | 16.808 | 0.018 |
| 54 | 3331.41357 | 0.967 | 16.382 | 0.014 |
| 55 | 3331.47876 | 0.194 | 16.435 | 0.015 |
| 56 | 3331.49292 | 0.244 | 16.504 | 0.015 |
| 57 | 3342.23535 | 0.698 | 16.761 | 0.032 |
| 58 | 3342.24609 | 0.735 | 16.756 | 0.029 |
| 59 | 3342.25684 | 0.773 | 16.719 | 0.027 |
| 60 | 3342.26807 | 0.812 | 16.614 | 0.026 |
| 61 | 3342.29858 | 0.918 | 16.363 | 0.020 |
| 62 | 3342.30908 | 0.955 | 16.363 | 0.020 |
| 63 | 3342.31982 | 0.993 | 16.349 | 0.021 |
| 64 | 3342.33057 | 0.030 | 16.339 | 0.020 |

15. RR102605

| | Dayval | Phase | Vint | Vinterr |
|---|---|---|---|---|
| 1 | 1086.49329 | 0.959 | 17.951 | 0.091 |
| 2 | 1119.40234 | 0.491 | 18.299 | 0.145 |
| 3 | 1121.39685 | 0.099 | 17.791 | 0.107 |
| 4 | 1142.33862 | 0.982 | 17.785 | 0.093 |
| 5 | 1144.33252 | 0.589 | 18.527 | 0.148 |
| 6 | 1172.25635 | 0.102 | 17.947 | 0.106 |
| 7 | 1173.25366 | 0.906 | 18.165 | 0.132 |
| 8 | 1174.25098 | 0.710 | 18.559 | 0.164 |
| 9 | 1175.24817 | 0.514 | 18.593 | 0.176 |
| 10 | 1179.23694 | 0.730 | 18.372 | 0.200 |
| 11 | 1442.52234 | 0.005 | 17.861 | 0.104 |
| 12 | 1496.36926 | 0.412 | 18.216 | 0.159 |
| 13 | 1504.34729 | 0.845 | 18.591 | 0.183 |
| 14 | 1526.28687 | 0.533 | 18.512 | 0.156 |
| 15 | 1527.28381 | 0.336 | 18.319 | 0.141 |
| 16 | 1528.28137 | 0.140 | 18.042 | 0.126 |
| 17 | 1529.27905 | 0.945 | 17.918 | 0.122 |
| 18 | 1530.27637 | 0.749 | 18.626 | 0.181 |
| 19 | 1531.27319 | 0.553 | 18.328 | 0.164 |
| 20 | 1550.22168 | 0.830 | 18.617 | 0.180 |
| 21 | 1552.21631 | 0.438 | 18.357 | 0.167 |
| 22 | 1818.49048 | 0.120 | 17.996 | 0.138 |
| 23 | 1832.45154 | 0.375 | 18.446 | 0.197 |
| 24 | 1850.40088 | 0.845 | 18.392 | 0.176 |
| 25 | 1851.39832 | 0.649 | 18.487 | 0.223 |
| 26 | 1854.38953 | 0.060 | 17.956 | 0.125 |
| 27 | 1855.38721 | 0.865 | 18.319 | 0.161 |
| 28 | 1856.38391 | 0.668 | 18.395 | 0.168 |
| 29 | 1874.33484 | 0.140 | 17.924 | 0.154 |
| 30 | 1875.33215 | 0.945 | 17.905 | 0.131 |
| 31 | 1880.31799 | 0.964 | 17.951 | 0.122 |
| 32 | 1886.30127 | 0.787 | 18.564 | 0.210 |
| 33 | 1902.25793 | 0.653 | 18.525 | 0.211 |
| 34 | 1904.25244 | 0.261 | 18.315 | 0.136 |
| 35 | 1932.17651 | 0.774 | 18.605 | 0.243 |
| 36 | 1935.16846 | 0.187 | 18.165 | 0.179 |
| 37 | 1936.16577 | 0.991 | 17.941 | 0.140 |
| 38 | 1910.23584 | 0.084 | 18.126 | 0.137 |
| 39 | 2202.43726 | 0.668 | 18.476 | 0.277 |
| 40 | 2230.36011 | 0.179 | 18.083 | 0.175 |
| 41 | 2262.27222 | 0.907 | 17.953 | 0.154 |
| 42 | 2263.26904 | 0.710 | 18.541 | 0.293 |
| 43 | 2290.19604 | 0.421 | 18.504 | 0.299 |
| 44 | 2295.18262 | 0.441 | 18.438 | 0.235 |
| 45 | 3357.18628 | 0.573 | 18.700 | 0.061 |
| 46 | 3357.20435 | 0.606 | 18.401 | 0.066 |
| 47 | 3363.09302 | 0.258 | 18.254 | 0.042 |
| 48 | 3363.11084 | 0.290 | 18.315 | 0.044 |
| 49 | 3363.16431 | 0.387 | 18.492 | 0.041 |
| 50 | 3363.18213 | 0.419 | 18.395 | 0.051 |
| 51 | 3363.23438 | 0.514 | 18.397 | 0.051 |
| 52 | 3363.25195 | 0.546 | 18.442 | 0.045 |
| 53 | 3363.31860 | 0.666 | 18.502 | 0.043 |
| 54 | 3363.33618 | 0.698 | 18.491 | 0.044 |
| 55 | 3363.38794 | 0.792 | 18.335 | 0.052 |
| 56 | 3363.40576 | 0.824 | 18.349 | 0.043 |
| 57 | 3622.33789 | 0.224 | 18.190 | 0.039 |
| 58 | 3622.35059 | 0.247 | 18.229 | 0.035 |
| 59 | 3622.46680 | 0.457 | 18.423 | 0.040 |
| 60 | 3622.48096 | 0.483 | 18.477 | 0.038 |
| 61 | 3666.21948 | 0.605 | 18.866 | 0.112 |
| 62 | 3666.23389 | 0.631 | 18.689 | 0.088 |
| 63 | 3666.31396 | 0.776 | 18.671 | 0.048 |
| 64 | 3666.36133 | 0.861 | 18.395 | 0.042 |
| 65 | 3666.37549 | 0.887 | 18.086 | 0.049 |
| 66 | 3666.38965 | 0.913 | 17.986 | 0.042 |
| 67 | 3666.40381 | 0.938 | 17.911 | 0.030 |
| 68 | 3666.42065 | 0.969 | 17.798 | 0.030 |
| 69 | 3666.43506 | 0.995 | 17.746 | 0.035 |
| 70 | 3685.31177 | 0.142 | 17.925 | 0.040 |
| 71 | 3685.34009 | 0.193 | 18.123 | 0.036 |
| 72 | 3685.35425 | 0.219 | 18.159 | 0.037 |

16. RR103617

| | Dayval | Phase | Vint | Vinterr |
|---|---|---|---|---|
| 1 | 1086.50037 | 0.840 | 18.282 | 0.105 |
| 2 | 1119.40942 | 0.381 | 18.103 | 0.107 |
| 3 | 1121.40405 | 0.202 | 17.895 | 0.102 |
| 4 | 1142.34570 | 0.818 | 18.325 | 0.122 |
| 5 | 1144.33960 | 0.638 | 18.239 | 0.127 |
| 6 | 1172.26343 | 0.129 | 17.851 | 0.094 |
| 7 | 1173.26074 | 0.539 | 18.107 | 0.132 |
| 8 | 1174.25806 | 0.950 | 17.894 | 0.106 |
| 9 | 1175.25525 | 0.360 | 18.156 | 0.153 |
| 10 | 1179.24402 | 0.001 | 17.502 | 0.113 |
| 11 | 1528.28845 | 0.633 | 18.129 | 0.136 |
| 12 | 1530.28345 | 0.454 | 18.120 | 0.126 |
| 13 | 1578.15332 | 0.153 | 17.780 | 0.107 |
| 14 | 3342.20093 | 0.935 | 18.052 | 0.066 |
| 15 | 3351.13062 | 0.564 | 18.326 | 0.041 |
| 16 | 3351.20728 | 0.672 | 18.216 | 0.038 |
| 17 | 3351.33057 | 0.847 | 18.430 | 0.036 |
| 18 | 3351.34839 | 0.872 | 18.360 | 0.040 |
| 19 | 3352.09473 | 0.927 | 17.873 | 0.054 |
| 20 | 3352.11255 | 0.952 | 17.765 | 0.088 |
| 21 | 3356.10938 | 0.605 | 18.307 | 0.044 |
| 22 | 3356.12744 | 0.631 | 18.279 | 0.042 |
| 23 | 3356.19385 | 0.724 | 18.217 | 0.045 |
| 24 | 3356.23877 | 0.788 | 18.351 | 0.044 |
| 25 | 3356.28687 | 0.856 | 18.444 | 0.047 |
| 26 | 3356.33301 | 0.921 | 18.009 | 0.032 |
| 27 | 3356.38599 | 0.996 | 17.564 | 0.029 |
| 28 | 3356.40381 | 0.021 | 17.590 | 0.030 |

| | | | |
|---|---|---|---|
| 29 3622.43628 | 0.254 | 17.916 | 0.035 |
| 30 3622.45093 | 0.275 | 18.029 | 0.035 |
| 31 3622.49731 | 0.341 | 18.029 | 0.037 |
| 32 3622.51196 | 0.361 | 18.113 | 0.036 |
| 33 3622.52612 | 0.381 | 18.191 | 0.038 |
| 34 3622.54028 | 0.401 | 18.176 | 0.060 |
| 35 3641.28809 | 0.915 | 18.237 | 0.072 |
| 36 3641.30249 | 0.936 | 17.960 | 0.054 |
| 37 3641.31665 | 0.956 | 17.807 | 0.044 |
| 38 3641.33081 | 0.976 | 17.726 | 0.045 |
| 39 3641.37109 | 0.032 | 17.578 | 0.040 |
| 40 3641.38525 | 0.053 | 17.704 | 0.043 |
| 41 3641.41968 | 0.101 | 17.738 | 0.039 |
| 42 3641.43408 | 0.122 | 17.913 | 0.036 |
| 43 3641.47070 | 0.173 | 17.871 | 0.042 |
| 44 3641.48486 | 0.194 | 17.951 | 0.045 |
| 45 3641.53833 | 0.269 | 17.988 | 0.047 |

17. RR105742

| Dayval | Phase | Vint | Vinterr |
|---|---|---|---|
| 1 1086.51526 | 0.944 | 16.622 | 0.030 |
| 2 1119.42432 | 0.387 | 16.701 | 0.035 |
| 3 1121.41895 | 0.474 | 16.649 | 0.034 |
| 4 1142.36060 | 0.391 | 16.742 | 0.036 |
| 5 1144.35449 | 0.477 | 16.823 | 0.041 |
| 6 1172.27832 | 0.704 | 16.971 | 0.049 |
| 7 1173.27563 | 0.748 | 16.982 | 0.047 |
| 8 1174.27295 | 0.792 | 16.928 | 0.049 |
| 9 1175.27014 | 0.835 | 16.956 | 0.056 |
| 10 1179.25903 | 0.010 | 16.501 | 0.046 |
| 11 1496.39124 | 0.939 | 16.514 | 0.037 |
| 12 1504.36938 | 0.289 | 16.722 | 0.042 |
| 13 1526.30896 | 0.251 | 16.677 | 0.044 |
| 14 1527.30579 | 0.294 | 16.689 | 0.043 |
| 15 1528.30334 | 0.339 | 16.773 | 0.039 |
| 16 1529.30103 | 0.384 | 16.797 | 0.048 |
| 17 1530.29846 | 0.428 | 16.888 | 0.045 |
| 18 1531.29517 | 0.470 | 16.908 | 0.050 |
| 19 1550.24329 | 0.302 | 16.762 | 0.043 |
| 20 1552.23828 | 0.391 | 16.847 | 0.051 |
| 21 1578.16821 | 0.533 | 16.999 | 0.048 |
| 22 1818.51245 | 0.095 | 16.481 | 0.046 |
| 23 1832.47351 | 0.706 | 16.943 | 0.062 |
| 24 1854.41150 | 0.663 | 17.041 | 0.057 |
| 25 1855.40930 | 0.709 | 16.924 | 0.048 |
| 26 1856.40601 | 0.751 | 16.815 | 0.046 |
| 27 1874.35681 | 0.539 | 16.958 | 0.069 |
| 28 1875.35413 | 0.583 | 16.971 | 0.067 |
| 29 1880.33923 | 0.798 | 16.638 | 0.040 |
| 30 1886.32324 | 0.062 | 16.517 | 0.046 |
| 31 1902.27991 | 0.764 | 16.729 | 0.052 |
| 32 1904.27441 | 0.852 | 16.499 | 0.038 |
| 33 1935.19043 | 0.211 | 16.669 | 0.047 |
| 34 1936.18774 | 0.255 | 16.791 | 0.050 |
| 35 1910.25745 | 0.112 | 16.646 | 0.042 |
| 36 2202.45923 | 0.950 | 16.564 | 0.052 |
| 37 2207.44531 | 0.168 | 16.618 | 0.052 |
| 38 2216.42017 | 0.561 | 17.005 | 0.074 |
| 39 2230.38208 | 0.175 | 16.650 | 0.056 |
| 40 2237.36206 | 0.479 | 16.932 | 0.079 |
| 41 2243.34546 | 0.740 | 16.898 | 0.068 |
| 42 2262.29419 | 0.575 | 16.972 | 0.083 |
| 43 2263.29102 | 0.617 | 16.921 | 0.090 |
| 44 2289.22070 | 0.758 | 16.753 | 0.081 |
| 45 2290.21802 | 0.802 | 16.687 | 0.071 |
| 46 2295.20459 | 0.021 | 16.541 | 0.058 |
| 47 2569.45435 | 0.067 | 16.467 | 0.584 |
| 48 3351.17480 | 0.980 | 16.566 | 0.016 |
| 49 3351.22803 | 0.143 | 16.501 | 0.014 |
| 50 3351.37451 | 0.590 | 17.016 | 0.018 |
| 51 3351.38892 | 0.634 | 16.997 | 0.018 |
| 52 3357.24829 | 0.517 | 17.018 | 0.055 |
| 53 3357.26245 | 0.560 | 17.019 | 0.045 |
| 54 3363.13086 | 0.471 | 16.924 | 0.017 |
| 55 3363.14502 | 0.515 | 16.991 | 0.018 |
| 56 3363.20093 | 0.686 | 17.023 | 0.020 |
| 57 3363.21533 | 0.729 | 16.975 | 0.019 |
| 58 3363.27100 | 0.899 | 16.579 | 0.014 |
| 59 3363.28516 | 0.943 | 16.526 | 0.014 |
| 60 3363.35498 | 0.156 | 16.559 | 0.015 |
| 61 3363.36938 | 0.199 | 16.613 | 0.015 |
| 62 3363.42456 | 0.368 | 16.796 | 0.017 |
| 63 3363.43872 | 0.411 | 16.841 | 0.017 |

18. RR114832

| Dayval | Phase | Vint | Vinterr |
|---|---|---|---|
| 1 1119.46143 | 0.426 | 15.436 | 0.017 |
| 2 1121.45605 | 0.762 | 15.675 | 0.018 |
| 3 1142.39673 | 0.791 | 15.677 | 0.019 |
| 4 1172.31335 | 0.834 | 15.675 | 0.022 |
| 5 1173.31067 | 0.502 | 15.557 | 0.019 |
| 6 1174.30798 | 0.170 | 14.987 | 0.013 |
| 7 1175.30505 | 0.838 | 15.699 | 0.027 |
| 8 1179.29370 | 0.510 | 15.558 | 0.024 |
| 9 1496.42761 | 0.993 | 15.127 | 0.016 |
| 10 1504.40576 | 0.338 | 15.318 | 0.017 |
| 11 1527.34106 | 0.703 | 15.661 | 0.022 |
| 12 1528.33875 | 0.372 | 15.373 | 0.018 |
| 13 1529.33630 | 0.041 | 14.638 | 0.012 |
| 14 1530.33374 | 0.709 | 15.684 | 0.023 |
| 15 1531.33044 | 0.376 | 15.381 | 0.018 |
| 16 1550.27771 | 0.070 | 14.694 | 0.012 |
| 17 1552.27271 | 0.407 | 15.423 | 0.022 |
| 18 1578.20166 | 0.780 | 15.668 | 0.020 |
| 19 1590.16919 | 0.798 | 15.652 | 0.024 |
| 20 1851.45654 | 0.864 | 15.750 | 0.027 |
| 21 1854.44849 | 0.869 | 15.746 | 0.027 |
| 22 1855.44617 | 0.538 | 15.584 | 0.022 |
| 23 1856.44287 | 0.205 | 15.062 | 0.015 |
| 24 1874.39294 | 0.231 | 15.129 | 0.020 |
| 25 1875.39026 | 0.900 | 15.798 | 0.028 |
| 26 1880.37512 | 0.238 | 15.119 | 0.016 |
| 27 1886.35840 | 0.246 | 15.175 | 0.019 |
| 28 1932.23230 | 0.981 | 15.121 | 0.024 |
| 29 1935.22412 | 0.986 | 15.087 | 0.016 |
| 30 1936.22131 | 0.654 | 15.629 | 0.025 |
| 31 1910.29199 | 0.281 | 15.238 | 0.018 |
| 32 2202.49634 | 0.064 | 14.690 | 0.019 |
| 33 2207.48218 | 0.404 | 15.458 | 0.027 |
| 34 2216.45703 | 0.416 | 15.449 | 0.029 |
| 35 2237.39795 | 0.445 | 15.501 | 0.030 |
| 36 2243.38135 | 0.453 | 15.495 | 0.031 |
| 37 2262.32935 | 0.149 | 14.977 | 0.020 |
| 38 2289.25464 | 0.188 | 15.055 | 0.024 |
| 39 2290.25146 | 0.855 | 15.732 | 0.040 |
| 40 2295.23828 | 0.197 | 15.075 | 0.023 |
| 41 2318.17603 | 0.565 | 15.619 | 0.027 |
| 42 2323.16260 | 0.907 | 15.790 | 0.029 |
| 43 2569.49170 | 0.952 | 15.654 | 0.390 |
| 44 3342.21509 | 0.518 | 15.495 | 0.018 |
| 45 3342.22241 | 0.530 | 15.561 | 0.019 |
| 46 3342.28027 | 0.627 | 15.571 | 0.016 |
| 47 3342.28760 | 0.639 | 15.606 | 0.015 |
| 48 3342.34302 | 0.732 | 15.582 | 0.017 |
| 49 3342.35010 | 0.744 | 15.580 | 0.016 |
| 50 3356.14600 | 0.821 | 15.686 | 0.016 |
| 51 3356.15405 | 0.834 | 15.674 | 0.016 |
| 52 3356.20679 | 0.923 | 15.525 | 0.016 |
| 53 3356.25342 | 0.001 | 14.557 | 0.012 |
| 54 3356.30151 | 0.081 | 14.738 | 0.013 |
| 55 3356.30908 | 0.094 | 14.792 | 0.013 |
| 56 3356.31665 | 0.107 | 14.825 | 0.012 |
| 57 3356.34741 | 0.158 | 14.985 | 0.012 |
| 58 3356.35498 | 0.171 | 15.000 | 0.013 |
| 59 3356.36255 | 0.183 | 15.035 | 0.013 |

19. GR Com

| Dayval | Phase | Vint | Vinterr |
|---|---|---|---|
| 1 1119.47278 | 0.198 | 16.203 | 0.027 |
| 2 1121.46729 | 0.020 | 15.851 | 0.022 |
| 3 1142.40796 | 0.150 | 16.140 | 0.026 |
| 4 1172.32458 | 0.481 | 16.628 | 0.041 |
| 5 1173.32190 | 0.392 | 16.473 | 0.037 |
| 6 1174.31921 | 0.303 | 16.349 | 0.033 |
| 7 1175.31628 | 0.214 | 16.220 | 0.033 |
| 8 1179.30493 | 0.858 | 16.615 | 0.043 |

| | | | |
|---|---|---|---|
| 9 1496.43884 | 0.600 | 16.650 | 0.054 |
| 10 1504.41699 | 0.889 | 16.688 | 0.039 |
| 11 1526.35486 | 0.930 | 16.314 | 0.032 |
| 12 1527.35229 | 0.842 | 16.762 | 0.049 |
| 13 1528.34998 | 0.753 | 16.658 | 0.049 |
| 14 1529.34753 | 0.665 | 16.678 | 0.041 |
| 15 1530.34497 | 0.577 | 16.656 | 0.042 |
| 16 1531.34167 | 0.487 | 16.655 | 0.042 |
| 17 1550.28894 | 0.796 | 16.748 | 0.045 |
| 18 1552.28394 | 0.619 | 16.701 | 0.048 |
| 19 1578.21289 | 0.309 | 16.414 | 0.034 |
| 20 1590.18042 | 0.243 | 16.303 | 0.037 |
| 21 1832.52112 | 0.654 | 16.652 | 0.051 |
| 22 1851.46777 | 0.963 | 16.025 | 0.031 |
| 23 1854.45972 | 0.697 | 16.695 | 0.044 |
| 24 1855.45740 | 0.609 | 16.624 | 0.043 |
| 25 1856.45410 | 0.519 | 16.632 | 0.036 |
| 26 1875.40149 | 0.829 | 16.769 | 0.059 |
| 27 1880.38635 | 0.381 | 16.488 | 0.040 |
| 28 1886.36963 | 0.848 | 16.616 | 0.050 |
| 29 1902.32617 | 0.426 | 16.552 | 0.077 |
| 30 1919.27832 | 0.912 | 16.453 | 0.082 |
| 31 1932.24353 | 0.758 | 16.757 | 0.065 |
| 32 1934.23755 | 0.580 | 16.657 | 0.056 |
| 33 1935.23535 | 0.492 | 16.674 | 0.047 |
| 34 1936.23254 | 0.403 | 16.607 | 0.044 |
| 35 1942.21594 | 0.869 | 16.690 | 0.150 |
| 36 1910.30322 | 0.713 | 16.666 | 0.050 |
| 37 2202.50757 | 0.681 | 16.741 | 0.074 |
| 38 2207.49341 | 0.236 | 16.242 | 0.047 |
| 39 2216.46826 | 0.435 | 16.568 | 0.056 |
| 40 2237.40918 | 0.565 | 16.756 | 0.068 |
| 41 2243.39258 | 0.032 | 15.966 | 0.038 |
| 42 2262.34058 | 0.343 | 16.457 | 0.055 |
| 43 2263.33667 | 0.252 | 16.306 | 0.054 |
| 44 2289.26587 | 0.941 | 16.084 | 0.047 |
| 45 2290.26270 | 0.852 | 16.820 | 0.087 |
| 46 2318.18726 | 0.365 | 16.414 | 0.048 |
| 47 2323.17383 | 0.921 | 16.169 | 0.038 |
| 48 2569.50293 | 0.976 | 16.005 | 0.498 |
| 49 3351.29761 | 0.175 | 16.062 | 0.018 |
| 50 3351.30908 | 0.197 | 16.105 | 0.018 |
| 51 3361.11035 | 0.980 | 15.852 | 0.018 |
| 52 3361.12109 | 0.000 | 15.614 | 0.016 |
| 53 3361.19629 | 0.144 | 15.982 | 0.018 |
| 54 3361.20703 | 0.165 | 16.029 | 0.018 |
| 55 3361.27588 | 0.297 | 16.307 | 0.020 |
| 56 3361.28662 | 0.317 | 16.346 | 0.021 |
| 57 3361.35840 | 0.455 | 16.535 | 0.023 |
| 58 3361.36914 | 0.475 | 16.562 | 0.023 |
| 59 3361.43872 | 0.609 | 16.674 | 0.024 |
| 60 3361.44946 | 0.630 | 16.682 | 0.024 |

20. RR120525

| Dayval | Phase | Vint | Vinterr |
|---|---|---|---|
| 1 1119.47327 | 0.918 | 16.097 | 0.026 |
| 2 1121.46777 | 0.839 | 16.129 | 0.025 |
| 3 1142.40845 | 0.004 | 15.013 | 0.014 |
| 4 1172.32507 | 0.814 | 16.082 | 0.030 |
| 5 1173.32239 | 0.774 | 16.020 | 0.028 |
| 6 1174.31970 | 0.735 | 16.070 | 0.027 |
| 7 1175.31677 | 0.695 | 16.111 | 0.035 |
| 8 1179.30542 | 0.535 | 16.054 | 0.033 |
| 9 1496.43933 | 0.953 | 15.456 | 0.022 |
| 10 1504.41760 | 0.637 | 16.078 | 0.030 |
| 11 1526.35547 | 0.762 | 16.072 | 0.029 |
| 12 1527.35291 | 0.723 | 16.078 | 0.030 |
| 13 1528.35046 | 0.684 | 16.046 | 0.032 |
| 14 1529.34814 | 0.645 | 16.080 | 0.029 |
| 15 1530.34546 | 0.606 | 16.105 | 0.031 |
| 16 1531.34216 | 0.565 | 16.083 | 0.030 |
| 17 1550.28943 | 0.811 | 16.122 | 0.030 |
| 18 1552.28442 | 0.733 | 16.074 | 0.033 |
| 19 1578.21338 | 0.704 | 16.080 | 0.027 |
| 20 1590.18091 | 0.229 | 15.646 | 0.024 |
| 21 1832.52161 | 0.620 | 16.085 | 0.033 |
| 22 1851.46826 | 0.865 | 16.187 | 0.037 |
| 23 1854.46021 | 0.746 | 16.092 | 0.031 |
| 24 1855.45789 | 0.708 | 16.080 | 0.031 |
| 25 1856.45459 | 0.667 | 16.092 | 0.027 |
| 26 1875.40210 | 0.913 | 16.058 | 0.036 |
| 27 1880.38684 | 0.712 | 16.091 | 0.030 |
| 28 1886.37012 | 0.474 | 16.019 | 0.034 |
| 29 1902.32666 | 0.841 | 16.104 | 0.051 |
| 30 1919.27893 | 0.166 | 15.551 | 0.038 |
| 31 1932.24402 | 0.653 | 16.070 | 0.039 |
| 32 1934.23804 | 0.573 | 16.103 | 0.037 |
| 33 1935.23584 | 0.534 | 16.067 | 0.034 |
| 34 1936.23315 | 0.494 | 16.024 | 0.034 |
| 35 1942.21643 | 0.256 | 15.775 | 0.085 |
| 36 1910.30383 | 0.523 | 16.076 | 0.033 |
| 37 2202.50806 | 0.934 | 15.868 | 0.043 |
| 38 2207.49414 | 0.736 | 16.117 | 0.044 |
| 39 2216.46875 | 0.378 | 15.874 | 0.036 |
| 40 2237.40991 | 0.544 | 16.104 | 0.043 |
| 41 2243.39307 | 0.306 | 15.779 | 0.035 |
| 42 2262.34106 | 0.554 | 16.070 | 0.049 |
| 43 2263.33716 | 0.512 | 16.078 | 0.046 |
| 44 2289.26636 | 0.483 | 16.057 | 0.051 |
| 45 2290.26318 | 0.442 | 15.954 | 0.050 |
| 46 2318.18774 | 0.336 | 15.826 | 0.032 |
| 47 2323.17432 | 0.138 | 15.465 | 0.022 |
| 48 3641.35059 | 0.393 | 15.839 | 0.019 |
| 49 3641.35913 | 0.410 | 15.849 | 0.019 |
| 50 3641.39990 | 0.490 | 16.001 | 0.018 |
| 51 3641.40869 | 0.507 | 16.001 | 0.018 |
| 52 3641.45093 | 0.590 | 16.026 | 0.017 |
| 53 3641.45972 | 0.607 | 16.045 | 0.017 |
| 54 3641.50879 | 0.704 | 16.099 | 0.019 |
| 55 3641.51758 | 0.721 | 16.075 | 0.019 |
| 56 3641.52710 | 0.740 | 16.064 | 0.018 |
| 57 3641.55444 | 0.794 | 15.991 | 0.021 |
| 58 3683.36133 | 0.977 | 15.025 | 0.010 |
| 59 3683.37012 | 0.994 | 14.966 | 0.015 |
| 60 3683.37866 | 0.011 | 15.028 | 0.012 |
| 61 3683.38721 | 0.028 | 15.061 | 0.015 |
| 62 3683.39600 | 0.045 | 15.124 | 0.027 |
| 63 3683.40454 | 0.062 | 15.152 | 0.070 |

21. GS Com

| Dayval | Phase | Vint | Vinterr |
|---|---|---|---|
| 1 1119.48645 | 0.821 | 16.900 | 0.042 |
| 2 1121.48096 | 0.589 | 16.757 | 0.038 |
| 3 1142.42163 | 0.141 | 16.189 | 0.029 |
| 4 1172.33826 | 0.646 | 16.789 | 0.045 |
| 5 1173.33557 | 0.529 | 16.700 | 0.044 |
| 6 1174.33289 | 0.413 | 16.625 | 0.040 |
| 7 1175.32996 | 0.296 | 16.461 | 0.038 |
| 8 1179.31860 | 0.830 | 16.846 | 0.053 |
| 9 1496.45251 | 0.818 | 16.852 | 0.053 |
| 10 1504.43066 | 0.887 | 16.801 | 0.046 |
| 11 1526.36853 | 0.323 | 16.527 | 0.044 |
| 12 1527.36597 | 0.207 | 16.308 | 0.036 |
| 13 1528.36365 | 0.091 | 16.082 | 0.029 |
| 14 1529.36121 | 0.975 | 15.989 | 0.027 |
| 15 1530.35864 | 0.859 | 16.911 | 0.047 |
| 16 1531.35461 | 0.740 | 16.772 | 0.049 |
| 17 1550.30237 | 0.528 | 16.765 | 0.048 |
| 18 1552.29761 | 0.296 | 16.518 | 0.044 |
| 19 1578.22656 | 0.270 | 16.420 | 0.035 |
| 20 1590.19409 | 0.873 | 16.819 | 0.065 |
| 21 1593.18579 | 0.524 | 16.795 | 0.091 |
| 22 1832.53479 | 0.596 | 16.754 | 0.066 |
| 23 1851.48145 | 0.381 | 16.585 | 0.051 |
| 24 1854.47339 | 0.033 | 15.801 | 0.024 |
| 25 1855.47107 | 0.917 | 16.790 | 0.048 |
| 26 1856.46777 | 0.799 | 16.742 | 0.045 |
| 27 1875.41516 | 0.587 | 16.836 | 0.065 |
| 28 1879.40259 | 0.118 | 16.144 | 0.045 |
| 29 1880.40002 | 0.002 | 15.759 | 0.025 |
| 30 1886.38330 | 0.303 | 16.459 | 0.049 |
| 31 1902.33984 | 0.441 | 16.699 | 0.068 |
| 32 1919.29199 | 0.459 | 16.773 | 0.087 |
| 33 1932.25720 | 0.947 | 16.207 | 0.047 |
| 34 1934.25122 | 0.713 | 16.820 | 0.063 |
| 35 1935.24902 | 0.598 | 16.759 | 0.055 |

| | | | | |
|---|---|---|---|---|
| 36 | 1936.24622 | 0.482 | 16.729 | 0.062 |
| 37 | 1942.22961 | 0.783 | 16.814 | 0.062 |
| 38 | 1910.31689 | 0.507 | 16.825 | 0.051 |
| 39 | 2202.52124 | 0.410 | 16.599 | 0.079 |
| 40 | 2207.50708 | 0.827 | 16.812 | 0.069 |
| 41 | 2216.48193 | 0.778 | 16.782 | 0.076 |
| 42 | 2237.42285 | 0.331 | 16.543 | 0.077 |
| 43 | 2243.40625 | 0.632 | 16.857 | 0.074 |
| 44 | 2262.35425 | 0.420 | 16.671 | 0.067 |
| 45 | 2263.35034 | 0.302 | 16.717 | 0.111 |
| 46 | 2289.27954 | 0.275 | 16.416 | 0.063 |
| 47 | 2290.27637 | 0.158 | 16.196 | 0.054 |
| 48 | 2295.26294 | 0.576 | 16.839 | 0.081 |
| 49 | 2318.20093 | 0.901 | 16.948 | 0.066 |
| 50 | 2323.18750 | 0.319 | 16.499 | 0.053 |
| 51 | 3361.13428 | 0.748 | 16.759 | 0.031 |
| 52 | 3361.14526 | 0.768 | 16.748 | 0.027 |
| 53 | 3361.21851 | 0.907 | 16.775 | 0.023 |
| 54 | 3361.22949 | 0.927 | 16.629 | 0.022 |
| 55 | 3361.29883 | 0.058 | 15.981 | 0.016 |
| 56 | 3361.30957 | 0.078 | 16.016 | 0.017 |
| 57 | 3361.38110 | 0.214 | 16.278 | 0.017 |
| 58 | 3361.39185 | 0.234 | 16.291 | 0.017 |
| 59 | 3361.46143 | 0.365 | 16.537 | 0.019 |
| 60 | 3361.47217 | 0.386 | 16.567 | 0.020 |

22. DV Com

| | Dayval | Phase | Vint | Vinterr |
|---|---|---|---|---|
| 1 | 1119.49963 | 0.856 | 15.229 | 0.015 |
| 2 | 1121.49414 | 0.544 | 15.116 | 0.013 |
| 3 | 1142.43494 | 0.263 | 14.794 | 0.011 |
| 4 | 1172.35144 | 0.578 | 15.115 | 0.015 |
| 5 | 1173.34875 | 0.422 | 15.019 | 0.012 |
| 6 | 1174.34607 | 0.266 | 14.789 | 0.011 |
| 7 | 1175.34314 | 0.110 | 14.504 | 0.009 |
| 8 | 1179.33179 | 0.485 | 15.068 | 0.015 |
| 9 | 1496.46570 | 0.861 | 15.244 | 0.016 |
| 10 | 1504.44397 | 0.612 | 15.140 | 0.014 |
| 11 | 1526.38184 | 0.175 | 14.652 | 0.011 |
| 12 | 1527.37927 | 0.019 | 14.250 | 0.009 |
| 13 | 1528.37683 | 0.864 | 15.237 | 0.015 |
| 14 | 1529.37451 | 0.709 | 15.126 | 0.015 |
| 15 | 1530.37183 | 0.553 | 15.104 | 0.016 |
| 16 | 1531.36780 | 0.394 | 15.006 | 0.014 |
| 17 | 1550.31555 | 0.428 | 15.026 | 0.015 |
| 18 | 1552.31079 | 0.118 | 14.510 | 0.011 |
| 19 | 1578.23975 | 0.060 | 14.348 | 0.009 |
| 20 | 1590.20728 | 0.188 | 14.649 | 0.013 |
| 21 | 1851.49463 | 0.304 | 14.842 | 0.014 |
| 22 | 1854.48657 | 0.836 | 15.242 | 0.018 |
| 23 | 1855.48425 | 0.681 | 15.134 | 0.014 |
| 24 | 1856.48096 | 0.524 | 15.118 | 0.014 |
| 25 | 1875.42847 | 0.557 | 15.117 | 0.020 |
| 26 | 1879.41589 | 0.930 | 14.763 | 0.014 |
| 27 | 1880.41321 | 0.774 | 15.108 | 0.016 |
| 28 | 1886.39661 | 0.837 | 15.206 | 0.020 |
| 29 | 1919.30518 | 0.685 | 15.119 | 0.025 |
| 30 | 1932.27039 | 0.657 | 15.125 | 0.024 |
| 31 | 1934.26453 | 0.344 | 14.931 | 0.015 |
| 32 | 1935.26221 | 0.189 | 14.662 | 0.013 |
| 33 | 1936.25952 | 0.033 | 14.271 | 0.010 |
| 34 | 1942.24280 | 0.096 | 14.473 | 0.012 |
| 35 | 1910.33020 | 0.090 | 14.456 | 0.010 |
| 36 | 2202.53442 | 0.372 | 14.943 | 0.022 |
| 37 | 2216.49512 | 0.185 | 14.640 | 0.017 |
| 38 | 2243.41943 | 0.968 | 14.395 | 0.014 |
| 39 | 2262.36743 | 0.002 | 14.225 | 0.013 |
| 40 | 2263.36353 | 0.844 | 15.107 | 0.028 |
| 41 | 2289.29224 | 0.786 | 15.165 | 0.024 |
| 42 | 2290.28955 | 0.630 | 15.123 | 0.025 |
| 43 | 2295.27612 | 0.850 | 15.236 | 0.026 |
| 44 | 2318.21411 | 0.262 | 14.797 | 0.016 |
| 45 | 2323.20068 | 0.482 | 15.062 | 0.019 |
| 46 | 3361.16040 | 0.655 | 15.067 | 0.014 |
| 47 | 3361.16772 | 0.669 | 15.088 | 0.013 |
| 48 | 3361.24121 | 0.804 | 15.153 | 0.011 |
| 49 | 3361.24854 | 0.818 | 15.149 | 0.011 |
| 50 | 3361.32349 | 0.956 | 14.382 | 0.008 |
| 51 | 3361.33081 | 0.970 | 14.237 | 0.008 |
| 52 | 3361.40381 | 0.105 | 14.446 | 0.009 |
| 53 | 3361.41113 | 0.118 | 14.470 | 0.009 |
| 54 | 3361.48389 | 0.253 | 14.735 | 0.009 |
| 55 | 3361.49097 | 0.266 | 14.740 | 0.009 |

23. RR131403

| | Dayval | Phase | Vint | Vinterr |
|---|---|---|---|---|
| 1 | 1119.52100 | 0.656 | 13.975 | 0.006 |
| 2 | 1121.51562 | 0.996 | 13.674 | 0.005 |
| 3 | 1142.45630 | 0.550 | 13.986 | 0.006 |
| 4 | 1172.37292 | 0.633 | 13.996 | 0.007 |
| 5 | 1173.37024 | 0.802 | 13.833 | 0.006 |
| 6 | 1174.36743 | 0.972 | 13.672 | 0.006 |
| 7 | 1175.36462 | 0.141 | 13.719 | 0.006 |
| 8 | 1179.35327 | 0.818 | 13.796 | 0.006 |
| 9 | 1212.26257 | 0.412 | 13.929 | 0.012 |
| 10 | 1496.48682 | 0.746 | 13.895 | 0.007 |
| 11 | 1504.46448 | 0.101 | 13.681 | 0.006 |
| 12 | 1526.40308 | 0.828 | 13.763 | 0.006 |
| 13 | 1527.40063 | 0.998 | 13.669 | 0.006 |
| 14 | 1528.39832 | 0.169 | 13.731 | 0.006 |
| 15 | 1529.39587 | 0.339 | 13.856 | 0.007 |
| 16 | 1530.39319 | 0.509 | 13.989 | 0.007 |
| 17 | 1531.38904 | 0.674 | 13.959 | 0.009 |
| 18 | 1550.33704 | 0.895 | 13.681 | 0.006 |
| 19 | 1552.33130 | 0.234 | 13.770 | 0.007 |
| 20 | 1578.26111 | 0.645 | 13.983 | 0.007 |
| 21 | 1593.22046 | 0.189 | 13.765 | 0.009 |
| 22 | 1851.51611 | 0.116 | 13.702 | 0.006 |
| 23 | 1854.50806 | 0.626 | 13.985 | 0.007 |
| 24 | 1856.50244 | 0.964 | 13.683 | 0.006 |
| 25 | 1879.43726 | 0.857 | 13.739 | 0.007 |
| 26 | 1880.43469 | 0.027 | 13.667 | 0.006 |
| 27 | 1886.41760 | 0.042 | 13.666 | 0.007 |
| 28 | 1919.32666 | 0.635 | 13.978 | 0.010 |
| 29 | 1932.29187 | 0.842 | 13.775 | 0.007 |
| 30 | 1934.28589 | 0.179 | 13.730 | 0.007 |
| 31 | 1935.28308 | 0.348 | 13.868 | 0.007 |
| 32 | 1936.28088 | 0.520 | 13.982 | 0.008 |
| 33 | 1942.26416 | 0.536 | 13.986 | 0.008 |
| 34 | 1910.35156 | 0.110 | 13.703 | 0.006 |
| 35 | 3361.17725 | 0.190 | 13.754 | 0.007 |
| 36 | 3361.18457 | 0.213 | 13.766 | 0.007 |
| 37 | 3361.25684 | 0.443 | 13.955 | 0.006 |
| 38 | 3361.26392 | 0.466 | 13.982 | 0.006 |
| 39 | 3361.33936 | 0.705 | 13.964 | 0.006 |
| 40 | 3361.34644 | 0.728 | 13.947 | 0.006 |
| 41 | 3361.41992 | 0.961 | 13.698 | 0.006 |
| 42 | 3361.42700 | 0.984 | 13.691 | 0.006 |
| 43 | 3361.49976 | 0.215 | 13.756 | 0.006 |
| 44 | 3361.50708 | 0.239 | 13.796 | 0.007 |

24. EZ Com

| | Dayval | Phase | Vint | Vinterr |
|---|---|---|---|---|
| 1 | 1119.52344 | 0.694 | 16.881 | 0.046 |
| 2 | 1121.51807 | 0.203 | 16.631 | 0.036 |
| 3 | 1142.45850 | 0.045 | 16.488 | 0.032 |
| 4 | 1172.37537 | 0.679 | 16.930 | 0.051 |
| 5 | 1173.37268 | 0.434 | 16.855 | 0.045 |
| 6 | 1174.36987 | 0.188 | 16.634 | 0.042 |
| 7 | 1175.36707 | 0.942 | 16.549 | 0.043 |
| 8 | 1179.35571 | 0.960 | 16.611 | 0.038 |
| 9 | 1212.26489 | 0.859 | 17.088 | 0.138 |
| 10 | 1496.48926 | 0.911 | 16.895 | 0.058 |
| 11 | 1504.46692 | 0.947 | 16.489 | 0.036 |
| 12 | 1526.40552 | 0.545 | 16.898 | 0.057 |
| 13 | 1527.40308 | 0.300 | 16.788 | 0.043 |
| 14 | 1528.40076 | 0.055 | 16.501 | 0.037 |
| 15 | 1529.39832 | 0.810 | 17.089 | 0.054 |
| 16 | 1530.39563 | 0.565 | 16.850 | 0.052 |
| 17 | 1531.39148 | 0.317 | 16.729 | 0.053 |
| 18 | 1550.33948 | 0.653 | 16.963 | 0.059 |
| 19 | 1552.33374 | 0.162 | 16.517 | 0.044 |
| 20 | 1578.26355 | 0.782 | 16.935 | 0.058 |
| 21 | 1590.23108 | 0.837 | 16.892 | 0.069 |
| 22 | 1593.22278 | 0.101 | 16.552 | 0.068 |
| 23 | 1613.16943 | 0.194 | 16.562 | 0.035 |

| | | | | |
|---|---|---|---|---|
| 24 | 1851.51843 | 0.535 | 17.048 | 0.070 |
| 25 | 1854.51050 | 0.799 | 17.016 | 0.057 |
| 26 | 1856.50488 | 0.308 | 16.844 | 0.047 |
| 27 | 1879.43970 | 0.659 | 16.937 | 0.061 |
| 28 | 1880.43701 | 0.413 | 16.845 | 0.054 |
| 29 | 1886.42004 | 0.939 | 16.435 | 0.043 |
| 30 | 1919.32910 | 0.838 | 16.720 | 0.067 |
| 31 | 1932.29419 | 0.649 | 17.020 | 0.068 |
| 32 | 1934.28833 | 0.157 | 16.625 | 0.054 |
| 33 | 1935.28552 | 0.911 | 16.512 | 0.044 |
| 34 | 1936.28333 | 0.667 | 16.975 | 0.058 |
| 35 | 1942.26660 | 0.194 | 16.687 | 0.052 |
| 36 | 1910.35400 | 0.048 | 16.512 | 0.038 |
| 37 | 2216.51904 | 0.702 | 16.834 | 0.078 |
| 38 | 2243.44336 | 0.072 | 16.484 | 0.058 |
| 39 | 2262.39136 | 0.408 | 16.933 | 0.080 |
| 40 | 2263.38721 | 0.160 | 16.741 | 0.071 |
| 41 | 2289.31592 | 0.778 | 16.882 | 0.082 |
| 42 | 2290.31348 | 0.533 | 16.984 | 0.087 |
| 43 | 2295.29980 | 0.306 | 16.796 | 0.071 |
| 44 | 2318.23804 | 0.662 | 16.979 | 0.066 |
| 45 | 2323.22437 | 0.435 | 16.858 | 0.077 |
| 46 | 3453.18506 | 0.441 | 16.925 | 0.019 |
| 47 | 3453.19946 | 0.466 | 16.939 | 0.018 |
| 48 | 3453.24146 | 0.540 | 16.999 | 0.020 |
| 49 | 3453.26245 | 0.577 | 16.994 | 0.020 |
| 50 | 3453.31104 | 0.662 | 16.967 | 0.023 |
| 51 | 3453.32520 | 0.687 | 16.932 | 0.028 |
| 52 | 3468.15088 | 0.771 | 16.893 | 0.019 |
| 53 | 3468.16504 | 0.796 | 16.900 | 0.019 |
| 54 | 3468.20898 | 0.873 | 16.835 | 0.019 |
| 55 | 3468.22339 | 0.899 | 16.792 | 0.020 |
| 56 | 3468.26587 | 0.973 | 16.545 | 0.023 |
| 57 | 3468.28003 | 0.998 | 16.525 | 0.022 |

25. RR132347

| | Dayval | Phase | Vint | Vinterr |
|---|---|---|---|---|
| 1 | 1119.52783 | 0.048 | 16.771 | 0.047 |
| 2 | 1121.52234 | 0.049 | 16.880 | 0.047 |
| 3 | 1142.46289 | 0.057 | 16.753 | 0.052 |
| 4 | 1496.49353 | 0.199 | 16.954 | 0.070 |
| 5 | 1504.47119 | 0.202 | 16.941 | 0.067 |
| 6 | 1526.40979 | 0.211 | 16.964 | 0.076 |
| 7 | 1527.40747 | 0.211 | 17.029 | 0.071 |
| 8 | 1528.40503 | 0.211 | 17.102 | 0.072 |
| 9 | 1529.40271 | 0.212 | 17.052 | 0.071 |
| 10 | 1530.40002 | 0.212 | 17.031 | 0.067 |
| 11 | 1531.39587 | 0.213 | 17.028 | 0.078 |
| 12 | 1550.34375 | 0.220 | 17.070 | 0.068 |
| 13 | 1552.33813 | 0.221 | 17.033 | 0.082 |
| 14 | 1578.26794 | 0.231 | 17.094 | 0.072 |
| 15 | 1593.22717 | 0.237 | 16.984 | 0.113 |
| 16 | 1614.17114 | 0.246 | 17.074 | 0.078 |
| 17 | 1851.52283 | 0.341 | 17.170 | 0.083 |
| 18 | 1854.51477 | 0.342 | 17.148 | 0.080 |
| 19 | 1856.50916 | 0.343 | 17.147 | 0.069 |
| 20 | 1879.44397 | 0.352 | 17.118 | 0.091 |
| 21 | 1880.44141 | 0.352 | 17.093 | 0.074 |
| 22 | 1886.42432 | 0.355 | 17.146 | 0.086 |
| 23 | 1919.33337 | 0.368 | 17.188 | 0.114 |
| 24 | 1932.29858 | 0.373 | 17.164 | 0.094 |
| 25 | 1934.29260 | 0.374 | 17.103 | 0.087 |
| 26 | 1935.28979 | 0.374 | 17.193 | 0.083 |
| 27 | 1942.27100 | 0.377 | 17.075 | 0.079 |
| 28 | 1910.35840 | 0.364 | 17.207 | 0.082 |
| 29 | 2216.52319 | 0.487 | 16.949 | 0.094 |
| 30 | 2243.44775 | 0.497 | 17.021 | 0.094 |
| 31 | 2262.39575 | 0.505 | 17.113 | 0.108 |
| 32 | 2289.32031 | 0.516 | 16.964 | 0.119 |
| 33 | 2290.31787 | 0.516 | 17.138 | 0.115 |
| 34 | 2295.30420 | 0.518 | 17.039 | 0.100 |
| 35 | 2318.24219 | 0.527 | 17.027 | 0.085 |
| 36 | 2323.22876 | 0.529 | 16.936 | 0.078 |
| 37 | 3453.15161 | 0.981 | 17.378 | 0.033 |
| 38 | 3453.16577 | 0.981 | 17.335 | 0.029 |
| 39 | 3453.21704 | 0.981 | 17.369 | 0.030 |
| 40 | 3453.23120 | 0.981 | 17.292 | 0.028 |
| 41 | 3453.27979 | 0.981 | 17.328 | 0.030 |
| 42 | 3453.29395 | 0.981 | 17.287 | 0.030 |
| 43 | 3454.14966 | 0.982 | 17.377 | 0.033 |
| 44 | 3454.16431 | 0.982 | 17.361 | 0.031 |
| 45 | 3454.22144 | 0.982 | 17.349 | 0.031 |
| 46 | 3454.29224 | 0.982 | 17.299 | 0.029 |
| 47 | 3454.30640 | 0.982 | 17.411 | 0.033 |

26. RR143313

| | Dayval | Phase | Vint | Vinterr |
|---|---|---|---|---|
| 1 | 1142.51270 | 0.972 | 17.640 | 0.075 |
| 2 | 1172.42871 | 0.346 | 18.064 | 0.112 |
| 3 | 1173.42590 | 0.625 | 18.205 | 0.116 |
| 4 | 1174.42322 | 0.904 | 17.828 | 0.108 |
| 5 | 1175.42029 | 0.183 | 17.858 | 0.093 |
| 6 | 1179.40881 | 0.299 | 18.024 | 0.111 |
| 7 | 1212.31702 | 0.511 | 18.200 | 0.202 |
| 8 | 1228.27344 | 0.980 | 17.669 | 0.088 |
| 9 | 1254.20361 | 0.244 | 17.783 | 0.104 |
| 10 | 1255.20093 | 0.524 | 18.191 | 0.564 |
| 11 | 1258.19287 | 0.362 | 18.232 | 0.219 |
| 12 | 1504.52100 | 0.351 | 18.085 | 0.123 |
| 13 | 1526.45886 | 0.491 | 18.335 | 0.145 |
| 14 | 1527.45667 | 0.771 | 18.103 | 0.122 |
| 15 | 1528.45435 | 0.051 | 17.776 | 0.083 |
| 16 | 1529.45190 | 0.331 | 18.018 | 0.112 |
| 17 | 1530.44922 | 0.611 | 18.261 | 0.113 |
| 18 | 1531.44507 | 0.887 | 17.796 | 0.100 |
| 19 | 1550.39233 | 0.191 | 18.043 | 0.133 |
| 20 | 1552.38660 | 0.749 | 18.199 | 0.131 |
| 21 | 1578.31567 | 0.011 | 17.738 | 0.092 |
| 22 | 1593.27429 | 0.199 | 17.904 | 0.151 |
| 23 | 1612.22314 | 0.507 | 18.278 | 0.116 |
| 24 | 1613.22058 | 0.787 | 18.121 | 0.107 |
| 25 | 1614.21790 | 0.066 | 17.718 | 0.109 |
| 26 | 1615.21521 | 0.346 | 18.161 | 0.124 |
| 27 | 1616.21252 | 0.625 | 18.241 | 0.155 |
| 28 | 1617.20984 | 0.904 | 17.663 | 0.434 |
| 29 | 1620.20166 | 0.742 | 18.162 | 0.139 |
| 30 | 1621.19910 | 0.022 | 17.695 | 0.112 |
| 31 | 1623.19373 | 0.581 | 18.307 | 0.216 |
| 32 | 1879.49316 | 0.360 | 18.045 | 0.135 |
| 33 | 1886.47375 | 0.314 | 18.100 | 0.127 |
| 34 | 1904.42297 | 0.338 | 18.053 | 0.141 |
| 35 | 1919.38184 | 0.527 | 18.164 | 0.147 |
| 36 | 1932.34668 | 0.158 | 17.980 | 0.295 |
| 37 | 1934.34058 | 0.715 | 18.186 | 0.134 |
| 38 | 1935.33777 | 0.994 | 17.683 | 0.103 |
| 39 | 1936.33484 | 0.273 | 17.977 | 0.114 |
| 40 | 1942.31873 | 0.949 | 17.684 | 0.092 |
| 41 | 1910.40710 | 0.014 | 17.844 | 0.094 |
| 42 | 2243.49731 | 0.301 | 18.012 | 0.164 |
| 43 | 2262.44482 | 0.606 | 18.179 | 0.201 |
| 44 | 2263.44067 | 0.882 | 17.700 | 0.315 |
| 45 | 2289.36841 | 0.141 | 18.180 | 0.174 |
| 46 | 2290.36572 | 0.420 | 18.188 | 0.199 |
| 47 | 2318.28979 | 0.241 | 18.041 | 0.156 |
| 48 | 2323.27588 | 0.637 | 17.952 | 0.141 |
| 49 | 2326.26758 | 0.474 | 18.178 | 0.147 |
| 50 | 3454.18286 | 0.355 | 18.262 | 0.035 |
| 51 | 3454.20068 | 0.395 | 18.232 | 0.038 |
| 52 | 3454.25366 | 0.516 | 18.298 | 0.035 |
| 53 | 3454.27148 | 0.557 | 18.211 | 0.034 |
| 54 | 3454.32324 | 0.675 | 18.211 | 0.037 |
| 55 | 3454.34106 | 0.716 | 18.241 | 0.038 |
| 56 | 3469.17651 | 0.623 | 18.069 | 0.061 |
| 57 | 3469.19458 | 0.664 | 18.153 | 0.048 |
| 58 | 3469.23901 | 0.766 | 18.243 | 0.068 |
| 59 | 3469.25684 | 0.807 | 18.119 | 0.093 |
| 60 | 3474.19043 | 0.082 | 17.827 | 0.027 |
| 61 | 3474.20825 | 0.123 | 17.917 | 0.027 |
| 62 | 3474.26758 | 0.258 | 18.049 | 0.028 |
| 63 | 3474.28516 | 0.299 | 18.005 | 0.034 |
| 64 | 3481.14404 | 0.975 | 17.866 | 0.095 |
| 65 | 3481.16211 | 0.016 | 17.631 | 0.059 |
| 66 | 3481.20776 | 0.120 | 17.809 | 0.029 |
| 67 | 3481.22534 | 0.161 | 17.873 | 0.028 |
| 68 | 3481.26855 | 0.260 | 17.960 | 0.031 |
| 69 | 3481.28638 | 0.300 | 17.903 | 0.035 |

27. RR145439

| | Dayval | Phase | Vint | Vinterr |
|---|---|---|---|---|
| 1 | 1142.52759 | 0.006 | 14.517 | 0.009 |
| 2 | 1172.44360 | 0.093 | 14.595 | 0.011 |
| 3 | 1173.44092 | 0.695 | 15.006 | 0.013 |
| 4 | 1174.43811 | 0.298 | 14.816 | 0.013 |
| 5 | 1175.43518 | 0.901 | 14.698 | 0.010 |
| 6 | 1179.42371 | 0.312 | 14.823 | 0.012 |
| 7 | 1205.35071 | 0.986 | 14.558 | 0.011 |
| 8 | 1212.33203 | 0.208 | 14.723 | 0.017 |
| 9 | 1228.28833 | 0.856 | 14.846 | 0.013 |
| 10 | 1254.21851 | 0.535 | 14.941 | 0.014 |
| 11 | 1255.21582 | 0.138 | 14.683 | 0.048 |
| 12 | 1257.21045 | 0.344 | 14.845 | 0.013 |
| 13 | 1258.20789 | 0.947 | 14.583 | 0.014 |
| 14 | 1526.47375 | 0.149 | 14.702 | 0.012 |
| 15 | 1527.47168 | 0.753 | 15.036 | 0.014 |
| 16 | 1528.46924 | 0.357 | 14.871 | 0.013 |
| 17 | 1529.46680 | 0.960 | 14.612 | 0.011 |
| 18 | 1530.46411 | 0.563 | 14.955 | 0.014 |
| 19 | 1531.45996 | 0.164 | 14.699 | 0.012 |
| 20 | 1550.40662 | 0.618 | 14.967 | 0.016 |
| 21 | 1552.40149 | 0.825 | 14.980 | 0.016 |
| 22 | 1578.33057 | 0.502 | 14.935 | 0.016 |
| 23 | 1593.28918 | 0.546 | 14.994 | 0.017 |
| 24 | 1612.23804 | 0.004 | 14.546 | 0.010 |
| 25 | 1613.23547 | 0.607 | 14.962 | 0.013 |
| 26 | 1614.23279 | 0.210 | 14.759 | 0.013 |
| 27 | 1615.22998 | 0.813 | 14.983 | 0.014 |
| 28 | 1616.22742 | 0.416 | 14.900 | 0.015 |
| 29 | 1620.21667 | 0.829 | 14.943 | 0.015 |
| 30 | 1621.21399 | 0.432 | 14.893 | 0.015 |
| 31 | 1623.20862 | 0.638 | 14.933 | 0.021 |
| 32 | 1879.50806 | 0.605 | 14.941 | 0.017 |
| 33 | 1886.48865 | 0.826 | 14.987 | 0.015 |
| 34 | 1919.39673 | 0.721 | 14.999 | 0.016 |
| 35 | 1932.36157 | 0.560 | 15.005 | 0.074 |
| 36 | 1934.35559 | 0.765 | 15.055 | 0.017 |
| 37 | 1935.35266 | 0.368 | 14.870 | 0.015 |
| 38 | 1936.34973 | 0.971 | 14.527 | 0.011 |
| 39 | 1942.33362 | 0.589 | 14.978 | 0.014 |
| 40 | 1910.42200 | 0.295 | 14.811 | 0.013 |
| 41 | 1997.18542 | 0.756 | 15.013 | 0.015 |
| 42 | 2243.51147 | 0.693 | 15.027 | 0.021 |
| 43 | 2262.45972 | 0.150 | 14.713 | 0.017 |
| 44 | 2263.45532 | 0.750 | 14.960 | 0.030 |
| 45 | 2289.38330 | 0.426 | 14.875 | 0.022 |
| 46 | 2290.38062 | 0.029 | 14.596 | 0.016 |
| 47 | 2295.36670 | 0.043 | 14.574 | 0.015 |
| 48 | 2318.30469 | 0.913 | 14.556 | 0.013 |
| 49 | 2323.29077 | 0.928 | 14.598 | 0.013 |
| 50 | 2326.28247 | 0.736 | 15.021 | 0.019 |
| 51 | 3093.14233 | 0.363 | 14.891 | 0.019 |
| 52 | 3093.15186 | 0.378 | 14.881 | 0.018 |
| 53 | 3097.15088 | 0.806 | 15.022 | 0.019 |
| 54 | 3097.16162 | 0.823 | 14.983 | 0.012 |
| 55 | 3109.18384 | 0.147 | 14.672 | 0.017 |
| 56 | 3109.19409 | 0.163 | 14.704 | 0.014 |
| 57 | 3109.20703 | 0.184 | 14.734 | 0.014 |
| 58 | 3109.22925 | 0.220 | 14.764 | 0.014 |
| 59 | 3109.24023 | 0.238 | 14.784 | 0.014 |
| 60 | 3109.25098 | 0.255 | 14.805 | 0.014 |
| 61 | 3109.27319 | 0.291 | 14.843 | 0.016 |
| 62 | 3109.28931 | 0.317 | 14.864 | 0.017 |
| 63 | 3109.29980 | 0.334 | 14.860 | 0.016 |
| 64 | 3112.19360 | 0.985 | 14.535 | 0.013 |
| 65 | 3112.20459 | 0.002 | 14.521 | 0.013 |
| 66 | 3385.22778 | 0.851 | 14.857 | 0.027 |
| 67 | 3385.23511 | 0.863 | 14.781 | 0.031 |

28. RR151628

| | Dayval | Phase | Vint | Vinterr |
|---|---|---|---|---|
| 1 | 1172.46069 | 0.630 | 17.920 | 0.132 |
| 2 | 1173.45789 | 0.374 | 17.883 | 0.098 |
| 3 | 1174.45508 | 0.117 | 17.689 | 0.095 |
| 4 | 1175.45215 | 0.861 | 18.131 | 0.122 |
| 5 | 1179.44055 | 0.835 | 18.151 | 0.123 |
| 6 | 1205.36658 | 0.168 | 17.847 | 0.101 |
| 7 | 1212.34753 | 0.374 | 17.834 | 0.139 |
| 8 | 1228.30322 | 0.274 | 17.919 | 0.099 |
| 9 | 1254.23230 | 0.612 | 17.918 | 0.137 |
| 10 | 1255.22961 | 0.356 | 17.832 | 0.529 |
| 11 | 1257.22424 | 0.844 | 18.139 | 0.137 |
| 12 | 1258.22156 | 0.588 | 18.047 | 0.159 |
| 13 | 1526.49109 | 0.672 | 18.074 | 0.122 |
| 14 | 1527.48889 | 0.417 | 18.022 | 0.125 |
| 15 | 1528.48645 | 0.162 | 17.729 | 0.102 |
| 16 | 1529.48242 | 0.903 | 17.968 | 0.100 |
| 17 | 1530.48132 | 0.650 | 18.148 | 0.109 |
| 18 | 1531.47717 | 0.391 | 18.014 | 0.121 |
| 19 | 1550.42322 | 0.519 | 17.836 | 0.151 |
| 20 | 1552.41760 | 0.007 | 17.520 | 0.095 |
| 21 | 1578.34607 | 0.344 | 18.005 | 0.148 |
| 22 | 1593.30408 | 0.499 | 18.129 | 0.175 |
| 23 | 1612.25208 | 0.631 | 18.041 | 0.110 |
| 24 | 1613.24951 | 0.375 | 17.952 | 0.101 |
| 25 | 1614.24683 | 0.118 | 17.633 | 0.102 |
| 26 | 1615.24390 | 0.862 | 17.937 | 0.143 |
| 27 | 1616.24133 | 0.606 | 17.964 | 0.122 |
| 28 | 1617.23865 | 0.350 | 17.728 | 0.241 |
| 29 | 1620.23022 | 0.581 | 17.937 | 0.134 |
| 30 | 1621.22778 | 0.325 | 17.871 | 0.130 |
| 31 | 1623.22229 | 0.813 | 17.991 | 0.192 |
| 32 | 1879.52563 | 0.974 | 17.683 | 0.097 |
| 33 | 1886.50610 | 0.179 | 17.748 | 0.103 |
| 34 | 1910.43872 | 0.027 | 17.673 | 0.085 |
| 35 | 1919.41321 | 0.719 | 18.116 | 0.133 |
| 36 | 1934.37134 | 0.875 | 17.940 | 0.132 |
| 37 | 1935.36853 | 0.618 | 18.104 | 0.140 |
| 38 | 1936.36548 | 0.361 | 17.914 | 0.136 |
| 39 | 1942.34912 | 0.824 | 18.235 | 0.141 |
| 40 | 1997.19873 | 0.732 | 18.211 | 0.130 |
| 41 | 2263.47241 | 0.326 | 17.976 | 0.265 |
| 42 | 2290.39648 | 0.405 | 18.149 | 0.200 |
| 43 | 2295.38257 | 0.123 | 17.551 | 0.138 |
| 44 | 2318.31958 | 0.230 | 17.907 | 0.134 |
| 45 | 2323.30566 | 0.948 | 17.657 | 0.116 |
| 46 | 2326.29688 | 0.179 | 17.611 | 0.117 |
| 47 | 3685.38184 | 0.617 | 18.097 | 0.040 |
| 48 | 3685.39624 | 0.642 | 18.132 | 0.043 |
| 49 | 3685.41040 | 0.667 | 18.240 | 0.044 |
| 50 | 3685.44971 | 0.736 | 18.055 | 0.038 |
| 51 | 3685.46411 | 0.761 | 18.076 | 0.040 |
| 52 | 3685.51807 | 0.855 | 18.207 | 0.037 |
| 53 | 3685.53247 | 0.880 | 17.945 | 0.037 |

29. RR162318

| | Dayval | Phase | Vint | Vinterr |
|---|---|---|---|---|
| 1 | 1173.50452 | 0.797 | 15.151 | 0.013 |
| 2 | 1174.49976 | 0.693 | 15.138 | 0.014 |
| 3 | 1175.49878 | 0.600 | 15.242 | 0.015 |
| 4 | 1179.48718 | 0.205 | 15.157 | 0.014 |
| 5 | 1205.41321 | 0.644 | 15.154 | 0.015 |
| 6 | 1212.39417 | 0.957 | 15.333 | 0.015 |
| 7 | 1228.34973 | 0.384 | 15.262 | 0.017 |
| 8 | 1237.32471 | 0.499 | 15.322 | 0.017 |
| 9 | 1254.27881 | 0.832 | 15.205 | 0.015 |
| 10 | 1255.27576 | 0.733 | 15.133 | 0.062 |
| 11 | 1257.27051 | 0.537 | 15.339 | 0.019 |
| 12 | 1258.26794 | 0.440 | 15.359 | 0.017 |
| 13 | 1263.25427 | 0.949 | 15.361 | 0.019 |
| 14 | 3685.42676 | 0.930 | 15.295 | 0.018 |
| 15 | 3685.43555 | 0.955 | 15.346 | 0.018 |
| 16 | 3685.49536 | 0.129 | 15.216 | 0.018 |
| 17 | 3685.50415 | 0.154 | 15.175 | 0.018 |

30. RR165009

| | Dayval | Phase | Vint | Vinterr |
|---|---|---|---|---|
| 1 | 1205.43384 | 0.899 | 15.614 | 0.020 |
| 2 | 1228.36951 | 0.078 | 14.979 | 0.014 |
| 3 | 1237.34399 | 0.800 | 15.760 | 0.021 |
| 4 | 1254.29736 | 0.499 | 15.649 | 0.022 |
| 5 | 1255.29419 | 0.246 | 15.367 | 0.079 |
| 6 | 1257.28894 | 0.740 | 15.693 | 0.025 |
| 7 | 1258.28589 | 0.486 | 15.613 | 0.023 |
| 8 | 1263.27246 | 0.222 | 15.305 | 0.020 |

| | | | | |
|---|---|---|---|---|
| 9 | 1550.49097 | 0.381 | 15.537 | 0.026 |
| 10 | 1552.48511 | 0.874 | 15.603 | 0.025 |
| 11 | 1578.41187 | 0.293 | 15.376 | 0.025 |
| 12 | 1593.36987 | 0.497 | 15.645 | 0.023 |
| 13 | 1612.31750 | 0.690 | 15.687 | 0.021 |
| 14 | 1613.31482 | 0.437 | 15.573 | 0.019 |
| 15 | 1614.31165 | 0.184 | 15.221 | 0.017 |
| 16 | 1615.30908 | 0.931 | 15.257 | 0.018 |
| 17 | 1616.30652 | 0.678 | 15.689 | 0.024 |
| 18 | 1620.29492 | 0.665 | 15.667 | 0.023 |
| 19 | 1621.29272 | 0.413 | 15.561 | 0.024 |
| 20 | 1623.28711 | 0.907 | 15.221 | 0.025 |
| 21 | 1919.48010 | 0.788 | 15.718 | 0.022 |
| 22 | 1935.43567 | 0.739 | 15.697 | 0.025 |
| 23 | 1936.43262 | 0.486 | 15.608 | 0.022 |
| 24 | 1942.41602 | 0.967 | 14.927 | 0.016 |
| 25 | 1997.26306 | 0.050 | 14.925 | 0.013 |
| 26 | 2295.44946 | 0.423 | 15.606 | 0.028 |
| 27 | 2323.37183 | 0.338 | 15.408 | 0.022 |
| 28 | 2326.36304 | 0.578 | 15.639 | 0.027 |
| 29 | 3112.21753 | 0.263 | 15.221 | 0.026 |
| 30 | 3112.22974 | 0.284 | 15.321 | 0.013 |
| 31 | 3112.24292 | 0.307 | 15.350 | 0.011 |
| 32 | 3112.36768 | 0.526 | 15.606 | 0.013 |
| 33 | 3112.37866 | 0.545 | 15.603 | 0.014 |
| 34 | 3113.16455 | 0.922 | 15.382 | 0.014 |
| 35 | 3113.17529 | 0.941 | 15.197 | 0.012 |
| 36 | 3113.21851 | 0.017 | 14.765 | 0.009 |
| 37 | 3113.22925 | 0.035 | 14.821 | 0.009 |
| 38 | 3113.26660 | 0.101 | 14.976 | 0.010 |
| 39 | 3113.27734 | 0.120 | 15.016 | 0.010 |
| 40 | 3113.31470 | 0.185 | 15.148 | 0.010 |
| 41 | 3113.31934 | 0.193 | 15.194 | 0.011 |
| 42 | 3113.36401 | 0.272 | 15.292 | 0.011 |
| 43 | 3113.37500 | 0.291 | 15.327 | 0.012 |
| 44 | 3097.17529 | 0.912 | 15.146 | 0.036 |
| 45 | 3385.25513 | 0.579 | 15.677 | 0.034 |
| 46 | 3385.26270 | 0.592 | 15.698 | 0.030 |
| 47 | 3385.34668 | 0.740 | 15.565 | 0.031 |
| 48 | 3385.35425 | 0.753 | 15.629 | 0.025 |

31. RR165831

| | Dayval | Phase | Vint | Vinterr |
|---|---|---|---|---|
| 1 | 1205.43970 | 0.560 | 15.115 | 0.015 |
| 2 | 1552.49097 | 0.157 | 14.875 | 0.016 |
| 3 | 1578.41760 | 0.227 | 14.977 | 0.021 |
| 4 | 1593.37573 | 0.077 | 14.772 | 0.013 |
| 5 | 1612.32324 | 0.555 | 15.129 | 0.014 |
| 6 | 1613.32068 | 0.213 | 14.967 | 0.013 |
| 7 | 1614.31738 | 0.868 | 14.689 | 0.012 |
| 8 | 1615.31494 | 0.525 | 15.131 | 0.018 |
| 9 | 1616.31226 | 0.183 | 14.945 | 0.015 |
| 10 | 1617.30957 | 0.840 | 14.735 | 0.044 |
| 11 | 1620.30078 | 0.808 | 14.691 | 0.013 |
| 12 | 1621.29846 | 0.467 | 15.133 | 0.017 |
| 13 | 1623.29297 | 0.780 | 14.720 | 0.015 |
| 14 | 1919.48596 | 0.886 | 14.676 | 0.012 |
| 15 | 1936.43848 | 0.049 | 14.707 | 0.013 |
| 16 | 1942.42188 | 0.989 | 14.636 | 0.012 |
| 17 | 1997.26892 | 0.107 | 14.761 | 0.012 |
| 18 | 2295.45532 | 0.522 | 15.152 | 0.023 |
| 19 | 2323.37769 | 0.910 | 14.705 | 0.015 |
| 20 | 2326.36890 | 0.879 | 14.711 | 0.016 |
| 21 | 3685.48096 | 0.587 | 15.080 | 0.010 |
| 22 | 3685.48828 | 0.614 | 15.053 | 0.010 |
| 23 | 3685.54736 | 0.831 | 14.714 | 0.010 |
| 24 | 3685.55469 | 0.858 | 14.725 | 0.011 |
| 25 | 3685.56201 | 0.885 | 14.686 | 0.018 |

32. V375 Her

| | Dayval | Phase | Vint | Vinterr |
|---|---|---|---|---|
| 1 | 1205.44995 | 0.740 | 16.501 | 0.037 |
| 2 | 1228.38562 | 0.898 | 16.384 | 0.035 |
| 3 | 1237.36011 | 0.786 | 16.546 | 0.039 |
| 4 | 1254.31287 | 0.686 | 16.538 | 0.038 |
| 5 | 1255.31030 | 0.563 | 16.492 | 0.191 |
| 6 | 1257.30469 | 0.316 | 16.314 | 0.037 |
| 7 | 1258.30200 | 0.192 | 16.045 | 0.031 |
| 8 | 1263.28833 | 0.575 | 16.557 | 0.043 |
| 9 | 1269.27173 | 0.834 | 16.624 | 0.054 |
| 10 | 1578.42786 | 0.575 | 16.498 | 0.057 |
| 11 | 1593.38599 | 0.721 | 16.517 | 0.043 |
| 12 | 1612.33350 | 0.375 | 16.361 | 0.032 |
| 13 | 1613.33081 | 0.252 | 16.190 | 0.027 |
| 14 | 1614.32764 | 0.128 | 15.946 | 0.027 |
| 15 | 1615.32520 | 0.005 | 15.594 | 0.024 |
| 16 | 1616.32251 | 0.881 | 16.534 | 0.044 |
| 17 | 1617.31982 | 0.758 | 16.462 | 0.106 |
| 18 | 1620.31104 | 0.386 | 16.343 | 0.035 |
| 19 | 1621.30872 | 0.264 | 16.212 | 0.037 |
| 20 | 1623.30310 | 0.017 | 15.607 | 0.026 |
| 21 | 1935.45068 | 0.386 | 16.391 | 0.038 |
| 22 | 1936.44788 | 0.263 | 16.207 | 0.038 |
| 23 | 1942.43213 | 0.523 | 16.513 | 0.039 |
| 24 | 1997.27905 | 0.729 | 16.525 | 0.036 |
| 25 | 2305.43726 | 0.592 | 16.465 | 0.054 |
| 26 | 2323.38672 | 0.368 | 16.271 | 0.046 |
| 27 | 2326.37866 | 0.997 | 15.540 | 0.024 |
| 28 | 3097.19580 | 0.447 | 16.444 | 0.021 |
| 29 | 3097.20605 | 0.467 | 16.347 | 0.033 |
| 30 | 3126.14429 | 0.920 | 16.054 | 0.019 |
| 31 | 3126.15503 | 0.940 | 15.777 | 0.018 |
| 32 | 3126.36157 | 0.329 | 16.305 | 0.028 |
| 33 | 3129.15210 | 0.580 | 16.524 | 0.022 |
| 34 | 3129.16284 | 0.600 | 16.506 | 0.026 |
| 35 | 3129.23804 | 0.742 | 16.506 | 0.027 |
| 36 | 3129.24902 | 0.762 | 16.524 | 0.032 |
| 37 | 3129.30981 | 0.877 | 16.613 | 0.049 |
| 38 | 3129.32056 | 0.897 | 16.401 | 0.039 |
| 39 | 3385.28467 | 0.546 | 16.357 | 0.059 |
| 40 | 3385.29565 | 0.566 | 16.568 | 0.042 |
| 41 | 3385.38062 | 0.726 | 16.531 | 0.026 |
| 42 | 3385.39160 | 0.747 | 16.516 | 0.021 |
| 43 | 3481.17505 | 0.983 | 15.649 | 0.054 |
| 44 | 3481.18604 | 0.004 | 15.565 | 0.016 |
| 45 | 3481.23657 | 0.099 | 15.857 | 0.015 |
| 46 | 3481.24731 | 0.119 | 15.908 | 0.015 |

33. RR171524

| | Dayval | Phase | Vint | Vinterr |
|---|---|---|---|---|
| 1 | 1205.45142 | 0.407 | 17.985 | 0.120 |
| 2 | 1228.38708 | 0.835 | 18.299 | 0.143 |
| 3 | 1237.36157 | 0.219 | 17.834 | 0.094 |
| 4 | 1254.31445 | 0.057 | 17.310 | 0.069 |
| 5 | 1255.31177 | 0.989 | 17.582 | 0.374 |
| 6 | 1257.30615 | 0.852 | 18.136 | 0.155 |
| 7 | 1258.30347 | 0.784 | 18.130 | 0.142 |
| 8 | 1263.28979 | 0.443 | 18.243 | 0.133 |
| 9 | 1269.27332 | 0.033 | 17.284 | 0.081 |
| 10 | 1578.42944 | 0.883 | 18.461 | 0.230 |
| 11 | 1593.38757 | 0.857 | 18.396 | 0.158 |
| 12 | 1612.33508 | 0.559 | 18.369 | 0.129 |
| 13 | 1613.33240 | 0.491 | 18.219 | 0.119 |
| 14 | 1614.32922 | 0.422 | 18.083 | 0.133 |
| 15 | 1615.32666 | 0.354 | 17.971 | 0.126 |
| 16 | 1616.32410 | 0.286 | 17.912 | 0.119 |
| 17 | 1617.32129 | 0.218 | 17.651 | 0.221 |
| 18 | 1620.31250 | 0.012 | 17.305 | 0.077 |
| 19 | 1621.31030 | 0.945 | 18.532 | 0.189 |
| 20 | 1623.30469 | 0.808 | 18.291 | 0.157 |
| 21 | 1935.45227 | 0.452 | 18.626 | 0.222 |
| 22 | 1936.44946 | 0.384 | 18.090 | 0.136 |
| 23 | 1942.43359 | 0.976 | 17.861 | 0.092 |
| 24 | 1997.28064 | 0.217 | 17.790 | 0.091 |
| 25 | 2295.46704 | 0.817 | 18.246 | 0.240 |
| 26 | 2305.43872 | 0.133 | 17.709 | 0.125 |
| 27 | 2323.38843 | 0.902 | 18.446 | 0.209 |
| 28 | 3126.17261 | 0.932 | 18.415 | 0.094 |
| 29 | 3126.18359 | 0.954 | 18.448 | 0.237 |
| 30 | 3126.37524 | 0.325 | 18.185 | 0.088 |
| 31 | 3129.19385 | 0.785 | 18.340 | 0.045 |
| 32 | 3129.26782 | 0.928 | 18.207 | 0.089 |
| 33 | 3129.33789 | 0.064 | 17.427 | 0.057 |
| 34 | 3453.34180 | 0.674 | 18.272 | 0.034 |
| 35 | 3453.35986 | 0.709 | 18.331 | 0.036 |
| 36 | 3453.38062 | 0.749 | 18.251 | 0.040 |

| | | | | |
|---|---|---|---|---|
| 37 | 3453.39844 | 0.784 | 18.296 | 0.039 |
| 38 | 3453.41626 | 0.819 | 18.463 | 0.043 |
| 39 | 3453.43408 | 0.853 | 18.301 | 0.045 |
| 40 | 3474.14722 | 0.975 | 17.345 | 0.023 |
| 41 | 3474.16528 | 0.010 | 17.328 | 0.022 |
| 42 | 3474.22485 | 0.125 | 17.619 | 0.027 |
| 43 | 3474.24268 | 0.160 | 17.717 | 0.027 |
| 44 | 3474.31982 | 0.309 | 18.000 | 0.030 |
| 45 | 3474.33740 | 0.344 | 18.049 | 0.034 |
| 46 | 3474.39746 | 0.460 | 18.210 | 0.036 |
| 47 | 3474.41504 | 0.494 | 18.304 | 0.041 |

34. V385 Her

| | Dayval | Phase | Vint | Vinterr |
|---|---|---|---|---|
| 1 | 1578.43030 | 0.014 | 14.674 | 0.015 |
| 2 | 1593.38831 | 0.336 | 15.175 | 0.017 |
| 3 | 1612.33569 | 0.211 | 15.019 | 0.013 |
| 4 | 1613.33301 | 0.099 | 14.895 | 0.012 |
| 5 | 1614.32983 | 0.987 | 14.749 | 0.013 |
| 6 | 1615.32727 | 0.875 | 14.948 | 0.016 |
| 7 | 1616.32471 | 0.764 | 15.351 | 0.021 |
| 8 | 1623.30518 | 0.981 | 14.766 | 0.014 |
| 9 | 1935.45325 | 0.008 | 14.791 | 0.016 |
| 10 | 1936.45044 | 0.896 | 14.801 | 0.015 |
| 11 | 1942.43457 | 0.227 | 15.008 | 0.016 |
| 12 | 1997.28101 | 0.074 | 14.787 | 0.013 |
| 13 | 2295.46802 | 0.667 | 15.312 | 0.028 |
| 14 | 2305.43970 | 0.548 | 15.415 | 0.026 |
| 15 | 2323.38916 | 0.534 | 15.351 | 0.024 |
| 16 | 3097.22217 | 0.724 | 15.421 | 0.017 |
| 17 | 3099.38257 | 0.814 | 15.178 | 0.014 |
| 18 | 3099.39380 | 0.836 | 15.061 | 0.013 |
| 19 | 3099.42529 | 0.895 | 14.900 | 0.015 |
| 20 | 3126.38818 | 0.948 | 14.807 | 0.015 |
| 21 | 3128.13574 | 0.256 | 15.102 | 0.013 |
| 22 | 3128.14795 | 0.279 | 15.123 | 0.012 |
| 23 | 3128.15918 | 0.301 | 15.160 | 0.013 |
| 24 | 3128.22778 | 0.430 | 15.247 | 0.012 |
| 25 | 3128.23853 | 0.451 | 15.243 | 0.012 |
| 26 | 3128.30933 | 0.585 | 15.316 | 0.013 |
| 27 | 3128.32007 | 0.605 | 15.330 | 0.013 |
| 28 | 3385.30786 | 0.191 | 15.025 | 0.019 |
| 29 | 3385.31519 | 0.205 | 15.013 | 0.019 |
| 30 | 3385.40283 | 0.371 | 15.221 | 0.028 |
| 31 | 3385.41040 | 0.385 | 15.286 | 0.034 |

35. RR171907

| | Dayval | Phase | Vint | Vinterr |
|---|---|---|---|---|
| 1 | 1578.43250 | 0.705 | 17.853 | 0.171 |
| 2 | 1593.39050 | 0.356 | 17.845 | 0.117 |
| 3 | 1612.33789 | 0.449 | 17.876 | 0.104 |
| 4 | 1613.33521 | 0.559 | 17.819 | 0.106 |
| 5 | 1614.33203 | 0.668 | 17.839 | 0.121 |
| 6 | 1615.32947 | 0.779 | 17.927 | 0.136 |
| 7 | 1616.32690 | 0.889 | 17.987 | 0.134 |
| 8 | 1620.31531 | 0.329 | 17.830 | 0.125 |
| 9 | 1621.31299 | 0.440 | 17.720 | 0.144 |
| 10 | 1623.30737 | 0.660 | 17.826 | 0.123 |
| 11 | 1935.45544 | 0.165 | 17.404 | 0.106 |
| 12 | 1936.45264 | 0.275 | 17.564 | 0.106 |
| 13 | 1942.43677 | 0.938 | 17.337 | 0.087 |
| 14 | 1997.28320 | 0.993 | 17.260 | 0.084 |
| 15 | 2295.47021 | 0.956 | 17.219 | 0.113 |
| 16 | 2305.44189 | 0.056 | 17.236 | 0.110 |
| 17 | 2323.39136 | 0.037 | 17.266 | 0.097 |

36. RR172059

| | Dayval | Phase | Vint | Vinterr |
|---|---|---|---|---|
| 1 | 1205.45532 | 0.862 | 14.713 | 0.012 |
| 2 | 1228.39099 | 0.503 | 14.901 | 0.013 |
| 3 | 1237.36548 | 0.884 | 14.679 | 0.011 |
| 4 | 1254.31836 | 0.272 | 14.774 | 0.013 |
| 5 | 1255.31567 | 0.649 | 14.888 | 0.055 |
| 6 | 1257.31006 | 0.400 | 14.886 | 0.014 |
| 7 | 1258.30737 | 0.776 | 14.760 | 0.012 |
| 8 | 1269.27722 | 0.911 | 14.689 | 0.014 |
| 9 | 1578.43335 | 0.461 | 14.885 | 0.018 |
| 10 | 1593.39136 | 0.097 | 14.681 | 0.012 |
| 11 | 1612.33887 | 0.238 | 14.761 | 0.011 |
| 12 | 1613.33630 | 0.614 | 14.901 | 0.012 |
| 13 | 1614.33313 | 0.988 | 14.675 | 0.012 |
| 14 | 1615.33057 | 0.365 | 14.841 | 0.014 |
| 15 | 1616.32800 | 0.741 | 14.826 | 0.013 |
| 16 | 1620.31641 | 0.243 | 14.670 | 0.012 |
| 17 | 1621.31409 | 0.620 | 14.804 | 0.015 |
| 18 | 1623.30859 | 0.372 | 14.841 | 0.014 |
| 19 | 1935.45605 | 0.048 | 14.659 | 0.014 |
| 20 | 1936.45325 | 0.424 | 14.870 | 0.015 |
| 21 | 1942.43750 | 0.682 | 14.886 | 0.014 |
| 22 | 1997.28455 | 0.349 | 14.846 | 0.012 |
| 23 | 2295.47095 | 0.764 | 14.833 | 0.019 |
| 24 | 2305.44263 | 0.520 | 14.911 | 0.017 |
| 25 | 2323.39233 | 0.283 | 14.783 | 0.016 |
| 26 | 2326.38379 | 0.410 | 14.864 | 0.016 |
| 27 | 3454.35938 | 0.814 | 14.698 | 0.010 |
| 28 | 3454.37402 | 0.864 | 14.657 | 0.010 |
| 29 | 3454.39746 | 0.943 | 14.638 | 0.009 |
| 30 | 3454.41211 | 0.992 | 14.623 | 0.009 |
| 31 | 3454.43457 | 0.068 | 14.636 | 0.009 |
| 32 | 3454.44995 | 0.120 | 14.600 | 0.014 |
| 33 | 3469.14136 | 0.853 | 14.691 | 0.036 |
| 34 | 3469.15649 | 0.905 | 14.683 | 0.015 |
| 35 | 3469.20630 | 0.074 | 14.673 | 0.015 |
| 36 | 3469.22998 | 0.154 | 14.660 | 0.016 |
| 37 | 3469.26880 | 0.285 | 14.857 | 0.021 |
| 38 | 3469.28369 | 0.335 | 14.765 | 0.021 |
| 39 | 3469.32520 | 0.476 | 14.924 | 0.024 |
| 40 | 3469.34009 | 0.526 | 14.941 | 0.042 |
| 41 | 3473.25293 | 0.772 | 14.701 | 0.021 |
| 42 | 3473.26807 | 0.823 | 14.722 | 0.010 |
| 43 | 3540.12109 | 0.133 | 14.657 | 0.011 |
| 44 | 3540.12622 | 0.151 | 14.670 | 0.011 |
| 45 | 3540.13159 | 0.169 | 14.665 | 0.011 |
| 46 | 3540.13867 | 0.193 | 14.672 | 0.011 |
| 47 | 3540.14404 | 0.210 | 14.699 | 0.011 |
| 48 | 3540.14917 | 0.228 | 14.747 | 0.011 |
| 49 | 3540.15430 | 0.245 | 14.729 | 0.011 |
| 50 | 3540.15942 | 0.263 | 14.733 | 0.011 |
| 51 | 3540.16455 | 0.280 | 14.742 | 0.011 |

37. RR173043

| | Dayval | Phase | Vint | Vinterr |
|---|---|---|---|---|
| 1 | 1205.46216 | 0.837 | 15.774 | 0.025 |
| 2 | 1228.39783 | 0.976 | 15.286 | 0.018 |
| 3 | 1237.37231 | 0.720 | 15.896 | 0.025 |
| 4 | 1254.32520 | 0.699 | 15.886 | 0.026 |
| 5 | 1255.32251 | 0.230 | 15.727 | 0.098 |
| 6 | 1257.31689 | 0.284 | 15.798 | 0.027 |
| 7 | 1258.31421 | 0.814 | 15.630 | 0.022 |
| 8 | 1263.30042 | 0.458 | 15.860 | 0.026 |
| 9 | 1269.28394 | 0.630 | 15.879 | 0.029 |
| 10 | 1292.22168 | 0.804 | 15.807 | 0.028 |
| 11 | 1578.43970 | 0.643 | 15.903 | 0.039 |
| 12 | 1593.39819 | 0.568 | 15.880 | 0.027 |
| 13 | 1612.34570 | 0.608 | 15.907 | 0.023 |
| 14 | 1613.34302 | 0.138 | 15.607 | 0.020 |
| 15 | 1614.33984 | 0.659 | 15.885 | 0.026 |
| 16 | 1615.33740 | 0.192 | 15.694 | 0.023 |
| 17 | 1616.33472 | 0.723 | 15.848 | 0.027 |
| 18 | 1617.33203 | 0.252 | 15.643 | 0.032 |
| 19 | 1620.32324 | 0.828 | 15.763 | 0.024 |
| 20 | 1621.32092 | 0.365 | 15.789 | 0.033 |
| 21 | 1623.31531 | 0.421 | 15.868 | 0.027 |
| 22 | 1935.46289 | 0.022 | 15.299 | 0.021 |
| 23 | 1936.46008 | 0.549 | 15.898 | 0.032 |
| 24 | 1942.44434 | 0.734 | 15.899 | 0.027 |
| 25 | 1980.33728 | 0.777 | 15.773 | 0.036 |
| 26 | 1997.29126 | 0.777 | 15.839 | 0.023 |
| 27 | 2295.47754 | 0.982 | 15.577 | 0.030 |
| 28 | 2305.44946 | 0.256 | 15.705 | 0.030 |
| 29 | 2323.39893 | 0.755 | 15.877 | 0.032 |
| 30 | 2326.39062 | 0.338 | 15.807 | 0.031 |
| 31 | 3097.23804 | 0.483 | 15.841 | 0.017 |
| 32 | 3099.28662 | 0.490 | 15.803 | 0.019 |
| 33 | 3099.31250 | 0.944 | 15.486 | 0.012 |
| 34 | 3099.32520 | 0.170 | 15.605 | 0.014 |

| | | | | |
|---|---|---|---|---|
| 35 | 3099.33936 | 0.416 | 15.814 | 0.013 |
| 36 | 3099.41113 | 0.679 | 15.833 | 0.015 |
| 37 | 3112.25635 | 0.460 | 15.867 | 0.016 |
| 38 | 3112.26733 | 0.652 | 15.847 | 0.027 |
| 39 | 3112.35498 | 0.193 | 15.588 | 0.016 |
| 40 | 3112.39185 | 0.839 | 15.616 | 0.013 |
| 41 | 3112.40234 | 0.026 | 15.330 | 0.013 |
| 42 | 3112.41357 | 0.220 | 15.675 | 0.014 |
| 43 | 3112.42432 | 0.411 | 15.812 | 0.016 |
| 44 | 3130.33960 | 0.309 | 15.698 | 0.028 |
| 45 | 3130.34351 | 0.376 | 15.815 | 0.028 |
| 46 | 3130.34717 | 0.442 | 15.795 | 0.035 |
| 47 | 3130.35107 | 0.509 | 15.792 | 0.034 |
| 48 | 3130.35498 | 0.576 | 15.918 | 0.034 |
| 49 | 3130.35913 | 0.651 | 15.878 | 0.031 |
| 50 | 3130.36328 | 0.725 | 15.847 | 0.036 |
| 51 | 3130.36768 | 0.802 | 15.823 | 0.035 |
| 52 | 3130.37207 | 0.876 | 15.633 | 0.035 |
| 53 | 3130.37646 | 0.954 | 15.472 | 0.031 |
| 54 | 3385.42041 | 0.851 | 15.790 | 0.027 |
| 55 | 3385.42456 | 0.921 | 15.624 | 0.028 |
| 56 | 3385.42847 | 0.989 | 15.332 | 0.021 |
| 57 | 3385.43213 | 0.056 | 15.282 | 0.025 |

38. RR174152

| | Dayval | Phase | Vint | Vinterr |
|---|---|---|---|---|
| 1 | 1205.46985 | 0.205 | 15.661 | 0.022 |
| 2 | 1228.40552 | 0.659 | 16.093 | 0.029 |
| 3 | 1237.38000 | 0.488 | 16.053 | 0.029 |
| 4 | 1254.33276 | 0.389 | 15.934 | 0.028 |
| 5 | 1255.33020 | 0.148 | 15.545 | 0.101 |
| 6 | 1257.32458 | 0.665 | 16.082 | 0.035 |
| 7 | 1258.32190 | 0.424 | 15.992 | 0.030 |
| 8 | 1263.30823 | 0.219 | 15.670 | 0.025 |
| 9 | 1269.29175 | 0.773 | 16.102 | 0.030 |
| 10 | 1292.22937 | 0.230 | 15.692 | 0.027 |
| 11 | 1578.44739 | 0.054 | 15.290 | 0.024 |
| 12 | 1593.40588 | 0.437 | 15.977 | 0.030 |
| 13 | 1612.35352 | 0.856 | 16.229 | 0.030 |
| 14 | 1613.35083 | 0.615 | 16.112 | 0.028 |
| 15 | 1614.34766 | 0.373 | 15.897 | 0.030 |
| 16 | 1615.34509 | 0.133 | 15.511 | 0.022 |
| 17 | 1616.34253 | 0.892 | 16.178 | 0.034 |
| 18 | 1617.33972 | 0.651 | 16.074 | 0.039 |
| 19 | 1620.33093 | 0.927 | 15.812 | 0.027 |
| 20 | 1621.32861 | 0.686 | 16.070 | 0.033 |
| 21 | 1623.32312 | 0.204 | 15.669 | 0.023 |
| 22 | 1935.47070 | 0.762 | 16.064 | 0.039 |
| 23 | 1936.46777 | 0.521 | 16.074 | 0.037 |
| 24 | 1942.45203 | 0.076 | 15.372 | 0.020 |
| 25 | 1980.34509 | 0.910 | 16.076 | 0.040 |
| 26 | 1997.29907 | 0.813 | 16.180 | 0.030 |
| 27 | 2035.19604 | 0.655 | 16.099 | 0.038 |
| 28 | 2305.45728 | 0.335 | 15.867 | 0.036 |
| 29 | 2323.40674 | 0.994 | 15.195 | 0.020 |
| 30 | 2326.39844 | 0.270 | 15.764 | 0.034 |
| 31 | 3097.27417 | 0.921 | 15.795 | 0.015 |
| 32 | 3113.19458 | 0.001 | 15.180 | 0.011 |
| 33 | 3113.20532 | 0.020 | 15.226 | 0.011 |
| 34 | 3113.24243 | 0.085 | 15.420 | 0.011 |
| 35 | 3113.25317 | 0.104 | 15.447 | 0.013 |
| 36 | 3113.29053 | 0.170 | 15.612 | 0.012 |
| 37 | 3113.30151 | 0.190 | 15.627 | 0.018 |
| 38 | 3113.33960 | 0.257 | 15.754 | 0.013 |
| 39 | 3113.35059 | 0.276 | 15.801 | 0.013 |
| 40 | 3113.38818 | 0.342 | 15.880 | 0.015 |
| 41 | 3113.39917 | 0.362 | 15.828 | 0.031 |
| 42 | 3385.44385 | 0.187 | 15.602 | 0.015 |
| 43 | 3385.45483 | 0.207 | 15.644 | 0.036 |

39. RR174240

| | Dayval | Phase | Vint | Vinterr |
|---|---|---|---|---|
| 1 | 1205.47046 | 0.060 | 16.226 | 0.033 |
| 2 | 1228.40613 | 0.635 | 16.883 | 0.054 |
| 3 | 1237.38062 | 0.685 | 16.896 | 0.048 |
| 4 | 1254.33337 | 0.893 | 16.974 | 0.056 |
| 5 | 1255.33081 | 0.788 | 17.018 | 0.244 |
| 6 | 1257.32520 | 0.577 | 16.881 | 0.062 |
| 7 | 1258.32251 | 0.472 | 16.816 | 0.050 |
| 8 | 1263.30872 | 0.945 | 16.629 | 0.050 |
| 9 | 1269.29236 | 0.313 | 16.639 | 0.047 |
| 10 | 1292.22998 | 0.891 | 16.634 | 0.051 |
| 11 | 1578.44800 | 0.666 | 16.941 | 0.081 |
| 12 | 1593.40649 | 0.085 | 16.244 | 0.032 |
| 13 | 1612.35400 | 0.083 | 16.302 | 0.029 |
| 14 | 1613.35132 | 0.977 | 16.218 | 0.029 |
| 15 | 1614.34814 | 0.871 | 16.757 | 0.052 |
| 16 | 1615.34570 | 0.766 | 16.884 | 0.062 |
| 17 | 1616.34302 | 0.661 | 16.879 | 0.056 |
| 18 | 1617.34033 | 0.556 | 16.894 | 0.065 |
| 19 | 1620.33154 | 0.239 | 16.592 | 0.051 |
| 20 | 1621.32922 | 0.134 | 16.489 | 0.053 |
| 21 | 1623.32361 | 0.923 | 16.502 | 0.046 |
| 22 | 1935.47119 | 0.961 | 16.348 | 0.046 |
| 23 | 1936.46838 | 0.855 | 16.962 | 0.067 |
| 24 | 1942.45264 | 0.224 | 16.541 | 0.041 |
| 25 | 1980.34558 | 0.216 | 16.582 | 0.061 |
| 26 | 1997.29968 | 0.426 | 16.824 | 0.046 |
| 27 | 2035.19666 | 0.425 | 16.773 | 0.067 |
| 28 | 2305.45776 | 0.884 | 16.791 | 0.063 |
| 29 | 2323.40747 | 0.986 | 16.086 | 0.038 |
| 30 | 2326.39893 | 0.669 | 16.931 | 0.073 |
| 31 | 3129.21362 | 0.907 | 16.493 | 0.024 |
| 32 | 3129.22461 | 0.928 | 16.461 | 0.026 |
| 33 | 3129.28589 | 0.044 | 16.292 | 0.024 |
| 34 | 3129.29663 | 0.064 | 16.376 | 0.033 |
| 35 | 3129.36060 | 0.186 | 16.556 | 0.032 |
| 36 | 3129.37158 | 0.207 | 16.539 | 0.025 |
| 37 | 3175.11230 | 0.108 | 16.323 | 0.016 |
| 38 | 3175.12329 | 0.129 | 16.340 | 0.017 |
| 39 | 3175.16992 | 0.217 | 16.482 | 0.021 |
| 40 | 3175.18115 | 0.239 | 16.546 | 0.019 |
| 41 | 3181.09253 | 0.469 | 16.891 | 0.024 |
| 42 | 3181.10327 | 0.490 | 16.842 | 0.023 |
| 43 | 3181.11401 | 0.510 | 16.833 | 0.025 |
| 44 | 3181.12476 | 0.531 | 16.800 | 0.021 |
| 45 | 3181.20288 | 0.679 | 16.871 | 0.026 |
| 46 | 3181.21558 | 0.703 | 16.933 | 0.024 |
| 47 | 3181.22656 | 0.724 | 16.930 | 0.028 |
| 48 | 3181.23730 | 0.744 | 16.868 | 0.026 |
| 49 | 3186.08960 | 0.963 | 16.278 | 0.017 |
| 50 | 3186.10059 | 0.984 | 16.229 | 0.016 |
| 51 | 3186.11133 | 0.005 | 16.226 | 0.015 |
| 52 | 3186.12231 | 0.025 | 16.200 | 0.017 |
| 53 | 3186.13354 | 0.047 | 16.254 | 0.017 |
| 54 | 3186.14453 | 0.067 | 16.284 | 0.015 |
| 55 | 3186.15527 | 0.088 | 16.316 | 0.018 |
| 56 | 3186.18091 | 0.136 | 16.408 | 0.019 |
| 57 | 3186.19214 | 0.158 | 16.434 | 0.020 |
| 58 | 3186.20288 | 0.178 | 16.485 | 0.020 |
| 59 | 3186.21362 | 0.199 | 16.532 | 0.027 |
| 60 | 3186.22437 | 0.219 | 16.559 | 0.030 |
| 61 | 3186.23535 | 0.240 | 16.502 | 0.022 |
| 62 | 3385.47046 | 0.759 | 16.854 | 0.057 |
| 63 | 3385.48486 | 0.787 | 16.888 | 0.027 |

40. RR174420

| | Dayval | Phase | Vint | Vinterr |
|---|---|---|---|---|
| 1 | 1205.47156 | 0.488 | 15.842 | 0.025 |
| 2 | 1228.40723 | 0.315 | 15.715 | 0.022 |
| 3 | 1237.38171 | 0.115 | 15.529 | 0.022 |
| 4 | 1254.33459 | 0.075 | 15.519 | 0.022 |
| 5 | 1255.33191 | 0.720 | 15.726 | 0.097 |
| 6 | 1257.32629 | 0.009 | 15.538 | 0.023 |
| 7 | 1258.32361 | 0.654 | 15.819 | 0.025 |
| 8 | 1263.30994 | 0.878 | 15.584 | 0.022 |
| 9 | 1269.29346 | 0.746 | 15.666 | 0.024 |
| 10 | 1292.23108 | 0.578 | 15.869 | 0.028 |
| 11 | 1578.44910 | 0.638 | 15.799 | 0.036 |
| 12 | 1593.40771 | 0.308 | 15.729 | 0.024 |
| 13 | 1612.35522 | 0.558 | 15.860 | 0.023 |
| 14 | 1613.35254 | 0.203 | 15.615 | 0.021 |
| 15 | 1614.34937 | 0.846 | 15.602 | 0.021 |
| 16 | 1615.34680 | 0.492 | 15.837 | 0.027 |
| 17 | 1616.34424 | 0.137 | 15.574 | 0.022 |
| 18 | 1617.34143 | 0.782 | 15.649 | 0.026 |

| | | | | |
|---|---|---|---|---|
| 19 | 1620.33264 | 0.714 | 15.727 | 0.025 |
| 20 | 1621.33044 | 0.360 | 15.742 | 0.027 |
| 21 | 1623.32483 | 0.650 | 15.800 | 0.025 |
| 22 | 1935.47241 | 0.476 | 15.599 | 0.024 |
| 23 | 1936.46960 | 0.120 | 15.692 | 0.026 |
| 24 | 1942.45374 | 0.991 | 15.820 | 0.026 |
| 25 | 1980.34680 | 0.484 | 15.569 | 0.028 |
| 26 | 1997.30078 | 0.447 | 15.573 | 0.021 |
| 27 | 2035.19775 | 0.951 | 15.816 | 0.029 |
| 28 | 2305.45898 | 0.693 | 15.609 | 0.030 |
| 29 | 2323.40845 | 0.296 | 15.846 | 0.031 |
| 30 | 2326.40015 | 0.229 | 15.794 | 0.030 |
| 31 | 3464.37500 | 0.178 | 15.546 | 0.021 |
| 32 | 3464.38257 | 0.198 | 15.562 | 0.021 |
| 33 | 3468.17700 | 0.261 | 15.642 | 0.015 |
| 34 | 3468.18799 | 0.290 | 15.662 | 0.016 |
| 35 | 3468.23340 | 0.411 | 15.776 | 0.016 |
| 36 | 3468.24414 | 0.440 | 15.814 | 0.016 |
| 37 | 3468.28833 | 0.556 | 15.836 | 0.017 |
| 38 | 3468.29907 | 0.585 | 15.861 | 0.016 |
| 39 | 3468.34814 | 0.715 | 15.710 | 0.022 |
| 40 | 3468.35913 | 0.744 | 15.663 | 0.024 |
| 41 | 3468.42163 | 0.910 | 15.522 | 0.017 |
| 42 | 3468.43237 | 0.939 | 15.543 | 0.016 |
| 43 | 3487.28369 | 0.933 | 15.530 | 0.016 |
| 44 | 3487.29517 | 0.963 | 15.499 | 0.016 |
| 45 | 3487.30566 | 0.991 | 15.465 | 0.016 |
| 46 | 3487.31641 | 0.020 | 15.542 | 0.017 |

41. RR175017

| | Dayval | Phase | Vint | Vinterr |
|---|---|---|---|---|
| 1 | 1228.41284 | 0.666 | 13.204 | 0.005 |
| 2 | 1237.38721 | 0.579 | 13.282 | 0.005 |
| 3 | 1254.33948 | 0.970 | 13.362 | 0.006 |
| 4 | 1255.33679 | 0.406 | 13.267 | 0.018 |
| 5 | 1257.33118 | 0.275 | 13.174 | 0.005 |
| 6 | 1258.32837 | 0.710 | 13.176 | 0.005 |
| 7 | 1263.31458 | 0.884 | 13.248 | 0.005 |
| 8 | 1292.23474 | 0.496 | 13.352 | 0.006 |
| 9 | 1593.41333 | 0.846 | 13.210 | 0.005 |
| 10 | 1612.36023 | 0.108 | 13.261 | 0.005 |
| 11 | 1613.35754 | 0.543 | 13.339 | 0.005 |
| 12 | 1614.35437 | 0.977 | 13.378 | 0.005 |
| 13 | 1615.35181 | 0.413 | 13.277 | 0.005 |
| 14 | 1616.34924 | 0.848 | 13.212 | 0.005 |
| 15 | 1617.34644 | 0.283 | 13.075 | 0.008 |
| 16 | 1620.33752 | 0.586 | 13.276 | 0.005 |
| 17 | 1621.33521 | 0.022 | 13.376 | 0.005 |
| 18 | 1623.32959 | 0.891 | 13.262 | 0.005 |
| 19 | 1942.45972 | 0.072 | 13.321 | 0.005 |
| 20 | 1980.35181 | 0.592 | 13.267 | 0.006 |
| 21 | 1997.30518 | 0.986 | 13.378 | 0.006 |
| 22 | 2035.20093 | 0.512 | 13.363 | 0.006 |
| 23 | 2305.46484 | 0.381 | 13.217 | 0.006 |
| 24 | 2323.41406 | 0.207 | 13.151 | 0.006 |
| 25 | 2326.40552 | 0.512 | 13.324 | 0.006 |
| 26 | 3463.32422 | 0.366 | 13.222 | 0.009 |
| 27 | 3463.33667 | 0.384 | 13.242 | 0.009 |
| 28 | 3463.38770 | 0.457 | 13.345 | 0.009 |
| 29 | 3463.40039 | 0.475 | 13.354 | 0.009 |
| 30 | 3464.39209 | 0.902 | 13.263 | 0.009 |
| 31 | 3464.40430 | 0.920 | 13.291 | 0.009 |
| 32 | 3473.30249 | 0.723 | 13.176 | 0.010 |
| 33 | 3473.31299 | 0.738 | 13.163 | 0.010 |
| 34 | 3473.43896 | 0.919 | 13.297 | 0.011 |
| 35 | 3473.44971 | 0.935 | 13.312 | 0.011 |
| 36 | 3546.08276 | 0.443 | 13.304 | 0.012 |
| 37 | 3546.08594 | 0.447 | 13.312 | 0.011 |
| 38 | 3546.11694 | 0.492 | 13.352 | 0.011 |
| 39 | 3546.11328 | 0.487 | 13.331 | 0.011 |
| 40 | 3546.11987 | 0.496 | 13.320 | 0.011 |
| 41 | 3546.12305 | 0.501 | 13.325 | 0.011 |
| 42 | 3546.12598 | 0.505 | 13.320 | 0.011 |
| 43 | 3546.12915 | 0.510 | 13.340 | 0.011 |
| 44 | 3546.13232 | 0.514 | 13.356 | 0.011 |
| 45 | 3546.14990 | 0.540 | 13.342 | 0.011 |

42. RR181101

| | Dayval | Phase | Vint | Vinterr |
|---|---|---|---|---|
| 1 | 1228.42737 | 0.697 | 17.475 | 0.066 |
| 2 | 1237.40161 | 0.456 | 17.306 | 0.065 |
| 3 | 1254.35388 | 0.781 | 17.292 | 0.083 |
| 4 | 1255.35132 | 0.977 | 16.639 | 0.190 |
| 5 | 1257.34558 | 0.368 | 17.123 | 0.074 |
| 6 | 1258.34290 | 0.563 | 17.391 | 0.068 |
| 7 | 1263.32874 | 0.541 | 17.369 | 0.080 |
| 8 | 1269.31213 | 0.715 | 17.349 | 0.072 |
| 9 | 1292.24915 | 0.217 | 16.822 | 0.051 |
| 10 | 1317.18164 | 0.112 | 16.516 | 0.055 |
| 11 | 1593.42773 | 0.337 | 17.259 | 0.066 |
| 12 | 1612.37476 | 0.053 | 16.552 | 0.038 |
| 13 | 1613.37207 | 0.249 | 17.106 | 0.057 |
| 14 | 1614.36877 | 0.444 | 17.367 | 0.077 |
| 15 | 1615.36621 | 0.640 | 17.431 | 0.082 |
| 16 | 1617.36084 | 0.032 | 16.853 | 0.171 |
| 17 | 1620.35193 | 0.617 | 17.449 | 0.084 |
| 18 | 1621.34875 | 0.812 | 17.420 | 0.086 |
| 19 | 1623.34399 | 0.205 | 17.056 | 0.065 |
| 20 | 1980.36621 | 0.279 | 17.252 | 0.071 |
| 21 | 1997.31958 | 0.606 | 17.507 | 0.068 |
| 22 | 2035.21533 | 0.043 | 16.683 | 0.055 |
| 23 | 2036.21265 | 0.239 | 17.253 | 0.083 |
| 24 | 2057.15625 | 0.352 | 17.195 | 0.105 |
| 25 | 2323.42847 | 0.617 | 17.487 | 0.098 |
| 26 | 2326.41992 | 0.203 | 17.070 | 0.074 |
| 27 | 3128.17358 | 0.465 | 17.384 | 0.032 |
| 28 | 3128.18555 | 0.491 | 17.429 | 0.033 |
| 29 | 3128.25659 | 0.648 | 17.419 | 0.023 |
| 30 | 3128.33984 | 0.831 | 17.228 | 0.019 |
| 31 | 3128.41333 | 0.993 | 16.365 | 0.030 |
| 32 | 3169.12036 | 0.619 | 17.425 | 0.032 |
| 33 | 3169.13452 | 0.651 | 17.425 | 0.027 |
| 34 | 3169.20850 | 0.813 | 17.492 | 0.025 |
| 35 | 3169.22290 | 0.845 | 17.305 | 0.025 |
| 36 | 3169.29614 | 0.007 | 16.367 | 0.024 |
| 37 | 3180.09839 | 0.790 | 17.463 | 0.029 |
| 38 | 3180.11279 | 0.822 | 17.386 | 0.026 |
| 39 | 3180.19482 | 0.003 | 16.358 | 0.017 |
| 40 | 3180.20923 | 0.034 | 16.508 | 0.018 |
| 41 | 3180.25708 | 0.139 | 16.803 | 0.022 |
| 42 | 3180.27051 | 0.169 | 16.892 | 0.023 |
| 43 | 3187.10742 | 0.222 | 17.036 | 0.022 |
| 44 | 3187.12207 | 0.255 | 17.130 | 0.020 |
| 45 | 3187.13672 | 0.287 | 17.196 | 0.022 |
| 46 | 3187.15161 | 0.320 | 17.178 | 0.025 |
| 47 | 3187.16650 | 0.353 | 17.225 | 0.025 |
| 48 | 3187.18091 | 0.384 | 17.280 | 0.024 |
| 49 | 3187.19580 | 0.417 | 17.326 | 0.028 |
| 50 | 3187.21021 | 0.449 | 17.335 | 0.030 |
| 51 | 3187.22437 | 0.480 | 17.419 | 0.029 |
| 52 | 3187.23853 | 0.511 | 17.429 | 0.025 |
| 53 | 3187.25269 | 0.542 | 17.406 | 0.026 |

43. V532 Her

| | Dayval | Phase | Vint | Vinterr |
|---|---|---|---|---|
| 1 | 1228.42761 | 0.852 | 16.000 | 0.027 |
| 2 | 1237.40186 | 0.426 | 15.735 | 0.023 |
| 3 | 1254.35413 | 0.734 | 15.872 | 0.029 |
| 4 | 1255.35156 | 0.576 | 15.814 | 0.103 |
| 5 | 1257.34583 | 0.259 | 15.559 | 0.023 |
| 6 | 1258.34314 | 0.101 | 15.252 | 0.016 |
| 7 | 1263.32898 | 0.309 | 15.598 | 0.023 |
| 8 | 1269.31250 | 0.360 | 15.665 | 0.023 |
| 9 | 1292.24951 | 0.720 | 15.856 | 0.025 |
| 10 | 1317.18188 | 0.767 | 15.861 | 0.036 |
| 11 | 1593.42798 | 0.948 | 15.312 | 0.017 |
| 12 | 1612.37500 | 0.940 | 15.345 | 0.016 |
| 13 | 1613.37231 | 0.782 | 15.944 | 0.025 |
| 14 | 1614.36914 | 0.623 | 15.835 | 0.025 |
| 15 | 1617.36108 | 0.149 | 15.421 | 0.052 |
| 16 | 1620.35229 | 0.673 | 15.843 | 0.026 |
| 17 | 1621.34912 | 0.514 | 15.795 | 0.032 |
| 18 | 1623.34424 | 0.199 | 15.453 | 0.021 |
| 19 | 1980.36646 | 0.561 | 15.805 | 0.032 |

| | | | | |
|---|---|---|---|---|
| 20 | 1997.31995 | 0.871 | 15.914 | 0.027 |
| 21 | 2035.21570 | 0.859 | 15.976 | 0.032 |
| 22 | 2036.21289 | 0.700 | 15.851 | 0.031 |
| 23 | 2057.15674 | 0.380 | 15.647 | 0.038 |
| 24 | 2323.42871 | 0.142 | 15.360 | 0.023 |
| 25 | 2326.42017 | 0.666 | 15.885 | 0.031 |
| 26 | 3128.20020 | 0.424 | 15.730 | 0.018 |
| 27 | 3128.21191 | 0.446 | 15.747 | 0.018 |
| 28 | 3128.27515 | 0.563 | 15.800 | 0.018 |
| 29 | 3128.29443 | 0.598 | 15.814 | 0.019 |
| 30 | 3128.35864 | 0.717 | 15.845 | 0.019 |
| 31 | 3128.36963 | 0.737 | 15.873 | 0.019 |
| 32 | 3128.42603 | 0.841 | 15.940 | 0.020 |
| 33 | 3097.28540 | 0.329 | 15.693 | 0.020 |
| 34 | 3169.15405 | 0.059 | 15.195 | 0.016 |
| 35 | 3169.16504 | 0.079 | 15.248 | 0.017 |
| 36 | 3169.24487 | 0.227 | 15.516 | 0.018 |
| 37 | 3169.25562 | 0.247 | 15.532 | 0.018 |
| 38 | 3175.13623 | 0.107 | 15.304 | 0.016 |
| 39 | 3175.14697 | 0.127 | 15.344 | 0.017 |
| 40 | 3175.19189 | 0.210 | 15.487 | 0.017 |
| 41 | 3175.20264 | 0.230 | 15.512 | 0.017 |

44. RR183606

| | Dayval | Phase | Vint | Vinterr |
|---|---|---|---|---|
| 1 | 1228.44482 | 0.734 | 17.000 | 0.050 |
| 2 | 1237.41907 | 0.271 | 16.608 | 0.038 |
| 3 | 1254.37134 | 0.289 | 16.673 | 0.044 |
| 4 | 1255.36877 | 0.349 | 16.734 | 0.264 |
| 5 | 1257.36267 | 0.468 | 16.926 | 0.057 |
| 6 | 1258.36035 | 0.528 | 16.956 | 0.050 |
| 7 | 1263.34619 | 0.827 | 16.904 | 0.059 |
| 8 | 1269.32959 | 0.187 | 16.447 | 0.035 |
| 9 | 1292.26660 | 0.566 | 16.992 | 0.057 |
| 10 | 1317.19910 | 0.067 | 16.070 | 0.041 |
| 11 | 1593.44519 | 0.689 | 16.958 | 0.050 |
| 12 | 1612.39136 | 0.825 | 17.053 | 0.050 |
| 13 | 1613.38953 | 0.887 | 17.018 | 0.058 |
| 14 | 1615.38293 | 0.005 | 15.836 | 0.028 |
| 15 | 1616.38013 | 0.064 | 16.051 | 0.029 |
| 16 | 1617.37720 | 0.124 | 16.278 | 0.039 |
| 17 | 1620.36951 | 0.305 | 16.646 | 0.051 |
| 18 | 1621.36621 | 0.364 | 16.729 | 0.047 |
| 19 | 1623.36145 | 0.485 | 16.876 | 0.061 |
| 20 | 1980.38354 | 0.960 | 16.548 | 0.046 |
| 21 | 1997.33716 | 0.980 | 15.955 | 0.027 |
| 22 | 2035.23291 | 0.259 | 16.605 | 0.045 |
| 23 | 2057.17383 | 0.581 | 17.075 | 0.083 |
| 24 | 2323.44604 | 0.600 | 16.923 | 0.072 |
| 25 | 2326.43750 | 0.780 | 16.977 | 0.069 |
| 26 | 3126.40332 | 0.212 | 16.456 | 0.023 |
| 27 | 3126.41406 | 0.235 | 16.560 | 0.029 |
| 28 | 3126.42505 | 0.257 | 16.610 | 0.028 |
| 29 | 3129.38916 | 0.380 | 16.719 | 0.034 |
| 30 | 3129.40308 | 0.409 | 16.703 | 0.075 |
| 31 | 3130.38794 | 0.443 | 16.813 | 0.023 |
| 32 | 3130.39868 | 0.465 | 16.881 | 0.027 |
| 33 | 3130.40942 | 0.487 | 16.907 | 0.028 |
| 34 | 3130.42017 | 0.510 | 16.917 | 0.027 |
| 35 | 3169.18066 | 0.574 | 16.995 | 0.024 |
| 36 | 3169.19165 | 0.597 | 16.984 | 0.028 |
| 37 | 3169.27026 | 0.760 | 16.965 | 0.028 |
| 38 | 3169.28125 | 0.782 | 16.990 | 0.029 |
| 39 | 3174.09814 | 0.732 | 16.926 | 0.025 |
| 40 | 3174.11133 | 0.759 | 17.009 | 0.025 |
| 41 | 3174.12231 | 0.782 | 17.041 | 0.023 |
| 42 | 3174.18677 | 0.915 | 16.882 | 0.023 |
| 43 | 3174.19775 | 0.938 | 16.597 | 0.020 |
| 44 | 3174.24658 | 0.039 | 15.990 | 0.016 |
| 45 | 3174.25757 | 0.061 | 16.028 | 0.016 |
| 46 | 3454.38599 | 0.703 | 16.992 | 0.021 |
| 47 | 3454.42285 | 0.779 | 16.947 | 0.021 |

45. RR183918

| | Dayval | Phase | Vint | Vinterr |
|---|---|---|---|---|
| 1 | 1228.44702 | 0.313 | 16.668 | 0.041 |
| 2 | 1237.42126 | 0.954 | 16.541 | 0.036 |
| 3 | 1254.37354 | 0.834 | 17.068 | 0.063 |
| 4 | 1255.37097 | 0.239 | 16.611 | 0.168 |
| 5 | 1257.36487 | 0.047 | 16.316 | 0.035 |
| 6 | 1258.36255 | 0.453 | 16.792 | 0.043 |
| 7 | 1263.34839 | 0.476 | 16.817 | 0.049 |
| 8 | 1269.33191 | 0.904 | 16.918 | 0.051 |
| 9 | 1292.26892 | 0.213 | 16.533 | 0.039 |
| 10 | 1317.20129 | 0.333 | 16.673 | 0.052 |
| 11 | 1593.44739 | 0.456 | 16.741 | 0.048 |
| 12 | 1612.39355 | 0.143 | 16.429 | 0.034 |
| 13 | 1613.39172 | 0.549 | 16.834 | 0.049 |
| 14 | 1615.38513 | 0.357 | 16.685 | 0.048 |
| 15 | 1616.38232 | 0.762 | 17.024 | 0.056 |
| 16 | 1617.37939 | 0.166 | 16.477 | 0.043 |
| 17 | 1620.37170 | 0.381 | 16.707 | 0.046 |
| 18 | 1621.36841 | 0.785 | 17.013 | 0.059 |
| 19 | 1623.36365 | 0.596 | 16.856 | 0.052 |
| 20 | 1980.38574 | 0.500 | 16.868 | 0.051 |
| 21 | 1997.33936 | 0.381 | 16.785 | 0.042 |
| 22 | 2035.23511 | 0.761 | 16.993 | 0.066 |
| 23 | 2057.17603 | 0.667 | 16.867 | 0.068 |
| 24 | 2323.44824 | 0.740 | 16.968 | 0.064 |
| 25 | 2326.43970 | 0.954 | 16.590 | 0.047 |
| 26 | 3473.34888 | 0.499 | 16.814 | 0.022 |
| 27 | 3473.35962 | 0.514 | 16.868 | 0.022 |
| 28 | 3473.39526 | 0.564 | 16.848 | 0.023 |
| 29 | 3473.40649 | 0.580 | 16.893 | 0.023 |
| 30 | 3478.25171 | 0.405 | 16.763 | 0.018 |
| 31 | 3478.30493 | 0.480 | 16.830 | 0.019 |
| 32 | 3478.31909 | 0.500 | 16.855 | 0.019 |
| 33 | 3478.35645 | 0.552 | 16.892 | 0.020 |
| 34 | 3478.37061 | 0.572 | 16.892 | 0.020 |
| 35 | 3478.40698 | 0.624 | 16.881 | 0.020 |
| 36 | 3478.42114 | 0.644 | 16.886 | 0.020 |
| 37 | 3516.15967 | 0.802 | 17.031 | 0.021 |
| 38 | 3516.19824 | 0.856 | 17.048 | 0.023 |
| 39 | 3516.21094 | 0.875 | 17.012 | 0.023 |
| 40 | 3516.25439 | 0.936 | 16.588 | 0.019 |
| 41 | 3516.26733 | 0.954 | 16.536 | 0.019 |
| 42 | 3516.28027 | 0.972 | 16.446 | 0.019 |
| 43 | 3516.32471 | 0.035 | 16.305 | 0.019 |
| 44 | 3516.33789 | 0.053 | 16.321 | 0.017 |

46. RR184019

| | Dayval | Phase | Vint | Vinterr |
|---|---|---|---|---|
| 1 | 1228.44775 | 0.437 | 14.679 | 0.011 |
| 2 | 1237.42200 | 0.896 | 14.482 | 0.010 |
| 3 | 1254.37427 | 0.098 | 14.439 | 0.012 |
| 4 | 1255.37170 | 0.817 | 14.303 | 0.038 |
| 5 | 1257.36560 | 0.251 | 14.279 | 0.010 |
| 6 | 1258.36328 | 0.970 | 14.754 | 0.012 |
| 7 | 1263.34912 | 0.559 | 14.566 | 0.011 |
| 8 | 1269.33252 | 0.866 | 14.403 | 0.010 |
| 9 | 1292.26953 | 0.380 | 14.453 | 0.011 |
| 10 | 1317.20203 | 0.332 | 14.351 | 0.012 |
| 11 | 1593.44812 | 0.227 | 14.276 | 0.009 |
| 12 | 1612.39429 | 0.864 | 14.398 | 0.009 |
| 13 | 1613.39246 | 0.584 | 14.519 | 0.010 |
| 14 | 1615.38586 | 0.017 | 14.729 | 0.013 |
| 15 | 1616.38306 | 0.735 | 14.278 | 0.010 |
| 16 | 1617.38013 | 0.452 | 14.726 | 0.014 |
| 17 | 1620.37244 | 0.607 | 14.371 | 0.011 |
| 18 | 1621.36914 | 0.324 | 14.368 | 0.010 |
| 19 | 1623.36438 | 0.762 | 14.264 | 0.009 |
| 20 | 1980.38647 | 0.808 | 14.289 | 0.010 |
| 21 | 1997.34009 | 0.014 | 14.745 | 0.012 |
| 22 | 2035.23584 | 0.297 | 14.305 | 0.011 |
| 23 | 2057.17676 | 0.096 | 14.486 | 0.013 |
| 24 | 2323.44897 | 0.807 | 14.251 | 0.010 |
| 25 | 2326.44043 | 0.960 | 14.614 | 0.013 |
| 26 | 3463.34912 | 0.547 | 14.590 | 0.009 |
| 27 | 3463.36597 | 0.593 | 14.413 | 0.008 |
| 28 | 3463.41113 | 0.716 | 14.231 | 0.007 |
| 29 | 3463.42651 | 0.758 | 14.220 | 0.007 |
| 30 | 3473.27734 | 0.606 | 14.381 | 0.007 |
| 31 | 3473.29224 | 0.646 | 14.307 | 0.007 |
| 32 | 3473.32007 | 0.722 | 14.220 | 0.007 |
| 33 | 3473.33447 | 0.762 | 14.207 | 0.007 |
| 34 | 3473.36963 | 0.857 | 14.306 | 0.008 |

| | | | |
|---|---|---|---|
| 35 3473.38379 | 0.896 | 14.416 | 0.008 |
| 36 3473.41626 | 0.984 | 14.670 | 0.009 |
| 37 3473.43042 | 0.023 | 14.650 | 0.009 |

47. RR184315

| Dayval | Phase | Vint | Vinterr |
|---|---|---|---|
| 1 1228.44971 | 0.786 | 16.214 | 0.030 |
| 2 1237.42407 | 0.460 | 16.453 | 0.034 |
| 3 1254.37634 | 0.291 | 16.194 | 0.037 |
| 4 1255.37378 | 0.811 | 16.263 | 0.150 |
| 5 1257.36768 | 0.849 | 16.313 | 0.036 |
| 6 1258.36523 | 0.370 | 16.284 | 0.032 |
| 7 1263.35120 | 0.967 | 16.600 | 0.043 |
| 8 1269.33459 | 0.084 | 16.486 | 0.039 |
| 9 1292.27161 | 0.034 | 16.549 | 0.038 |
| 10 1317.20410 | 0.025 | 16.564 | 0.048 |
| 11 1593.45020 | 0.953 | 16.540 | 0.038 |
| 12 1612.39636 | 0.822 | 16.221 | 0.028 |
| 13 1613.39453 | 0.343 | 16.243 | 0.030 |
| 14 1616.38513 | 0.900 | 16.326 | 0.035 |
| 15 1617.38220 | 0.419 | 16.507 | 0.059 |
| 16 1620.37439 | 0.979 | 16.519 | 0.042 |
| 17 1621.37122 | 0.498 | 16.493 | 0.036 |
| 18 1623.36646 | 0.538 | 16.568 | 0.040 |
| 19 1980.38855 | 0.548 | 16.554 | 0.039 |
| 20 1997.34204 | 0.381 | 16.355 | 0.031 |
| 21 2035.23779 | 0.125 | 16.376 | 0.039 |
| 22 2057.17871 | 0.557 | 16.516 | 0.041 |
| 23 2323.45093 | 0.288 | 16.205 | 0.037 |
| 24 2326.44238 | 0.846 | 16.249 | 0.036 |

48. RR184421

| Dayval | Phase | Vint | Vinterr |
|---|---|---|---|
| 1 1228.45056 | 0.242 | 16.949 | 0.046 |
| 2 1237.42480 | 0.184 | 16.948 | 0.043 |
| 3 1254.37708 | 0.189 | 16.941 | 0.054 |
| 4 1255.37451 | 0.072 | 17.099 | 0.243 |
| 5 1257.36841 | 0.836 | 17.097 | 0.060 |
| 6 1258.36609 | 0.720 | 16.982 | 0.048 |
| 7 1263.35193 | 0.133 | 17.035 | 0.051 |
| 8 1269.33545 | 0.430 | 17.308 | 0.059 |
| 9 1292.27234 | 0.735 | 17.077 | 0.056 |
| 10 1317.20483 | 0.809 | 17.139 | 0.067 |
| 11 1593.45093 | 0.370 | 17.199 | 0.059 |
| 12 1612.39709 | 0.138 | 17.077 | 0.050 |
| 13 1613.39526 | 0.024 | 17.380 | 0.059 |
| 14 1616.38586 | 0.669 | 17.017 | 0.056 |
| 15 1617.38293 | 0.551 | 17.237 | 0.081 |
| 16 1620.37512 | 0.201 | 16.973 | 0.055 |
| 17 1621.37195 | 0.083 | 17.045 | 0.054 |
| 18 1623.36719 | 0.850 | 17.218 | 0.060 |
| 19 1980.38928 | 0.915 | 17.271 | 0.060 |
| 20 1997.34290 | 0.924 | 17.325 | 0.066 |
| 21 2035.23865 | 0.471 | 17.140 | 0.065 |
| 22 2057.17944 | 0.897 | 17.205 | 0.072 |
| 23 2323.45166 | 0.626 | 16.990 | 0.067 |
| 24 2326.44312 | 0.273 | 16.942 | 0.056 |
| 25 3468.31860 | 0.159 | 16.911 | 0.019 |
| 26 3468.33325 | 0.201 | 16.930 | 0.023 |
| 27 3468.37451 | 0.320 | 16.904 | 0.019 |
| 28 3468.40698 | 0.414 | 17.106 | 0.022 |
| 29 3481.30103 | 0.688 | 16.975 | 0.020 |
| 30 3481.31519 | 0.729 | 16.968 | 0.023 |
| 31 3481.35547 | 0.845 | 17.107 | 0.024 |
| 32 3481.36743 | 0.880 | 17.157 | 0.025 |
| 33 3481.40283 | 0.982 | 17.374 | 0.025 |
| 34 3481.41724 | 0.023 | 17.282 | 0.024 |

49. RR184747

| Dayval | Phase | Vint | Vinterr |
|---|---|---|---|
| 1 1228.45288 | 0.921 | 16.965 | 0.052 |
| 2 1237.42725 | 0.660 | 17.326 | 0.060 |
| 3 1254.37952 | 0.836 | 17.167 | 0.068 |
| 4 1255.37683 | 0.141 | 17.111 | 0.241 |
| 5 1257.37085 | 0.749 | 17.367 | 0.082 |
| 6 1258.36841 | 0.054 | 17.067 | 0.052 |
| 7 1263.35425 | 0.576 | 17.305 | 0.071 |
| 8 1269.33777 | 0.403 | 17.295 | 0.063 |
| 9 1292.27478 | 0.407 | 17.218 | 0.067 |
| 10 1317.20728 | 0.022 | 17.120 | 0.067 |
| 11 1593.45337 | 0.382 | 17.169 | 0.067 |
| 12 1612.39941 | 0.166 | 17.071 | 0.050 |
| 13 1613.39758 | 0.472 | 17.365 | 0.063 |
| 14 1616.38831 | 0.384 | 17.292 | 0.068 |
| 15 1617.38525 | 0.688 | 17.497 | 0.123 |
| 16 1620.37756 | 0.602 | 17.517 | 0.086 |
| 17 1621.37439 | 0.906 | 17.087 | 0.057 |
| 18 1623.36963 | 0.516 | 17.436 | 0.089 |
| 19 1980.39160 | 0.541 | 17.263 | 0.069 |
| 20 1997.34521 | 0.718 | 17.378 | 0.064 |
| 21 2035.24097 | 0.290 | 17.184 | 0.068 |
| 22 2036.23816 | 0.594 | 17.268 | 0.081 |
| 23 2057.18188 | 0.991 | 17.030 | 0.065 |
| 24 2326.44556 | 0.218 | 17.181 | 0.071 |
| 25 3474.35864 | 0.816 | 17.226 | 0.019 |
| 26 3474.37646 | 0.839 | 17.131 | 0.019 |
| 27 3480.26538 | 0.542 | 17.258 | 0.019 |
| 28 3480.28345 | 0.566 | 17.254 | 0.019 |
| 29 3480.32031 | 0.614 | 17.299 | 0.019 |
| 30 3480.33789 | 0.637 | 17.298 | 0.018 |
| 31 3480.37158 | 0.681 | 17.283 | 0.020 |
| 32 3480.38940 | 0.704 | 17.326 | 0.020 |
| 33 3480.42358 | 0.749 | 17.346 | 0.021 |
| 34 3480.44141 | 0.772 | 17.307 | 0.023 |
| 35 3488.25293 | 0.991 | 17.076 | 0.023 |
| 36 3488.27051 | 0.014 | 17.083 | 0.021 |
| 37 3488.28833 | 0.037 | 17.096 | 0.022 |
| 38 3488.35083 | 0.119 | 17.104 | 0.022 |
| 39 3488.36841 | 0.142 | 17.081 | 0.020 |
| 40 3488.42798 | 0.220 | 17.108 | 0.019 |
| 41 3539.10425 | 0.510 | 17.294 | 0.020 |
| 42 3539.11841 | 0.528 | 17.314 | 0.018 |
| 43 3539.19141 | 0.624 | 17.360 | 0.026 |
| 44 3539.20337 | 0.640 | 17.377 | 0.024 |
| 45 3539.28882 | 0.751 | 17.402 | 0.026 |
| 46 3539.29956 | 0.765 | 17.389 | 0.027 |
| 47 3563.07349 | 0.864 | 17.111 | 0.020 |
| 48 3563.08545 | 0.880 | 17.042 | 0.018 |
| 49 3563.12256 | 0.929 | 16.946 | 0.020 |
| 50 3563.13477 | 0.945 | 16.914 | 0.017 |
| 51 3563.14844 | 0.962 | 16.883 | 0.018 |
| 52 3563.16089 | 0.979 | 16.852 | 0.019 |
| 53 3563.17407 | 0.996 | 16.850 | 0.019 |
| 54 3563.18652 | 0.012 | 16.858 | 0.034 |
| 55 3606.05566 | 0.090 | 16.992 | 0.020 |
| 56 3606.07007 | 0.109 | 17.038 | 0.019 |
| 57 3607.05078 | 0.391 | 17.292 | 0.031 |
| 58 3607.06519 | 0.410 | 17.281 | 0.026 |
| 59 3607.07983 | 0.429 | 17.305 | 0.027 |
| 60 3607.09692 | 0.452 | 17.386 | 0.032 |
| 61 3607.11108 | 0.471 | 17.337 | 0.034 |
| 62 3607.12573 | 0.489 | 17.358 | 0.041 |
| 63 3607.13989 | 0.508 | 17.504 | 0.041 |
| 64 3607.15405 | 0.527 | 17.392 | 0.042 |
| 65 3622.05103 | 0.013 | 16.894 | 0.015 |
| 66 3622.06519 | 0.032 | 16.919 | 0.016 |
| 67 3622.07935 | 0.051 | 16.935 | 0.017 |
| 68 3622.09375 | 0.069 | 16.973 | 0.017 |

50. GS Lyr

| Dayval | Phase | Vint | Vinterr |
|---|---|---|---|
| 1 1237.43896 | 0.095 | 12.528 | 0.003 |
| 2 1254.39075 | 0.102 | 12.651 | 0.004 |
| 3 1255.38855 | 0.102 | 12.646 | 0.010 |
| 4 1257.38245 | 0.103 | 12.713 | 0.004 |
| 5 1258.38000 | 0.103 | 12.744 | 0.003 |
| 6 1263.36572 | 0.105 | 12.822 | 0.004 |
| 7 1269.34888 | 0.108 | 12.897 | 0.004 |
| 8 1292.28589 | 0.117 | 12.749 | 0.004 |
| 9 1317.21802 | 0.127 | 12.793 | 0.004 |
| 10 1612.41113 | 0.245 | 12.904 | 0.004 |
| 11 1613.40930 | 0.245 | 12.895 | 0.004 |
| 12 1615.40247 | 0.246 | 12.886 | 0.004 |
| 13 1616.39990 | 0.247 | 12.957 | 0.004 |
| 14 1617.39697 | 0.247 | 12.963 | 0.004 |
| 15 1620.38916 | 0.248 | 12.960 | 0.004 |

| | | | |
|---|---|---|---|
| 16 1621.38599 | 0.249 | 12.939 | 0.004 |
| 17 1623.38123 | 0.249 | 13.011 | 0.004 |
| 18 1997.35669 | 0.399 | 13.003 | 0.004 |
| 19 2035.25195 | 0.414 | 12.472 | 0.003 |
| 20 2036.24902 | 0.414 | 12.511 | 0.003 |
| 21 2057.19263 | 0.423 | 12.956 | 0.005 |
| 22 2061.18188 | 0.424 | 12.993 | 0.005 |
| 23 2062.17920 | 0.425 | 12.976 | 0.005 |
| 24 3097.30200 | 0.839 | 12.799 | 0.008 |
| 25 3126.43628 | 0.851 | 13.017 | 0.010 |
| 26 3126.44214 | 0.851 | 13.000 | 0.008 |
| 27 3126.44971 | 0.851 | 13.010 | 0.008 |
| 28 3128.39478 | 0.851 | 13.044 | 0.008 |
| 29 3128.40088 | 0.851 | 13.041 | 0.008 |
| 30 3128.43628 | 0.851 | 13.022 | 0.009 |
| 31 3128.44263 | 0.851 | 13.017 | 0.009 |
| 32 3128.44849 | 0.851 | 13.018 | 0.008 |
| 33 3174.13818 | 0.870 | 12.673 | 0.010 |
| 34 3174.14160 | 0.870 | 12.688 | 0.013 |
| 35 3174.20532 | 0.870 | 12.688 | 0.013 |
| 36 3174.20776 | 0.870 | 12.689 | 0.013 |
| 37 3174.26562 | 0.870 | 12.688 | 0.013 |
| 38 3174.26807 | 0.870 | 12.685 | 0.011 |
| 39 3175.15649 | 0.870 | 12.693 | 0.013 |
| 40 3175.15918 | 0.870 | 12.697 | 0.013 |
| 41 3175.21045 | 0.870 | 12.688 | 0.013 |
| 42 3175.21387 | 0.870 | 12.683 | 0.011 |
| 43 3181.13501 | 0.872 | 12.762 | 0.013 |
| 44 3181.13794 | 0.872 | 12.757 | 0.013 |
| 45 3187.26660 | 0.875 | 12.847 | 0.011 |
| 46 3187.27075 | 0.875 | 12.839 | 0.011 |
| 47 3194.10986 | 0.878 | 12.971 | 0.010 |
| 48 3194.11401 | 0.878 | 12.960 | 0.010 |
| 49 3195.08643 | 0.878 | 12.980 | 0.010 |
| 50 3195.09058 | 0.878 | 12.979 | 0.010 |
| 51 3201.11133 | 0.880 | 13.000 | 0.012 |
| 52 3201.11450 | 0.880 | 12.983 | 0.012 |
| 53 3203.13745 | 0.881 | 12.964 | 0.012 |
| 54 3204.08447 | 0.882 | 12.938 | 0.012 |
| 55 3204.08765 | 0.882 | 12.943 | 0.012 |
| 56 3205.11963 | 0.882 | 12.913 | 0.012 |
| 57 3205.12305 | 0.882 | 12.912 | 0.012 |
| 58 3206.08105 | 0.882 | 12.921 | 0.012 |
| 59 3206.08350 | 0.882 | 12.905 | 0.012 |
| 60 3209.20923 | 0.884 | 12.874 | 0.008 |
| 61 3209.21753 | 0.884 | 12.879 | 0.013 |
| 62 3211.06836 | 0.884 | 12.846 | 0.013 |
| 63 3211.07861 | 0.884 | 12.880 | 0.012 |
| 64 3217.07349 | 0.887 | 12.862 | 0.012 |
| 65 3217.07617 | 0.887 | 12.834 | 0.010 |
| 66 3223.07373 | 0.889 | 12.870 | 0.012 |
| 67 3223.07666 | 0.889 | 12.865 | 0.012 |
| 68 3231.04224 | 0.892 | 12.834 | 0.012 |
| 69 3231.04468 | 0.892 | 12.818 | 0.012 |
| 70 3245.05640 | 0.898 | 12.776 | 0.013 |
| 71 3245.05884 | 0.898 | 12.779 | 0.013 |
| 72 3262.05078 | 0.905 | 12.790 | 0.013 |
| 73 3262.05371 | 0.905 | 12.806 | 0.012 |
| 74 3453.45239 | 0.981 | 12.908 | 0.012 |
| 75 3453.45508 | 0.981 | 12.931 | 0.013 |
| 76 3463.44629 | 0.985 | 13.039 | 0.012 |
| 77 3463.44897 | 0.985 | 13.012 | 0.012 |
| 78 3464.41504 | 0.986 | 13.022 | 0.014 |
| 79 3464.41748 | 0.986 | 13.013 | 0.014 |
| 80 3465.43262 | 0.986 | 13.040 | 0.012 |
| 81 3465.43506 | 0.986 | 13.036 | 0.012 |
| 82 3468.44287 | 0.987 | 13.040 | 0.012 |
| 83 3468.44531 | 0.987 | 13.043 | 0.012 |
| 84 3469.35059 | 0.988 | 13.111 | 0.044 |
| 85 3469.35327 | 0.988 | 13.043 | 0.027 |
| 86 3473.45630 | 0.989 | 13.063 | 0.014 |
| 87 3473.45898 | 0.989 | 13.074 | 0.015 |
| 88 3474.45288 | 0.990 | 13.054 | 0.012 |
| 89 3474.45801 | 0.990 | 13.044 | 0.014 |
| 90 3480.45312 | 0.992 | 13.128 | 0.012 |
| 91 3480.45776 | 0.992 | 13.129 | 0.013 |
| 92 3481.45068 | 0.993 | 13.196 | 0.013 |
| 93 3481.45557 | 0.993 | 13.202 | 0.014 |
| 94 3487.45532 | 0.995 | 13.362 | 0.012 |
| 95 3487.46069 | 0.995 | 13.358 | 0.013 |
| 96 3488.43945 | 0.995 | 13.382 | 0.012 |
| 97 3488.44482 | 0.995 | 13.368 | 0.012 |
| 98 3516.34741 | 0.007 | 13.314 | 0.012 |
| 99 3516.35376 | 0.007 | 13.312 | 0.012 |
| 100 3539.30786 | 0.016 | 13.362 | 0.011 |
| 101 3539.31079 | 0.016 | 13.326 | 0.011 |
| 102 3540.25122 | 0.016 | 13.314 | 0.013 |
| 103 3540.25366 | 0.016 | 13.333 | 0.012 |
| 104 3545.25317 | 0.018 | 13.360 | 0.012 |
| 105 3545.25562 | 0.018 | 13.365 | 0.011 |
| 106 3546.10229 | 0.018 | 13.408 | 0.011 |
| 107 3546.13843 | 0.018 | 13.371 | 0.011 |
| 108 3563.09497 | 0.025 | 13.347 | 0.011 |
| 109 3563.10059 | 0.025 | 13.344 | 0.011 |
| 110 3569.06152 | 0.028 | 13.384 | 0.011 |
| 111 3569.06738 | 0.028 | 13.399 | 0.011 |
| 112 3606.03784 | 0.042 | 13.231 | 0.012 |
| 113 3606.04321 | 0.042 | 13.220 | 0.011 |
| 114 3607.03271 | 0.043 | 13.245 | 0.015 |
| 115 3607.03857 | 0.043 | 13.204 | 0.012 |
| 116 3622.03247 | 0.049 | 12.828 | 0.014 |
| 117 3622.03955 | 0.049 | 12.835 | 0.012 |

51. V427 Lyr

| Dayval | Phase | Vint | Vinterr |
|---|---|---|---|
| 1 1237.44556 | 0.529 | 16.664 | 0.040 |
| 2 1254.39734 | 0.453 | 16.645 | 0.053 |
| 3 1255.39502 | 0.803 | 16.744 | 0.193 |
| 4 1257.38892 | 0.499 | 16.632 | 0.051 |
| 5 1258.38611 | 0.848 | 16.742 | 0.044 |
| 6 1269.35547 | 0.682 | 16.691 | 0.046 |
| 7 1292.29248 | 0.703 | 16.713 | 0.050 |
| 8 1317.22461 | 0.422 | 16.608 | 0.050 |
| 9 1355.12305 | 0.679 | 16.753 | 0.038 |
| 10 1612.41772 | 0.650 | 16.699 | 0.043 |
| 11 1613.41589 | 0.001 | 15.767 | 0.023 |
| 12 1615.40906 | 0.695 | 16.779 | 0.056 |
| 13 1616.40649 | 0.044 | 15.913 | 0.025 |
| 14 1617.40344 | 0.392 | 16.590 | 0.041 |
| 15 1620.39575 | 0.439 | 16.668 | 0.047 |
| 16 1621.39246 | 0.787 | 16.832 | 0.054 |
| 17 1623.38770 | 0.486 | 16.632 | 0.046 |
| 18 1980.40979 | 0.331 | 16.587 | 0.043 |
| 19 1997.36328 | 0.259 | 16.477 | 0.037 |
| 20 2036.25562 | 0.857 | 16.617 | 0.046 |
| 21 2057.19922 | 0.183 | 16.378 | 0.045 |
| 22 2061.18823 | 0.578 | 16.671 | 0.050 |
| 23 2062.18555 | 0.927 | 15.756 | 0.025 |
| 24 2082.13257 | 0.905 | 16.157 | 0.035 |
| 25 3097.31470 | 0.825 | 16.599 | 0.029 |
| 26 3129.42432 | 0.448 | 16.643 | 0.056 |
| 27 3129.43579 | 0.475 | 16.742 | 0.088 |
| 28 3194.12744 | 0.834 | 16.654 | 0.026 |
| 29 3194.13867 | 0.861 | 16.572 | 0.026 |
| 30 3194.17822 | 0.954 | 15.861 | 0.019 |
| 31 3194.18896 | 0.980 | 15.799 | 0.017 |
| 32 3194.21875 | 0.049 | 15.903 | 0.018 |
| 33 3194.22949 | 0.075 | 15.974 | 0.022 |
| 34 3194.26001 | 0.147 | 16.147 | 0.025 |
| 35 3194.27075 | 0.172 | 16.177 | 0.026 |
| 36 3195.10498 | 0.137 | 16.117 | 0.019 |
| 37 3195.11572 | 0.162 | 16.171 | 0.020 |
| 38 3195.14551 | 0.232 | 16.294 | 0.021 |
| 39 3195.15625 | 0.258 | 16.332 | 0.023 |
| 40 3195.18579 | 0.327 | 16.341 | 0.025 |
| 41 3195.19653 | 0.352 | 16.460 | 0.025 |
| 42 3195.22656 | 0.423 | 16.551 | 0.027 |
| 43 3195.23730 | 0.448 | 16.623 | 0.032 |
| 44 3474.43408 | 0.003 | 15.744 | 0.015 |
| 45 3474.44482 | 0.028 | 15.803 | 0.017 |

52. V926 Cyg

| Dayval | Phase | Vint | Vinterr |
|---|---|---|---|
| 1 1255.41357 | 0.610 | 15.334 | 0.053 |
| 2 1257.40747 | 0.105 | 15.032 | 0.014 |
| 3 1258.40454 | 0.353 | 15.222 | 0.014 |

| | | | | |
|---|---|---|---|---|
| 4 | 1263.39038 | 0.593 | 15.162 | 0.021 |
| 5 | 1269.37366 | 0.083 | 14.995 | 0.013 |
| 6 | 1292.31018 | 0.795 | 15.009 | 0.016 |
| 7 | 1317.24158 | 0.005 | 14.932 | 0.016 |
| 8 | 1354.14185 | 0.202 | 15.144 | 0.011 |
| 9 | 1355.13928 | 0.451 | 15.313 | 0.013 |
| 10 | 1612.43628 | 0.554 | 15.264 | 0.017 |
| 11 | 1613.43323 | 0.802 | 15.024 | 0.014 |
| 12 | 1615.42761 | 0.298 | 15.100 | 0.015 |
| 13 | 1616.42468 | 0.546 | 15.300 | 0.017 |
| 14 | 1617.42200 | 0.795 | 14.990 | 0.016 |
| 15 | 1620.41418 | 0.541 | 15.232 | 0.018 |
| 16 | 1621.41101 | 0.788 | 15.052 | 0.016 |
| 17 | 1623.40613 | 0.287 | 15.070 | 0.017 |
| 18 | 1980.42834 | 0.229 | 15.177 | 0.015 |
| 19 | 1997.38147 | 0.452 | 15.354 | 0.016 |
| 20 | 2035.27551 | 0.885 | 15.036 | 0.016 |
| 21 | 2036.27283 | 0.134 | 15.052 | 0.016 |
| 22 | 2061.20508 | 0.346 | 15.288 | 0.018 |
| 23 | 2062.20215 | 0.595 | 15.374 | 0.018 |
| 24 | 2063.19946 | 0.843 | 15.126 | 0.016 |
| 25 | 2082.14868 | 0.567 | 15.434 | 0.022 |
| 26 | 3097.36401 | 0.468 | 15.279 | 0.029 |
| 27 | 3194.15088 | 0.736 | 15.134 | 0.017 |
| 28 | 3194.15820 | 0.760 | 15.075 | 0.017 |
| 29 | 3194.16553 | 0.784 | 15.065 | 0.017 |
| 30 | 3194.19873 | 0.892 | 14.967 | 0.017 |
| 31 | 3194.20605 | 0.916 | 14.965 | 0.015 |
| 32 | 3194.24023 | 0.027 | 14.974 | 0.017 |
| 33 | 3194.24756 | 0.051 | 14.997 | 0.019 |
| 34 | 3195.12549 | 0.910 | 14.976 | 0.017 |
| 35 | 3195.13281 | 0.934 | 14.959 | 0.016 |
| 36 | 3195.16602 | 0.042 | 14.983 | 0.017 |
| 37 | 3195.17334 | 0.066 | 14.980 | 0.016 |
| 38 | 3195.20654 | 0.175 | 15.084 | 0.018 |
| 39 | 3195.21387 | 0.198 | 15.098 | 0.019 |
| 40 | 3195.24707 | 0.307 | 15.247 | 0.021 |
| 41 | 3195.25439 | 0.330 | 15.250 | 0.022 |
| 42 | 3474.29834 | 0.271 | 15.143 | 0.012 |
| 43 | 3474.30591 | 0.296 | 15.162 | 0.013 |
| 44 | 3488.30420 | 0.893 | 15.018 | 0.013 |
| 45 | 3488.31128 | 0.917 | 14.986 | 0.012 |
| 46 | 3488.38232 | 0.148 | 15.032 | 0.014 |
| 47 | 3488.38965 | 0.172 | 15.045 | 0.013 |

53. RR210716

| | Dayval | Phase | Vint | Vinterr |
|---|---|---|---|---|
| 1 | 1269.43628 | 0.541 | 13.063 | 0.004 |
| 2 | 1292.37280 | 0.805 | 12.767 | 0.004 |
| 3 | 1317.30371 | 0.615 | 12.841 | 0.005 |
| 4 | 1354.20337 | 0.696 | 12.755 | 0.003 |
| 5 | 1355.20068 | 0.969 | 13.170 | 0.004 |
| 6 | 1359.18982 | 0.059 | 13.009 | 0.005 |
| 7 | 1378.13916 | 0.238 | 12.733 | 0.004 |
| 8 | 1379.13660 | 0.511 | 13.129 | 0.004 |
| 9 | 1742.14258 | 0.679 | 12.771 | 0.005 |
| 10 | 2035.33765 | 0.771 | 12.743 | 0.004 |
| 11 | 2036.33472 | 0.043 | 13.088 | 0.005 |
| 12 | 2061.26685 | 0.855 | 12.842 | 0.004 |
| 13 | 2062.26416 | 0.128 | 12.835 | 0.004 |
| 14 | 2063.26099 | 0.399 | 12.934 | 0.005 |
| 15 | 2094.17798 | 0.848 | 12.691 | 0.005 |
| 16 | 2110.13525 | 0.210 | 12.750 | 0.005 |
| 17 | 2113.12744 | 0.028 | 13.167 | 0.006 |
| 18 | 2121.10620 | 0.209 | 12.736 | 0.005 |
| 19 | 3465.32153 | 0.221 | 12.761 | 0.012 |
| 20 | 3465.32959 | 0.240 | 12.729 | 0.012 |
| 21 | 3465.35718 | 0.303 | 12.786 | 0.011 |
| 22 | 3465.36133 | 0.312 | 12.784 | 0.011 |
| 23 | 3465.36938 | 0.330 | 12.816 | 0.011 |
| 24 | 3465.39307 | 0.384 | 12.895 | 0.011 |
| 25 | 3465.40088 | 0.402 | 12.919 | 0.011 |
| 26 | 3517.14795 | 0.316 | 12.765 | 0.015 |
| 27 | 3517.15161 | 0.325 | 12.795 | 0.013 |
| 28 | 3517.21948 | 0.479 | 13.128 | 0.010 |
| 29 | 3517.22339 | 0.488 | 13.143 | 0.010 |
| 30 | 3517.29492 | 0.651 | 12.837 | 0.011 |
| 31 | 3517.29858 | 0.660 | 12.810 | 0.011 |
| 32 | 3517.36816 | 0.818 | 12.782 | 0.011 |
| 33 | 3517.37207 | 0.827 | 12.798 | 0.011 |
| 34 | 3517.47339 | 0.058 | 13.045 | 0.020 |
| 35 | 3517.47705 | 0.066 | 13.019 | 0.015 |

54. RR212011

| | Dayval | Phase | Vint | Vinterr |
|---|---|---|---|---|
| 1 | 1354.21448 | 0.779 | 16.628 | 0.034 |
| 2 | 1355.21167 | 0.001 | 16.408 | 0.032 |
| 3 | 1359.20044 | 0.891 | 16.663 | 0.050 |
| 4 | 1378.14771 | 0.121 | 16.425 | 0.034 |
| 5 | 1379.14502 | 0.344 | 16.439 | 0.043 |
| 6 | 2035.35254 | 0.885 | 16.595 | 0.046 |
| 7 | 2061.28003 | 0.672 | 16.605 | 0.048 |
| 8 | 2062.27710 | 0.895 | 16.617 | 0.047 |
| 9 | 2063.27393 | 0.116 | 16.386 | 0.049 |
| 10 | 2094.18774 | 0.017 | 16.398 | 0.050 |
| 11 | 2110.14355 | 0.578 | 16.549 | 0.050 |
| 12 | 2113.13525 | 0.246 | 16.391 | 0.053 |
| 13 | 2121.11328 | 0.027 | 16.335 | 0.053 |

55. RR212110

| | Dayval | Phase | Vint | Vinterr |
|---|---|---|---|---|
| 1 | 1354.21509 | 0.986 | 15.182 | 0.014 |
| 2 | 1355.21240 | 0.053 | 15.207 | 0.014 |
| 3 | 1359.20105 | 0.320 | 15.473 | 0.025 |
| 4 | 1378.14844 | 0.591 | 15.601 | 0.019 |
| 5 | 1379.14575 | 0.658 | 15.743 | 0.029 |
| 6 | 2035.35315 | 0.762 | 15.524 | 0.023 |
| 7 | 2061.28076 | 0.500 | 15.576 | 0.022 |
| 8 | 2062.27783 | 0.567 | 15.583 | 0.023 |
| 9 | 2063.27466 | 0.632 | 15.609 | 0.024 |
| 10 | 2094.18848 | 0.705 | 15.585 | 0.026 |
| 11 | 2110.14429 | 0.775 | 15.505 | 0.025 |
| 12 | 2113.13599 | 0.976 | 15.204 | 0.019 |
| 13 | 2121.11401 | 0.512 | 15.572 | 0.028 |

56. RR213430

| | Dayval | Phase | Vint | Vinterr |
|---|---|---|---|---|
| 1 | 1292.39307 | 0.371 | 16.841 | 0.055 |
| 2 | 1317.32349 | 0.181 | 16.724 | 0.056 |
| 3 | 1354.22192 | 0.905 | 16.943 | 0.046 |
| 4 | 1355.21924 | 0.898 | 16.870 | 0.047 |
| 5 | 1359.20825 | 0.868 | 16.791 | 0.063 |
| 6 | 1378.15698 | 0.729 | 16.693 | 0.042 |
| 7 | 1404.08752 | 0.541 | 17.064 | 0.066 |
| 8 | 1405.08496 | 0.534 | 17.184 | 0.056 |
| 9 | 1742.16040 | 0.022 | 17.115 | 0.091 |
| 10 | 1758.11755 | 0.906 | 16.882 | 0.062 |
| 11 | 2035.35767 | 0.842 | 16.769 | 0.054 |
| 12 | 2061.28613 | 0.647 | 16.793 | 0.054 |
| 13 | 2062.28320 | 0.640 | 16.814 | 0.051 |
| 14 | 2063.28003 | 0.631 | 16.804 | 0.061 |
| 15 | 2094.19604 | 0.403 | 17.009 | 0.066 |
| 16 | 2110.15308 | 0.287 | 16.770 | 0.066 |
| 17 | 2113.14502 | 0.265 | 16.737 | 0.063 |
| 18 | 2121.12378 | 0.207 | 16.768 | 0.069 |
| 19 | 3487.36841 | 0.003 | 17.268 | 0.022 |
| 20 | 3487.38281 | 0.046 | 17.128 | 0.021 |
| 21 | 3487.43115 | 0.191 | 16.795 | 0.018 |
| 22 | 3487.44556 | 0.234 | 16.746 | 0.018 |
| 23 | 3516.18115 | 0.463 | 17.184 | 0.028 |
| 24 | 3516.22485 | 0.594 | 16.847 | 0.023 |
| 25 | 3516.23779 | 0.633 | 16.859 | 0.022 |
| 26 | 3516.29517 | 0.806 | 16.788 | 0.021 |
| 27 | 3516.30811 | 0.844 | 16.891 | 0.022 |
| 28 | 3516.36230 | 0.007 | 17.225 | 0.024 |
| 29 | 3516.37524 | 0.046 | 17.103 | 0.022 |
| 30 | 3516.43677 | 0.230 | 16.804 | 0.021 |
| 31 | 3516.44971 | 0.269 | 16.735 | 0.020 |
| 32 | 3545.19043 | 0.513 | 17.161 | 0.028 |
| 33 | 3545.20044 | 0.544 | 17.025 | 0.026 |
| 34 | 3545.21045 | 0.574 | 16.939 | 0.025 |
| 35 | 3545.22046 | 0.604 | 16.836 | 0.025 |

57. RR214612

| | Dayval | Phase | Vint | Vinterr |
|---|---|---|---|---|
| 1 | 1292.40125 | 0.970 | 15.108 | 0.018 |

| | | | | |
|---|---|---|---|---|
| 2 | 1317.33167 | 0.025 | 14.920 | 0.017 |
| 3 | 1354.22998 | 0.268 | 15.167 | 0.014 |
| 4 | 1355.22742 | 0.951 | 15.182 | 0.014 |
| 5 | 1359.21631 | 0.680 | 15.446 | 0.022 |
| 6 | 1378.16516 | 0.644 | 15.437 | 0.017 |
| 7 | 1379.16260 | 0.327 | 15.162 | 0.022 |
| 8 | 1403.09839 | 0.704 | 15.453 | 0.024 |
| 9 | 1404.09570 | 0.386 | 15.277 | 0.017 |
| 10 | 1405.09302 | 0.069 | 14.793 | 0.012 |
| 11 | 1742.16858 | 0.679 | 15.438 | 0.025 |
| 12 | 1758.12573 | 0.597 | 15.425 | 0.022 |
| 13 | 2035.36572 | 0.271 | 15.216 | 0.018 |
| 14 | 2061.29419 | 0.010 | 14.833 | 0.015 |
| 15 | 2062.29150 | 0.692 | 15.465 | 0.023 |
| 16 | 2063.28833 | 0.373 | 15.305 | 0.019 |
| 17 | 2094.20435 | 0.525 | 15.432 | 0.023 |
| 18 | 2110.16138 | 0.443 | 15.355 | 0.025 |
| 19 | 2113.15332 | 0.490 | 15.396 | 0.023 |
| 20 | 2121.13184 | 0.949 | 15.318 | 0.025 |
| 21 | 3465.34204 | 0.488 | 15.347 | 0.016 |
| 22 | 3465.34961 | 0.500 | 15.333 | 0.016 |
| 23 | 3465.37842 | 0.549 | 15.399 | 0.015 |
| 24 | 3465.38623 | 0.562 | 15.384 | 0.015 |
| 25 | 3465.40967 | 0.601 | 15.405 | 0.016 |
| 26 | 3465.41699 | 0.614 | 15.422 | 0.016 |
| 27 | 3503.29224 | 0.506 | 15.435 | 0.056 |
| 28 | 3503.30591 | 0.529 | 15.390 | 0.014 |
| 29 | 3517.13110 | 0.850 | 15.404 | 0.019 |
| 30 | 3517.13843 | 0.863 | 15.379 | 0.028 |
| 31 | 3517.20532 | 0.975 | 14.966 | 0.017 |
| 32 | 3517.21265 | 0.988 | 14.906 | 0.018 |
| 33 | 3517.28101 | 0.103 | 14.989 | 0.014 |
| 34 | 3517.28833 | 0.115 | 15.020 | 0.013 |
| 35 | 3517.35376 | 0.226 | 15.135 | 0.014 |
| 36 | 3517.36108 | 0.238 | 15.150 | 0.014 |
| 37 | 3517.43604 | 0.364 | 15.288 | 0.019 |
| 38 | 3517.44336 | 0.377 | 15.300 | 0.016 |

58. RR215735

| | Dayval | Phase | Vint | Vinterr |
|---|---|---|---|---|
| 1 | 1292.40918 | 0.661 | 17.581 | 0.096 |
| 2 | 1317.33960 | 0.318 | 17.266 | 0.077 |
| 3 | 1354.23792 | 0.733 | 17.647 | 0.069 |
| 4 | 1355.23523 | 0.879 | 17.772 | 0.085 |
| 5 | 1359.22424 | 0.465 | 17.476 | 0.090 |
| 6 | 1378.17310 | 0.247 | 17.113 | 0.055 |
| 7 | 1379.17053 | 0.394 | 17.002 | 0.082 |
| 8 | 1403.10632 | 0.910 | 17.544 | 0.140 |
| 9 | 1404.10364 | 0.057 | 16.471 | 0.040 |
| 10 | 1405.10095 | 0.203 | 16.980 | 0.047 |
| 11 | 1411.08508 | 0.083 | 16.634 | 0.037 |
| 12 | 1742.17651 | 0.679 | 17.555 | 0.123 |
| 13 | 1758.13367 | 0.023 | 16.408 | 0.040 |
| 14 | 2035.37366 | 0.717 | 17.659 | 0.095 |
| 15 | 2061.30225 | 0.522 | 17.559 | 0.092 |
| 16 | 2062.29932 | 0.668 | 17.681 | 0.089 |
| 17 | 2063.29614 | 0.813 | 17.773 | 0.107 |
| 18 | 2094.21216 | 0.353 | 17.421 | 0.089 |
| 19 | 2113.16113 | 0.136 | 16.800 | 0.059 |
| 20 | 2121.13989 | 0.308 | 17.169 | 0.092 |
| 21 | 3231.05518 | 0.139 | 16.802 | 0.019 |
| 22 | 3231.06934 | 0.170 | 16.894 | 0.017 |
| 23 | 3231.12793 | 0.295 | 17.244 | 0.022 |
| 24 | 3231.14258 | 0.327 | 17.281 | 0.024 |
| 25 | 3231.20898 | 0.470 | 17.508 | 0.031 |
| 26 | 3231.22339 | 0.501 | 17.527 | 0.026 |
| 27 | 3231.28174 | 0.627 | 17.560 | 0.039 |
| 28 | 3231.29590 | 0.657 | 17.607 | 0.045 |
| 29 | 3234.04712 | 0.578 | 17.534 | 0.035 |
| 30 | 3234.06152 | 0.609 | 17.555 | 0.029 |
| 31 | 3234.11035 | 0.715 | 17.549 | 0.031 |
| 32 | 3234.12476 | 0.745 | 17.549 | 0.031 |
| 33 | 3234.17236 | 0.848 | 17.773 | 0.028 |
| 34 | 3234.18701 | 0.879 | 17.710 | 0.028 |
| 35 | 3234.23389 | 0.980 | 16.329 | 0.015 |
| 36 | 3234.24829 | 0.011 | 16.332 | 0.015 |
| 37 | 3245.06543 | 0.293 | 17.219 | 0.024 |
| 38 | 3245.07959 | 0.323 | 17.265 | 0.027 |
| 39 | 3245.15088 | 0.476 | 17.494 | 0.028 |
| 40 | 3245.16504 | 0.507 | 17.448 | 0.041 |
| 41 | 3246.16040 | 0.649 | 17.526 | 0.036 |
| 42 | 3246.17456 | 0.680 | 17.470 | 0.035 |
| 43 | 3246.22290 | 0.784 | 17.598 | 0.030 |
| 44 | 3246.23706 | 0.814 | 17.742 | 0.036 |
| 45 | 3247.07837 | 0.625 | 17.607 | 0.054 |
| 46 | 3247.08643 | 0.642 | 17.697 | 0.053 |

59. RR215817

| | Dayval | Phase | Vint | Vinterr |
|---|---|---|---|---|
| 1 | 1292.40967 | 0.289 | 15.321 | 0.019 |
| 2 | 1317.33997 | 0.743 | 15.614 | 0.025 |
| 3 | 1354.23840 | 0.977 | 14.791 | 0.011 |
| 4 | 1355.23572 | 0.875 | 15.227 | 0.014 |
| 5 | 1359.22473 | 0.468 | 15.485 | 0.022 |
| 6 | 1378.17358 | 0.536 | 15.409 | 0.017 |
| 7 | 1379.17102 | 0.435 | 15.497 | 0.027 |
| 8 | 1403.10669 | 0.995 | 14.695 | 0.021 |
| 9 | 1404.10413 | 0.894 | 15.385 | 0.018 |
| 10 | 1405.10144 | 0.792 | 15.569 | 0.018 |
| 11 | 1411.08545 | 0.183 | 14.900 | 0.012 |
| 12 | 1742.17700 | 0.400 | 15.466 | 0.023 |
| 13 | 1758.13416 | 0.773 | 15.544 | 0.022 |
| 14 | 2035.37415 | 0.487 | 15.432 | 0.020 |
| 15 | 2061.30273 | 0.840 | 15.515 | 0.023 |
| 16 | 2062.29980 | 0.739 | 15.629 | 0.023 |
| 17 | 2063.29663 | 0.636 | 15.588 | 0.025 |
| 18 | 2094.21265 | 0.483 | 15.518 | 0.025 |
| 19 | 2110.16943 | 0.856 | 15.470 | 0.018 |
| 20 | 2113.16162 | 0.552 | 15.482 | 0.025 |
| 21 | 2121.14038 | 0.739 | 15.481 | 0.024 |
| 22 | 3641.03833 | 0.793 | 15.485 | 0.016 |
| 23 | 3641.04712 | 0.810 | 15.384 | 0.017 |
| 24 | 3660.05054 | 0.982 | 14.719 | 0.023 |
| 25 | 3660.05786 | 0.996 | 14.621 | 0.020 |
| 26 | 3660.10718 | 0.090 | 14.706 | 0.029 |
| 27 | 3660.11450 | 0.104 | 14.748 | 0.022 |
| 28 | 3666.05713 | 0.415 | 15.391 | 0.022 |
| 29 | 3666.06421 | 0.429 | 15.420 | 0.012 |
| 30 | 3666.09302 | 0.483 | 15.489 | 0.029 |
| 31 | 3667.04614 | 0.298 | 15.244 | 0.063 |
| 32 | 3667.05347 | 0.312 | 15.213 | 0.029 |
| 33 | 3667.08008 | 0.362 | 15.282 | 0.039 |
| 34 | 3667.08740 | 0.376 | 15.387 | 0.060 |

60. RR220055

| | Dayval | Phase | Vint | Vinterr |
|---|---|---|---|---|
| 1 | 1292.41150 | 0.980 | 15.057 | 0.017 |
| 2 | 1317.34180 | 0.079 | 15.224 | 0.017 |
| 3 | 1354.24023 | 0.790 | 15.912 | 0.021 |
| 4 | 1355.23755 | 0.674 | 15.956 | 0.021 |
| 5 | 1359.22656 | 0.210 | 15.505 | 0.024 |
| 6 | 1378.17542 | 0.010 | 15.016 | 0.013 |
| 7 | 1379.17285 | 0.894 | 15.864 | 0.027 |
| 8 | 1403.10864 | 0.115 | 15.243 | 0.024 |
| 9 | 1404.10596 | 0.999 | 15.050 | 0.013 |
| 10 | 1405.10327 | 0.883 | 15.950 | 0.026 |
| 11 | 1411.08728 | 0.189 | 15.442 | 0.018 |
| 12 | 1742.17883 | 0.705 | 15.873 | 0.036 |
| 13 | 1758.13599 | 0.852 | 15.986 | 0.029 |
| 14 | 2035.37598 | 0.630 | 15.930 | 0.027 |
| 15 | 2061.30444 | 0.615 | 15.903 | 0.030 |
| 16 | 2062.30176 | 0.499 | 15.931 | 0.028 |
| 17 | 2063.29858 | 0.382 | 15.804 | 0.026 |
| 18 | 2094.21460 | 0.791 | 16.002 | 0.031 |
| 19 | 2110.17139 | 0.937 | 15.758 | 0.023 |
| 20 | 2113.16357 | 0.590 | 15.961 | 0.033 |
| 21 | 2121.14209 | 0.664 | 15.968 | 0.034 |
| 22 | 3481.33228 | 0.410 | 15.768 | 0.014 |
| 23 | 3481.34302 | 0.431 | 15.782 | 0.041 |
| 24 | 3481.38306 | 0.507 | 15.858 | 0.024 |
| 25 | 3481.39185 | 0.523 | 15.871 | 0.024 |
| 26 | 3481.43311 | 0.601 | 15.902 | 0.015 |
| 27 | 3481.44385 | 0.621 | 15.904 | 0.014 |
| 28 | 3503.26978 | 0.856 | 15.954 | 0.021 |
| 29 | 3503.28052 | 0.876 | 16.021 | 0.016 |
| 30 | 3503.31714 | 0.945 | 15.452 | 0.011 |

| | Dayval | Phase | Vint | Vinterr |
|---|---|---|---|---|
| 31 | 3503.32861 | 0.967 | 15.205 | 0.014 |
| 32 | 3503.39355 | 0.090 | 15.212 | 0.018 |
| 33 | 3503.40576 | 0.113 | 15.256 | 0.054 |
| 34 | 3517.10303 | 0.990 | 15.020 | 0.019 |
| 35 | 3517.11133 | 0.006 | 15.011 | 0.014 |
| 36 | 3517.12036 | 0.023 | 15.065 | 0.014 |
| 37 | 3517.19141 | 0.158 | 15.378 | 0.016 |
| 38 | 3517.19580 | 0.166 | 15.417 | 0.017 |
| 39 | 3517.25635 | 0.280 | 15.597 | 0.012 |
| 40 | 3517.26807 | 0.302 | 15.637 | 0.012 |
| 41 | 3517.33252 | 0.424 | 15.782 | 0.013 |
| 42 | 3517.34326 | 0.444 | 15.820 | 0.013 |
| 43 | 3517.41235 | 0.575 | 15.892 | 0.013 |
| 44 | 3517.42334 | 0.596 | 15.890 | 0.016 |
| 45 | 3563.20288 | 0.085 | 15.223 | 0.021 |
| 46 | 3563.21313 | 0.105 | 15.269 | 0.020 |
| 47 | 3563.22339 | 0.124 | 15.317 | 0.043 |
| 48 | 3563.25049 | 0.175 | 15.408 | 0.018 |
| 49 | 3563.25928 | 0.191 | 15.477 | 0.025 |
| 50 | 3563.26978 | 0.211 | 15.423 | 0.016 |

61. RR220245

| | Dayval | Phase | Vint | Vinterr |
|---|---|---|---|---|
| 1 | 1292.41284 | 0.138 | 13.885 | 0.008 |
| 2 | 1317.34314 | 0.448 | 14.027 | 0.009 |
| 3 | 1354.24158 | 0.632 | 13.913 | 0.006 |
| 4 | 1355.23889 | 0.205 | 13.811 | 0.006 |
| 5 | 1359.22791 | 0.495 | 14.057 | 0.009 |
| 6 | 1378.17676 | 0.377 | 13.951 | 0.007 |
| 7 | 1379.17407 | 0.950 | 13.841 | 0.007 |
| 8 | 1403.10986 | 0.697 | 13.816 | 0.007 |
| 9 | 1404.10730 | 0.270 | 13.844 | 0.007 |
| 10 | 1405.10461 | 0.843 | 13.840 | 0.006 |
| 11 | 1411.08862 | 0.280 | 13.864 | 0.007 |
| 12 | 1414.08069 | 0.998 | 13.981 | 0.008 |
| 13 | 1742.18005 | 0.375 | 13.971 | 0.010 |
| 14 | 1758.13721 | 0.540 | 14.016 | 0.008 |
| 15 | 2035.37732 | 0.719 | 13.866 | 0.008 |
| 16 | 2061.30566 | 0.605 | 13.974 | 0.008 |
| 17 | 2062.30298 | 0.177 | 13.843 | 0.008 |
| 18 | 2063.29980 | 0.748 | 13.861 | 0.008 |
| 19 | 2094.21582 | 0.501 | 14.068 | 0.010 |
| 20 | 2113.16479 | 0.384 | 13.983 | 0.009 |
| 21 | 2121.14355 | 0.966 | 14.030 | 0.010 |
| 22 | 3478.28223 | 0.753 | 13.840 | 0.008 |
| 23 | 3478.29419 | 0.797 | 13.879 | 0.008 |
| 24 | 3478.33350 | 0.937 | 14.047 | 0.008 |
| 25 | 3478.34521 | 0.980 | 14.072 | 0.008 |
| 26 | 3478.38452 | 0.120 | 13.933 | 0.008 |
| 27 | 3478.39624 | 0.162 | 13.899 | 0.008 |
| 28 | 3478.43506 | 0.302 | 13.904 | 0.008 |
| 29 | 3478.44702 | 0.344 | 13.937 | 0.008 |

62. RR221023

| | Dayval | Phase | Vint | Vinterr |
|---|---|---|---|---|
| 1 | 1292.41809 | 0.768 | 16.792 | 0.060 |
| 2 | 1317.34851 | 0.695 | 16.765 | 0.059 |
| 3 | 1354.24683 | 0.190 | 16.328 | 0.028 |
| 4 | 1355.24414 | 0.987 | 16.474 | 0.037 |
| 5 | 1359.23315 | 0.175 | 16.271 | 0.042 |
| 6 | 1378.18201 | 0.323 | 16.454 | 0.041 |
| 7 | 1379.17944 | 0.121 | 16.153 | 0.049 |
| 8 | 1403.11523 | 0.255 | 16.402 | 0.041 |
| 9 | 1404.11255 | 0.053 | 16.356 | 0.037 |
| 10 | 1405.10986 | 0.850 | 16.709 | 0.043 |
| 11 | 1411.09399 | 0.634 | 16.739 | 0.043 |
| 12 | 1414.08594 | 0.026 | 15.919 | 0.029 |
| 13 | 1742.18542 | 0.295 | 16.505 | 0.048 |
| 14 | 1758.14258 | 0.052 | 15.934 | 0.032 |
| 15 | 2035.38257 | 0.667 | 16.794 | 0.060 |
| 16 | 2061.31104 | 0.393 | 16.592 | 0.054 |
| 17 | 2062.30835 | 0.190 | 16.313 | 0.041 |
| 18 | 2063.30518 | 0.986 | 16.268 | 0.044 |
| 19 | 2094.22119 | 0.700 | 16.781 | 0.066 |
| 20 | 2121.14868 | 0.226 | 16.471 | 0.057 |
| 21 | 3641.05664 | 0.258 | 16.562 | 0.020 |
| 22 | 3641.06567 | 0.275 | 16.541 | 0.020 |
| 23 | 3660.06665 | 0.516 | 16.794 | 0.023 |
| 24 | 3660.07520 | 0.532 | 16.773 | 0.025 |
| 25 | 3660.12354 | 0.619 | 16.848 | 0.039 |
| 26 | 3660.13232 | 0.634 | 16.760 | 0.055 |
| 27 | 3666.07471 | 0.343 | 16.700 | 0.025 |
| 28 | 3666.08325 | 0.359 | 16.676 | 0.027 |
| 29 | 3666.10938 | 0.406 | 16.704 | 0.028 |
| 30 | 3667.06274 | 0.124 | 16.413 | 0.032 |
| 31 | 3667.07153 | 0.140 | 16.414 | 0.027 |
| 32 | 3673.10205 | 0.007 | 16.145 | 0.064 |
| 33 | 3673.11060 | 0.023 | 16.165 | 0.060 |
| 34 | 3681.06152 | 0.351 | 16.630 | 0.027 |
| 35 | 3681.07031 | 0.367 | 16.670 | 0.025 |
| 36 | 3681.07935 | 0.383 | 16.668 | 0.024 |
| 37 | 3681.08813 | 0.399 | 16.713 | 0.029 |
| 38 | 3683.06567 | 0.963 | 16.591 | 0.055 |
| 39 | 3683.07446 | 0.979 | 16.424 | 0.030 |

63. RR222036

| | Dayval | Phase | Vint | Vinterr |
|---|---|---|---|---|
| 1 | 1023.16327 | 0.324 | 15.075 | 0.012 |
| 2 | 1292.43213 | 0.277 | 15.070 | 0.018 |
| 3 | 1317.36292 | 0.788 | 15.078 | 0.017 |
| 4 | 1354.25940 | 0.381 | 15.098 | 0.013 |
| 5 | 1355.25671 | 0.721 | 15.095 | 0.013 |
| 6 | 1359.24536 | 0.083 | 15.269 | 0.018 |
| 7 | 1378.19214 | 0.549 | 15.306 | 0.016 |
| 8 | 1379.18945 | 0.890 | 15.148 | 0.015 |
| 9 | 1401.12769 | 0.377 | 15.134 | 0.015 |
| 10 | 1403.12231 | 0.058 | 15.307 | 0.016 |
| 11 | 1404.11963 | 0.399 | 15.181 | 0.015 |
| 12 | 1405.11682 | 0.739 | 15.084 | 0.013 |
| 13 | 1411.10010 | 0.782 | 15.059 | 0.013 |
| 14 | 1414.09167 | 0.803 | 15.064 | 0.015 |
| 15 | 1742.19556 | 0.837 | 15.114 | 0.018 |
| 16 | 1758.15088 | 0.283 | 15.077 | 0.017 |
| 17 | 2035.39697 | 0.958 | 15.297 | 0.020 |
| 18 | 2061.32495 | 0.809 | 15.091 | 0.017 |
| 19 | 2062.32227 | 0.149 | 15.169 | 0.018 |
| 20 | 2063.31885 | 0.488 | 15.355 | 0.020 |
| 21 | 2094.23267 | 0.040 | 15.343 | 0.022 |
| 22 | 2113.17920 | 0.507 | 15.347 | 0.023 |
| 23 | 2121.15723 | 0.230 | 15.101 | 0.021 |
| 24 | 3488.33154 | 0.882 | 15.135 | 0.012 |
| 25 | 3488.34253 | 0.908 | 15.190 | 0.012 |
| 26 | 3488.41040 | 0.067 | 15.280 | 0.012 |
| 27 | 3488.42114 | 0.092 | 15.225 | 0.012 |
| 28 | 3485.41040 | 0.026 | 15.341 | 0.016 |
| 29 | 3485.44556 | 0.108 | 15.216 | 0.016 |
| 30 | 3485.45630 | 0.134 | 15.196 | 0.021 |
| 31 | 3517.17017 | 0.564 | 15.242 | 0.016 |
| 32 | 3517.18140 | 0.590 | 15.250 | 0.015 |
| 33 | 3517.23901 | 0.726 | 15.096 | 0.013 |
| 34 | 3517.25000 | 0.751 | 15.074 | 0.012 |
| 35 | 3517.31470 | 0.903 | 15.220 | 0.012 |
| 36 | 3517.32568 | 0.929 | 15.258 | 0.012 |
| 37 | 3517.38843 | 0.076 | 15.260 | 0.012 |
| 38 | 3517.39917 | 0.101 | 15.219 | 0.012 |
| 39 | 3517.46094 | 0.246 | 15.062 | 0.014 |
| 40 | 3517.47168 | 0.271 | 15.080 | 0.014 |

64. RR223619

| | Dayval | Phase | Vint | Vinterr |
|---|---|---|---|---|
| 1 | 1023.17419 | 0.441 | 16.778 | 0.042 |
| 2 | 1292.44312 | 0.494 | 16.811 | 0.058 |
| 3 | 1317.37378 | 0.237 | 16.620 | 0.057 |
| 4 | 1354.27039 | 0.535 | 16.737 | 0.040 |
| 5 | 1355.26758 | 0.165 | 16.555 | 0.040 |
| 6 | 1359.25623 | 0.683 | 16.688 | 0.051 |
| 7 | 1378.20312 | 0.647 | 16.726 | 0.047 |
| 8 | 1379.20044 | 0.277 | 16.707 | 0.046 |
| 9 | 1401.13867 | 0.130 | 16.635 | 0.044 |
| 10 | 1403.13330 | 0.389 | 16.727 | 0.051 |
| 11 | 1404.13049 | 0.019 | 16.511 | 0.040 |
| 12 | 1405.12769 | 0.649 | 16.792 | 0.044 |
| 13 | 1411.11108 | 0.427 | 16.747 | 0.046 |
| 14 | 1412.10815 | 0.056 | 16.548 | 0.045 |
| 15 | 1414.10266 | 0.316 | 16.738 | 0.051 |
| 16 | 1417.09436 | 0.205 | 16.744 | 0.087 |

| | | | | |
|---|---|---|---|---|
| 17 | 1742.20654 | 0.520 | 16.794 | 0.064 |
| 18 | 2035.40796 | 0.685 | 16.778 | 0.061 |
| 19 | 2061.33594 | 0.058 | 16.559 | 0.053 |
| 20 | 2062.33325 | 0.688 | 16.750 | 0.056 |
| 21 | 2063.32983 | 0.316 | 16.752 | 0.054 |
| 22 | 2094.24365 | 0.837 | 16.709 | 0.064 |
| 23 | 2113.19019 | 0.801 | 16.827 | 0.069 |
| 24 | 2121.16821 | 0.839 | 16.563 | 0.069 |
| 25 | 3516.40991 | 0.014 | 16.538 | 0.015 |
| 26 | 3516.42310 | 0.036 | 16.505 | 0.016 |
| 27 | 3516.47266 | 0.117 | 16.589 | 0.018 |
| 28 | 3516.48560 | 0.138 | 16.730 | 0.044 |
| 29 | 3540.22534 | 0.935 | 16.579 | 0.041 |
| 30 | 3540.23486 | 0.950 | 16.524 | 0.043 |
| 31 | 3545.12061 | 0.935 | 16.554 | 0.022 |
| 32 | 3545.13013 | 0.951 | 16.495 | 0.021 |
| 33 | 3545.13989 | 0.966 | 16.495 | 0.019 |
| 34 | 3545.14917 | 0.981 | 16.492 | 0.020 |
| 35 | 3545.15845 | 0.997 | 16.492 | 0.020 |
| 36 | 3569.08057 | 0.092 | 16.579 | 0.019 |
| 37 | 3569.09009 | 0.107 | 16.592 | 0.019 |
| 38 | 3569.11353 | 0.145 | 16.592 | 0.020 |
| 39 | 3569.12305 | 0.161 | 16.594 | 0.019 |
| 40 | 3569.14502 | 0.197 | 16.666 | 0.020 |
| 41 | 3569.15430 | 0.212 | 16.676 | 0.020 |
| 42 | 3569.17285 | 0.242 | 16.696 | 0.020 |
| 43 | 3569.18237 | 0.258 | 16.704 | 0.019 |
| 44 | 3569.20068 | 0.288 | 16.710 | 0.020 |
| 45 | 3569.21021 | 0.303 | 16.721 | 0.020 |
| 46 | 3569.22803 | 0.332 | 16.729 | 0.020 |
| 47 | 3569.23730 | 0.348 | 16.717 | 0.021 |
| 48 | 3622.10132 | 0.741 | 16.818 | 0.021 |
| 49 | 3622.11084 | 0.756 | 16.855 | 0.020 |
| 50 | 3622.16479 | 0.844 | 16.866 | 0.022 |
| 51 | 3622.17407 | 0.860 | 16.877 | 0.020 |
| 52 | 3622.18359 | 0.875 | 16.777 | 0.028 |
| 53 | 3622.22632 | 0.945 | 16.551 | 0.018 |
| 54 | 3622.23560 | 0.960 | 16.491 | 0.017 |
| 55 | 3622.24512 | 0.976 | 16.480 | 0.018 |
| 56 | 3622.25391 | 0.990 | 16.440 | 0.017 |

65. RR224735

| | Dayval | Phase | Vint | Vinterr |
|---|---|---|---|---|
| 1 | 1023.18201 | 0.233 | 13.424 | 0.005 |
| 2 | 1292.45093 | 0.993 | 13.626 | 0.007 |
| 3 | 1317.38159 | 0.708 | 13.451 | 0.006 |
| 4 | 1354.27820 | 0.962 | 13.607 | 0.005 |
| 5 | 1355.27551 | 0.591 | 13.605 | 0.005 |
| 6 | 1359.26404 | 0.105 | 13.570 | 0.006 |
| 7 | 1378.21094 | 0.046 | 13.664 | 0.006 |
| 8 | 1379.20825 | 0.675 | 13.474 | 0.005 |
| 9 | 1401.14648 | 0.501 | 13.658 | 0.006 |
| 10 | 1403.14111 | 0.759 | 13.406 | 0.005 |
| 11 | 1404.13831 | 0.388 | 13.509 | 0.005 |
| 12 | 1405.13562 | 0.016 | 13.679 | 0.006 |
| 13 | 1411.11890 | 0.788 | 13.400 | 0.005 |
| 14 | 1412.11597 | 0.416 | 13.512 | 0.007 |
| 15 | 1414.11047 | 0.673 | 13.487 | 0.006 |
| 16 | 1417.10217 | 0.559 | 13.679 | 0.009 |
| 17 | 1742.21436 | 0.515 | 13.666 | 0.007 |
| 18 | 1758.16943 | 0.571 | 13.608 | 0.006 |
| 19 | 2035.41577 | 0.359 | 13.476 | 0.006 |
| 20 | 2061.34375 | 0.702 | 13.463 | 0.006 |
| 21 | 2062.34106 | 0.331 | 13.447 | 0.006 |
| 22 | 2094.25146 | 0.443 | 13.616 | 0.007 |
| 23 | 2113.19800 | 0.384 | 13.535 | 0.007 |
| 24 | 2147.10352 | 0.754 | 13.421 | 0.007 |
| 25 | 3480.30835 | 0.922 | 13.556 | 0.011 |
| 26 | 3480.31421 | 0.937 | 13.613 | 0.016 |
| 27 | 3480.36035 | 0.059 | 13.627 | 0.010 |
| 28 | 3480.36621 | 0.074 | 13.601 | 0.010 |
| 29 | 3480.41211 | 0.195 | 13.433 | 0.010 |
| 30 | 3480.41821 | 0.211 | 13.420 | 0.010 |
| 31 | 3480.47241 | 0.354 | 13.454 | 0.012 |
| 32 | 3480.47827 | 0.369 | 13.445 | 0.015 |

66. RR230520

| | Dayval | Phase | Vint | Vinterr |
|---|---|---|---|---|
| 1 | 1023.19440 | 0.297 | 17.089 | 0.052 |
| 2 | 1055.10547 | 0.396 | 17.296 | 0.051 |
| 3 | 1354.29053 | 0.236 | 17.009 | 0.043 |
| 4 | 1355.28784 | 0.145 | 16.773 | 0.040 |
| 5 | 1359.27649 | 0.782 | 17.422 | 0.096 |
| 6 | 1378.22327 | 0.059 | 16.508 | 0.033 |
| 7 | 1379.22058 | 0.969 | 16.500 | 0.042 |
| 8 | 1401.15881 | 0.973 | 16.475 | 0.037 |
| 9 | 1403.15344 | 0.792 | 17.497 | 0.070 |
| 10 | 1404.15076 | 0.702 | 17.420 | 0.078 |
| 11 | 1411.13123 | 0.067 | 16.497 | 0.037 |
| 12 | 1412.12830 | 0.976 | 16.420 | 0.039 |
| 13 | 1414.12292 | 0.795 | 17.452 | 0.087 |
| 14 | 1417.11450 | 0.523 | 17.671 | 0.162 |
| 15 | 2035.42822 | 0.388 | 17.240 | 0.075 |
| 16 | 2061.35620 | 0.031 | 16.374 | 0.041 |
| 17 | 2062.35327 | 0.941 | 17.211 | 0.068 |
| 18 | 2094.26367 | 0.038 | 16.445 | 0.046 |
| 19 | 2113.21045 | 0.315 | 17.090 | 0.075 |
| 20 | 2121.18799 | 0.589 | 17.493 | 0.124 |
| 21 | 2147.11572 | 0.232 | 17.022 | 0.097 |
| 22 | 3174.15967 | 0.679 | 17.394 | 0.031 |
| 23 | 3174.17480 | 0.709 | 17.392 | 0.031 |
| 24 | 3174.22119 | 0.797 | 17.401 | 0.029 |
| 25 | 3174.23535 | 0.825 | 17.505 | 0.030 |
| 26 | 3174.31836 | 0.983 | 16.343 | 0.020 |
| 27 | 3174.33276 | 0.011 | 16.337 | 0.019 |
| 28 | 3174.40259 | 0.145 | 16.746 | 0.024 |
| 29 | 3174.42969 | 0.197 | 16.868 | 0.025 |
| 30 | 3174.46411 | 0.263 | 17.001 | 0.028 |
| 31 | 3174.47852 | 0.290 | 17.127 | 0.030 |
| 32 | 3180.13379 | 0.118 | 16.718 | 0.022 |
| 33 | 3180.14819 | 0.146 | 16.795 | 0.020 |
| 34 | 3180.22754 | 0.297 | 17.112 | 0.023 |
| 35 | 3180.29053 | 0.418 | 17.292 | 0.027 |
| 36 | 3180.30493 | 0.446 | 17.298 | 0.027 |
| 37 | 3180.35522 | 0.542 | 17.349 | 0.027 |
| 38 | 3180.36938 | 0.569 | 17.433 | 0.028 |
| 39 | 3180.42285 | 0.672 | 17.410 | 0.031 |
| 40 | 3180.43726 | 0.699 | 17.460 | 0.031 |
| 41 | 3503.36011 | 0.989 | 16.373 | 0.027 |
| 42 | 3503.37427 | 0.016 | 16.281 | 0.033 |

67. RR232138

| | Dayval | Phase | Vint | Vinterr |
|---|---|---|---|---|
| 1 | 1023.20575 | 0.170 | 16.356 | 0.029 |
| 2 | 1055.11682 | 0.083 | 16.469 | 0.033 |
| 3 | 1317.40417 | 0.134 | 16.388 | 0.041 |
| 4 | 1354.30188 | 0.691 | 16.335 | 0.031 |
| 5 | 1355.29919 | 0.220 | 16.300 | 0.032 |
| 6 | 1359.28784 | 0.333 | 16.412 | 0.048 |
| 7 | 1378.23462 | 0.374 | 16.475 | 0.033 |
| 8 | 1379.23193 | 0.903 | 16.542 | 0.038 |
| 9 | 1401.17017 | 0.529 | 16.614 | 0.039 |
| 10 | 1403.16479 | 0.587 | 16.434 | 0.037 |
| 11 | 1405.15906 | 0.643 | 16.411 | 0.035 |
| 12 | 1411.14258 | 0.815 | 16.371 | 0.035 |
| 13 | 1412.13965 | 0.343 | 16.391 | 0.043 |
| 14 | 1413.13672 | 0.871 | 16.495 | 0.034 |
| 15 | 1417.12585 | 0.986 | 16.719 | 0.082 |
| 16 | 1435.07605 | 0.500 | 16.630 | 0.041 |
| 17 | 1742.23804 | 0.334 | 16.346 | 0.047 |
| 18 | 1758.19324 | 0.790 | 16.337 | 0.037 |
| 19 | 2035.43958 | 0.770 | 16.293 | 0.036 |
| 20 | 2061.36743 | 0.513 | 16.600 | 0.045 |
| 21 | 2062.36475 | 0.041 | 16.542 | 0.047 |
| 22 | 2094.27515 | 0.953 | 16.517 | 0.053 |
| 23 | 2096.26880 | 0.008 | 16.553 | 0.055 |
| 24 | 2110.22998 | 0.407 | 16.421 | 0.056 |
| 25 | 2113.22192 | 0.993 | 16.559 | 0.053 |
| 26 | 2121.19922 | 0.221 | 16.363 | 0.054 |
| 27 | 2147.12720 | 0.963 | 16.614 | 0.063 |
| 28 | 3540.10059 | 0.959 | 16.510 | 0.024 |
| 29 | 3540.11035 | 0.984 | 16.546 | 0.023 |
| 30 | 3540.17529 | 0.149 | 16.380 | 0.019 |
| 31 | 3540.18506 | 0.173 | 16.279 | 0.021 |

| | | | |
|---|---|---|---|
| 32 3540.26782 | 0.384 | 16.242 | 0.032 |
| 33 3540.27734 | 0.407 | 16.474 | 0.028 |
| 34 3545.09814 | 0.631 | 16.366 | 0.023 |
| 35 3545.10767 | 0.655 | 16.384 | 0.021 |
| 36 3545.17261 | 0.820 | 16.273 | 0.021 |
| 37 3545.18213 | 0.844 | 16.307 | 0.020 |
| 38 3545.23828 | 0.986 | 16.595 | 0.019 |
| 39 3545.24756 | 0.010 | 16.587 | 0.021 |
| 40 3569.27148 | 0.924 | 16.439 | 0.018 |
| 41 3569.28101 | 0.949 | 16.473 | 0.019 |
| 42 3569.30298 | 0.004 | 16.528 | 0.019 |
| 43 3569.31226 | 0.028 | 16.507 | 0.020 |
| 44 3569.33105 | 0.076 | 16.443 | 0.019 |
| 45 3569.34058 | 0.100 | 16.381 | 0.019 |
| 46 3569.35864 | 0.146 | 16.349 | 0.018 |
| 47 3569.36816 | 0.169 | 16.332 | 0.019 |
| 48 3569.38159 | 0.204 | 16.261 | 0.017 |
| 49 3569.39087 | 0.227 | 16.241 | 0.018 |
| 50 3569.40039 | 0.251 | 16.249 | 0.018 |
| 51 3569.41602 | 0.291 | 16.289 | 0.019 |

68. RR233207

| Dayval | Phase | Vint | Vinterr |
|---|---|---|---|
| 1 1023.21289 | 0.542 | 17.509 | 0.068 |
| 2 1055.12390 | 0.599 | 17.531 | 0.065 |
| 3 1317.41150 | 0.157 | 17.069 | 0.066 |
| 4 1354.30920 | 0.412 | 17.458 | 0.059 |
| 5 1355.30652 | 0.851 | 17.628 | 0.084 |
| 6 1359.29517 | 0.608 | 17.614 | 0.085 |
| 7 1377.24402 | 0.513 | 17.549 | 0.069 |
| 8 1378.24194 | 0.954 | 16.841 | 0.042 |
| 9 1379.23926 | 0.393 | 17.410 | 0.072 |
| 10 1401.17749 | 0.056 | 16.861 | 0.049 |
| 11 1403.17212 | 0.935 | 17.027 | 0.053 |
| 12 1404.16943 | 0.374 | 17.337 | 0.076 |
| 13 1405.16638 | 0.813 | 17.667 | 0.084 |
| 14 1410.15234 | 0.010 | 16.770 | 0.046 |
| 15 1411.14990 | 0.449 | 17.431 | 0.067 |
| 16 1412.14697 | 0.888 | 17.469 | 0.094 |
| 17 1413.14404 | 0.328 | 17.297 | 0.063 |
| 18 1414.14148 | 0.767 | 17.629 | 0.092 |
| 19 1416.13574 | 0.645 | 17.463 | 0.114 |
| 20 1417.13318 | 0.085 | 16.922 | 0.102 |
| 21 1418.13013 | 0.524 | 17.543 | 0.254 |
| 22 1435.08337 | 0.992 | 16.744 | 0.043 |
| 23 1742.24536 | 0.318 | 17.297 | 0.080 |
| 24 1758.20044 | 0.346 | 17.351 | 0.078 |
| 25 2035.44678 | 0.494 | 17.402 | 0.084 |
| 26 2061.37476 | 0.916 | 17.263 | 0.077 |
| 27 2062.37207 | 0.355 | 17.227 | 0.082 |
| 28 2094.28247 | 0.411 | 17.476 | 0.100 |
| 29 2096.27612 | 0.289 | 17.294 | 0.084 |
| 30 2110.23730 | 0.439 | 17.352 | 0.106 |
| 31 2113.22900 | 0.757 | 17.658 | 0.116 |
| 32 2121.20654 | 0.271 | 17.212 | 0.106 |
| 33 2123.20093 | 0.149 | 17.083 | 0.073 |
| 34 2124.19800 | 0.588 | 17.493 | 0.119 |
| 35 2125.19531 | 0.028 | 16.770 | 0.084 |
| 36 2147.13452 | 0.692 | 17.474 | 0.167 |
| 37 2500.16821 | 0.224 | 17.162 | 0.109 |
| 38 3174.28735 | 0.177 | 17.114 | 0.021 |
| 39 3174.30151 | 0.198 | 17.168 | 0.021 |
| 40 3174.37012 | 0.297 | 17.304 | 0.022 |
| 41 3174.38501 | 0.318 | 17.303 | 0.023 |
| 42 3174.44604 | 0.406 | 17.437 | 0.027 |
| 43 3174.49463 | 0.476 | 17.460 | 0.053 |
| 44 3175.23169 | 0.540 | 17.520 | 0.028 |
| 45 3157.24707 | 0.583 | 17.462 | 0.028 |
| 46 3175.29736 | 0.635 | 17.501 | 0.028 |
| 47 3175.31177 | 0.656 | 17.518 | 0.031 |
| 48 3180.16553 | 0.661 | 17.540 | 0.033 |
| 49 3180.17993 | 0.682 | 17.530 | 0.029 |
| 50 3180.24316 | 0.773 | 17.636 | 0.027 |
| 51 3180.32397 | 0.890 | 17.541 | 0.028 |
| 52 3180.33838 | 0.910 | 17.387 | 0.027 |
| 53 3180.39185 | 0.988 | 16.741 | 0.018 |
| 54 3180.40625 | 0.009 | 16.719 | 0.017 |
| 55 3180.45435 | 0.078 | 16.846 | 0.021 |
| 56 3180.46851 | 0.098 | 16.941 | 0.024 |
| 57 3180.48291 | 0.119 | 16.981 | 0.023 |
| 58 3487.34204 | 0.007 | 16.688 | 0.019 |
| 59 3487.35620 | 0.028 | 16.743 | 0.017 |
| 60 3487.40723 | 0.101 | 16.918 | 0.018 |
| 61 3487.42139 | 0.122 | 16.947 | 0.019 |

69. RR235226

| Dayval | Phase | Vint | Vinterr |
|---|---|---|---|
| 1 1023.22705 | 0.316 | 17.569 | 0.065 |
| 2 1055.13806 | 0.476 | 17.699 | 0.077 |
| 3 1317.42566 | 0.641 | 17.810 | 0.104 |
| 4 1354.32336 | 0.265 | 17.493 | 0.061 |
| 5 1355.32068 | 0.958 | 17.298 | 0.058 |
| 6 1377.25818 | 0.191 | 17.436 | 0.061 |
| 7 1378.25610 | 0.885 | 17.667 | 0.085 |
| 8 1379.25342 | 0.578 | 17.738 | 0.099 |
| 9 1401.19165 | 0.812 | 17.834 | 0.110 |
| 10 1403.18628 | 0.198 | 17.392 | 0.075 |
| 11 1404.18359 | 0.890 | 17.645 | 0.090 |
| 12 1405.18054 | 0.582 | 17.629 | 0.084 |
| 13 1410.16650 | 0.045 | 17.239 | 0.052 |
| 14 1411.16406 | 0.738 | 17.735 | 0.084 |
| 15 1412.16113 | 0.430 | 17.710 | 0.135 |
| 16 1413.15808 | 0.122 | 17.345 | 0.056 |
| 17 1414.15564 | 0.815 | 17.921 | 0.114 |
| 18 1416.14978 | 0.200 | 17.365 | 0.103 |
| 19 1417.14734 | 0.893 | 17.684 | 0.176 |
| 20 1418.14429 | 0.585 | 17.926 | 0.290 |
| 21 1432.10571 | 0.281 | 17.592 | 0.085 |
| 22 1435.09753 | 0.359 | 17.623 | 0.077 |
| 23 1442.07812 | 0.206 | 17.422 | 0.077 |
| 24 1742.25952 | 0.686 | 17.710 | 0.098 |
| 25 1758.21460 | 0.766 | 17.874 | 0.101 |
| 26 1768.18652 | 0.690 | 17.763 | 0.112 |
| 27 2035.46094 | 0.319 | 17.583 | 0.094 |
| 28 2061.38892 | 0.325 | 17.631 | 0.092 |
| 29 2062.38623 | 0.018 | 17.147 | 0.075 |
| 30 2063.38232 | 0.709 | 17.908 | 0.096 |
| 31 2094.29590 | 0.176 | 17.412 | 0.092 |
| 32 2096.29028 | 0.561 | 17.768 | 0.132 |
| 33 2110.25122 | 0.256 | 17.526 | 0.112 |
| 34 2113.24292 | 0.334 | 17.578 | 0.114 |
| 35 2121.22070 | 0.874 | 17.844 | 0.152 |
| 36 2123.21509 | 0.259 | 17.479 | 0.111 |
| 37 2124.21216 | 0.951 | 17.216 | 0.110 |
| 38 2125.20947 | 0.644 | 17.804 | 0.145 |
| 39 2170.08496 | 0.809 | 17.966 | 0.143 |
| 40 2500.18237 | 0.063 | 17.224 | 0.116 |
| 41 3232.19482 | 0.463 | 17.897 | 0.039 |
| 42 3232.21021 | 0.489 | 17.696 | 0.043 |
| 43 3232.23462 | 0.531 | 17.678 | 0.042 |
| 44 3232.24927 | 0.556 | 17.788 | 0.040 |
| 45 3245.10107 | 0.368 | 17.629 | 0.032 |
| 46 3245.11597 | 0.393 | 17.691 | 0.032 |
| 47 3245.17920 | 0.501 | 17.700 | 0.043 |
| 48 3245.19336 | 0.525 | 17.794 | 0.066 |
| 49 3246.18994 | 0.216 | 17.471 | 0.030 |
| 50 3246.20410 | 0.240 | 17.490 | 0.027 |
| 51 3246.25073 | 0.320 | 17.588 | 0.031 |
| 52 3246.26514 | 0.344 | 17.537 | 0.029 |
| 53 3247.10278 | 0.765 | 17.859 | 0.051 |
| 54 3247.11060 | 0.779 | 17.810 | 0.057 |
| 55 3273.05127 | 0.807 | 17.606 | 0.099 |
| 56 3273.06616 | 0.832 | 17.881 | 0.042 |
| 57 3273.15356 | 0.980 | 17.131 | 0.060 |
| 58 3273.18384 | 0.031 | 17.199 | 0.030 |
| 59 3273.23096 | 0.111 | 17.314 | 0.038 |
| 60 3273.24512 | 0.136 | 17.283 | 0.054 |
| 61 3485.36694 | 0.157 | 17.381 | 0.046 |
| 62 3485.38135 | 0.181 | 17.459 | 0.043 |
| 63 3545.26953 | 0.826 | 17.882 | 0.037 |
| 64 3545.28027 | 0.844 | 17.794 | 0.035 |
| 65 3545.37231 | 0.001 | 17.101 | 0.027 |
| 66 3545.38330 | 0.019 | 17.183 | 0.025 |
| 67 3545.45752 | 0.145 | 17.371 | 0.030 |
| 68 3545.46826 | 0.163 | 17.423 | 0.028 |

RA: 00 21 01.3

Dec: 28 05 18.0

<V> = 16.837

<B-V> = 0.60

P = 0.276682 days

Epoch = 3539.373

Type: W UMa

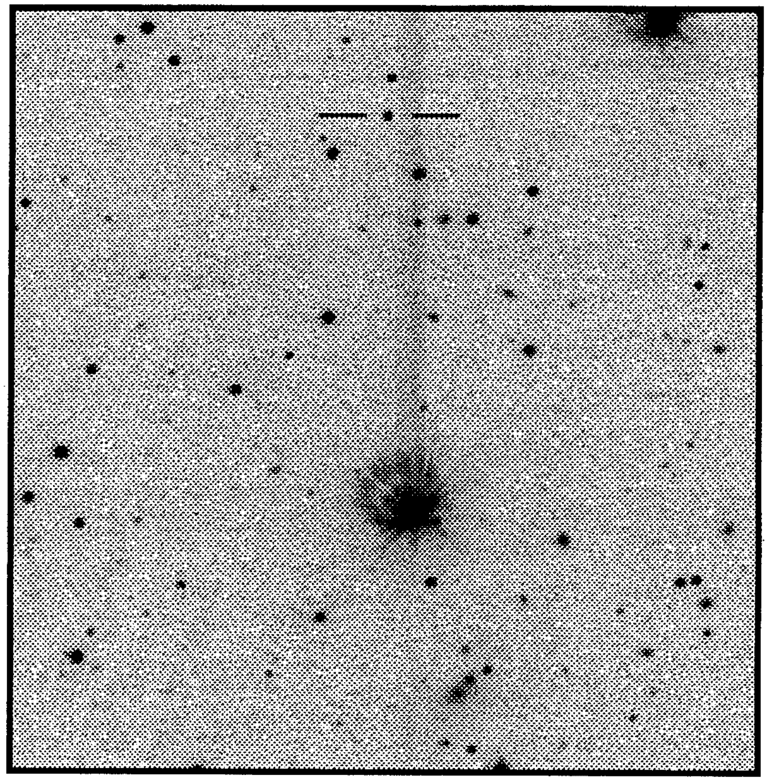

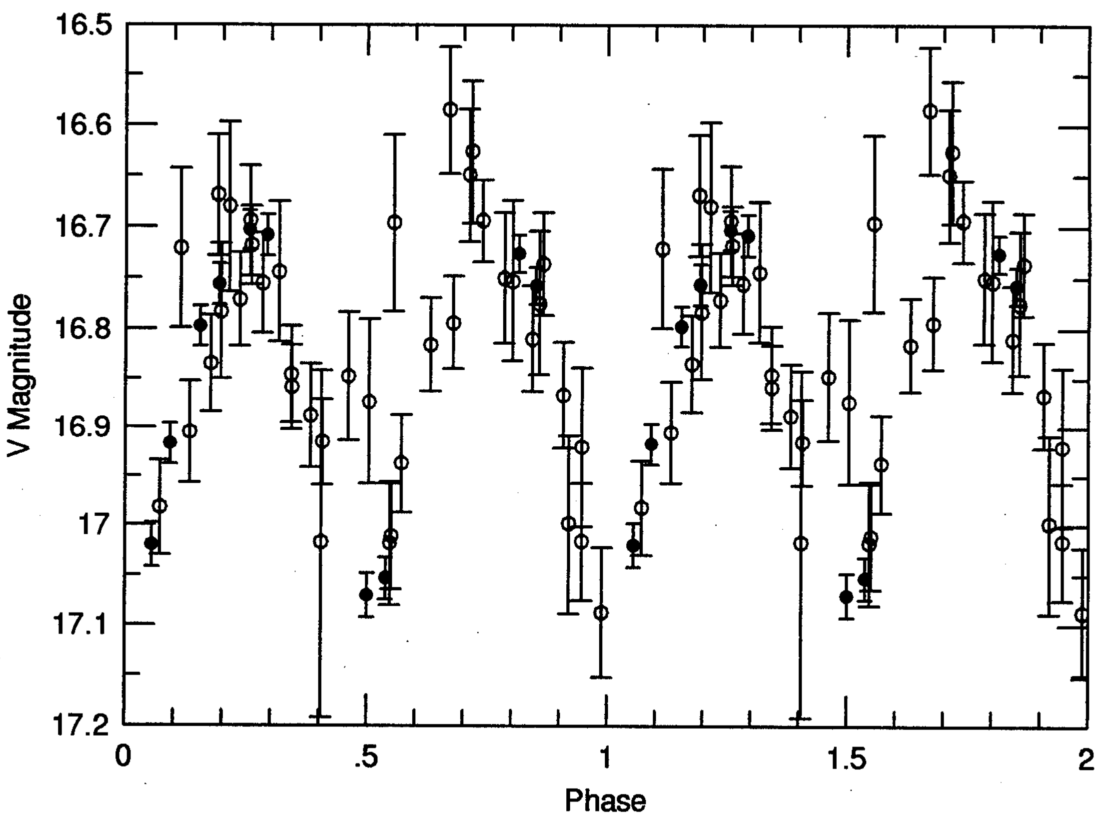

RA : 01 13 58.1
Dec: 28 02 47.1
<V> = 16.415
<B-V> = 0.47
P = 0.383472 days
Epoch = 3539.565
Type: W UMa

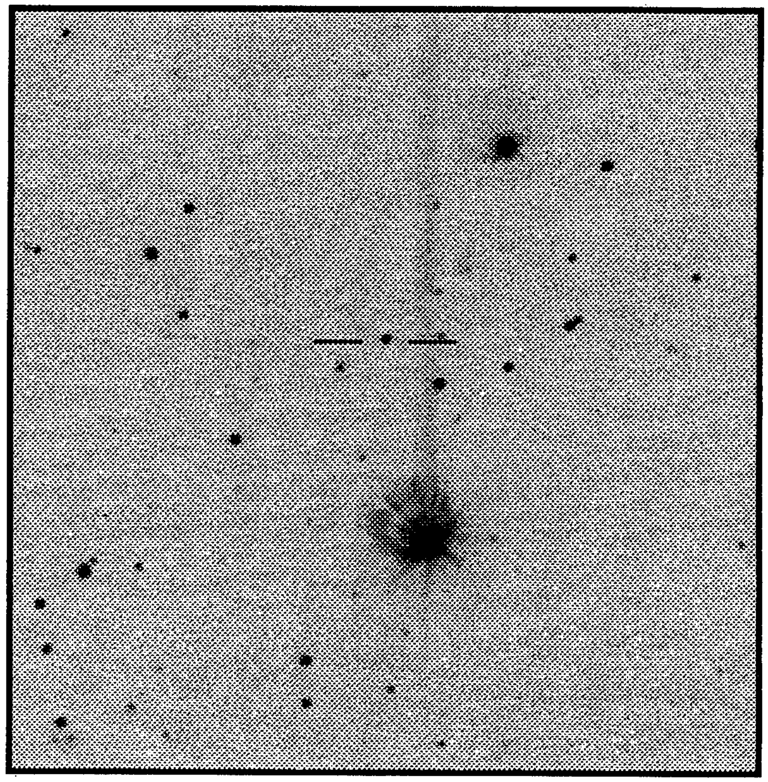

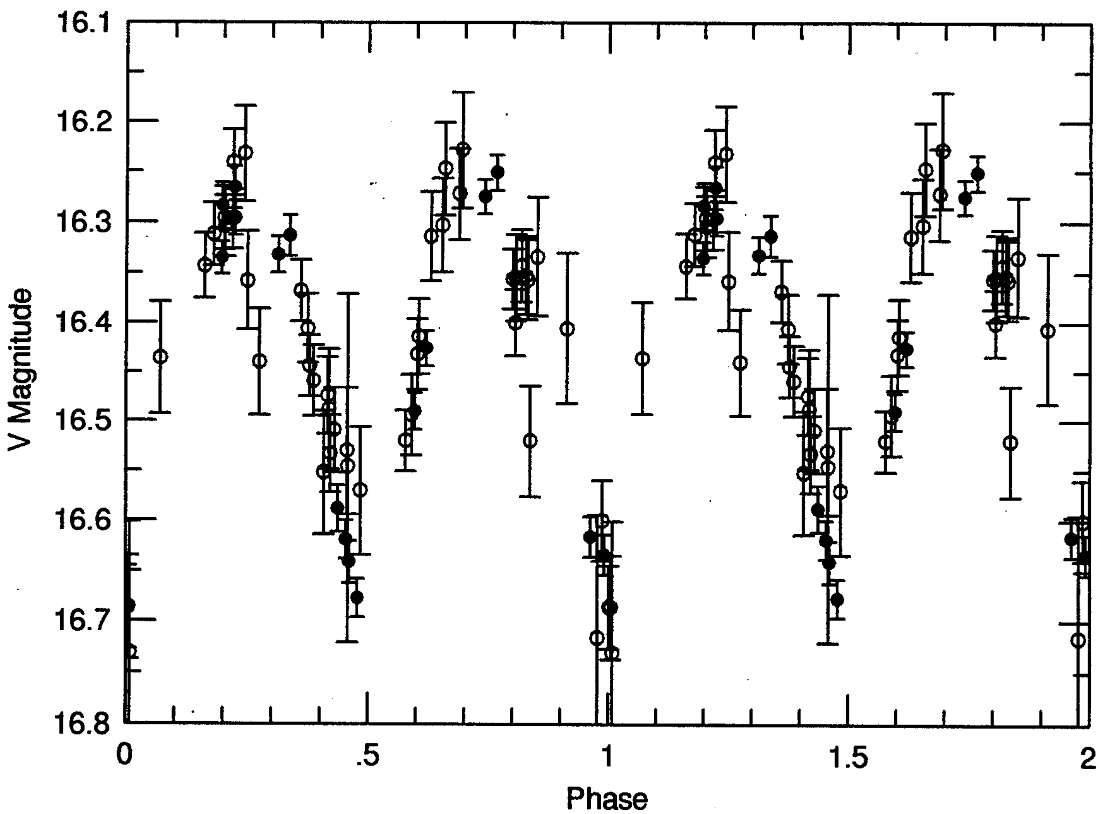

RA : 01 26 59.2

Dec: 28 03 54.3

<V> = 16.580

<B-V> = 0.80

P = 0.349120 days

Epoch = 3546.52

Type: W UMa

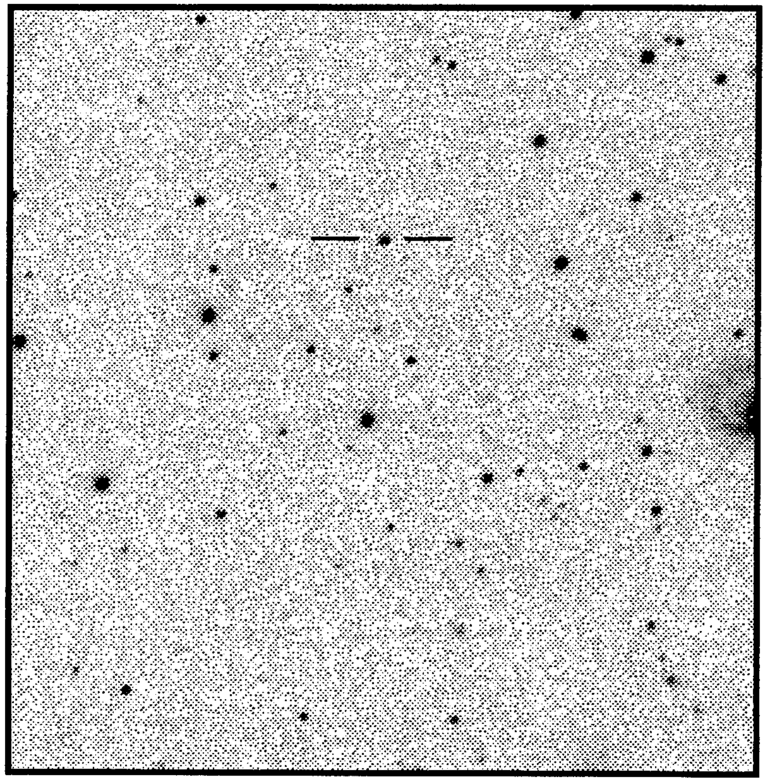

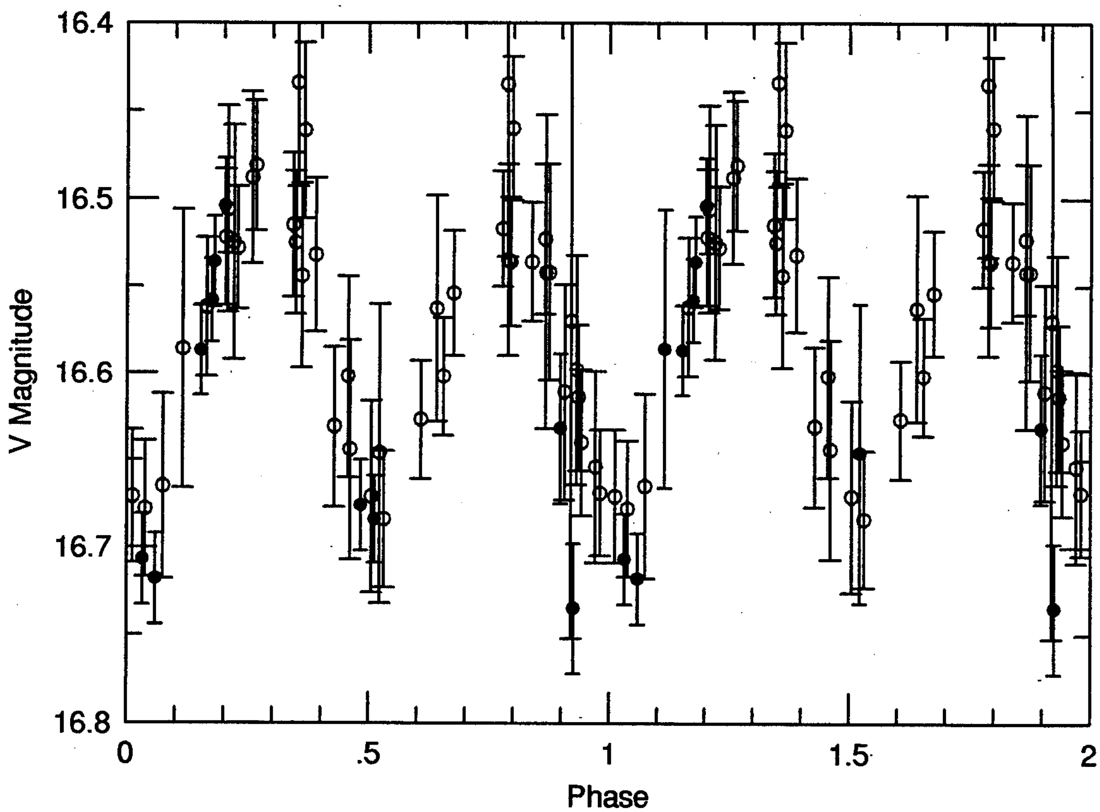

RA : 01 58 55.9

Dec: 27 58 09.5

<V> = 17.081

<B-V> = 0.20

P = 0.497854 days

Epoch = 3641.220

Type: RRab

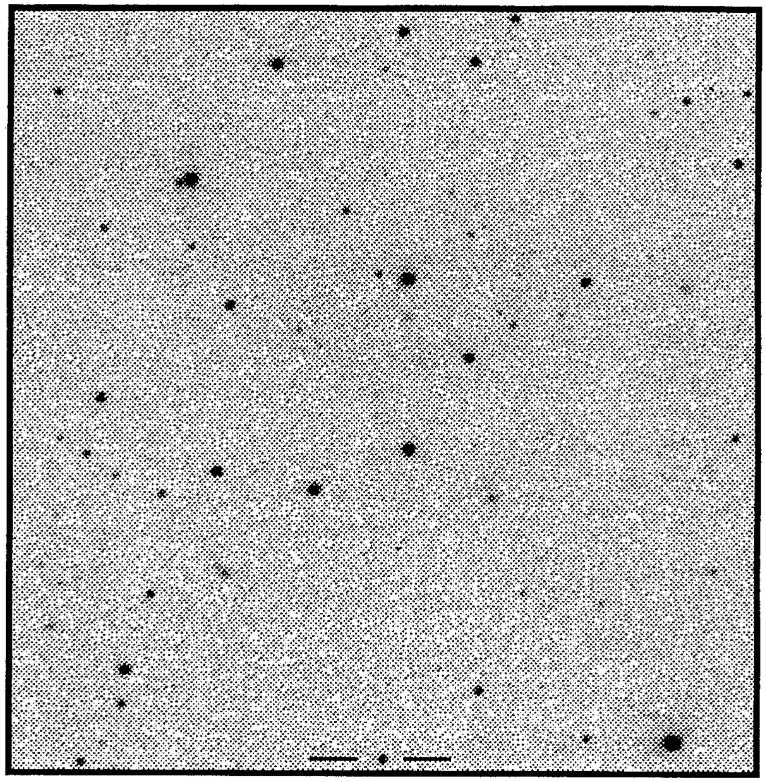

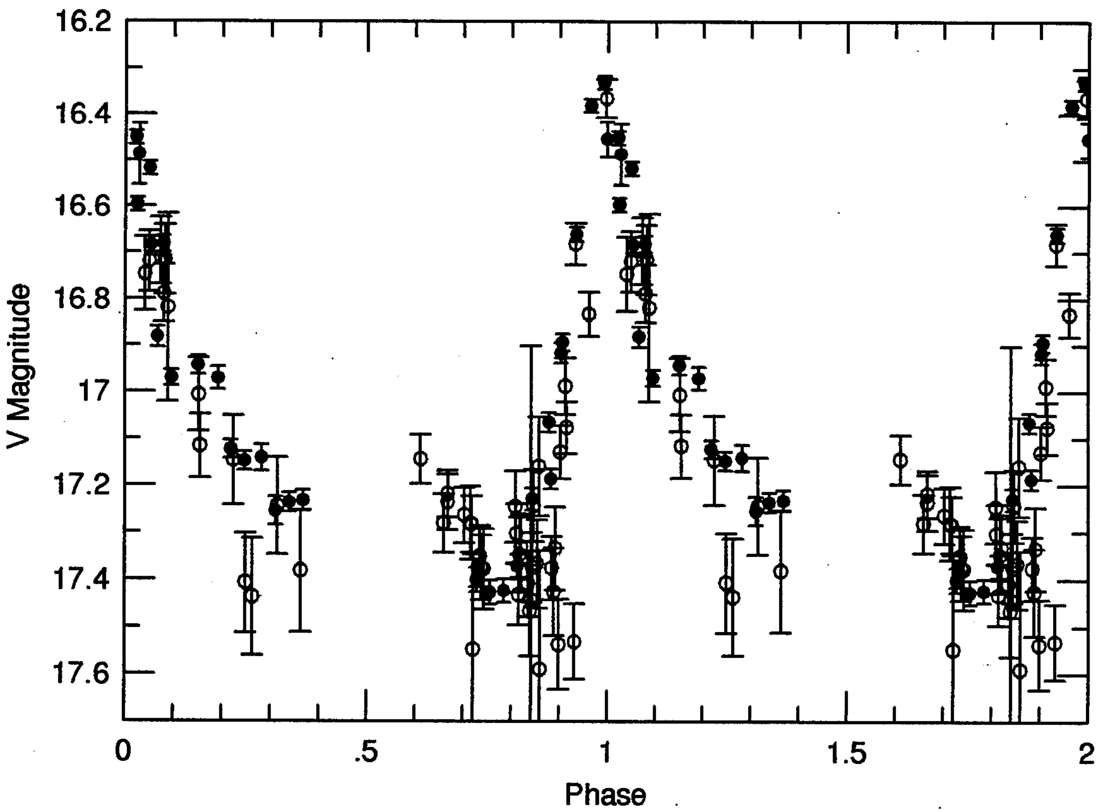

RA : 02 01 50.4
Dec: 28 04 22.6
<V> = 17.517
<B-V> = 0.40
P = 0.461291 days
Epoch = 3559.380
Type: RRab B

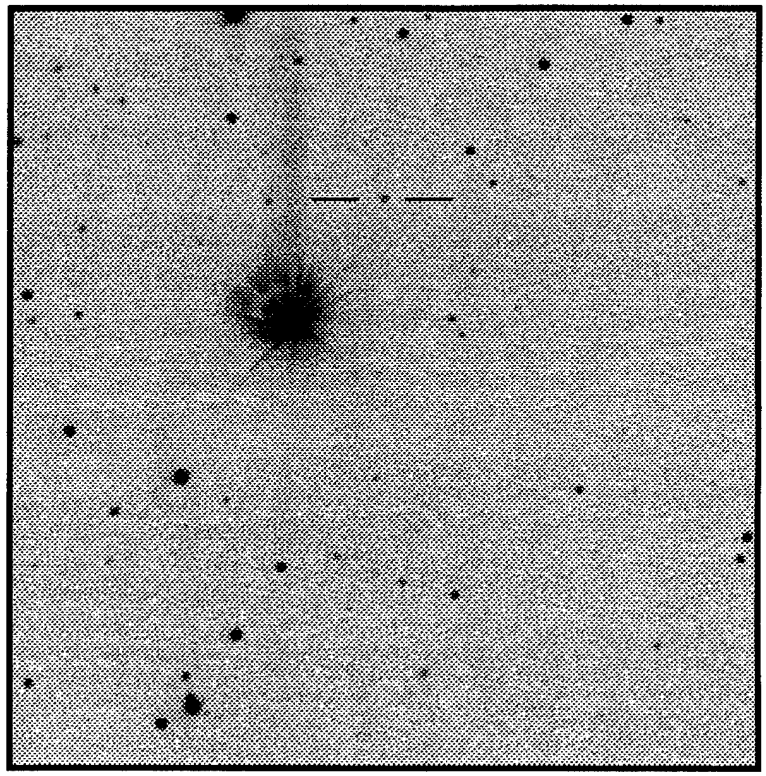

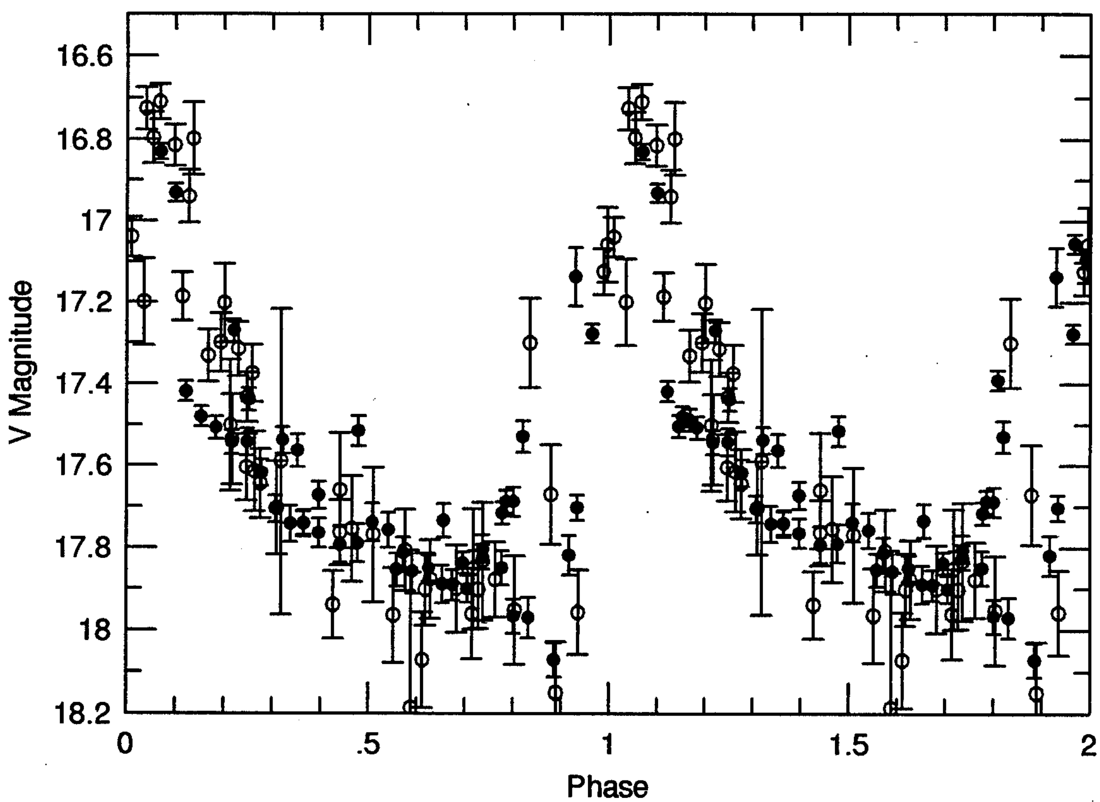

RA : 02 31 40.3

Dec: 27 59 47.3

<V> = 13.947

<B-V> = 0.78

P = 0.265461 days

Epoch = 3539.429

Type: W UMa

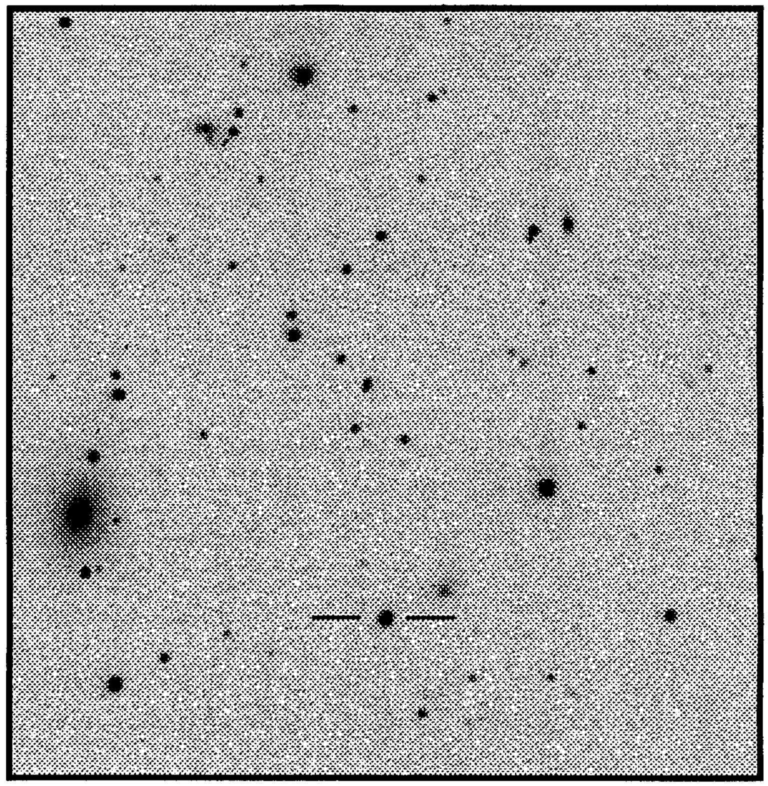

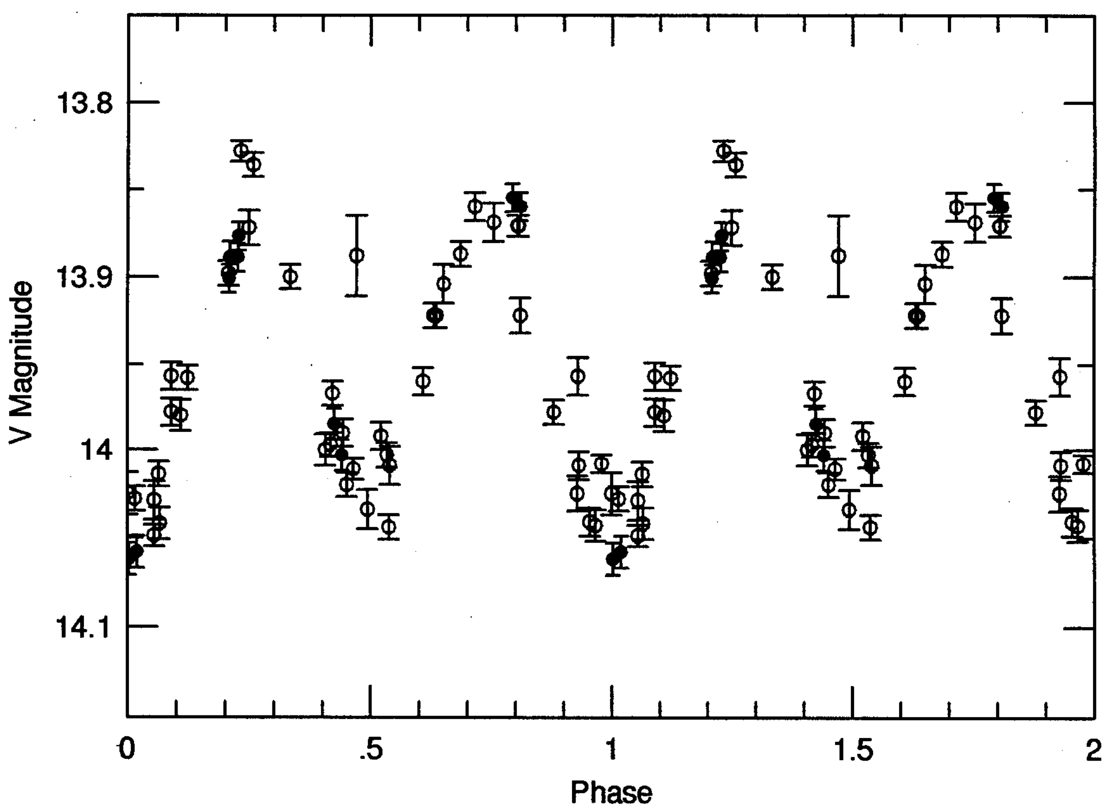

RA : 03 46 21.7

Dec: 28 01 24.7

<V> = 17.905

<B-V> = 0.45

P = 0.561891 days

Epoch = 3685.125

Type: RRab

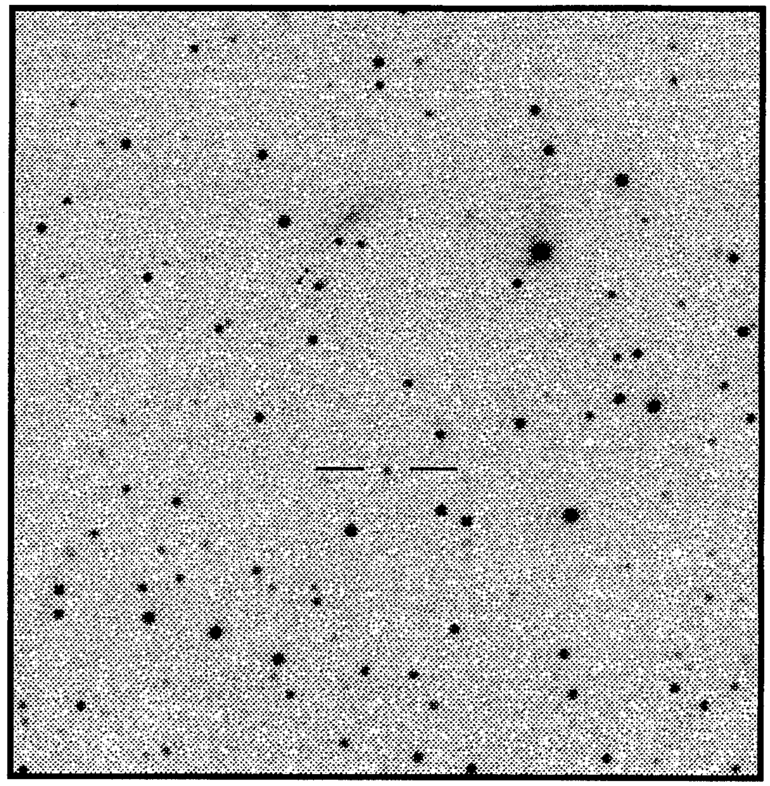

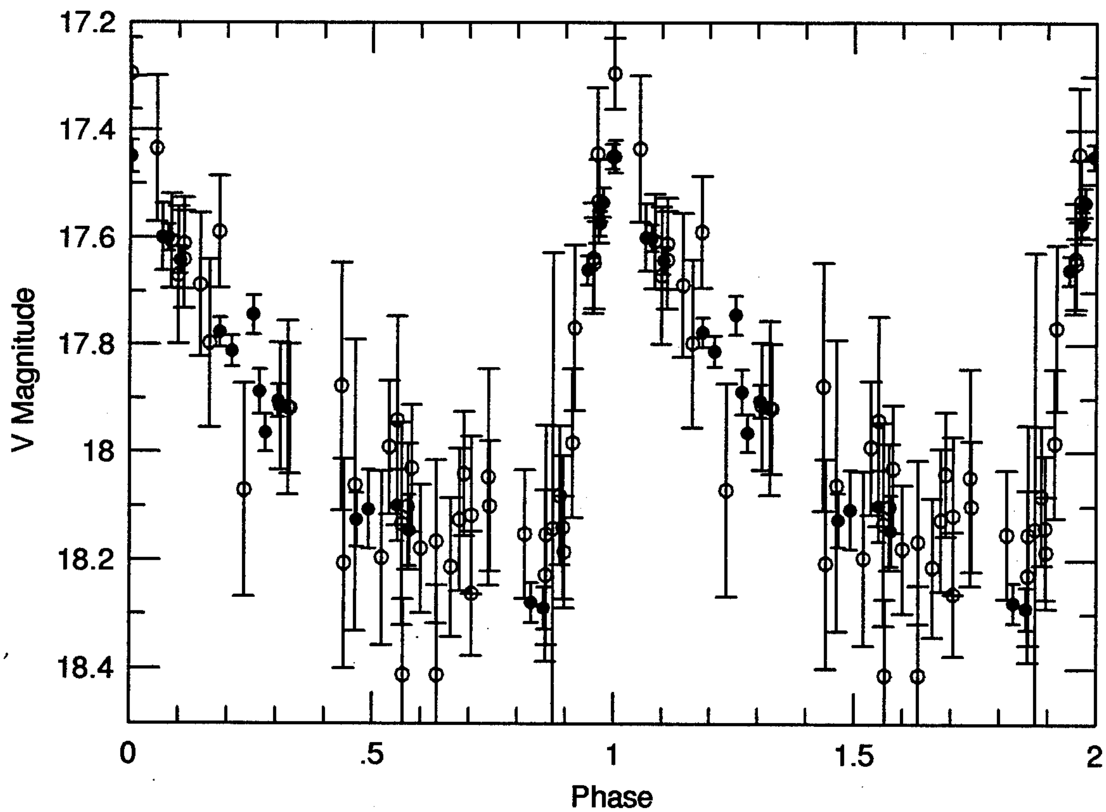

RA : 04 02 57.9
Dec: 28 01 30.5
<V> = 17.711
<B-V> = 0.60
P = 0.319400 days
Epoch = 3546.455
Type: W UMa

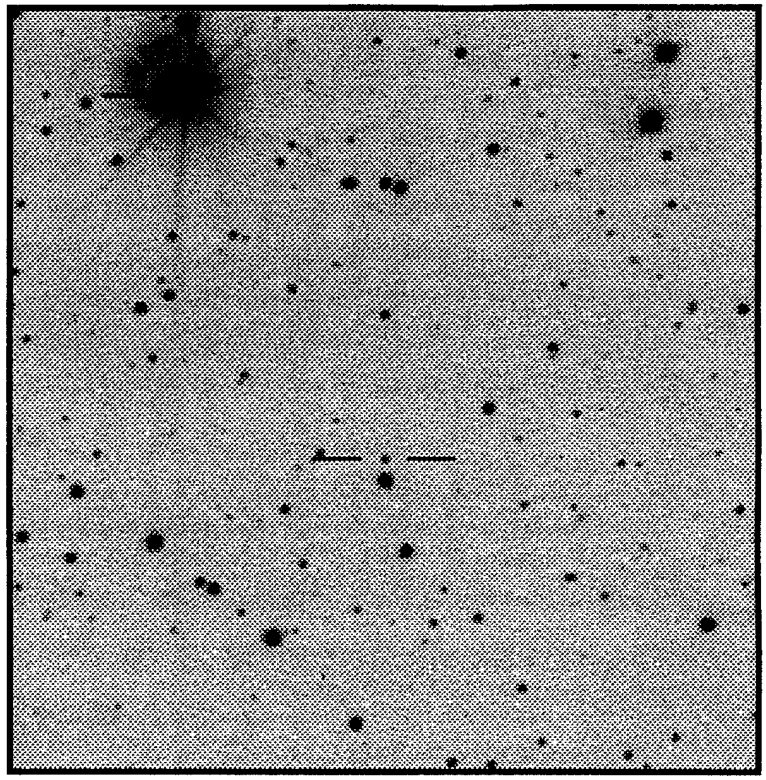

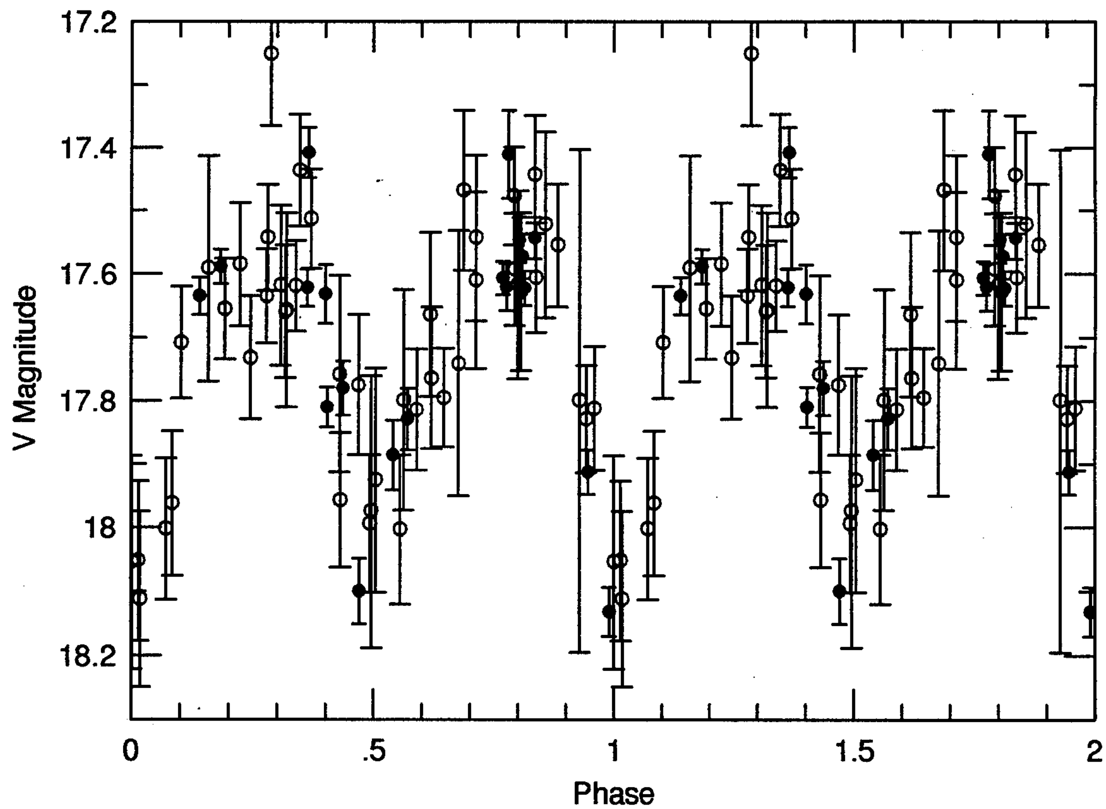

RA: 05 57 22.1
Dec: 28 02 31.0
<V> = 12.739
<B-V> = 0.80
P = 1.79325 days
Epoch = 3299.884
Type: Cepheid
CN Tau

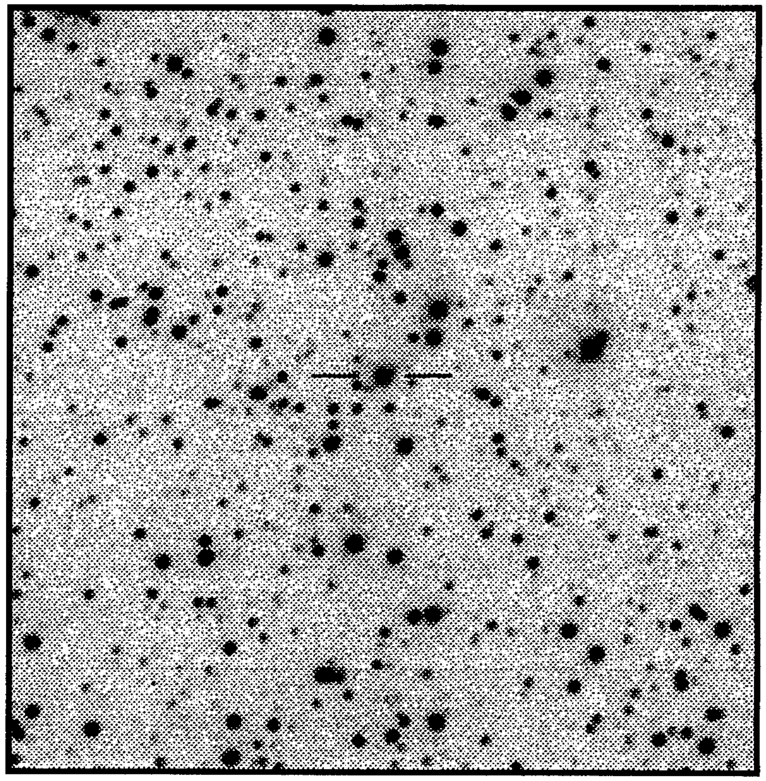

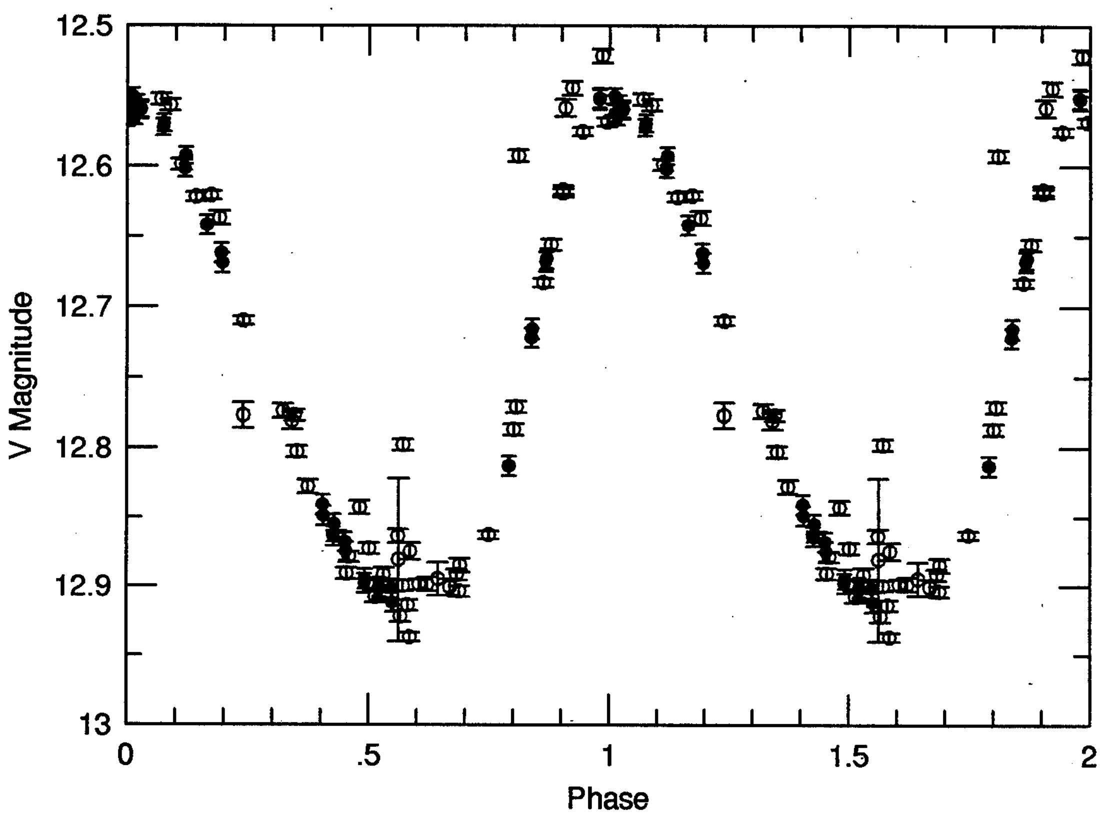

RA : 06 49 46.1

Dec: 28 04 59.5

<V> = 18.267

<B-V> = 0.75

P = 0.269392 days

Epoch = 3622.235

Type: W UMa

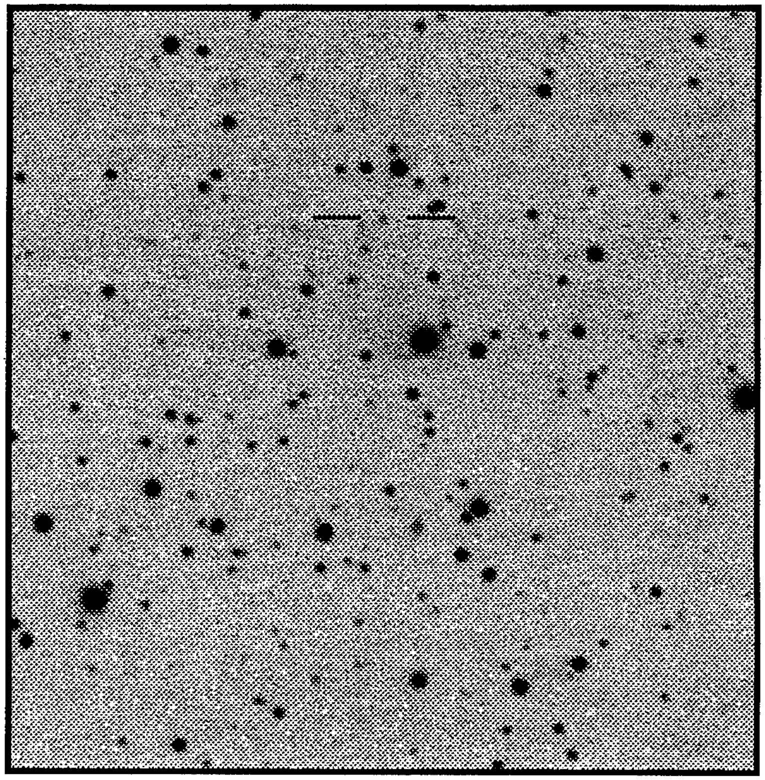

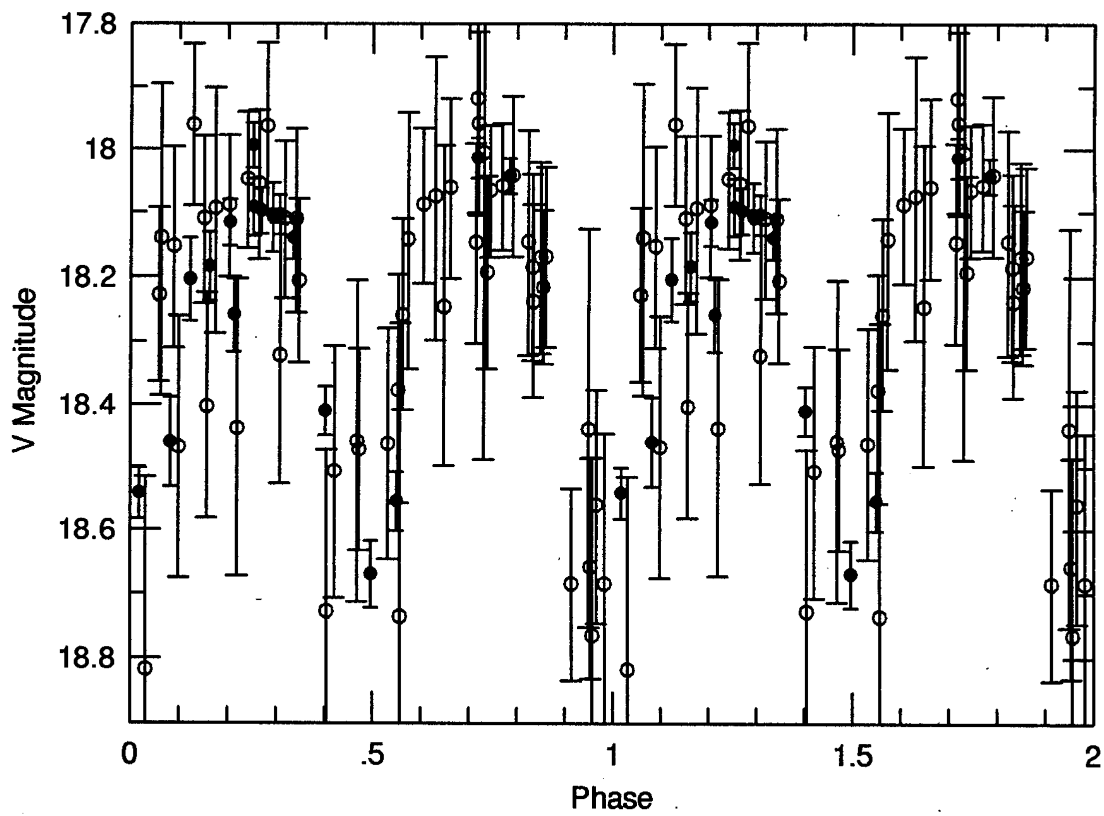

RA : 07 53 50.3

Dec: 28 01 58.2

<V> = 16.085

<B-V> = 0.33

P = 0.632536 days

Epoch = 3308.3

Type: RRab

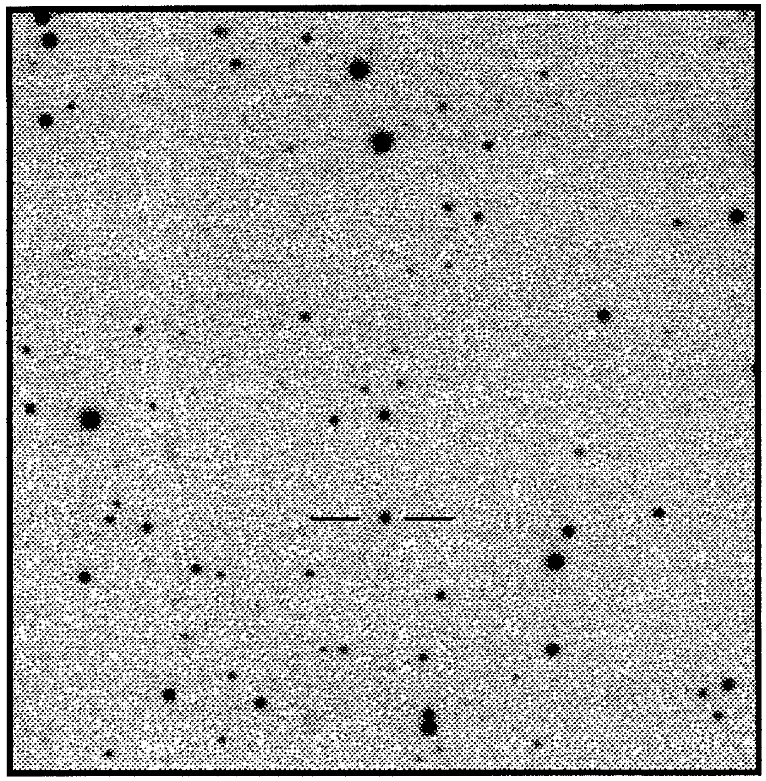

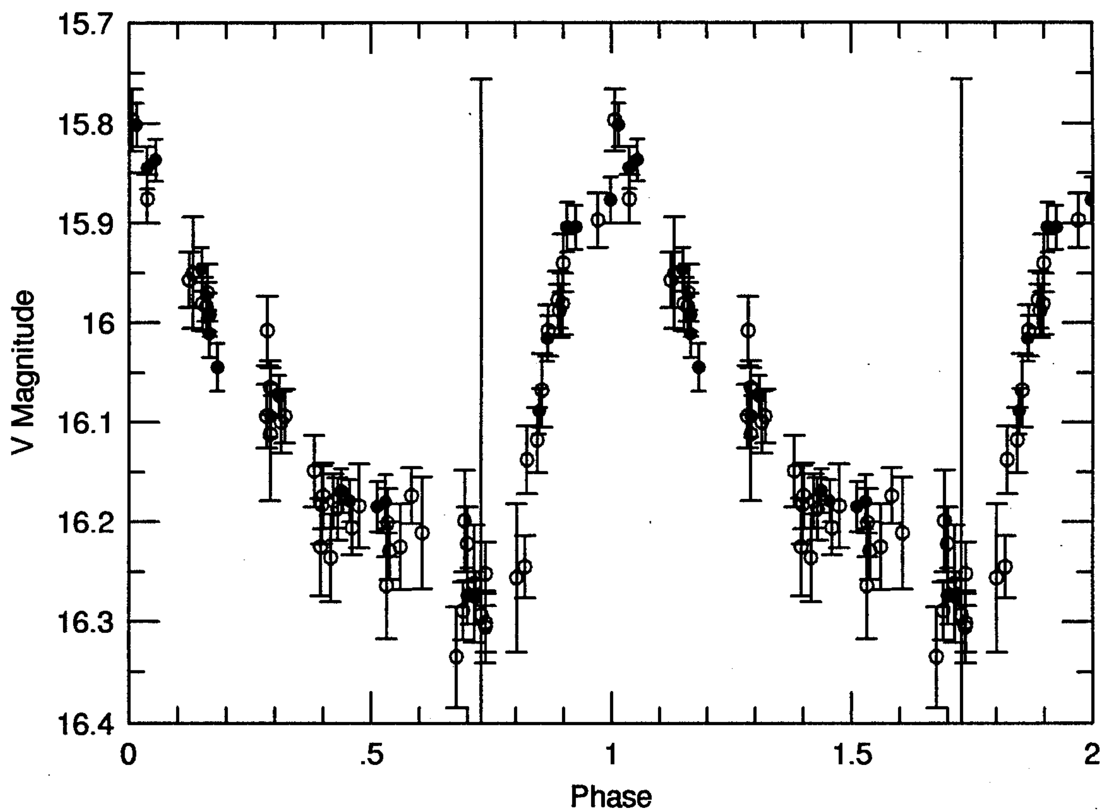

RA : 08 46 51.7

Dec: 28 02 45.3

<V> = 16.344

<B-V> = 0.21

P = 0.552704 days

Epoch = 3307.320

Type: RRab B

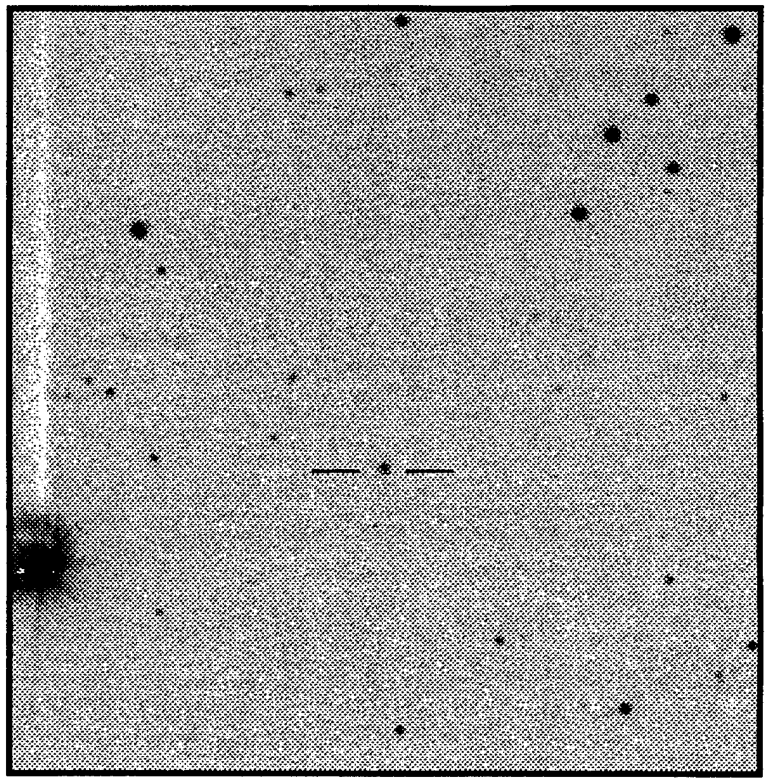

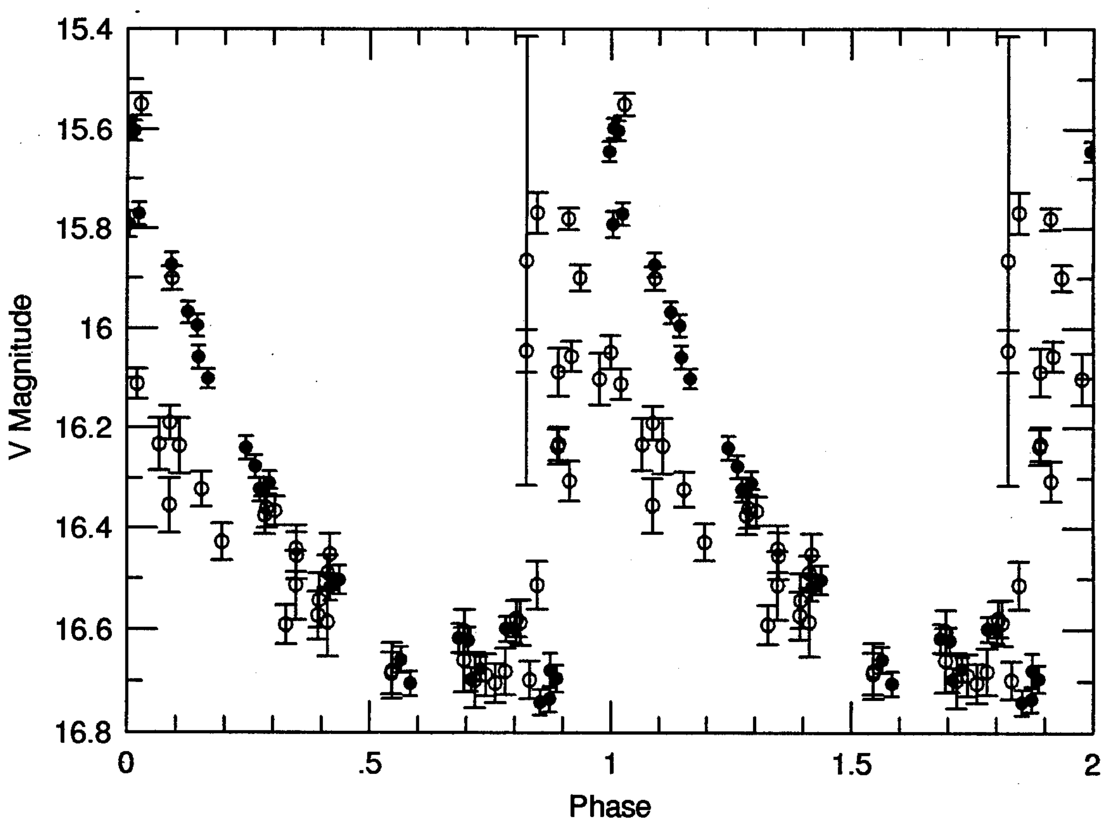

RA : 09 01 17.7
Dec: 28 01 31.3
<V> = 16.255
<B-V> = 0.30
P = 0.513581 days
Epoch = 3331.312
Type: RRab B

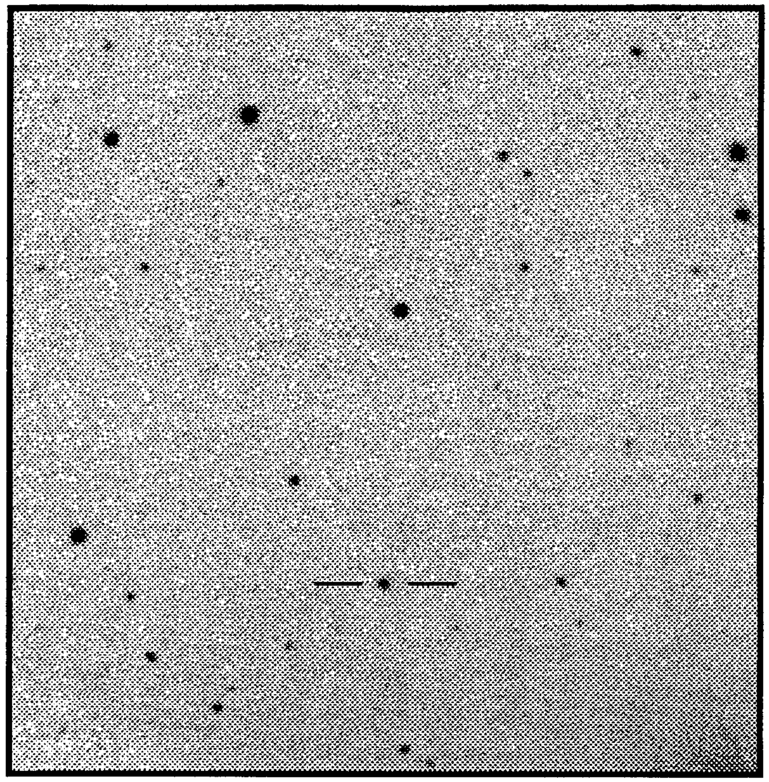

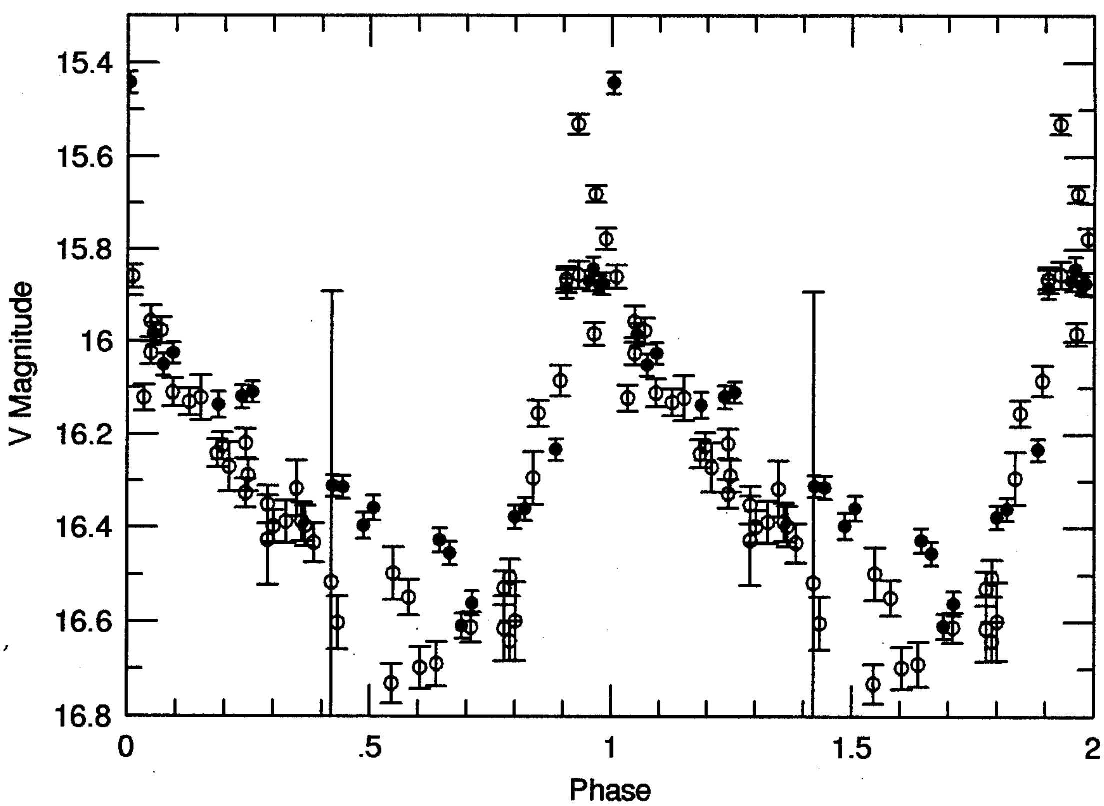

RA : 09 56 59.1

Dec: 28 02 02.6

<V> = 16.571

<B-V> = 0.07

P = 0.286813 days

Epoch = 3342.322

Type: RRc

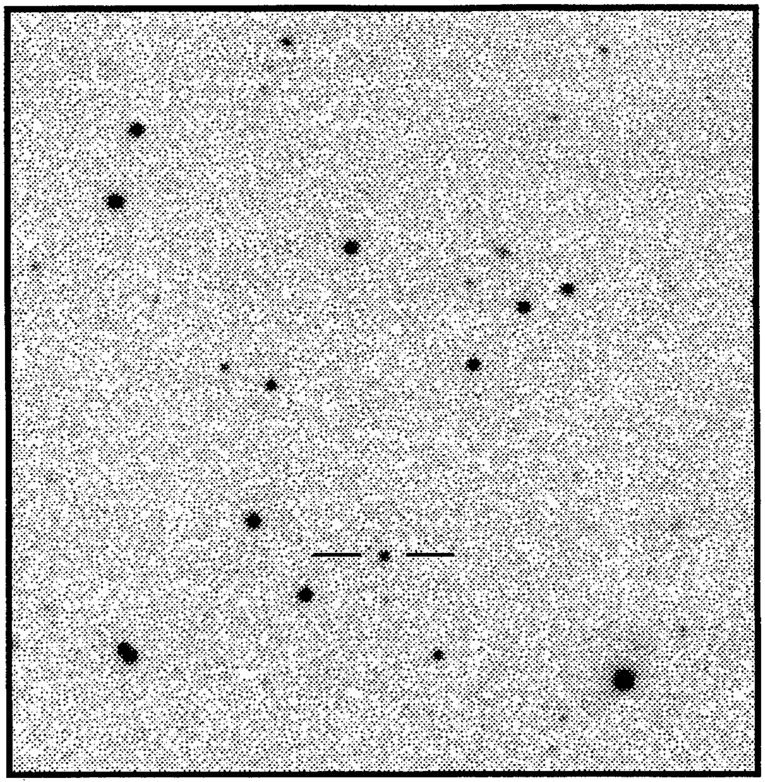

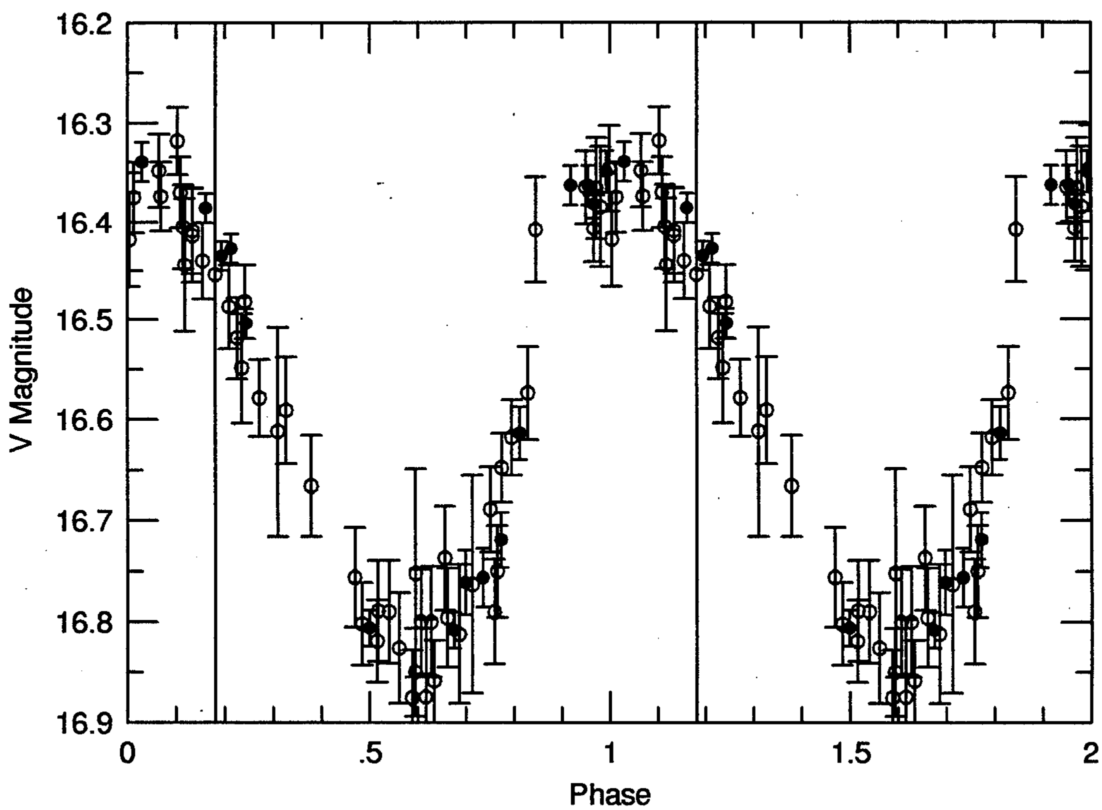

RA : 10 26 04.7
Dec: 28 02 51.5
<V> = 18.250
<B-V> = 0.32
P = 0.552801 days
Epoch = 3666.438
Type: RRab

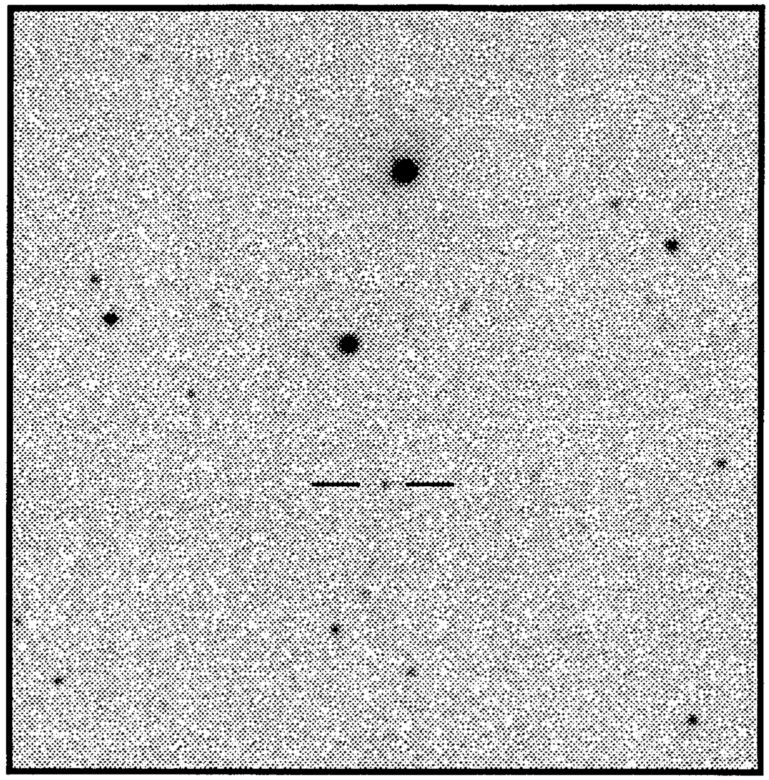

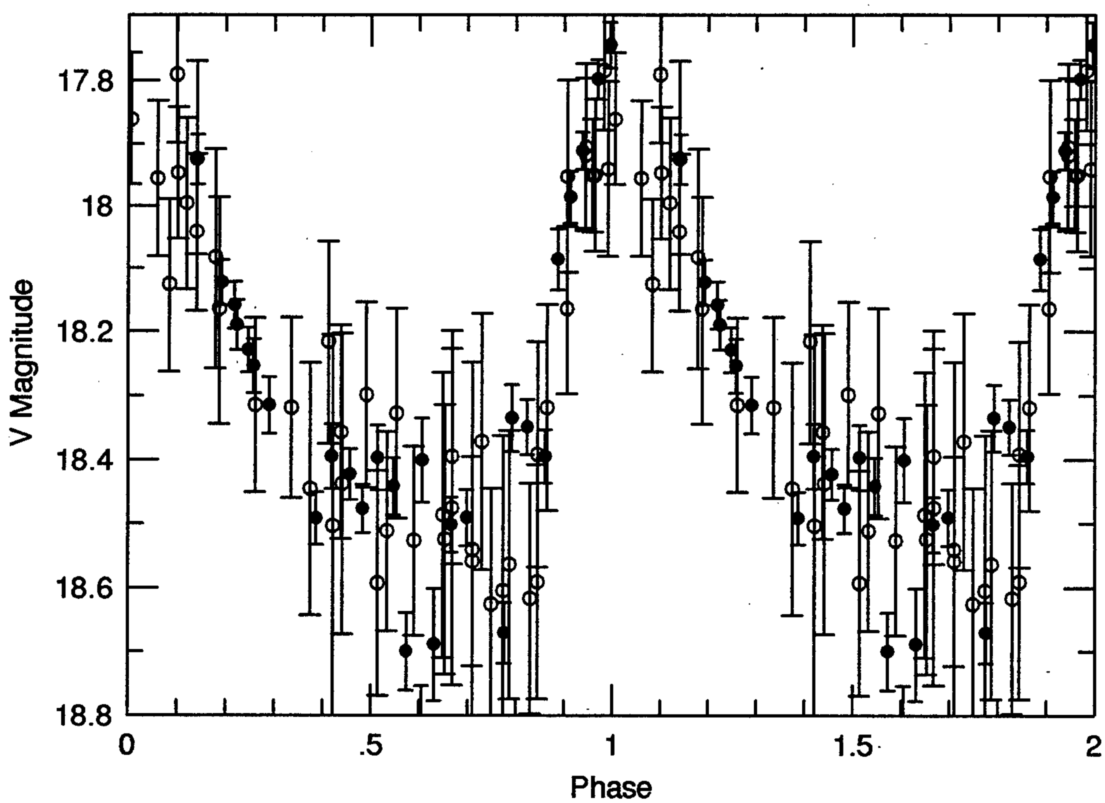

RA : 10 36 17.2
Dec: 27 59 07.7
<V> = 18.037
<B-V> = 0.24
P = 0.707095 days
Epoch = 3461.348
Type: RRab

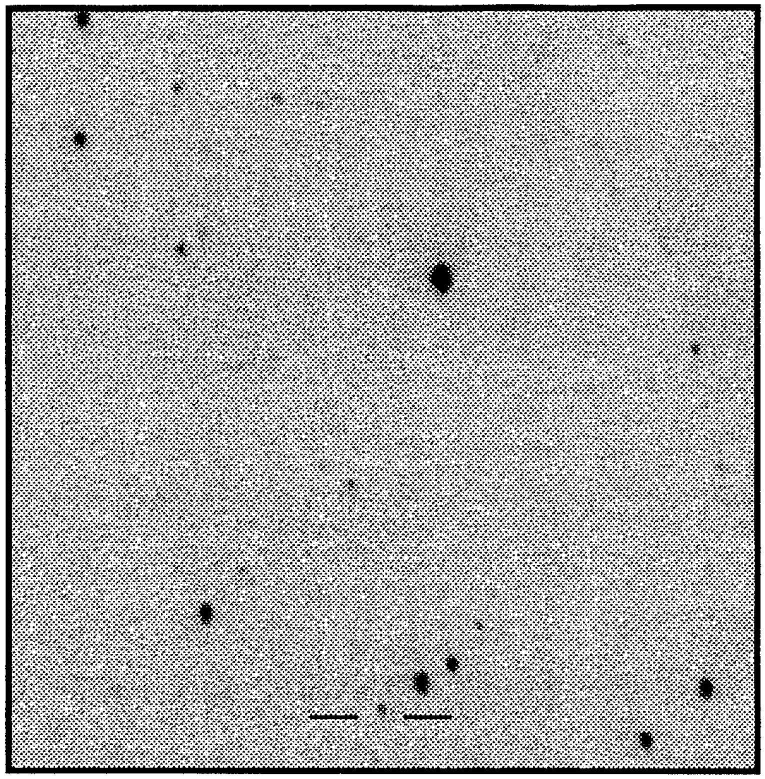

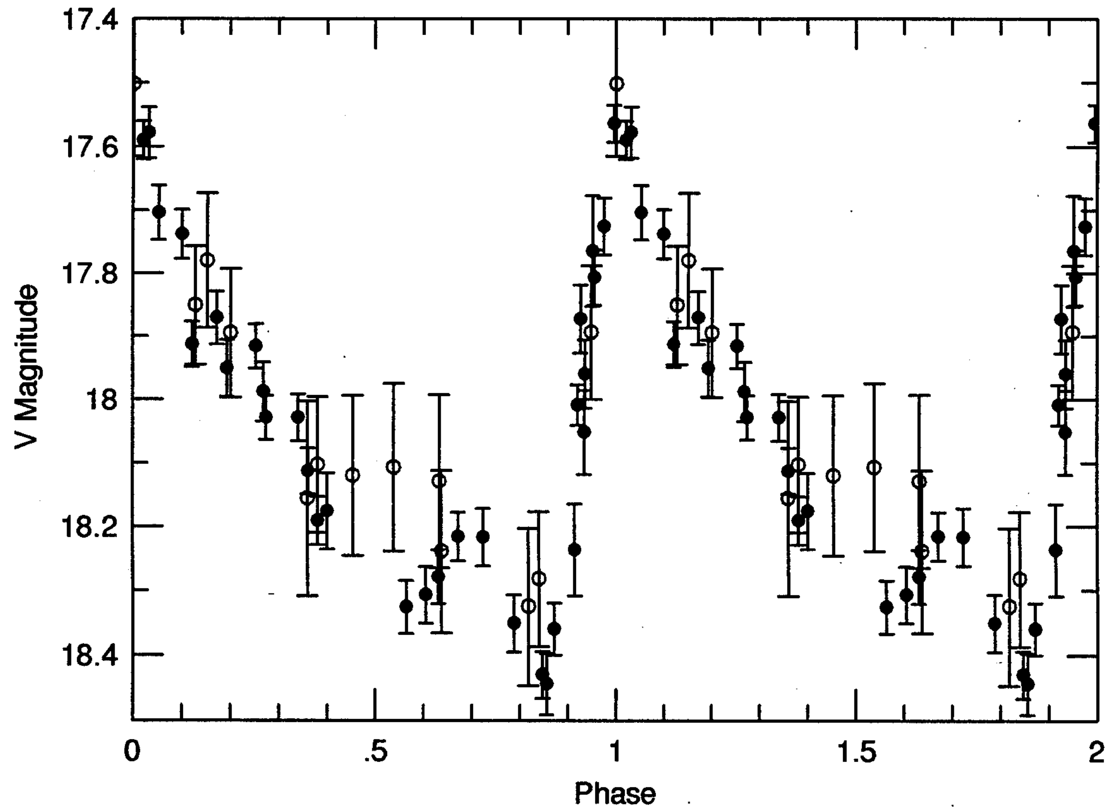

RA : 10 57 41.6
Dec: 28 02 46.0
<V> = 16.740
<B-V> = 0.12
P = 0.327640 days
Epoch = 3363.304
Type: RRc

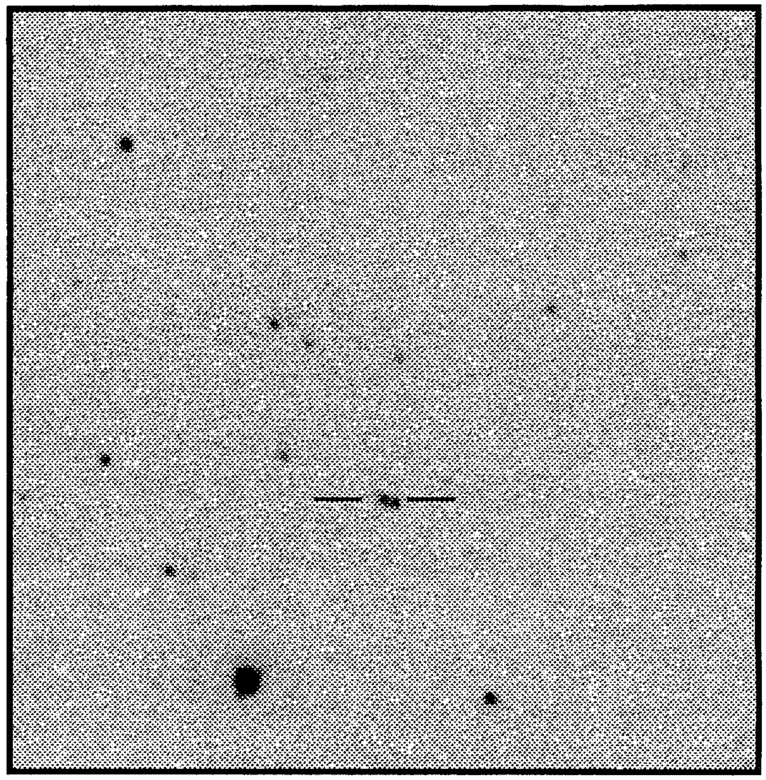

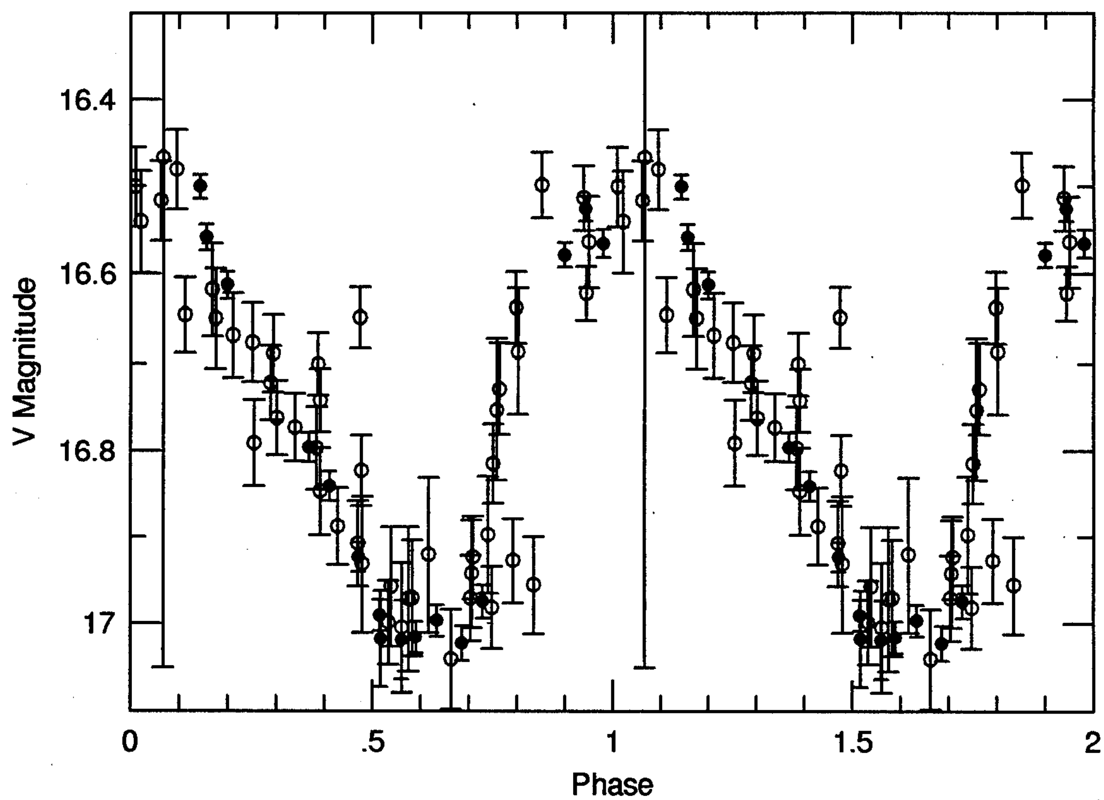

RA : 11 48 32.1
Dec: 28 04 36.1
<V> = 15.305
<B-V> = 0.36
P = 0.597821 days
Epoch = 3356.253
Type: RRab

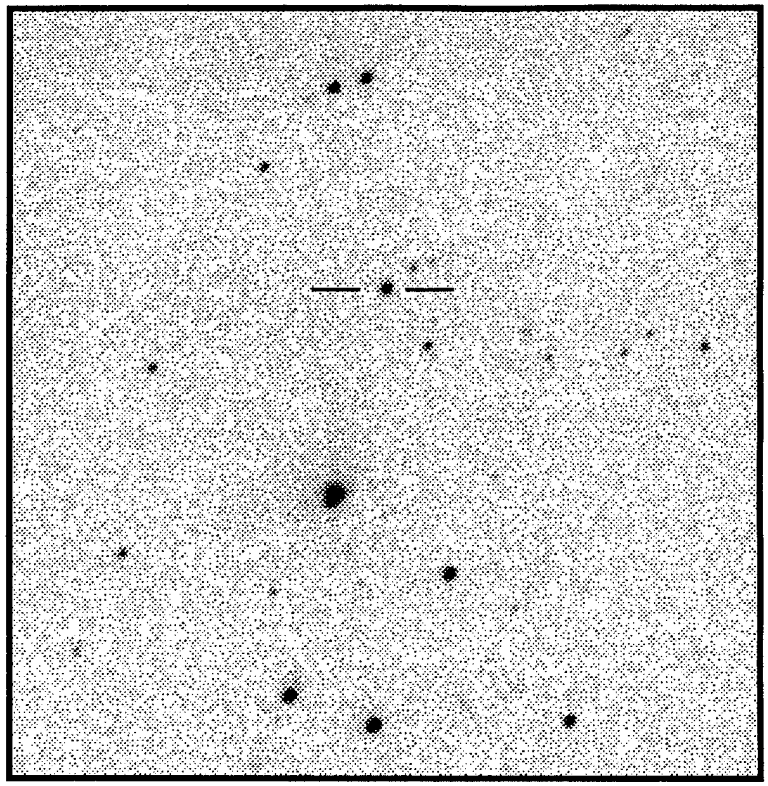

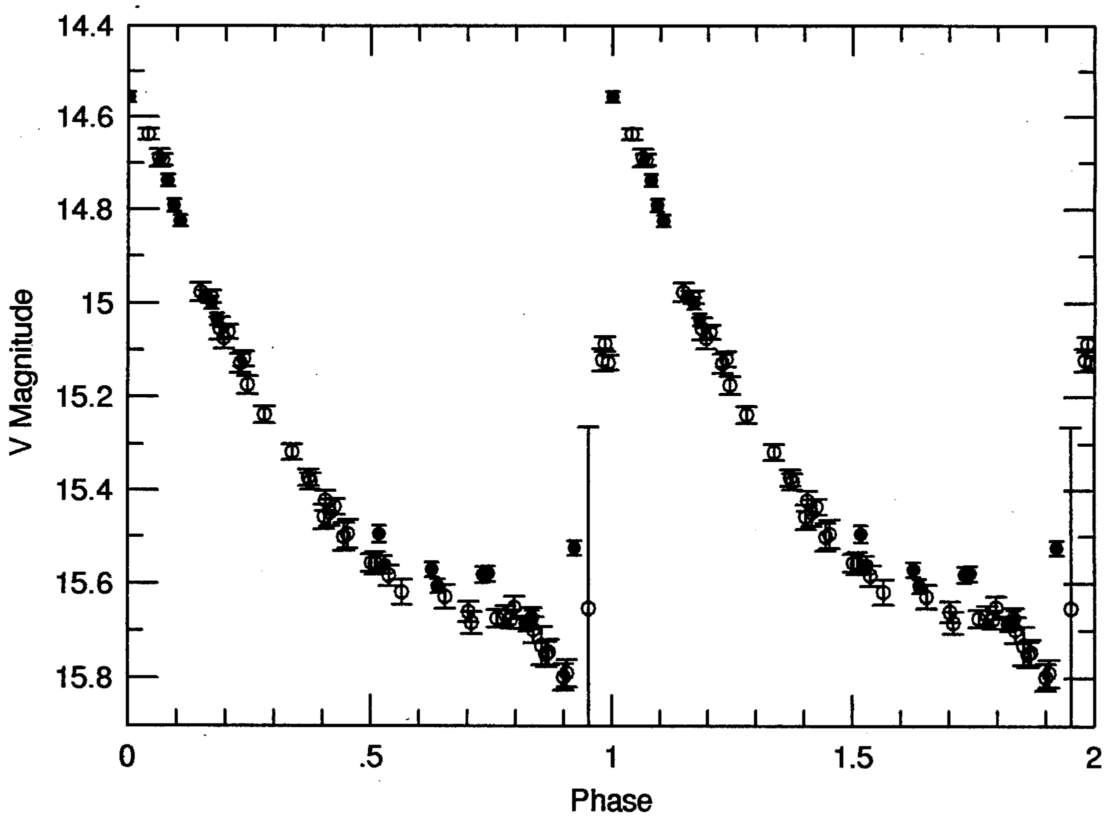

RA: 12 04 40.4

Dec: 28 01 08.5

<V> = 16.364

<B-V> = 0.20

P = 0.521823 days

Epoch = 3361.121

Type: RRab

GR Com

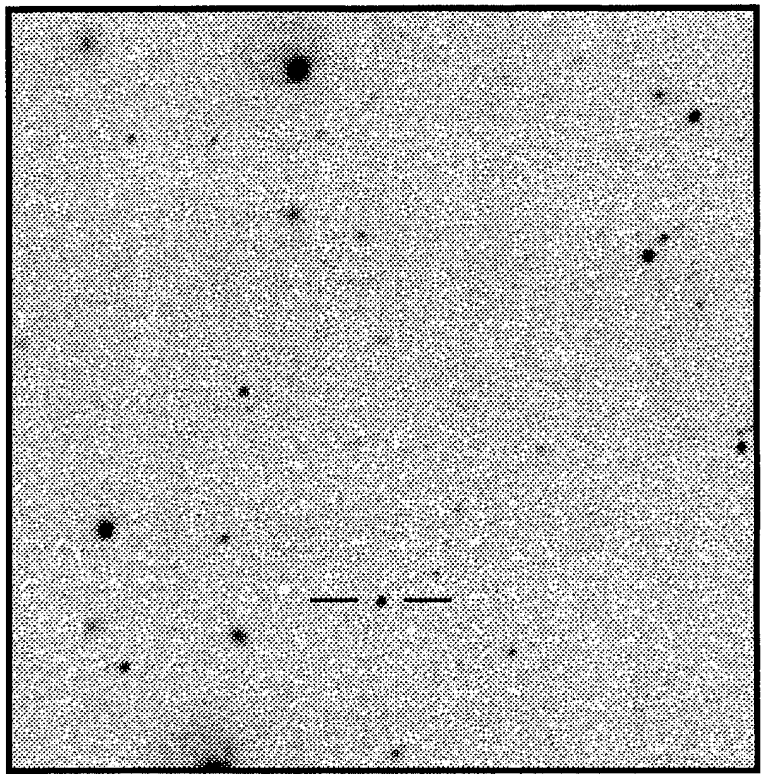

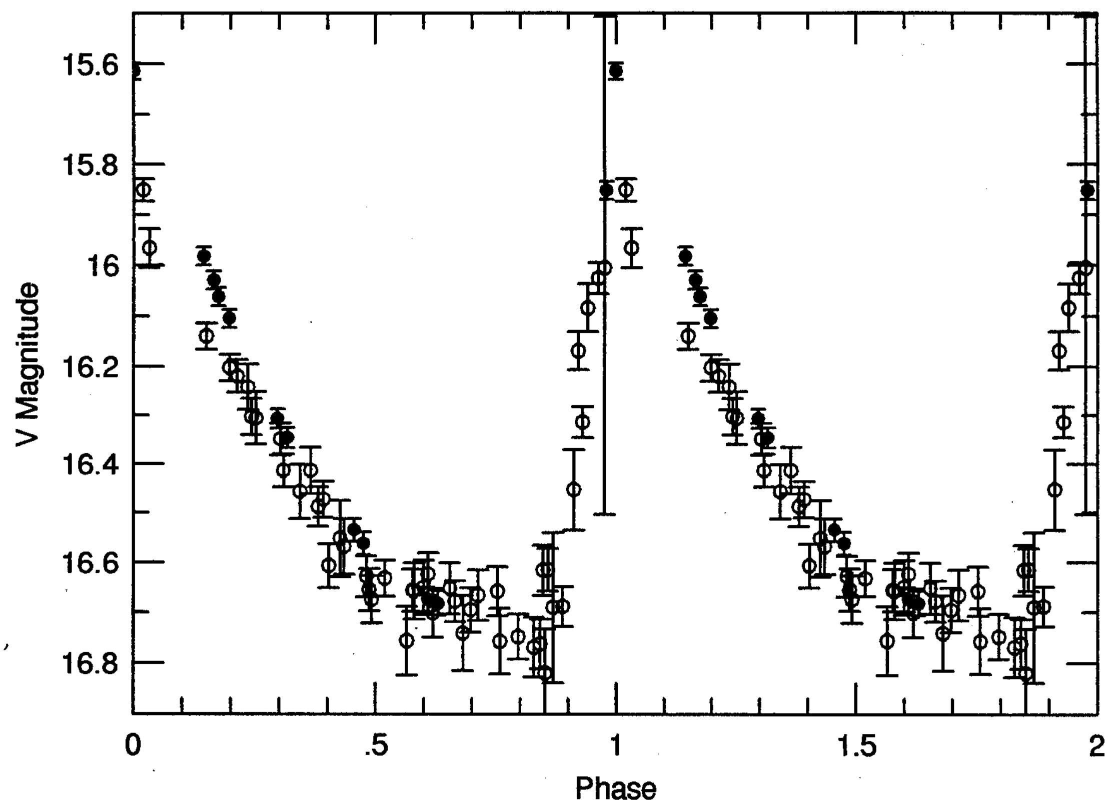

RA : 12 05 25.4
Dec: 28 03 28.8
<V> = 15.737
<B-V> = 0.32
P = 0.508702 days
Epoch = 3683.373
Type: RRab

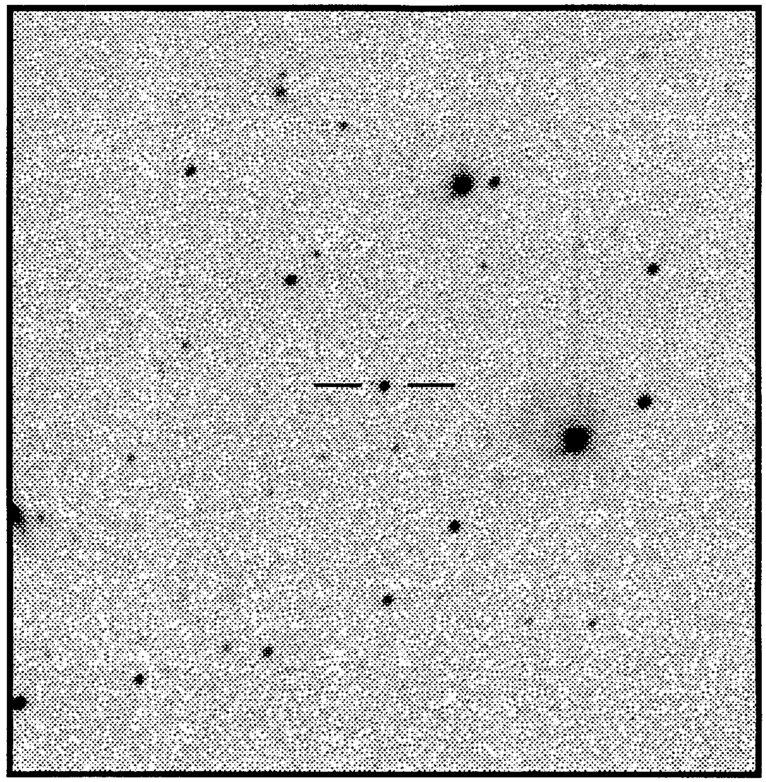

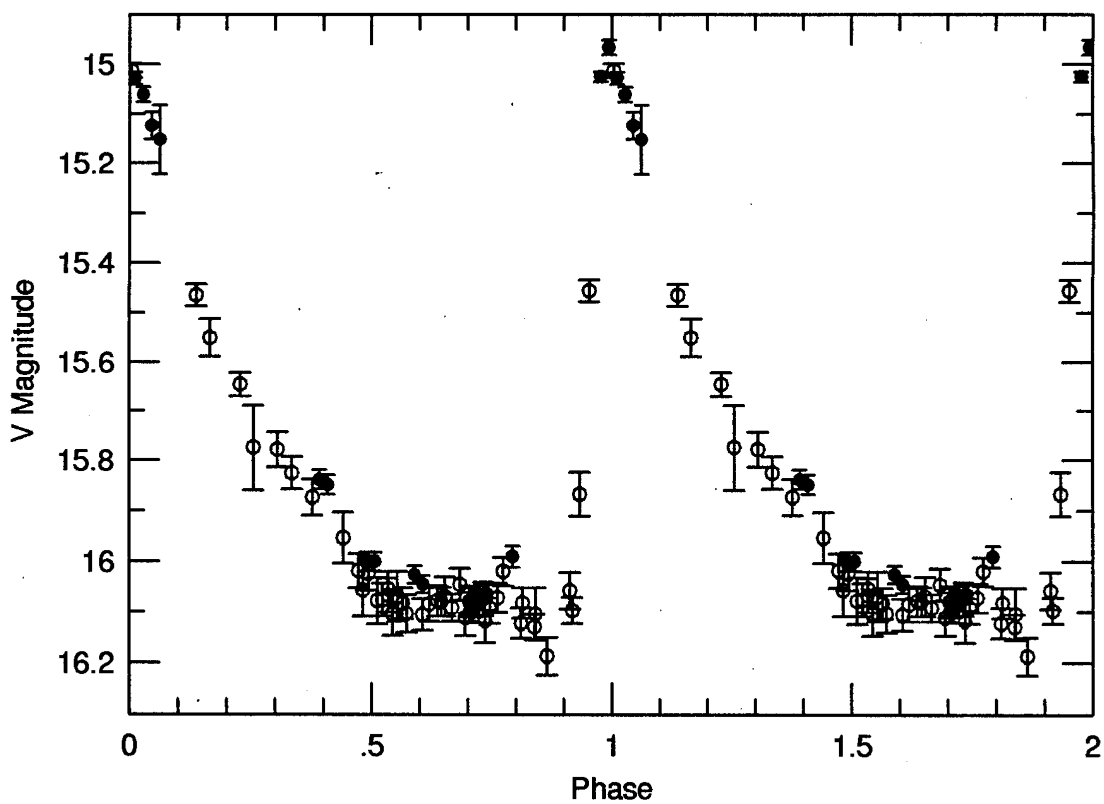

RA : 12 24 18.6

Dec: 28 03 17.4

<V> = 16.470

<B-V> = 0.33

P = 0.529449 days

Epoch = 3361.268

Type: RRab

GS Com

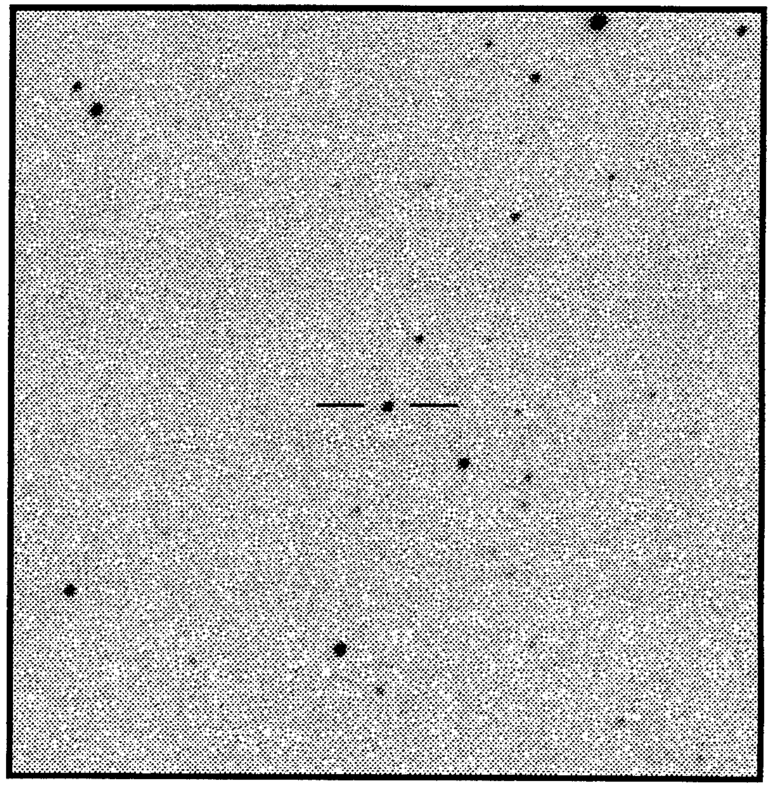

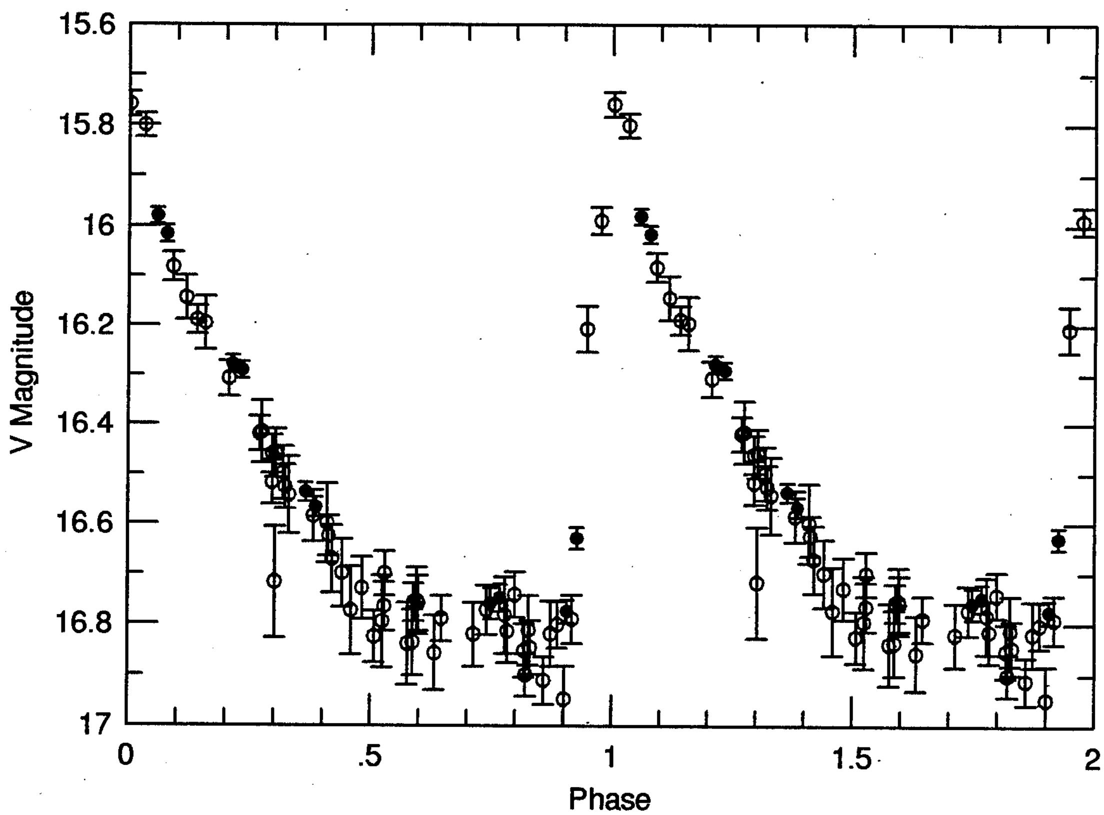

RA : 12 43 17.6

Dec: 28 05 21.7

<V> = 14.820

<B-V> = 0.35

P = 0.540837 days

Epoch = 3361.347

Type: RRab

DV Com

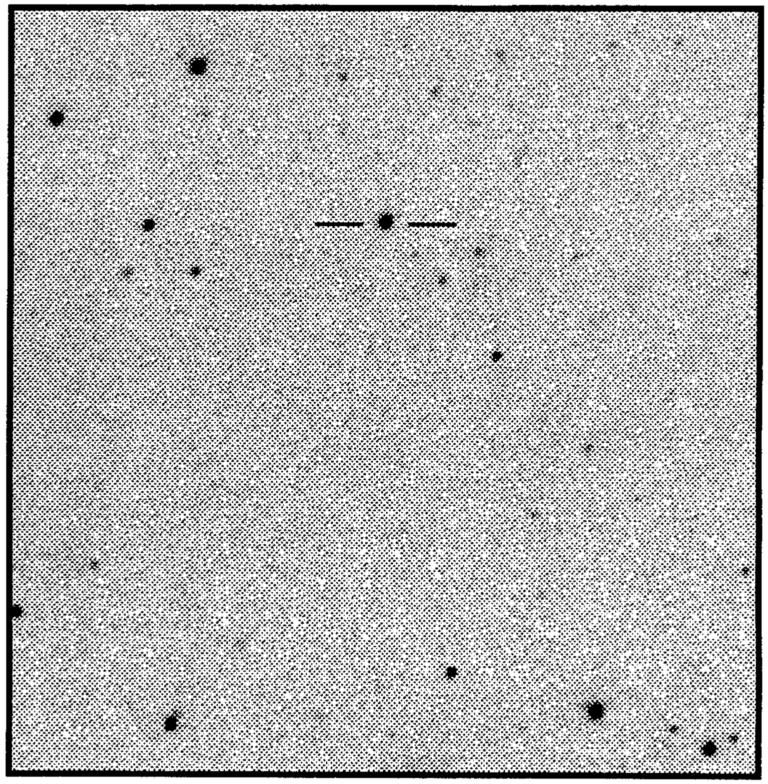

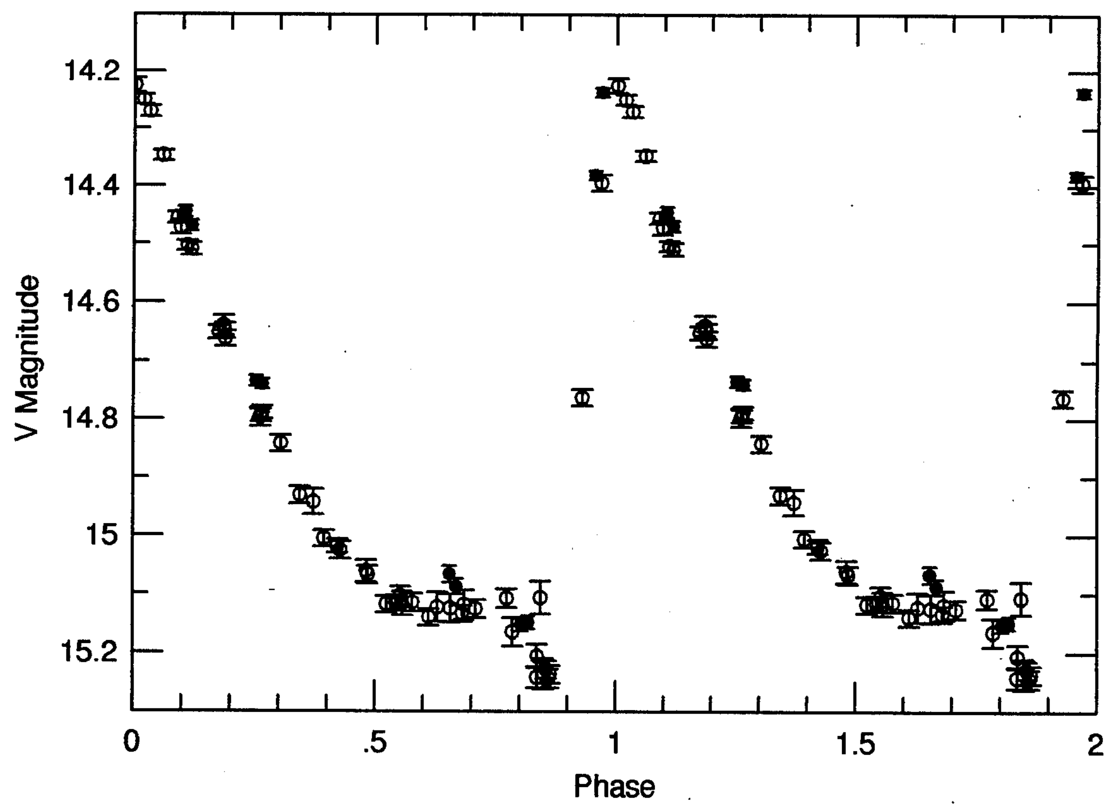

RA : 13 14 03.3
Dec: 28 00 26.7
<V> = 13.825
<B-V> = 0.05
P = 0.314639 days
Epoch = 3361.432
Type: RRc

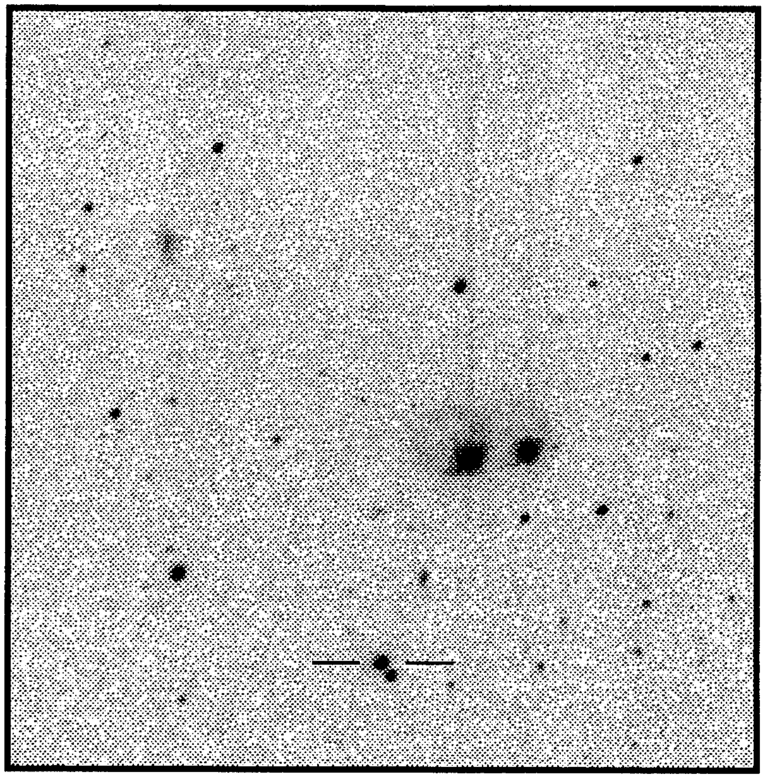

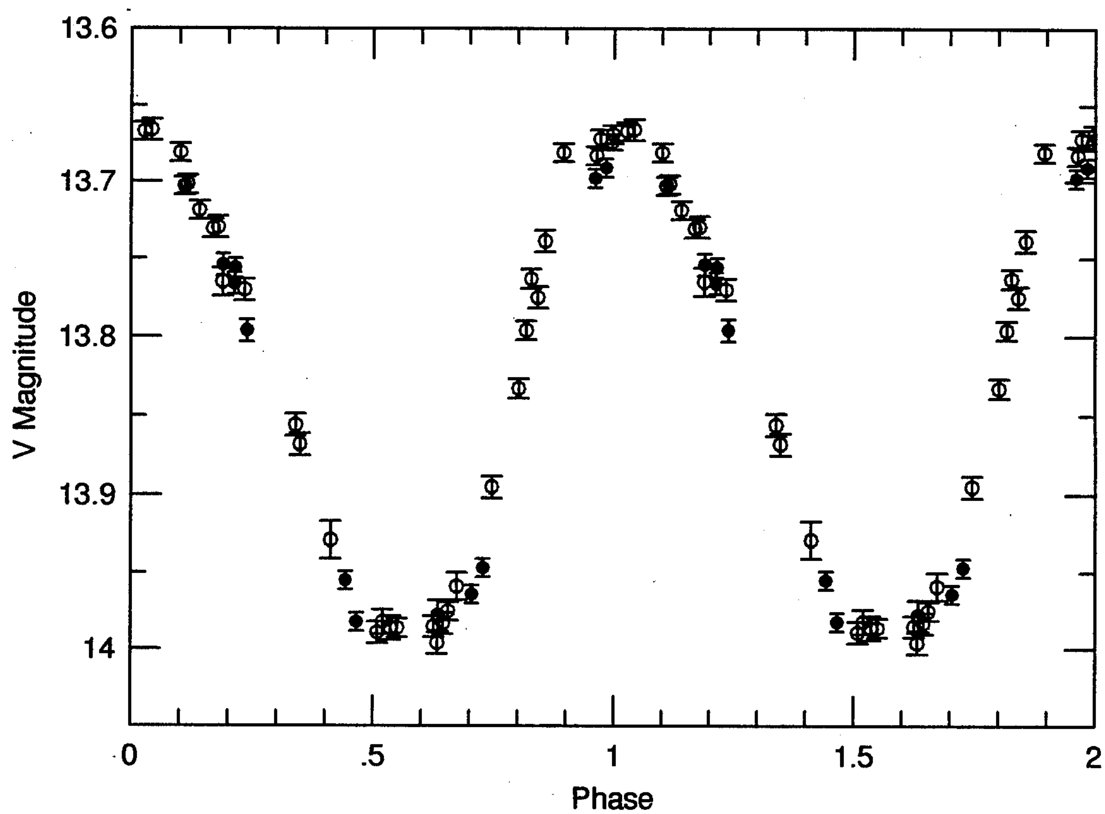

RA : 13 17 32.5

Dec: 28 01 39.4

<V> = 16.770

<B-V> = 0.35

P = 0.568389 days

Epoch = 3468.281

Type: RRab B

EZ Com

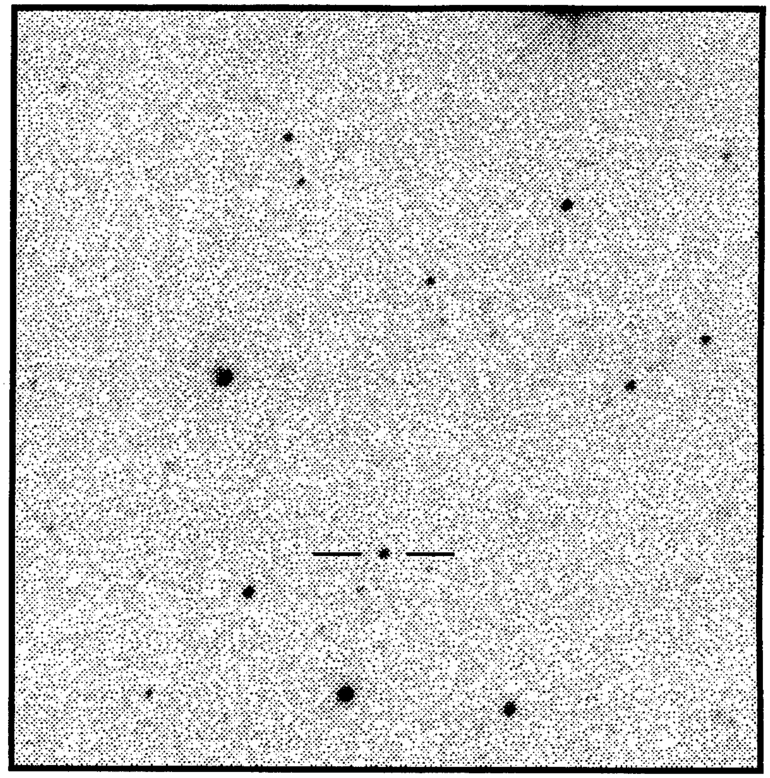

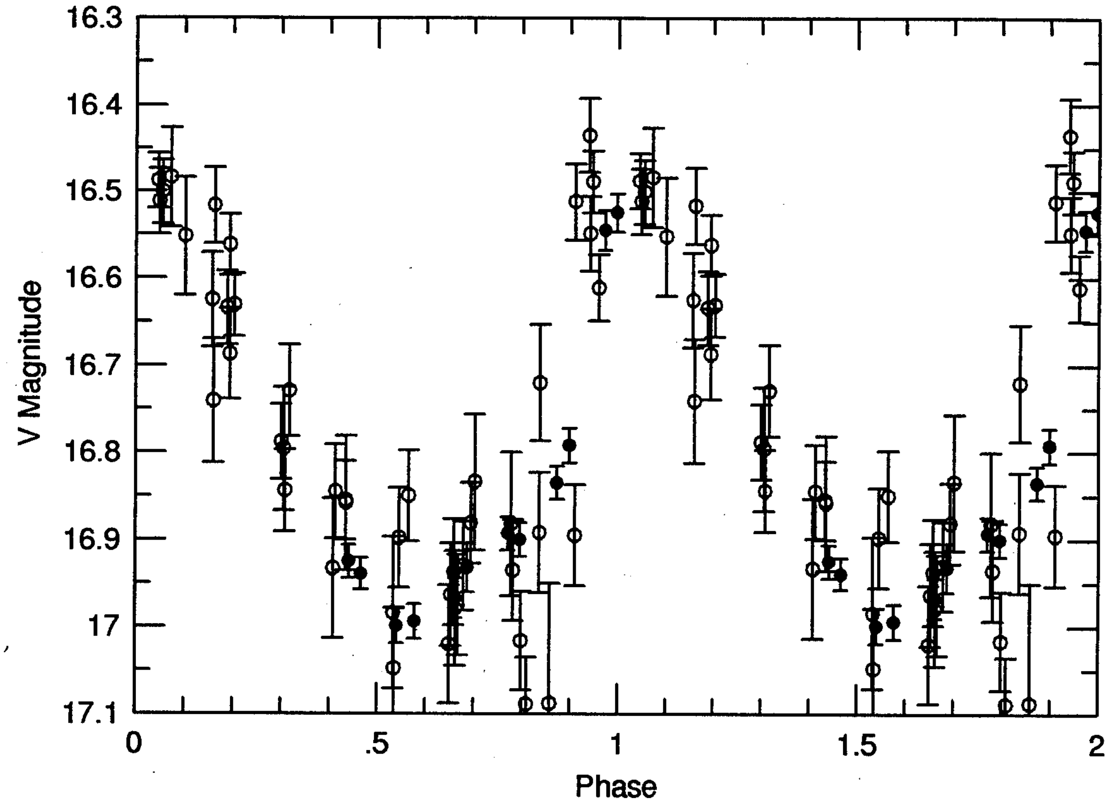

RA : 13 23 46.7

Dec: 28 06 32.5

<V> = 17.056

<B-V> = 0.60

Type: AGN/QSO

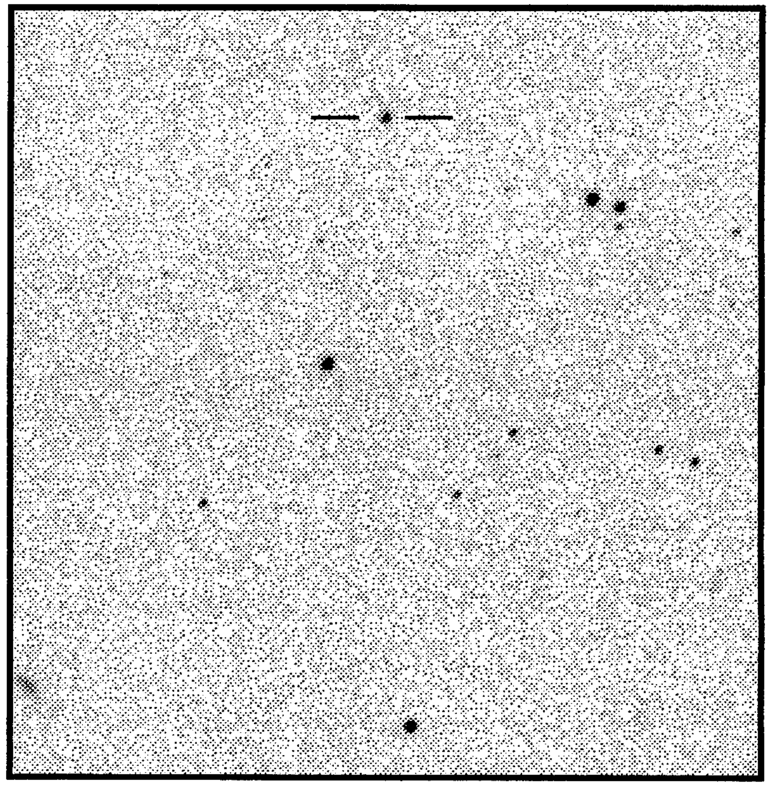

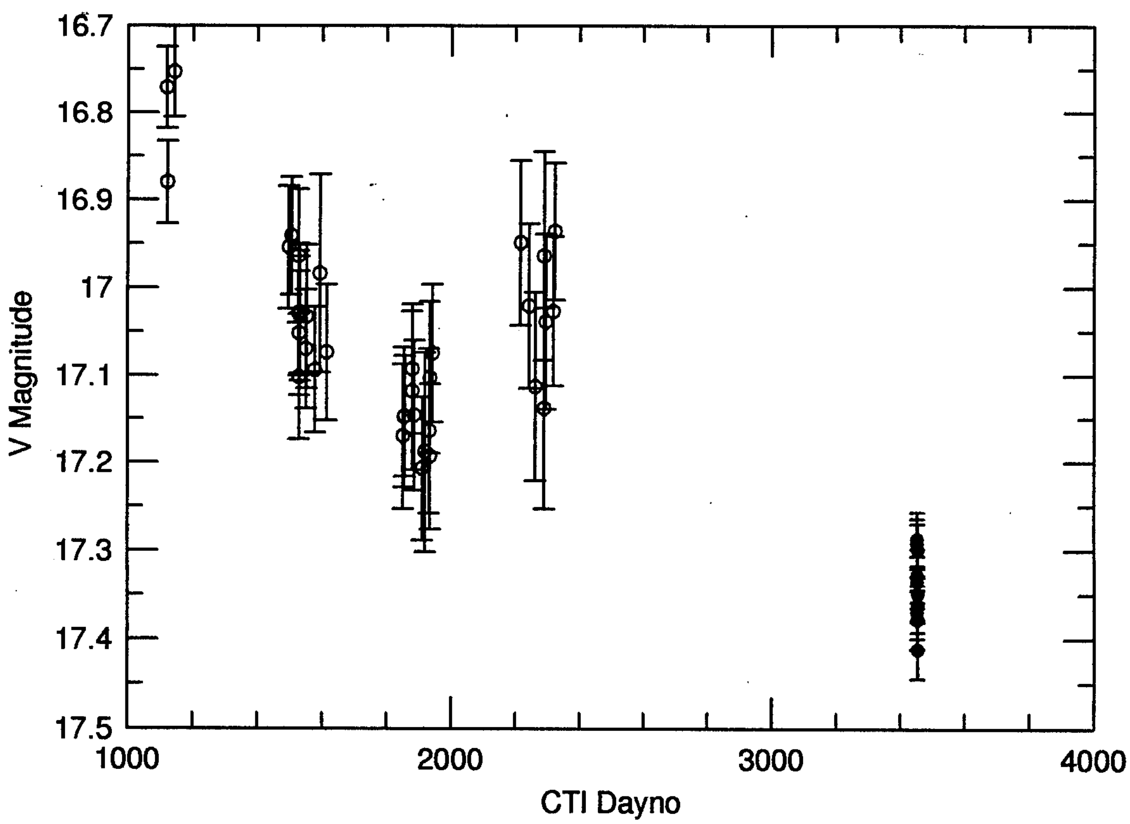

RA: 14 33 13.2
Dec: 28 01 17.0
<V> = 17.995
<B-V> = 0.40
P = 0.437536 days
Epoch = 3481.155
Type: RRab

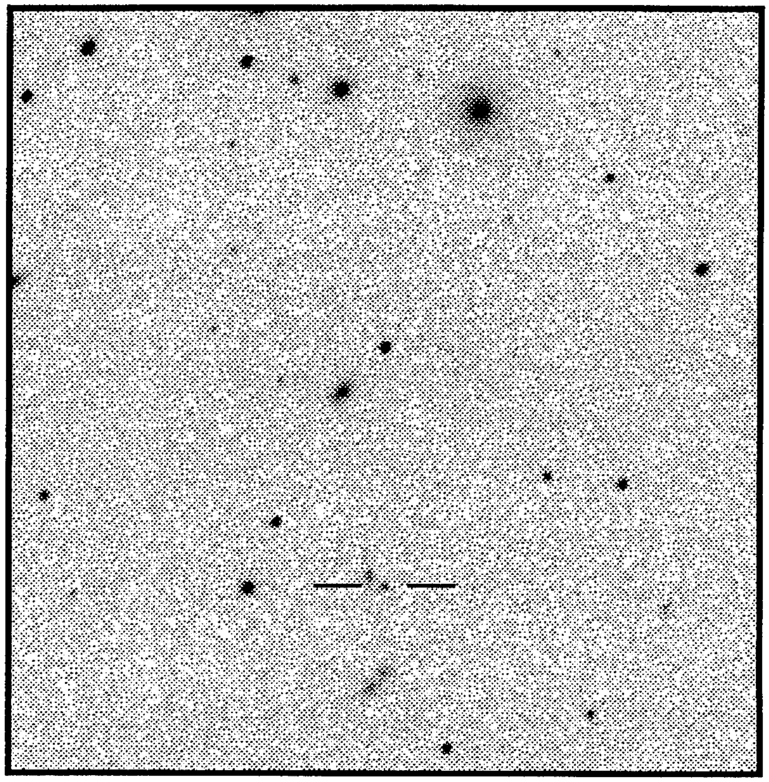

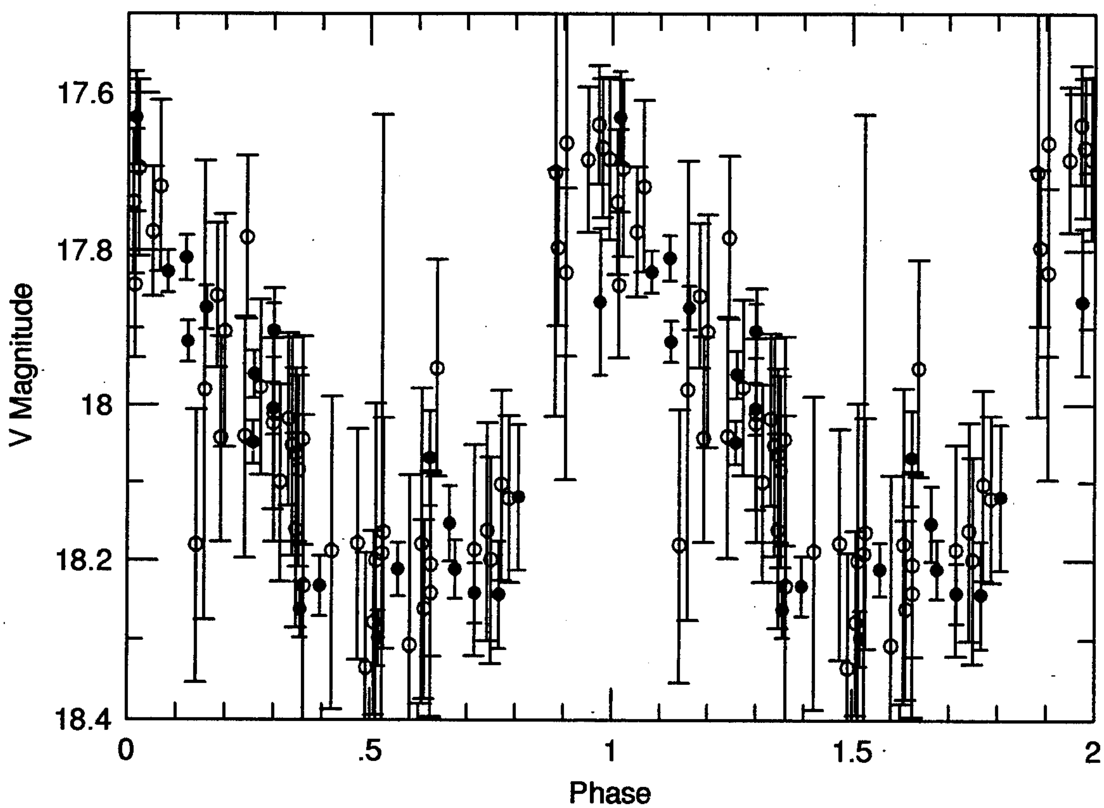

RA : 14 54 39.0

Dec: 28 05 32.8

<V> = 14.810

<B-V> = 0.36

P = 0.622135 days

Epoch = 3112.203

Type: RRab

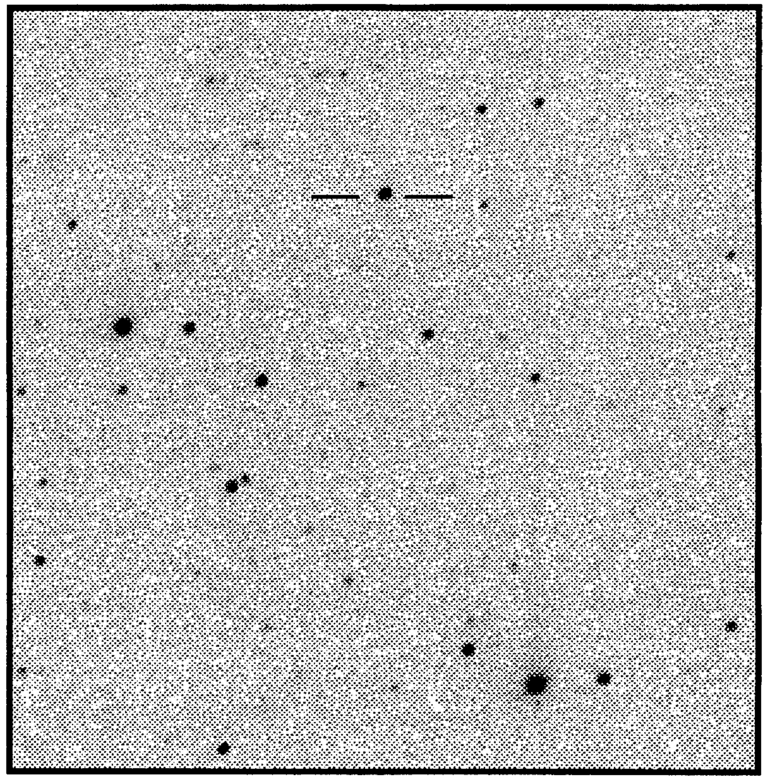

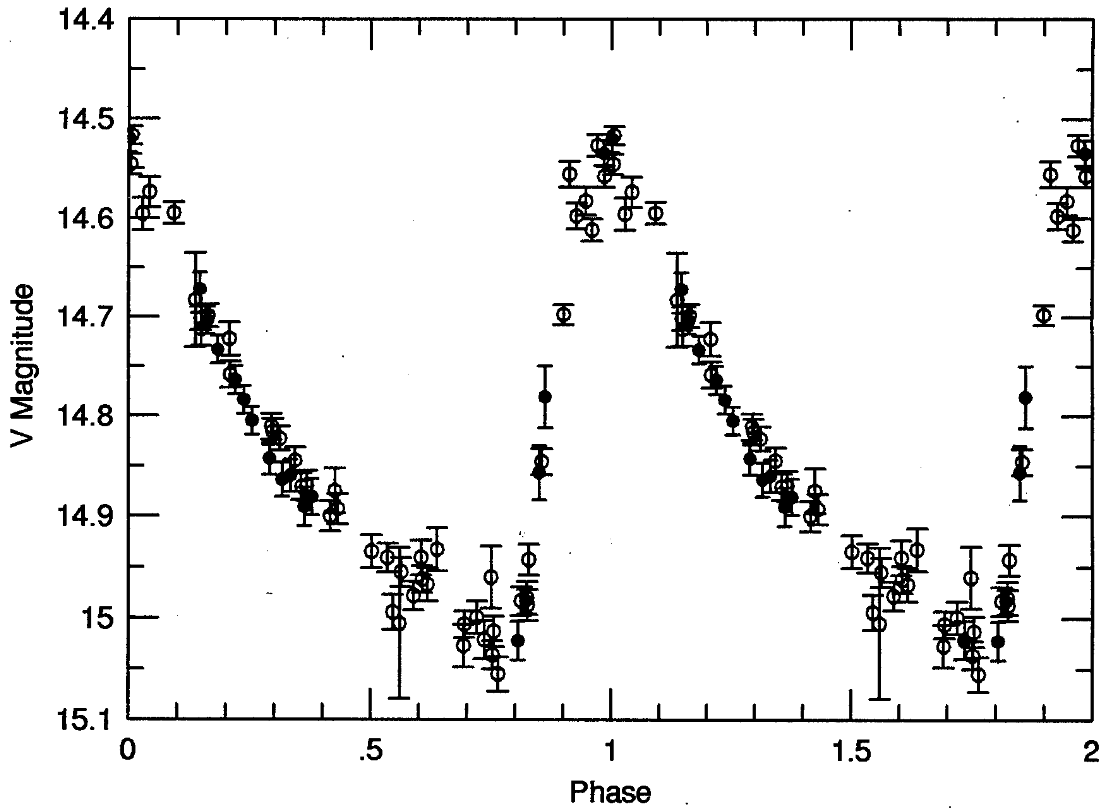

RA : 15 16 28.1

Dec: 28 00 41.6

<V> = 17.897

<B-V> = 0.30

P = 0.571900 days

Epoch = 3685.029

Type: RRab

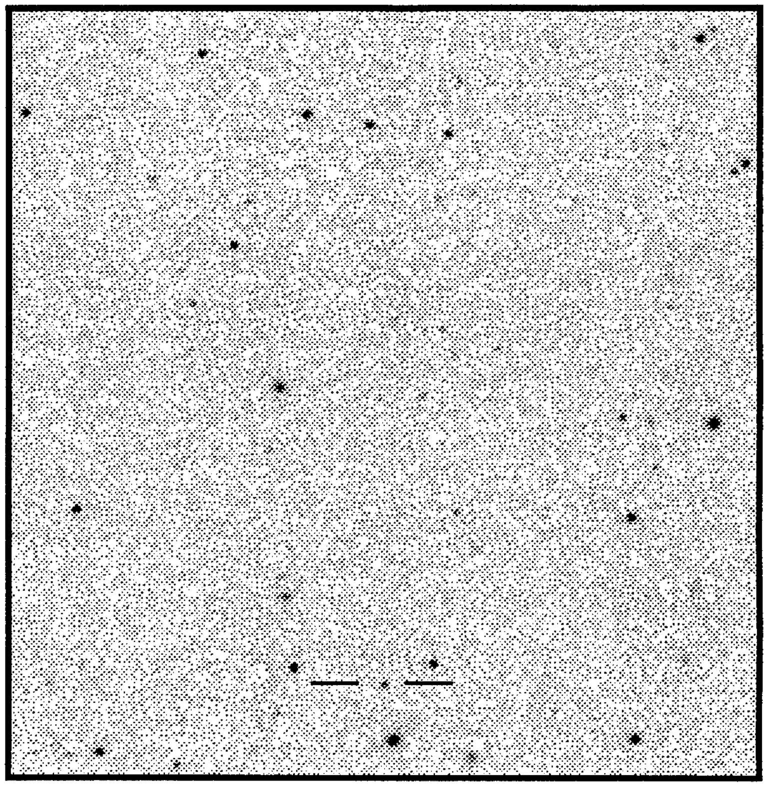

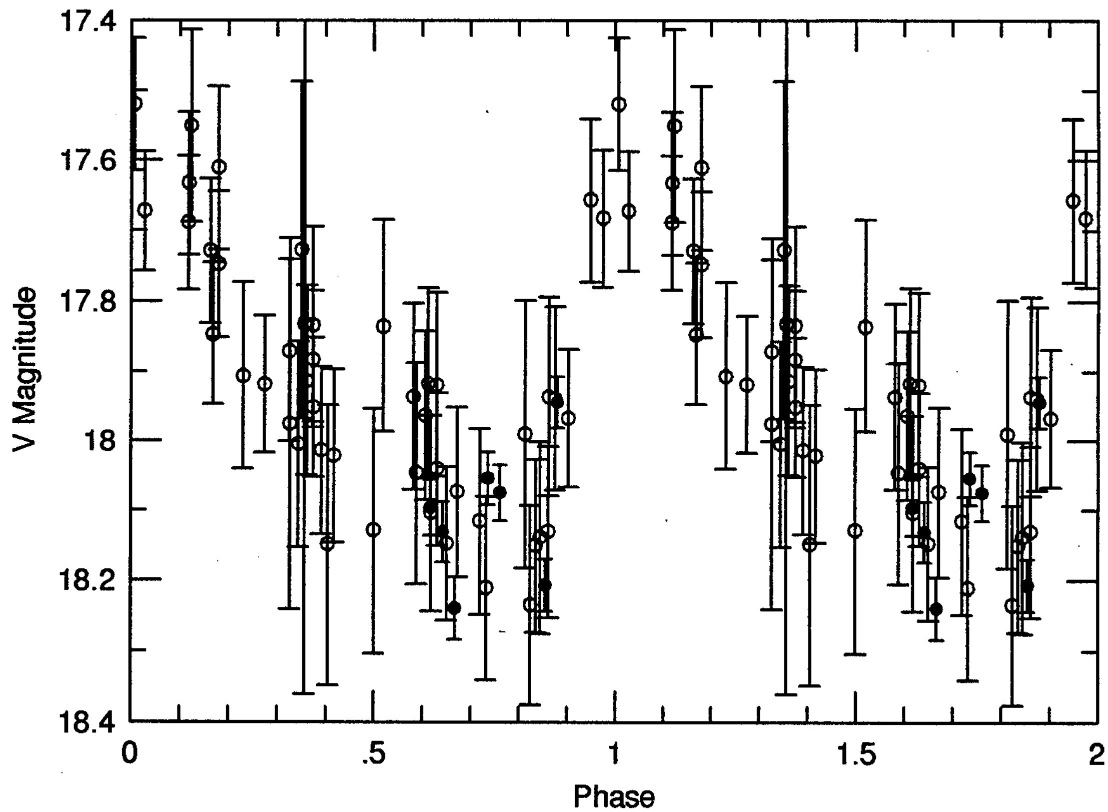

RA : 16 23 17.6
Dec: 27 58 28.9
<V> = 15.234
<B-V> = 0.47
P = 0.343669 days
Epoch = 3685.451
Type: W UMa

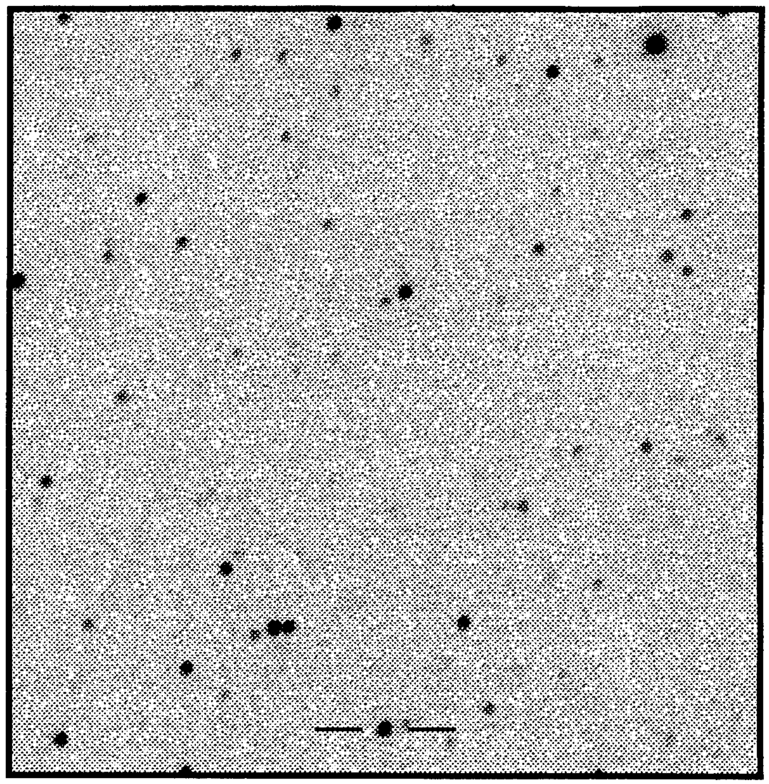

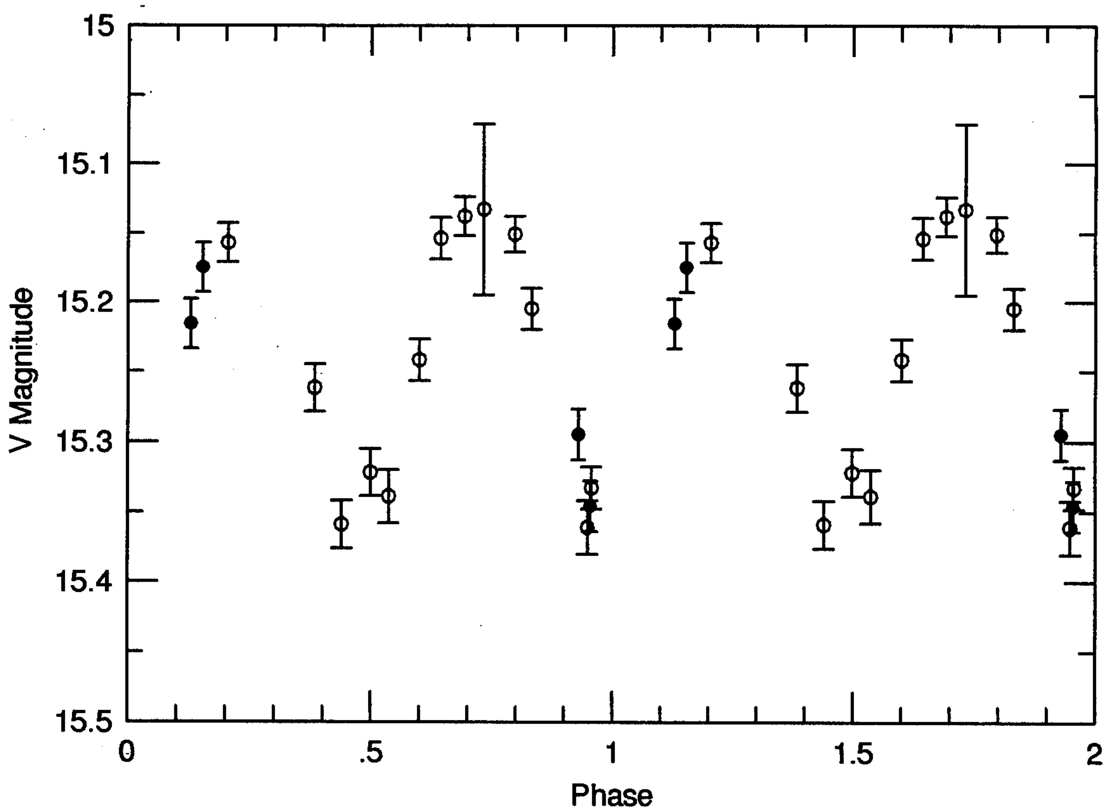

RA : 16 50 08.8
Dec: 27 59 55.0
<V> = 15.368
<B-V> = 0.33
P = 0.570831 days
Epoch = 3113.209
Type: RRab

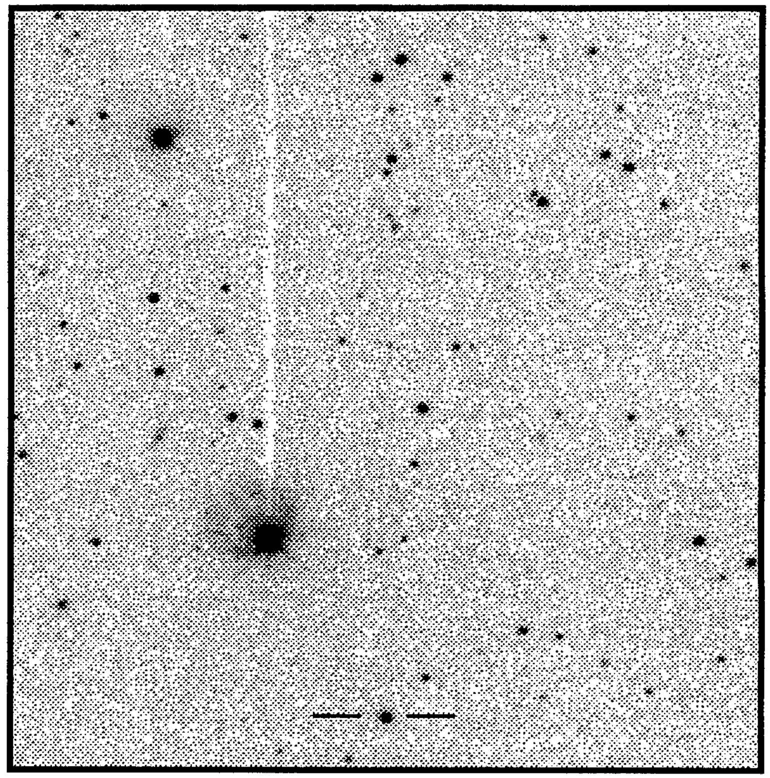

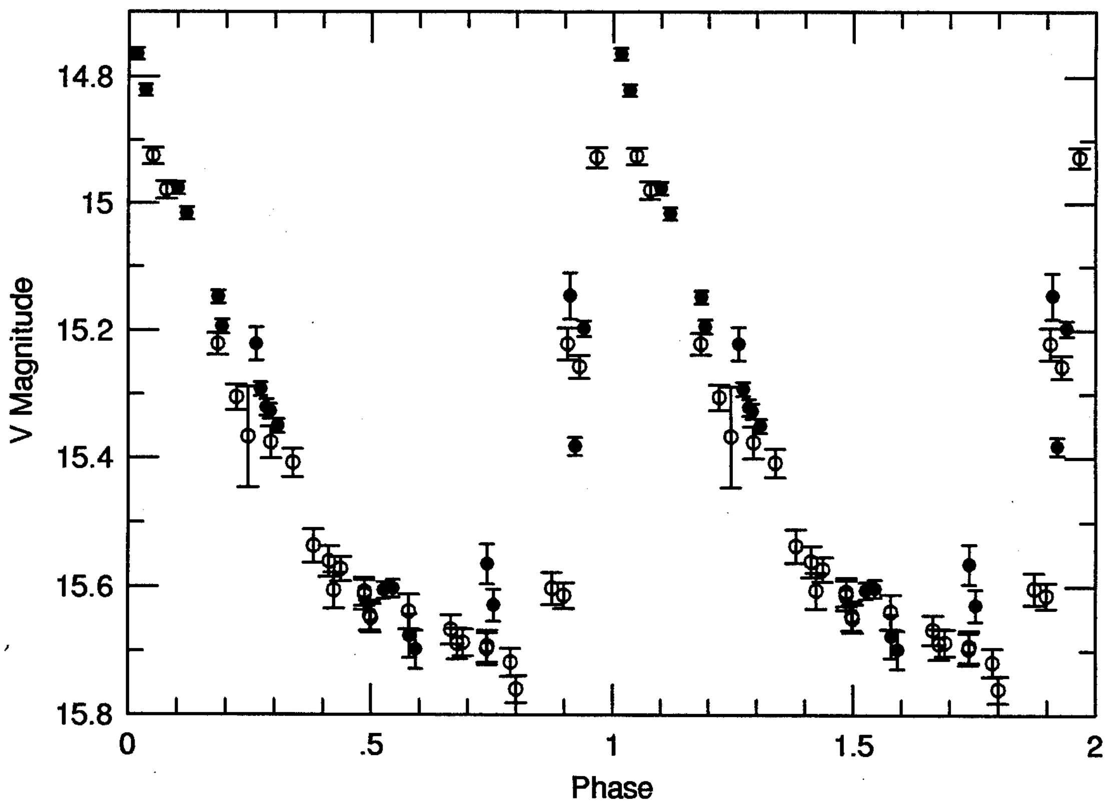

RA : 16 58 30.7
Dec: 28 06 00.7
<V> = 14.884
<B-V> = 0.30
P = 0.272711 days
Epoch = 3685.586
Type: RRc?

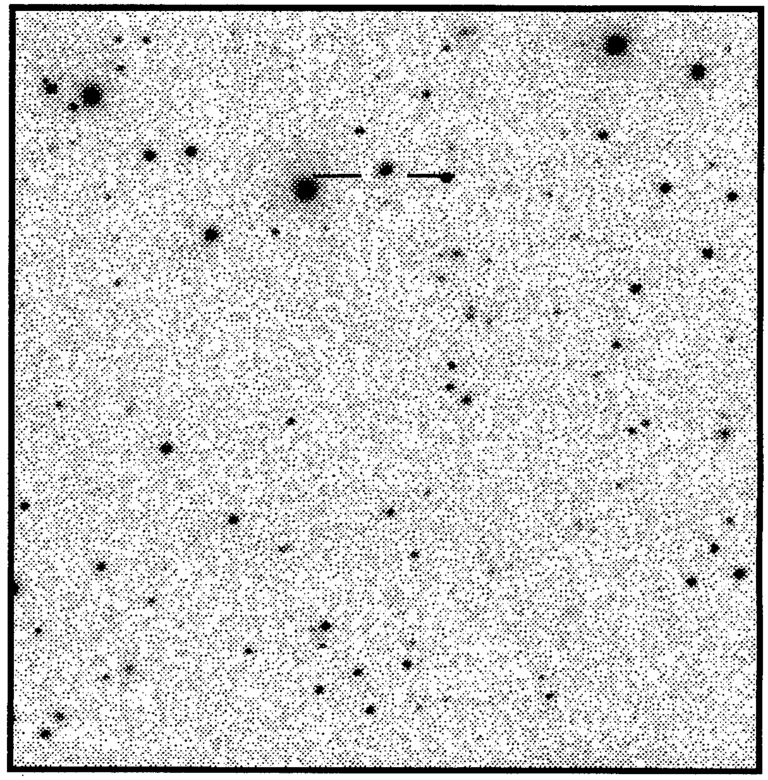

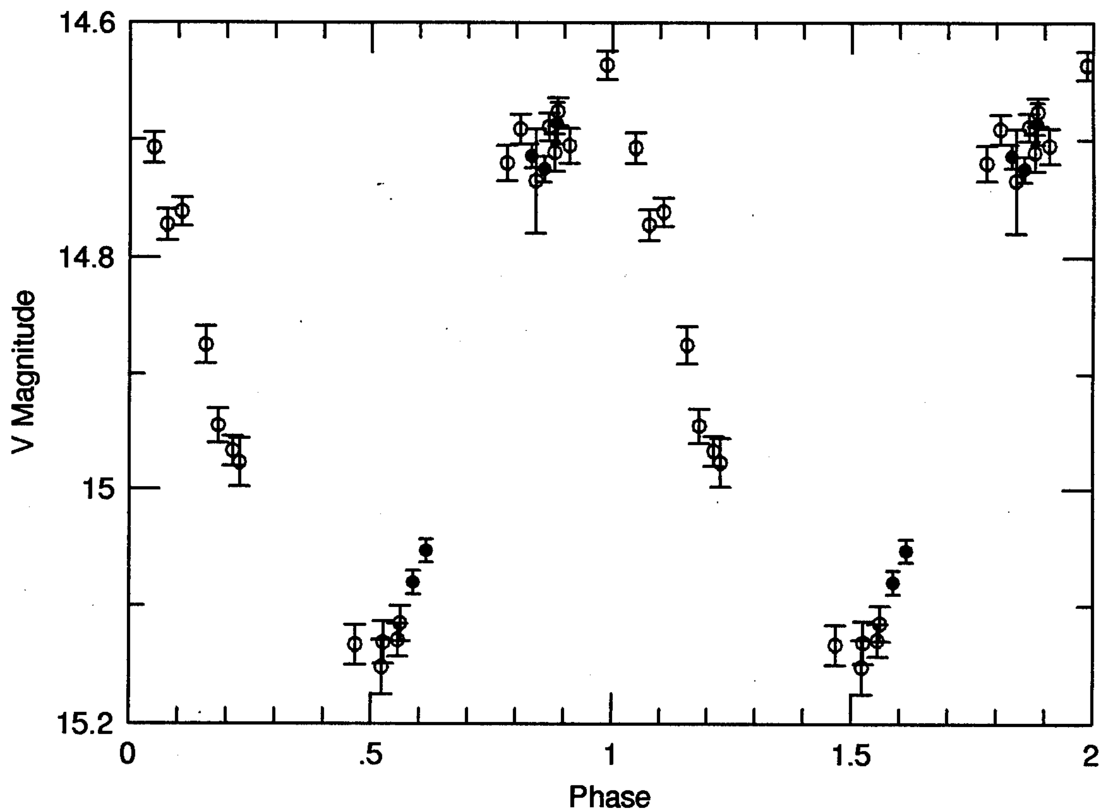

RA: 17 13 10.9

Dec: 28 00 10.3

<V> = 16.202

<B-V> = 0.30

P = 0.531433 days

Epoch = 3481.184

Type: RRab

V375 Her

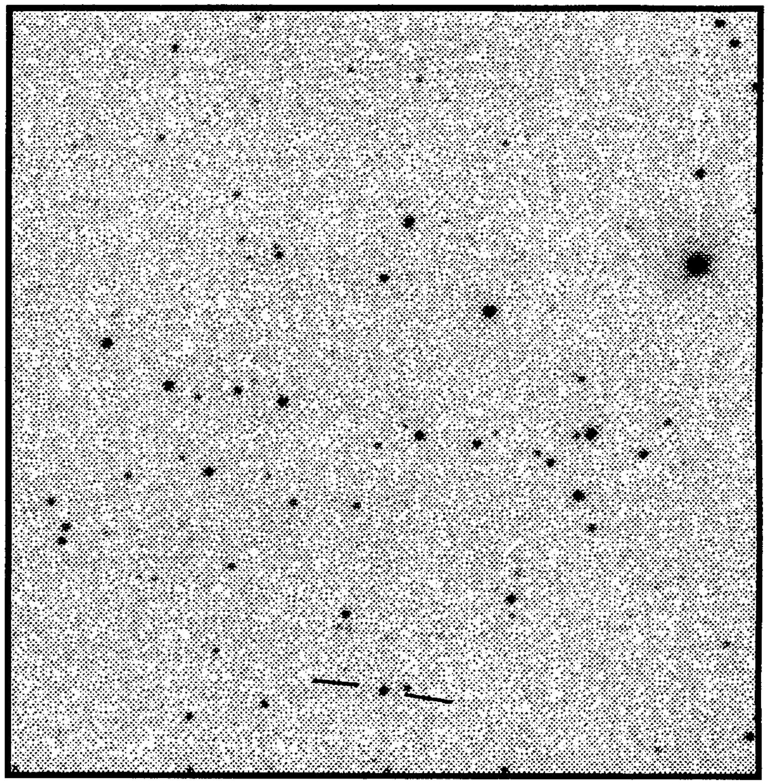

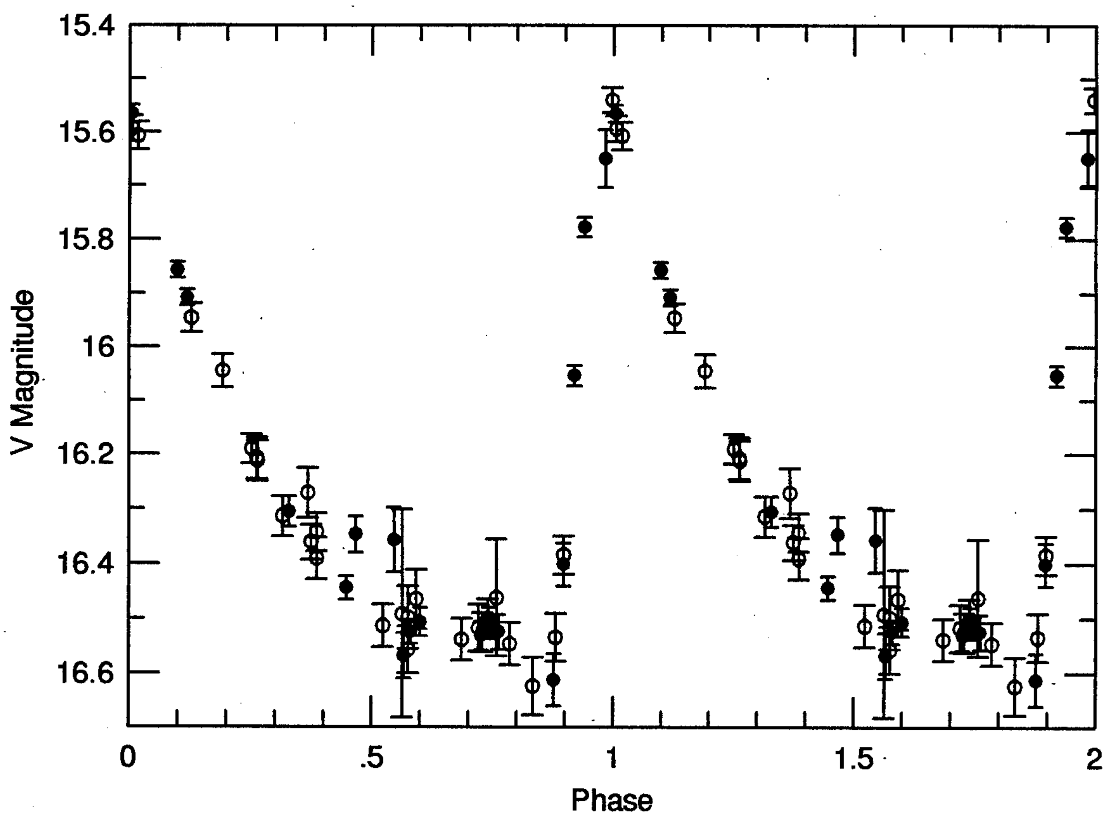

RA : 17 15 23.9
Dec: 28 00 43.0
<V> = 17.998
<B-V> = 0.35
P = 0.516250 days
Epoch = 3474.160
Type: RRab

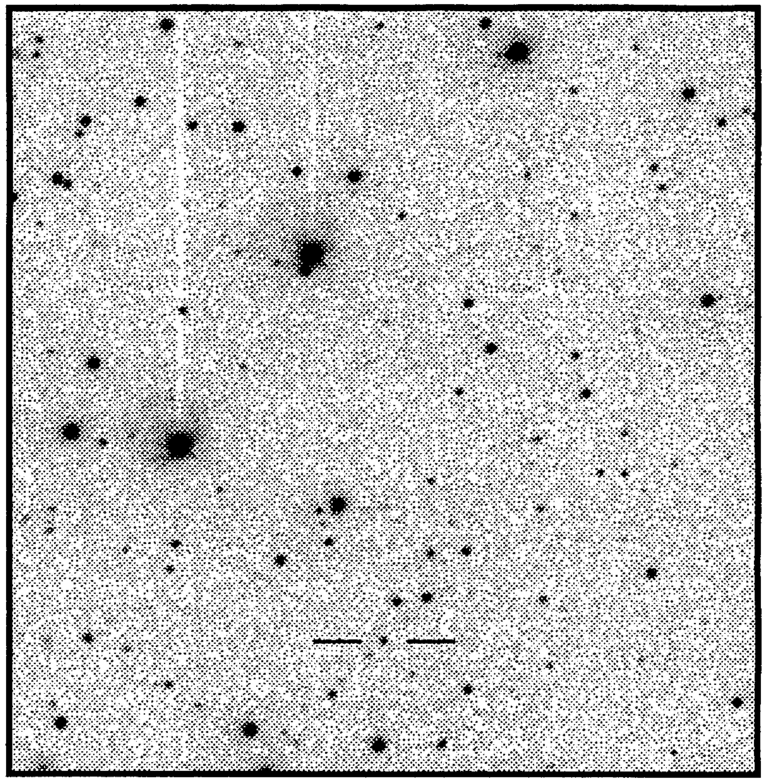

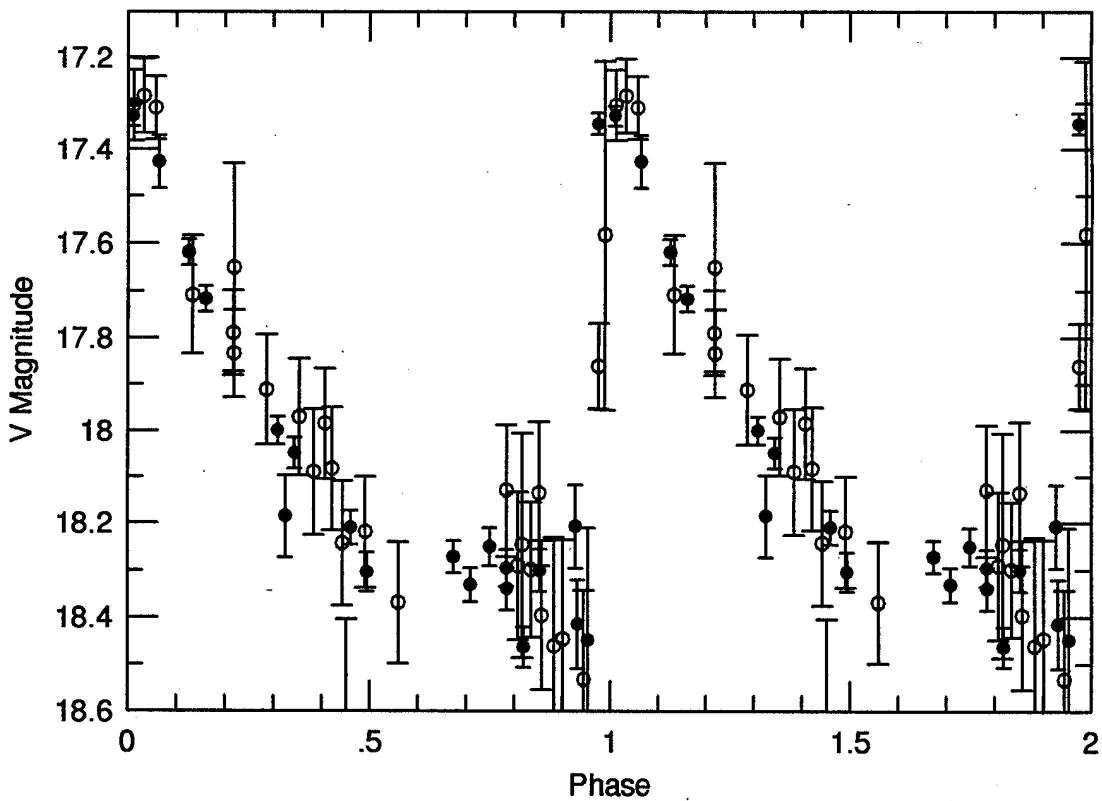

RA: 17 15 57.0
Dec: 28 06 44.6
<V> = 15.090
<B-V> = 0.45
P = 0.528145 days
Epoch = 3385.207
Type: RRab
V385 Her

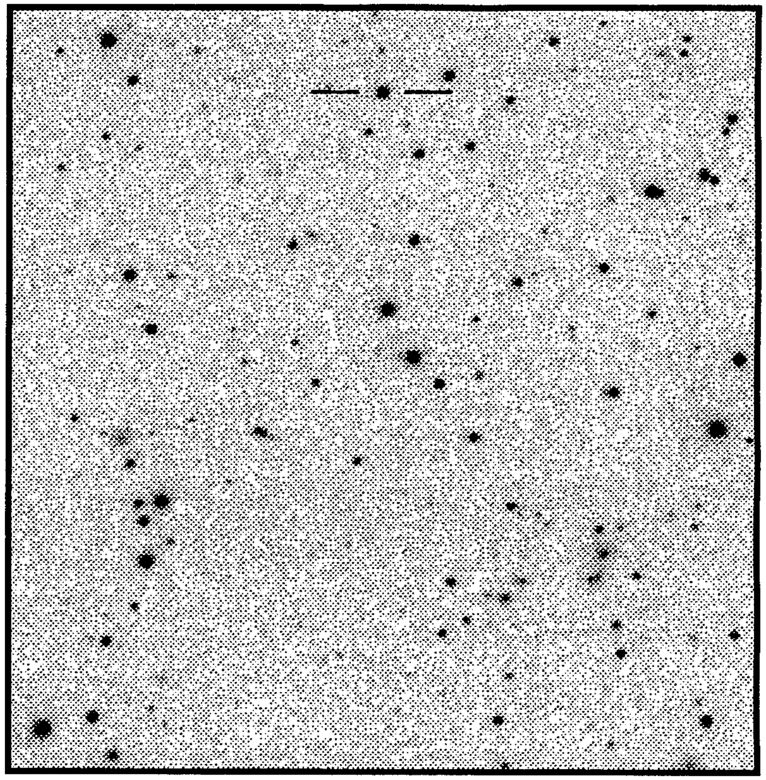

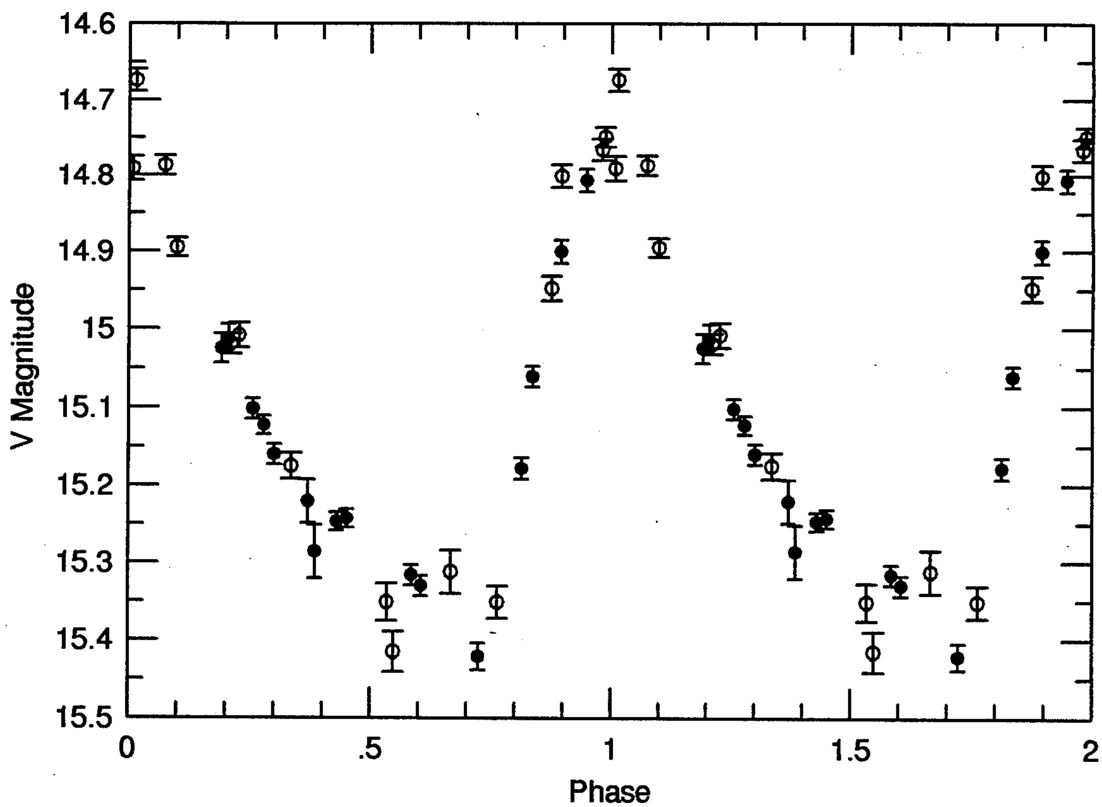

RA : 17 19 06.6
Dec: 28 06 28.2
<V> = 17.637
<B-V> = 0.6
P = 0.47259 days
Epoch = 3385.248
Type: RRab?

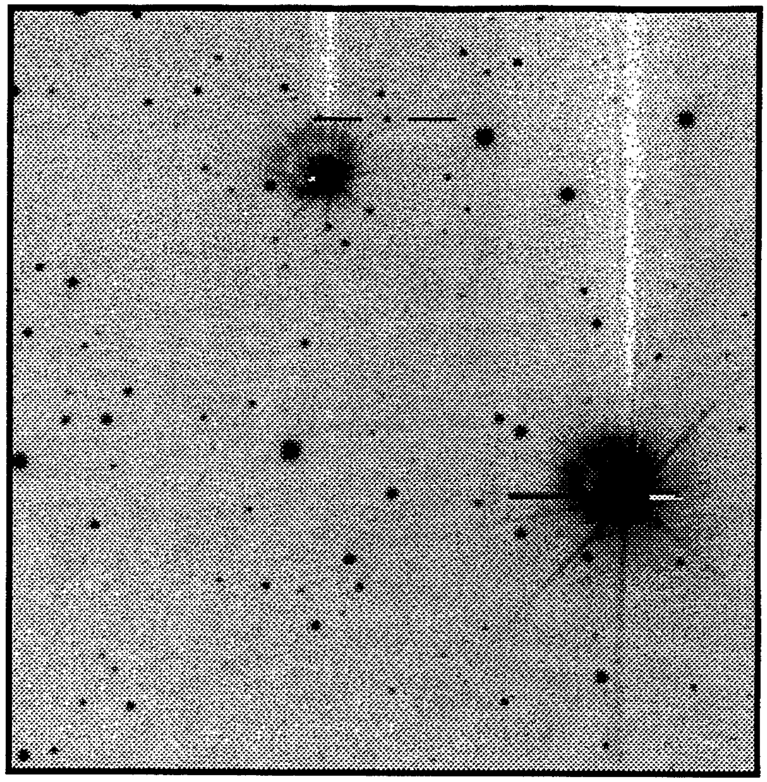

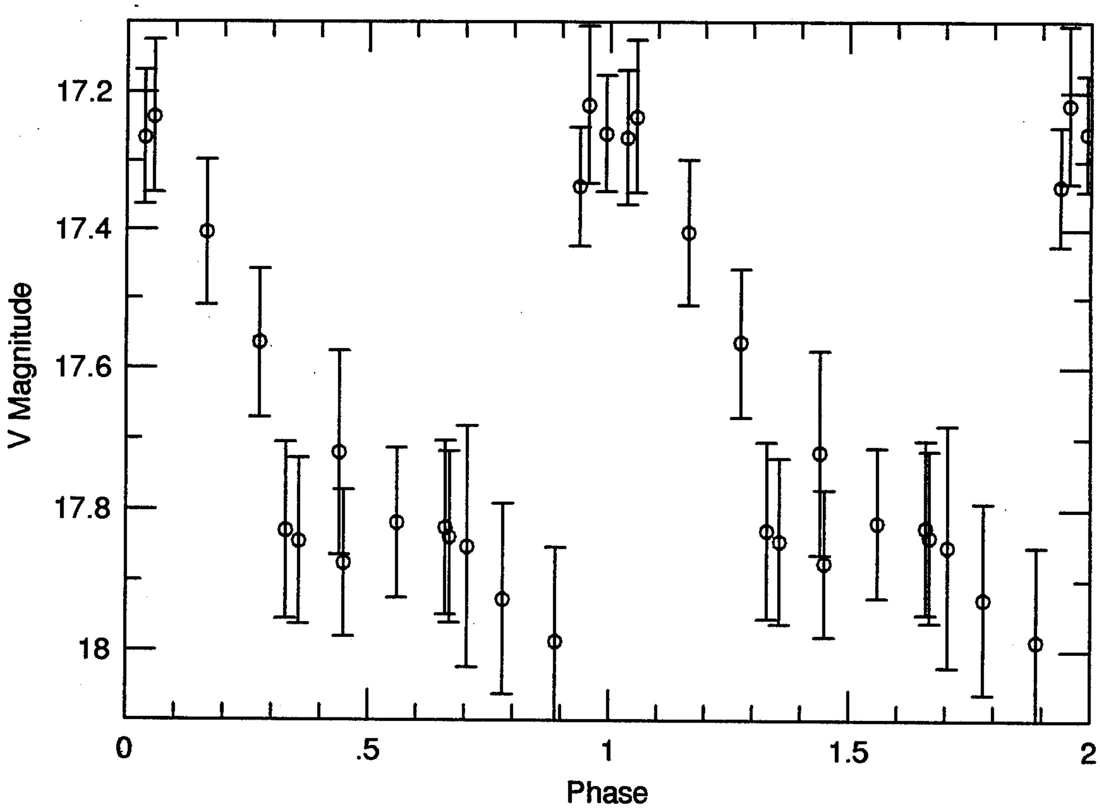

RA : 17 20 58.6

Dec: 28 01 15.2

<V> = 14.768

<B-V> = 0.15

P = 0.295405 days

Epoch = 3469.480

Type: RRc

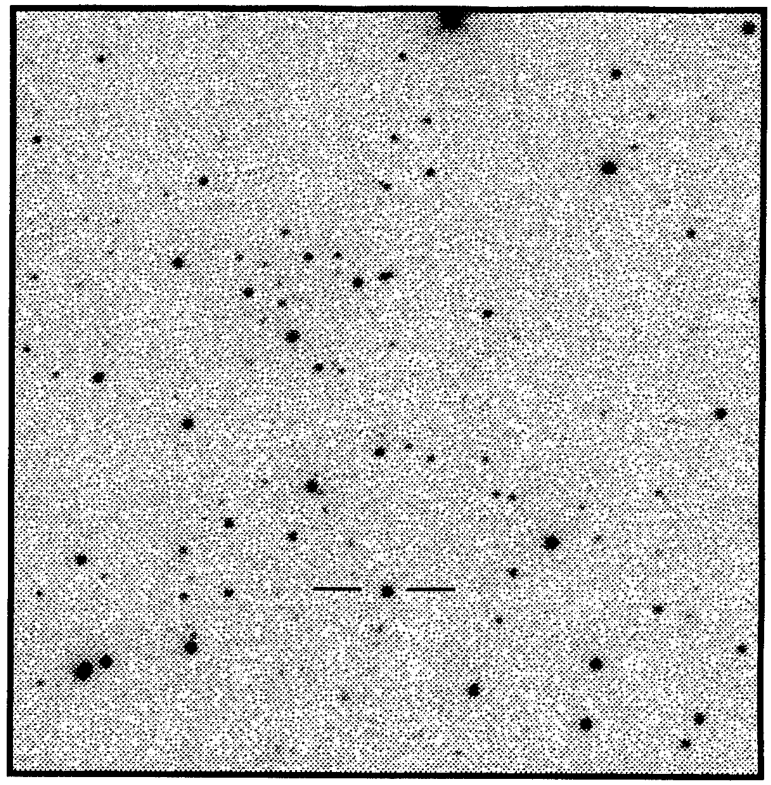

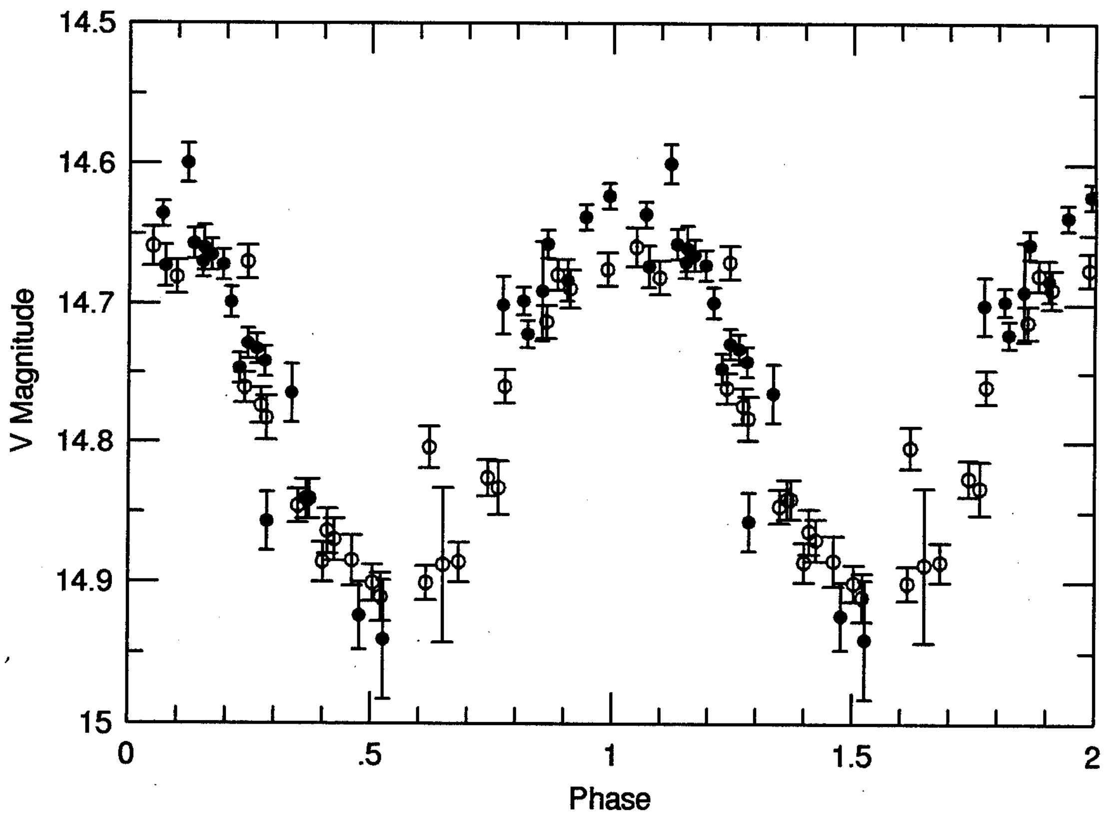

RA: 17 30 43.1
Dec: 28 03 48.3
<V> = 15.686
<B-V> = 0.15
P = 0.0568927 days
Epoch = 3385.429
Type: SX Phe

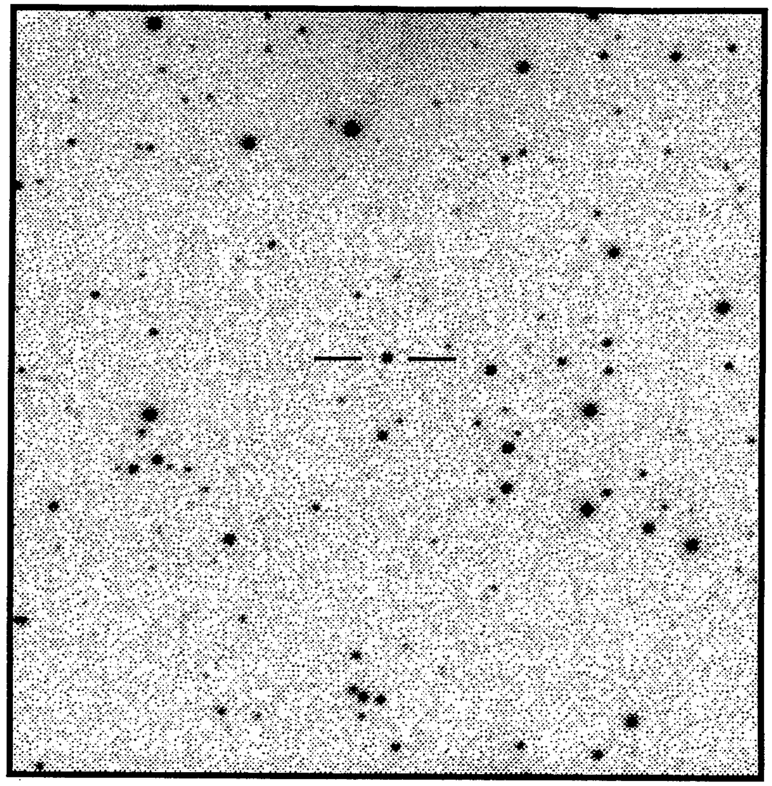

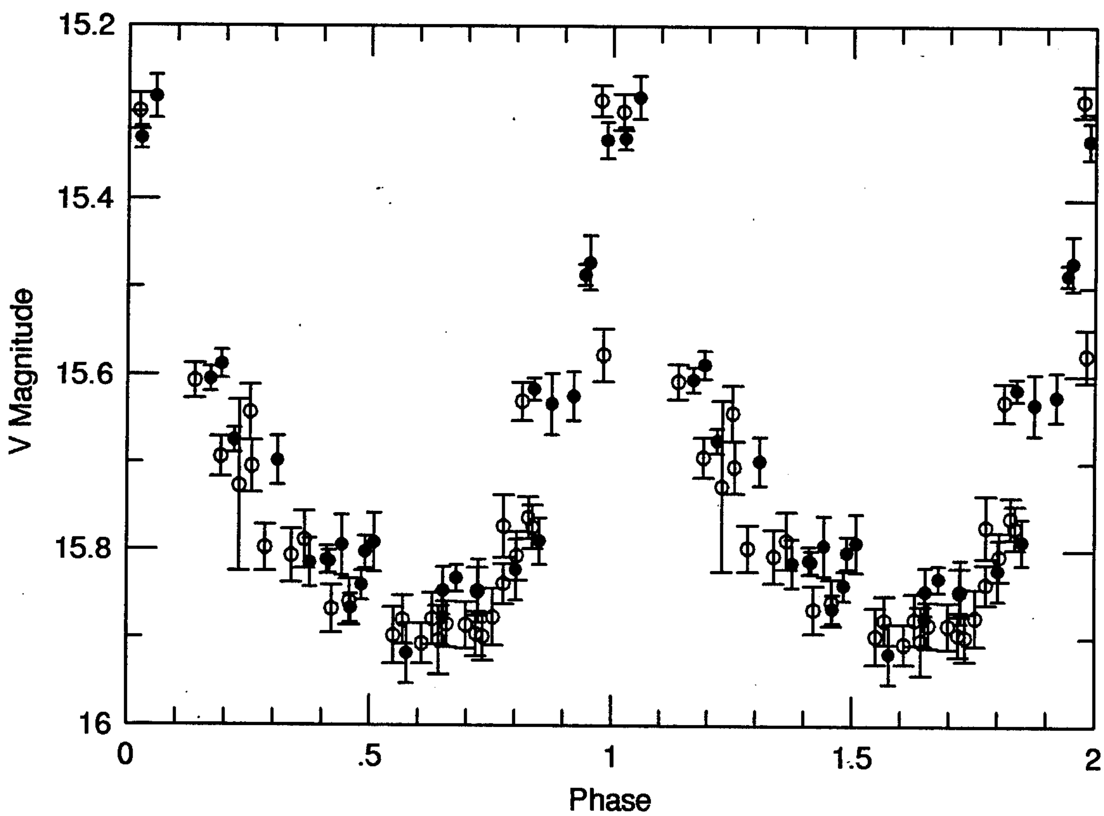

RA : 17 41 51.5
Dec: 28 03 53.2
<V> = 15.807
<B-V> = 0.30
P = 0.566966 days
Epoch = 3113.194
Type: RRab

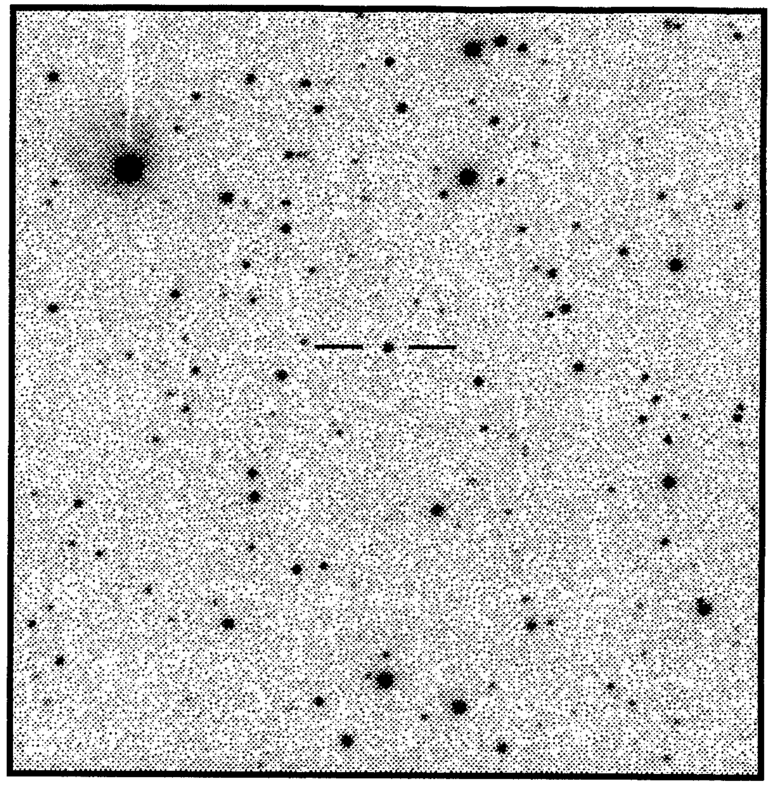

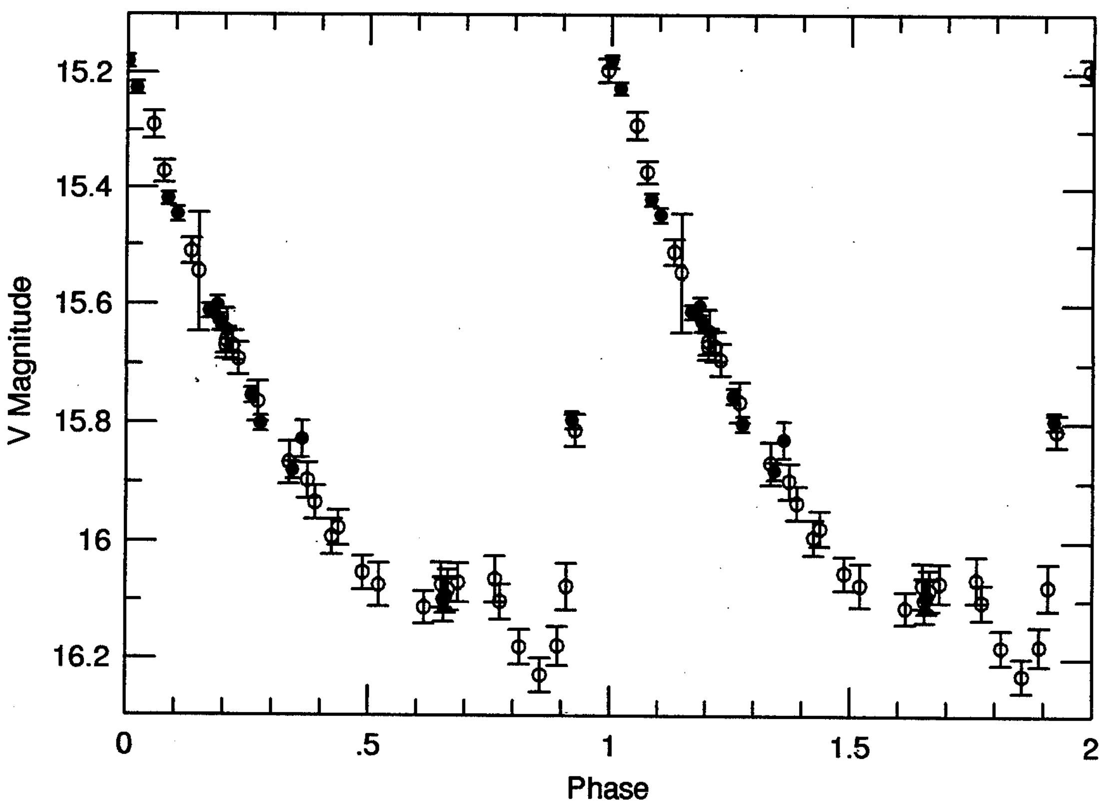

RA : 17 42 40.2

Dec: 28 04 44.7

<V> = 16.642

<B-V> = 0.30

P = 0.526354 days

Epoch = 3186.109

Type: RRab

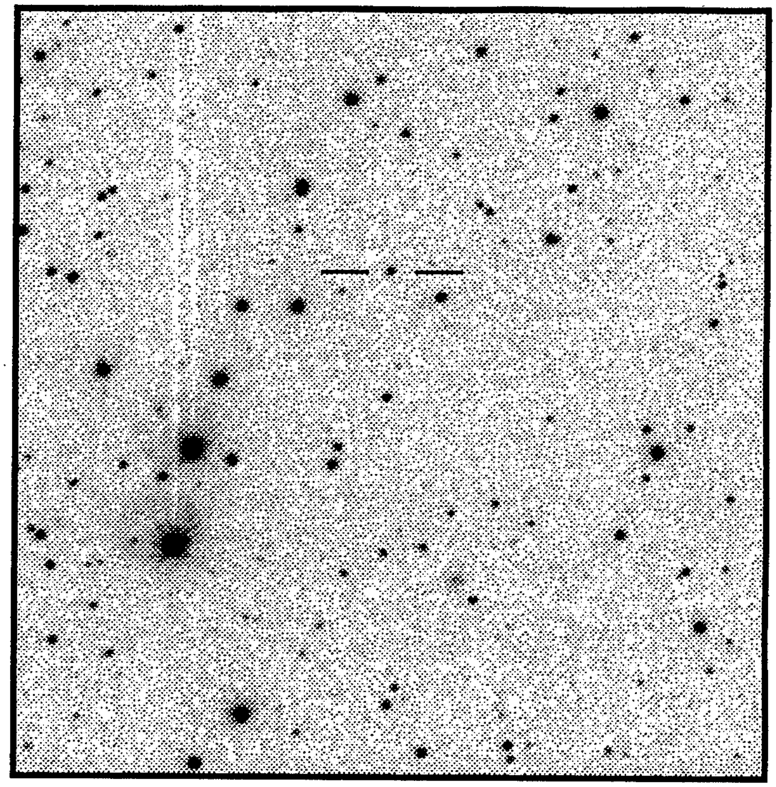

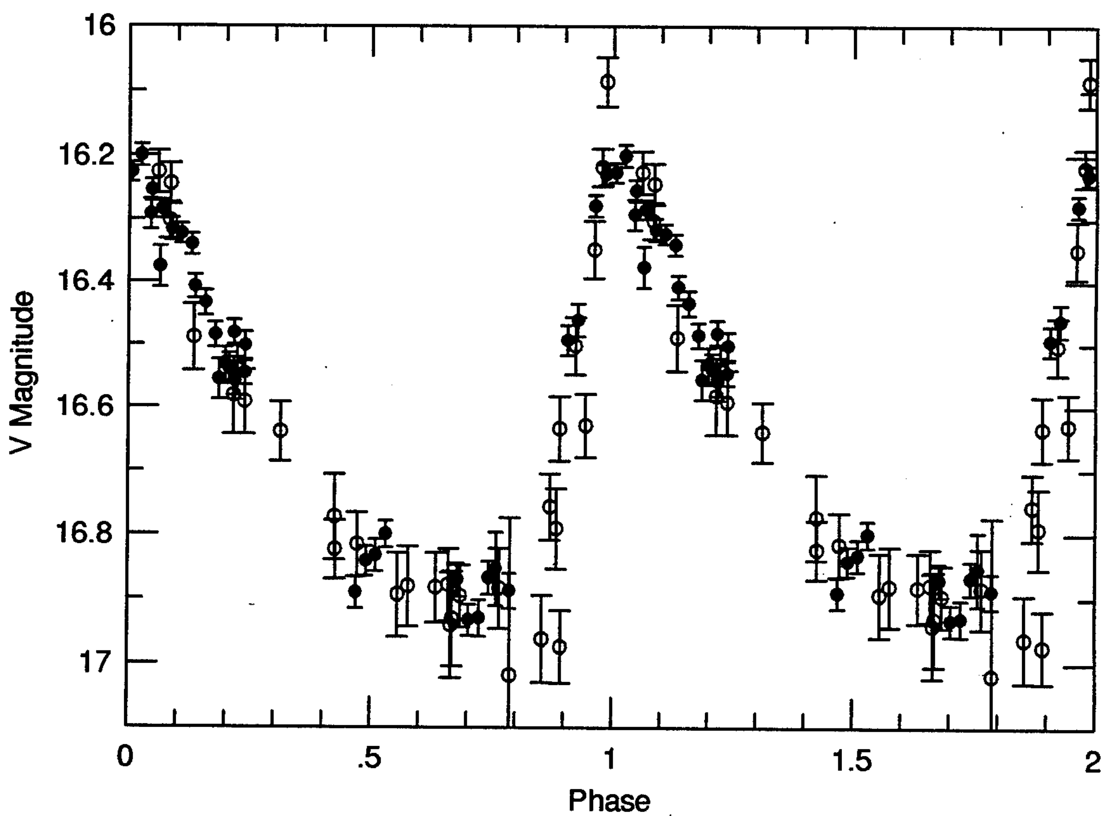

RA : 17 44 19.7
Dec: 28 01 21.6
<V> = 15.666
<B-V> = 0.22
P = 0.377069 days
Epoch = 3487.309
Type: RRc

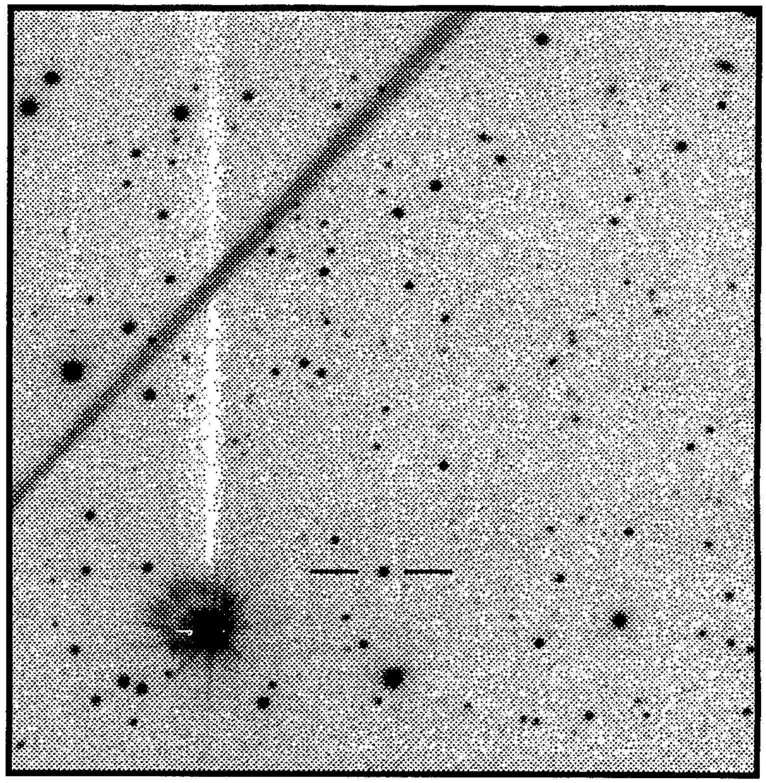

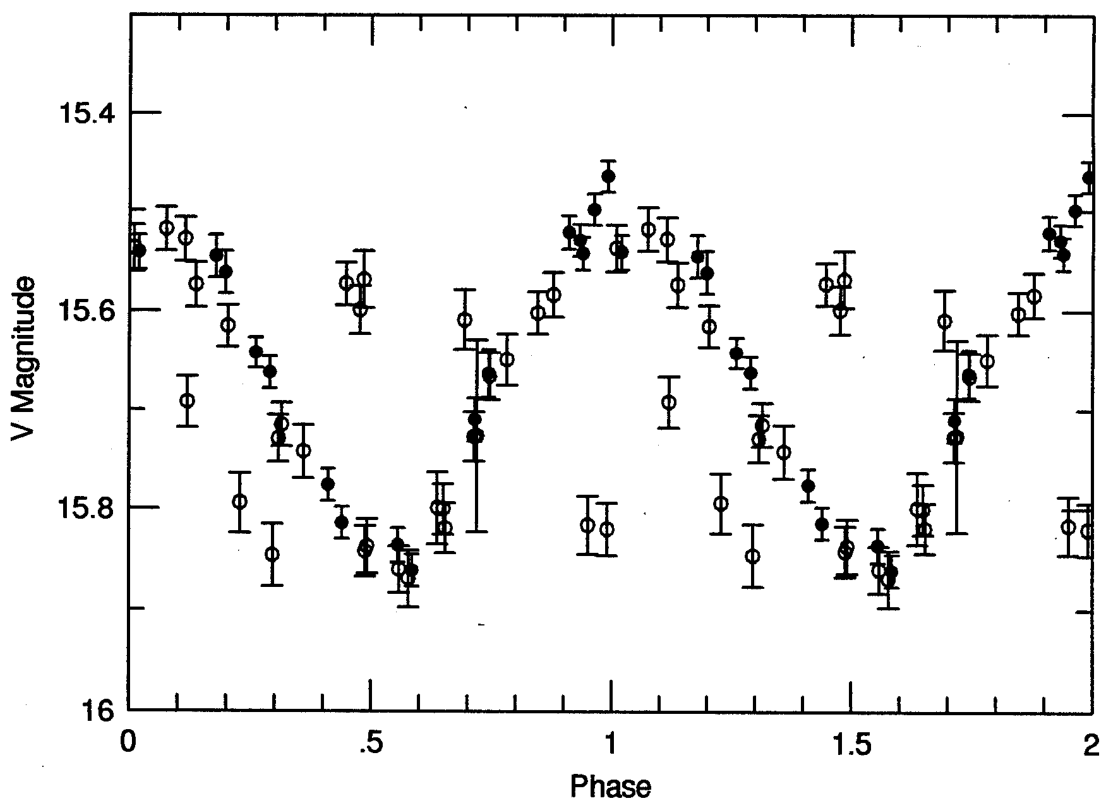

RA : 17 50 17.0

Dec: 28 01 00.0

<V> = 13.244

<B-V> = 0.28

P = 0.695000 days

Epoch = 3474.19

Type: W UMa

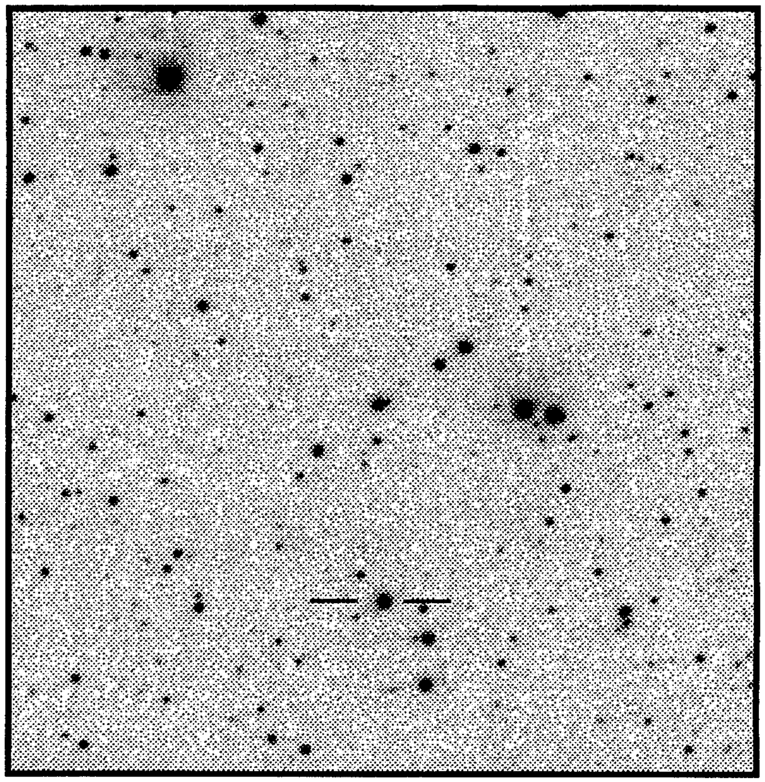

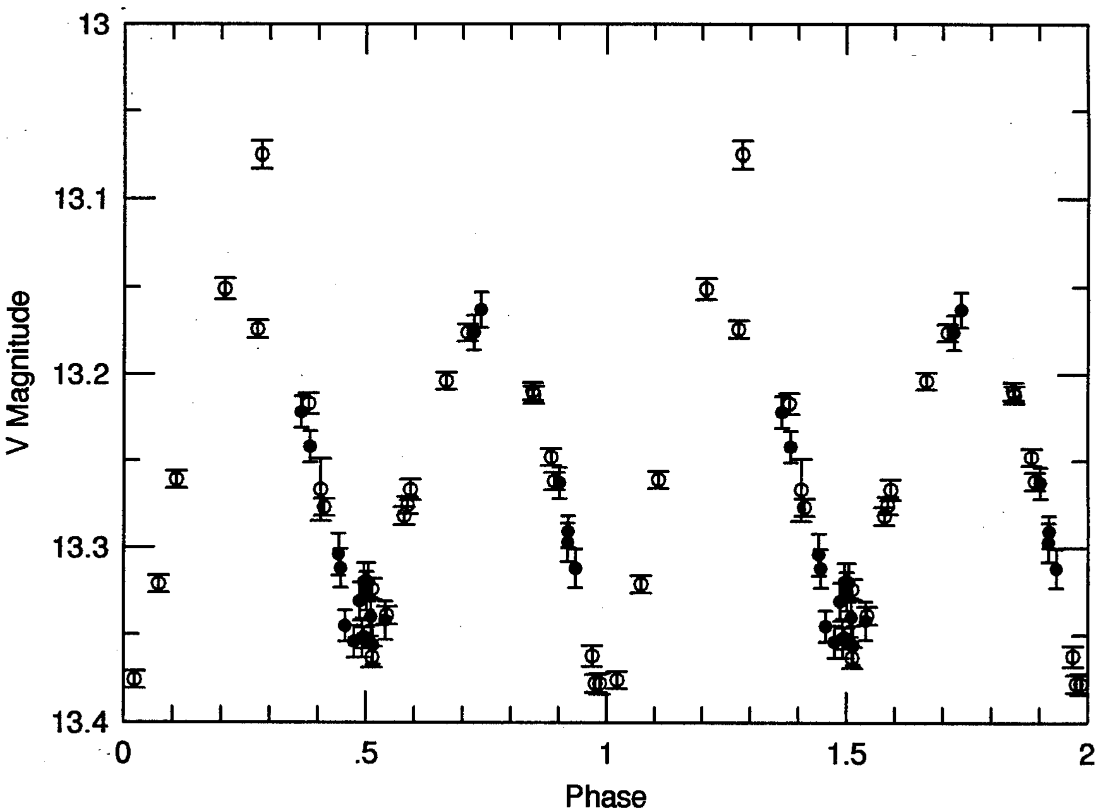

RA : 18 11 01.2

Dec: 27 59 27.4

<V> = 17.072

<B-V> = 0.38

P = 0.454185 days

Epoch = 3181.102

Type: RRab

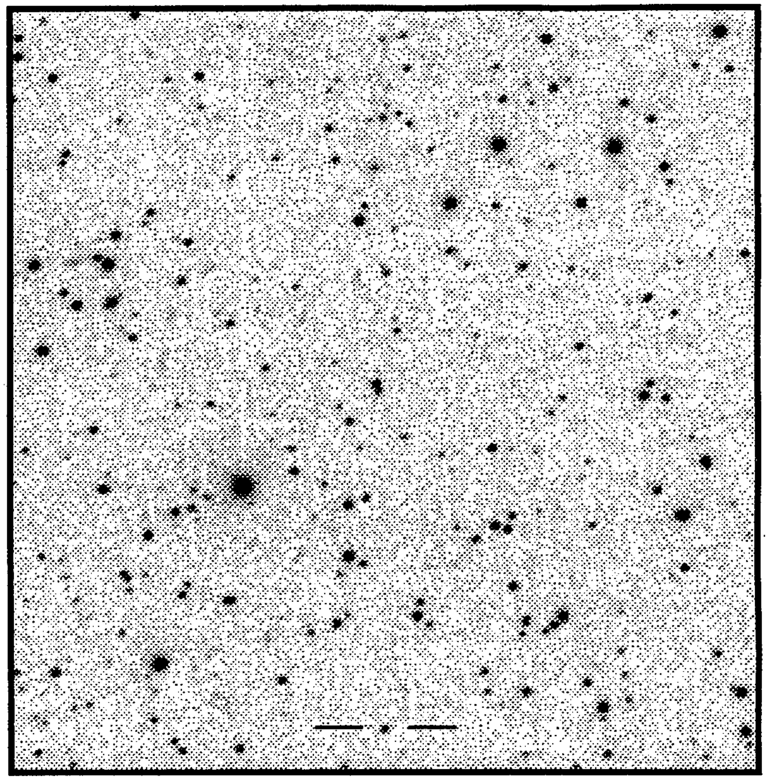

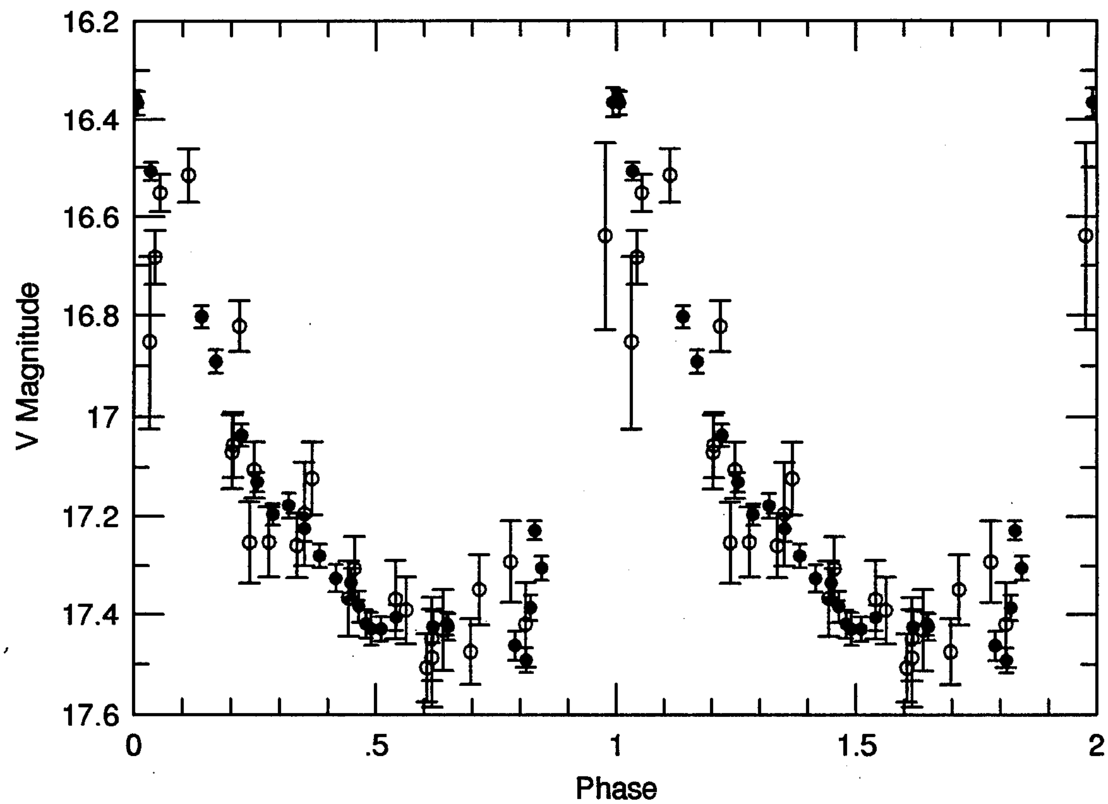

RA : 18 11 26.7

Dec: 28 03 45.4

<V> = 15.610

<B-V> = 0.43

P = 0.541466 days

Epoch = 3169.122

Type: RRab

V532 Her

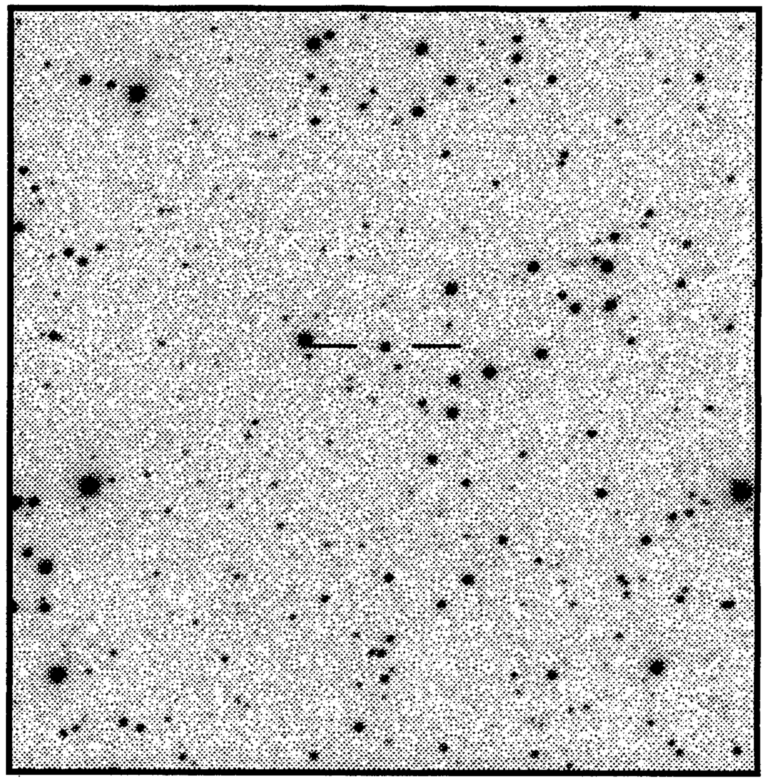

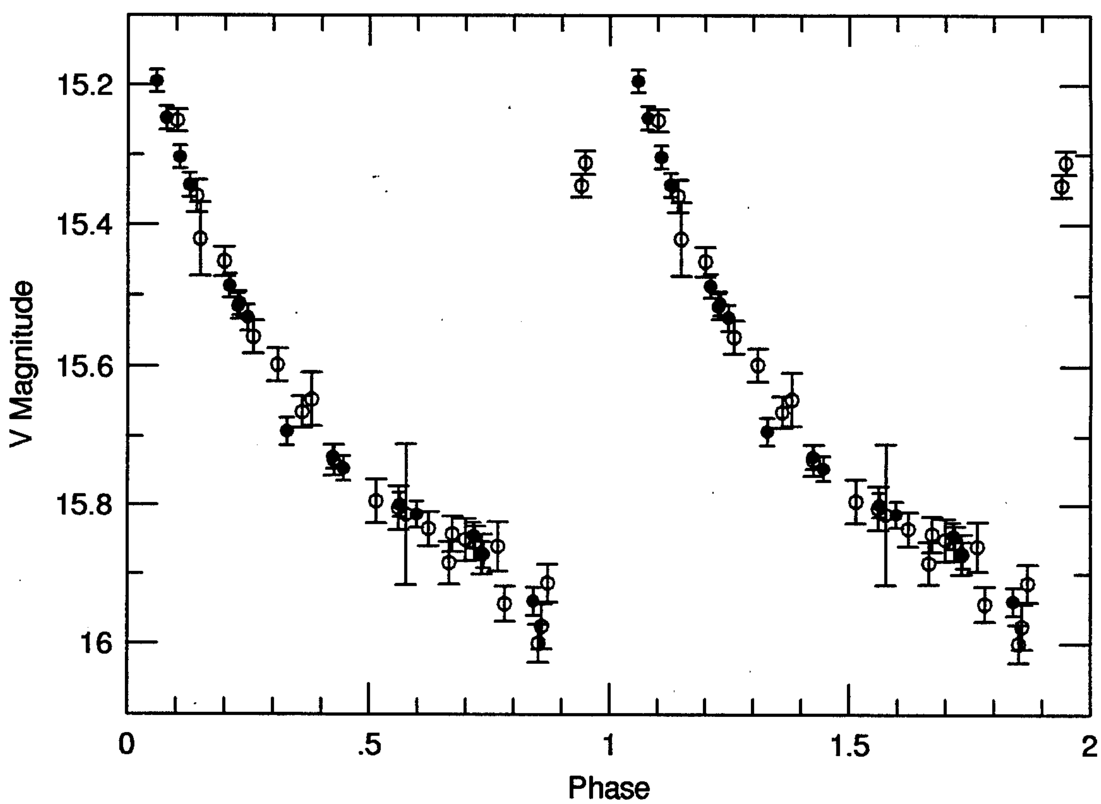

RA : 18 36 06.3
Dec: 28 03 21.6
<V> = 16.621
<B-V> = 0.49
P = 0.484114 days
Epoch = 3175.196
Type: RRab

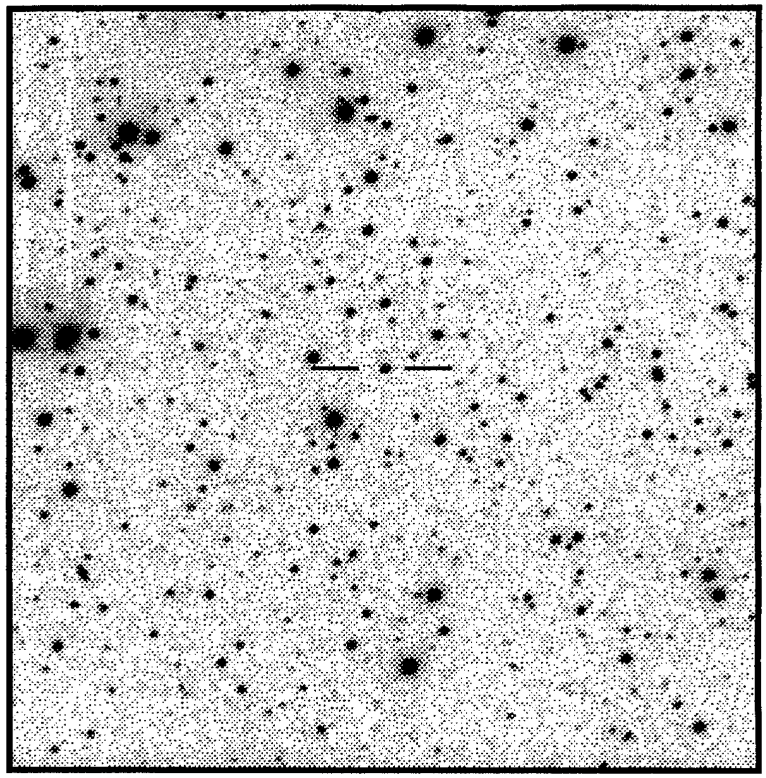

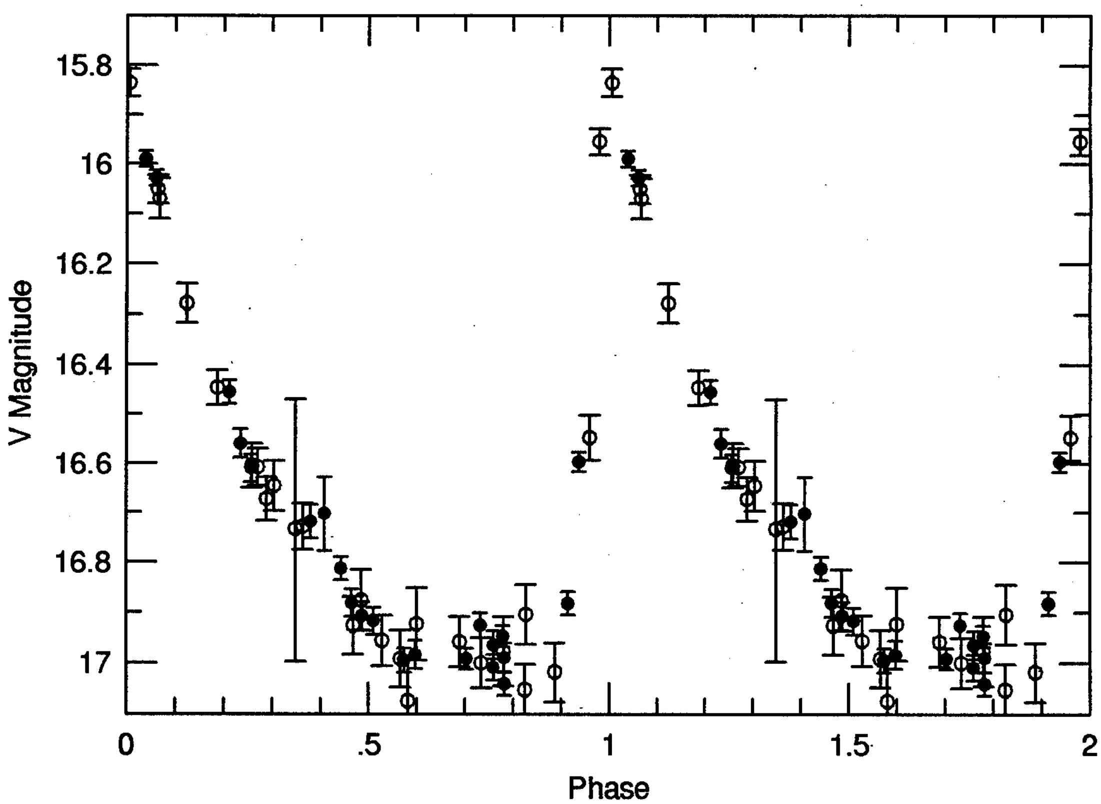

RA : 18 39 18.3
Dec: 28 04 16.6
<V> = 16.698
<B-V> = 0.55
P = 0.709921 days
Epoch = 3516.300
Type: RRab

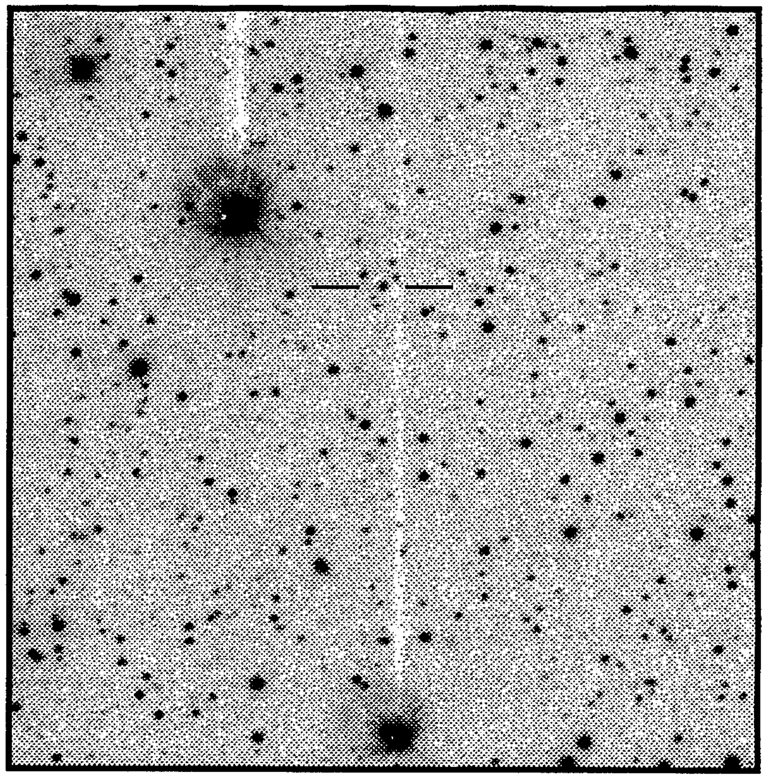

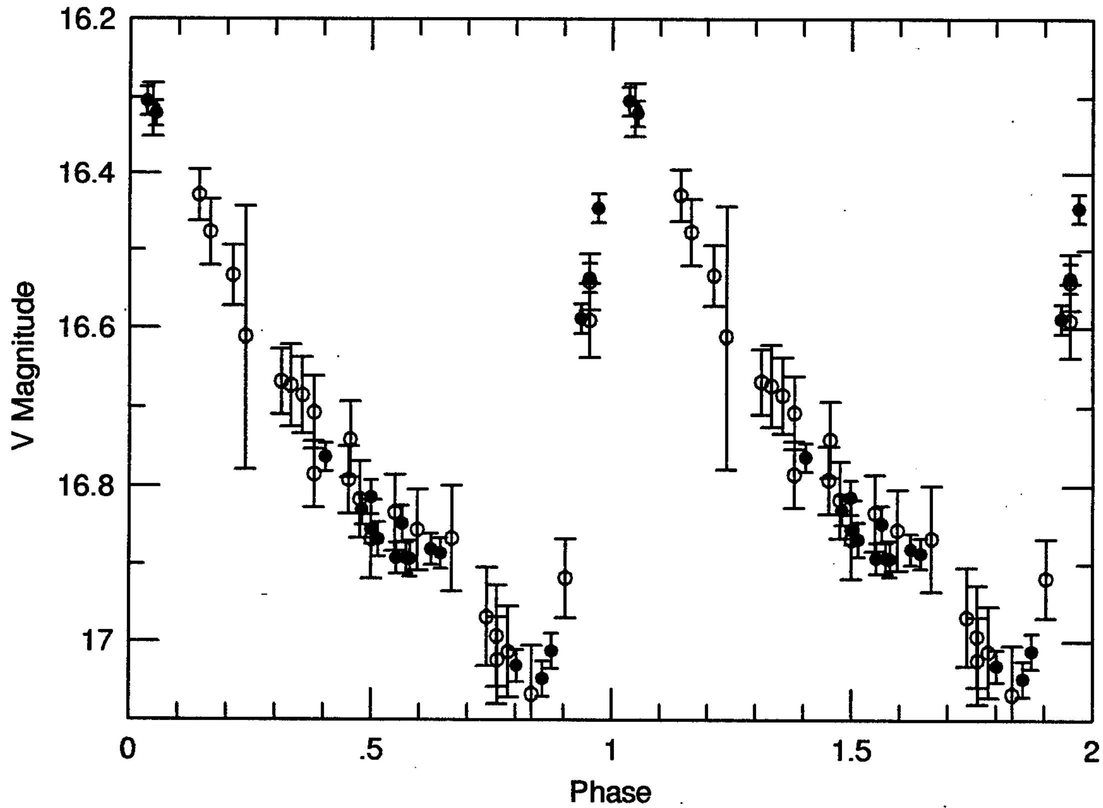

RA: 18 40 18.8
Dec: 28 00 54.1
<V> = 14.427
<B-V> = 0.52
P = 0.366912 days
Epoch = 3473.422
Type: W UMa

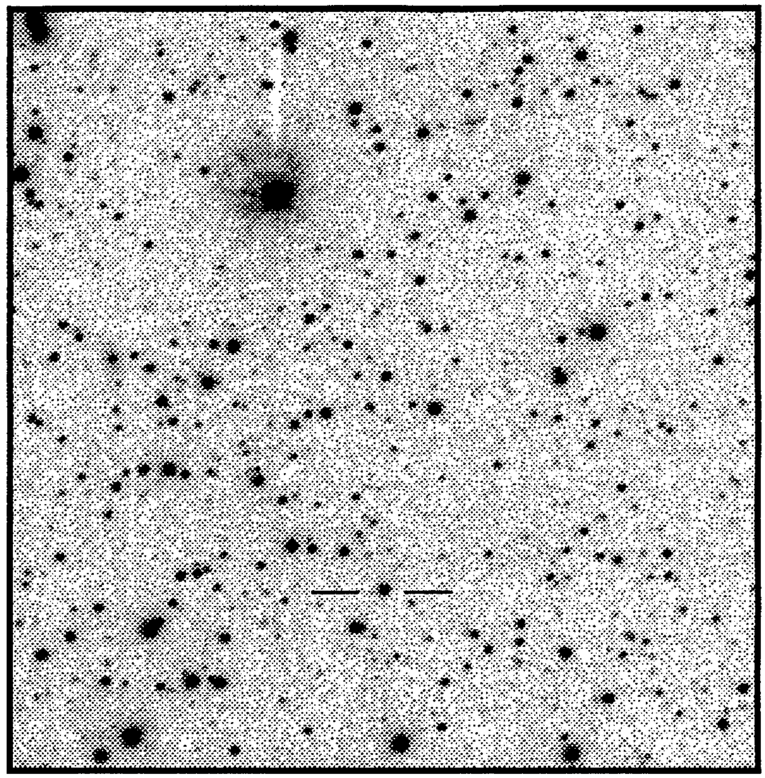

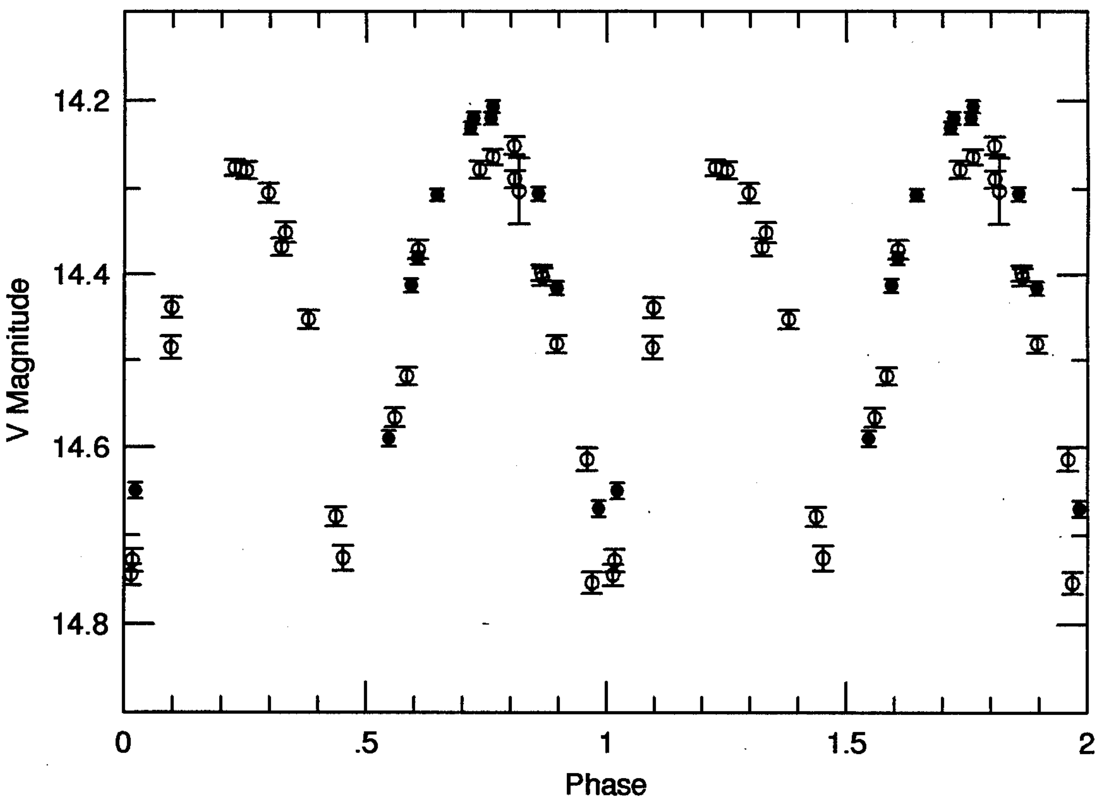

RA : 18 43 15.3
Dec: 28 01 14.7
<V> = 16.373
<B-V> = 0.66
P = 0.656278 days
Epoch = 3473.717
Type: W UMa

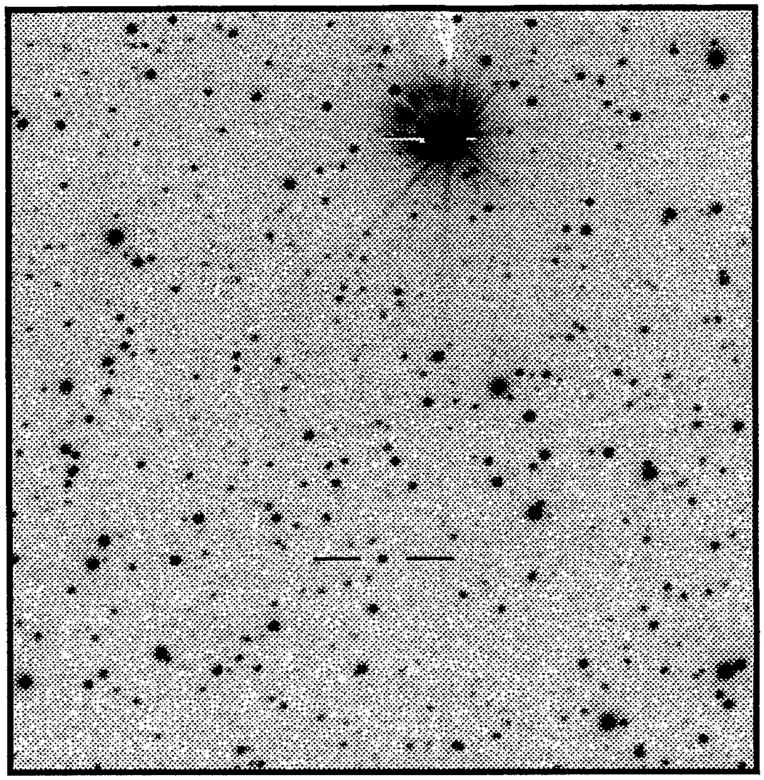

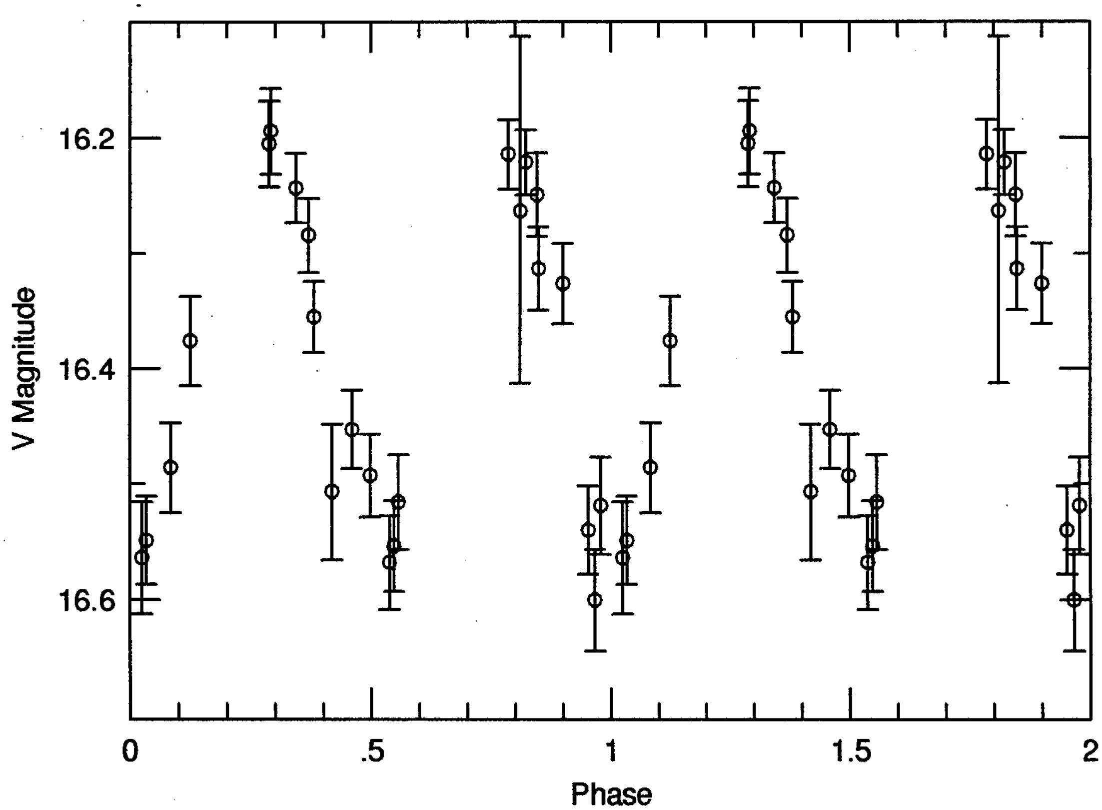

RA : 18 44 20.6
Dec: 27 59 36.6
<V> = 17.103
<B-V> = 0.45
P = 0.345930 days
Epoch = 3481.409
Type: W UMa

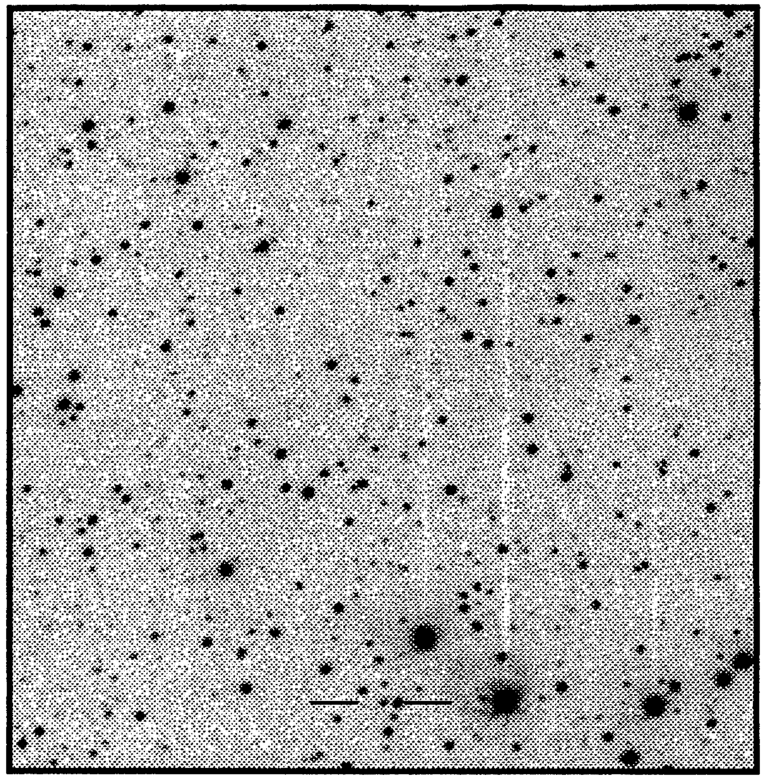

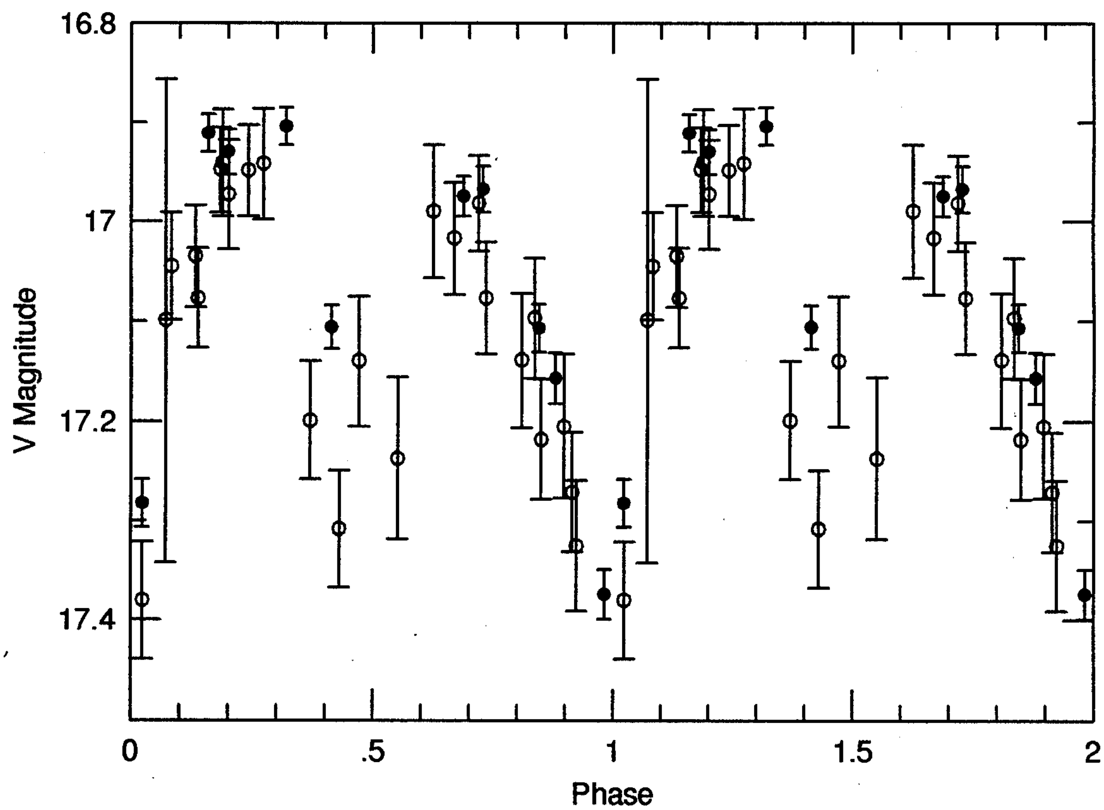

RA : 18 47 46.9
Dec: 28 04 47.0
<V> = 17.175
<B-V> = 0.65
P = 0.764461 days
Epoch = 3488.260
Type: RRab B

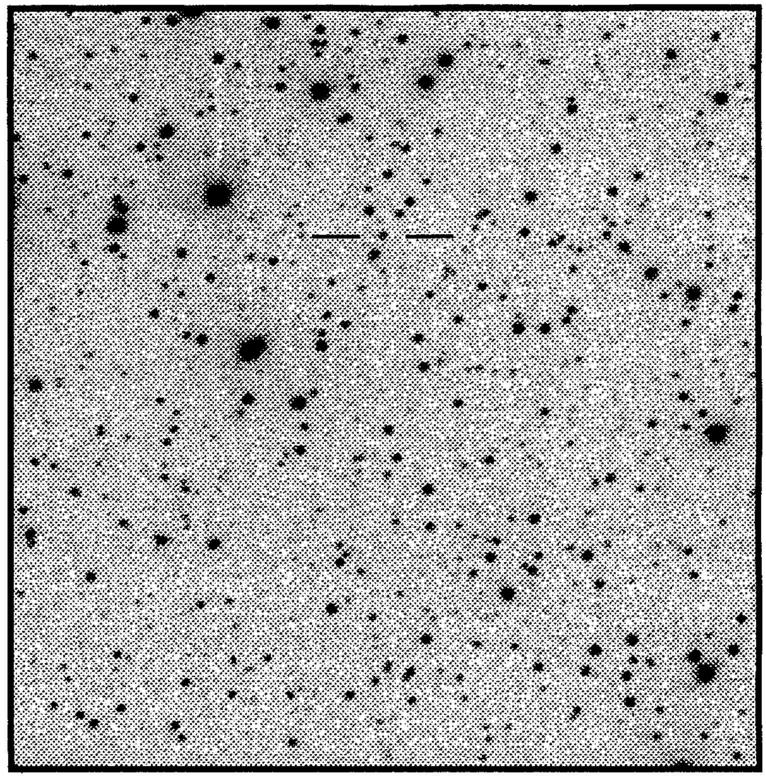

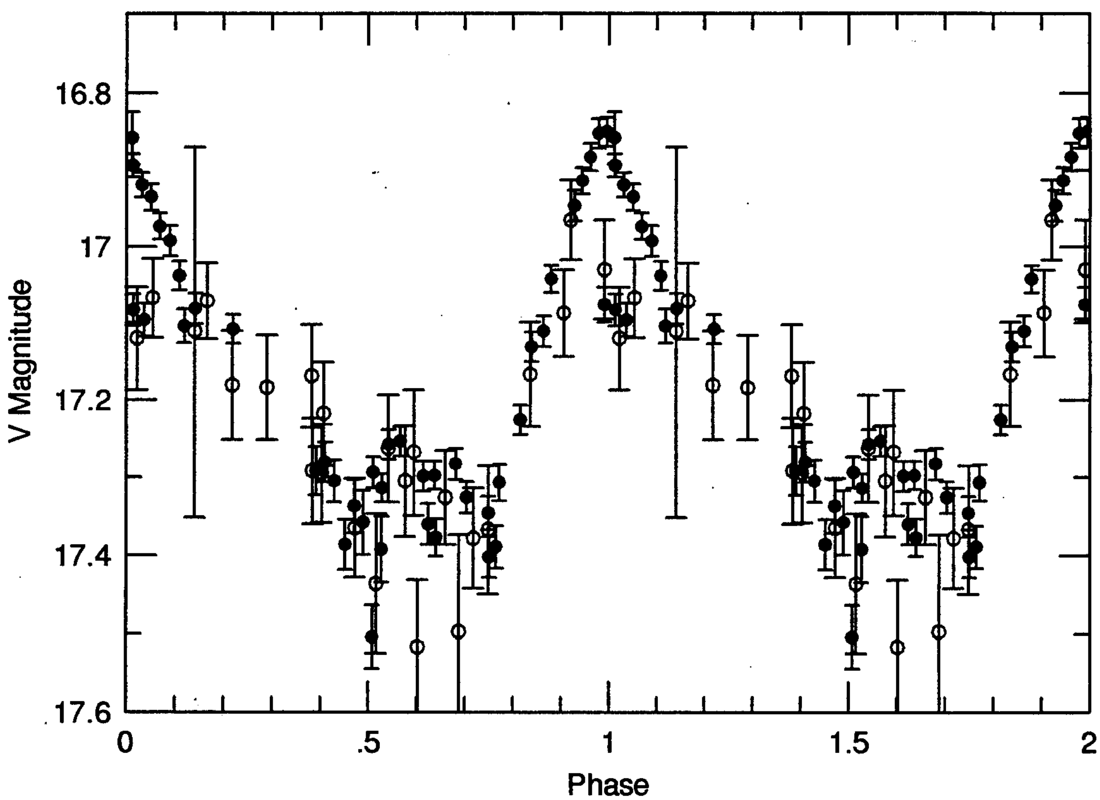

RA : 19 03 50.4

Dec: 28 00 44.9

<V> = 12.976

<B-V> = 1.75

Type: Irregular

GS Lyr

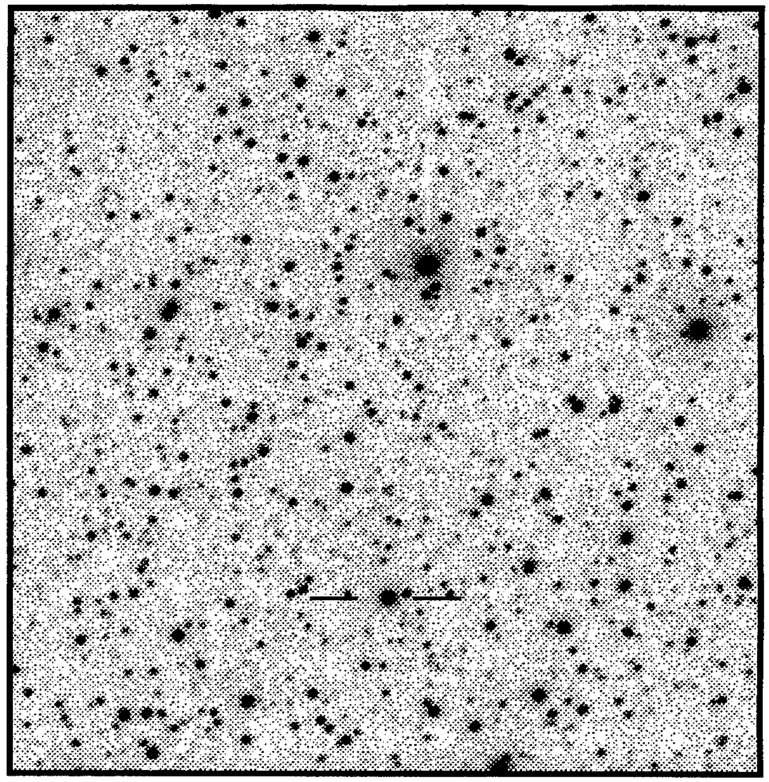

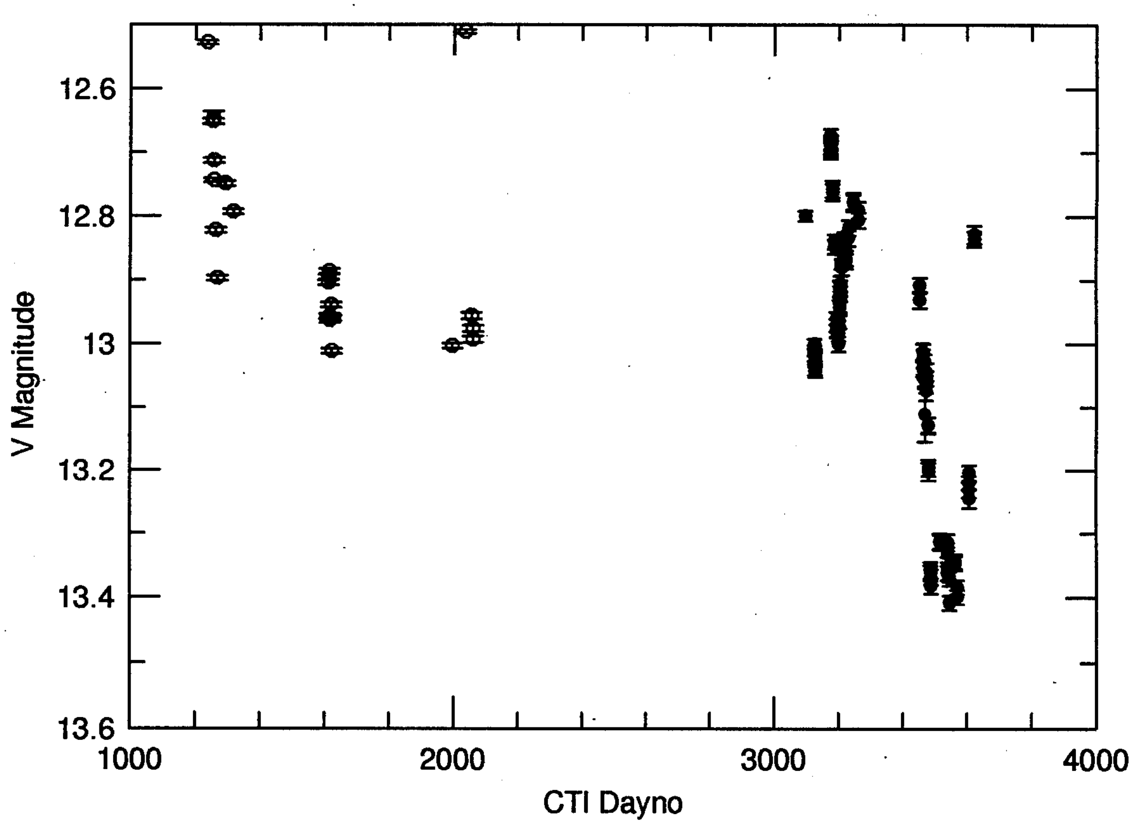

RA: 19 13 11.8

Dec: 28 00 51.5

<V> = 16.359

<B-V> = 0.60

P = 0.424599 days

Epoch = 3474.433

Type: RRab

V427 Lyr

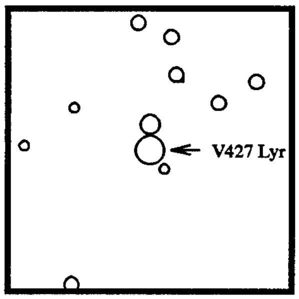


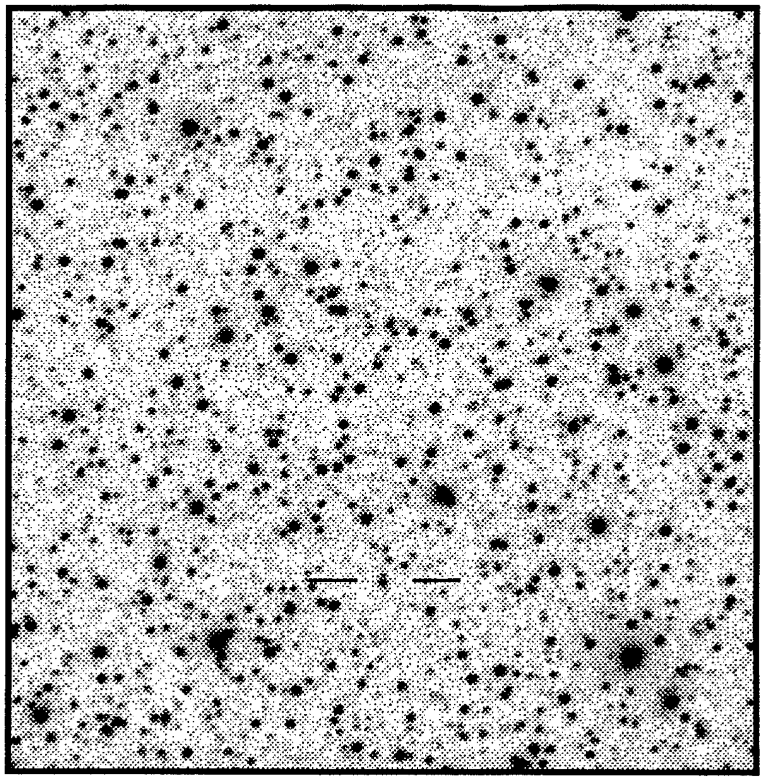

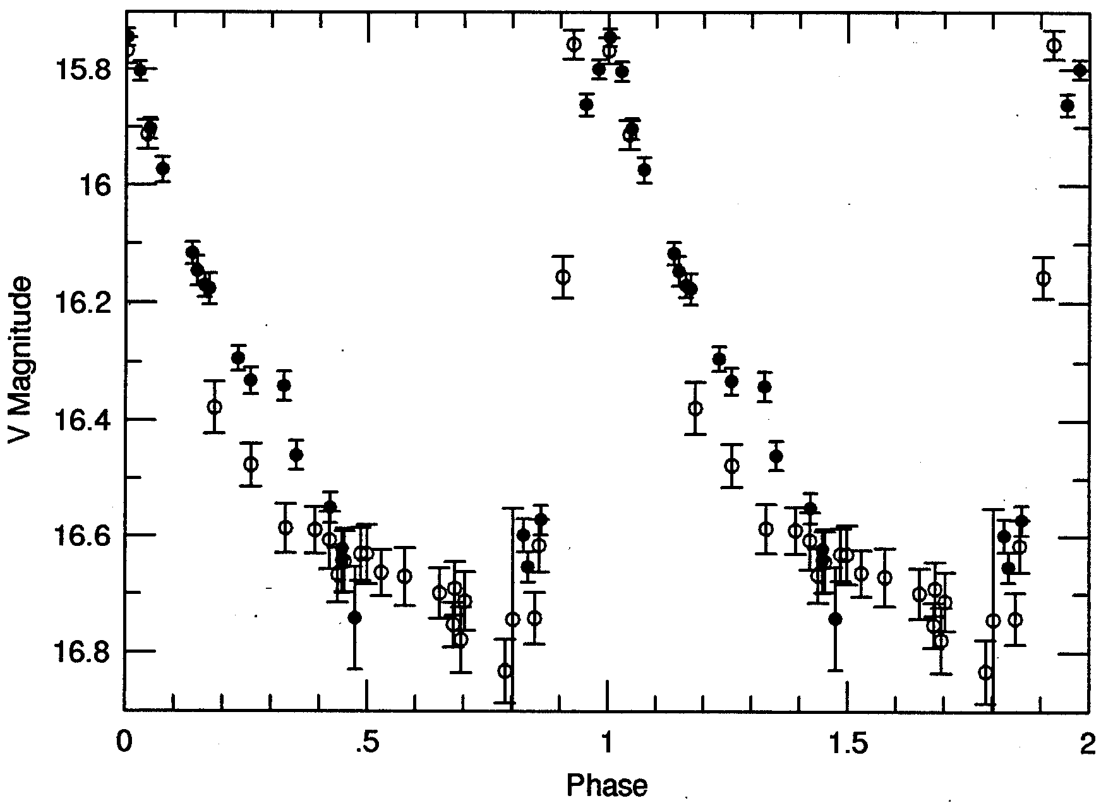

RA : 19 38 06.6

Dec: 27 59 09.9

<V> = 15.131

<B-V> = 0.60

P = 0.306999 days

Epoch = 3488.337

Type: RRc

V926 Cyg

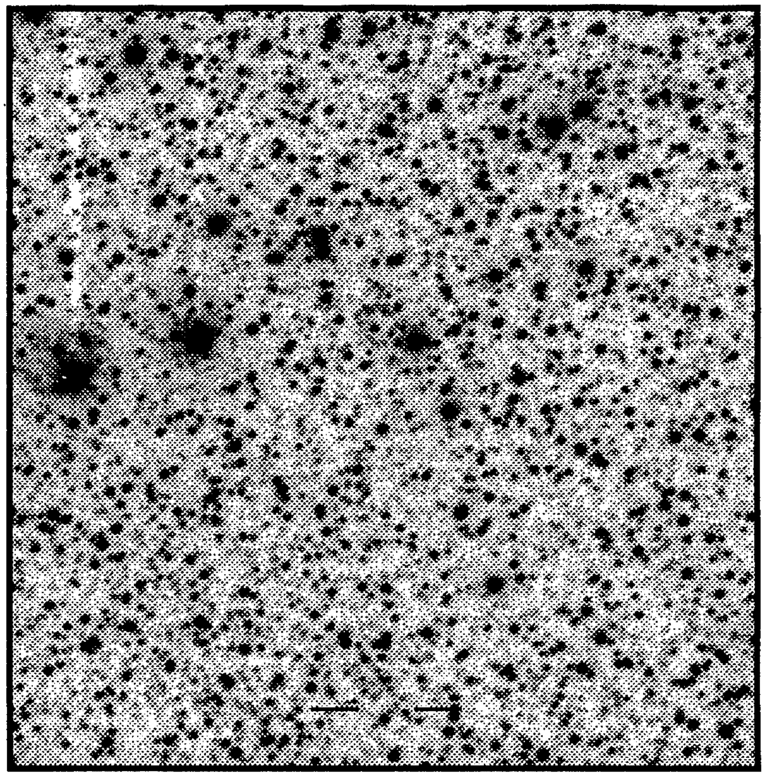

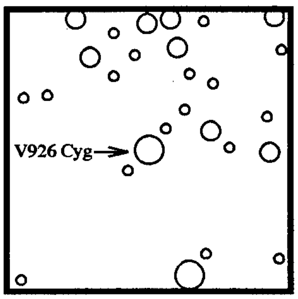


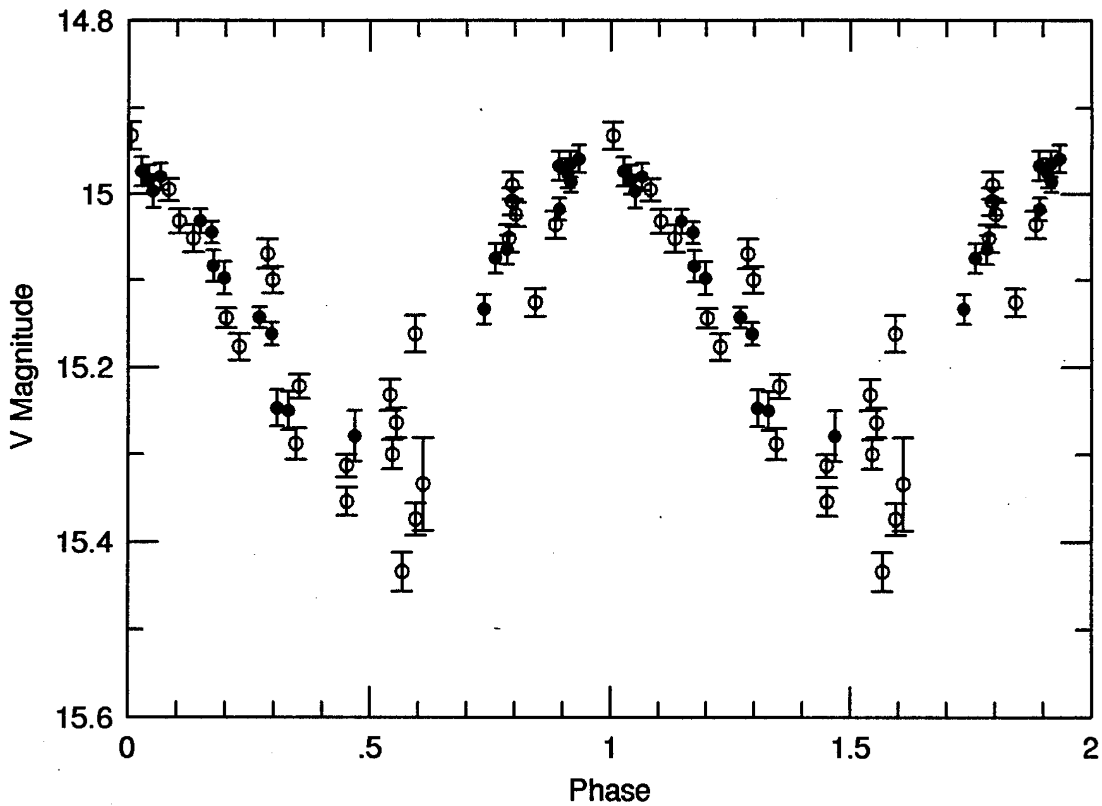

RA : 21 07 16.1

Dec: 28 02 29.2

<V> = 12.894

<B-V> = 0.42

P = 0.438854 days

Epoch = 3517.448

Type: W UMa

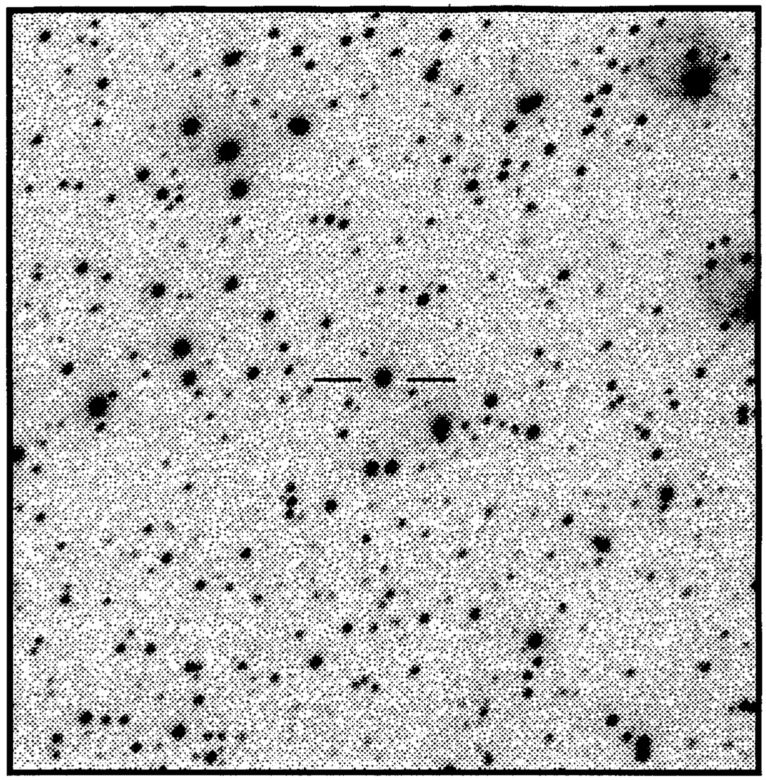

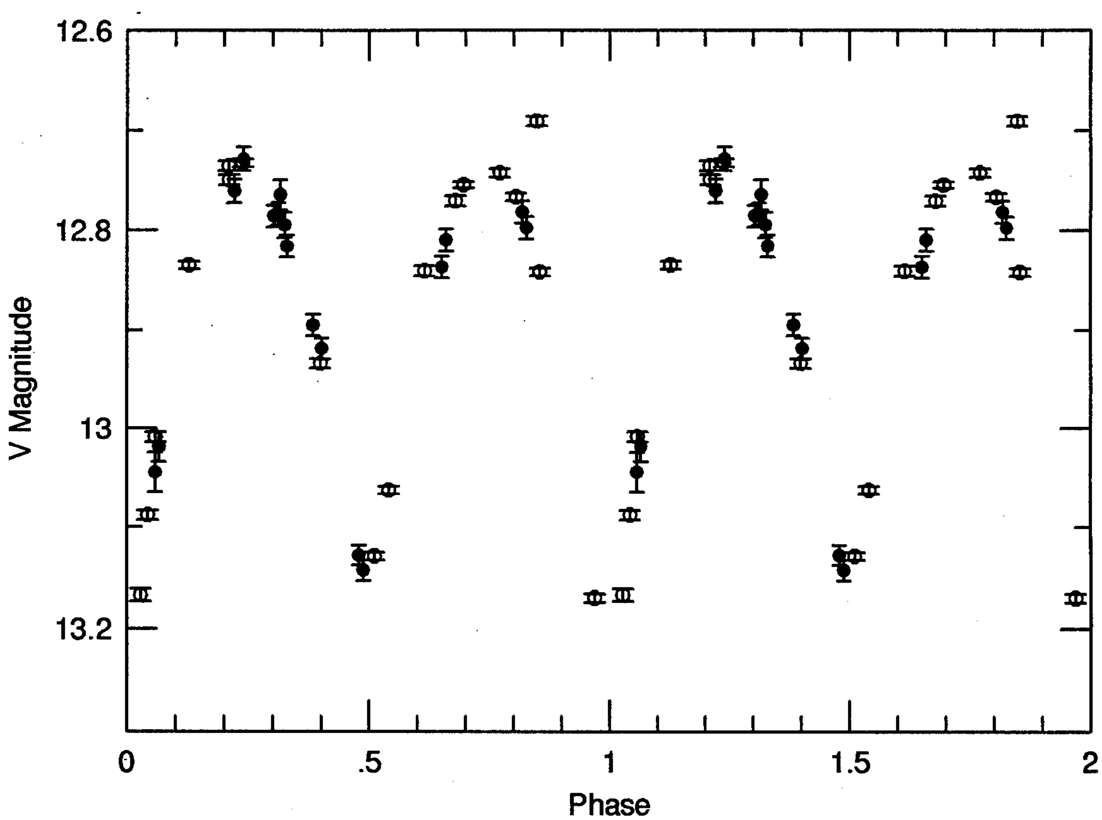

RA : 21 20 11.2
Dec: 28 06 09.3
<V> = 16.493
<B-V> = 0.43
P = 0.448676 days
Epoch = 3517.381
Type: RR

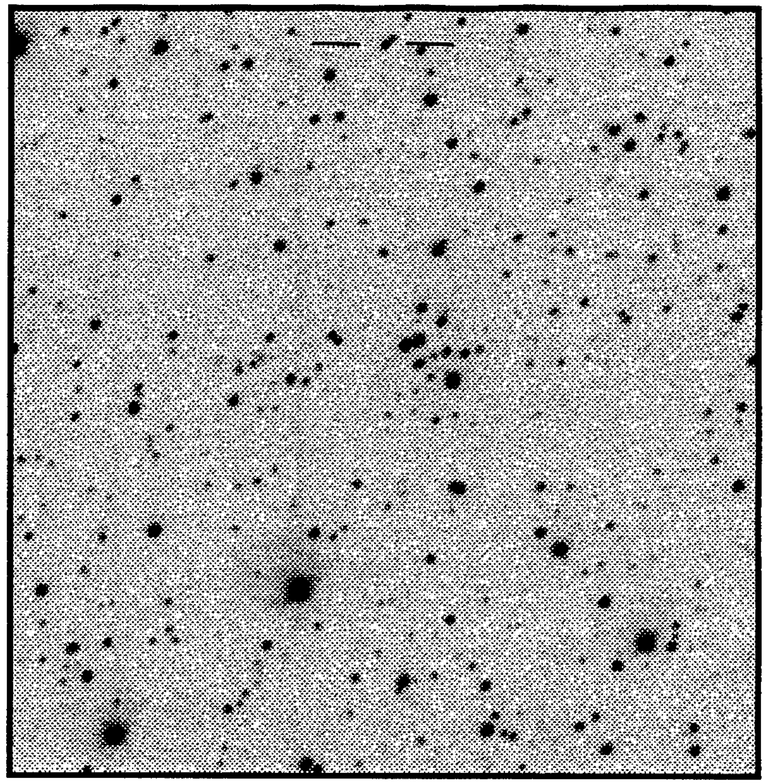

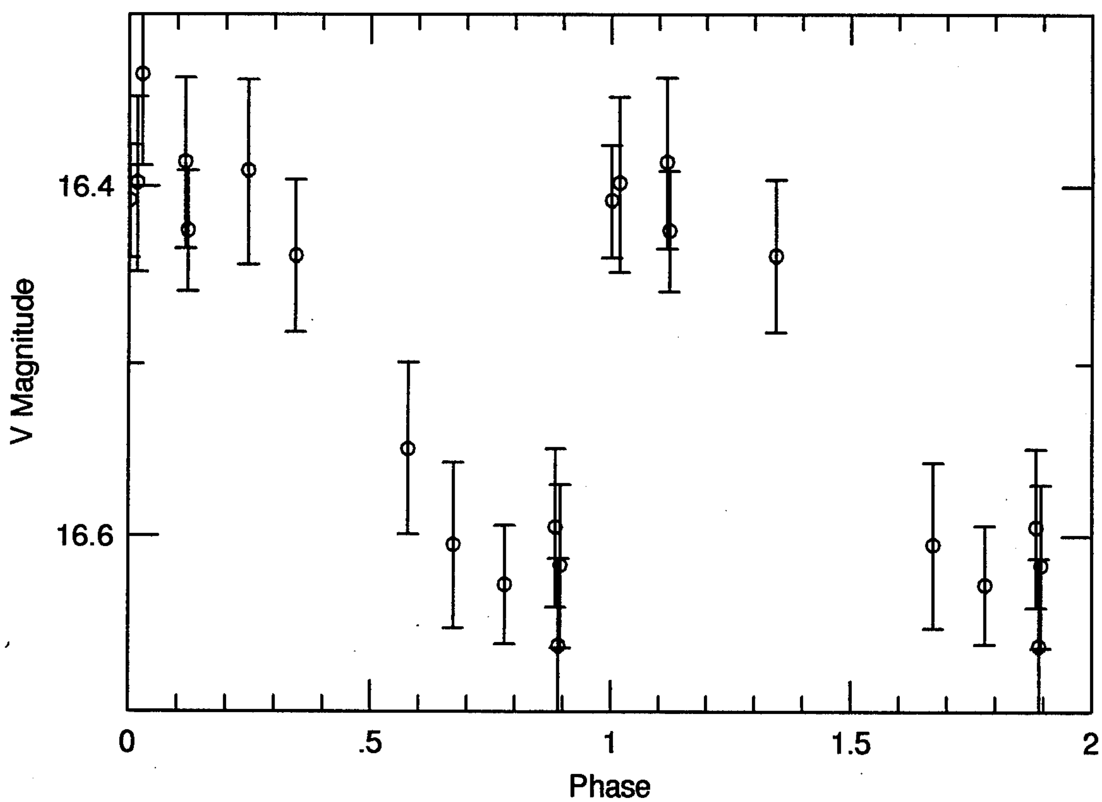

RA : 21 21 10.2
Dec: 28 05 56.5
<V> = 15.423
<B-V> = 0.25
P = 0.325160 days
Epoch = 3517.511
Type: RRc

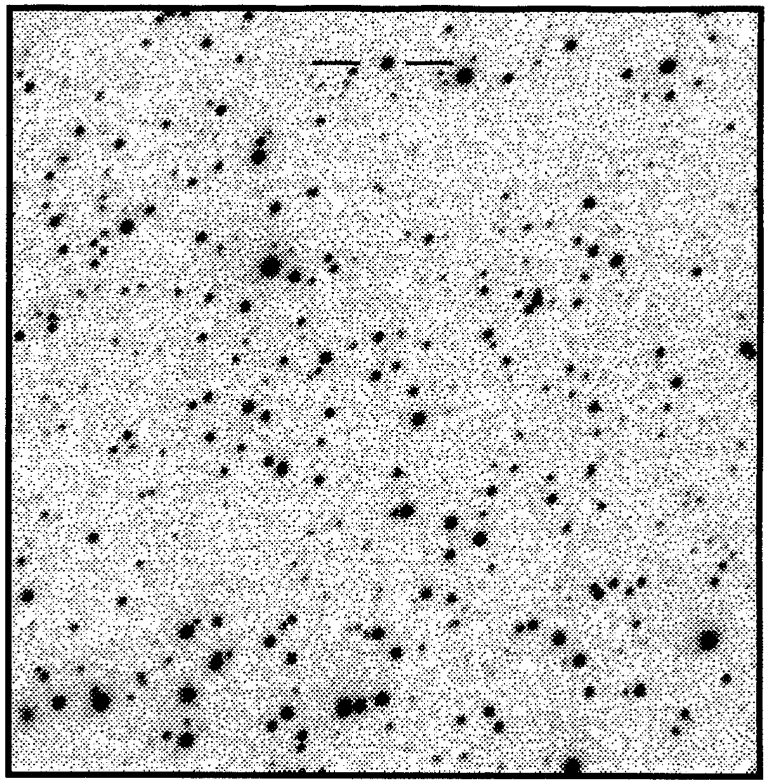

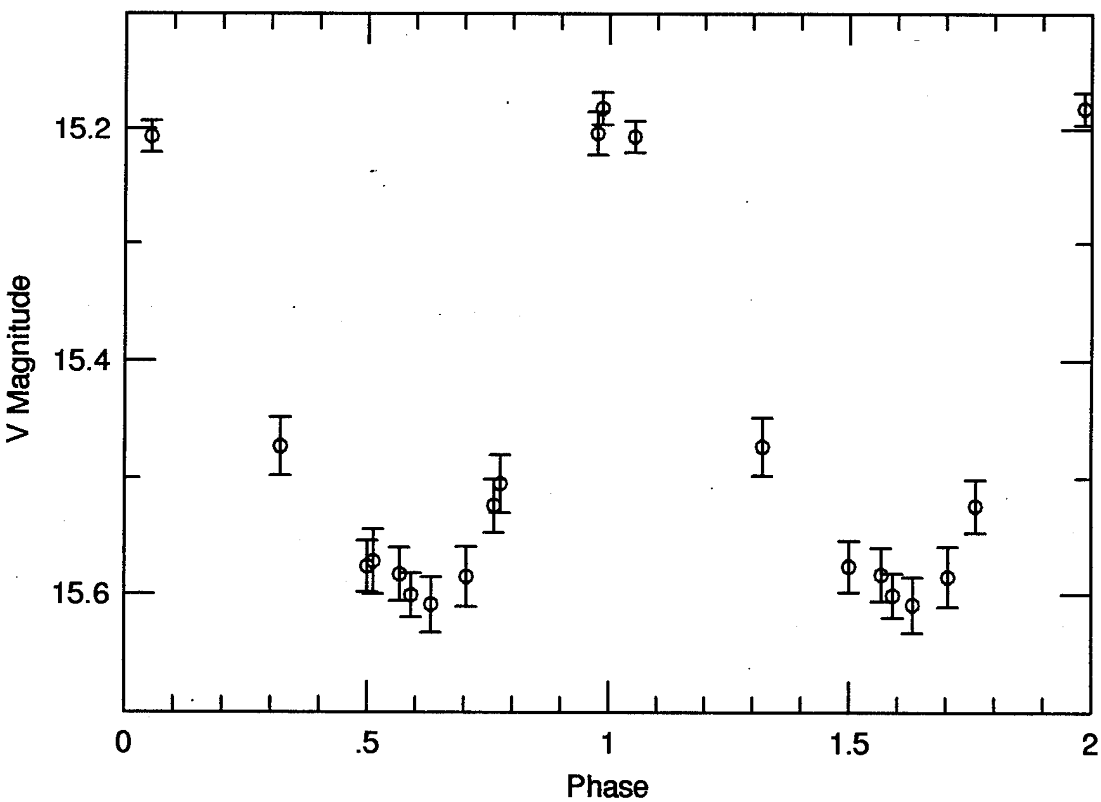

RA : 21 34 29.8
Dec: 28 01 56.9
<V> = 16.892
<B-V> = 0.70
P = 0.333247 days
Epoch = 3516.360
Type: W UMa

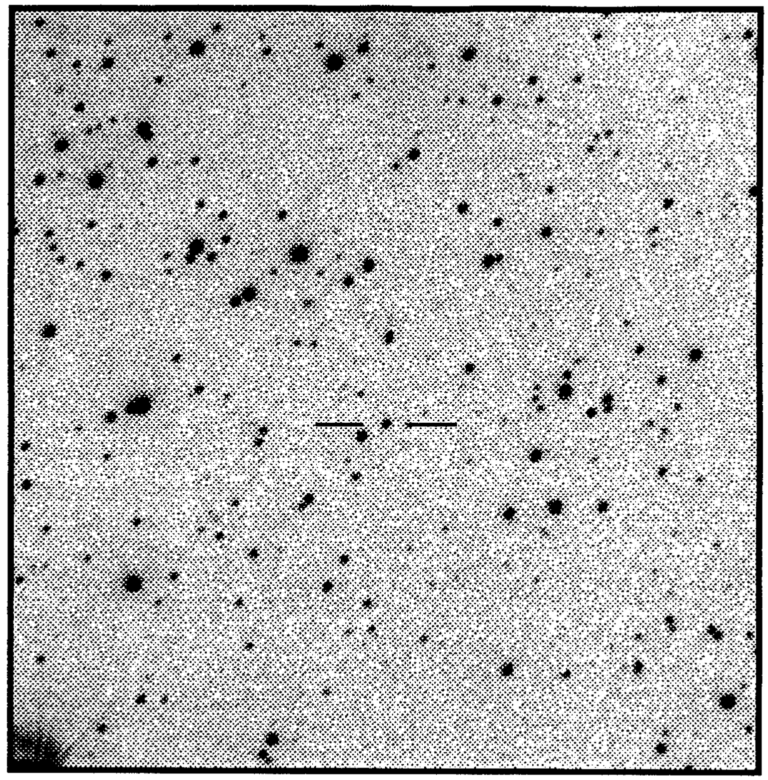

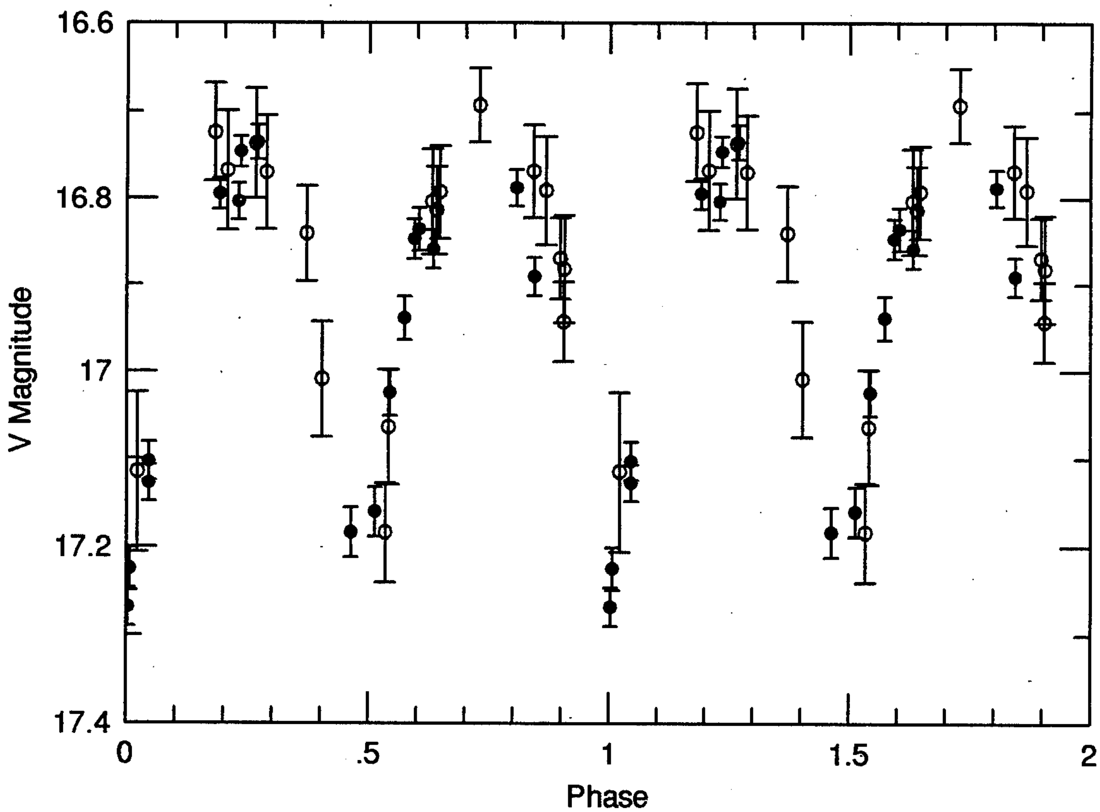

RA : 21 46 11.6
Dec: 28 00 57.2
<V> = 15.233
<B-V> = 0.45
P = 0.592806 days
Epoch = 3517.220
Type: RRab

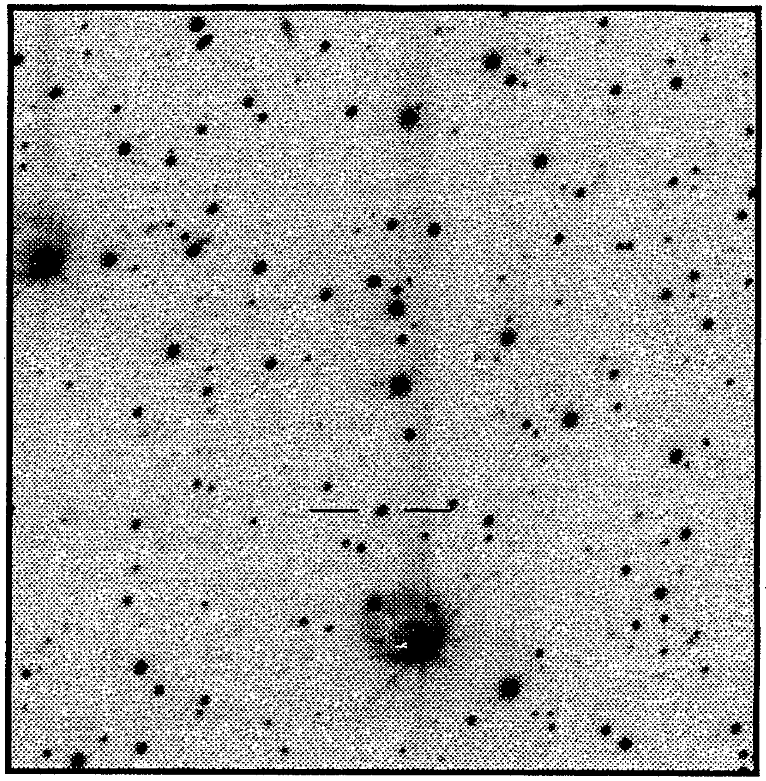

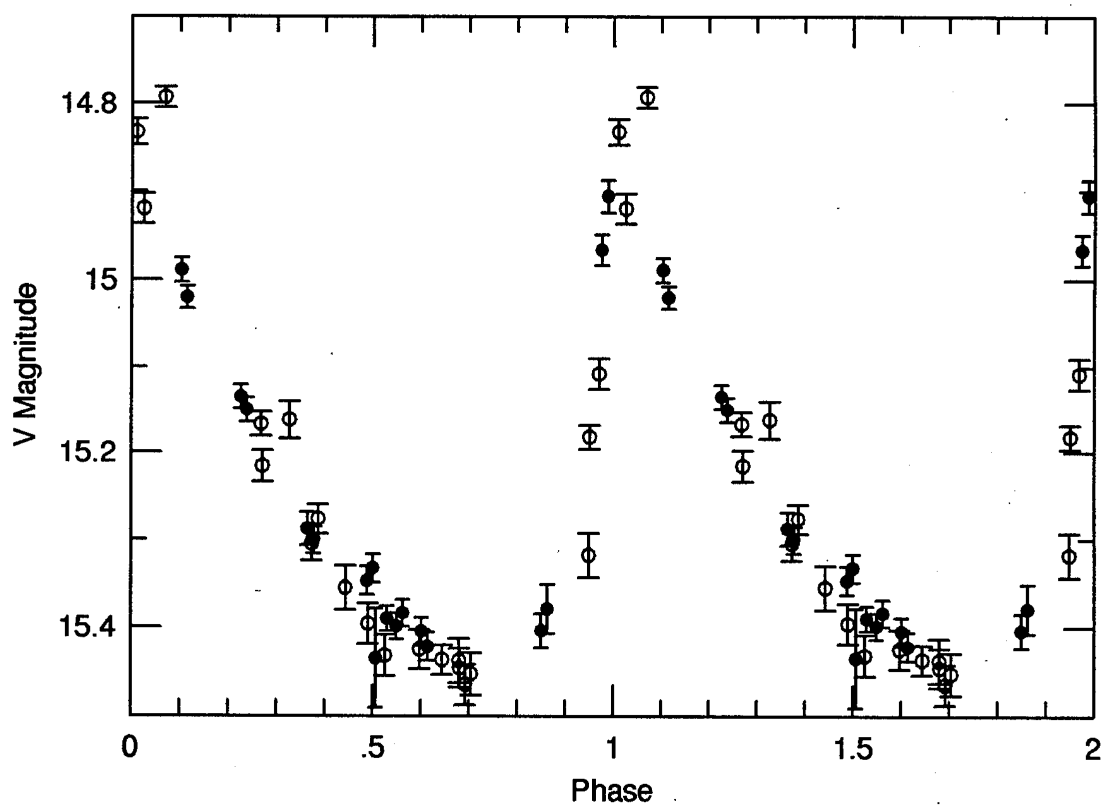

RA : 21 57 35.4
Dec: 28 02 37.5
<V> = 17.137
<B-V> = 0.38
P = 0.464627 days
Epoch = 3234.243
Type: RRab

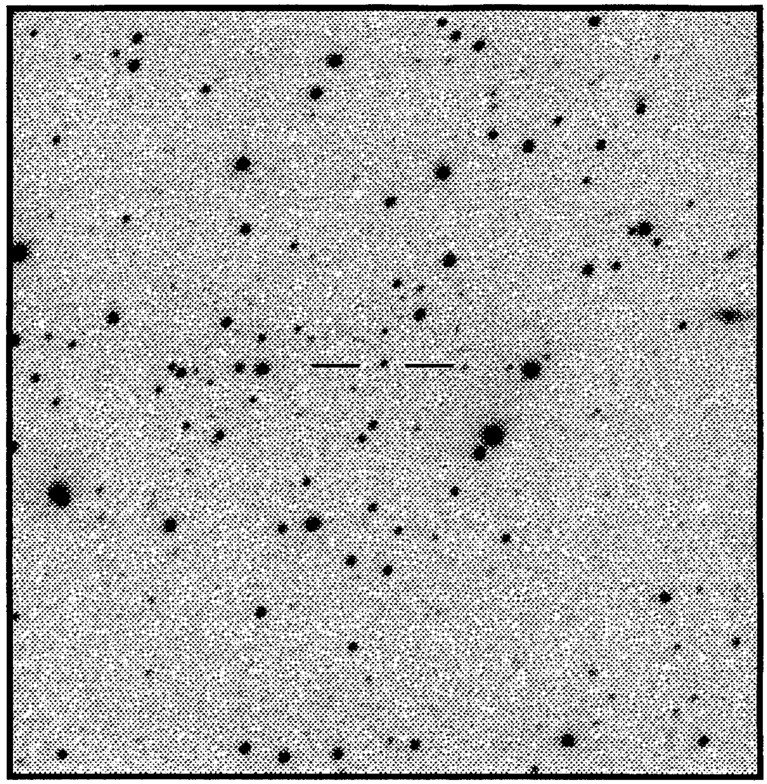

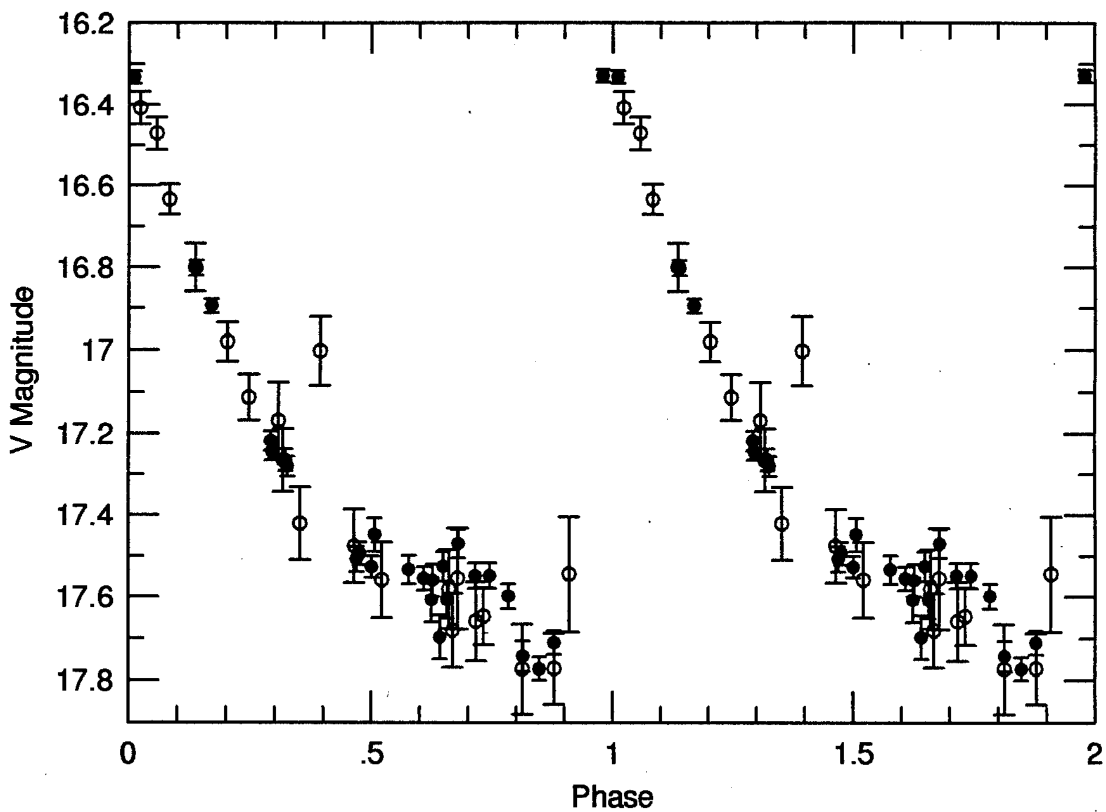

RA : 21 58 16.5
Dec: 27 58 09.5
<V> = 15.192
<B-V> = 0.35
P = 0.525361 days
Epoch = 3660.060
Type: RRab

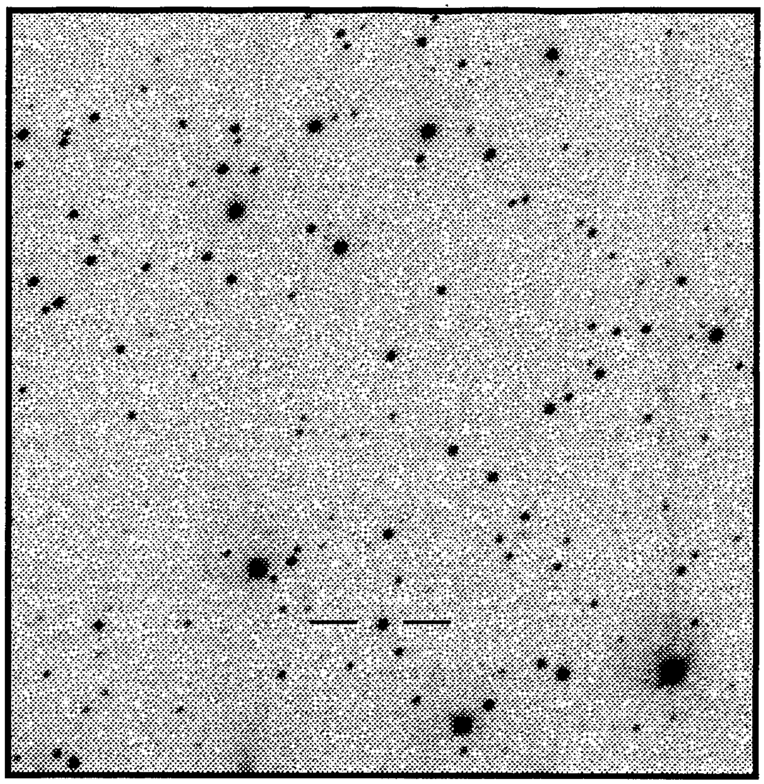

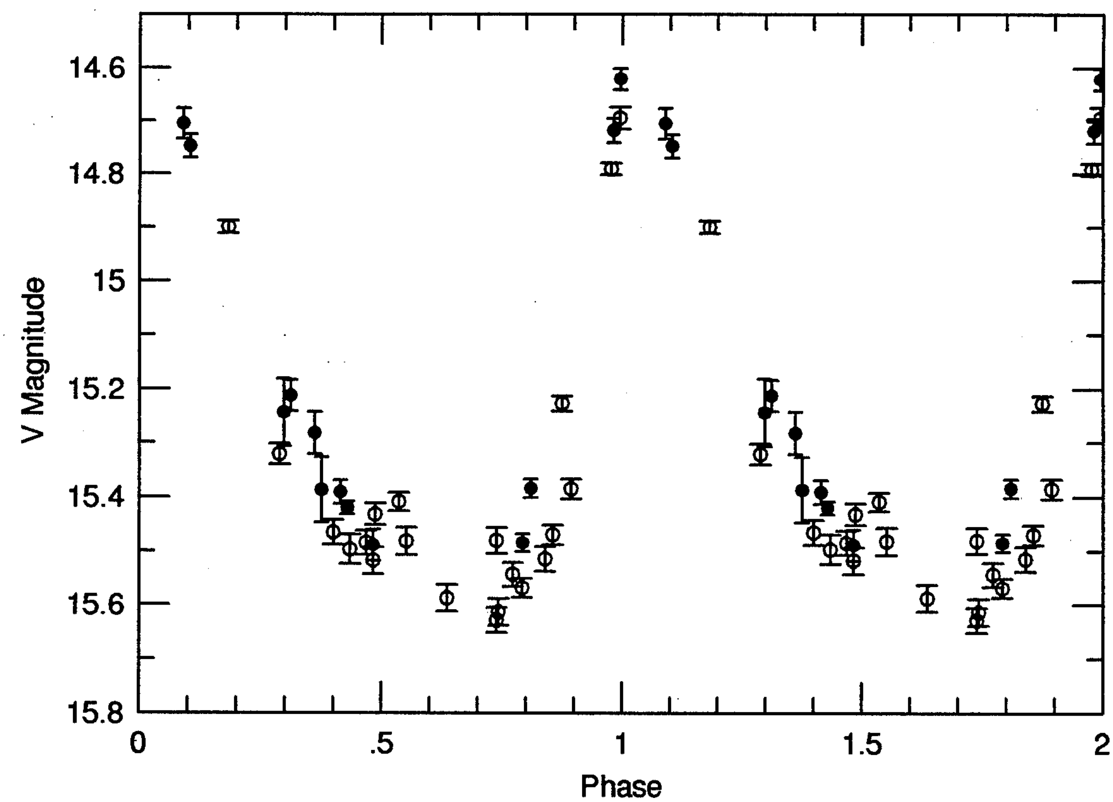

RA : 22 00 54.8

Dec: 28 00 20.1

<V> = 15.630

<B-V> = 0.38

P = 0.529309 days

Epoch = 3517.108

Type: RRab

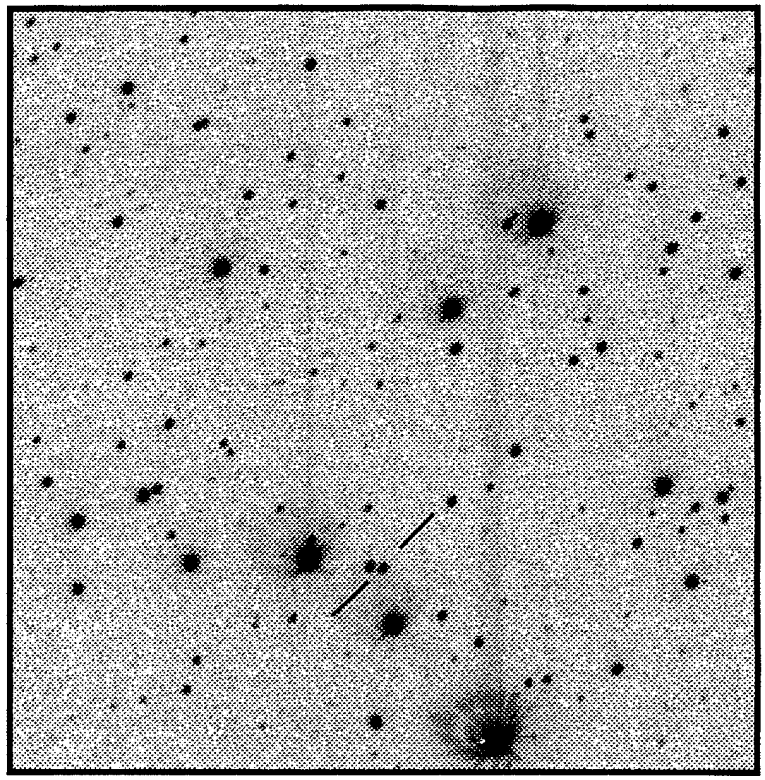

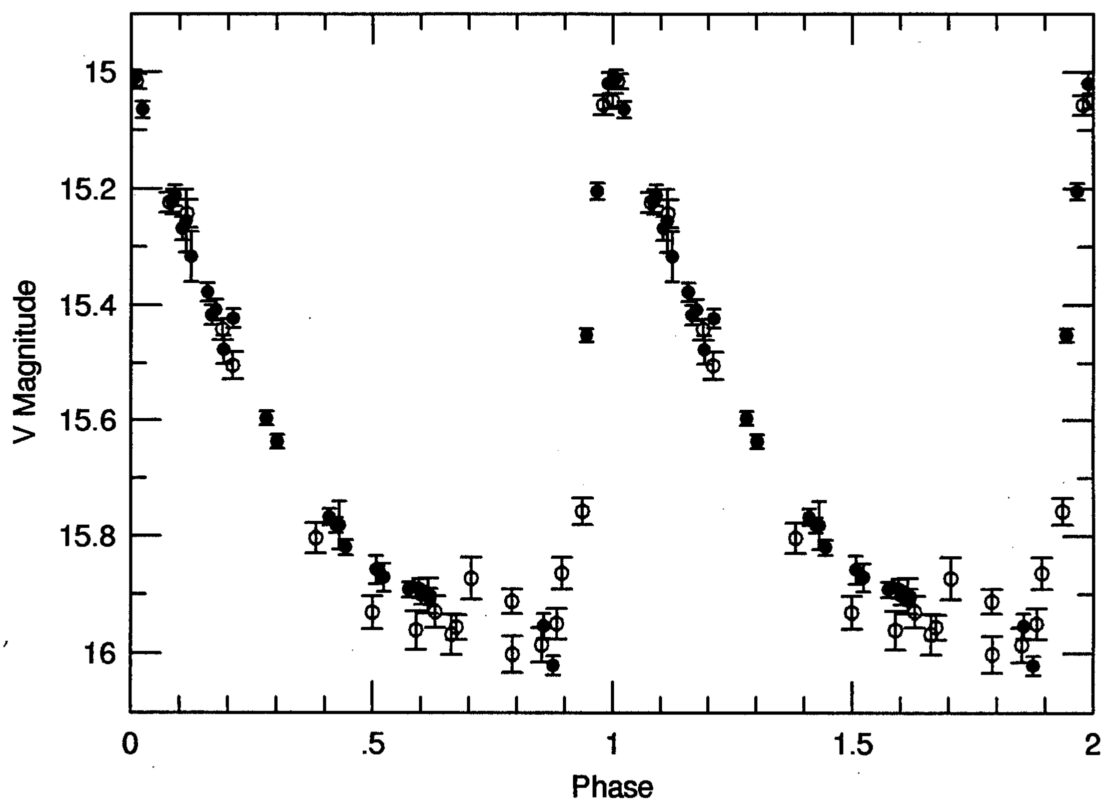

RA : 22 02 44.8
Dec: 27 59 04.0
<V> = 13.927
<B-V> = 0.79
P = 0.279144 days
Epoch = 3478.351
Type: W UMa

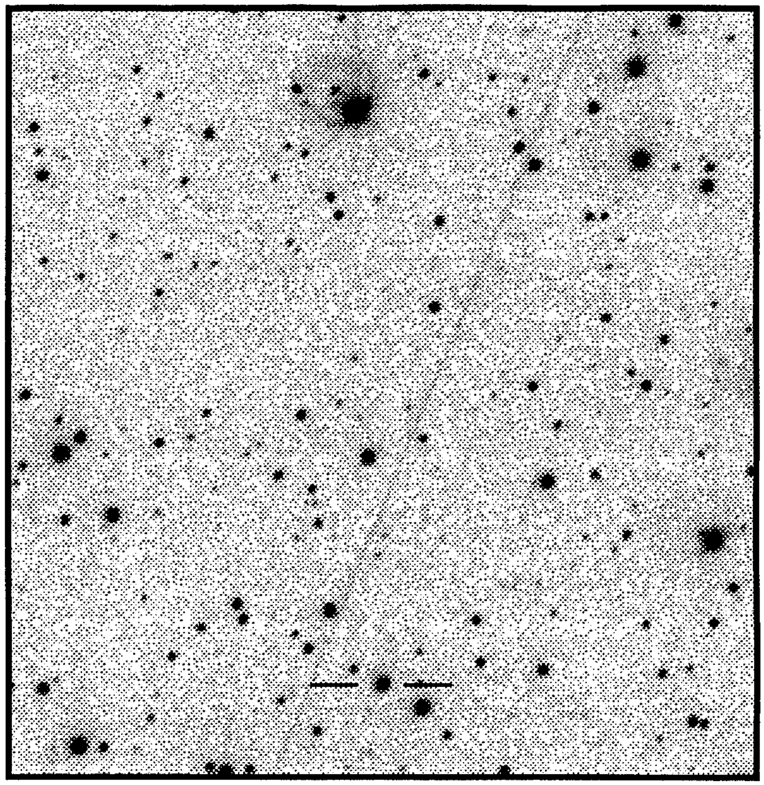

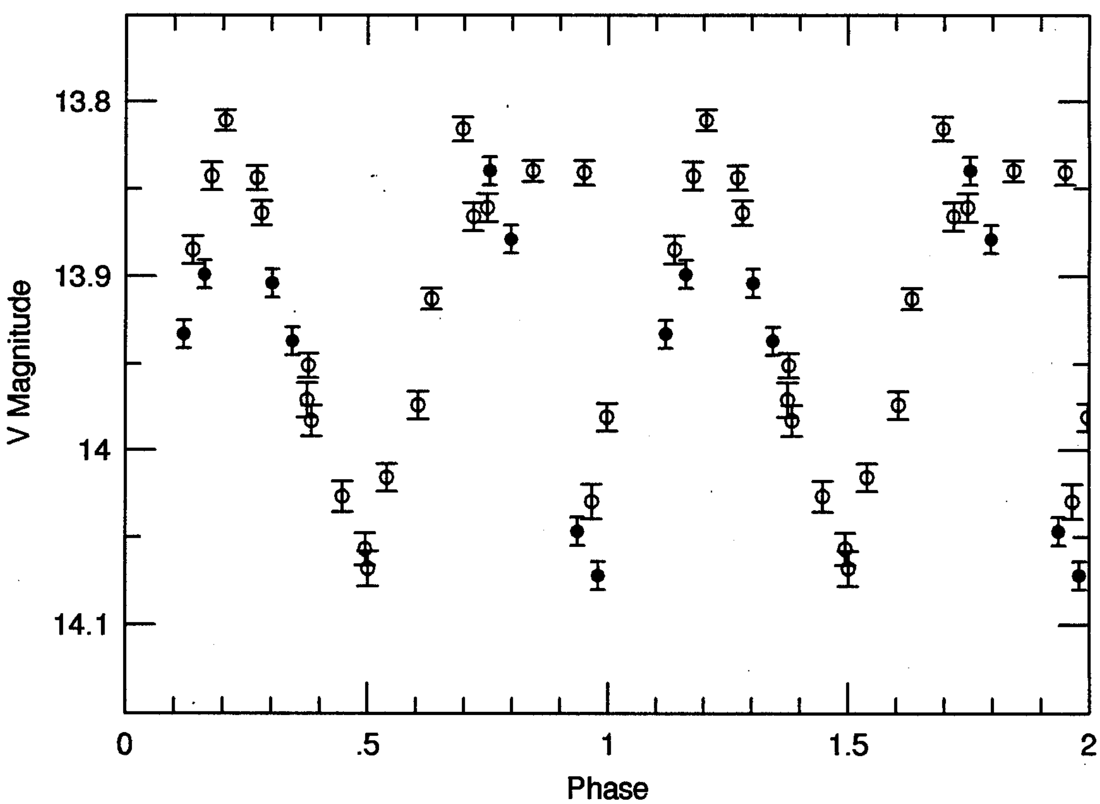

RA : 22 10 22.8

Dec: 28 04 16.2

<V> = 16.566

<B-V> = 0.30

P = 0.554907 days

Epoch = 3673.098

Type: RRab B

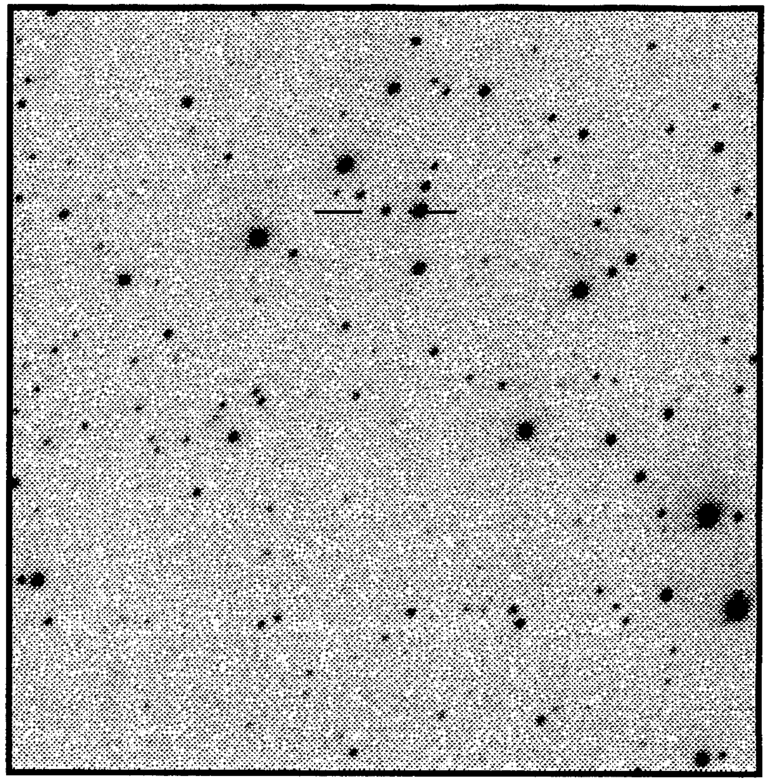

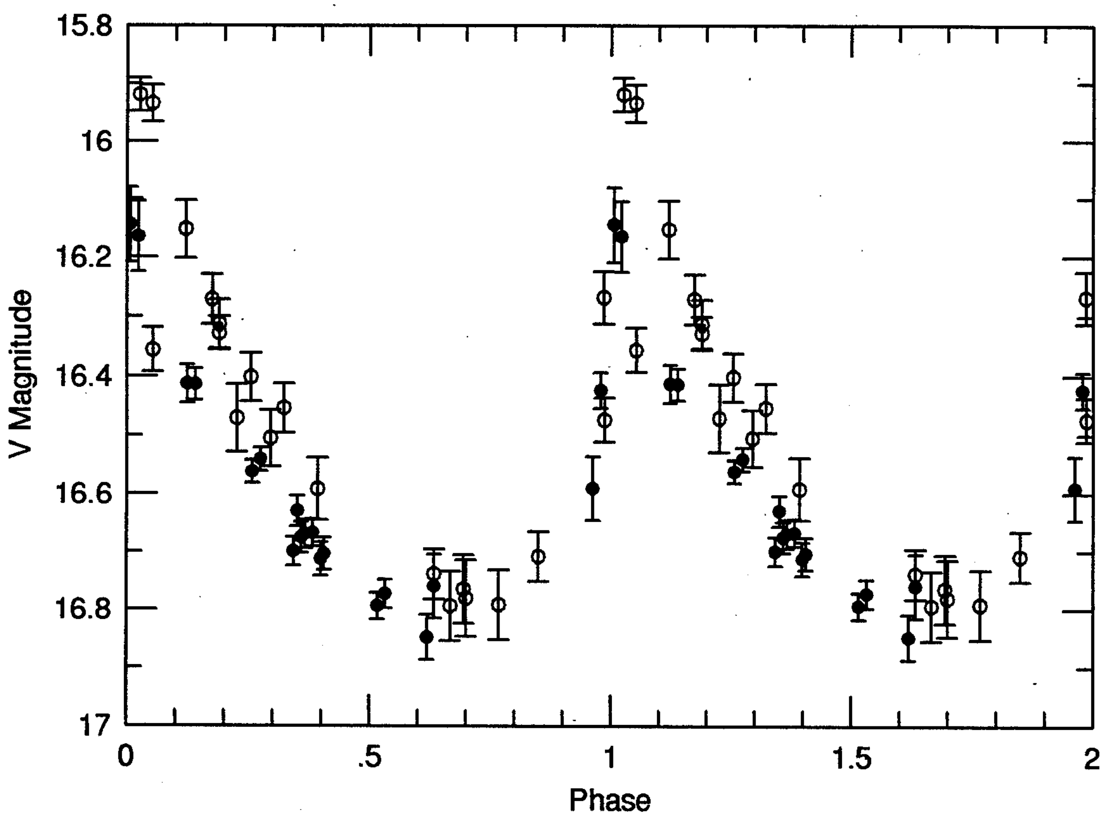

RA : 22 20 36.4

Dec: 27 59 39.2

<V> = 15.185

<B-V> = 0.35

P = 0.426090 days

Epoch = 3517.356

Type: W UMa

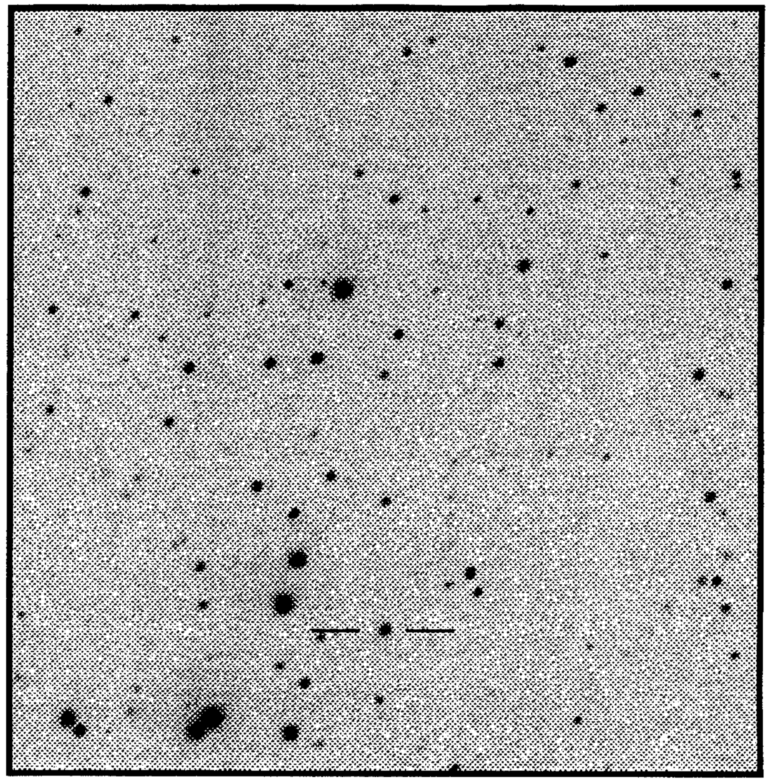

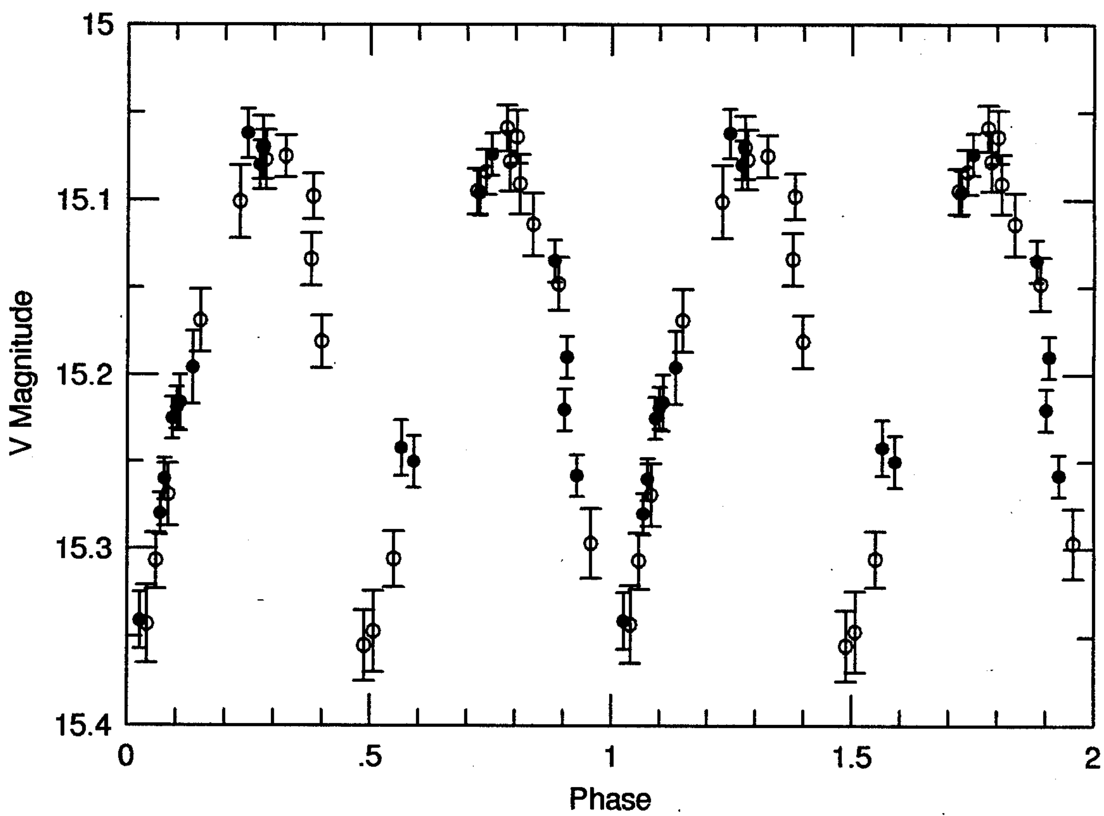

RA : 22 36 18.9

Dec: 27 58 38.4

<V> = 16.693

<B-V> = 0.45

P = 0.611901 days

Epoch = 3622.260

Type: RRab

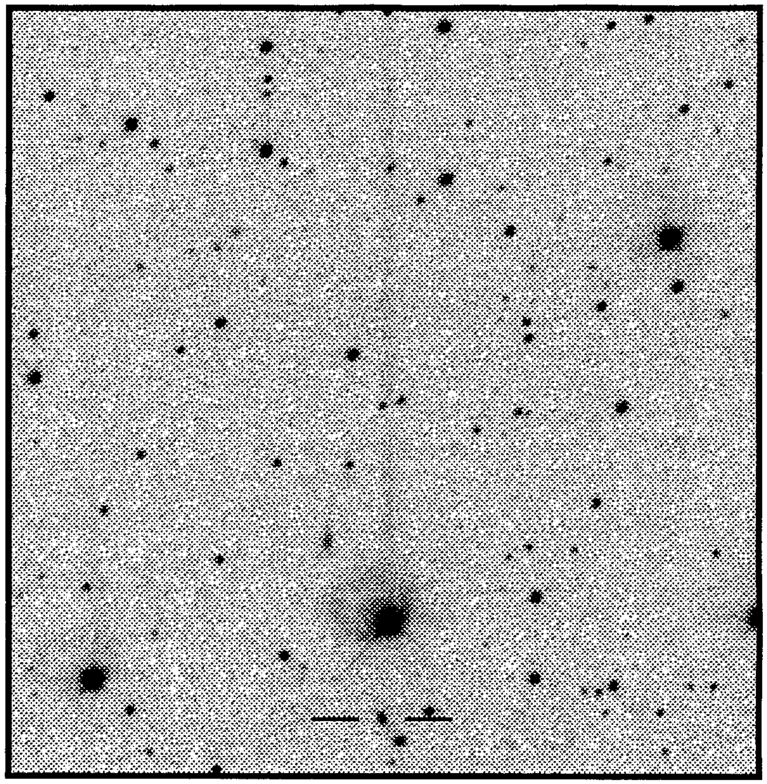

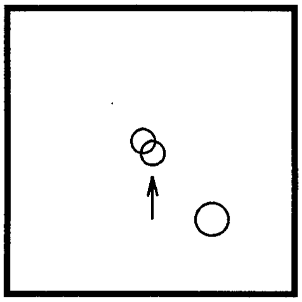

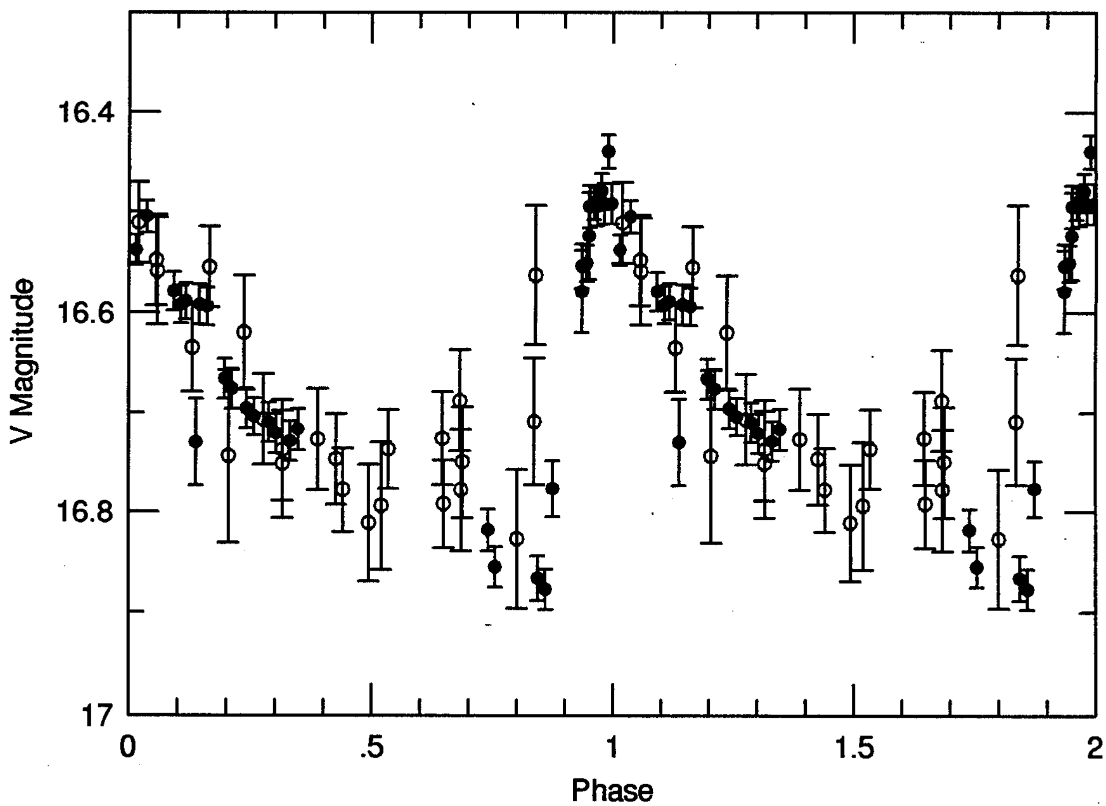

RA : 22 47 34.7

Dec: 28 01 20.8

<V> = 13.525

<B-V> = 0.40

P = 0.379380 days

Epoch = 3480.338

Type: W UMa

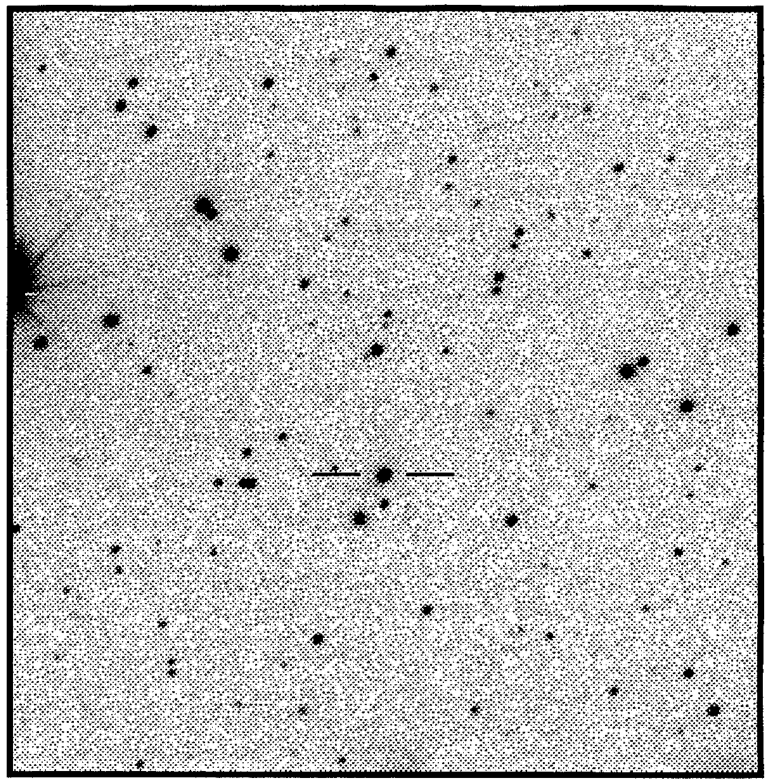

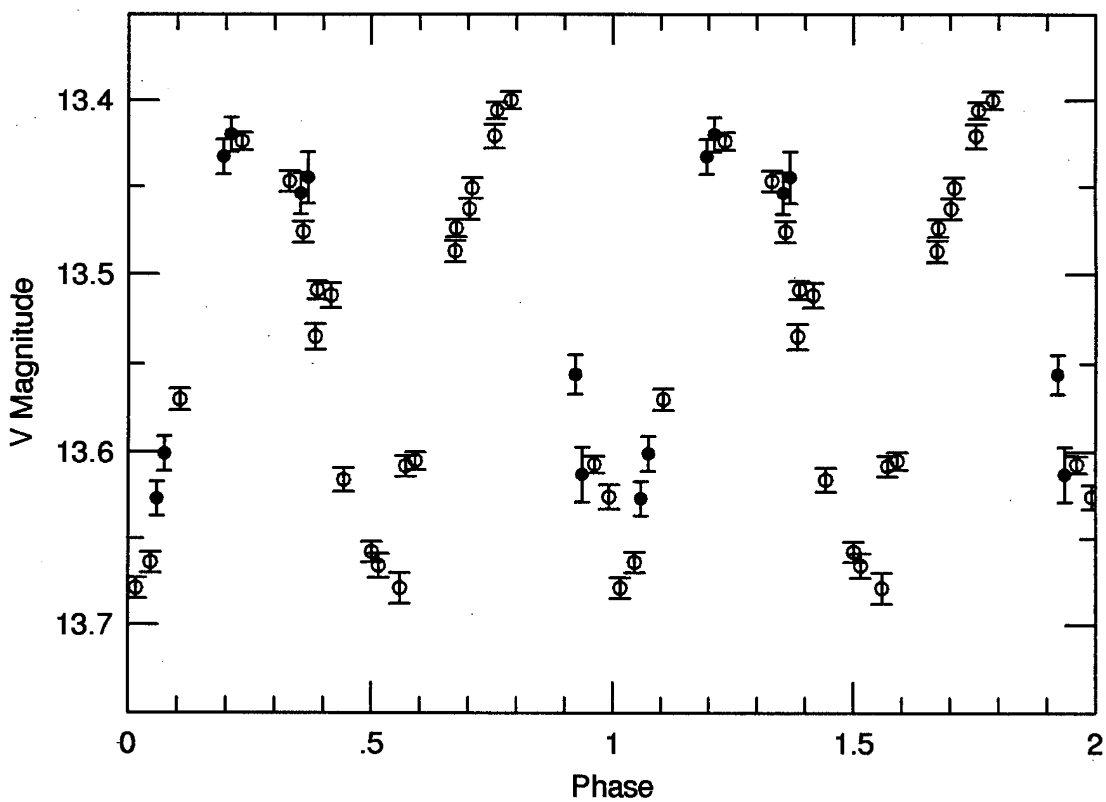

RA : 23 05 19.7

Dec: 28 05 44.1

<V> = 17.064

<B-V> = 0.30

P = 0.522284 days

Epoch = 3174.327

Type: RRab

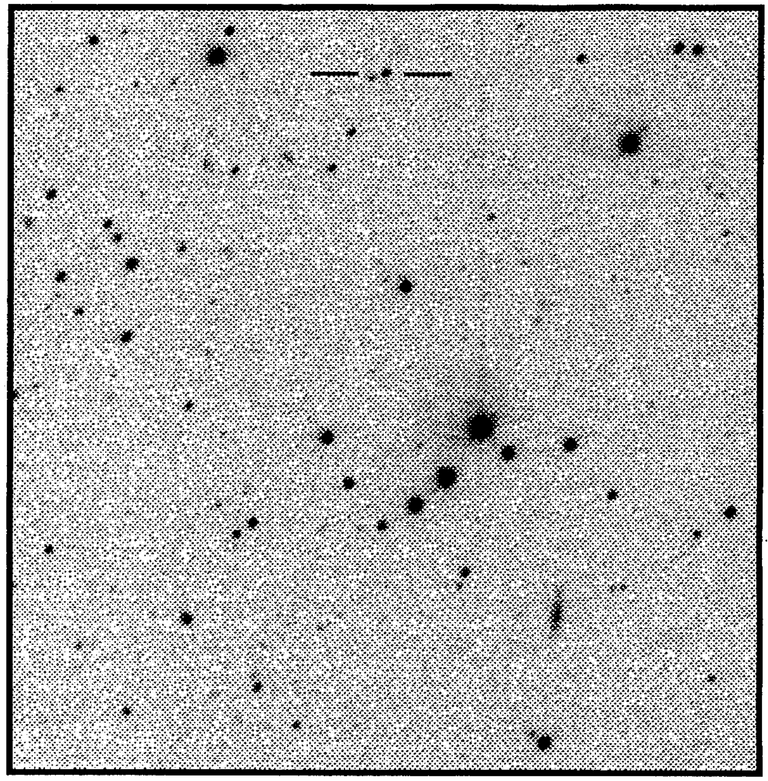

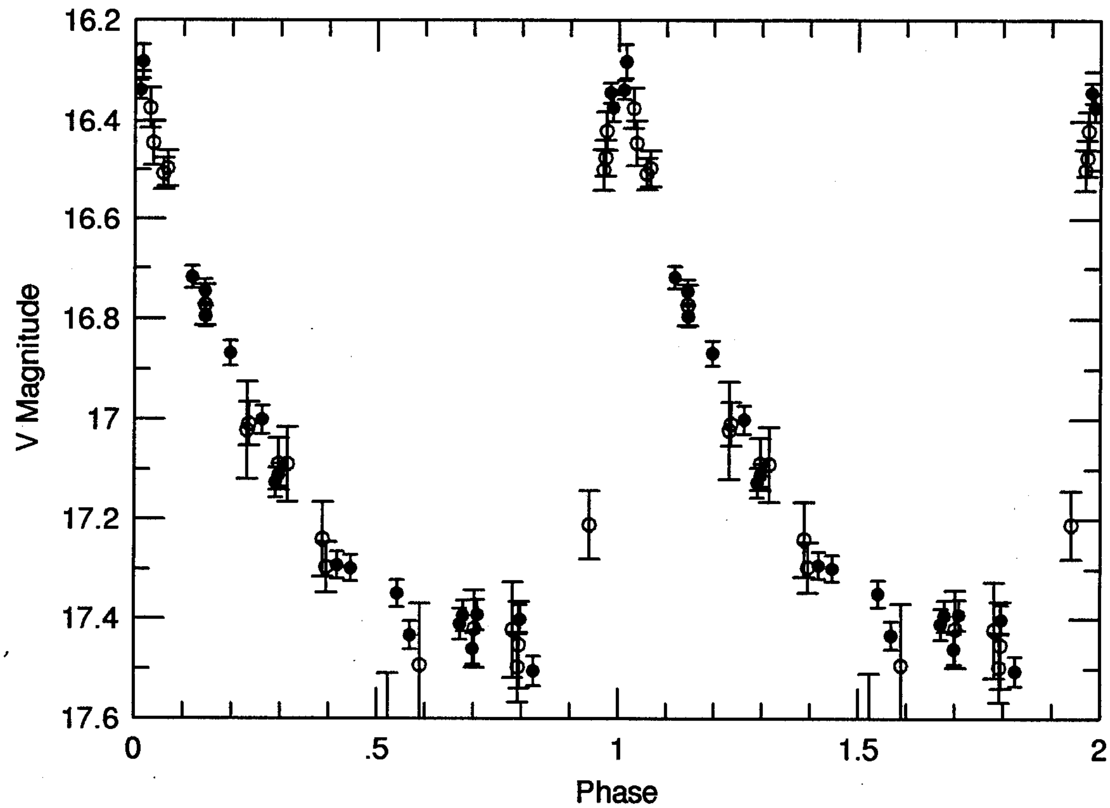

RA : 23 21 38.0
Dec: 28 01 25.6
<V> = 16.411
<B-V> = 0.40
P = 0.394387 days
Epoch = 3545.638
Type: W UMa

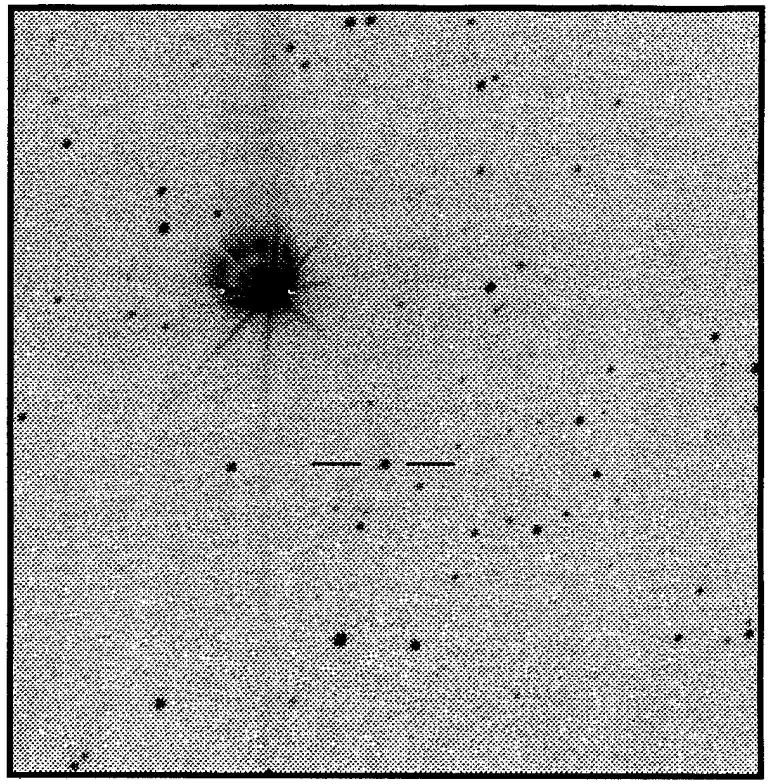

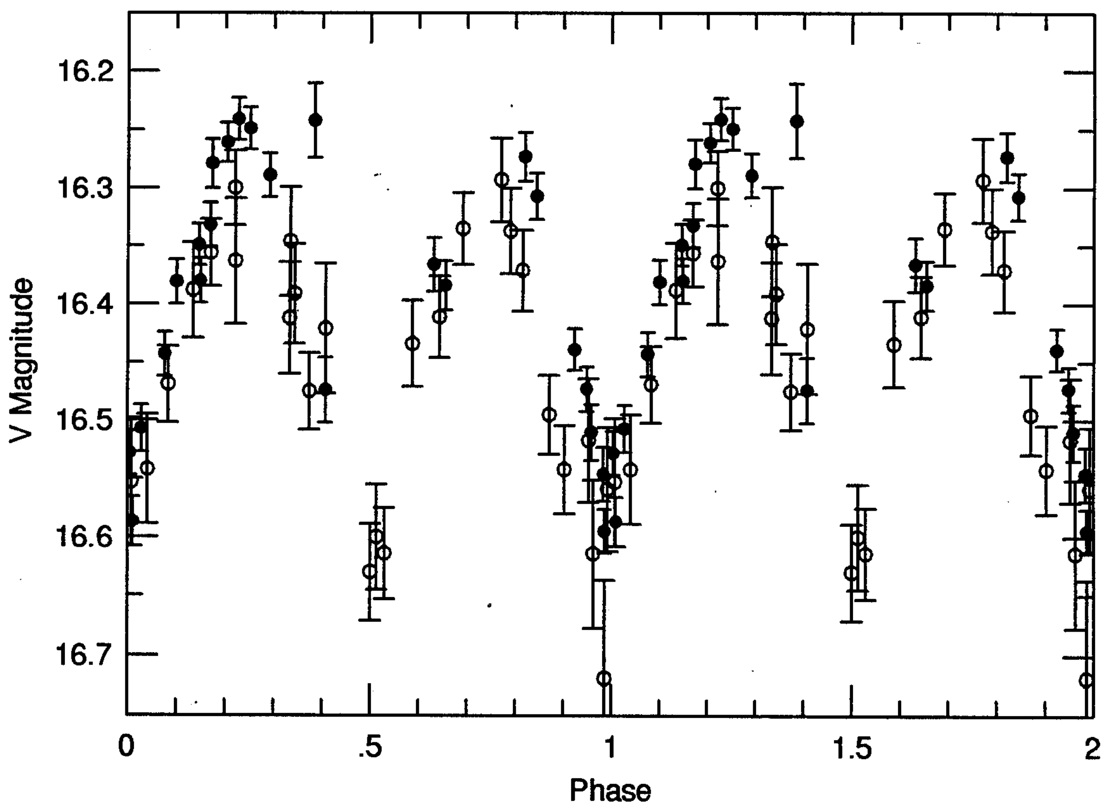

RA : 23 32 06.7
Dec: 28 02 10.9
<V> = 17.265
<B-V> = 0.44
P = 0.692859 days
Epoch = 3187.329
Type: RRab

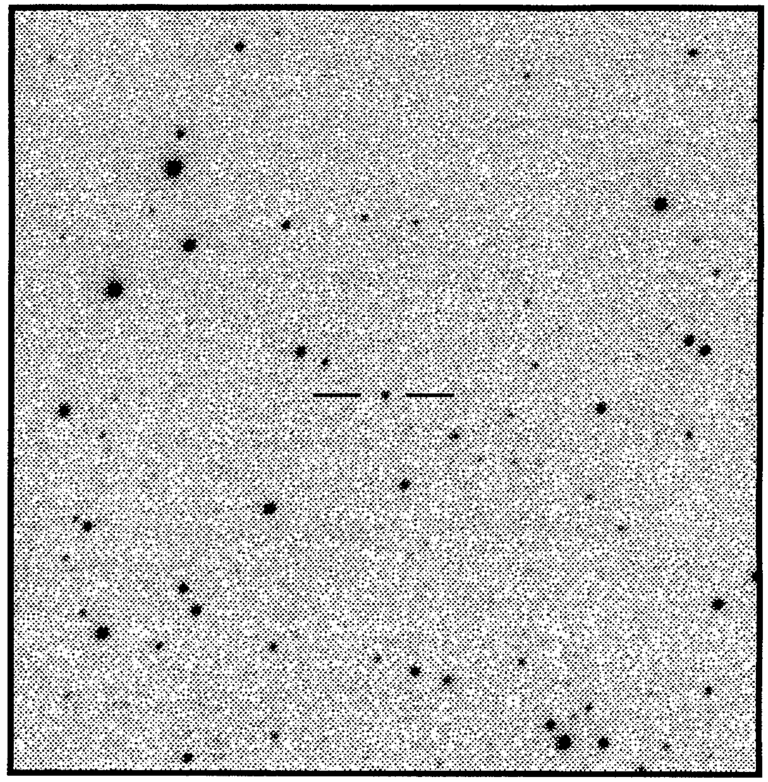

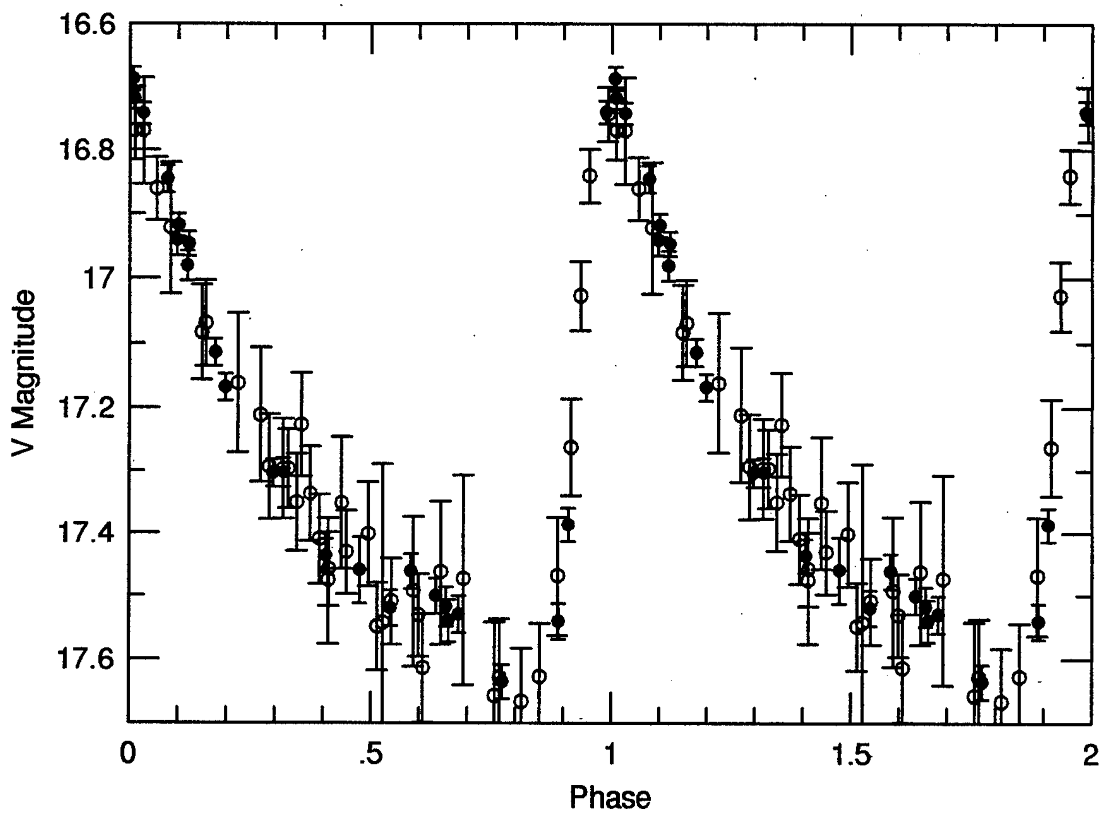

RA : 23 52 26.0

Dec: 28 01 18.9

<V> = 17.565

<B-V> = 0.48

P = 0.589192 days

Epoch = 3545.372

Type: RRab

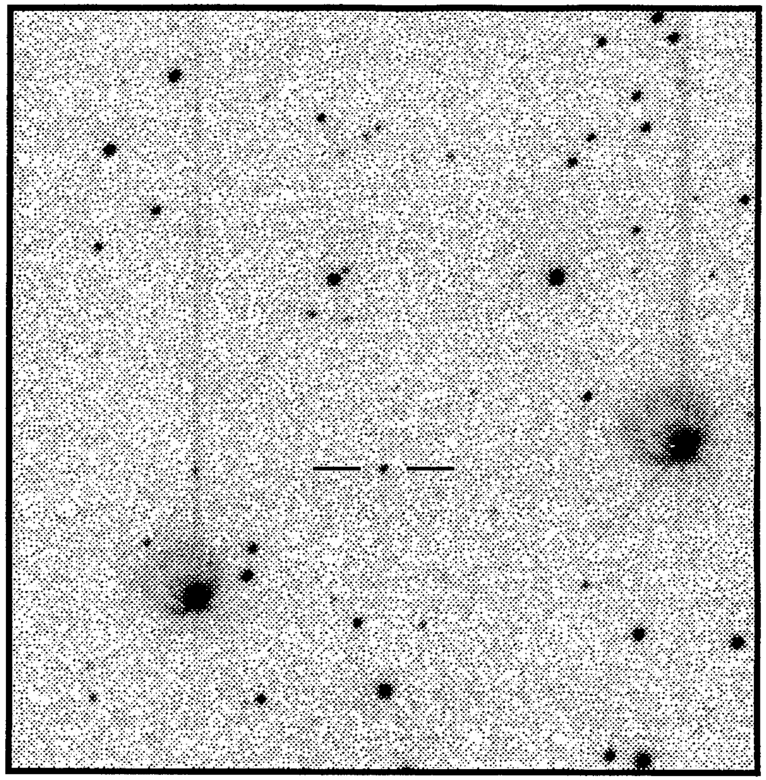

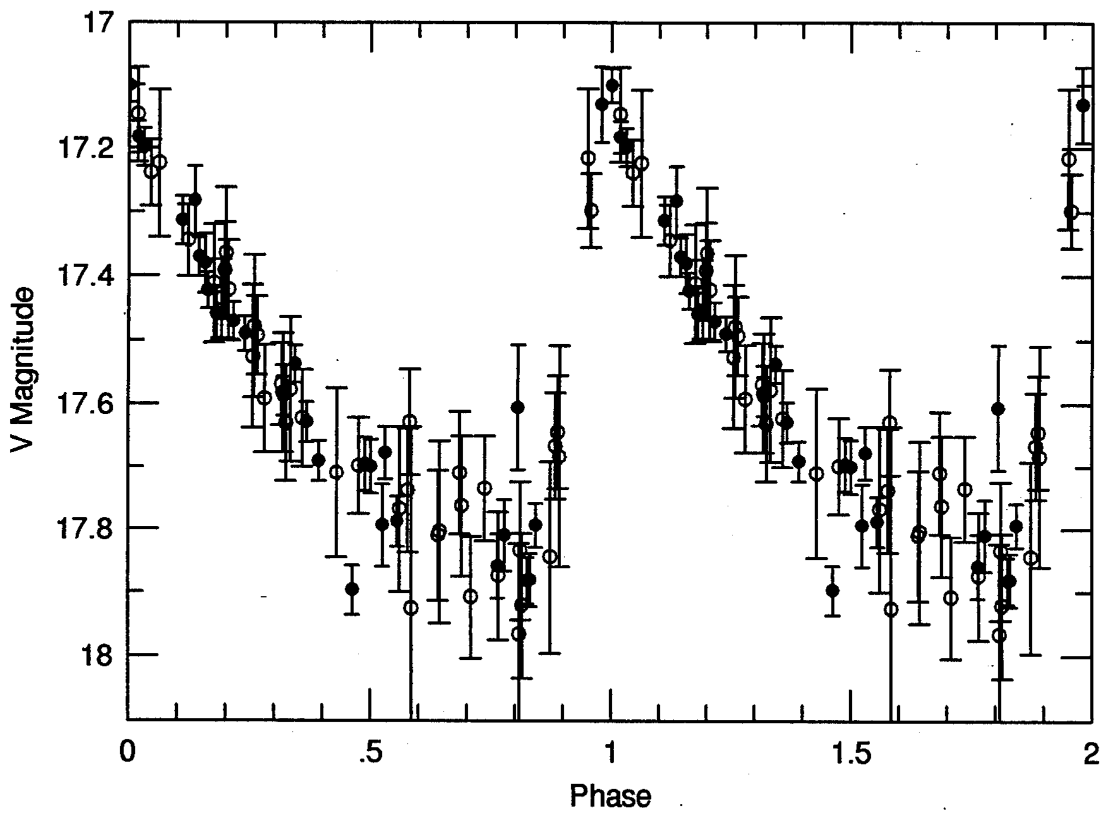

# References

## Chapter 1

## Chapter 2


Baker, J.G., "On Improving the Effectiveness of Large Telescopes," IEEE Trans. on Aerospace and Electronic Systems Vol. AES-5, No. 2, p. 261, 1969.

Benedict, G.F., McGraw, J.T., Hess, T.R., Cawson, M.G.M., Keane, M.J., "Relative Astrometry with the Steward Observatory CCD/Transit Instrument," Bulletin of the American Astonomical Society Vol. 21, No. 4, p. 1109, 1989.

Benedict, G.F., McGraw, J.T., Hess, T.R., Cawson, M.G.M., Keane, M.J., "Relative Astrometry with the Steward Observatory CCD/Transit Instrument," Astronomical Journal **101**, p. 279, 1991.

Borra, E.F., Content, R., Drinkwater, M.J., Szapiel, S., "A Deffraction Limited f/2 1.5 meter Diameter Liquid Mirror," Astrophysical Journal Letters **346**, p. L41, 1989.

Borra, E.F., Content, R., Girard, L., Szapiel, S., Tremblay, L.M., "Liquid Mirrors: Optical Shop Tests and Contributions to the Technology," Astrophysical Journal **393**, p. 829, 1992.

Cawson, M.G.M., McGraw, J.T., Keane, M.J., "A Relational Database Approach to Astronomical Research," SPIE Proc. Vol. 627, p. 70, 1986.

Cawson, M.G.M., McGraw, J.T., Keane, M.J., "The CCD/Transit Instrument (CTI) Data-Analysis System," SPIE Proc. Vol. 627, p. 79, 1986.

Content, R., Borra, E.F., Drinkwater, M.J., Poirier, S., Poisson, E., Beauchemin, M., Boily, E., Gauthier, A., Tremblay, L.M., "A Search for Optical Flares and Flashes with a Liquid Mirror Telescope," Astronomical Journal **97** (3), p. 917, 1989.

Delporte, E., Délimitation Scientifique des Constellations (Tables et Cartes), (Cambridge, At the University Press, 1930).

Dixon, R.S., Gearhart, M.R., and Schmidtke, P.C., Atlas of Sky Overlay Maps (for the Palomar Sky Survey), (The Ohio State Radio Observatory, 1981).

Hoffleit, D., Bright Star Catalogue, 5th revised edition (Yale University Observatory, 1982).

Jones, K.G. (editor), Webb Society Deep-Sky Observer's Handbook Volume 5: Clusters of Galaxies, (Enslow Publishing, 1981).

Kent, S.M., Ramella, M., Nonino, M., "A Small Drift Scan Survey for Galaxies in the Northern Sky," Astronomical Journal **105** (2), p. 393, 1993.

Kent, S.M., Stoughton, C., Newberg, H., Loveday, J., Petravick, D., Gurbani, V., Berman, E., Sergey, G., Lupton, R., Sloan Digital Sky Survey, Report #FNAL/C-94/084, (Batavia, Ill.: Fermi National Accelerator Laboratory, 1994).

Kholopov, P.N., Samus, N.N., Frolov, M.S., Goranskij, V.P., Gorynya, N.A., Kireeva, N.N., Kukarkina, N.P., Kurochkin, N.E., Medvedeva, G.I., Perova, N.B., and Shugarov, S.Y., General Catalogue of Variable Stars, 4th edition (Moscow: Nauka Publishing House, 1985-88).

Kirkpatrick, J.D., McGraw, J.T., "The CCD/Transit Instrument (CTI) Blue Object Survey," IAU Colloquium #114 (White Dwarfs), p. 167, 1988.

Kirkpatrick, J.D., Henry, T.J., McCarthy, D.W., McGraw, J.T., "Constraining the Faint End of the Stellar Luminosity Function Through a Systematic Search for M Dwarfs," Bulletin of the American Astronomical Society, Vol. 22, No. 4, p. 1204, 1990.

Kirkpatrick, J.D., Spectroscopic and Photometric Studies of Main Sequence M Stars and a Search for Late Type Dwarfs in the Solar Vicinity, Phd dissertation, (Department of Astronomy, The University of Arizona, 1992).

Kirkpatrick, J.D., "The Luminosity Function of Field M Dwarfs: Evidence for a Population of Substellar Objects," Bulletin of the American Astronomical Society Vol. 26, No. 2, p. 944, 1994.

Kirkpatrick, J.D., "The Luminosity Function at the End of the Main Sequence: Results of a Deep, Large-Area, CCD Survey for Cool Dwarfs," Astrophysical Journal Supplement Series **94**, p. 749, 1994.

Kron, R., "Digital Optical Sky Surveys," Bulletin of the American Astronomical Society Vol. 26, No. 2, p. 915, 1994.

McGraw, J.T., Angel, J.R.P., and Sargent, T.A., "A CCD Transit-telescope Survey for Galactic and Extragalactic Variability and Polarization," SPIE Proc. Vol. 264, p. 20,

1980.

McGraw, J.T., Stockman, H.S., Angel, J.R.P., Epps, H., and Williams, J.T., "The CCD/transit instrument (CTI) deep photometric and polarimetric survey - a progress report," SPIE Proc. Vol. 331, p. 137, 1983.

McGraw, J.T., Cawson, M.G.M., Keane, M.J., "Operation of the CCD/Transit Instrument (CTI)," SPIE Proc. Vol. 627, p. 60, 1986.

McGraw, J.T., Cawson, M.G.M., Kirkpatrick, J.D., Haemmerle, V., "A Strip Search for Quasars: The CCD/Transit Instrument (CTI) Quasar Survey," Proceedings of a Workshop on Optical Surveys for Quasars, p. 163, 1988.

McGraw, J.T., Hess, T.R., Green, E.M., Bridges, C.T., Benedict, G.F., "Photometric and Positional Calibration of the CCD/Transit Instrument (CTI) Strip of the Sky," Bulletin of the American Astronomical Society Vol. 21, No. 3, p. 1021, 1989.

McGraw, J.T., "A Strip Search of the Universe," Variable Stars and Galaxies, ASP Conference Series, Vol. 30, p. 77 (San Francisco: Astronomical Society of the Pacific, 1992).

McGraw, J.T., "The Lunar Transit Telescope (LTT): An Early Lunar Based Science and Engineering Mission," Engineering, Construction and Operations in Space III, p. 1865, 1992.

McGraw, J.T. (editor), Proceedings of the Lunar Ultraviolet Telescope Experiment (LUTE) Science Workshop, (Institute for Astrophysics, The University of New Mexico, 1993).

McGraw, J.T., Wetterer, C.J., Hess, T.R., Green, E.M., "Photometric Standard Stars in the CCD/Transit Instrument (CTI) Survey," Bulletin of the American Astronomical Society Vol. 26, No. 2, p. 899, 1994.

Paul, M., "Corrective Systems for Astronomical Reflectors," Rev. d'Optique Vol. 14, p. 169, 1935.

Stoughton, C., Annis, J., Kent, S., Kron, R., Loveday, J., McKay, T., Newberg, H., "First Data from the Fermilab Drift Scan Camera," Bulletin of the American Astronomical Society Vol. 26, No. 2, p. 897, 1994.

Sulentic, J.W. and Tifft, W.G., The Revised New General Catalogue of Nonstellar Astronomical Objects, (Tucson: The University of Arizona Press, 1973).

Veron-Cetty, M.P., and Veron, P., "A Catalogue of Quasars and

Active Galactic Nuclei, 4th edition," E.S.O. Sci. Rep. **7**, 1989.

Wetterer, C.J., McGraw, J.T., Hess, T.R., Grashuis, R., "Variable Stars in the CCD/Transit Instrument (CTI) Survey," Bulletin of the American Astronomical Society Vol. 26, No. 2, p. 899, 1994.

Wetterer, C.J., The CCD/Transit Instrument Atlas and Database Guide, Supplement to PhD Dissertation, (Department of Physics and Astronomy, University of New Mexico, 1995).

Zwicky, F., Herzog, E., Wild, P., Karpowicz, M., Kowal, C.T., The Catalogue of Galaxies and Clusters of Galaxies, (California Institute of Technology, 1961-68).

, The National Geographic Society - Palomar Observatory Sky Survey, (California Institute of Technology, 1954).

, Smithsonian Astrophysical Observatory Star Catalog, (Washington, Smithsonian Institution, 1966-1990).

(variable star original finder chart references)

Bond, H.E., Kron, R.G. and Spinrad, H., "GQ Comae and V396 Herculis: Two Low-Redshift Optically Variable QSOs," Astrophysical Journal **213** (1), p. 1, 1977. (GQ Com)

Erleksova, G.E., "EQ Vulpeculae," Переменные звезды, Прцложенце **2** №10, p. 248, 1975. (EQ Vul)

Hoffmeister, C., "Untersuchung der Schtaube des Positions-Fadenmikrometers *Heyde 3013*," Mitteilungen der Sternwarte zu Sonneberg Nr. 6, 1924. (UU Lyr)

Hoffmeister, C., "Relative Koordinaten, Örter und Karten neuer Veränderlicher," Mitteilungen der Sternwarte zu Sonneberg Nr. 17, 1930. (CE Lyr and CV Lyr)

Hoffmeister, C., "Relative Koordinaten, Örter und Karten neuer Veränderlicher," Mitteilungen der Sternwarte zu Sonneberg Nr. 22, 1933. (GS Lyr)

Hoffmeister, C., "89 neue veränderliche Sterne," Astronomische Nachrichten **284**, p. 275, 1959. (V375 Her and V385 Her)

Hoffmeister, C., "Mitteilungen über neuentdeckte Veränderliche Sterne (S9727-S10152)," Astronomische Nachrichten **290** H1-2, p. 43, 1967. (KW Vul)

Pinto, G. and Romano, G., "Researches with the Schmidt Telescope VI - The Variable Stars around Gamma Comae," Memorie della Società Astronomica Italiana **44** №1, p. 53, 1973. (GR Com and GS Com)

Kurochkin, N.E., "New Variable Stars in the Region of M56," Переменные звезды **17** №128, p. 186, 1970. (V427 Lyr)

Kinman, T., Wirtanen, C.A. and Janes, K.A., "An RR Lyrae Star Survey with the Lick 20 inch Astrograph. IV. A Survey of Three Fields Near the North Galactic Pole," Astrophysical Journal Supplement **119**, p. 379, 1966 (DV Com and EZ Com)

Meinunger, L., "Über Veränderliche in einigen T-Assoziationen," Mitteilungen über Veränderliche Sterne **3** H5, p. 137, 1966. (CN Tau)

Miller, W.J. and Wachmann, A.A., "Six New Variable Stars in the Cygnus Cloud, VV 125-130," Ricerche Astronomiche **6** №22, p. 497, 1964. (V926 Cyg)

Miller, W.J., "Eleven Variable Stars in the Cygnus Cloud, VV 151-161," Ricerche Astronomiche **7** №4, p. 197, 1965. (V911 Cyg)

Miller, W.J., "Ten New Variable Stars in the Cygnus Cloud, VV 191-200," Ricerche Astronomiche **7** №10, p. , 1967. (V1140 Cyg)

Rügemer, H., "Neue Veränderliche Sterne," Astronomische Nachrichten **248**, p. 409, 1933. (EP Tau)

Shaganian, B.L. and Shaganian, V.B., "On Three Longperiod Variable Stars in the Region of M56," Переменные звезды, Приложение **3** №18, p. 748, 1979. (TY Lyr)

Vogt, N. and Bateson, F.M., "An Atlas of Southern and Equitorial Dwarf Novae," Astronomy and Astrophysics Supplement **48** (3), p. 383, 1982. (IR Gem)

Wachmann, A.A., "Die Veränderlichen im Südteil der Cygnuswolke - Teil II," Astronomische Abhandlungen der Hamburger Sternwarte, Band VI Nr. 2, 1963. (PP Lyr)

Wachmann, A.A., "Die Veränderlichen im Südteil der Cygnuswolke - Teil III," Astronomische Abhandlungen der Hamburger Sternwarte, Band VI Nr. 3, 1964. (EH Cyg and AI Cyg)

, Mitteilungen über Veränderliche Sterne №299, 1957. (V532 Her)

Chapter 3

Cawson, M.G.M., McGraw, J.T., Keane, M.J., "A Relational Database Approach to Astronomical Research," SPIE Proc. Vol. 627, p. 70, 1986.

Cawson, M.G.M., McGraw, J.T., Keane, M.J., "The CCD/Transit Instrument (CTI) Data-Analysis System," SPIE Proc. Vol. 627, p. 79, 1986.

Dieckvoss, W., Kox, H., Gunther, A., and Brosterhus, E., AGK3 Star Catalog of Positions and Proper Motions North of -2.5 degree Declination (Hamburg-Bergedorf, 1975).

Lasker, B.M., Sturch, C.R., McLean, B.J., Russell, J.L., Jenkner, H., Shara, M.M., "The Guide Star Catalog I. Astronomical Foundations and Image Processing," Astronomical Journal **99**(6), p. 2019, 1990.

McGraw, J.T., Hess, T.R., Green, E.M., Bridges, C.T., Benedict, G.F., "Photometric and Positional Calibration of the CCD/Transit Instrument (CTI) Strip of the Sky," Bulletin of the American Astronomical Society Vol. 21, No. 3, p. 1021, 1989.

McGraw, J.T., "A Strip Search of the Universe," Variable Stars and Galaxies, ASP Conference Series, Vol. 30, p. 77 (San Francisco: Astronomical Society of the Pacific, 1992).

Wetterer, C.J., The CCD/Transit Instrument Atlas and Database Guide, Supplement to PhD Dissertation, (Department of Physics and Astronomy, University of New Mexico, 1995).

Chapter 4

Allen, R.H., Star Names: Their Lore and Meaning (New York: Dover Publications, 1963).

Bevington, P.R., Data Reduction and Error Analysis for the Physical Sciences (New York: McGraw-Hill Book Company, 1969).

Campbell, L. and Jacchia, L., The Story of Variable Stars (Philidelphia: The Blakiston Company, 1941).

Cox, J.P., Theory of Stellar Pulsation (Princeton: Princeton University Press, 1980).

Hawkins, M.R.S., "A Study of the Galactic halo from a complete sample of RR Lyrae variables to B = 21," Monthly Notices for the Royal Astronomical Society **206**, p.433, 1984.

Jacoby, G.H., Branch, D., Ciardullo, R., Davies, R.L., Harris, W.E., Pierce, M.J., Pritchet, C.J., Tonry, J.L., Welch, D.L., "A Critical Review of Selected Techniques for Measuring Extragalactic Distances," Publications of the Astronomical Society of the Pacific **104**, p. 599, 1992.

Kholopov, P.N., Samus, N.N., Frolov, M.S., Goranskij, V.P., Gorynya, N.A., Kireeva, N.N., Kukarkina, N.P., Kurochkin, N.E., Medvedeva, G.I., Perova, N.B., and Shugarov, S.Y., General Catalogue of Variable Stars, 4th edition (Moscow: Nauka Publishing House, 1985-88).

Madore, B.F., Freedman, W.L., " The Cepheid Distance Scale," Publications of the Astronomical Society of the Pacific **103**, p. 933, 1991.

Petit, M., Variable Stars (English translation, New York: John Wiley & Sons Ltd., 1987).

Saha, A. and Hoessel, J.G., "RR Lyrae stars in Local Group galaxies I: NGC 185," Astronomical Journal **99** (1), p. 97, 1990.

Stobie, R.S., Bishop, I.S., King, D.L., "Variable Stars in the South Galactic Cap," Monthly Notices of the Royal Astronomical Society **222**, p. 473, 1986.

Chapter 5

Barnes III, T.G., Hawley, S.L., "On Absolute Magnitues of RR Lyrae Stars," Astrophysical Journal **307**, p. L9, 1986.

Beckert, D.C. and Newberry M.V., "The Design and Testing of Filter-Detector Systems using Synthetic Photometry," Publications of the Astronomical Society of the Pacific **101**, p. 849, 1989.

Burstein, D., and Heiles, C., "Reddenings Derived form HI and Galaxy Counts: Accuracy and Maps," Astronomical Journal **87** (8), p. 1165, 1982.

Carney, B.W., Storm, J., Jones , R.V., "The Baade-Wesselink Method and the Distances to RR Lyrae Stars. VIII. Comparisons with Other Techniques and Implications for Globular Cluster Distances and Ages," Astrophysical Journal **386**, p. 663, 1992.

Cox, J.P., Theory of Stellar Pulsation (Princeton: Princeton University Press, 1980).

Hawley, S.L., Jeffreys, W.H., Barnes III, T.G., "Absolute Magnitudes and Kinematic Properties of RR Lyrae Stars,"

Astrophysical Journal **302**, p. 626, 1986.

Kholopov, P.N., Samus, N.N., Frolov, M.S., Goranskij, V.P., Gorynya, N.A., Kireeva, N.N., Kukarkina, N.P., Kurochkin, N.E., Medvedeva, G.I., Perova, N.B., and Shugarov, S.Y., General Catalogue of Variable Stars, 4th edition (Moscow: Nauka Publishing House, 1985-88).

Kukarkin, B.V., Kholopov, P.N., Artiukhina, N.M., Fedorovich, V.P., Frolov, M.S., Goranskij, V.P., Gorynya, N.A., Karitskaya, E.A., Kirreeva, N.N., Kukarkina, N.P., Kurochkin, N.E., Medvedeva, G.I., Perova, N.B., Ponomareva, G.A., Samus, N.N., and Shugarov, S.Y., New Catalogue of Suspected Variable Stars (Moscow: Nauka Publishing Office, 1982).

Lafler, J., and Kinman, T.D., "An RR Lyrae Star Survey with the Lick 20-inch Astrograph II. The Calculation of RR Lyrae Periods by Electronic Computer," Astrophysical Journal Supplement **11** p. 216, 1965.

Laubscher, B., Gregory, S., Bauer, T., Zeilik, M., Burns, J., "A CCD Camera System at Capilla Peak Observatory, New Mexico," Publications of the Astronomical Society of the Pacific **100**, p. 131, 1988.

Layden, A.C., Hanson, R.B., Hawley, S.L., "Absolute Magnitudes and Kinematics of RR Lyrae Stars via Statistical Parallax," Bulletin of the American Astronomical Society Vol. 26, No. 2, p. 911, 1994.

Lee, Y-W, "Evidence for an Old Galactic Bulge from RR Lyrae Stars in Baade's Window: Implications for the Formation of the Galaxy and the Age of the Universe," Astronomical Journal **104** (5), p. 1780, 1992.

Mihalas, D. and Binney, J., Galactic Astronomy: Structure and Kinematics, second edition (New York: W.H. Freeman and Company, 1981).

Nemec, J.M., Linnell Nemec, A.F., Lutz, T.E., "Period-Luminosity-Metallicity Relations, Pulsation Modes, Absolute Magnitudes, and Distances for Population II Variable Stars," Astronomical Journal **108**, p. 222, 1994.

Newberry, M.V., "Signal-to-Noise Considerations for Sky-Subtracted CCD Data," Publications of the Astronomical Society of the Pacific **103**, p. 122, 1991.

Saha, A. and Hoessel, J.G., "RR Lyrae stars in Local Group galaxies I: NGC 185," Astronomical Journal **99** (1), p. 97, 1990.

Sandage, A., "Evidence for a Period-Luminosity-Amplitude Relation for RR Lyrae Stars," Astrophysical Journal **244**, p. L23, 1981.

Sandage, A., Katem, B., Sandage, M., "The Oosterhoff Period Groups and the Age of Globular Clusters. I. Photometry of Cluster Variables in M15," Astrophysical Jouranl Supplement **46**, p. L41, 1981.

Sandage, A., "The Oosterhoff Period Groups and the Age of Globular Clusters. II. Properties of RR Lyrae Stars in Six Clusters: The P-L-A Realation," Astrophysical Jouranl **248**, p. 161, 1981.

Sandage, A., "The Oosterhoff Period Groups and the Age of Globular Clusters. III. The Age of the Globular Cluster System," Astrophysical Jouranl **252**, p. 553, 1982.

Sandage, A., Katem, B., Sandage, M., "The Oosterhoff Period Groups and the Age of Globular Clusters. IV. Field RR Lyrae Stars: Age of the Galactic Disk," Astrophysical Jouranl Supplement **252**, p. 574, 1982.

Stellingwerf, R.F., "Period Determination using Phase Dispersion Minimization," Astrophysical Journal **224**, p. 953, 1978.

Szeidl, B. "Multiple Periodic Variable Stars," IAU Colloquium No. 29, edited by W.S. Fitch (Reidel, Dordrecht), p. 133, 1976.

Tsesevich, V.P. "RR Lyrae Stars," in Pulsating Stars (edited by B.V. Kukarkin), English translation (New York: Halsted Press, 1975).

Tyson, J.A., "The Shift-and-Stare Technique and a Large Area CCD Mosaic," CCDs in Astronomy, ASP Conference series, Vol. 8, p. 1, (San Francisco: Astronomical Society of the Pacific, 1990).

, The Astronomical Almanac for the year 1993 (Washington D.C.: United States Government Printing, 1992).

(Capilla Peak research references)

Beckert, D.C., Cox, D., Gordon, S., Jaderlund, E., Mann, E., Zeilik, M., "1989 BVR photometry of CG Cygni", IBVS #3398, 1989.

Beckert, D.C. and Newberry M.V., "The Design and Testing of Filter-Detector Systems using Synthetic Photometry,"

Publications of the Astronomical Society of the Pacific **101**, p. 849, 1989.

Beckert, D.C., Gordon, S., Jaderlund, E., Mann, E., Zeilik, M., "CG Cygni redux : more 1989 BVR data", IBVS #3556, 1991.

Bryja, C., Lawrence, G., "Photometry of Suspected Low Mass Hyades Cluster Members," Bulletin of the American Astronomical Society, Vol. 23, No. 2, p. 908, 1991.

Bryja, C., Jones, T.J., Humphreys, R.M., Lawrence, G., Pennington, R.L., Zumach, W., "Candidate Brown Dwarfs in the Hyades," Astrophysical Journal **388**, p. L23, 1992.

Deeg, H-J., Brinks, E., Duric, N., Klein, U., Skillman, E., "New 325 MHz Observations of HII Galaxies: The Mechanisms That Shape the Unusual Radio Spectra," Astrophysical Journal **410**, p. 626, 1993.

Gordon, S., Hall, S., Ledlow, M., Mann, E., Zeilik, M., "1989 BVR light curves of RT And," IBVS #3469, 1990.

Gisler, G., Laubscher, B., Chabot, N., Boudreaux, K., Grashuis, R., "Multi-filter Optical Observations of SL9 Impact Spots on Jupiter," Bulletin of the American Astronomical Society Vol. 26, No. 4, p. 1374, 1994.

Gregory, S.A., Deeg, H.-J., Morrison, G., Crane, M., Grashuis, R., Lacey, C., "Galaxian Nuclear Spectral Types as a Function of Environment," Bulletin of the American Astronomical Society Vol. 22 No. 2, p. 881, 1990.

Hayes, J.J.E., Sadun, A.C., and R. Grashuis, "Narrow-band images of Arp 213," Bulletin of the American Astronomical Society Vol. 25 No. 4, p. 1248, 1993.

Kidger, M., et al., "Multiband Monitoring of OJ287 in 1993/94," Bulletin of the American Astronomical Society Vol. 26, No. 4, p. 1506, 1994.

Laubscher, B., Gregory, S., Bauer, T., Zeilik, M., Burns, J., "A CCD Camera System at Capilla Peak Observatory, New Mexico," Publications of the Astronomical Society of the Pacific **100**, p. 131, 1988.

Laubscher, B., Gregory, S., "Galaxy alignments in the Perseus supercluster," Bulletin of the American Astronomical Society Vol. 25, No. 2, p. 913, 1993.

Laubscher, B., "Problems with Galaxy Position Angles," Bulletin of the American Astronomical Society Vol. 26, No. 2, p. 963, 1994.

Odewahn, S.C., "Properties of the Magellanic-type spirals. I - Surface photometry of NGC 4618 and NGC 4625," Astronomical Journal **101**, p. 829, 1991.

Odewahn, S.C., Bryja, C., Humphreys ,R.M., "Improved CCD Standard Fields," Publications of the Astronomical Society of the Pacific **104**, p. 553, 1992.

Sadun, A., "Optical Variability of the Blazar OJ 287," Bulletin of the American Astronomical Society Vol. 26, No. 4, p. 1467, 1994.

Schmidt, B.P., Kirshner, R.P., Eastman, R.G., Grashuis, R., Dell'Antonio, I., Caldwell, N., Foltz, C., Huchra, J.P., Milone, A.A.E., "The Unusual Supernoa SN 1993J in M81," Nature **364**, p. 600, 1993.

Schmidt, B.P., Kirshner, R.P., Eastman, R.G., Phillips, M.M., Suntzeff, N.B., Hamuy, M., Aviles, R., Filippenko, A.V., Ho, L., Matheson, T., Grashuis, R., Maza, J., Kirkpatrick, J.D., Kuijken, K. Zucker, D., Bolte, M., Tyson, N., "The Expanding Photosphere Method Applied to SN 1992am at cz = 14600 km $s^{-1}$," Astronomical Journal **107**, p. 1444, 1994.

Summers, D.L., Zeilik, M., "Starspot activity on the RS CVn candidate 1E 1919+0427," Bulletin of the American Astronomical Society, Vol. 22, No. 4, p. 1295, 1990.

Summers, D.L., Zeilik, M., Jaderlund, E., Hoeppe, G., Collins, A., "1991 V-band photometry of an eclipsing binary: 1E 1919+0427," IBVS #3708, 1992.

Takalo, L.O., Pursimo, T., Sillanpää, A., Lehto, H., Nilsson, K., Kidger, M., deDiego, J.A., Gonzales-Perez, J.N., Rodriguez-Espinoza, J-M., Mahoney, T., Boltwood, P., Dultzin-Hacyan, D., Benitez, E., Turner, G.W., Robertson, J.W., Honeycutt, R.K., Efimov, T.S., Shakhovskoy, N., Charles, P.A., Schramm, K.J., Borgeest, U., Linde, J.V., Sadun, A., Grashuis, R., "The Light Curve of Blazar 3C 66A," Bulletin of the American Astronomical Society Vol. 26, No. 4, p. 1507, 1994.

Taylor, C., Brinks, E., Grashuis, R., Skillman, E., "An Optical and Radio Atlas of Companions to Dwarf Galaxies," to be published in Astrophysical Journal Supplement Series, 1995.

Wetterer, C.J., McGraw, J.T., Hess, T.R., Grashuis, R., "Variable Stars in the CCD/Transit Instrument (CTI) Survey," Bulletin of the American Astronomical Society Vol. 26, No. 2, p. 899, 1994.

Zeilik, M., DeBlasi, D., Rhodes, M., Budding, E., "A Half-Century of Starspot Activity on SV Camelopardalis," Bulletin

of the American Astronomical Society Vol. 19., No. 4, p. 1086, 1987.

Zeilik, M., Beckert, D., DeBlasi, C., Ledlow, M., Rhodes, M., Williams, T., "1987 BVRI Photometry of RT And," IBVS #3173, 1988.

Zeilik, M., Cox, D., DeBlasi, D., Ledlow, M., Rhodes, M., Williams, T., "1988 BVRI Photometry of XY UMa," IBVS #3200, 1988.

Zeilik, M., DeBlasi, D., Rhodes, M., Budding, E., "A Half-Century of Starspot Activity on SV Camelopardalis," The Astrophysical Journal **332**, p. 293, 1988.

Zeilik, M., Beckert, D., Cox, D., Dolby, J., Ledlow, M., Newberry, M., Rhodes, M., "1989 V-band light curve of RT And," IBVS #3301, 1989.

Zeilik, M., Cox, D.A., DeBlasi, C., Rhodes, M., Budding, E., "Long-Term Starspot Activity of Short-Period RS CVn Stars, Part II, RT Andromedae," The Astrophysical Journal **345**, p.991, 1989.

Zeilik, M., DeBlasi, C.B., Gordon, S., Ledlow, M., "1990 BVR photometry of XY UMa," IBVS #3535, 1990.

Zeilik, M., Gordon, S., Cox, D., Beckert, D., "Long-term starspot activity of short-period RS CVn stars : CG Cygni," Bulletin of the American Astronomical Society, Vol. 22, No. 2, p. 830, 1990.

Zeilik, M., Ledlow, M., Rhodes, M., Arevardo, M.J., Budding, E., "Long-Term Starspot Activity of Short-Period RS CVn Stars, Part III, BH Virginis," The Astrophysical Journal **354**, p.352, 1990.

Zeilik, M., Cox, D.A., De Blasi, C., Rhodes, M., Budding, E., "Long-Term Starspot Activity of Short-Period RS CVn Stars, Part IV, WY Cancri," The Astrophysical Journal **363**, p.467, 1990.

Zeilik, M., Heckert, P., Ledlow, M., Summers, D.L., Jaderlund, E., Boudreau, K., M., "1991 BVR photometry of CG Cygni," IBVS #3663, 1991.

Zeilik, M., Deeg, H.J., "Long-term starspot activity of short-period RS CVn stars : XY UMa," Bulletin of the American Astronomical Society, Vol. 23, No. 2, p. 880, 1991.

Zeilik, M., Gordon, S., Jaderlund, E., Ledlow, M., Summers, D.L., Heckert, P.A., Budding, E., Banks, T.S., "Long-term

Starspot Activity of Short-Period RS Canum Venaticorum Stars. V. CG Cygni," Astrophysical Journal **421**, p. 303, 1994.

Chapter 6

Blanco, B.M., "RR Lyrae Variables in Baade's Window," Astronomical Journal **89**, p. 1836, 1984.

Blanco, B.M., "RR Lyare Variables in a Galactic Bulge Window," Astronomical Journal **103**, p. 1872, 1992.

Hartwick, F.D.A., Barlow, D.J., Hesser, J.E., "Variable Stars in the Bulge of the Galaxy in a Field Around NGC 6304," Astronomical Journal **86**, p. 1044, 1981.

Hawkins, M.R.S., "A Study of the Galactic halo from a complete sample of RR Lyrae variables to B = 21," Monthly Notices for the Royal Astronomical Society **206**, p.433, 1984.

Kinman, T.D., "An RR Lyrae Star Survey with the Lick 20-inch Astrograph I. Methods of Observation and Reduction," Astrophysical Journal Supplement Series **11**, p. 199, 1965.

Kinman, T.D., Wirtanen, C.A., and Janes, K.A. "An RR Lyrae Star Survey with the Lick 20-inch Astrograph III. A Survey of Part of the Variable Star Field MWF 361," Astrophysical Journal Supplement Series **11**, p. 223, 1965.

Kinman, T.D., Wirtanen, C.A., and Janes, K.A. "An RR Lyrae Star Survey with the Lick 20-inch Astrograph IV. A Survey of Three Fields Near the North Galactic Pole," Astrophysical Journal Supplement Series **13**, p. 379, 1966.

Kinman, T.D., Mahaffey, C.T., and Wirtanen, C.A. "An RR Lyrae Star Survey with the Lick 20-inch Astrograph V. A Survey of Three Fields at Intermediate Latitudes Towards the Galactic Anti-Center," Astronomcal Journal **87**, p. 314, 1982.

Kinman, T.D., Wong-Swanson, B., Wenz, M., Harlan, E.A., "An RR Lyrae Star Survey with the Lick Astrograph VI. New Photometric Observations and Ephemerides for the Variables in the Field RR I (MWF 361A)," Astronomcal Journal **89**, p. 1200, 1984.

Lafler, J., and Kinman, T.D., "An RR Lyrae Star Survey with the Lick 20-inch Astrograph II. The Calculation of RR Lyrae Periods by Electronic Computer," Astrophysical Journal Supplement Series **11**, p. 216, 1965.

Layden, A.C., Hanson, R.B., Hawley, S.L., "Absolute Magnitudes and Kinematics of RR Lyrae Stars via Statistical Parallax," Bulletin of the American Astronomical Society Vol. 26, No. 2,

p. 911, 1994.

Merrifield, M.R., "The Rotation Curve of the Milky Way to $2.5R_0$ from the Thickness of the HI Layer," Astronomical Journal **103**, p. 1552, 1992.

Oort, J.H., and Plaut, L., "The Distance to the Galactic Centre Derived form RR Lyrae Variables, the Distribution of these Variables in the Galaxy's Inner Region and Halo, and a Redicussion of the Galactic Rotation Constants," Astronomy and Astrophysics **41**, p. 71, 1975.

Plaut, L., "Variable Stars in a Field Centered at $l = 0°$, $b = +29°$ (Field 1 of the Palomar-Groningen Variable-Star Survey)," Bulletin of the Astronomical Institute of the Netherlands Supplement **1**, p. 105, 1966.

Plaut, L., "Variable Stars in a Field Centered at $l = 4°$, $b = +12°$ (Field 2 of the Palomar-Groningen Variable-Star Survey) Part 1: Introduction and RR Lyrae-Type Variables," Bulletin of the Astronomical Institute of the Netherlands Supplement **2**, p. 293, 1968.

Plaut, L., "Variable Stars in a Field Centered at $l = 4°$, $b = +12°$ (Field 2 of the Palomar-Groningen Variable-Star Survey)," Bulletin of the Astronomical Institute of the Netherlands Supplement **3**, p. 1, 1968.

Plaut, L., "Variable Stars in a Field Centered at $l = 0°$, $b = -10°$ (Field 3 of the Palomar-Groningen Variable-Star Survey $\alpha_{1950} = 18^h24^m04^s$, $\delta_{1950} = -33° 58.6'$)," Astronomy and Astrophysics **8**, p. 341, 1970.

Plaut, L., "Variable Stars in a Field Centered at $l = 0°$, $b = -10°$ (Field 3 of the Palomar-Groningen Variable-Star Survey)," Astronomy and Astrophysics Supplement **4**, p. 73, 1971.

Plaut, L., "Palomar-Groningen Variable Star Survey. VI. B and V Observations of Twenty RR Lryae Variables and Some Related Problems," Astronomy and Astrophysics Supplement **12**, p. 351, 1973.

Preston, G.W., Shectman, S.A., and Beers, T.C., "Detection of a Galactic Color Gradient for Blue Horizontal-Branch Stars of the Halo Field and Implications for the Halo Age and Denisty Distrubutions," Astrophysical Journal **375**, p. 121, 1991.

Reid, M.J., in The Center of the Galaxy, IAU Symposium No. 136, (Kluwer, Dordrecht, 1989).

Saha, A., "A Search for Distant Halo RR Lyrae Stars," Astrophysical Journal **283**, p. 580, 1984.

Saha, A., and Oke, J.B., "Spectroscopy and Spectrophotometry of Distant Halo RR Lyrae Stars," Astrophysical Journal **285**, p. 688, 1984.

Saha, A., "RR Lyrae Stars and the Distant Galactic Halo: Distribution, Chemical Composition, Kinematics, and Dynamics," Astrophysical Journal **289**, p. 310, 1985.

Stobie, R.S., Bishop, I.S., King, D.L., "Variable Stars in the South Galactic Cap," Monthly Notices of the Royal Astronomical Society **222**, p. 473, 1986.

Suntzeff, N.B., Kinman, T.D., Kraft, R.P., "Metal Abundances of RR Lyrae Variables in Selected Galactic Star Fields. V. The Lick Astrographic Fields at Intermediate Galactic Latitudes," Astrophysical Journal **367**, p. 528, 1991.

van den Bergh, S., "UBV Photometry in the Nuclear Bulge of the Galaxy," Astronomical Journal **76**, p. 1082, 1971.

Zinn, R., "The Globular Cluster System of the Galaxy. IV. The Halo and Disk Subsystems," Astrophysical Journal **293**, p. 424, 1985.

Chapter 7

Armandroff, T.E., DaCosta, G.S., "The Radial Velocity, Velocity Dispersion, and Mass-to-Light Ratio of the Sculptor Dwarf Galaxy," Astronomical Journal **92**, p. 777, 1986.

Benedict, G.F., and Shelus, P.J., "Applications of Automated Invenotry Techniques to Astrometry," Proceedings of I.A.U. Colloquium No. 48 on Modern Astronomy (Institute of Astronomy, Vienna, 1978).

Benedict, G.F., McGraw, J.T., Hess, T.R., Cawson, M.G.M., Keane, M.J., "Relative Astrometry with the Steward Observatory CCD/Transit Insturment," Astronomical Journal **101**, p. 279, 1991.

Frenk, C.S., White, S.D.M., "The kinematics and dynamics of the Galactic globular cluster system," Monthly Notices of the Royal Astronomical Society **193**, p. 295, 1980.

Harris, W.E., "Spatial structure of the globular cluster system and the distance to the Galactic center," Astronomical Journal **81**, p. 1095, 1976.

Hartwick, F.D.A., Sargent, W.L.W., "Radial Velocities for Outlying Satellites and their Implications for the Mass of the Galaxy," Astrophysical Journal **221**, p. 512, 1978.

Hawkins, M.R.S., "Direct evidence for a massive Galactic halo," Nature **303**, p. 406, 1983.

Hawkins, M.R.S., "A Study of the Galactic halo from a complete sample of RR Lyrae variables to B = 21," Monthly Notices for the Royal Astronomical Society **206**, p.433, 1984.

Hesser, J.E., Shawl, S.J., Meyer, J.E., "Systematic Reinvestigation of the Radial Velocities of the Galactic Globular Clusters: Image-Tube Results," Publications of the Astronomical Society of the Pacific **98**, p.403, 1986.

Jeffreys, W.H., Fitzpatrick, M.J., McArthur, B.E., Gaussfit - A System for Least Squares and Robust Estimation: User's Manual (Department of Astronomy, University of Texas, Austin, 1989).

Kulessa, A.S., Lynden-Bell, D., "The mass of the Milky Way Galaxy," Monthly Notices for the Royal Astronomical Society **255**, p. 105, 1992.

Layden, A.C., "The Metallicities and Kinematics of RR Lyrae Variables. I. New Observations of Local Stars," Astronomical Journal **108**, p. 1016, 1994.

Little, B., Tremaine, S., "Distant Satellites as Probes of our Galaxy's Mass Distribution," Astrophysical Journal **320**, p. 493, 1987.

Liu, T., and Janes, K.A., "The Luminosity Scale of RR Lyrae Stars with the Baade-Wesselink Method. I. Photometry and Radial Velocities," Astrophysical Journal Supplement Series **69**, p. 593, 1989.

Lynden-Bell, D., Cannon, R.D., Godwin, P.J., "Slippery evidence on the Galaxy's invisible heavy halo," Monthly Notices of the Royal Astronomical Society **204**, p. 87P, 1983.

Merrifield, M.R., "The Rotation Curve of the Milky Way to $2.5R_0$ from the Thickness of the HI Layer," Astronomical Journal **103**, p. 1552, 1992.

Mihalas, D. and Binney, J., Galactic Astronomy: Structure and Kinematics, second edition (New York: W.H. Freeman and Company, 1981).

Oke, J.B., Giver, L.P., and Searle, L., "An Analysis of the Absolute Energy Distribution in the Spectrum of SU Draconis," Astrophysical Journal **136**, p. 393, 1962.

Oke, J.B., "A Spectrophotometric Study of X Arietis," Astrophysical Journal **145**, p. 468, 1966.

Olszewski, E.W., Peterson, R.C., Aaronson, M., "High-Precision Radial Velocities for Faint Giants: Radial Velocities of Extreme Halo Systems and the Mass of the Galaxy," Astrophysical Journal **302**, p. L45, 1986.

Peterson, R.C., "Radial Velocities of Remote Globular Clusters: Stalking the Missing Mass," Astrophysical Journal **297**, p. 309, 1985.

Peterson, R.C., Latham, D.W., "The Radial Velocity and Velocity Dispersion of the Remote Globular Cluster Palomar 15: Constraints on the Mass of the Galaxy," Astrophysical Journal **336**, p. 178, 1989.

Saha, A., and Oke, J.B., "Spectroscopy and Spectrophotometry of Distant Halo RR Lyrae Stars," Astrophysical Journal **285**, p. 688, 1984.

Saha, A., "RR Lyrae Stars and the Distant Galactic Halo: Distribution, Chemical Composition, Kinematics, and Dynamics," Astrophysical Journal **289**, p. 310, 1985.

Webbink, R.F., "A Catalog of Radial Velocities in Galactic Globular Clusters," Astrophysical Journal Supplement **45**, p. 259, 1981.

Zaritsky, D., Olszewski, E.W., Schommer, R.A., Peterson, R.C., Aaronson, M., "Velocities of Stars in Remote Galactic Satellites and the Mass of the Galaxy," Astrophysical Journal **345**, p. 769, 1989.

Appendix 1

Appendix 2

Wetterer, C.J., The CCD/Transit Instrument Atlas and Database Guide, Supplement to PhD Dissertation, (Department of Physics and Astronomy, University of New Mexico, 1995).

Appendix 3

RR LYRAE VARIABLE STARS IN THE CCD/TRANSIT INSTRUMENT SURVEY

by

Charles J. Wetterer

Captain, US Air Force

343 pages

PhD, Physics, University of New Mexico, 1995

## ABSTRACT

RR Lyrae variable stars have long been recognized as important tools in probing the mass, chemical distribution and kinematics of the Galaxy from the inner recesses of the nuclear bulge to the outer environs of the distant Galactic halo. This dissertation chronicles an RR Lyrae variable star survey from a thorough description of the initial observations with the CCD/Transit Instrument (CTI), to an examination of RR Lyrae space density and the Galactic mass using the discovered RR Lyrae stars.

The RR Lyrae space density as a function of Galactocentric distance is shown to be a power-law function ($R^{-3 \text{ to } -3.5}$) and consistant with an ellipsoidal distribution in the nuclear bulge and more spherically symmetric distribution in the Galactic halo. The unique area of the CTI survey and comparison to other RR Lyrae surveys verifies this function is valid throughout the Galactic halo and over the range of Galactocentric distances sampled ($0.6 < R < 40$ kpc). Local underdensities and overdensities of RR Lyrae stars are

discussed, including a possible resonance with the Magallenic Clouds ($R \approx 50$ kpc).

The Galactic mass estimated using radial velocities of RR Lyrae stars discovered in the CTI survey does not support the existence of a massive dark Galactic halo. This result is compared to the mass as determined from the radial velocities of other halo objects. Depending on the type of orbits assumed, the radial velocities of RR Lyrae stars, globular clusters, and dwarf elliptical galaxies can be used to support the notion that a massive dark halo exists (i.e. the mass-to-light ratio increases for increasing Galactocentric distance), or that no excessive dark matter exists in the Galactic halo (i.e. the mass-to-light ratio remains constant for increasing Galactocentric distance).

## References (primary)

### Chapter 2


Cawson, M.G.M., McGraw, J.T., Keane, M.J., "A Relational Database Approach to Astronomical Research," SPIE Proc. Vol. 627, p. 70, 1986.

Cawson, M.G.M., McGraw, J.T., Keane, M.J., "The CCD/Transit Instrument (CTI) Data-Analysis System," SPIE Proc. Vol. 627, p. 79, 1986.

Delporte, E., Délimitation Scientifique des Constellations (Tables et Cartes), (Cambridge, At the University Press, 1930).

Dixon, R.S., Gearhart, M.R., and Schmidtke, P.C., Atlas of Sky Overlay Maps (for the Palomar Sky Survey), (The Ohio State Radio Observatory, 1981).

Hoffleit, D., Bright Star Catalogue, 5th revised edition (Yale University Observatory, 1982).

Jones, K.G. (editor), Webb Society Deep-Sky Observer's Handbook Volume 5: Clusters of Galaxies, (Enslow Publishing, 1981).

Kholopov, P.N., Samus, N.N., Frolov, M.S., Goranskij, V.P., Gorynya, N.A., Kireeva, N.N., Kukarkina, N.P., Kurochkin, N.E., Medvedeva, G.I., Perova, N.B., and Shugarov, S.Y., General Catalogue of Variable Stars, 4th edition (Moscow: Nauka Publishing House, 1985-88).

McGraw, J.T., Angel, J.R.P., and Sargent, T.A., "A CCD Transit-telescope Survey for Galactic and Extragalactic Variability and Polarization," SPIE Proc. Vol. 264, p. 20, 1980.

McGraw, J.T., Stockman, H.S., Angel, J.R.P., Epps, H., and Williams, J.T., "The CCD/transit instrument (CTI) deep photometric and polarimetric survey - a progress report," SPIE Proc. Vol. 331, p. 137, 1983.

McGraw, J.T., Cawson, M.G.M., Keane, M.J., "Operation of the CCD/Transit Instrument (CTI)," SPIE Proc. Vol. 627, p. 60, 1986.

McGraw, J.T., Hess, T.R., Green, E.M., Bridges, C.T., Benedict, G.F., "Photometric and Positional Calibration of the CCD/Transit Instrument (CTI) Strip of the Sky," Bulletin of the American Astronomical Society Vol. 21, No. 3, p. 1021, 1989.

McGraw, J.T., "A Strip Search of the Universe," Variable Stars and Galaxies, ASP Conference Series, Vol. 30, p. 77 (San Francisco: Astronomical Society of the Pacific, 1992).

McGraw, J.T., Wetterer, C.J., Hess, T.R., Green, E.M., "Photometric Standard Stars in the CCD/Transit Instrument (CTI) Survey," Bulletin of the American Astronomical Society Vol. 26, No. 2, p. 899, 1994.

Paul, M., "Corrective Systems for Astronomical Reflectors," Rev. d'Optique Vol. 14, p. 169, 1935.

Sulentic, J.W. and Tifft, W.G., The Revised New General Catalogue of Nonstellar Astronomical Objects, (Tucson: The University of Arizona Press, 1973).

Veron-Cetty, M.P., and Veron, P., "A Catalogue of Quasars and Active Galactic Nuclei, 4th edition," E.S.O. Sci. Rep. 7, 1989.

Wetterer, C.J., McGraw, J.T., Hess, T.R., Grashuis, R., "Variable Stars in the CCD/Transit Instrument (CTI) Survey," Bulletin of the American Astronomical Society Vol. 26, No. 2, p. 899, 1994.

Wetterer, C.J., The CCD/Transit Instrument Atlas and Database Guide, Supplement to PhD Dissertation, (Department of Physics and Astronomy, University of New Mexico, 1995).

Zwicky, F., Herzog, E., Wild, P., Karpowicz, M., Kowal, C.T., The Catalogue of Galaxies and Clusters of Galaxies, (California Institute of Technology, 1961-68).

, The National Geographic Society - Palomar Observatory Sky Survey, (California Institute of Technology, 1954).

, Smithsonian Astrophysical Observatory Star Catalog, (Washington, Smithsonian Institution, 1966-1990).

Chapter 3

Cawson, M.G.M., McGraw, J.T., Keane, M.J., "A Relational Database Approach to Astronomical Research," SPIE Proc. Vol. 627, p. 70, 1986.

Cawson, M.G.M., McGraw, J.T., Keane, M.J., "The CCD/Transit Instrument (CTI) Data-Analysis System," SPIE Proc. Vol. 627, p. 79, 1986.

Dieckvoss, W., Kox, H., Gunther, A., and Brosterhus, E., AGK3 Star Catalog of Positions and Proper Motions North of -2.5 degree Declination (Hamburg-Bergedorf, 1975).

Lasker, B.M., Sturch, C.R., McLean, B.J., Russell, J.L., Jenkner, H., Shara, M.M., "The Guide Star Catalog I. Astronomical Foundations and Image Processing," Astronomical Journal **99**(6), p. 2019, 1990.

McGraw, J.T., Hess, T.R., Green, E.M., Bridges, C.T., Benedict, G.F., "Photometric and Positional Calibration of the CCD/Transit Instrument (CTI) Strip of the Sky," Bulletin of the American Astronomical Society Vol. 21, No. 3, p. 1021, 1989.

McGraw, J.T., "A Strip Search of the Universe," Variable Stars and Galaxies, ASP Conference Series, Vol. 30, p. 77 (San Francisco: Astronomical Society of the Pacific, 1992).

Wetterer, C.J., <u>The CCD/Transit Instrument Atlas and Database Guide</u>, Supplement to PhD Dissertation, (Department of Physics and Astronomy, University of New Mexico, 1995).

<u>Chapter 4</u>

Allen, R.H., <u>Star Names: Their Lore and Meaning</u> (New York: Dover Publications, 1963).

Bevington, P.R., <u>Data Reduction and Error Analysis for the Physical Sciences</u> (New York: McGraw-Hill Book Company, 1969).

Campbell, L. and Jacchia, L., <u>The Story of Variable Stars</u> (Philidelphia: The Blakiston Company, 1941).

Cox, J.P., <u>Theory of Stellar Pulsation</u> (Princeton: Princeton University Press, 1980).

Hawkins, M.R.S., "A Study of the Galactic halo from a complete sample of RR Lyrae variables to B = 21," Monthly Notices for the Royal Astronomical Society **206**, p.433, 1984.

Kholopov, P.N., Samus, N.N., Frolov, M.S., Goranskij, V.P., Gorynya, N.A., Kireeva, N.N., Kukarkina, N.P., Kurochkin, N.E., Medvedeva, G.I., Perova, N.B., and Shugarov, S.Y., <u>General Catalogue of Variable Stars</u>, 4th edition (Moscow: Nauka Publishing House, 1985-88).

Petit, M., <u>Variable Stars</u> (English translation, New York: John Wiley & Sons Ltd., 1987).

Saha, A. and Hoessel, J.G., "RR Lyrae stars in Local Group galaxies I: NGC 185," Astronomical Journal **99** (1), p. 97, 1990.

Stobie, R.S., Bishop, I.S., King, D.L., "Variable Stars in the South Galactic Cap," Monthly Notices of the Royal Astronomical Society **222**, p. 473, 1986.

<u>Chapter 5</u>

Barnes III, T.G., Hawley, S.L., "On Absolute Magnitues of RR Lyrae Stars," Astrophysical Journal **307**, p. L9, 1986.

Beckert, D.C. and Newberry M.V., "The Design and Testing of Filter-Detector Systems using Synthetic Photometry," Publications of the Astronomical Society of the Pacific **101**, p. 849, 1989.

Burstein, D., and Heiles, C., "Reddenings Derived form HI and Galaxy Counts: Accuracy and Maps," Astronomical Journal **87** (8), p. 1165, 1982.

Carney, B.W., Storm, J., Jones , R.V., "The Baade-Wesselink Method and the Distances to RR Lyrae Stars. VIII. Comparisons with Other Techniques and Implications for Globular Cluster Distances and Ages," Astrophysical Journal **386**, p. 663, 1992.

Cox, J.P., <u>Theory of Stellar Pulsation</u> (Princeton: Princeton University Press, 1980).

Hawley, S.L., Jeffreys, W.H., Barnes III, T.G., "Absolute Magnitudes and Kinematic Properties of RR Lyrae Stars," Astrophysical Journal **302**, p. 626, 1986.

Kholopov, P.N., Samus, N.N., Frolov, M.S., Goranskij, V.P., Gorynya, N.A., Kireeva, N.N., Kukarkina, N.P., Kurochkin, N.E., Medvedeva, G.I., Perova, N.B., and Shugarov, S.Y., <u>General Catalogue of Variable Stars</u>, 4th edition (Moscow: Nauka Publishing House, 1985-88).

Kukarkin, B.V., Kholopov, P.N., Artiukhina, N.M., Fedorovich, V.P., Frolov, M.S., Goranskij, V.P., Gorynya, N.A., Karitskaya, E.A., Kirreeva, N.N., Kukarkina, N.P., Kurochkin, N.E., Medvedeva, G.I., Perova, N.B., Ponomareva, G.A., Samus, N.N., and Shugarov, S.Y., <u>New Catalogue of Suspected Variable Stars</u> (Moscow: Nauka Publishing Office, 1982).

Lafler, J., and Kinman, T.D., "An RR Lyrae Star Survey with the Lick 20-inch Astrograph II. The Calculation of RR Lyrae Periods by Electronic Computer," Astrophysical Journal Supplement **11** p. 216, 1965.

Laubscher, B., Gregory, S., Bauer, T., Zeilik, M., Burns, J., "A CCD Camera System at Capilla Peak Observatory, New Mexico," Publications of the Astronomical Society of the Pacific **100**, p. 131, 1988.

Layden, A.C., Hanson, R.B., Hawley, S.L., "Absolute Magnitudes and Kinematics of RR Lyrae Stars via Statistical Parallax," Bulletin of the American Astronomical Society Vol. 26, No. 2, p. 911, 1994.

Lee, Y-W, "Evidence for an Old Galactic Bulge from RR Lyrae Stars in Baade's Window: Implications for the Formation of the Galaxy and the Age of the Universe," Astronomical Journal **104** (5), p. 1780, 1992.

Mihalas, D. and Binney, J., Galactic Astronomy: Structure and Kinematics, second edition (New York: W.H. Freeman and Company, 1981).

Nemec, J.M., Linnell Nemec, A.F., Lutz, T.E., "Period-Luminosity-Metallicity Relations, Pulsation Modes, Absolute Magnitudes, and Distances for Population II Variable Stars," Astronomical Journal **108**, p. 222, 1994.

Newberry, M.V., "Signal-to-Noise Considerations for Sky-Subtracted CCD Data," Publications of the Astronomical Society of the Pacific **103**, p. 122, 1991.

Saha, A. and Hoessel, J.G., "RR Lyrae stars in Local Group galaxies I: NGC 185," Astronomical Journal **99** (1), p. 97, 1990.

Sandage, A., "Evidence for a Period-Luminosity-Amplitude Relation for RR Lyrae Stars," Astrophysical Journal **244**, p. L23, 1981.

Sandage, A., Katem, B., Sandage, M., "The Oosterhoff Period Groups and the Age of Globular Clusters. I. Photometry of Cluster Variables in M15," Astrophysical Jouranl Supplement **46**, p. L41, 1981.

Sandage, A., "The Oosterhoff Period Groups and the Age of Globular Clusters. II. Properties of RR Lyrae Stars in Six Clusters: The P-L-A Realation," Astrophysical Jouranl **248**, p. 161, 1981.

Sandage, A., "The Oosterhoff Period Groups and the Age of Globular Clusters. III. The Age of the Globular Cluster System," Astrophysical Jouranl **252**, p. 553, 1982.

Sandage, A., Katem, B., Sandage, M., "The Oosterhoff Period Groups and the Age of Globular Clusters. IV. Field RR Lyrae Stars: Age of the Galactic Disk," Astrophysical Jouranl Supplement **252**, p. 574, 1982.

Stellingwerf, R.F., "Period Determination using Phase Dispersion Minimization," Astrophysical Journal **224**, p. 953, 1978.

Szeidl, B. "Multiple Periodic Variable Stars," IAU Colloquium No. 29, edited by W.S. Fitch (Reidel, Dordrecht), p. 133, 1976.

Tsesevich, V.P. "RR Lyrae Stars," in Pulsating Stars (edited

by B.V. Kukarkin), English translation (New York: Halsted Press, 1975).

Tyson, J.A., "The Shift-and-Stare Technique and a Large Area CCD Mosaic," CCDs in Astronomy, ASP Conference series, Vol. 8, p. 1, (San Francisco: Astronomical Society of the Pacific, 1990).

, The Astronomical Almanac for the year 1993 (Washington D.C.: United States Government Printing, 1992).

Chapter 6

Blanco, B.M., "RR Lyrae Variables in Baade's Window," Astronomical Journal **89**, p. 1836, 1984.

Blanco, B.M., "RR Lyare Variables in a Galactic Bulge Window," Astronomical Journal **103**, p. 1872, 1992.

Hartwick, F.D.A., Barlow, D.J., Hesser, J.E., "Variable Stars in the Bulge of the Galaxy in a Field Around NGC 6304," Astronomical Journal **86**, p. 1044, 1981.

Hawkins, M.R.S., "A Study of the Galactic halo from a complete sample of RR Lyrae variables to B = 21," Monthly Notices for the Royal Astronomical Society **206**, p.433, 1984.

Kinman, T.D., "An RR Lyrae Star Survey with the Lick 20-inch Astrograph I. Methods of Observation and Reduction," Astrophysical Journal Supplement Series **11**, p. 199, 1965.

Kinman, T.D., Wirtanen, C.A., and Janes, K.A. "An RR Lyrae Star Survey with the Lick 20-inch Astrograph III. A Survey of Part of the Variable Star Field MWF 361," Astrophysical Journal Supplement Series **11**, p. 223, 1965.

Kinman, T.D., Wirtanen, C.A., and Janes, K.A. "An RR Lyrae Star Survey with the Lick 20-inch Astrograph IV. A Survey of Three Fields Near the North Galactic Pole," Astrophysical Journal Supplement Series **13**, p. 379, 1966.

Kinman, T.D., Mahaffey, C.T., and Wirtanen, C.A. "An RR Lyrae Star Survey with the Lick 20-inch Astrograph V. A Survey of Three Fields at Intermediate Latitudes Towards the Galactic Anti-Center," Astronomcal Journal **87**, p. 314, 1982.

Kinman, T.D., Wong-Swanson, B., Wenz, M., Harlan, E.A., "An RR Lyrae Star Survey with the Lick Astrograph VI. New Photometric Observations and Ephemerides for the Variables in the Field RR I (MWF 361A)," Astronomcal Journal **89**, p. 1200, 1984.

Lafler, J., and Kinman, T.D., "An RR Lyrae Star Survey with

the Lick 20-inch Astrograph II. The Calculation of RR Lyrae Periods by Electronic Computer," Astrophysical Journal Supplement Series **11**, p. 216, 1965.

Layden, A.C., Hanson, R.B., Hawley, S.L., "Absolute Magnitudes and Kinematics of RR Lyrae Stars via Statistical Parallax," Bulletin of the American Astronomical Society Vol. 26, No. 2, p. 911, 1994.

Merrifield, M.R., "The Rotation Curve of the Milky Way to $2.5R_0$ from the Thickness of the HI Layer," Astronomical Journal **103**, p. 1552, 1992.

Oort, J.H., and Plaut, L., "The Distance to the Galactic Centre Derived form RR Lyrae Variables, the Distribution of these Variables in the Galaxy's Inner Region and Halo, and a Redicussion of the Galactic Rotation Constants," Astronomy and Astrophysics **41**, p. 71, 1975.

Plaut, L., "Variable Stars in a Field Centered at $l = 0°$, $b = +29°$ (Field 1 of the Palomar-Groningen Variable-Star Survey)," Bulletin of the Astronomical Institute of the Netherlands Supplement **1**, p. 105, 1966.

Plaut, L., "Variable Stars in a Field Centered at $l = 4°$, $b = +12°$ (Field 2 of the Palomar-Groningen Variable-Star Survey) Part 1: Introduction and RR Lyrae-Type Variables," Bulletin of the Astronomical Institute of the Netherlands Supplement **2**, p. 293, 1968.

Plaut, L., "Variable Stars in a Field Centered at $l = 4°$, $b = +12°$ (Field 2 of the Palomar-Groningen Variable-Star Survey)," Bulletin of the Astronomical Institute of the Netherlands Supplement **3**, p. 1, 1968.

Plaut, L., "Variable Stars in a Field Centered at $l = 0°$, $b = -10°$ (Field 3 of the Palomar-Groningen Variable-Star Survey $\alpha_{1950} = 18^h24^m04^s$, $\delta_{1950} = -33° 58.6'$)," Astronomy and Astrophysics **8**, p. 341, 1970.

Plaut, L., "Variable Stars in a Field Centered at $l = 0°$, $b = -10°$ (Field 3 of the Palomar-Groningen Variable-Star Survey)," Astronomy and Astrophysics Supplement **4**, p. 73, 1971.

Plaut, L., "Palomar-Groningen Variable Star Survey. VI. B and V Observations of Twenty RR Lryae Variables and Some Related Problems," Astronomy and Astrophysics Supplement **12**, p. 351, 1973.

Preston, G.W., Shectman, S.A., and Beers, T.C., "Detection of a Galactic Color Gradient for Blue Horizontal-Branch Stars of the Halo Field and Implications for the Halo Age and Denisty Distrubutions," Astrophysical Journal **375**, p. 121, 1991.

Reid, M.J., in The Center of the Galaxy, IAU Symposium No. 136, (Kluwer, Dordrecht, 1989).

Saha, A., "A Search for Distant Halo RR Lyrae Stars," Astrophysical Journal **283**, p. 580, 1984.

Saha, A., and Oke, J.B., "Spectroscopy and Spectrophotometry of Distant Halo RR Lyrae Stars," Astrophysical Journal **285**, p. 688, 1984.

Saha, A., "RR Lyrae Stars and the Distant Galactic Halo: Distribution, Chemical Composition, Kinematics, and Dynamics," Astrophysical Journal **289**, p. 310, 1985.

Stobie, R.S., Bishop, I.S., King, D.L., "Variable Stars in the South Galactic Cap," Monthly Notices of the Royal Astronomical Society **222**, p. 473, 1986.

Suntzeff, N.B., Kinman, T.D., Kraft, R.P., "Metal Abundances of RR Lyrae Variables in Selected Galactic Star Fields. V. The Lick Astrographic Fields at Intermediate Galactic Latitudes," Astrophysical Journal **367**, p. 528, 1991.

van den Bergh, S., "UBV Photometry in the Nuclear Bulge of the Galaxy," Astronomical Journal **76**, p. 1082, 1971.

Zinn, R., "The Globular Cluster System of the Galaxy. IV. The Halo and Disk Subsystems," Astrophysical Journal **293**, p. 424, 1985.

## Chapter 7

Armandroff, T.E., DaCosta, G.S., "The Radial Velocity, Velocity Dispersion, and Mass-to-Light Ratio of the Sculptor Dwarf Galaxy," Astronomical Journal **92**, p. 777, 1986.

Benedict, G.F., and Shelus, P.J., "Applications of Automated Invenotry Techniques to Astrometry," Proceedings of I.A.U. Colloquium No. 48 on Modern Astronomy (Institute of Astronomy, Vienna, 1978).

Benedict, G.F., McGraw, J.T., Hess, T.R., Cawson, M.G.M., Keane, M.J., "Relative Astrometry with the Steward Observatory CCD/Transit Insturment," Astronomical Journal **101**, p. 279, 1991.

Frenk, C.S., White, S.D.M., "The kinematics and dynamics of the Galactic globular cluster system," Monthly Notices of the Royal Astronomical Society **193**, p. 295, 1980.

Harris, W.E., "Spatial structure of the globular cluster system and the distance to the Galactic center," Astronomical Journal **81**, p. 1095, 1976.

Hartwick, F.D.A., Sargent, W.L.W., "Radial Velocities for Outlying Satellites and their Implications for the Mass of the Galaxy," Astrophysical Journal **221**, p. 512, 1978.

Hawkins, M.R.S., "Direct evidence for a massive Galactic halo," Nature **303**, p. 406, 1983.

Hawkins, M.R.S., "A Study of the Galactic halo from a complete sample of RR Lyrae variables to B = 21," Monthly Notices for the Royal Astronomical Society **206**, p.433, 1984.

Hesser, J.E., Shawl, S.J., Meyer, J.E., "Systematic Reinvestigation of the Radial Velocities of the Galactic Globular Clusters: Image-Tube Results," Publications of the Astronomical Society of the Pacific **98**, p.403, 1986.

Jeffreys, W.H., Fitzpatrick, M.J., McArthur, B.E., Gaussfit - A System for Least Squares and Robust Estimation: User's Manual (Department of Astronomy, University of Texas, Austin, 1989).

Kulessa, A.S., Lynden-Bell, D., "The mass of the Milky Way Galaxy," Monthly Notices for the Royal Astronomical Society **255**, p. 105, 1992.

Layden, A.C., "The Metallicities and Kinematics of RR Lyrae Variables. I. New Observations of Local Stars," Astronomical Journal **108**, p. 1016, 1994.

Little, B., Tremaine, S., "Distant Satellites as Probes of our Galaxy's Mass Distribution," Astrophysical Journal **320**, p. 493, 1987.

Liu, T., and Janes, K.A., "The Luminosity Scale of RR Lyrae Stars with the Baade-Wesselink Method. I. Photometry and Radial Velocities," Astrophysical Journal Supplement Series **69**, p. 593, 1989.

Lynden-Bell, D., Cannon, R.D., Godwin, P.J., "Slippery evidence on the Galaxy's invisible heavy halo," Monthly Notices of the Royal Astronomical Society **204**, p. 87P, 1983.

Merrifield, M.R., "The Rotation Curve of the Milky Way to $2.5R_0$ from the Thickness of the HI Layer," Astronomical Journal **103**, p. 1552, 1992.

Mihalas, D. and Binney, J., Galactic Astronomy: Structure and Kinematics, second edition (New York: W.H. Freeman and Company, 1981).

Oke, J.B., Giver, L.P., and Searle, L., "An Analysis of the Absolute Energy Distribution in the Spectrum of SU Draconis," Astrophysical Journal **136**, p. 393, 1962.

Oke, J.B., "A Spectrophotometric Study of X Arietis," Astrophysical Journal **145**, p. 468, 1966.

Olszewski, E.W., Peterson, R.C., Aaronson, M., "High-Precision Radial Velocities for Faint Giants: Radial Velocities of Extreme Halo Systems and the Mass of the Galaxy," Astrophysical Journal **302**, p. L45, 1986.

Peterson, R.C., "Radial Velocities of Remote Globular Clusters: Stalking the Missing Mass," Astrophysical Journal **297**, p. 309, 1985.

Peterson, R.C., Latham, D.W., "The Radial Velocity and Velocity Dispersion of the Remote Globular Cluster Palomar 15: Constraints on the Mass of the Galaxy," Astrophysical Journal **336**, p. 178, 1989.

Saha, A., and Oke, J.B., "Spectroscopy and Spectrophotometry of Distant Halo RR Lyrae Stars," Astrophysical Journal **285**, p. 688, 1984.

Saha, A., "RR Lyrae Stars and the Distant Galactic Halo: Distribution, Chemical Composition, Kinematics, and Dynamics," Astrophysical Journal **289**, p. 310, 1985.

Webbink, R.F., "A Catalog of Radial Velocities in Galactic Globular Clusters," Astrophysical Journal Supplement **45**, p. 259, 1981.

Zaritsky, D., Olszewski, E.W., Schommer, R.A., Peterson, R.C., Aaronson, M., "Velocities of Stars in Remote Galactic Satellites and the Mass of the Galaxy," Astrophysical Journal **345**, p. 769, 1989.

## References (secondary)

### Chapter 2

Baker, J.G., "On Improving the Effectiveness of Large Telescopes," IEEE Trans. on Aerospace and Electronic Systems Vol. AES-5, No. 2, p. 261, 1969.

Benedict, G.F., McGraw, J.T., Hess, T.R., Cawson, M.G.M., Keane, M.J., "Relative Astrometry with the Steward Observatory CCD/Transit Instrument," Bulletin of the American Astonomical Society Vol. 21, No. 4, p. 1109, 1989.

Benedict, G.F., McGraw, J.T., Hess, T.R., Cawson, M.G.M., Keane, M.J., "Relative Astrometry with the Steward Observatory CCD/Transit Instrument," Astronomical Journal **101**, p. 279, 1991.

Bond, H.E., Kron, R.G. and Spinrad, H., "GQ Comae and V396 Herculis: Two Low-Redshift Optically Variable QSOs," Astrophysical Journal **213** (1), p. 1, 1977.

Borra, E.F., Content, R., Drinkwater, M.J., Szapiel, S., "A Deffraction Limited f/2 1.5 meter Diameter Liquid Mirror," Astrophysical Journal Letters **346**, p. L41, 1989.

Borra, E.F., Content, R., Girard, L., Szapiel, S., Tremblay, L.M., "Liquid Mirrors: Optical Shop Tests and Contributions to the Technology," Astrophysical Journal **393**, p. 829, 1992.

Content, R., Borra, E.F., Drinkwater, M.J., Poirier, S., Poisson, E., Beauchemin, M., Boily, E., Gauthier, A., Tremblay, L.M., "A Search for Optical Flares and Flashes with a Liquid Mirror Telescope," Astronomical Journal **97** (3), p. 917, 1989.

Erleksova, G.E., "EQ Vulpeculae," Переменнье звездьі, Прцложенце **2** №10, p. 248, 1975.

Hoffmeister, C., "Untersuchung der Schtaube des Positions-Fadenmikrometers *Heyde 3013*," Mitteilungen der Sternwarte zu Sonneberg Nr. 6, 1924.

Hoffmeister, C., "Relative Koordinaten, Örter und Karten neuer Veränderlicher," Mitteilungen der Sternwarte zu Sonneberg Nr. 17, 1930.

Hoffmeister, C., "Relative Koordinaten, Örter und Karten neuer Veränderlicher," Mitteilungen der Sternwarte zu Sonneberg Nr. 22, 1933.

Hoffmeister, C., "89 neue veränderliche Sterne," Astronomische Nachrichten **284**, p. 275, 1959.

Hoffmeister, C., "Mitteilungen über neuentdeckte Veränderliche Sterne (S9727-S10152)," Astronomische Nachrichten **290** H1-2, p. 43, 1967.

Kent, S.M., Ramella, M., Nonino, M., "A Small Drift Scan Survey for Galaxies in the Northern Sky," Astronomical Journal **105** (2), p. 393, 1993.

Kent, S.M., Stoughton, C., Newberg, H., Loveday, J., Petravick, D., Gurbani, V., Berman, E., Sergey, G., Lupton, R., Sloan Digital Sky Survey, Report #FNAL/C-94/084, (Batavia, Ill.: Fermi National Accelerator Laboratory, 1994).

Kron, R., "Digital Optical Sky Surveys," Bulletin of the American Astronomical Society Vol. 26, No. 2, p. 915, 1994.

Kurochkin, N.E., "New Variable Stars in the Region of M56," Переменнье звездьі **17** №128, p. 186, 1970.

Kinman, T., Wirtanen, C.A. and Janes, K.A., "An RR Lyrae Star Survey with the Lick 20 inch Astrograph. IV. A Survey of Three Fields Near the North Galactic Pole," Astrophysical Journal Supplement **119**, p. 379, 1966.

Kirkpatrick, J.D., McGraw, J.T., "The CCD/Transit Instrument (CTI) Blue Object Survey," IAU Colloquium #114 (White Dwarfs), p. 167, 1988.

Kirkpatrick, J.D., Henry, T.J., McCarthy, D.W., McGraw, J.T., "Constraining the Faint End of the Stellar Luminosity Function Through a Systematic Search for M Dwarfs," Bulletin of the American Astronomical Society, Vol. 22, No. 4, p. 1204, 1990.

Kirkpatrick, J.D., Spectroscopic and Photometric Studies of Main Sequence M Stars and a Search for Late Type Dwarfs in the Solar Vicinity, Phd dissertation, (Department of Astronomy, The University of Arizona, 1992).

Kirkpatrick, J.D., "The Luminosity Function of Field M Dwarfs: Evidence for a Population of Substellar Objects," Bulletin of the American Astronomical Society Vol. 26, No. 2, p. 944, 1994.

Kirkpatrick, J.D., "The Luminosity Function at the End of the Main Sequence: Results of a Deep, Large-Area, CCD Survey for Cool Dwarfs," Astrophysical Journal Supplement Series **94**, p. 749, 1994.

McGraw, J.T., Cawson, M.G.M., Kirkpatrick, J.D., Haemmerle, V., "A Strip Search for Quasars: The CCD/Transit Instrument (CTI) Quasar Survey," Proceedings of a Workshop on Optical Surveys for Quasars, p. 163, 1988.

McGraw, J.T., "The Lunar Transit Telescope (LTT): An Early Lunar Based Science and Engineering Mission," Engineering, Construction and Operations in Space III, p. 1865, 1992.

McGraw, J.T. (editor), Proceedings of the Lunar Ultraviolet Telescope Experiment (LUTE) Science Workshop, (Institute for Astrophysics, The University of New Mexico, 1993).

Meinunger, L., "Über Veränderliche in einigen T-Assoziationen," Mitteilungen über Veränderliche Sterne **3** H5, p. 137, 1966.

Miller, W.J. and Wachmann, A.A., "Six New Variable Stars in the Cygnus Cloud, VV 125-130," Ricerche Astronomiche **6** №22, p. 497, 1964.

Miller, W.J., "Eleven Variable Stars in the Cygnus Cloud, VV 151-161," Ricerche Astronomiche **7** №4, p. 197, 1965.

Miller, W.J., "Ten New Variable Stars in the Cygnus Cloud, VV

191-200," Ricerche Astronomiche **7** №10, p. , 1967.

Pinto, G. and Romano, G., "Researches with the Schmidt Telescope VI - The Variable Stars around Gamma Comae," Memorie della Società Astronomica Italiana **44** №1, p. 53, 1973.

Rügemer, H., "Neue Veränderliche Sterne," Astronomische Nachrichten **248**, p. 409, 1933.

Shaganian, B.L. and Shaganian, V.B., "On Three Longperiod Variable Stars in the Region of M56," Переменные звезды, Прцложенце **3** №18, p. 748, 1979.

Stoughton, C., Annis, J., Kent, S., Kron, R., Loveday, J., McKay, T., Newberg, H., "First Data from the Fermilab Drift Scan Camera," Bulletin of the American Astronomical Society Vol. 26, No. 2, p. 897, 1994.

Vogt, N. and Bateson, F.M., "An Atlas of Southern and Equitorial Dwarf Novae," Astronomy and Astrophysics Supplement **48** (3), p. 383, 1982.

Wachmann, A.A., "Die Veränderlichen im Südteil der Cygnuswolke - Teil II," Astronomische Abhandlungen der Hamburger Sternwarte, Band VI Nr. 2, 1963.

Wachmann, A.A., "Die Veränderlichen im Südteil der Cygnuswolke - Teil III," Astronomische Abhandlungen der Hamburger Sternwarte, Band VI Nr. 3, 1964.

, Mitteilungen über Veränderliche Sterne №299, 1957.

Chapter 4

Jacoby, G.H., Branch, D., Ciardullo, R., Davies, R.L., Harris, W.E., Pierce, M.J., Pritchet, C.J., Tonry, J.L., Welch, D.L., "A Critical Review of Selected Techniques for Measuring Extragalactic Distances," Publications of the Astronomical Society of the Pacific **104**, p. 599, 1992.

Madore, B.F., Freedman, W.L., " The Cepheid Distance Scale," Publications of the Astronomical Society of the Pacific **103**, p. 933, 1991.

Chapter 5

Beckert, D.C., Cox, D., Gordon, S., Jaderlund, E., Mann, E., Zeilik, M., "1989 BVR photometry of CG Cygni", IBVS #3398, 1989.

Beckert, D.C. and Newberry M.V., "The Design and Testing of Filter-Detector Systems using Synthetic Photometry,"

Publications of the Astronomical Society of the Pacific **101**, p. 849, 1989.

Beckert, D.C., Gordon, S., Jaderlund, E., Mann, E., Zeilik, M., "CG Cygni redux : more 1989 BVR data", IBVS #3556, 1991.

Bryja, C., Lawrence, G., "Photometry of Suspected Low Mass Hyades Cluster Members," Bulletin of the American Astronomical Society, Vol. 23, No. 2, p. 908, 1991.

Bryja, C., Jones, T.J., Humphreys, R.M., Lawrence, G., Pennington, R.L., Zumach, W., "Candidate Brown Dwarfs in the Hyades," Astrophysical Journal **388**, p. L23, 1992.

Deeg, H-J., Brinks, E., Duric, N., Klein, U., Skillman, E., "New 325 MHz Observations of HII Galaxies: The Mechanisms That Shape the Unusual Radio Spectra," Astrophysical Journal **410**, p. 626, 1993.

Gordon, S., Hall, S., Ledlow, M., Mann, E., Zeilik, M., "1989 BVR light curves of RT And," IBVS #3469, 1990.

Gisler, G., Laubscher, B., Chabot, N., Boudreaux, K., Grashuis, R., "Multi-filter Optical Observations of SL9 Impact Spots on Jupiter," Bulletin of the American Astronomical Society Vol. 26, No. 4, p. 1374, 1994.

Gregory, S.A., Deeg, H.-J., Morrison, G., Crane, M., Grashuis, R., Lacey, C., "Galaxian Nuclear Spectral Types as a Function of Environment," Bulletin of the American Astronomical Society Vol. 22 No. 2, p. 881, 1990.

Hayes, J.J.E., Sadun, A.C., and R. Grashuis, "Narrow-band images of Arp 213," Bulletin of the American Astronomical Society Vol. 25 No. 4, p. 1248, 1993.

Kidger, M., et al., "Multiband Monitoring of OJ287 in 1993/94," Bulletin of the American Astronomical Society Vol. 26, No. 4, p. 1506, 1994.

Laubscher, B., Gregory, S., Bauer, T., Zeilik, M., Burns, J., "A CCD Camera System at Capilla Peak Observatory, New Mexico," Publications of the Astronomical Society of the Pacific **100**, p. 131, 1988.

Laubscher, B., Gregory, S., "Galaxy alignments in the Perseus supercluster," Bulletin of the American Astronomical Society Vol. 25, No. 2, p. 913, 1993.

Laubscher, B., "Problems with Galaxy Position Angles," Bulletin of the American Astronomical Society Vol. 26, No. 2, p. 963, 1994.

Odewahn, S.C., "Properties of the Magellanic-type spirals. I -

Surface photometry of NGC 4618 and NGC 4625," Astronomical Journal **101**, p. 829, 1991.

Odewahn, S.C., Bryja, C., Humphreys ,R.M., "Improved CCD Standard Fields," Publications of the Astronomical Society of the Pacific **104**, p. 553, 1992.

Sadun, A., "Optical Variability of the Blazar OJ 287," Bulletin of the American Astronomical Society Vol. 26, No. 4, p. 1467, 1994.

Schmidt, B.P., Kirshner, R.P., Eastman, R.G., Grashuis, R., Dell'Antonio, I., Caldwell, N., Foltz, C., Huchra, J.P., Milone, A.A.E., "The Unusual Supernoa SN 1993J in M81," Nature **364**, p. 600, 1993.

Schmidt, B.P., Kirshner, R.P., Eastman, R.G., Phillips, M.M., Suntzeff, N.B., Hamuy, M., Aviles, R., Filippenko, A.V., Ho, L., Matheson, T., Grashuis, R., Maza, J., Kirkpatrick, J.D., Kuijken, K. Zucker, D., Bolte, M., Tyson, N., "The Expanding Photosphere Method Applied to SN 1992am at cz = 14600 km $s^{-1}$," Astronomical Journal **107**, p. 1444, 1994.

Summers, D.L., Zeilik, M., "Starspot activity on the RS CVn candidate 1E 1919+0427," Bulletin of the American Astronomical Society, Vol. 22, No. 4, p. 1295, 1990.

Summers, D.L., Zeilik, M., Jaderlund, E., Hoeppe, G., Collins, A., "1991 V-band photometry of an eclipsing binary: 1E 1919+0427," IBVS #3708, 1992.

Takalo, L.O., Pursimo, T., Sillanpää, A., Lehto, H., Nilsson, K., Kidger, M., deDiego, J.A., Gonzales-Perez, J.N., Rodriguez-Espinoza, J-M., Mahoney, T., Boltwood, P., Dultzin-Hacyan, D., Benitez, E., Turner, G.W., Robertson, J.W., Honeycutt, R.K., Efimov, T.S., Shakhovskoy, N., Charles, P.A., Schramm, K.J., Borgeest, U., Linde, J.V., Sadun, A., Grashuis, R., "The Light Curve of Blazar 3C 66A," Bulletin of the American Astronomical Society Vol. 26, No. 4, p. 1507, 1994.

Taylor, C., Brinks, E., Grashuis, R., Skillman, E., "An Optical and Radio Atlas of Companions to Dwarf Galaxies," to be published in Astrophysical Journal Supplement Series, 1995.

Wetterer, C.J., McGraw, J.T., Hess, T.R., Grashuis, R., "Variable Stars in the CCD/Transit Instrument (CTI) Survey," Bulletin of the American Astronomical Society Vol. 26, No. 2, p. 899, 1994.

Zeilik, M., DeBlasi, D., Rhodes, M., Budding, E., "A Half-Century of Starspot Activity on SV Camelopardalis," Bulletin of the American Astronomical Society Vol. 19., No. 4, p. 1086, 1987.

Zeilik, M., Beckert, D., DeBlasi, C., Ledlow, M., Rhodes, M., Williams, T., "1987 BVRI Photometry of RT And," IBVS #3173, 1988.

Zeilik, M., Cox, D., DeBlasi, D., Ledlow, M., Rhodes, M., Williams, T., "1988 BVRI Photometry of XY UMa," IBVS #3200, 1988.

Zeilik, M., DeBlasi, D., Rhodes, M., Budding, E., "A Half-Century of Starspot Activity on SV Camelopardalis," The Astrophysical Journal **332**, p. 293, 1988.

Zeilik, M., Beckert, D., Cox, D., Dolby, J., Ledlow, M., Newberry, M., Rhodes, M., "1989 V-band light curve of RT And," IBVS #3301, 1989.

Zeilik, M., Cox, D.A., DeBlasi, C., Rhodes, M., Budding, E., "Long-Term Starspot Activity of Short-Period RS CVn Stars, Part II, RT Andromedae," The Astrophysical Journal **345**, p.991, 1989.

Zeilik, M., DeBlasi, C.B., Gordon, S., Ledlow, M., "1990 BVR photometry of XY UMa," IBVS #3535, 1990.

Zeilik, M., Gordon, S., Cox, D., Beckert, D., "Long-term starspot activity of short-period RS CVn stars : CG Cygni," Bulletin of the American Astronomical Society, Vol. 22, No. 2, p. 830, 1990.

Zeilik, M., Ledlow, M., Rhodes, M., Arevardo, M.J., Budding, E., "Long-Term Starspot Activity of Short-Period RS CVn Stars, Part III, BH Virginis," The Astrophysical Journal **354**, p.352, 1990.

Zeilik, M., Cox, D.A., De Blasi, C., Rhodes, M., Budding, E., "Long-Term Starspot Activity of Short-Period RS CVn Stars, Part IV, WY Cancri," The Astrophysical Journal **363**, p.467, 1990.

Zeilik, M., Heckert, P., Ledlow, M., Summers, D.L., Jaderlund, E., Boudreau, K., M., "1991 BVR photometry of CG Cygni," IBVS #3663, 1991.

Zeilik, M., Deeg, H.J., "Long-term starspot activity of short-period RS CVn stars : XY UMa," Bulletin of the American Astronomical Society, Vol. 23, No. 2, p. 880, 1991.

Zeilik, M., Gordon, S., Jaderlund, E., Ledlow, M., Summers, D.L., Heckert, P.A., Budding, E., Banks, T.S., "Long-term Starspot Activity of Short-Period RS Canum Venaticorum Stars. V. CG Cygni," Astrophysical Journal **421**, p. 303, 1994.